A Modelling and Experimental Study of Evaporating Two-Phase Flow on the Shellside of Shell-and-Tube Heat Exchangers

A thesis submitted to the University of Strathclyde department of Mechanical Engineering for the fulfilment of the degree of Doctor of Philosophy

April 2005

By

Gavin H. Doo

Acknowledgements

I would like to thank J.M. McNaught at the National Engineering Laboratory (NEL) in East Kilbride and Dr W. Dempster from the Department of Mechanical Engineering at Strathclyde University for their technical support, supervision and advice throughout the course of this project. I would also like to thank Tom Clark at NEL for his assistance with the experimental facility.

In addition I gratefully acknowledge the financial support I have received for the project from both the EPSRC and NEL, and also the financial support for the test work provided by Hyprotech UK Ltd.

Finally, special thanks to Monica. Your constant support has been a huge help in enabling me to finish this thesis.

Abstract

The thesis describes the results of a research programme involving both experimental and modelling work to study evaporation on the shellside of shell-and-tube heat exchangers. The particular focus is on the study of evaporation over a range of mass fluxes typical of operating practice. Current design procedures make simplifying assumptions (such as a uniform gas/liquid distribution across the entire cross section of the shellside) which are thought to be inaccurate. The experimental work was conducted on a TEMA E-type shell and tube evaporator. The evaporator has 97 tubes of length 1240 mm, and the unit is large enough to represent full-scale industrial exchangers. Geometrical considerations such as baffle orientation and presence of sealing strips were also tested. The results show that there is a drop in the heat transfer performance at lower mass fluxes and higher vapour outlet qualities. It is suggested that the sudden drop in heat transfer performance at lower mass fluxes is caused by a change in flow pattern on the shellside of the heat exchanger. Evidence suggests that there is a possible transition from a homogeneous to a stratified two-phase flow. Support for this conclusion is that the transition in heat transfer performance appears to coincide with a change in the behaviour of the measured two-phase pressure drop multiplier. The thesis also describes the development of a model for shellside heat transfer and pressure drop which allows for the effects of separated flow and also attempts to predict the apparent transition in two-phase flow pattern. Knowledge of the existence of the transition and its prediction is important in avoiding unexpected poor performance in practice. A close correspondence is found when the predictions from the developed model are compared with the data from the experimental programme.

Nomenclature

Symbol	Quantity	Units
A_f	Geometric / 'Non frictional' two-phase Multiplier	-
A, S	Cross sectional area / flow area	m^2
B	Factor in two-phase multiplier correlations	-
b	Value in equation 8.24	-
C	Constant in equation 2.52	-
D, d	Diameter	m
E	Wetting factor due to entrainment in Model-C	-
F_b	Boiling correction factor	-
F_c	Boiling correction factor	-
f	Friction factor	-
g_n	Acceleration due to gravity	m/s^2
H	Height	m
h	Specific enthalpy	J/kg
j	Mixed flow superficial velocity	m/s
K	Slip ratio	-
$\dot{M}$	Mass flowrate	kg/s
$\dot{m}$	Mass flux	kg/m^2s
n	Number of velocity heads in shellside pressure drop network/	-
	Exponent in equation 2.5	-
p, P	Pressure	Pa
P_t	Tube pitch	m
$\dot{Q}$	Heat duty / Heat load	W
$\dot{q}$	Heat flux	W/m^2
R_l	Liquid volume fraction	-
r	Radius	m
S	Suppression factor in equation 2.4	-
s	Height above base of shell at which baffle begins (Model-B)	m
T	Temperature	^0C, K
U	Overall heat transfer coefficient	W/m^2K
u_c	Combined standard uncertainty	-
u_i	Instrument uncertainty	-
u_m	Measurement uncertainty	-
u(y)	Standard uncertainty in parameter y	-

$\dot{V}$	Volumetric flowrate	m^3/s
$\dot{v}$	Superficial velocity	m/s
$\dot{v}_g^*$	Wallis dimensionless gas velocity	-
X	Lockhart-Martinelli parameter, also empirical parameter in Stephan-Abdelsalam correlation	-
x	Vapour quality, vapour mass fraction	-
α	Heat transfer coefficient	W/m^2K
β	Volumetric vapour/gas fraction	-
Δ	Difference operator	-
Δh_l	Specific latent heat of vaporisation	J/kg
ε_g	Void fraction	-
ϕ_l^2	Two-phase pressure drop multiplier based on liquid-phase flowing alone	-
ϕ_{lo}^2	Two-phase pressure drop multiplier based on total flow with liquid properties	-
η	Dynamic viscosity	Ns/m^2
λ	Thermal conductivity	W/mK
ρ	Density	kg/m^3
σ	Surface tension	N/m
ψ	Dimensionless parameter in Figures 2.8 and 2.10	-

Subscripts

acc	Acceleration term
b	Bulk property, bubble(diameter), baffle
bc	Boundary condition
boil	Boiling term
c, crit	Critical parameter
cb	Convective boiling
eq	Equivalent(diameter)
evap	Evaporating flow
exp	Expanded
fc	Forced convective
g, G, V, VAP	Gas/Vapour phase
go	Total flow with gas/vapour properties
H	Homogeneous

i	Inner
l, L, LIQ	Liquid phase
lo	Total flow with liquid properties
Model-A	Parameter calculated in Model-A
Model-B	Parameter calculated in Model-B
Model-C	Parameter calculated in Model-C
nb	Nucleate boiling
nc	Natural convection
o	Outer
s	Static (pressure), Shellside
Sat	Saturated conditions
sg	Superficial gas property
sl	Superficial liquid property
t	Tubeside
tot, TOT	Total
tp, TP	Two-phase
w	Wall

Abbreviations

HTFS	Heat Transfer and Fluid Flow Service
HTRI	Heat Transfer Research Inc.
NEL	National Engineering Laboratory
TASC	HTFS Shell-and-Tube Heat Exchanger Design Program
TEMA	Tubular Exchanger Manufacturer's Association

Table of Contents

CHAPTER 1 – Introduction

The project is concerned with advancing the technology used in the thermal design of shell and tube heat exchangers in which evaporation occurs outside a bundle of tubes with the flow being directed by baffle plates. The shell and tube heat exchanger is very commonly used in chemical and process plant. This type of heat exchanger is by far the most popular for a number of practical reasons including; reliability, availability of established design standards and suitability for operation at high pressures.

Specific applications in which shellside evaporation occurs are feed-effluent exchangers and reboilers. In the feed-effluent exchanger the effluent from a process is used to heat and possibly vaporise the feed stream. The reboiler is used to vaporise a fraction of the bottom product from a distillation column. There are three principal types of reboiler: those which have no circulation of the liquid phase through the exchanger, those which have forced circulation and those which have natural circulation. The best example of the first type is the kettle reboiler where the evaporation takes place outside a bundle of tubes immersed in a pool of liquid and the exit vapour stream is produced by the migration of the vapour phase to the upper part of the shell. In the forced circulation case the process liquid is pumped through the shellside of the exchanger where the evaporation takes place producing an exit stream that is a mixture of liquid and vapour. In natural circulation, the liquid flow through the exchanger is maintained by the difference in density of the two-phase mixture of vapour and liquid in the exchanger and the single-phase liquid in the base of the distillation column. The dependence on the process of natural circulation requires an accurate thermal-hydraulic design for this type of reboiler.

Thermal design of a heat exchanger involves calculation of the surface area required to transfer a specified heat duty from a hot fluid to a cold fluid within imposed constraints such as pressure drop. It is very important to ensure that the design meets the required duty since operating penalties for underperformance may be severe. Once the heat exchanger is designed it may be necessary to conduct simulations to determine performance under off-design conditions. Nowadays these calculations are almost always performed using computer programs.

A computer model for the thermal performance of a heat exchanger needs to calculate heat transfer coefficients and pressure gradients. In two phase flow an incremental calculation is required because conditions such as the vapour quality on which heat transfer and pressure drop depend can vary along the exchanger.

The methods in the programs are based on research data that are validated, if possible against full-scale testing. The programs therefore offer enhanced accuracy and confidence in design. Shellside evaporation is a particularly complex process for which research and validation data are scarce, and this project was initiated to address the need both for more data and enhanced understanding of the thermal-hydraulic processes.

In the design of evaporators or reboilers there are two types of boiling to be considered: pool boiling and flow boiling. Pool boiling is the term used to describe nucleate boiling in a pool of liquid. In many practical cases the boiling process is a combination of nucleate boiling and convective boiling. Nucleate boiling describes the process by which heat is removed from the hot surface through the generation of vapour bubbles. In convective boiloing heat is removed by conduction/convection through a liquid layer on the heated surface and evaporation takes place at the liquid/vapour interface. The heat transfer coefficient in flow boiling is usually calculated by combining terms that describe the heat transfer due to nucleate boiling and that due to forced convection. The heat transfer coefficient due to nucleate boiling is generally larger than that due to forced convection and it is of concern to the designer of any evaporator/reboiler that the process of nucleate boiling can be sustained at the heated surface.

In the case of evaporation on the shell side of a shell and tube heat exchanger the heated surface consists of the outer surface of all the tubes in the tube bank. To sustain the process of nucleate boiling it is essential that the tubes in the tube bank are surrounded by the liquid phase to enable the generation of new bubbles. Many of the tubes may become dry if there is a change in the two-phase flow pattern which causes a separation of the liquid and vapour phases as areas of the tube bank become full of vapour. The heat transfer coefficients obtained in shellside evaporation are closely related to the local conditions of the two-phase flow. Unfortunately accurate prediction of local conditions in boiling two-phase flow on the shellside geometry is a very difficult task. The nature of shellside flow is very complex because of the many different directions the flow can take due to the shellside baffles and the required mechanical clearances between the tubes, the shell and the baffles. The flow is even more complex when there are two phases, especially when the fraction of the two phases are changing (as in boiling). As a result computer based models generally make the assumption that the two phases are sufficiently mixed to prevent dry patches of vapour around any of the tubes. This is related to another principal assumption that the vapour void fraction around one tube is identical to that around any other tube provided that they are at the same distance between the inlet and outlet of the shell. In order to test the validity of such assumptions it is necessary to produce more data for evaporating shellside flows.

One of the primary objectives of this study was to produce data for evaporating shellside flows which can be used to assess methods for the prediction of heat transfer and pressure drop. This data would be used to assess the current methods used in industry and will also provide means of testing future developments in modelling the behaviour of shellside two-phase flow beyond the scope of this project. An additional objective was to identify any limitations in current methods and if possible to produce an improved model for shellside evaporating flows.

The boiling and condensing test facility at the National Engineering Laboratory in East Kilbride was used throughout the project to generate a wide range of data for shellside evaporation. The facility contains a shell and tube evaporator which is large enough to represent conditions in a real industrial unit. The tests would be focussed on a wide range of operating conditions and changes in the shellside geometry. The principal changes made to the shellside geometry were the inclusion of sealing strips in the crossflow bypass lane and the orientation (horizontal / vertical) and pitch of the shellside baffles.

Data collected in the project would be compared with the HTFS shell and tube heat exchanger design software program TASC. This program is widely used throughout industry for designing shell and tube heat exchangers and would be used to represent the current most sophisticated available method.

Any limitations in the current methods that were highlighted by the comparison with the experimental data would be explored in an attempt to create an improved description of the shellside evaporating flow.

CHAPTER 2 – Literature Review

2.1 – Introduction

The principal objective of the literature review is to examine the existing open literature on the subject of two-phase flow (in particular evaporating two-phase flow) on the shellside of shell-and-tube heat exchangers. Existing procedures for the design of shellside evaporators such as the horizontal thermosyphon reboiler will be examined. These procedures will be assessed in terms of accuracy, applicability to a variety of conditions and scope for improvement. The aim of the literature review is to provide a starting point from which an improved model of shellside two-phase flow can be developed. Key areas of interest include the performance of shellside evaporators at relatively low mass fluxes (which may arise in off-design operation) and the possibility of non-uniform distribution of the liquid and vapour phases. The related problem of void fraction prediction in shellside evaporation will also be examined as it is likely that this will have a significant impact on the prediction of heat transfer and pressure drop performance.

2.2 – Shellside evaporation in baffled heat exchangers

The main focus of the current project is on the subject of shellside evaporation in baffled exchangers which may be used as feed-effluent exchangers, reboilers or any application involving vapour generation. Figure 2.1 shows some standard baffled shell types (Yilmaz, 1987) which can be used for shellside evaporation applications.

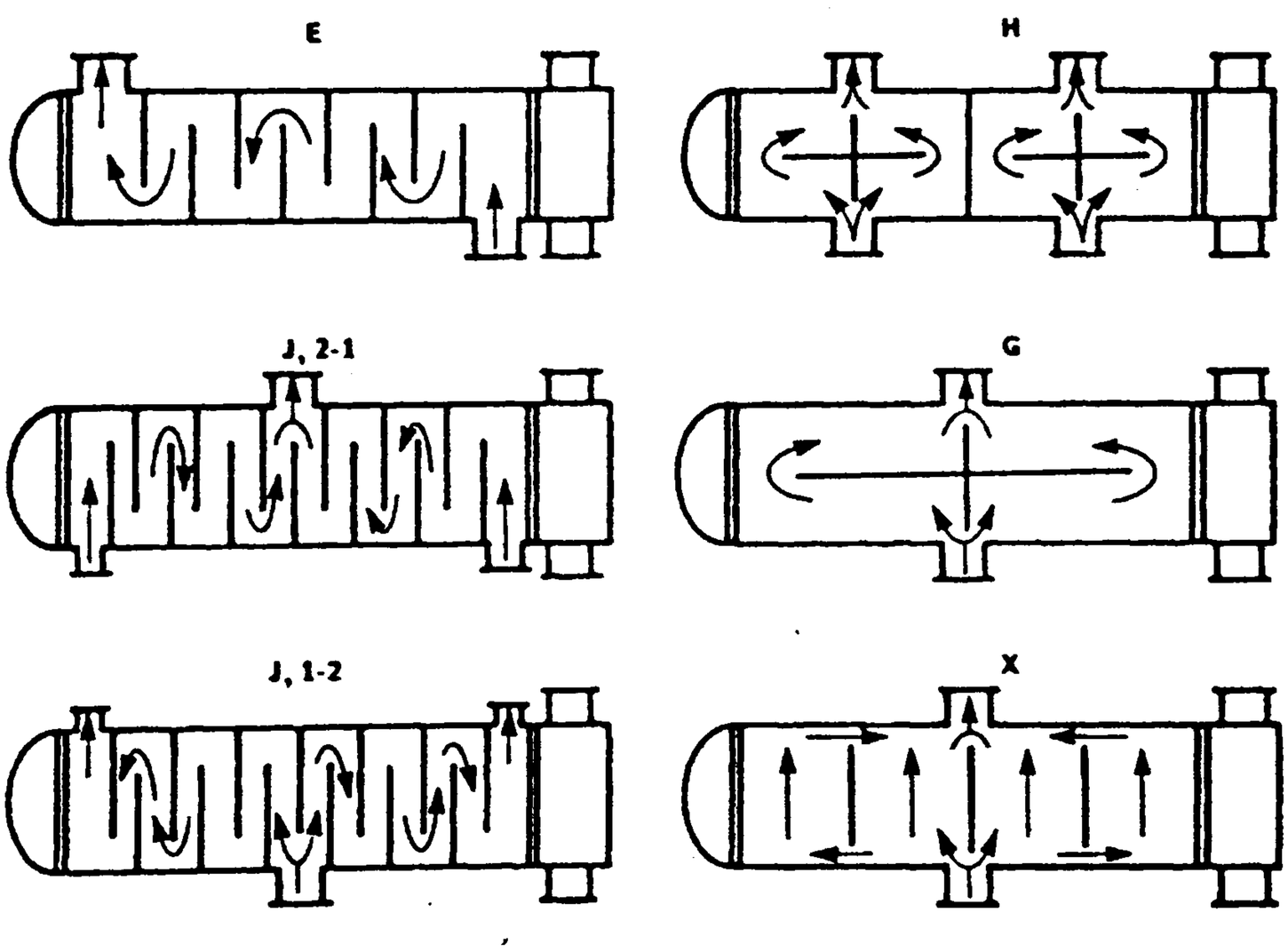

Figure 2.1 – Baffled heat exchanger shell types (Yilmaz, 1987)

The choice of the most appropriate shell type is dependant on the application of the heat exchanger in the particular situation. The following guidelines have been recommended (Yilmaz, 1987; Palen, 1990); for small shells the simple E-type configuration is effective. For larger exchangers, pressure drop limits due to the necessity for adequate circulation may require a J shell to be used. The X-shell type is generally preferable for vacuum service with narrow boiling ranges. G and H type shells have horizontal baffles that prevent shortcutting of fluid between the shellside nozzles and are preferable to X-shells for wide boiling mixtures. For identical conditions the X shell has the lowest pressure drop followed by H, G and J, the E shell has the highest pressure drop. In general the choice of shell often depends on balancing the pressure drop and heat transfer relationship, usually shells which produce a higher pressure drop will also produce the highest heat transfer rates.

As can be seen from Figure 2.1, the flow direction through the shell is largely controlled by the shellside baffles. The choice of baffle type can have a large effect on the shellside heat transfer and pressure drop. The baffle is chosen to control the flow direction between the inlet and outlet shellside nozzles. The standard type of baffle is the segmental baffle. These can be either single, double or triple segmental as indicated by Figure 2.2. Double or triple segmental baffles are often used to split the flow. Triple segmental baffles are sometimes used when there are strict limitations for pressure drop on the shellside.

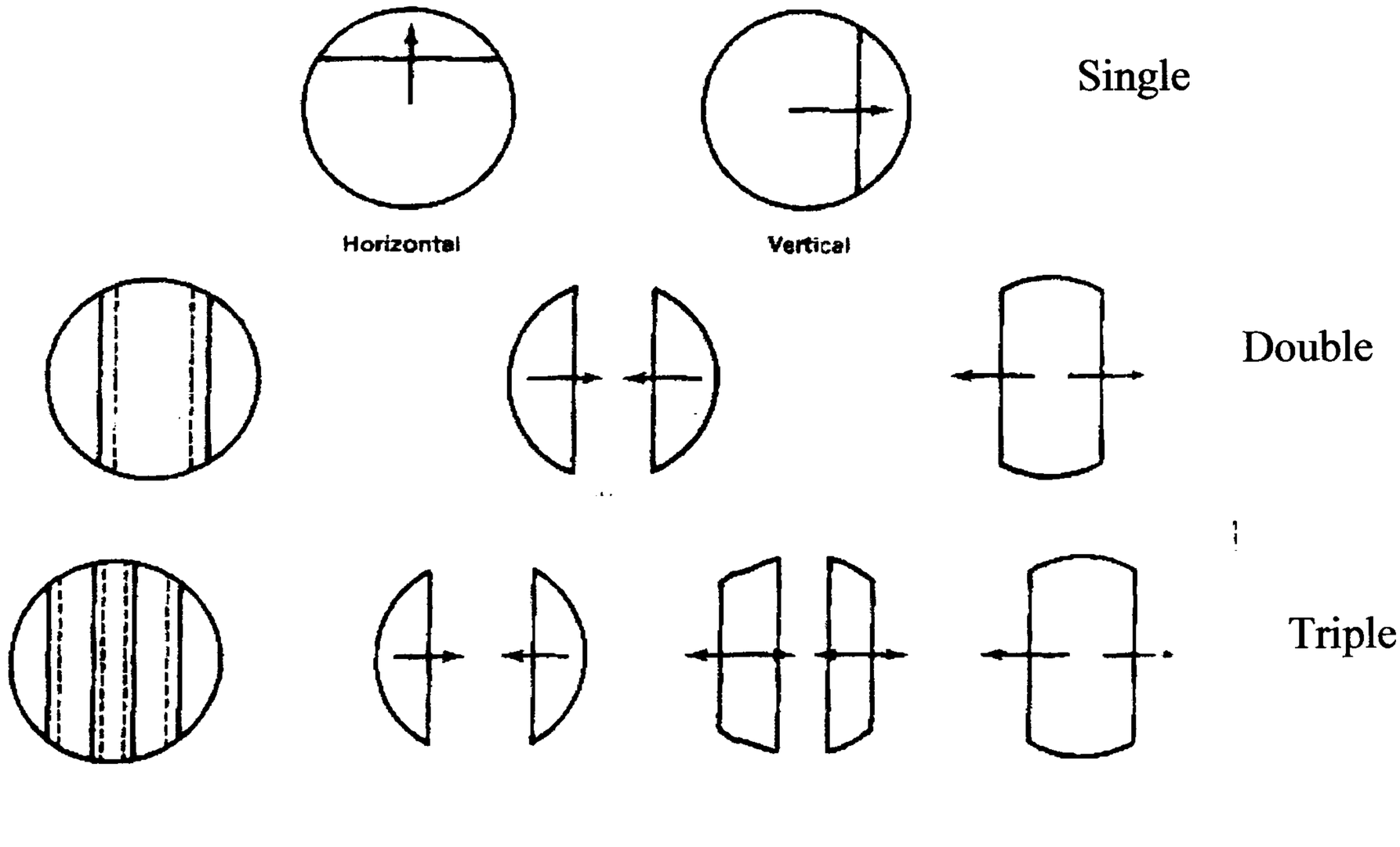

Figure 2.2 – Segmental baffle types (arrows indicate flow direction) – (Perry et al, 1997)

With the horizontal baffle, the predominant flow direction is up and down along the length of the shell. For the vertical cut, the flow will mainly be horizontally from side to side along the length of the shell. The choice of baffle type, baffle size and length (pitch) between shellside baffles are all important considerations which can have a significant impact on shellside pressure drop and heat transfer rates. Baffle size is usually quantified by a term called the baffle cut which refers to the ratio between the open segment height and the shell internal diameter. As a general rule the larger the baffle cut, the larger the space between shellside baffles and the smaller the area of the baffles (generally smaller with double and triple segmental baffles) the lower the shellside pressure drop. This is because with these arrangements there is less restriction to the flow between the shellside nozzles. A consequence of having little flow restriction is that the flow across the banks of tubes (termed crossflow) is at a lower velocity than with the arrangements where there is greater restriction (closely spaced baffles with small baffle cuts and large baffle areas). A higher crossflow velocity will lead to higher rates of heat transfer as the flow velocity has a large impact on the convective component of heat transfer. As a result the choice of type and layout of shellside baffles is usually a choice of balancing the importance of increasing crossflow velocity and heat transfer with the need to minimise shellside pressure drop. In arrangements such as the horizontal thermosyphon reboiler (Figure 2.3) a larger baffle pitch is usually desired to ensure that the shellside pressure drop is kept to a minimum. This is an important consideration as in such circumstances the process stream flowrate is driven by natural circulation and a large shellside pressure drop would require a large liquid level in the distillation column. This larger liquid level would imply a taller column and in turn increased capital costs.

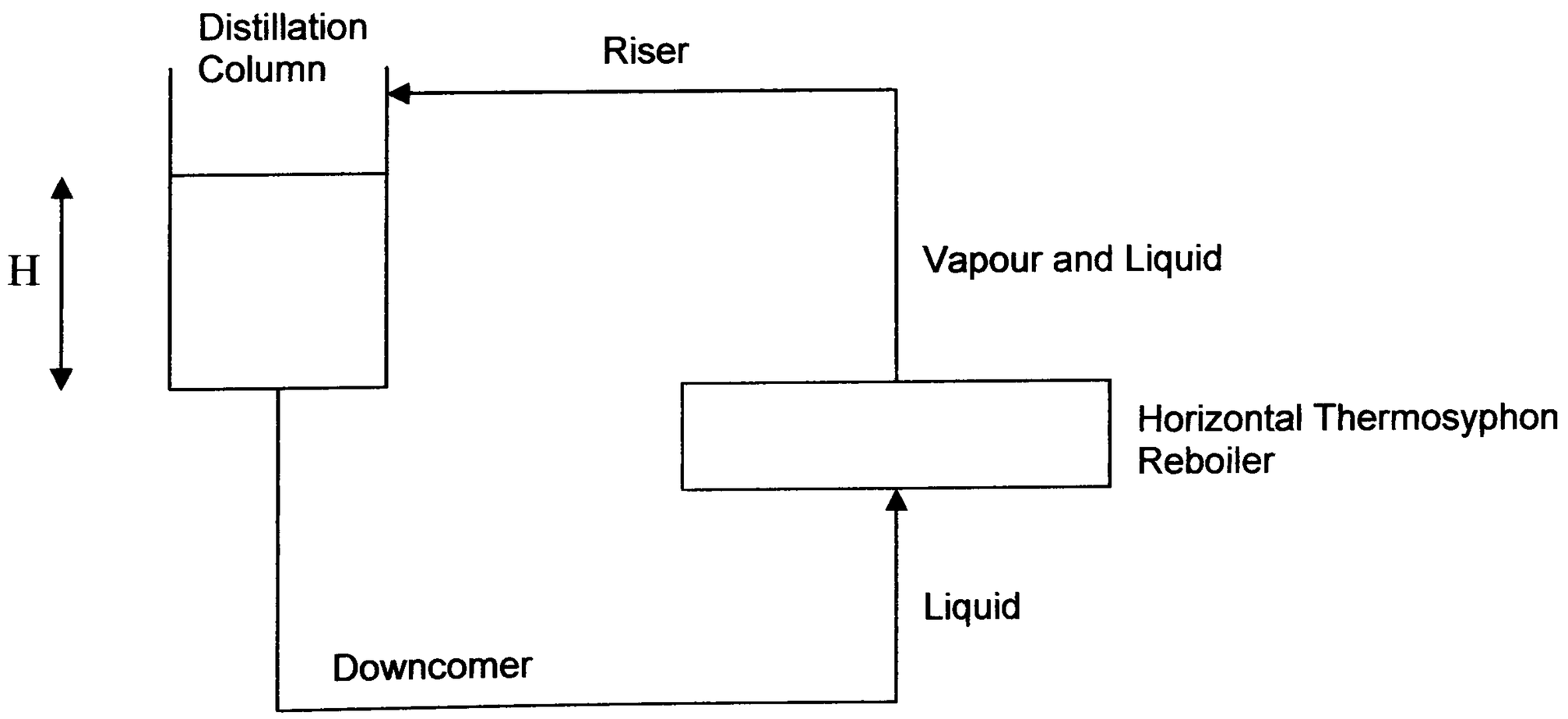

Figure 2.3 – Horizontal Thermosyphon reboiler arrangement

2.3 – Existing Data in the Literature on Shellside Two-Phase Flow

There has been a significant amount of study on the subject of two-phase flows in geometries that resemble the shellside of a shell and tube heat exchanger. The focus of this section is to examine the literature which may be considered the most applicable or relevant to the subject of boiling two-phase shellside flow. Studies involving non-boiling flows and two-phase flows in test sections where the geometry significantly differs from that of the typical shellside layout are also examined where they have been particularly influential in creating design methods for boiling two-phase shellside flow applications.

Many attempts have been made to study the behaviour of two-phase flow on the outside of bundles of horizontal tubes. Polley and Grant (Polley et al, 1973) and Grant, Findlay and Harris (Grant et al, 1974) studied two-phase air/water flowing vertically in a rectangular test section past a horizontal tube bank (Figure 2.4). The purpose of the particular test was to assess the influence of the crossflow bypass region on phase separation and two-phase pressure drop.

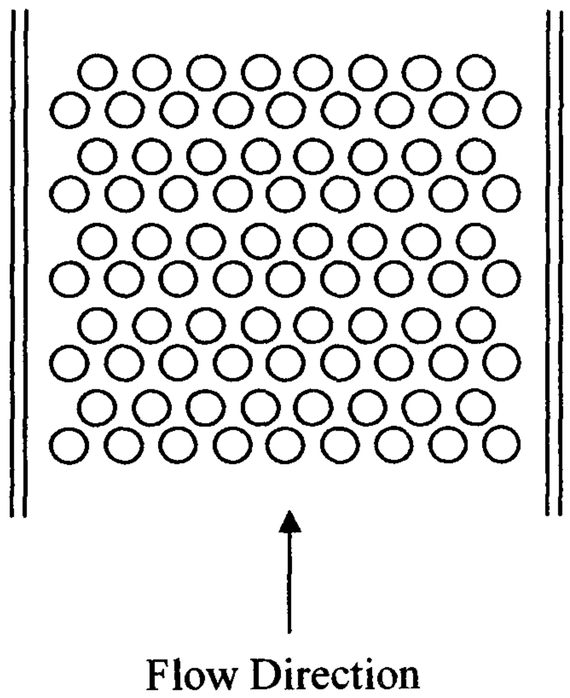

Figure 2.4 – Rectangular tube bundle test section

Many other tests have been carried out on rectangular test sections with and without bypass streams similar to the arrangement in Figure 2.4. A number of these tests (Cotchin, 1980; Cotchin et al, 1979; Dowlati et al, 1990, 1992, 1996; Grant et al, 1986; Schrage et al, 1988) focussed on developing methods for predicting pressure drop in two-phase crossflow. Generally these tests involved measuring the pressure drop of the two-phase flow and comparing this result with the pressure drop when only the liquid or vapour phase was flowing (generally the comparison is made with the liquid phase pressure drop). As a result of these studies, a number of correlations have been developed for a parameter called the 'two-phase pressure drop multiplier' which is used to describe the effects of two-phase flow on pressure drop. Another parameter which is closely linked to the prediction of the pressure drop and

heat transfer in two-phase flow is the vapour void fraction ε_g. This is defined as the fraction of the cross sectional area occupied by the vapour phase. Tests on the rectangular type tube bank geometry (Figure 2.4) have been carried out to measure the void fraction during two-phase crossflow (Dowlati et al, 1990, 1992, 1996; Feenstra et al, 2000; Grant et al, 1982, 1986; Schrage et al, 1988). Different methods have been identified for measuring the void fraction. In earlier studies (Grant et al, 1982, 1986; Schrage et al, 1988) the use of quick closing valves was preferred. These valves were used to control plates which almost instantaneously shut-off the flow into and out of a length of rectangular test section allowing the fraction of vapour and liquid remaining in the test section to be determined. In the more recent tests (Dowlati et al, 1990, 1992, 1996; Feenstra et al, 2000) gamma densitometers have been used to determine the fraction occupied by the liquid and vapour phases. Other tests that were carried out on the geometry of Figure 2.4 included tests to measure boiling heat transfer coefficients in vertical crossflow (Cornwell, 1990; Jensen et al, 1988; Roser et al, 1999) and tests to measure two-phase flow patterns (Hassan et al, 1990; Noghrehkar et al, 1999).

All of the above test data is useful for the purpose of designing a shell and tube heat exchanger with shellside boiling. The primary limitation of all this work for the objectives of the current project is that the test geometry displayed in Figure 2.4 can only truly represent the crossflow stream of a real heat exchanger. In a real shell and tube exchanger a large proportion of the flow is likely to be moving in different directions as the flow is directed between successive crossflow regions by shellside baffles. In addition there will be flows between various mechanical clearances between the tube bundle and the shell, the tubes and the baffles and the baffles and the shell, which are likely to affect the measured values of two-phase pressure drop and void fraction. To accurately recreate the conditions on the shellside of a real industrial heat exchanger it is necessary to undertake tests in a geometry which includes the baffles and mechanical clearances that would exist in the real case. Cornwell and Schuller (Cornwell et al, 1982) and Leong and Cornwell (Leong et al, 1979) have carried out flow boiling tests in a kettle reboiler. With this geometry there is a circular tube bundle, however the flow paths on the shellside are significantly different than those in baffled shellside geometry where the exit stream contains both vapour and liquid phases. Cotchin and Young (Cotchin et al, 1979) carried out a series of experimental tests on a TEMA E-type shell-and-tube heat exchanger. The fluids used were air and water and the tests were designed to produce methods for calculating the two-phase pressure drop in shellside geometries. Grant, Cotchin and White (Grant et al, 1987, 1989) also used an E-type heat exchanger as the test geometry when they carried out studies to examine two-phase pressure drop and flow patterns in shellside two-phase flow. Once again the test fluids used were air and water. The limitations of applying air/water data to predict the behaviour of a boiling two-

phase flow are that the vapour quality rarely varies as it does in the boiling case and the ratio of the vapour and liquid densities may be very different for air/water than for the boiling fluid. This could have significant implications as vapour and liquid densities are important characteristics in predicting the two-phase flow behaviour. From an analysis of the papers which contain data on the subject of two-phase flows in geometries closely resembling the shellside of a shell and tube heat exchanger, it is apparent that there is very little data on actual boiling two-phase flows. Recently HTFS have carried out commercial research and produced a small amount of data on shellside boiling two-phase flow in a TEMA E-type shell that has been unavailable in the open literature. The data represents limited measurements taken on one particular shell geometry and the results of the tests are contained within internal HTFS reports (Chu et al, 1998; McNaught et al, 1999). The data collected in these tests represents a starting point for testing methods for boiling shellside flow (Further analysis of these tests is contained in Chapter 5). To adequately assess existing methods far more data is required for boiling two-phase flows in geometries that are typically used in industry for such applications.

On the evidence of the literature most of the existing data on the subject of shellside two-phase flow is based on data from test sections which represent idealised crossflow. The majority of the data in more realistic shellside geometry is for flows of adiabatic air and water. There currently exists very little (none in the open literature) data for actual boiling flows in realistic shellside geometries. As a result, in order to assess existing commercial methods for predicting shellside two-phase boiling heat transfer coefficients and pressure drop there is a definite necessity to produce more test data for boiling two-phase flow on realistic shellside geometries.

2.4 – Development in areas related to shellside two-phase flow

2.4.1 – Introduction

The purpose of this section of the literature review is to examine areas which have been the subject of research in the open literature which may be of use in providing an improved description of shellside two-phase evaporating flow. The focus shall be on research which may help to describe the best approach to predicting shellside pressure drop and heat transfer. The heavily related problem of predicting the shellside vapour void fraction will also be examined.

2.4.2 – Predicting heat transfer in shellside two-phase flow

The calculation of the boiling heat transfer coefficient in shellside flow is based on a combination of two evaporative heat transfer processes. The two processes are defined as 'nucleate' and 'convective' boiling. Generally reboilers and shellside evaporators are designed to operate with predominantly nucleate boiling as the controlling mechanism. This is because the nucleate boiling coefficient is in most cases larger than the convective boiling term. The shellside boiling coefficient is calculated by combining these two parameters. This section examines some of the principal methods used for combining these terms.

Equation 2.1 shows one approach (Palen, 1990) in which the average boiling heat transfer coefficient is calculated using the nucleate boiling coefficient for a single-tube and terms for the convective boiling and natural convection.

$$\alpha_{boil} = \alpha_{nb(1)} F_b F_c + \alpha_{nc} \tag{2.1}$$

The factor F_b contains the convective boiling term and is given by equation 2.2.

$$F_b = \frac{F_c \alpha_{nb(1)} + \alpha_{cb}}{F_c \alpha_{nb(1)}} \tag{2.2}$$

F_c is the correction factor due to the presence of a mixture. For a pure component equation 2.1 reduces to.

$$\alpha_{boil} = \alpha_{nb(1)} F_b + \alpha_{nc} \tag{2.3}$$

The combination approach suggested by Yilmaz (Yilmaz, 1987) is similar to the tubeside model of Chen (Chen, 1966). It contains a suppression factor to the nucleate boiling term which accounts for the fact that the temperature difference for nucleate boiling is decreased when the convective boiling contribution is significant. The equation is presented in 2.4

$$\alpha_{boil} = S \alpha_{nb} + \alpha_{cb} \tag{2.4}$$

Another approach to describe the combination of the nucleate and convective boiling terms is the asymptotic method of equation 2.5 used by several authors.

$$\alpha_{boil} = \left(\alpha_{nb}{}^{n} + \alpha_{cb}{}^{n} \right)^{1/n} \tag{2.5}$$

For shellside boiling a value of $n = 2$ is recommended (Kutateladze, 1961; McNaught, 1994).

2.4.3 – Nucleate boiling term

Methods for describing the heat transfer coefficient due to nucleate boiling for a case with a flowing fluid (as on the shellside of a shell-and-tube heat exchanger) are examined in this section. The mechanism can be defined by considering a tube surrounded by a vertical

crossflow of liquid. As the heat flux increases from the tube side a point is reached where the convective heat transfer on the shellside is not strong enough to prevent the tube wall temperature rising above the saturation temperature of the shellside fluid. The elevated wall temperature superheats the liquid in contact with the wall and activates the nucleation sites generating bubbles (Figure 2.5).

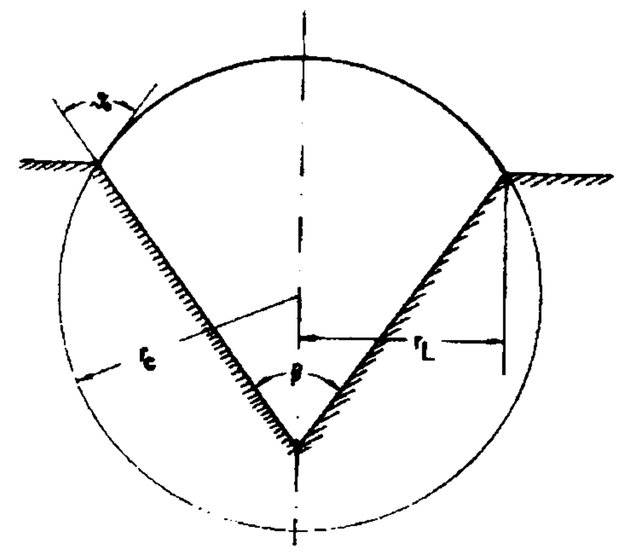

Figure 2.5 – Formation of a spherical bubble in a nucleation site

At first only some nucleation sites are activated and forced convection continues to be the controlling mechanism in the remaining areas. This condition is defined as partial nucleate boiling. As the heat flux is increased the number of nucleation sites activated increases and eventually the nucleate boiling mechanism dominates. This is defined as fully developed nucleate boiling. The nucleate boiling heat transfer coefficient is usually calculated using physical property based correlations and is generally presented in either the form of equation 2.6 or equation 2.7.

$$\alpha_{nb} = C_1 \left(\Delta T_b\right)^{m_1} \tag{2.6}$$

$$\alpha_{nb} = C_2 \left(q\right)^{m_2} \tag{2.7}$$

For typical non-enhanced commercial tubes the value of m_1 is in the range of 2-3 (Palen, 1990). Since $q = \alpha \Delta T$, the corresponding value of m_2 is in the range 2/3 – 3/4. For a large range of published correlations the value of m_2 is taken as 0.7(Palen, 1990).

Stephan and Abdelsalam (Stephan et al, 1980) presented a correlation (equation 2.8) based on dimensionless groups of applicable physical properties with the constants determined from a very large data set for a wide range of geometries ranging from wires to flat plates and cylinders.

$$\alpha_{nb} = \frac{\lambda_l}{d_b} \times 0.23 X_1^{\,0.674} X_5^{0.297} X_4^{0.371} X_{13}^{(-1.73)} X_2^{0.35} \tag{2.8}$$

Of the dimensionless groups X_1 is the most significant and contains the heat flux (q) which is raised to the power of 0.674 in equation 2.8. A simpler correlation which has been found to give reasonable results (Palen, 1990) is that of Mostinski (Mostinski, 1963).

$$\alpha_{nb(1)} = 0.00417 p_c^{0.69} F_p \tag{2.9}$$

$\alpha_{nb(1)}$ is the nucleate boiling coefficient for a single tube, p_c is the critical pressure and F_p is a pressure function correction factor. Palen suggests the use of equation 2.10 for mixtures and high pressures ($p / p_c > 0.2$) and the use of equation 2.11 for vacuum operation.

$$F_p = 1.8\left(\frac{p}{p_c}\right)^{0.17} \tag{2.10}$$

$$F_p = 2.1\left(\frac{p}{p_c}\right)^{0.27} + \left[9 + \frac{1}{1-(p/p_c)^2}\right]\left(\frac{p}{p_c}\right)^2 \tag{2.11}$$

Yilmaz (Yilmaz, 1987) suggests the addition of extra terms in the calculation of the nucleate boiling coefficient to account for enhanced tubes and for boiling mixtures as in equation 2.12.

$$\alpha_{nb} = \alpha_{nbr} F_m F_s F_e \tag{2.12}$$

α_{nbr} is the reference nucleate boiling coefficient, the subscripts, m , s and e indicate mixture, surface and fin efficiency respectively. For the boiling of mixtures a correlation based on the boiling range (BR) is used to determine the mixture boiling correction factor (F_m).

$$F_m = \frac{1}{\left(1 + 0.0235 q^{0.15} BR^{0.75}\right)} \tag{2.13}$$

The boiling surface correction factor (F_s) and the enhanced surface correction factor (F_e) take into account the change in the nucleate boiling heat transfer coefficient due to the condition of the surface and the presence of enhanced tubes.

2.4.4 – Convective boiling term

As the void fraction surrounding the outside of a tube increases the liquid layer surrounding the tube can become so thin that the mechanism of heat transfer changes. The simple conduction-convection mechanisms from the tube wall through the liquid layer can become more important than the nucleate boiling. In these circumstances the heat transfer coefficient must be calculated from correlations for forced convective boiling.

One estimate (equation 2.14) of the convective boiling term is given by Taborek (Taborek, 1974)

$$\alpha_{cb} = \left(\frac{\Delta p_{tpf}}{\Delta p_l}\right)^{m_3} \alpha_l \tag{2.14}$$

The coefficient α_l is calculated from ideal tube bank correlations for liquid flowing alone. The calculation of this term requires the flowrate through the tube bundle to be known. The value of m_3 in equation 2.14 ranges from about 0.4 – 0.5 and a value of 0.45 can be used as an approximation. Yilmaz (Yilmaz, 1987) presents equation 2.15 for the calculation of the convective boiling term.

$$\alpha_{cb} = F_{cb}\alpha_l \tag{2.15}$$

Where F_{cb} is correlated using equation 2.16

$$F_{cb} = \left(\frac{1}{R_l}\right)^{n/m} \tag{2.16}$$

R_l is the liquid volume fraction and n and m are constants which must be determined from experimental data. HTFS have their own proprietary method (McNaught, 1991) for determining the contribution from convective boiling based on the form of equation presented in 2.15. In this method the parameter F_{cb} is calculated using an equation that relates the contribution of the convective boiling term to the two-phase frictional pressure drop multiplier of equation 2.17.

$$\phi_l^2 = \frac{\Delta p_{TP}}{\Delta p_l} \tag{2.17}$$

2.4.5 – Prediction of Void Fraction in Shellside Two-phase Flow

There has been a significant amount of study on the subject of determining the void fraction during two-phase crossflow across banks of tubes. The accurate determination of void fraction is an important subject, as it has a strong influence on both the heat transfer and pressure drop during shellside boiling. The void fraction is defined as:

$$\varepsilon_g = \frac{A_G}{A_G + A_L} \tag{2.18}$$

Where A_G is the area occupied by gas and A_L is the area occupied by liquid at a given cross section of the flow.

The simplest model for void fraction is that calculated for homogeneous flow, the homogeneous void fraction is likely to be an accurate correlation when the two phases are well mixed, as is the case with bubbly flow. The expression for the homogeneous void fraction is:

$$\varepsilon_{gH} = \frac{\dot{V}_G}{\dot{V}_l + \dot{V}_G} \tag{2.19}$$

Where $\dot{V}_G$ and $\dot{V}_l$ are the volumetric flowrates of gas and liquid respectively. The problem with this model is that several studies have shown that it over predicts the void fraction at low mass- fluxes, during upward two-phase flows and also under predicts void fraction in down flows. When dealing with low pressures and high mass fluxes or high pressures the homogeneous equation can give reasonable results (Palen et al, 1990). When the two phases are not well mixed, other correlations are required which take account of the different phase velocities, and these models are generally referred to as separated flow models. There has been a considerable amount of work done to develop separated void fraction models for flow in tubes.

2.4.5(a) - Tubeside Flow

One of the earliest of these studies in two-phase flows by Lockhart and Martinelli (Lockhart et al, 1949) produced a set of maps for predicting the void fraction. The basis for their study was fitting an empirical correlation to a map on data of void fraction, and the correlation which proved the best fit to their data was:

$$\varepsilon_g = \frac{\phi_{ltt} - 1}{\phi_{ltt}} \tag{2.20}$$

Where ϕ_{ltt} is the two-phase frictional multiplier for turbulent-turbulent flow:

$$\phi_{ltt}^2 = 1 + \frac{20}{X} + \frac{1}{X^2} \tag{2.21}$$

X is the Martinelli Parameter

$$X^2 = \frac{\left(\frac{dp_f}{dz}\right)_l}{\left(\frac{dp_f}{dz}\right)_g} \tag{2.22}$$

It has been suggested that the maps for void fraction produced in the study take inadequate account of mass flux and other effects and are not generally recommended in the calculation of void fraction (Palen et al, 1990). In some other early studies the calculation has been attempted by measuring the extent to which the void fraction deviates from that of a homogeneous flow. This deviation is quantified by using a velocity ratio or Slip ratio between the phases, the larger the slip ratio the more separated the two-phases and the less homogeneous the flow. The slip ratio is defined as:

$K = \frac{u_g}{u_l}$ Where, u_g and u_l are the gas and liquid phase velocities. (2.23)

The void fraction itself can be calculated using:

$$\varepsilon_g = \frac{V_g}{K.V_l + V_g} \tag{2.24}$$

Chisholm suggests using a value of $K = \left(\frac{\rho_l}{\rho_H}\right)^{\frac{1}{2}}$ where ρ_H is defined as the homogeneous two-phase density and can be calculated from:

$$\frac{1}{\rho_H} = \frac{1-x}{\rho_l} + \frac{x}{\rho_g} \tag{2.25}$$

This calculation procedure is limited, and is unlikely to predict data accurately for conditions involving viscous flows, horizontal stratified flows and in general any condition where mass velocity effects would be significant (Chisholm, 1973). An alternative method for calculating the slip ratio between the two-phases and subsequently predicting the void fraction was presented by Premoli, 1971 (as presented in Hewitt 1990), known as the CISE correlation, in which the expression for Slip ratio is given as:

$$K = 1 + E_1\left(\frac{y}{1+y.E_2} - y.E_2\right)^{\frac{1}{2}} \tag{2.26}$$

Where,

$$y = \frac{\varepsilon_{gH}}{1-\varepsilon_{gH}},\ E_1 = 1.578.\mathrm{Re}_{lo}^{-0.19}\left(\frac{\rho_l}{\rho_g}\right)^{0.22} \text{ and } E_2 = 0.0273.We'.\mathrm{Re}_{lo}^{-0.51}\left(\frac{\rho_l}{\rho_g}\right)^{-0.08}$$

ρ_g and ρ_l are the gas and liquid phase densities, Re_{lo} and We' are:

$$\mathrm{Re}_{lo} = \frac{\dot{m}.D}{\eta_l} \text{ and } We' = \frac{\dot{m}^2.D}{\sigma.\rho_l}$$

Where m = mass flux, D = equivalent diameter of the channel, η_l = liquid phase viscosity and σ = surface tension. The CISE correlation is more applicable than the Martinelli or homogeneous models, but does not produce an accurate model for void fraction over a wide range of data. Grant (Grant, 1977) proposed an expression based on the previous work of Chisholm (Chisholm, 1973) and on data for void fraction in tubes (Figure 2.6) produced by Armand 1946 and 1955. The correlation presented was:

$$\varepsilon_g = C_A.\beta \tag{2.27}$$

Where C_A is the Armand co-efficient and

$$\beta = \frac{\dot{V}_g}{\dot{V}_g + \dot{V}_l}. \tag{2.28}$$

The correlation produced fairly accurate results when tested against their data for two-phase flow in tube bundles, given certain limiting conditions for the value of β . The limitation with the above correlation is mainly that it is based on data for void fraction in tubes and may suffer when applied to void fraction in a non-ideal tube bundle. The form of the correlation produced for in tube void fraction from which Grant et al had obtained their results, had been summarised by Butterworth (Butterworth, 1975). He had shown that the majority of in-tube void fraction models could be represented using the expression:

$$\frac{1-\varepsilon_g}{\varepsilon_g} = A\left(\frac{1-x}{x}\right)^p\left(\frac{\rho_G}{\rho_l}\right)^q\left(\frac{\mu_L}{\mu_G}\right)^r \tag{2.29}$$

The values of the constants A, p, q and r vary depending on the model being examined.

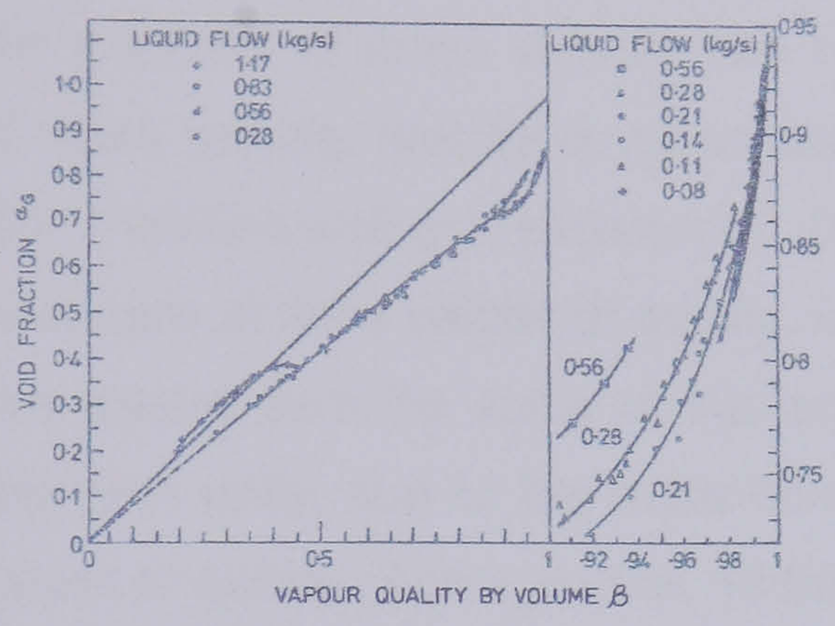

Figure 2.6 – Measured void fraction for flow in tubes of Armand 1946, 1955 (Grant, 1977)

2.4.5(b) – Flow in Tube Bundles

All of the above correlations were attempts to predict void fraction in tubeside flow. The problem of determining the void fraction in a tube bundle, where the hydrodynamics of the two-phase flow are markedly different has been the subject of more recent study. One attempt to assess the applicability of the in-tube models to the calculation of void fraction in a tube bundle (Grant and Cotchin, 1982) used measured values of liquid hold-up in a tube bundle test section. The conclusion of their investigation was that the existing model of predicting in tube void fraction gave reasonable predictions of the measured void fraction in the experimental tube bundle. They also pointed out however that the trend of liquid hold-up with vapour quality predicted by the model did not follow the trend of the measured liquid hold-up, and as a result the applicability of this model to other bundle geometries is questionable. Schrage et al (Schrage et al, 1988) conducted an experiment in order to determine the void fraction in a two-phase flow passing over a horizontal tube in a tube bundle. They attempted to simulate adiabatic and boiling conditions by introducing air upstream of a tube bundle in the adiabatic case and at each individual tube for the boiling case. They correlated the results of their experiment in terms of a reduced void fraction. This

was an attempt to reduce a scatter in results produced by differences in operating pressure. The correlation for reduced void fraction was defined as:

$$\frac{\varepsilon_g}{\varepsilon_{gH}} = 1 + 0.360.m^{-0.191} \ln x \text{ (Adiabatic)} \quad (2.30)$$

$$\frac{\varepsilon_g}{\varepsilon_{gH}} = 1 + 0.123.Fr^{-0.191} \ln x \text{ (Boiling)} \quad (2.31)$$

where ε_{gH} is the homogeneous void fraction at the particular conditions, m is the mass velocity (kg/m^{2}s) and x is the vapour quality. In the boiling expression Fr is the Froude number, and the value of the reduced void fraction would be obtained by integrating the expression across the length of the bundle. The main advantage of this correlation over previous attempts is that the influence of mass velocity has been considered. The authors concluded that the effect of mass velocity had been reasonably accounted for and that the values of reduced void fraction matched well with experiment. One drawback in the method is reduced void fraction values of zero at finite values of quality, which is physically impossible. In fact as the quality reduces toward zero the value of the reduced void fraction should go through a minimum then approach unity, due to the more homogeneous nature of the two-phase mixture at very low values of quality (Schrage et al, 1988). The authors were unable to locate this minimum turning point and arbitrarily set a boundary condition whereby the minimum value of reduced void fraction is set at 0.1 for any combination of mass velocity and quality.

Following on from the work of Schrage et al., Dowlati, Kawaji and Chan (Dowlati et al., 1990) examined the effect on the prediction of void fraction by changing the tube pitch to diameter ratio. From the results produced using a gamma densitometer to measure void fraction in their experimental tube bundle test rig, a correlation was produced to try and accurately predict the effect of mass velocity on the bundle average void fraction. The correlation was of the form:

$$\varepsilon_g = 1 - \frac{1}{\left(1 + C_1 \dot{v}*_g + C_2 \dot{v}*_g^2\right)^{\frac{1}{2}}} \quad (2.32)$$

Where $\dot{v}*_g$ is the dimensionless gas velocity, defined by Wallis (Wallis, 1969) as:

$$\dot{v}*_g = \frac{\rho_g^{0.5} \dot{v}_g}{\sqrt{gD\left(\rho_l - \rho_g\right)}} \quad (2.33)$$

$\dot{v}_g$ is the superficial gas velocity based on the minimum flow area, D is the rod diameter and the gas density is calculated at the average pressure in the test section. Dowlati et al found

the best fit to the data with values of the constants C_1 and C_2 taken as 35 and 1 respectively, and in addition they suggested that the value of C_2 be taken as 30 for $\dot{v}*_g$ values greater than or equal to 0.2. They concluded that their void fraction predictions accurately modelled the effect of mass velocity. They also noted that the correlation developed by Schrage et al under-predicted their void fraction data by up to 50%. The experiments of Dowlati et al were similar in nature to those carried out in the previous tests by Schrage et al and the reason for this large deviation in results is unclear. The success in accurately predicting the mass velocity effect on void fraction was attributed to the use of the dimensionless gas velocity term. This may be due to the dimensionless gas velocity being a factor of both the mass velocity and the quality, which can be easily seen if $\dot{v}*_g$ is written in alternative form:

$$\dot{v}*_g = \frac{\dot{m}x}{\sqrt{\rho_g g D(\rho_l - \rho_g)}} \quad \text{(Dowlati et al, 1990)} \qquad (2.34)$$

No discernible deviation in results was noted for changing the P/D ratio. Dowlati et al (Dowlati et al, 1992) continued the development of void fraction prediction by testing their previous correlation against a new correlation based on the Drift Flux model of Zuber and Findlay (Zuber et al, 1965). The introduction of the Drift Flux model to the problem was an attempt to account for the effect on void fraction of non-uniform velocity and void profiles and to address the effect of relative velocity between the phases due to slip by the drift velocity. The model used the weighted mean velocity:

$$\bar{u}_g = C_0\langle j\rangle + \bar{V}_{gj} \qquad (2.35)$$

Where $\langle j\rangle$ is the mixture mean velocity based on the volumetric flowrate and the minimum flow area and C_0 is the distribution parameter included to account for the non-uniform effects. $\bar{V}_{gj}$ is the drift velocity, which is described in the original Zuber and Findlay analysis as a term calculated to represent the difference between the gas phase velocity (u_g) and the mixed flow superficial velocity (j), weighted by the local void fraction. The parameters $\bar{V}_{gj}$, u_g and j are defined by the following equations:

$$\bar{V}_{gj} = \frac{\langle \varepsilon_g u_{gv}\rangle}{\langle \varepsilon_g\rangle} = \frac{(1/A)\int \varepsilon_g u_{gv} dA}{(1/A)\int \varepsilon_g dA} \qquad (2.36)$$

$$u_{gv} = u_g - j \qquad (2.37)$$

$$u_g = \frac{\dot{v}_g}{\varepsilon_g} \qquad (2.38)$$

$\dot{v}_g$ is the vapour superficial velocity based on the cross sectional area A.

$$j = \dot{v}_g + \dot{v}_l \tag{2.39}$$

In the analysis of Dowlati et al, values of C_0 and $\overline{V}_{gj}$ were obtained from plotting the data for $\overline{u}_g$ against $\langle j \rangle$ and using equation 2.35. The plots were approximately linear allowing the values of C_0 and $\overline{V}_{gj}$ to be easily extracted. Dowlati et al obtained the void fraction using the Zuber and Findlay definition of the weighted mean velocity as:

$$\overline{u}_g = \frac{\langle \dot{v}_g \rangle}{\langle \varepsilon_g \rangle} \tag{2.40}$$

Therefore the average bundle void fraction was calculated using the following expression:

$$\langle \varepsilon_g \rangle = \frac{\langle \dot{v}_g \rangle}{C_0 \langle j \rangle + \overline{V}_{gj}} \tag{2.41}$$

To see a clearer view of the effect of the functional components on the model, expressions for the values of $\langle j \rangle$ and $\langle \dot{v}_g \rangle$ were entered into the above equation, to produce:

$$\langle \varepsilon_g \rangle = \frac{1}{C_0 \left[1 + \frac{(1-x)}{x} \frac{\rho_g}{\rho_l} \right] + \frac{\overline{V}_{gj} \rho_g}{\dot{m} x}} \tag{2.42}$$

The results of the comparison between this model and the previous correlation of Dowlati et al. (1990) showed that they both obtained similar results for the void fraction prediction. Both of the methods proposed by Dowlati et al. (Dowlati et al, 1990, 1992) require the calculation of empirical constants. The models themselves are based on data for cross-flow of air-water mixtures across an ideal tube bundle. An improved correlation was developed (Dowlati et al, 1996) that was based on void fraction data for boiling R-113 across a tube bundle test section. They attempted to fit the previous correlation (Dowlati et al, 1990) and the Drift Flux correlation (above) to the data from the R-113 experiment.

$$\varepsilon_g = 1 - \frac{1}{\left(1 + C_1 \dot{v}*_g + C_2 \dot{v}*_g^2\right)^{\frac{1}{2}}} \tag{2.43}$$

They found values of the constants C_1 and C_2 of 10 and 1 were the best fit to the data. The refrigerant void fraction data was found to be significantly lower than the observed void fraction predicted by the air-water correlation. Dowlati et al concluded that since the mass velocities and system pressures were constant for the two experiments, the most prominent distinction was the gas density. It was speculated that the gas density had a large influence on the choice of constants for use in the void fraction correlation. They also speculated that the values of the constants could depend on fluid properties such as liquid density and

surface tension. It was noted that the effect of surface tension could be significant, as this affects the bubble size distribution and void fraction could be affected as the bubble rise velocity increases with bubble size. In their analysis of the Drift Flux model, for the R-113 data they observed that the drift flux velocity $\overline{V}_{gj}$ for R-113 was larger than the drift flux velocity of the air-water data. This suggests that empirical values for this term and possibly for the distribution parameter C_0 would have to be evaluated for each fluid.

More investigation on void fraction has been undertaken by Xu et al, (Xu et al, 1992). A correlation was developed that accurately fitted the air-water, vertical void fraction data of the Dowlati et al and previous studies. The correlation was analogous to the form defined previously by Butterworth and was in terms of the Martinelli Parameter and the liquid only Froude number. A further study (Xu et al. 1998) produced a similar correlation for horizontal cross-flow of air-water and air-oil mixtures across a tube bundle. The equation developed from a Martinelli type analysis to the form:

$$\frac{\varepsilon_g}{1-\varepsilon_g} = B^{(1+m)/(5-m)}\left[\left(\frac{\mu_g}{\mu_l}\right)^{\left(\frac{m}{2}\right)}\left(\frac{\rho_l}{\rho_g}\right)^{0.5}\left(\frac{x}{1-x}\right)^{(2-m)/2}\right]^{2/(2.5-0.5m)} \tag{2.44}$$

As in previous studies (Schrage et al 1988, Dowlati et al 1990, 1992) a value of m=0.2 was chosen as it provided the least scatter to the data. Thus the expression becomes:

$$\frac{\varepsilon_g}{1-\varepsilon_g} = B^{0.25} X_{tt}^{-0.833} \tag{2.45}$$

Where, the Martinelli parameter was defined as follows:

$$X_{tt} = \left(\frac{1-x}{x}\right)^{0.9}\left(\frac{\rho_g}{\rho_l}\right)^{0.5}\left(\frac{\mu_l}{\mu_g}\right)^{0.1} \tag{2.46}$$

The final correlation presented by Xu et al. included the liquid only Froude number:

$$\frac{\varepsilon_g}{1-\varepsilon_g} = C_1 Fr_{lo}^{C_2} X_{tt}^{-C_3} \tag{2.47}$$

Where, $Fr_{lo} = \frac{\dot{m}^2}{\rho_l^2 gD}$ The constants C_1=1.95, C_2=0.18 and C_3=0.833 were deemed to give the best fit to the data. The authors found that the correlation proved to fit well with their data and the data from previous studies in horizontal cross-flow by Grant et al. (Grant et al, 1979, 1984).

Feenstra et al, (Feenstra et al, 2000), presented a new approach for the calculation of void fraction in tube bundles. The purpose was to find a physically based model that could be

applied to any fluid and only needed input parameters that could be easily obtained. The model was developed from the definition of void fraction:

$$\varepsilon = \left(1 + S\frac{\rho_g}{\rho_l}\left(\frac{1}{x} - 1\right)\right)^{-1} \tag{2.48}$$

Feenstra et al suggest modelling the void fraction by a correlation for the slip velocity that is a function of the following parameters:

$$S = \frac{u_g}{u_l} = f\left[\Delta\rho, \rho, V_P, \eta_L, \sigma, g, a, P, D, \Delta p\right] \tag{2.49}$$

Where V_P is the pitch flow velocity. The authors used the Buckingham-Pi method and dimensional analysis to find a correlation using dimensionless groups that would give a good fit to the data. The correlation they found that gave the best fit to their data for upward crossflow through tube bundles, along with the data of Dowlati, Schrage and others was:

$$S = 1 + 25.7(Ri.Cap)^{0.5}(P/D)^{-1} \tag{2.50}$$

Where: $Ri = \frac{D\rho^2 g_n a}{G_P{}^2}$; a is the gap between the tubes, G_P is the pitch mass flux and

$$Cap = \frac{\eta_L U_G}{\sigma} \tag{2.51}$$

A comparison of the model with those presented by Schrage et al, and Dowlati et al, is shown in Figure 2.7, where the data are taken from the boiling Freon data of Dowlati et al, 1996. The correlation presented by Feenstra et al, provides a reasonably accurate measure of the void fraction data, but the author believes more work is required to determine the effect of the tube arrangement on the void fraction and suggests the possible inclusion of an Euler number term in equation 2.50. The correlation is largely fitted to data for the bubbly flow regime and its applicability to more separated flow models has not been tested.

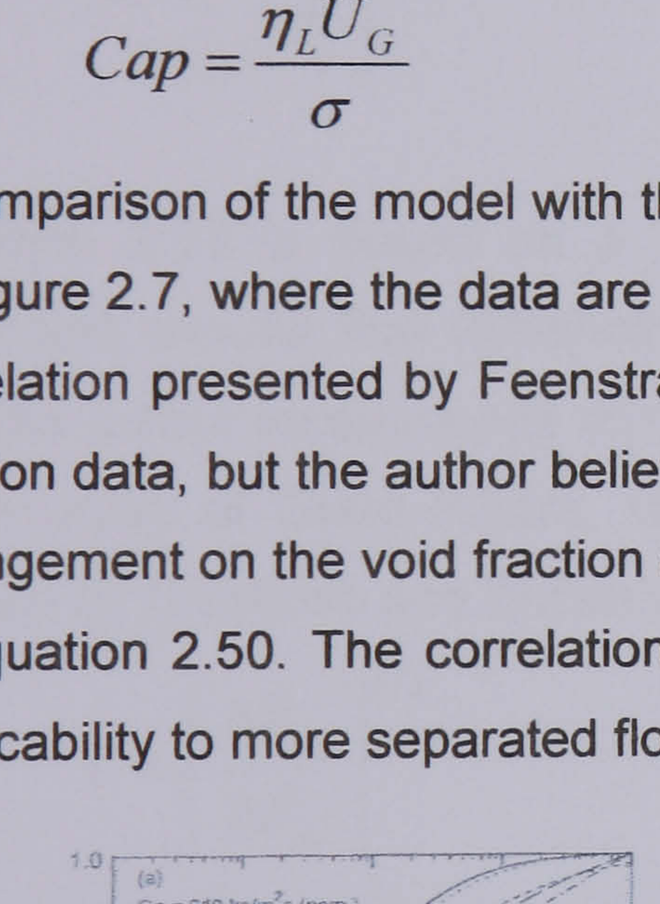

Figure 2.7 – Void fraction models for R-113 data of Dowlati, 1996 (Feenstra et al, 2000)

2.4.6 – Prediction of Two-phase Frictional Pressure Drop Multiplier in Crossflow

Many methods have been presented in the literature for calculating the two-phase frictional pressure drop multiplier for crossflow across tube bundles. This multiplier is used to correct the frictional pressure drop that would be expected in single-phase flow to describe the two-phase case. There are two principal forms of the multiplier, ϕ_l^2, which is used to scale the value of the frictional pressure drop based on the liquid phase of the two-phase flow flowing alone and ϕ_{lo}^2, which is used to scale the pressure drop that would be expected if the total two-phase flowrate were flowing with liquid properties.

The typical correlation presented for the calculation of two-phase multiplier is based on the Martinelli parameter and is shown by Chisholm (Chisholm, 1973) as:

$$\phi_l^2 = 1 + \frac{C}{X} + \frac{1}{X^2} \tag{2.52}$$

Where;

$$X = \left[\frac{\Delta P_l}{\Delta P_g}\right]^{1/2} \tag{2.53}$$

Equation 2.53 is based on a semi-empirical model derived from equations to describe separated annular flow (Chisholm, 1973). The value of C must be obtained from experiment and the author recommends using different values of C depending on the flow conditions. In the analysis of Grant (Grant, 1977), an alternative form is used based on the parameter defined by Chisholm and Sutherland (Chisholm et al, 1969-70):

$$\Gamma = \left[\frac{\Delta P_{go}}{\Delta P_{lo}}\right]^{1/2} \tag{2.54}$$

The resultant equation for the two-phase multiplier is:

$$\phi_{lo}^2 = 1 + (\Gamma^2 - 1)\left[Bx^{(2-n)/2}(1-x)^{(2-n)/2} + x^{(2-n)}\right] \tag{2.55}$$

Where:

$$B = \frac{C\Gamma - 2^{(2-n)} + 2}{\Gamma^2 - 1} \tag{2.56}$$

The value of the constant, n, used in the equation is obtained from a fit to friction factor data. From this approach Grant presented two models, one to describe homogeneous flow where the phases are well mixed and one to describe separated flow. These were to be used in

conjunction with a flow pattern map to get the best estimate of the pressure drop. For the homogeneous flow the equation derived was:

$$\phi_{lo}^2 = \left[1 + x\left[\frac{\rho_l}{\rho_g} - 1\right]\right]\left[1 + x\left[\frac{\eta_l}{\eta_g} - 1\right]\right]^{-n} \tag{2.57}$$

For the separated flow model Grant assumed zero interface shear and presented the equation:

$$\phi_{lo}^2 = \left[1 + x\left[\left(\frac{\eta_g}{\eta_l}\right)^{n/(2-n)}\left(\frac{\rho_l}{\rho_g}\right)^{n/(2-n)} - 1\right]\right]^{2-n} \tag{2.58}$$

Neither of these two methods accurately predicted the tube bank crossflow data and the authors suggested using equation 2.55, varying the value of B for the different flow paths, flow patterns and bundle geometries. This method requires an accurate estimation of the flow pattern when estimating pressure drop. Estimations of the value of B have been presented for various conditions. To calculate the two-phase pressure drop for vertically upward crossflow through an ideal tube bank, a value of 3.0 was used for B, for horizontal crossflow through an ideal tube bank B=0.6, 0.35 and 0.28 for rotated square, rotated triangular and square tube arrangement respectively. For vertically up and down crossflow between segmental baffles B=1.0, for horizontal side to side flow B=0.75 (spray and bubbly two-phase flow), B=0.35 (stratified and stratified spray flow). Cotchin (Cotchin, 1980), suggested calculating B for horizontal, side-to-side flow using an expression that accounted for mass-velocity effects. In a later study (Grant et al, 1986) it was suggested to use $B=0.7m^{0.53}$ for two-phase upward flow. A comparison of the homogeneous model and Grant correlation is presented in Figure 2.8(a) (Grant, 1977). It shows the horizontal crossflow pressure drop as predicted using a value of B=0.072 which was calculated using equation 2.59 at the experimental conditions and a value of n = 0.462 which was taken from a curve fit to single-phase friction factor data on the test geometry.

$$B = \frac{2^{2-n} - 2}{\Gamma + 1} \tag{2.59}$$

For vertical flow the pressure drop prediction is presented in Figure 2.8(b) (Grant, 1977). The value of B=1.0 is used. The use of equation 2.55 in this case is based on the assumption that the gravitational and mass velocity effects associated with upward and downward crossflow exactly cancel. This assumption can only be valid if the vapour distribution in upward and downward flow is the same. The parameter ψ in Figures 2.8(a) and (b) is defined by equation 2.60.

$$\psi = \frac{\frac{\Delta p_{ftp}}{\Delta p_{flo}} - 1}{\Gamma^2 - 1} \tag{2.60}$$

Where Δp_{ftp} is the friction pressure gradient for two-phase flow and Δp_{flo} is the pressure gradient for the total mass flowing with liquid properties.

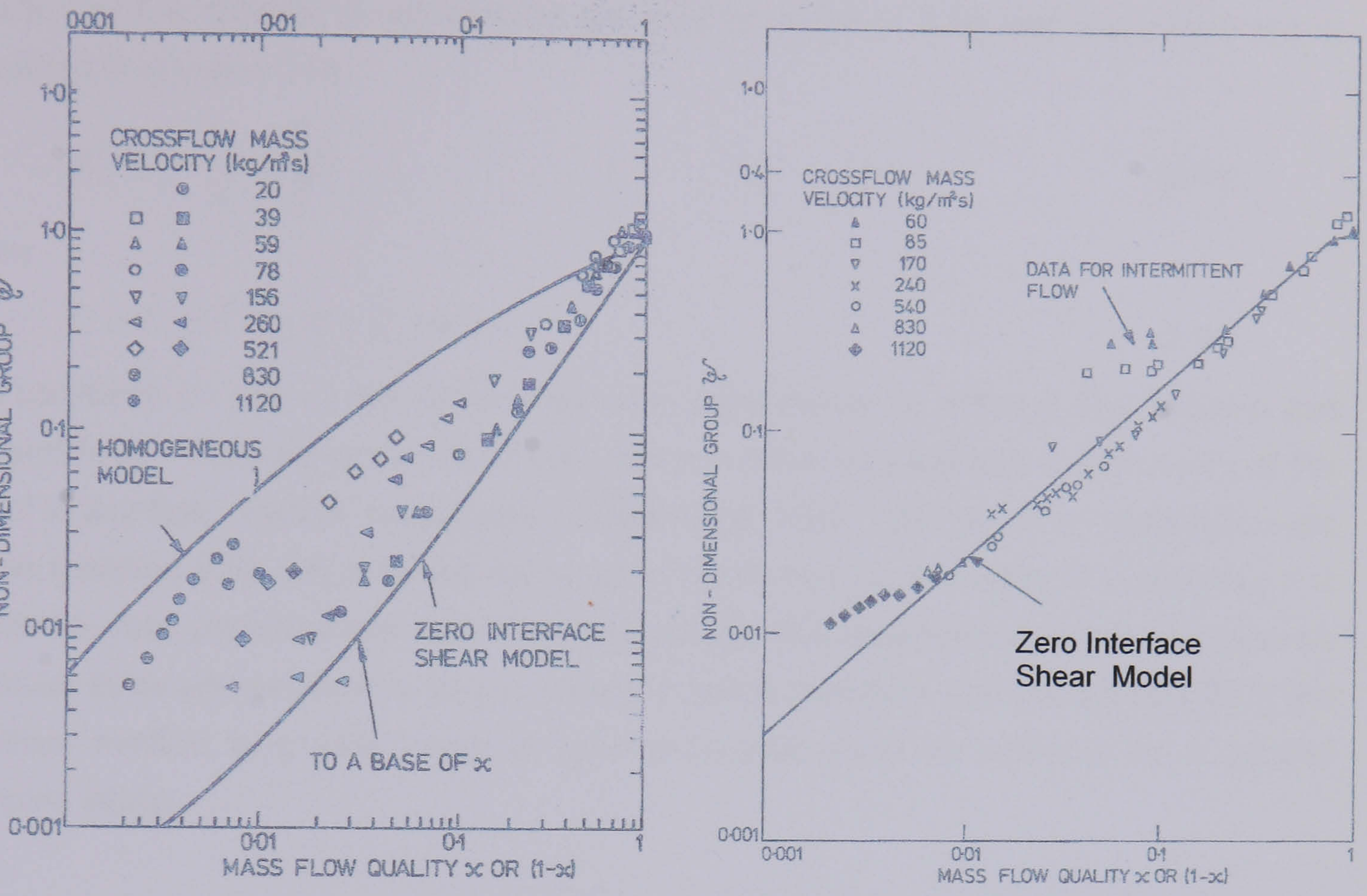

(a) – Horizontal crossflow (b) – Vertical crossflow

Figure 2.8 – Pressure Drop prediction in two-phase crossflow (Grant, 1977)

After a review of the literature on crossflow two-phase multipliers by the HTRI (Ishihara et al, 1980), a correlation based on equation 2.52 was presented. The authors suggested using equation 2.52 for Reynolds numbers Re >2000, and using the following equation for Re < 2000:

$$\phi_v^2 = 1 + CX + X^2 \tag{2.61}$$

Where

$$X = \left(\frac{\Delta P_l}{\Delta P_v}\right)^{0.5} = \left[\left(\frac{1-x}{x}\right)^{2-m}\left(\frac{\rho_v}{\rho_l}\right)\left(\frac{\eta_l}{\eta_v}\right)^m\right]^{0.5} \tag{2.62}$$

The authors used a value of m=0.2 in this equation which provided the least scatter of the data points. They also suggested that the value of the constant C could be calculated as a function of the parameters (X, γ and [1-x]/x). They introduced the parameter γ to account for mass velocity and geometric effects and suggested that it should be a function of the dimensionless gas velocity defined by Wallis (Wallis, 1969) and the tube pitch/diameter ratio.

A correlation for C was not presented but as a fit to their data Ishihara et al, chose C=8.0, which provided a reasonable fit but deviated from experimental results with values of X > 0.2 as shown in Figure 2.9. Further studies were undertaken by Schrage et al (Schrage et al, 1988) in which C values was plotted against X, mass velocity effects on the value of C were reported by the authors. A variation on the form of equation 2.52 was suggested and is presented in equation 2.63.

$$\phi_l^2 = 1 + \frac{C}{X} + \frac{C_5}{X^2} \tag{2.63}$$

where

$$C = C_1 Fr^{C_2} \ln X + C_3 Fr^{C_4} \tag{2.64}$$

The constants C_1 and C_5 are determined from experiments on different flow regimes and different fluids. Thus one drawback of this approach is the potential lack of applicability of the model to any fluid. Further researchers (Dowlati et al, 1990, 1992, Xu et al, 1999) continued to use equation 2.52 and provided some more information on the value of C and how it is affected by tube pitch/diameter ratio and mass velocity. The dependence on empirical data for particular fluids and geometries for the value of C raises questions over the applicability of the empirical method to a wide range of geometries that would be sufficient for a general shellside model.

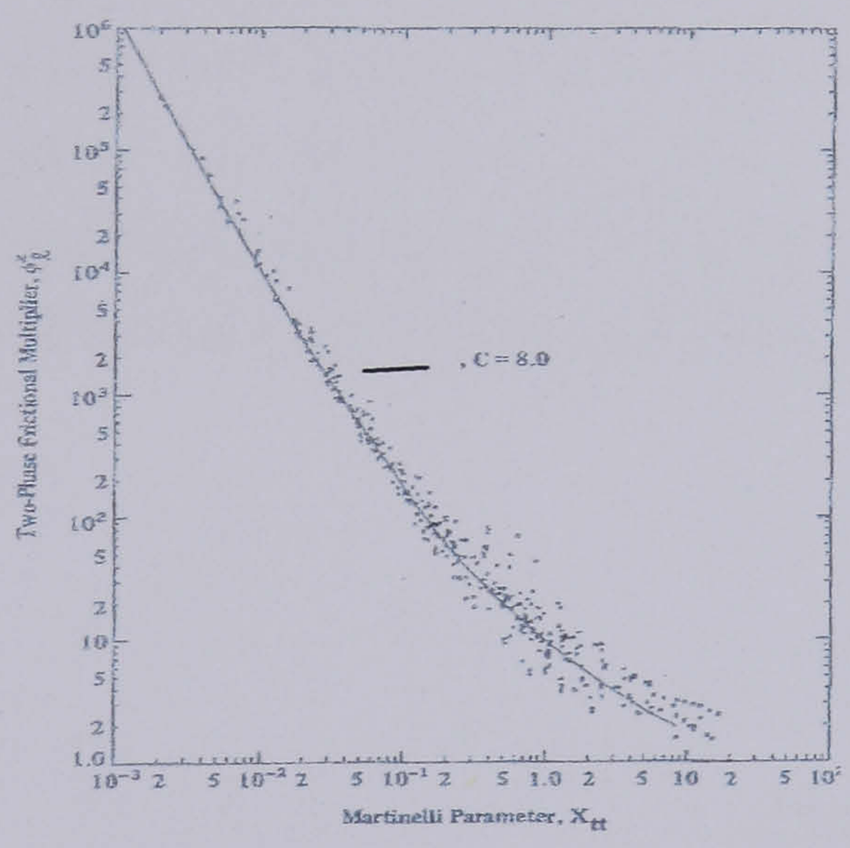

Figure 2.9 – Shellside pressure drop data (Ishihara et al, 1980)

2.4.7 – Prediction of Two-Phase Pressure Drop Multiplier in Longitudinal Flow

The longitudinal two-phase multiplier is used for describing the areas in the shellside flow where the predominant flow direction is parallel to the tubes (typically in the baffle windows between successive crossflow regions). To predict this parameter, Grant et al (Grant, 1977)

assumed that the friction factor is largely independent of Reynolds number and presented the equation:

$$\phi_{lo}^2 = 1 + (\Gamma^2 - 1)\left[Bx + (1-B)x^2\right] \tag{2.65}$$

Where

$$B = \frac{C\Gamma - 2}{\Gamma^2 - 1} \tag{2.66}$$

The homogeneous approach for longitudinal flow produced the equation:

$$\phi_{lo}^2 = 1 + x\left(\frac{\rho_l}{\rho_g} - 1\right) \tag{2.67}$$

Whereas, the zero interface shear, separated equation was:

$$\phi_{lo}^2 = 1 + x\left(\left(\frac{\rho_l}{\rho_g}\right)^{0.5} - 1\right) \tag{2.68}$$

Based on the experimental data available, Grant suggested using equation 2.65 with

$$B = \frac{2}{\Gamma + 1} \tag{2.69}$$

The comparison of horizontal flow data (Figure 2.10(a)) shows a good prediction using the zero interface shear model, which is not surprising as the tests were carried out with a stratified flow pattern. However the applicability of the zero interface shear model to the other flow patterns is still questionable. For the comparison with vertical flow (Figure 2.10(b)) a value of B = 0.25 leads to a reasonable prediction of up-and-down flow pressure drop, but the general applicability of this arbitrary selection is again questionable.

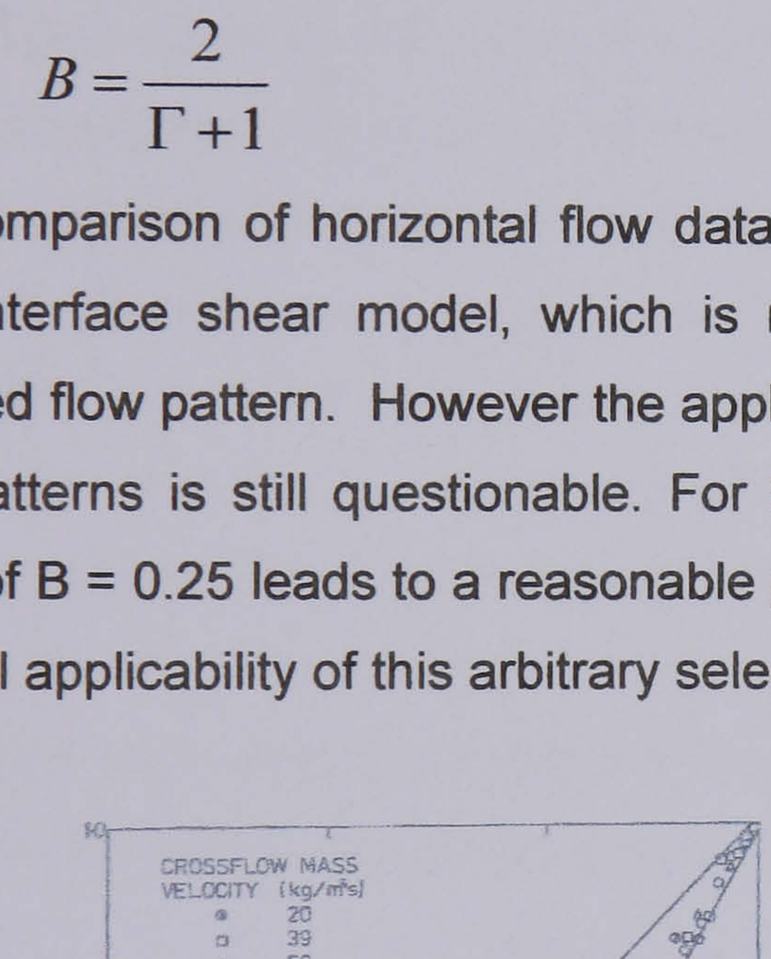

(a) – Horizontal longitudinal flow

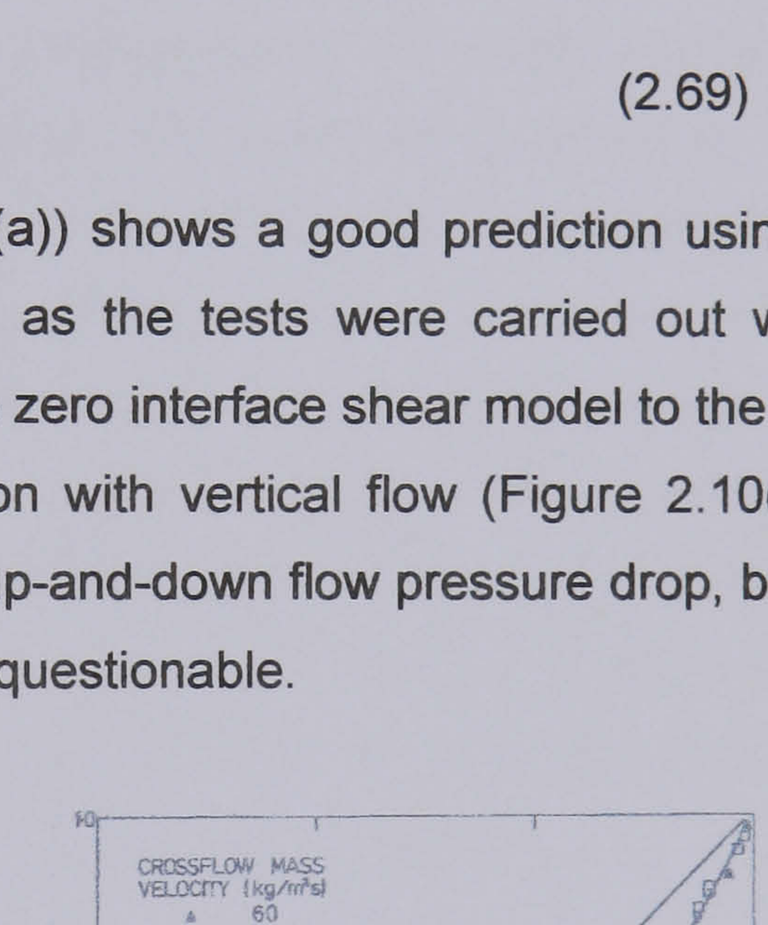

(b) – Vertical longitudinal flow

Figure 2.10 – Pressure drop prediction in longitudinal flow (Grant, 1977)

2.5 – Shellside Flow Models

Initial methods for predicting overall shellside evaporating heat transfer and pressure drop were reasonably simple. Fair (Fair, 1960) presented a general design procedure for thermosyphon reboilers. It was a reasonably flexible model that involved a series of trial and error calculations. Further to the early work of Fair, Hughmark (Hughmark, 1969) essentially extended the same method, adopting a simplified correlation for obtaining the inside co-efficient and some extra work on estimating the circulation rate in thermosyphon reboilers. Levy (Levy, 1966) produced correlations for liquid hold-up in thermosyphon reboilers and Collier and Hewitt, (Collier et al, 1961) and Chenoweth-Martin (Chenoweth et al, 1955) produced correlations for pressure drop. A summary of the work up to 1970 was produced by McKee (McKee, 1970). This contains a list of data sources on the vertical thermosyphon reboiler as well as a list of contributions made to the study of two-phase flow phenomenon, pressure drop and heat transfer. Fair and Klip (Fair et al, 1983) produced a model for Horizontal Reboiler design; it was based on fairly limited data and produced pressure drop correlations adapted from the vertical thermosyphon arrangement. The model incorporates the frictional pressure drop correlations produced by Grant and Chisholm (Grant et al, 1979), and the parameters such as two-phase density and void fraction used in gravitation and acceleration pressure drop based on the Martinelli parameter or the homogeneous model. The model considers two types of shell side flow, horizontal flow along the length of the exchanger, and vertical flow around the edges of a central horizontal baffle. There is no account taken of flows bypassing the tube bundle and the model has limited use for different shell types where the effects of baffle leakage may be more pronounced. The basis behind the design was using correlations from tube data. The authors used the Martinelli parameter based on horizontal tubes and a two-phase density based on vertical tube flow.

Contemporary designers generally use commercial design software to describe shellside evaporating conditions. The most popular commercial packages contain programmes that calculate overall shellside conditions based on a one-dimensional flow network used to describe the shellside geometry. The network model is based on a description of shellside flow first introduced by Tinker (Tinker, 1955).

Tinker identified a number of basic flow paths that could be used to describe the shellside flow in a shell & tube heat exchanger. The basis of the flow path split was that the shellside flow could be described as a combination of three distinct paths: crossflow, window flow and leakage flow. A physical representation of the flow paths is given in Figure 2.11.

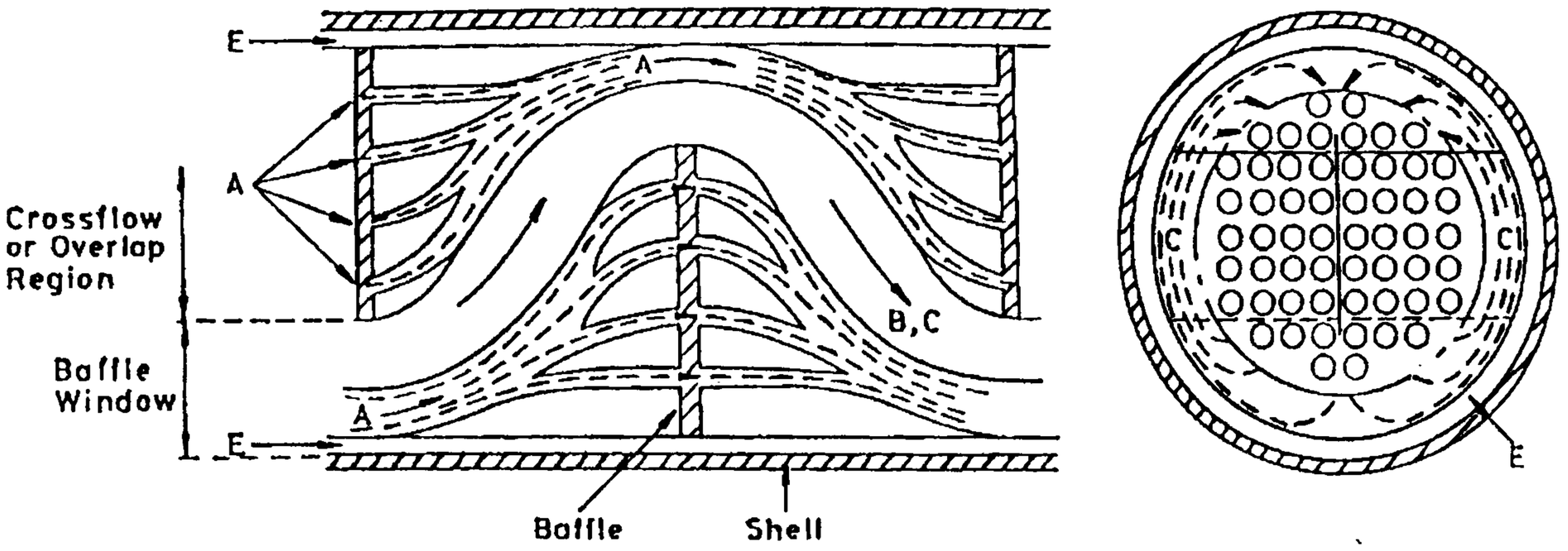

Flowstreams

A	=	Tube Baffle Leakage
B	=	Crossflow
C	=	Crossflow Bypass
E	=	Shell Baffle Leakage
W	=	A+B+C+E
	=	Window Flow in Baffle Window

Figure 2.11 – Tinker's representation of shellside flow (Tinker, 1955)

The flow paths in Tinker's flow model can be described as follows:

Tube baffle leakage: Flow in the manufacturing clearance between the outer diameter of the tubes and the shellside baffle.

Crossflow: Flow normal to the tube bundle (this is where most of the heat transfer takes place)

Crossflow bypass: The flow around the outside of the tube bundle in the same direction as the crossflow.

Shell baffle leakage: Flow in the necessary manufacturing clearance between the outside of the shellside baffle and the inside of the shell.

Window Flow: Flow predominantly parallel to the tubes in the tube bundle that flows in the region between successive crossflow paths, in the space not covered by the shellside baffles (baffle window).

Around the same time as the Tinker method was being developed, a less complicated flow path analysis configuration was suggested by Bell (as reported by Palen et al, 1969). Based on data produced at the University of Delaware experimental engineering facility, the Bell-Delaware method couldn't take into account interactions between the various flow streams, and has generally been considered less adaptable than the method of Tinker (Grant and Murray, 1972, Palen and Taborek, 1969, Moore, 1974).

The one-dimensional flow path network described by Tinker has been used by a number of authors to create models for single-phase liquid shellside pressure drop. Palen and Taborek (HTRI) further developed the Tinker shell-side flow model, to create what they termed the 'Stream Analysis' method (Palen et al, 1969). The Stream analysis method essentially employed the same streams as defined by Tinker, with the inclusion of an additional stream (labelled F) to account for flow past a tube-pass partition plate. The objective of their approach was to find the proportions of flow in each path to enable the solution of the pressure drop in each flow path by means of an equivalent piping frictional resistance network. The flowrates were given by a pressure drop equation of the form:

$$\Delta P_j = CK_j \left[\frac{\dot{M}_j}{S_j} \right]^2 \tag{2.70}$$

The pressure drop relations were also stated as:

$$\Delta P_C = \Delta P_F = \Delta P_B = \Delta P_X \tag{2.71}$$

$$\Delta P_A = \Delta P_E = \Delta P_X = \Delta P_W \tag{2.72}$$

Where subscript X refers to crossflow and subscript W refers to window flow. The other equation employed is the overall mass balance:

$$\dot{M} = \dot{M}_A + \dot{M}_B + \dot{M}_C + \dot{M}_E + \dot{M}_F . \tag{2.73}$$

The pressure drop expressions could be solved provided values were known for the resistance factors K. Since K values were calculated from in-tube correlations dependent on Reynolds number, the value of K would depend on the amount of flow, hence the equations would have to be solved by an iterative process. Essentially the most important part of the stream analysis method in terms of accurate design is the calculation of the resistance co-efficient K for each flow stream. For the crossflow stream (B) the calculation of resistance is the same as correlations developed for ideal tube bank data. The leakage streams (A and E) are calculated using correlations, which contain a frictional term and a geometric term (to account for acceleration/deceleration losses). The bundle bypass resistance co-efficient was based on data collected from the HTRI research data bank. The bypass channel proved difficult to find an accurate correlation with a high dependence on the bypass channel width and the possible presence of sealing strips and the K value for the pass-partition lane was calculated from a correlation based on data from the HTRI experimental facility. The drawbacks in the accuracy of the 'stream analysis' method lie largely in the dependence on the ideal tube bank data, and in the limited data to aid in describing the other flow paths.

A similar method to describe the shell-side two-phase frictional pressure drop was developed by Grant and Murray (Grant et al, 1972) for HTFS. The method was also based on the flow model suggested by Tinker. And the correlations were fitted to data used in the Bell-Delaware

project. The process of calculating the total shell-side pressure drop was a combination of calculating the pressure drop in the middle of the exchanger and also the end zones of the exchanger at the inlet and outlet nozzles. As in the stream analysis method the focus is on calculating the flow rates in each path based on a flow resistance network. The method for calculating the flow fractions in each of the flow paths is an iterative one. The procedure works as follows:

- Flow fractions are assumed in each flow path proportional to the flow areas
- Values for a resistance coefficient K are calculated from correlations for each flow path
- The values for K are used to re-estimate the mass flowrates in each flow path
- The overall mass balances are checked and mass fractions are re-estimated to obtain convergence

Friction factors used in the model were obtained using methods described by Butterworth (Butterworth et. al, 1971). The friction factor prediction accuracy is the most important part of the divided flow method. They were calculated using a fit to the friction factor data obtained from the experiments of Bergelin (Bergelin et al, 1958) and compared with data from the Bell/Delaware research project. The authors reported a significant improvement in the prediction of the shellside pressure drop. However as can be seen from Figure 2.12 the range of data suggests there is room for improvement in the pressure drop model.

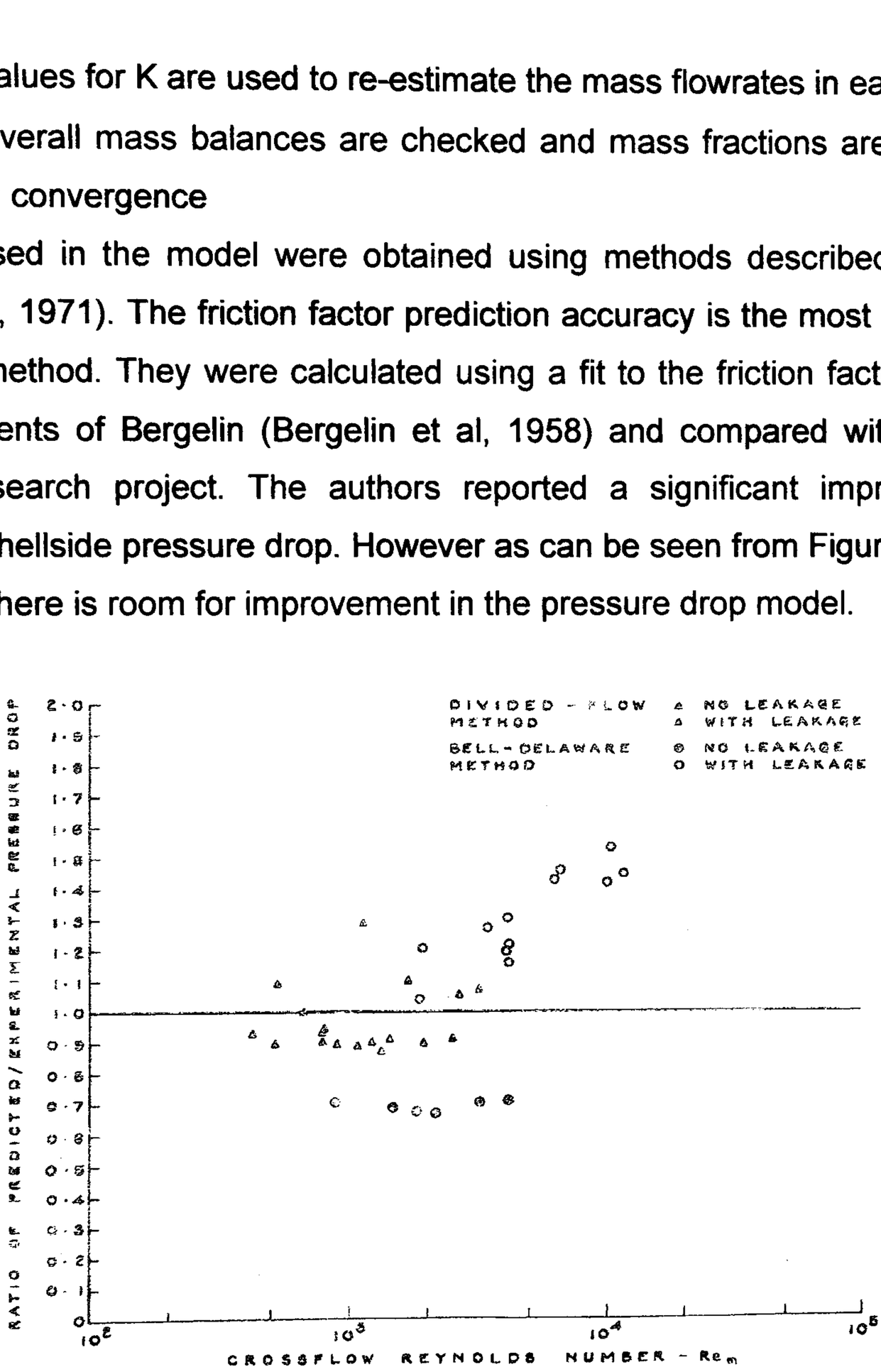

Figure 2.12 – Comparison of Divided flow and Bell-Delaware methods (Grant, 1977)

Another method for describing the shellside flow path pressure drop was developed around the same time as the divided flow method, also by HTFS. The method of Moore (Moore, 1974) is essentially a simplified version of the Grant and Murray Divided Flow method. The

purpose of the model was to improve the time it would take to process a calculation of the shell-side pressure drop. Another significant change to previous models is the definition of the characteristic length in the calculation of Reynolds number. The method of Moore uses the length between adjacent tubes as opposed to the tube outer diameter. This limits the importance of the pitch to diameter ratio in the calculations and relates the ideal tube bank data to the same reference. The method uses slightly different definitions for the flow streams with the pass-partition path being omitted and the inclusion of the window flow bypass stream (flow in the clearance between the tube bundle and the shell, flowing parallel to the tube bundle). The flow streams of the Moore method are:

1a) Crossflow

1b) Crossflow bypass

2a) Window flow

2b) Window flow bypass

3a) Shell-Baffle leakage

3b) Tube-Baffle leakage

The pressure drop constraints are similar to those of the previous flow stream models, namely:

$$\Delta P_{tot} = \Delta P_1 + \Delta P_2 = \Delta P_3 \quad \text{(1:crossflow, 2:windowflow, 3:leakage)} \tag{2.74}$$

$$\Delta P_{1a} = \Delta P_{1b} \text{ (1a:crossflow, 1b:crossflow bypass)} \tag{2.75}$$

For flowrates:

$$\dot{M}_{tot} = \dot{M}_1 + \dot{M}_3 \tag{2.76}$$

$$\dot{M}_1 = \dot{M}_2 . \tag{2.77}$$

For each stream the expression for pressure drop was given in terms of flowrate by the equation:

$$\Delta P = n \frac{\rho}{2} \left(\frac{\dot{M}}{\rho A} \right)^2 \tag{2.78}$$

Where n is the number of velocity heads lost in each stream. In the Moore method the velocity head term is combined with a modified flow area S.

$$S = \frac{A}{\sqrt{\frac{n}{2}}} \tag{2.79}$$

Therefore;

$$\Delta P = \frac{\dot{M}^2}{\rho S^2} \tag{2.80}$$

The total pressure drop was expressed in terms of modified flow areas by the expression

$$\Delta P = \frac{\dot{M}_{total}^2}{\rho . S_{total}^2} \tag{2.81}$$

Where:

$$S_{\text{total}} = \frac{S_2}{A_m} + S_{3a} + S_{3b} \tag{2.82}$$

And

$$A_m = \left(1 + \left\{\frac{S_2}{S_{1a} + S_{1b} + S_{1c}}\right\}^2 \left\{\frac{N_{rc} - N_{ss}}{N_{rc}} + \frac{N_{ss}}{N_{rc}}\left(\frac{S_{1a} + S_{1b} + S_{1c}}{S_{ss}}\right)^2\right\}\right)^{\frac{1}{2}} \tag{2.83}$$

Where N_{ss} is the number of sealing strips, N_{rc} is the number of tube rows crossed and S_{ss} is the modified area for the sealing strip row, which is taken to be equal to the modified crossflow area S_{1a}. The procedure for calculating the pressure drop is an iterative one, because the value of the modified flow area and the velocity head is dependent on the friction factor and in turn the friction factor is dependent on the flowrate. Thus the procedure involved calculating the flowrate for each iteration. This was done using the following equations:

$$\dot{M}_{1a} = \frac{\dot{M}_t S_{1a}}{S_t A_M}\left[\frac{S_{2a} + S_{2b}}{S_{1a} + S_{1b}}\right] \tag{2.84}$$

$$\dot{M}_{1b} = \frac{\dot{M}_t S_{1b}}{S_t A_M}\left[\frac{S_{2a} + S_{2b}}{S_{1a} + S_{1b}}\right] \tag{2.85}$$

$$\dot{M}_{2a} = \frac{\dot{M}_t S_{2a}}{S_t A_M} \tag{2.86}$$

$$\dot{M}_{2b} = \frac{\dot{M}_t S_{2b}}{S_t A_M} \tag{2.87}$$

$$\dot{M}_{3a} = \frac{\dot{M}_t S_{3a}}{S_t} \tag{2.88}$$

$$\dot{M}_{3b} = \frac{\dot{M}_t S_{3b}}{S_t} \tag{2.89}$$

The pressure drop is calculated from the iterative solution of equation (2.80). The main feature of the Moore method is the pressure drop of each flow path is linked to the number of velocity heads lost in each path. This is related both to the geometry of the flow path and to the friction factor associated with the flow path. The values of the parameters A and n used in the equations above (2.78)-(2.89) are calculated using a series of equations related to flow path. The friction factors used in the initial model presented by Moore were very simple and for window flow and leakage flow were taken from the Poiseuille equation and the 'commercial pipe' equation of Wilson et al. 1922 (as reported in Kern, 1950). Correlations for the crossflow friction factors were slightly more complicated, but again were simplified in comparison to the 'Divided Flow' method. Moore found that this approach did not introduce significant inaccuracies in the calculation of shell-side pressure drop.

The general shellside flow models outlined above have been applied to describe two-phase shellside flows by the use of two-phase multipliers to the single-phase friction factors calculated in each shellside flow path. The fundamental assumption of these two-phase models is that the vapour mass fraction in each flow path is identical at a given distance along the shell. Experiments such as those of Grant and Polley (Grant et al, 1974; Polley et al, 1974) have demonstrated that there may be a tendency for unequal distribution of the liquid and vapour phases in the crossflow and crossflow bypass flow paths. Such analysis suggests that the assumption of uniform vapour quality throughout the shellside flow paths may be inaccurate.

2.6 - Summary

Existing data on the subject of shellside two-phase flow in the open literature has been examined. Many studies have been made on rectangular test sections designed to represent the crossflow of a shellside geometry. A number of these have been focussed on producing data to test correlations for the two-phase pressure drop multiplier (Cotchin, 1980; Cotchin et al, 1979; Dowlati et al, 1990, 1992, 1996; Grant et al, 1986; Schrage et al, 1988). Tests have also been done to produce data for crossflow void fractions (Dowlati et al, 1990, 1992, 1996; Feenstra et al, 2000; Grant et al, 1982, 1986; Schrage et al, 1988). Boiling heat transfer has also been examined in the rectangular geometry (Cornwell, 1990; Jensen et al, 1988; Roser et al, 1999) and further studies have produced data for two-phase flow patterns (Hassan et al, 1990; Noghrehkar et al, 1999). The principal limitation with all these data sources is the potential lack of applicability to real shellside geometries where a significant part of the flow is

not in the ideal crossflow direction. The effects of the other flow paths (which will have a significant impact on the overall shellside model) are not accounted for.

Tests have been carried out on real baffled shellside geometries to produce data for pressure drop (Cotchin et al, 1979) and pressure drop and flow patterns (Grant et al, 1987, 1989) in air/water flows. A limited number of data points, unavailable in the open literature, have been produced for boiling two-phase flows (Chu et al, 1998; McNaught et al, 1999) as part of an HTFS research programme. However to adequately assess current shellside models there is a necessity to produce more data for boiling two-phase flows in accurate shellside geometries (which contain bypass and leakage flow paths).

An examination has also been made areas of research in the literature relevant to the study of shellside evaporation. Existing shellside heat transfer models assume a combination of nucleate and convective boiling as the dominant heat transfer process. A number of correlations for these parameters have been examined (Stephan et al, 1980; Mostinski, 1963; Palen, 1990; Yilmaz, 1987; McNaught, 1991). The lack of data available for boiling shellside flows makes it difficult to assess the validity of the assumption of nucleate and convective boiling and further to assess the accuracy of the individual correlations.

Several authors have produced work on predicting two-phase crossflow void fraction (Grant et al, 1982; Schrage et al, 1988; Dowlati et al, 1990, 1992, 1996; Xu et al, 1998; Feenstra, 2000) and correlations for two-phase pressure drop multiplier (Polley et al, 1973; Grant et al, 1974; Ishihara et al, 1980; Schrage et al, 1988; Dowlati et al, 1990, 1992, 1996; Xu et al, 1998). These studies may provide useful tools for developing an overall shellside method. The major limitation of these studies is the fact that they are based on empirical correlations fitted to experimental data for geometries that only represent the crossflow path of the shellside flow.

The current state of the art in modelling shellside flows involves using computer software that produce an overall description of the shellside flow by making iterative calculations throughout different sections (flow paths) of the shellside geometry. The principal models on which such computer programs are based have been examined (Tinker, 1955; Palen et al, 1969; Grant et al, 1972; Moore, 1974). Such models have been extended to describe two-phase shellside flow by employing two-phase multipliers in the calculation of pressure drop in the individual shellside flow paths. A standard assumption of the two-phase model is that the vapour mass fraction is uniform throughout the various flow paths. Evidence from experimental studies of two-phase flows in crossflow with bypass geometries (Grant et al, 1974; Polley et al, 1974) suggests that this assumption may lead to significant inaccuracies.

2.7 – Conclusion

From an examination of the literature it is clear at present that there is insufficient experimental data to test the effectiveness of the current most popular design methods for evaporating shellside two-phase flows. One of the principal objectives of the current project is to produce data for evaporating shellside flows which can be used for such an evaluation over a range of geometric and operating conditions.

A substantial amount of work in the literature has been focussed on predicting pressure drop and void fraction in crossflow across bundles of tubes. These may provide useful insights which could help improve current shellside methods. Comparison of the project experimental data with the current shellside design methods should help to indicate the areas in which improvements can be made.

It has been identified in the literature that the current design methods for two-phase shellside flows assume a uniform vapour quality throughout the shellside flow paths. Furthermore shellside heat transfer models assume the two-phases are sufficiently well distributed to allow the use of correlations for nucleate and convective boiling to determine the heat transfer coefficient. Experimental investigations on geometries similar to shellside conditions have suggested that such an assumption may be inaccurate. Phase maldistribution is likely to have a major impact on the prediction of shellside pressure drop (varying vapour quality in each flow path) and heat transfer (areas of tube bundle where there is no nucleate or convective boiling). The issue of phase maldistribution will therefore be an area of particular focus for the current project.

CHAPTER 3 – Experimental Outline

3.1 – Introduction

The previous chapter identified many key papers on the subject of two-phase flow on the shellside of shell & tube heat exchangers. On examination of the test data from the papers it became clear that there is very little data in the open literature for boiling two-phase flows on the shellside of real industrial exchanger geometries. Many of the models and correlations for two-phase pressure drop multipliers and flow methods are based on test data in rectangular tube bundle test sections (Dowlati et al, 1992, 1996; Cotchin et al, 1979; Taylor et al, 1987; Grant et al 1986; Xu et al, 1998) which can only truly represent the crossflow stream of a real exchanger. The majority of the other data from real exchanger geometries with bypass and leakage streams (Grant et al, 1986, 1987, 1989) present data for adiabatic flows of air/water and cannot truly represent the full range of qualities and conditions for a boiling two-phase flow. From a full review of the available open literature it was clear that to assess existing models and produce a new improved model it would be necessary to produce some experimental data for a boiling shellside two-phase flow on a real industrial exchanger geometry. Throughout the project experimental data were collected from the NEL boiling & condensing facility. The test evaporator is more closely related to a real heat exchanger than any other test facility identified in the open literature as the size and dimensions are close to those which would be used in the industrial applications. The test fluid used throughout was refrigerant R-134A. The purpose of the experimental programme was to produce sets of data that could be used for comparison with existing models and for creating an improved model for shellside evaporating flow.

3.2 – Test Facility Description and Operation

3.2.1 – Basic Facility Description

All the experimental work was carried out on the NEL 'Boiling and Condensing Test Facility'. A schematic of the facility is shown in Figure 3.1. The principal units are three shell-and-tube heat exchangers a separator vessel and an accumulator vessel. Two of the shell-and-tube exchangers are operated as condensers with the process fluid condensing on the shellside where the tubeside contains a flowing water/ethylene-glycol coolant mixture. The third exchanger is operated as an evaporator with the process fluid on the shellside and low pressure condensing steam on the tubeside. This shellside evaporator was used as the test section for the current project. The process fluid used in all tests was the refrigerant R134a (1,1,1,2–Tetraflouroethane). This fluid was chosen for the project as it has similar physical

properties to light hydrocarbons (which may be commonly used in industrial applications of such exchangers) whilst being less hazardous to deal with in a laboratory situation.

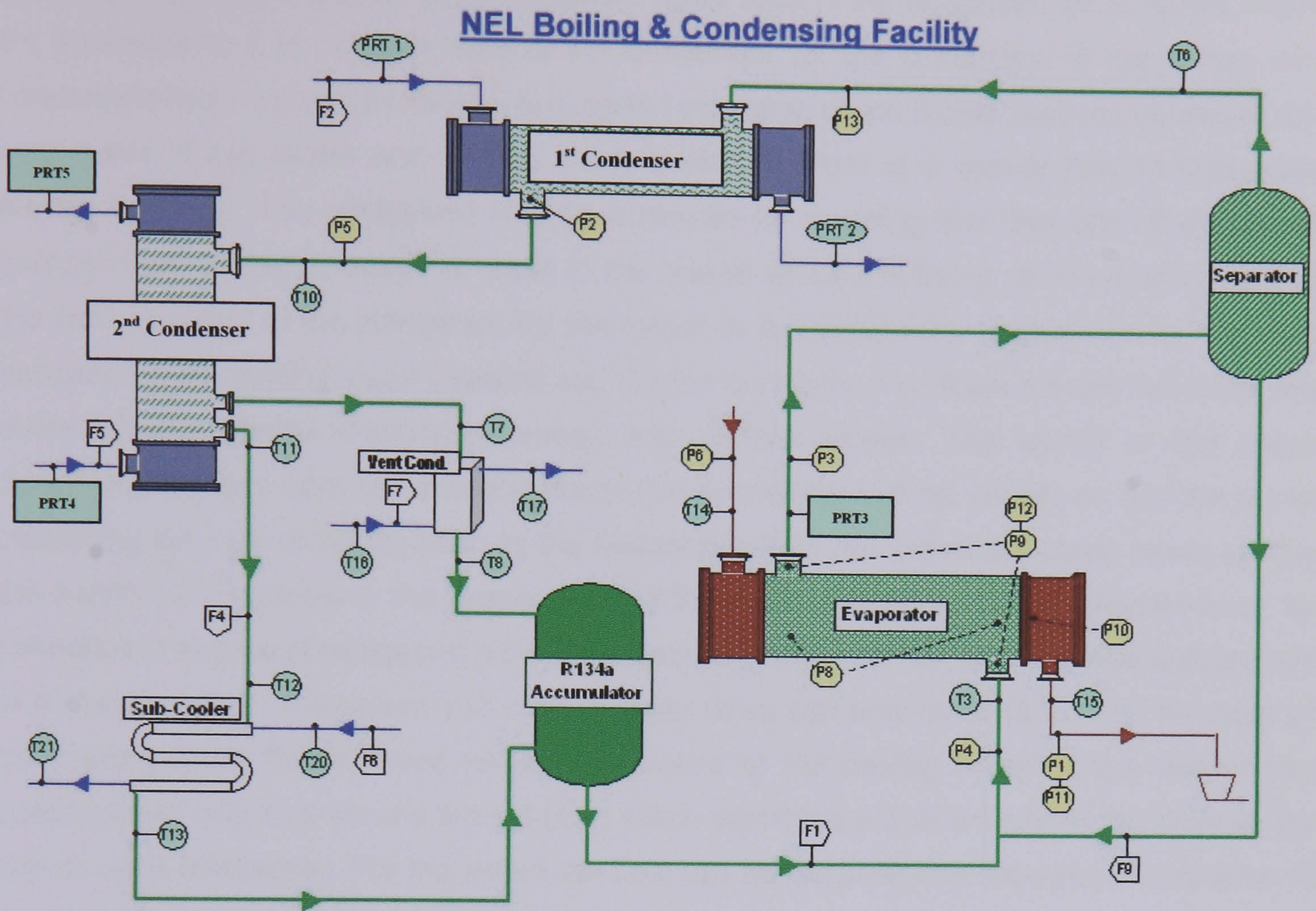

Figure 3.1 – Schematic diagram of NEL Boiling and Condensing Facility

3.2.2 – Operating Procedure

The first step in the operation was to fill the test facility with the refrigerant. The pressure in the facility was usually in the range from 5-7 bar after the refrigerant had been added. Initially the refrigerant accumulator vessel would contain the majority of the liquid R-134A. When the tests are to begin, the liquid refrigerant is pumped to the evaporator using a centrifugal pump. As there is not yet steam on the tubeside of the evaporator, the liquid refrigerant passes through the evaporator and separator and is returned to the evaporator via flow meter F9 by a second centrifugal pump.

Prior to steam entry, the tubeside is evacuated using a liquid ring vacuum pump, and the resultant low pressure allows the steam to condense at a saturation temperature of approximately 30°C. When the steam is introduced, the refrigerant begins to boil on the shellside and a vapour flow is generated through the top exit of the separator vessel. This flow is partially condensed on the shellside of the first condenser which is a twisted-tube shell-and-tube heat exchanger with the water/glycol coolant mixture flowing through the tubes. The

partially condensed refrigerant leaves this exchanger and passes to the second condenser. In this condenser (the vertical condenser in Figure 3.1) the remaining refrigerant vapour is condensed and the resultant liquid refrigerant flows back to the refrigerant accumulator. From the accumulator it is pumped back to the evaporator for the completion of the boiling and condensing loop around the facility. Successful operation of the facility involves balancing the heat loads of the steam and cooling water such that there is a steady flow of refrigerant around the loop. The refrigerant loop is sustained by ensuring that the rate of refrigerant pumped from the accumulator is equal to the rate at which it is being returned and also that the heat supplied to the refrigerant by the steam in the evaporator is balanced by the heat removed by the cooling water streams and the surroundings. The flows around the circuit are controlled by several centrifugal pumps and various valves. The speed of the pump controlling the flow from the accumulator to the evaporator can be varied, as can the pump controlling the rate of recirculation to the evaporator from the separator. Using these pumps the supply of refrigerant to the evaporator and the fraction of refrigerant re-circulated can be controlled. The rate of refrigerant exiting the second condenser can be controlled with the aid of a manual valve. The steam and cooling water flows can also be controlled. In the case of the cooling water this involves varying the speed of the cooling water pumps around the cooling water circuit or varying the set-point which controls the temperature of the water at the inlet to each condenser. For the steam the flow can be controlled by changing the position of the manual valves in the steam entry line.

The refrigerant flow around the facility is maintained with the aid of three sight glasses. The first of these sight glasses shows the level of liquid refrigerant in the liquid accumulator. If the level in the sight glass is falling it suggests that the refrigerant is being supplied to the evaporator at a rate faster than it is returning from the condensers. In this case the speed of the pump supplying the evaporator must be decreased to attempt to balance the refrigerant flows entering and exiting the accumulator. The second sight glass monitors the refrigerant level in the vertical condenser. If this level is rising it implies that the refrigerant is being condensed faster than it is being returned to the evaporator and indicates that the manual valve on the refrigerant exit line must be opened further to ensure the condenser does not begin to flood while the accumulator becomes empty. The third sight glass is used to ensure that the condensate level generated in the exit from the evaporator tubeside is steady. It is generally used to indicate that the condensate is being removed quickly enough to ensure the tubeside is not flooding and also to ensure that the condensate flowrate is steady while experimental data is being collected. If all three sight glass levels remain constant for a period of time it suggests that the heat input and output values to the refrigerant are balanced and the refrigerant loop will continue to circulate. When this steady refrigerant loop is established test data can be collected.

3.2.3 – Test Evaporator

The test evaporator in the facility was a TEMA AEW unit with single segmental baffles. Geometric details of the evaporator that were constant throughout all the experimental tests are given in Table 3.1. Figure 3.2(a) contains a picture of the tube bundle that was inside the evaporator shell during the tests. Figure 3.2(b) shows the shell-and-tube evaporator located in the test facility.

(a) – Tube Bundle with Baffles (Horizontal-cut)

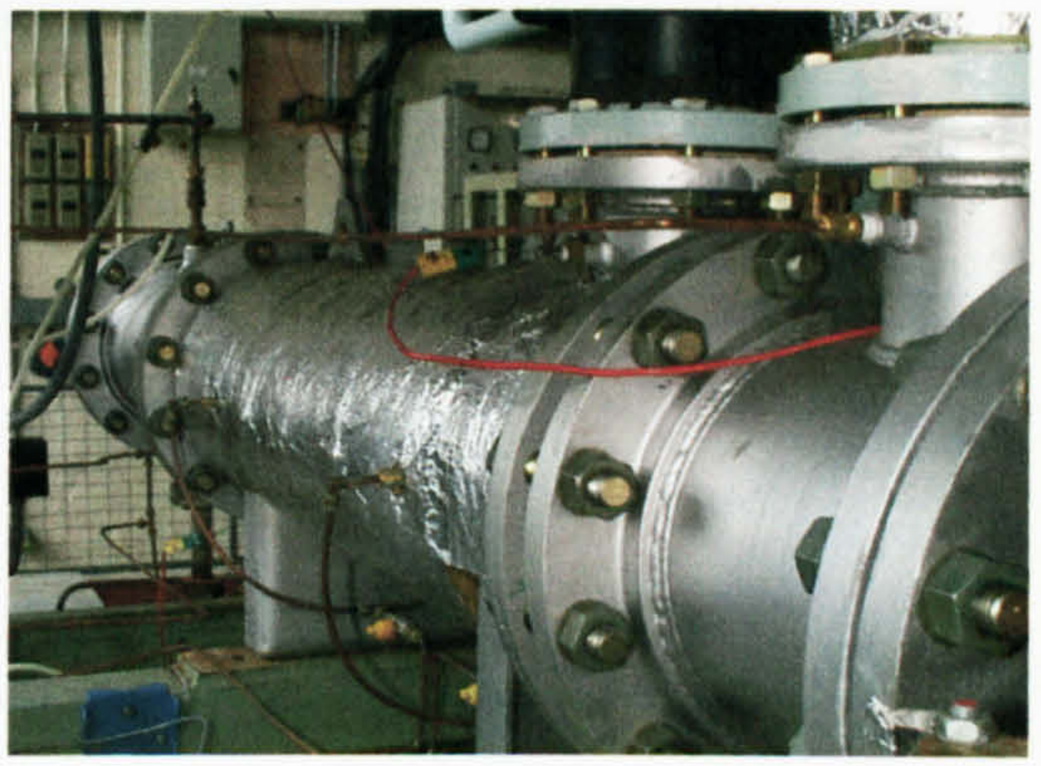

(b) – Test Evaporator in Facility

Figure 3.2 – Pictures of Test Evaporator and Interior Tube Bundle

Shell type	TEMA AEW
Shell inside diameter (mm)	254
Tube count	97
Number of tube passes	1
Tube outside diameter (mm)	15.88
Tube wall thickness (mm)	1.24
Tube material	Copper
Tube pitch (mm)	20.64
Tube layout angle (deg)	30
Tube length (mm)	1210
Baffle type	Single segmental
Baffle cut (%)	30
Baffle thickness (mm)	3
Shellside inlet nozzle i.d. (mm)	25
Impingement protection	None
Shellside outlet nozzle i.d. (mm)	100
Tubeside inlet nozzle i.d. (mm)	100
Tubeside outlet nozzle i.d. (mm)	25
Shell/bundle diametrical clearance (mm)	20.2
Baffle/tube diametrical clearance (mm)	0.42
Shell/baffle diametrical clearance(mm)	3.2

Table 3.1 – Evaporator Geometric Details

The evaporator tube bundle was removed and altered between the different series of experimental tests to assess the influence of certain geometrical parameters. The principal changes made involved the number of shellside baffles, the shellside baffle orientation (horizontal or vertical) and the presence of sealing strips in the crossflow bypass lane. The influence of baffle orientation on the flow path is indicated in Figure 3.3. With the horizontal baffle (3.3(a)) the process fluid enters the evaporator and travels vertically upwards and downwards between the shellside baffles to the exit. With the vertical baffle orientation (3.3(b)) the principal flow direction is horizontally from side to side.

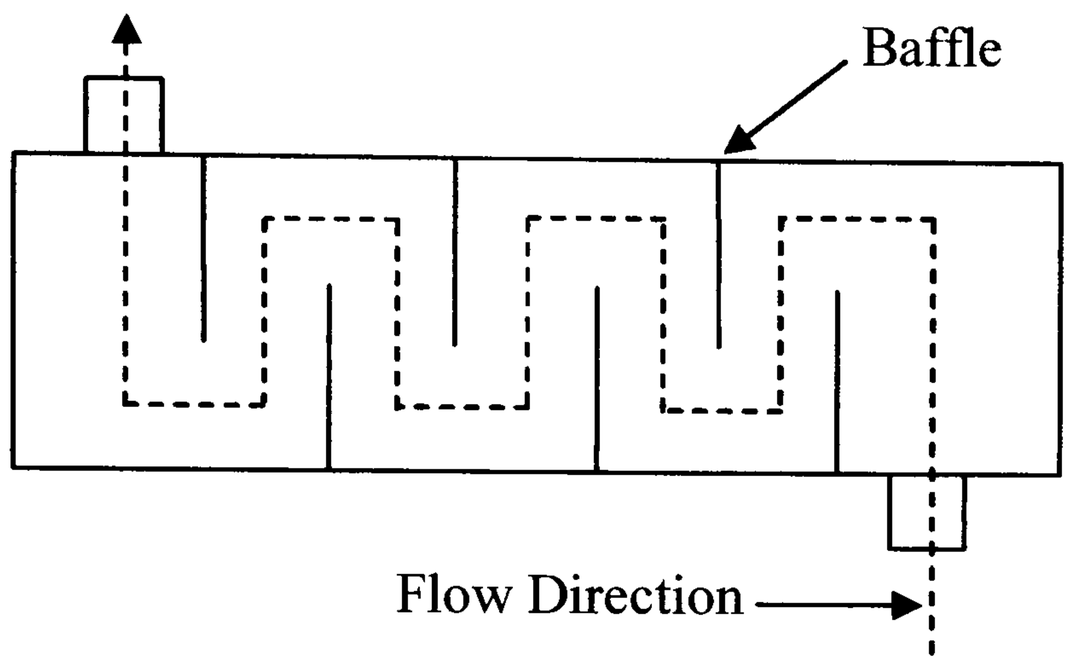

(a) – Side View of Exchanger with Horizontal Baffle Orientation

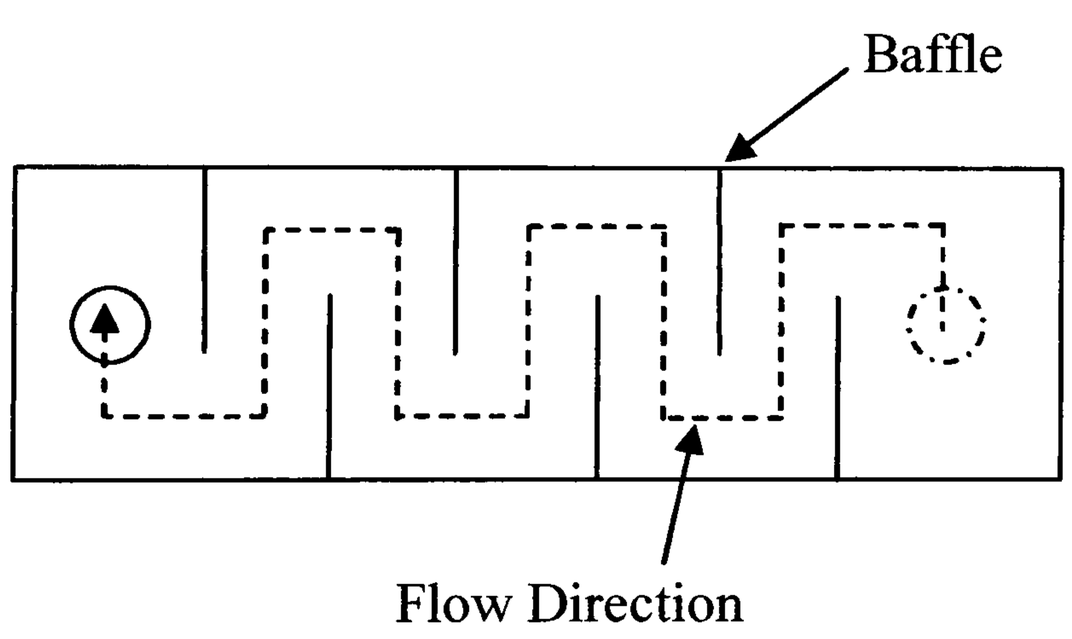

(b) – Plan View of Exchanger with Vertical Baffle Orientation.

Figure 3.3 – Influence of Baffle Orientation (Cut)

A cross sectional drawing of the tube bundle with and without sealing strips is shown in Figure 3.4 (further geometric details including the position and dimensions of the sealing strips are given in Appendix B). The purpose of the sealing strips is to force liquid that may be bypassing the tube bundle back towards the tubes in order to increase the flow of liquid in the crossflow path, where most of the heat transfer occurs.

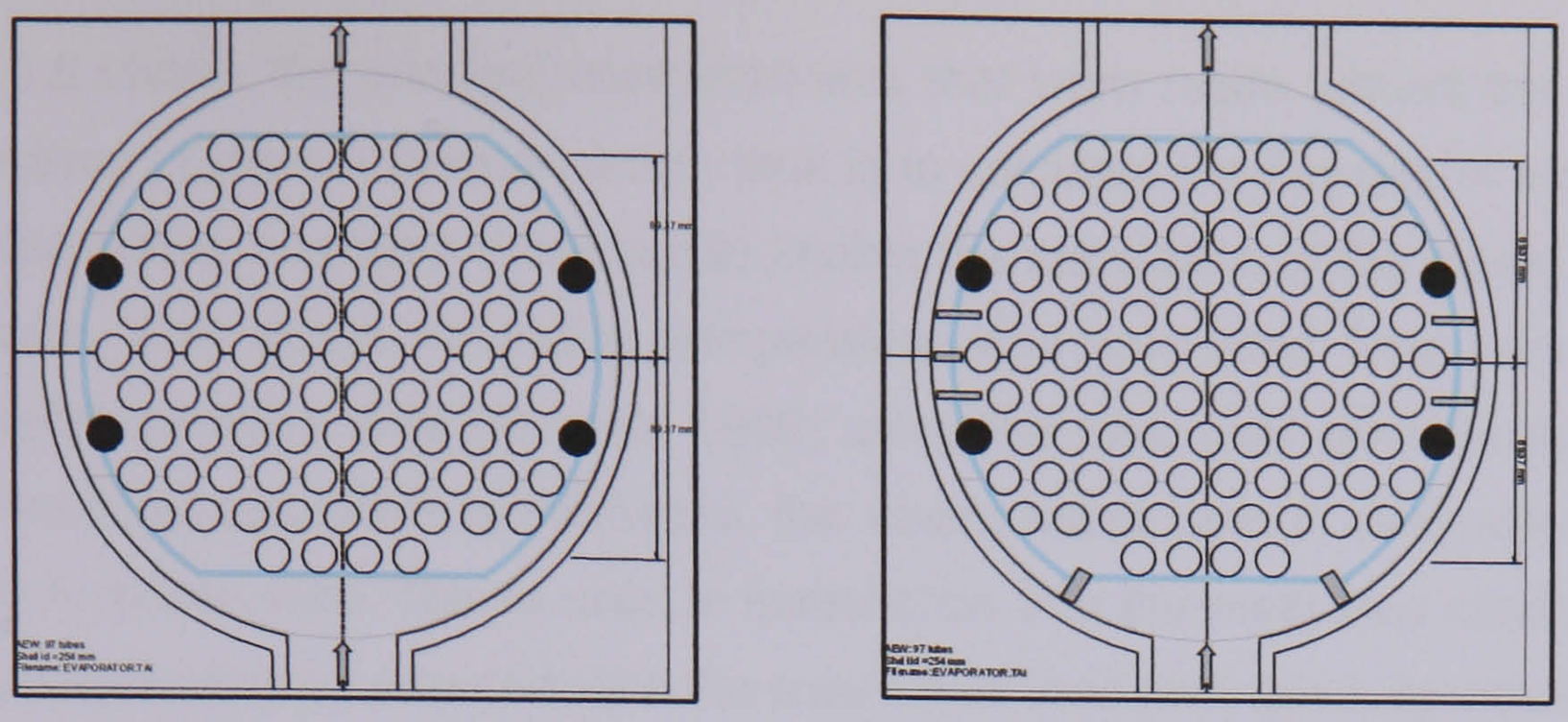

(a) – Without Sealing Strips (b) – With Sealing Strips

Figure 3.4 – Tube Bundle Cross Section With and Without Sealing Strips in Crossflow Bypass

3.3 – Principal Measurements

The location of the various instrumentation is indicated in Figure 3.1. In this section the principal measurements made during the experimental tests are highlighted.

3.3.1 - Test Evaporator

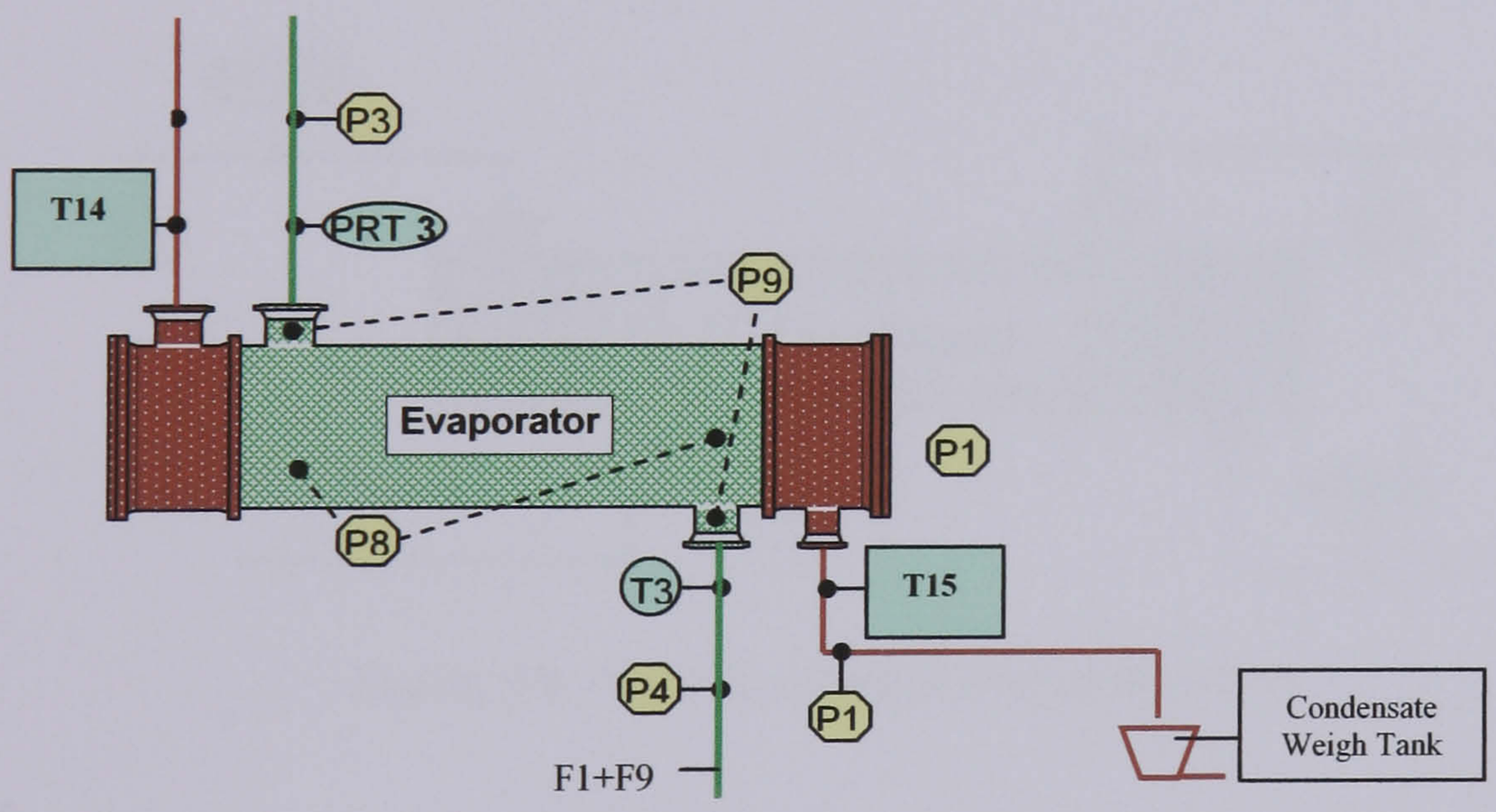

Figure 3.5 – Test Evaporator Instrumentation

Principal Measurements

Shellside Inlet Flowrate (F1), (F9)
Shellside Inlet Temperature (T3)
Shellside Outlet Temperature (PRT3)
Pressure Drop – nozzle to nozzle (P9)
Steam Condensate Collection Weight (Weigh Tank)
Tubeside Inlet Temperature (T14)
Condensate Outlet Temperature (T15)
Tubeside Outlet Pressure (P1)
Pressure Drop – Shellside Baffle Spaces (P8)

Figure 3.5 shows the principal measurements that were made around the test evaporator. The purpose of the condensate weigh tank is to calculate the flowrate of steam condensate generated during a particular test run to enable the calculation of the steam heat load in the evaporator. The steam saturation temperature was calculated from curve fits to steam pressure/temperature data (Robson, 1999) using the measured condensate outlet pressure (P1). From the saturation temperature, the steam latent heat is evaluated using a similar curve fit to steam data. This is used in conjunction with the measured condensate collection mass and collection time to calculate the steam heat load (kW) given by equation 3.1.

$$Q_{steam} = \left[\Delta h_{l(Tsat)} + \left(h_{g(Tin)} - h_{g(Tsat)}\right) + \left(h_{l(Tsat)} - h_{l(Tout)}\right)\right] M_{condensate} \qquad (3.1)$$

$\Delta h_{l(Tsat)}$ is the specific latent heat at the steam saturation temperature, $h_{g(Tin)}$ and $h_{g(Tsat)}$ are the specific enthalpies of the vapour at the inlet and saturation temperatures, $h_{l(Tsat)}$ and $h_{l(Tout)}$ are the liquid specific enthalpies at the saturation and outlet temperatures and $M_{condensate}$ is the mass flowrate of steam condensate calculated from the collected weight and the collection time.

3.3.2 – First Condenser

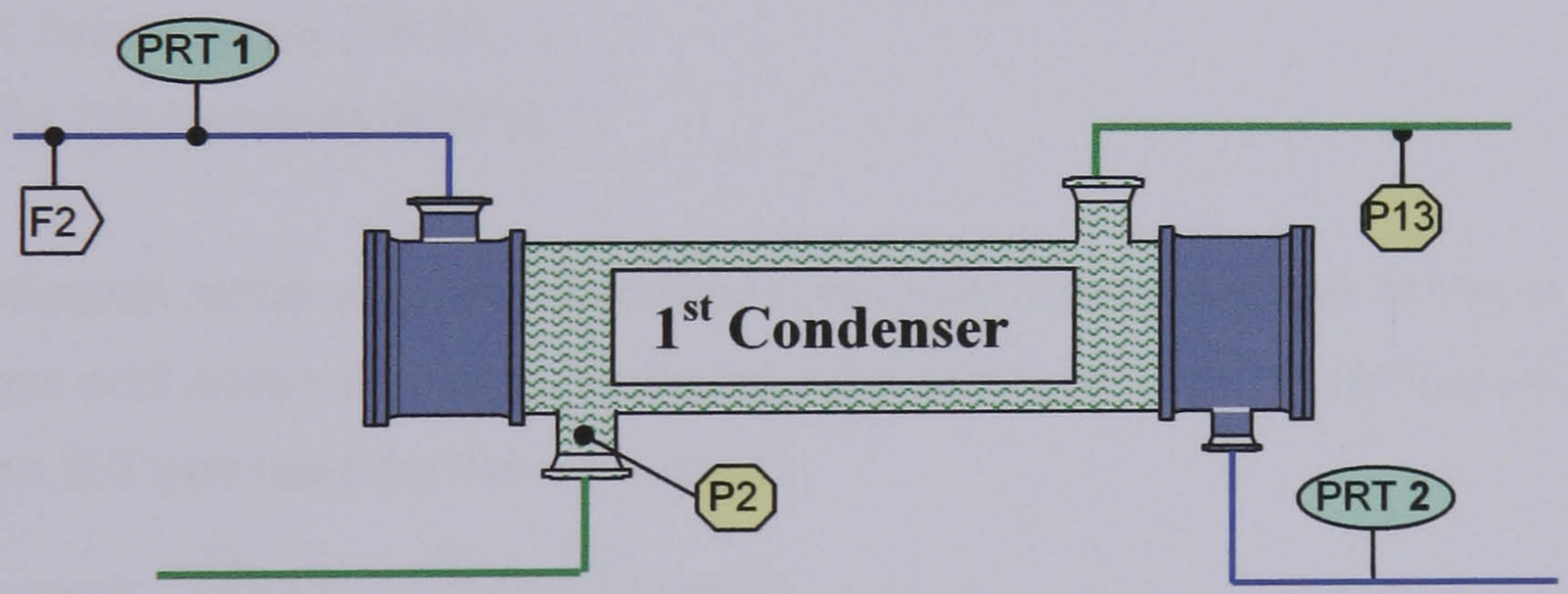

Figure 3.6 – First Condenser Instrumentation

Principal Measurements

Coolant Flowrate (F2)

Coolant Inlet Temperature (PRT1)

Coolant Outlet Temperature (PRT2)

The inlet and outlet temperatures and flowrate of the water/glycol coolant mixture stream were measured to enable the heat removed from the refrigerant to be calculated. The heat removed was calculated using equation 3.2. The specific enthalpies of the water/glycol mixture were calculated using a physical property programme ('Physprop') developed at NEL (Robson, 1999).

$$Q_{Cooling(1)} = \left(h_{l(Tout)} - h_{l(Tin)}\right) M_{Cooling(1)} \qquad (3.2)$$

3.3.3 – Second Condenser

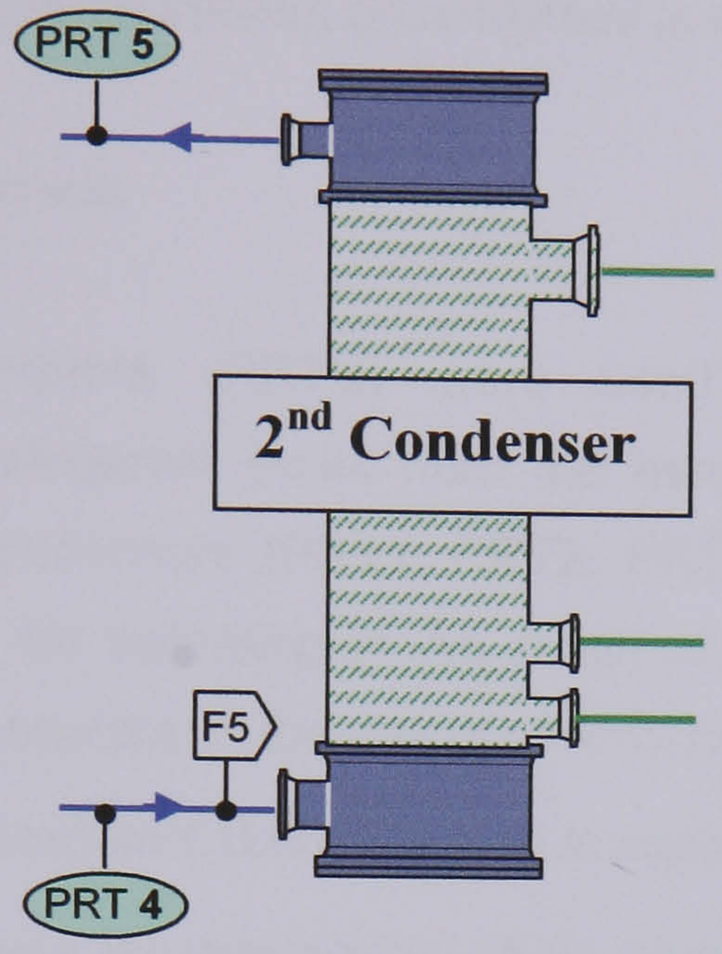

Figure 3.7 – Second Condenser Instrumentation

Principal Measurements

Coolant Flowrate (F5)

Coolant Inlet Temperature (PRT4)

Coolant Outlet Temperature (PRT5)

The measurements made around the vertical condenser were the same as those made at the first condenser and were used to calculate the heat removed from the refrigerant in the same way. Equation 3.3 was used for the calculation.

$$Q_{Cooling(2)} = \left(h_{l(Tout)} - h_{l(Tin)}\right) M_{Cooling(2)} \qquad (3.3)$$

Equations 3.1, 3.2 and 3.3 were used to check the overall heat balance for the refrigerant around the facility. Generally if the facility was operating at a steady state the total heat into the refrigerant stream would be balanced by the total heat removed. The heat balance was quantified using equation 3.4.

$$Q_{Balance} = \left[\frac{Q_{Steam} - \left(Q_{Cooling(1)} + Q_{Cooling(2)}\right)}{Q_{Steam}}\right] \times 100\% \qquad (3.4)$$

For all the test data the heat balance calculated from equation 3.4 was within the range $\pm 5\%$. With the possibility of some heat loss to the surroundings and some uncertainty in measurements it was assumed that a heat balance within this range would be a reasonable indicator that the facility was operating in a steady state.

3.4 – Instrumentation

This section describes the types of instrumentation used for the principal measurements outlined in the previous section. Further information on instrumentation such as the procedure for dealing with instrument and measurement uncertainties is outlined in Chapter 4.

3.4.1 – Temperature Measurement

Platinum resistance thermometers (PRT's) were used for the main temperature measurements such as the refrigerant outlet from the evaporator (PRT3) or the coolant stream temperatures at the condensers (PRT1, PRT2, PRT4 and PRT5). Type 16 PRT's were used which are suitable for operating in the range of -50°C to +350 °C. During the experimental tests they would operate in the range of 4 °C to 35 °C, at this temperature the manufacturer's tolerance is quoted as $\pm 0.05^0 C$. This is significantly more accurate than the commonly used K-type or T-type thermocouples which have an accuracy of $\pm 2.5^0 C$ and $\pm 0.5^0 C$ respectively.

3.4.2 – Pressure Measurement

The steam condensate outlet pressure reading (P1) was critical as it was used to determine the steam saturation temperature. The transducer used was a Seimens MF4 which has a quoted accuracy of $\pm 1\%$ and is generally used for the range of measured pressure from 0-0.07 bar. The differential pressure transducers for the critical shellside pressure drop measurements (P8 and P9) were Fisher-Rosemount M1151 Models and have a quoted accuracy of $\pm 0.1\%$ 0.25%???. They typically worked in a range of 0-0.1 bar. All three transducers were calibrated annually to accredited UKAS/NAMAS standards.

3.4.3 – Flow Measurement

Measurements of the flowrates to the evaporator (F1 and F9) are also critical and these were made using turbine flow meters which again were calibrated annually and which had an accuracy of $\pm 1\%$ over a range of flows which varied from 0.001 to 15 l/s.

3.4.4 – Steam Condensate Weight

The weigh scales used had an accuracy of $\pm 1\%$ over the range 0-60kg in 1g increments and were calibrated and checked annually under a maintenance contract.

3.5 – Data Recording and Archiving

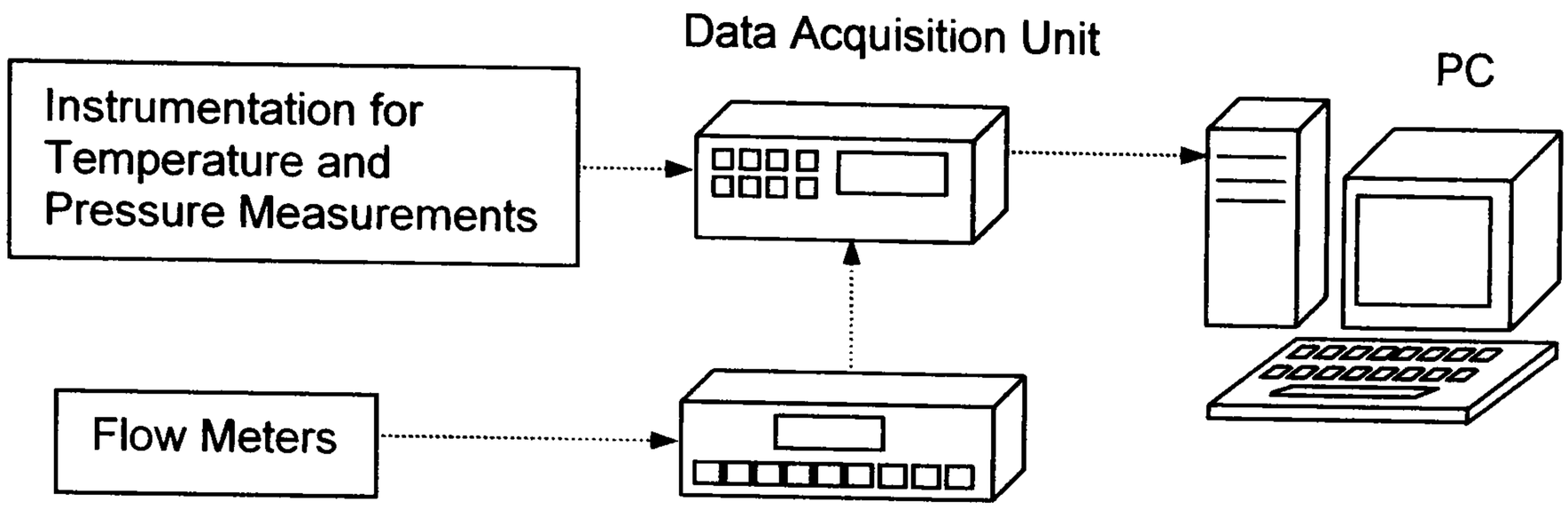

Figure 3.8 – Data Collection System

When steady state operation of the facility had been established, the process of data collection began. The test data was collected with the aid of a data acquisition unit and a PC. A diagram of the data collection system is presented in Figure 3.8. All temperature and pressure measuring devices were wired to a data acquisition unit which recorded the output signal from each device. The flow meters on the facility were wired to a frequency-to-voltage converter which produced a signal that was read by the data acquisition unit. Two data acquisition units were used to collect the data from all the instruments. These devices were the Hewlett-Packard 3497A and 3852A. The purpose of the data units was to measure the electronic signals output from all the instrumentation. For example a PRT operating in the facility would measure a temperature and produce an electrical resistance which would be measured by the data unit. The data unit was then connected to the facility PC. The PC contained a specific software program (Robson, 1998) designed for extracting the data collected by the data acquisition unit. The software took the readings from the data unit and converted them into meaningful results. For the PRT example, the electrical resistance stored by the data acquisition unit was converted to a temperature value in ^{0}C by the acquisition software on the PC. The PC was used to monitor the readings of the instruments continuously during operation.

The first step in the procedure of data collection was to instruct the PC software to begin recording data from the data acquisition unit. The unit scanned each instrument 10 times in sequence and the readings were passed to the PC where the average value and RMS error of each measurement was calculated. The next step was to begin collection of the steam condensate. The PC software was used to trigger the condensate collection system which used a two-way valve and a timer that were linked through an electrical circuit and operated by a single switch. Whilst data was not being collected the condensate was pumped back to the boiler. When the PC instructed the collection of the condensate the switch was triggered,

starting the timer and directing the condensate flow into the collection tank. When approximately 5kg of condensate has been collected the switch was triggered diverting the flow away from the collection tank and the timer stopped on the PC. The exact weight of the condensate was entered into the software program on the PC and the condensate flowrate is calculated. An output report (as in Figure 3.9) was produced of all the test run data collected from the instrumentation and steam condensate collection. The report contained all the instrument average measurements (of the 10 scans), the RMS error in the measurements and the refrigerant heat balance calculated using equation 3.4. Each one of these test runs was recorded with a date and time signature and stored on the facility PC. If the refrigerant heat balance was out with the range of $\pm 5\%$ the test data was rejected as it was unlikely that the data collected was representative of steady state conditions for the particular heat load and flowrates. If the heat balance was within the range the data was recorded and used for further analysis. The process of data analysis is the subject Chapter 4.

T12@1623 - Notepad

File Edit Search Help

```
NEL Boiling & Condensing Facility                                  Program Version = 2.30
=================================
TEST REPORT
-----------
Test Number      = 12
Test Date        = 15/11/2001
This Filename    = C:\BOILCOND\DATA\011115\T12@1623.TXT
Test Description:
Repeat Tests

Flowrates (Litre/sec)                                          | Start of scan = 16:23:19
=====================                                          |   End of scan = 16:23:30
F/M Chn. Description                    Stream        Average    RMS       Min.      Max.
-------------------------------------------------------------------------------------------
 1   51  E-shell Evap. S/s Inlet        R-134a        0.498      0.000     0.497       0.499
 2   52  Brown FinTube T/s Inlet        Wat/Gly       3.319      0.001     3.317       3.322
 4   54  Sub-Cooler Refrig. Inlet       R-134a        0.486      0.000     0.486       0.487
 5   55  Vert.Condenser T/s Inlet       Wat/Gly       9.898      0.002     9.895       9.901
 6   56  Sub-Cooler Coolant             Wat/Gly      -0.018      0.000    -0.018      -0.018
 7   57  Vent PHE Condenser Inlet       Wat/Gly       0.294      0.000     0.294       0.295
 9   53  Separator Recirculation        R-134a        3.503      0.007     3.491       3.513

Pressures (bar)   Dual Reading: Use P1 for < 0.2, P11=Ind.Only  | Start of scan = 16:23:12
===============   ************                                 |   End of scan = 16:23:19
P/T Chn. Description                    Stream  Units Average    RMS       Min.      Max.
-------------------------------------------------------------------------------------------
 1   40  E-shell Evap. T/s Outlet       Steam   abs.  0.0532     0.000     0.0532    0.0532
 2   41  Brown FinTube S/s Out.Noz.     R-134a  abs.  5.0051     0.00029   5.0047    5.0056
 3   42  E-shell Evap. S/s Outlet       R-134a  abs.  5.58363    0.00335   5.5807    5.5908
 4   46  E-shell Evap. S/s Inlet        R-134a  abs.  5.72254    0.00324   5.7166    5.7265
 5   44  Vert.Condenser S/s Inlet       R-134a  abs.  5.0173     0.00026   5.0168    5.0177
 6   45  E-shell Evap. T/s Inlet        Steam   abs. -0.34093    0.00684  -0.3515   -0.3302
 8   61  E-shell Evap. S/s Endzones     R-134a  dp.   0.01572    0.00017   0.0155    0.016
 9   62  E-shell Evap. S/s Nozzles      R-134a  dp.   0.11844    0.00058   0.11767   0.11936
10   63  E-shell Evap. T/s PD           Steam   dp.   0.00218    0.000     0.00218   0.00219
11   64  (P1)E-shell Evap. T/s Out.     Steam   abs.  0.0281     0.000     0.0281    0.0281
13   66  Brown FinTube S/s Inlet        R-134a  abs.  5.49352    0.00093   5.492     5.4948

Temperatures (°C)                                              | Start of scan = 16:23:07
=================                                              |   End of scan = 16:23:12
T/C Chn. Description                    Stream        Average    RMS       Min.      Max.
-------------------------------------------------------------------------------------------
 3   3   E-shell Evap. S/s Inlet        R-134a        18.56      0.0132    18.53     18.58
 6   6   Separator Vapour Outlet        R-134a        18.90      0.0366    18.79     18.91
 7   7   Vent PHE Condenser Inlet       R-134a        17.73      0.0115    17.72     17.74
 8   8   Vent PHE Condenser Outlet      R-134a        17.87      0.010     17.85     17.87
10   10  Vert.Condenser S/s Inlet       R-134a        15.74      0.0301    15.73     15.83
11   21  Vert.Condenser S/s Outlet      R-134a        9.62       0.010     9.60      9.62
12   22  Sub-Cooler Refrig. Inlet       R-134a        13.50      0.000     13.50     13.50
13   23  Sub-Cooler Refrig. Outlet      R-134a        13.39      0.0075    13.37     13.40
14   24  E-shell Evap. T/s Inlet        Steam         94.37      0.0091    94.36     94.38
15   25  E-shell Evap. T/s Outlet       Steam         19.68      0.0099    19.68     19.70
16   26  Vent PHE Condenser Inlet       Wat/Gly       5.76       0.0116    5.76      5.78
17   27  Vent PHE Condenser Outlet      Wat/Gly       5.53       0.0225    5.46      5.53
20   30  Sub-Cooler Coolant Inlet       Wat/Gly       15.23      0.0159    15.18     15.23
21   31  Sub-Cooler Coolant Outlet      Wat/Gly       15.90      0.0128    15.89     15.92
                                                               | Start of scan = 16:23:30
                                                               |   End of scan = 16:23:36
PRT Chn. Description                    Stream        Average    RMS       Min.      Max.
-------------------------------------------------------------------------------------------
 1   301 Brown FinTube T/s Inlet        Wat/Gly       7.21       0.0123    7.17      7.22
 2   300 Brown FinTube T/s Outlet       Wat/Gly       12.23      0.0034    12.23     12.24
 3   302 E-shell Evap. S/s Outlet       R-134a        19.37      0.0042    19.36     19.38
 4   303 Vert.Condenser T/s Inlet       Wat/Gly       5.27       0.0036    5.26      5.28
 5   304 Vert.Condenser T/s Outlet      Wat/Gly       6.64       0.0025    6.64      6.65

CALCULATIONS                                                   Properties Used in Calculations:
============                                                   Wat/Gly Mass Fr.= 25.0    %
Steam condensate weight  = 4.898    kg
            Time taken   = 110.18   sec
      Steam heat load    = 114.93   kW                         Calculated Properties:
                                                               R-134a Lat.heat = 182.37  kJ/kg
Heat received by R-134a  = 111.51   kW                         R-134a  Density = 1228.0  kg/m³
Heat received by C.W. in:
     Vertical Condenser  = 52.61    kW
          BF Condenser   = 64.85    kW
                 TOTAL   = 117.46   kW

Mass evaporated          = 0.630    kg/s
Recirc. mass flowrate
        from separator   = 4.302    kg/s                       Heat balance     = -2.20   %
```

Figure 3.9 – A typical data output report from an experimental test run

CHAPTER 4 – Data Processing and Uncertainty Analysis

4.1 – Introduction

The experimental measurements made on the test facility were described in Chapter 3. These measurements were used to calculate parameters (such as vapour quality and heat transfer coefficients) which were used to assess the performance of the test evaporator. The processing required to produce the relevant data from the test measurements is the subject of this chapter.

4.2 – Data Analysis Workbook

4.2.1 – Raw Data

The test data from each test run was stored on the facility PC in the form an output report. The output reports created were described briefly in Chapter 3 and an example of a typical report was presented in Figure 3.8. All of the relevant data for the test evaporator were extracted from these reports for more detailed analysis. The measurements extracted from the report are highlighted in Figure 4.1.

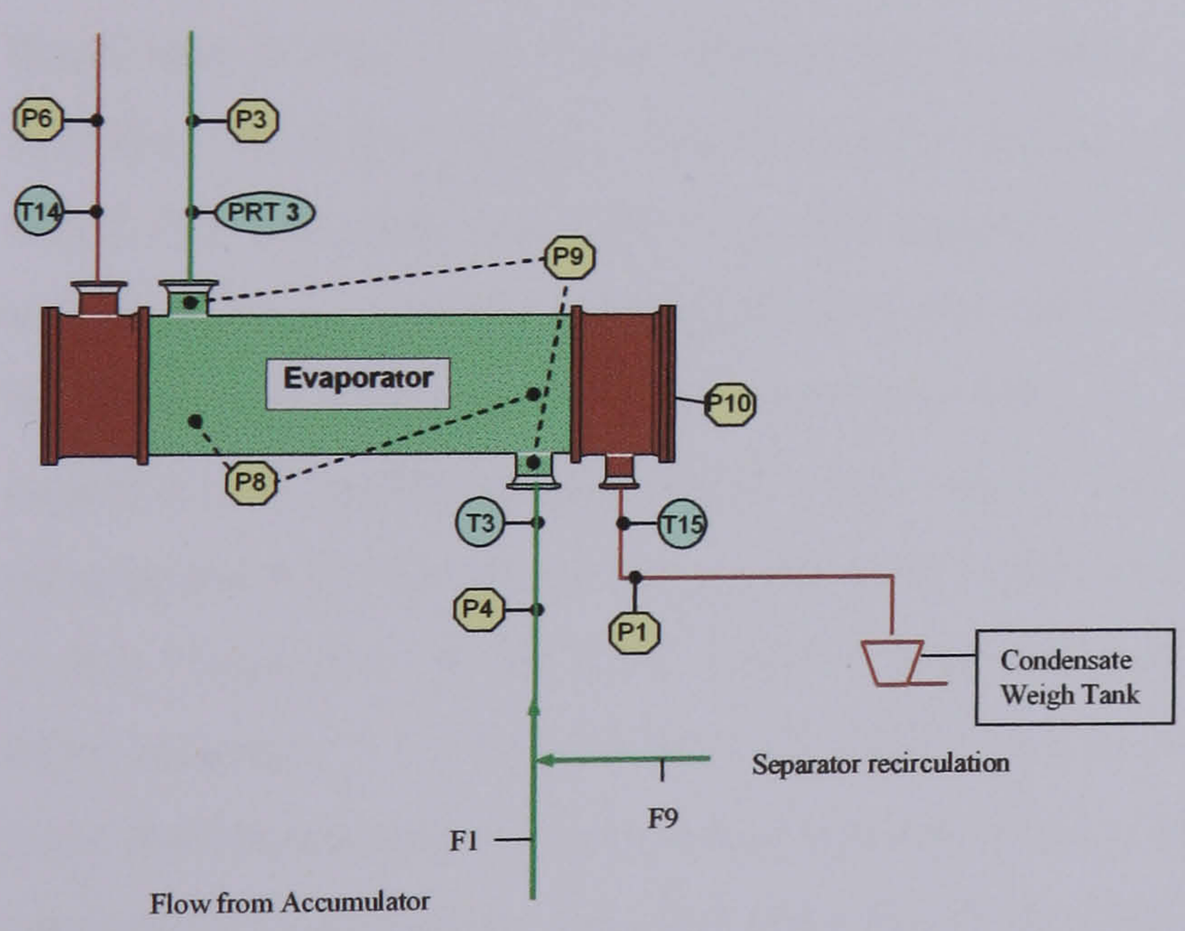

Extracted Measurements

Flowrate of R-134A which has been evaporated (F1)

Flowrate of R-134A which has been re-circulated (F9)

R-134A outlet temperature (PRT 3)

R-134A inlet pressure (P4)

R-134A outlet pressure (P3)

R-134A inlet temperature (T3)

Nozzle-to-nozzle shellside pressure drop (P9)

Steam condensate pressure (P1)

Shellside tube bundle pressure drop (P8)

Steam condensate temperature (T15)

Superheated steam entry temperature (T14)

Figure 4.1 – Measurements extracted from the data collected for each test run

The data from the test run output report were manually entered into a Microsoft Excel Analysis Workbook. The worksheet into which the data were entered was entitled 'Raw Data'. The layout of this worksheet is displayed in Figure 4.2.

Figure 4.2 – ‘Raw Data’ worksheet in analysis workbook

Each row in the ‘Raw Data’ worksheet contained all the measurement data extracted from one test run output report. The first two columns of each row contained the date and time at which the test data was collected. For example data collected on 4th of July 2000 at 3.43pm will be entered into the worksheet with the date and time reference 04/07/00; T@1543. The following 14 columns (C – P) contained the 11 extracted measurements from the output report and 3 additional calculated parameters. The 3 parameters were; the steam saturation temperature at the measured condensate outlet pressure (P1), the steam saturation pressure at the measured condensate outlet temperature (T15) and the steam heat load calculated from equation 3.1 (Chapter 3). The next 4 columns (Q - U) contained parameters calculated from the measured and calculated values in the preceding 14 columns. The purpose of these calculated parameters was to provide more information about the conditions in the test evaporator. The first of these values was the mass flow rate of R-134A evaporated in the test evaporator. This was calculated from equation 4.1 based on the assumption that the previously calculated heat load from the steam is absorbed in the process of heating and evaporating the refrigerant.

$$M_{evap} = \frac{Q_{Steam} - M_l\left(h_{l(Tsat)} - h_{l(Tin)}\right)}{\Delta h_{l(Tsat)}} \qquad (4.1)$$

M_l is the mass flowrate of R-134A liquid entering the evaporator, $h_{l(Tsat)}$ and $h_{l(Tin)}$ are the specific liquid enthalpies of R-134A at the saturation temperature and inlet temperatures respectively. $\Delta h_{l(Tsat)}$ is the specific latent heat of R-134A at the saturation temperature. All the refrigerant physical properties were calculated using the physical properties programme 'Physprop' (Robson, 1999). This calculated evaporated mass flow rate of R-134A was used in the calculation of the next parameter, the vapour quality at the exit of the test evaporator. The measured re-circulated flowrate from the separator (flow meter F9) was also used in the calculation. The exit vapour quality is given by equation 4.2.

$$x_{exit} = \frac{M_{evap}}{M_{evap} + V_{re-circ}\rho_l} \tag{4.2}$$

$V_{re-circ}$ is the volumetric flowrate of R-134A re-circulated and ρ_l is the R-134A liquid density at the measured evaporator outlet temperature (PRT 3). The other two calculated parameters were the total mass flowrate to the evaporator and the mass flux through the evaporator. The total mass flowrate is calculated from the measured volumetric flowrates to the evaporator (Flow meters F1 and F9) and is given by equation 4.3.

$$\dot{M}_{Tot} = \left(V_{acc} + V_{re-circ}\right)\rho_l \tag{4.3}$$

V_{acc} is the volumetric flowrate from the refrigerant accumulator and ρ_l was again calculated using the temperature of R-134A at the exit from the evaporator. The calculation of the mass flux through the evaporator is carried out using equation 4.4.

$$\dot{m}_{Tot} = \frac{\dot{M}_{Tot}}{A_{X-flow}} \tag{4.4}$$

A_{X-flow} is the shellside crossflow area which is specific to the geometry of the evaporator being used in the particular set of experimental tests. The method for calculating the crossflow area and the values of the crossflow area in each set of experimental tests are given in Chapter 5.

4.2.2 – Heat Transfer Coefficient

The measured data from the experimental tests were used to calculate the heat transfer coefficients in the shellside evaporator in a separate worksheet of the analysis workbook. The key measurements for the calculation are the pressure of the exit steam condensate from the tubeside of the evaporator (P1) and the R-134A temperature at the exit from the evaporator shellside (PRT 3). The measured steam condensate pressure was used to calculate the corresponding steam saturation temperature in the tubes. The saturation temperature was used as the mean tubeside temperature in the calculation of heat transfer coefficients. It was

assumed the majority of the heat transfer occurred during the condensation of steam at this temperature. The mean shellside temperature is taken as the refrigerant saturation temperature at outlet as the inlet R-134A to the evaporator may be subcooled below the saturation point. These temperatures are used to calculate the effective temperature difference between the tubeside and shellside of the evaporator. The effective temperature difference is given by equation 4.5.

$$\Delta T_{eff} = T_{Sat(Steam)} - T_{Sat(R-134A)} \tag{4.5}$$

The value of ΔT_{eff} is used to calculate the overall heat transfer coefficient from equation 4.6 with the aid of the available heat transfer area A_{HT} which is defined as the external surface area of the tubes in the tube bundle.

$$U_{Overall} = \frac{Q_{Steam}}{A_{HT}\Delta T_{eff}} \tag{4.6}$$

The heat transfer coefficient on the shellside was the parameter of prime interest during the experimental tests as it gives the best indication of the performance of the shellside evaporator. The shellside heat transfer coefficient (or boiling heat transfer coefficient) is related to the overall heat transfer coefficient by equation 4.7.

$$\frac{1}{U} = \frac{1}{\alpha_{boil}} + \frac{1}{\alpha_{Steam}} + \frac{1}{\alpha_{wall}} \tag{4.7}$$

The three terms on the right hand side of this equation represent the resistance to heat transfer on the shellside on the tubeside and in the tube wall. All of the coefficients were calculated with reference to the same heat transfer area as the overall coefficient. The values of the steam side and tube wall resistances were calculated using the HTFS TASC program. The values of α_{Steam} and α_{Wall} were much larger than the overall coefficient calculated from equation 4.6. As a result the value of the boiling heat transfer coefficient (calculated using equation 4.8) is predominantly influenced by the overall heat transfer coefficient U. The value of α_{Wall} calculated in TASC was around 289 kW/m^{2}K whereas α_{Steam} was in the range between 10–15 kW/m^2 depending on the particular test conditions. The value of U was in the range of 1-5 kW/m^2 throughout the tests.

$$\alpha_{boil} = \frac{1}{\left(\frac{1}{U}\right) - \left(\frac{1}{\alpha_{Steam}}\right) - \left(\frac{1}{\alpha_{wall}}\right)} \tag{4.8}$$

The final parameter calculated in the heat transfer coefficient worksheet is the heat flux. This term is calculated using the steam heat load and the available heat transfer area as in equation 4.9.

$$\dot{q} = \frac{Q_{Steam}}{A_{HT}} \tag{4.9}$$

4.2.3 – Pressure Drop

The locations of the principal differential pressure transducers (P8 and P9) are indicated in Figure 4.1. Transducer P8 was used to measure the pressure drop across the majority of the shellside baffle spaces, whereas the purpose of Transducer P9 was to measure the pressure drop between the inlet and outlet shellside nozzles. The transducer tapping points and location of the nozzle-to-nozzle pressure transducer are indicated in Figure 4.3.

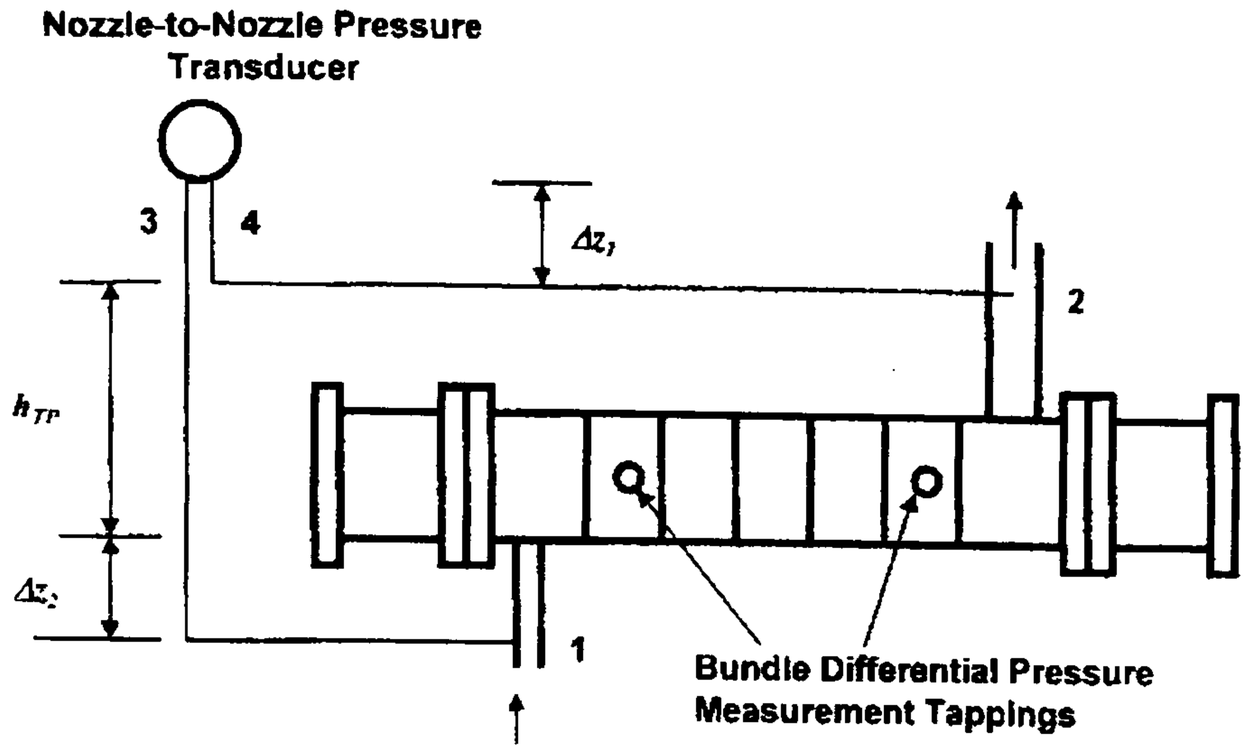

Figure 4.3 – Location of Differential Pressure Transducers

For the nozzle-to-nozzle transducer the tapping points of the transducer lines were flush with the walls of the inlet and outlet nozzles. This means that the pressure drop measured by the transducer was the static pressure drop between the nozzles. This term includes:

- Irreversible losses due to friction
- Accelerational change due to phase change
- Gravitational head due to the change in elevation across the pressure connections Allowance must be made for the fact that the shellside fluid has a different density from the liquid in the transmission lines from the nozzles to the transducer.
- Change in static pressure due to the fact the outlet nozzle is a larger diameter than the inlet nozzle.

In general the result of most interest is the irreversible losses as these must be used to assess the calculation of any shellside model. The static pressure drop between points 1 and 2 on Figure 4.3 is made up of the stagnation pressure drop and an additional dynamic pressure drop caused by the fact that the outlet nozzle is larger than the inlet. The static pressure drop between 1 and 2 is expressed in equation 4.10.

$$P_1 - P_2 = \Delta Po_{12} - \left(\rho_l u_1^2 - \rho_{TP2} u_2^2\right)/2 \tag{4.10}$$

The stagnation pressure drop term (ΔPo_{12}) in this equation includes the irreversible losses due to friction and the gravitational pressure drop between points 1 and 2. The pressure measured by the nozzle-to-nozzle transducer (transducer 1) is:

$$\Delta P_{Meas} = P_3 - P_4 \tag{4.11}$$

P_3 and P_4 differ from the static pressures at points 1 and 2 because they contain additional terms caused by the fact that the transducer is at a different height from the tappings. They can be related to P_1 and P_2 using the following equations.

$$P_3 = P_1 - (h_{TP} + \Delta z_1 + \Delta z_2)\rho_l g_n \tag{4.12}$$

$$P_4 = P_2 - \Delta z_1 \rho_l g_n \tag{4.13}$$

Therefore:

$$P_1 - P_2 = P_3 - P_4 + (h_{TP} + \Delta z_2)\rho_l g_n \tag{4.14}$$

From equations 4.14 and 4.10;

$$\Delta Po_{12} = P_3 - P_4 + (h_{TP} + \Delta z_2)\rho_l g_n + (\rho_l u_1^2 - \rho_{TP2} u_2^2)/2 \tag{4.15}$$

This equation 4.15 shows the stagnation pressure drop between tapping points 1 and 2. However to produce the value of the pressure drop between shellside nozzles it is first necessary to subtract the gravity terms that exist in equation 4.14 due to the fact that there is a height of tube between the tapping point and the shell. The resultant equation which is ready for comparison with the shellside prediction models is equation 4.16.

$$\Delta Po_{12} = P_3 - P_4 + h_{TP}\rho_l g_n - (h_{TP} - D_s)\rho_{TP2} g_n + (\rho_l u_1^2 - \rho_{TP2} u_2^2)/2 \tag{4.16}$$

To produce this result the two-phase density ρ_{TP} was calculated from equation 4.17 using the Zivi void fraction (Zivi, 1964) at the outlet nozzle from equation 4.18.

$$\rho_{TP} = \rho_l(1 - \varepsilon_g) + \rho_g \varepsilon_g \tag{4.17}$$

$$\varepsilon_g = \frac{1}{\left[1 + \left(\frac{1-x}{x}\right)\left(\frac{\rho_g}{\rho_l}\right)^{2/3}\right]} \tag{4.18}$$

4.3 – Uncertainties in Test Data

4.3.1 – Introduction

A detailed account of the procedure used to calculate the uncertainty in the measured and calculated experiemtal data is given in Appendix A. Also given in the appendix are the standard uncertainties for each measured and calculated data point throughout the series of

tests. The purpose of this section is to present a summary of the outcomes of the uncertainty analysis. The uncertainties presented are the combined expanded uncertainties (this includes both measurement and instrument uncertainties) expressed as a percentage of the measured data point. The 'expanded uncertainty' value describes the range within which 95.4% of new data would fall if the measurement was repeated at the same conditions.

4.3.2 – Uncertainty in measured parameters

The locations of the majority of the principal instrumentation and the measurements used for data analysis are presented in Figure 4.1 (F1, F9, PRT3, P9, P1 and P8). The steam condensate weight and collection time are also important parameters as they were used to calculate the steam heat load (Q_{Steam}). Table 4.1 presents the range of expanded uncertainties for the measured parameters for Tests 1, 2 and 3 (details of the experimental tests are contained in Chapter 5).

	Range of expanded uncertainty (%)		
Measurement	**Test 1**	**Test 2**	**Test 3**
R134a feed flowrate (F1)	3-6%	3-6%	3-6%
R134a recirc. flow (F9)	2-15%	1-7%	1-9%
Condensate weight	<0.05%	<0.05%	<0.05%
Collection time	<2.5%	<2%	1-2.5%
Shellside outlet temp (PRT3)	<0.3%	<0.25%	<0.25%
Nozzle-to-nozzle Δp (P9)	<20% (more than 70% of data)	<10%	<10% (more than 85% of data)
Steam outlet pressure (P1)	2-6%	2-6%	2-5%
Shellside bundle Δp (P8)	<20% (more than 70% of data)	<15%	<20% (more than 80% of data)

Table 4.1 – Range of expanded uncertainties in Experimental test measurements

The percentage expanded uncertainties displayed in Table 4.1 were calculated using equation 4.19 which converts the expanded uncertainty from the units of measurement (calculated using the method outlined in Appendix A) to a percentage by relating it to the associated measured data point.

$$u_{\exp(\%)} = \frac{u_{\exp(i)}}{y_{(i)}} \times 100\% \qquad (4.19)$$

$u_{\exp(i)}$ is the calculated expanded uncertainty in the measured units for a data point (i) and $y_{(i)}$ is the magnitude in the measured units of the data point (i). For the pressure drop results for P8 and P9 the range of percentage expanded uncertainties refers to the range within which the majority of the data lie and not the maximum value of the percentage

uncertainty. This distinction was required as there is a particularly large increase in the value of the percentage expanded uncertainty (from equation 4.19) as the measured pressure drop approaches zero. In reality the magnitude of the uncertainty in the units of pressure drop is very small (generally < 0.001 bar). A full list of the standard uncertainties for each data point is provided in Appendix A. Also given in the Appendix are plots of the important parameters extracted from the measured data complete with error bars of the expanded uncertainties. It can be seen from subsequent Chapters of the thesis (particularly Chapter 6) that the uncertainties in the measured values of parameters such as flow rate, temperature and pressure drop are very small in comparison to the deviation between measured values and those predicted by commercial design models (average predicted value of P8 pressure drop deviates from the measured value by around 140%). As a result, the measurements can be considered sufficiently accurate for the objective of assessing current methods by comparison of the experimental data with predicted values.

4.3.3 – Uncertainty in calculated values

Table 4.2 displays the range of the percentage expanded uncertainties for parameters calculated from the measured values referred to in Table 4.1. The parameters in Table 4.2 are the steam saturation temperature, the steam heat load, the shellside outlet vapour quality, the shellside mass flux and the boiling heat transfer coefficient. Full details of the calculation of these uncertainties along with lists of the standard uncertainties and plots containing the expanded uncertainties are given in Appendix A.

	Range of expanded uncertainty (%)		
Parameter	**Test 1**	**Test 2**	**Test 3**
Tsat	1-3.5%	1-3.5%	1-3%
Qsteam	1-2.5%	1-2%	1-2.5%
x (outlet)	1-7.5%	1-4%	1-5%
m	1-8%	1-5%	1-6%
boil coefficient	<20%	<31%	<25%

Table 4.2 – Range of expanded uncertainties in calculated parameters

The largest uncertainty in the calculated parameters is that of the boiling heat transfer coefficient α_{boil}. As can be seen the expanded uncertainty can be as high as 31% of the calculated value. In the calculation of the uncertainty in α_{boil} the percentage uncertainty in the prediction of the tube side coefficient α_{steam} was taken to be 20%. This value is considered by HTFS to be the maximum prediction uncertainty of the TASC method for tube side condensation (McNaught (HTFS), private communication). Full details of the tube side

condensation method used are detailed in HTFS Design Report 12 (Various Authors, 1988). The value of the boiling heat transfer coefficient α_{boil} is calculated using equation 4.8 and the value is affected mainly by the value of the overall coefficient U (calculated from equation 4.6).

In general the higher values of α_{boil} correspond to higher percentage uncertainties whereas uncertainties are much smaller at the lower magnitudes of the coefficient. The high value of α_{boil} corresponds with a high value of U which in turn corresponds with a low temperature difference. This low temperature difference can cause larger uncertainties as the calculated value of U becomes more sensitive to uncertainties in the predicted steam saturation temperature T_{sat} . The maximum uncertainties in Test 2 are higher than those in Tests 1 and 3 as the maximum value of the measured boiling heat transfer coefficient was larger for this series of tests. As with the measured pressure drop, the uncertainty in the measured boiling heat transfer coefficient is small compared with the accuracy of prediction models (average prediction deviates from the measured value by around 150%) and as such the measured values are sufficiently accurate for the purpose of testing the prediction methods of commercial design software.

CHAPTER 5 – Experimental Tests

5.1 – Introduction

From the review of the available open literature in Chapter 2 it was clear that to assess existing models and produce a new improved model it would be necessary to produce some experimental data for a boiling shellside two-phase flow on a real industrial heat exchanger geometry. Throughout the project experimental data were collected from the NEL boiling & condensing facility and a full description of the facility and the procedure for obtaining results is given in Chapters 3 & 4. The test evaporator geometry could most easily be altered by changing the baffle orientation (horizontal/vertical) which causes a change in the flow direction of the boiling flow from side-to-side flow to up-and-down flow. Other possible geometric changes were also explored (more detail on specific test geometries and location of instrumentation is given in Appendix B). The test fluid used throughout was refrigerant R-134a which has similar physical properties to light hydrocarbons that may be used in industrial applications. A series of experimental tests were arranged with the test evaporator to produce sets of data that could be used for comparison with existing models and for creating an improved shellside model.

5.2 – Test Background

The following section contains the experimental results collected throughout the duration of the project. In addition it contains previous test data collected from the experimental facility (Chu et al, 1998; McNaught et al, 1999, 2000) which was collected as part of a HTFS (Heat Transfer and Fluid Flow Service) research programme which is not available in the open literature.

5.2.1 – Test Details

The experimental tests were designed to replicate the typical operating range of a shellside evaporator. The focus was also on assessing the implications of phase separation for evaporators where the shellside flowrate was reasonably low; as can be the case in a horizontal thermosyphon reboiler. These reboilers usually operate with a recirculation ratio between 3 and 20 (Whalley, 1977). The recirculation ratios for all the experimental tests are given alongside other ranges and operating conditions in Table 5.1. Geometric details and additional information about the test facility are given in Chapter 3. Tests that were carried out during the current project have been assigned numbers (1, 2 and 3) whereas tests from the

previous research programme are identified by letters (A and B). Throughout all the tests the test fluid was Refrigerant R134-a (Tetraflouroethane).

	TEST A	TEST B	TEST 1	TEST 2	TEST 3
	Chu et al	McNaught et al			
Heat Load (kW)	70-170	70-266	108-255	120-220	146-230
Mean Temp Difference (K)	4-10	5.4-12.4	7.4-16.4	5.5-16.7	7.5-15
R-134A inlet pressure (bar)	6.9-8.6	6.7-8.7	5.8-9.3	5.6-8.13	6.43-7.39
Steam inlet pressure (bar)	0.045-0.074	0.038-0.09	0.041-0.101	0.038-0.094	0.048-0.087
R-134A mass flux (kg/m2s)	350-650	188-714	140-856	162-1023	108-504
Heat Flux (kW/m2)	12.5-30	16-45	19-44	24-37	26-37
Baffle pitch (mm)	156	156	156	156	260
Baffle orientation	Horizontal	Vertical	Horizontal	Vertical	Vertical
Sealing strips in bypass	No	No	Yes	Yes	No
Outlet vapour quality	0.059-0.65	0.07-0.52	0.11-0.68	0.09-0.5	0.11-0.56
Recirculation ratio	0.54-16	0.92-13.29	0.47-8.1	1-10.1	0.79-8.1

Table 5.1 – Experimental Test Details and Operating Ranges

Tests A and B were used as reference cases for assessing the effect of sealing strips in the crossflow bypass lane in Tests 1 and 2. In addition the purpose of Tests 1 and 2 was to produce data over a wider range of mass fluxes and to gain more data for further understanding the effect of baffle orientation. The purpose of Test 3 was to assess the effect of increased baffle pitch. With this geometry the shellside pressure drop is likely to be smaller and closer to that which may exist in a horizontal thermosyphon reboiler.

The mass fluxes in Table 5.1 above are calculated using the crossflow area described in section 5.3. One of the principal geometric variables in the tests is the baffle orientation. The influence of the baffle orientation was indicated in Figure 3.3. With the horizontal baffle the process fluid enters the evaporator and travels vertically upwards and downwards between the shellside baffles to the exit. With the vertical baffle orientation the principal flow direction is horizontally from side to side. Another geometric variable is the inclusion of sealing strips in the crossflow bypass stream. The purpose of the sealing strips is to force liquid that may be bypassing the tube bundle back towards the tubes in order to increase the flow of liquid in the crossflow path, where most of the heat transfer occurs. A cross sectional drawing of the tube bundle with and without sealing strips was shown in Figure 3.4.

Further information on the test geometries used and details such as the dimensions of sealing strips and locations of instrumentation are given in Appendix B.

5.3 – Test Results

The measurement and analysis procedure for the experimental test programme was outlined in Chapters 3 and 4. In this section the results from each set of experimental tests are presented. Values of the uncertainty in the measured parameters in Figures 5.2 – 5.10 are given in Appendix A.

5.3.1 – Heat Transfer

The analysis procedure for calculating the shellside 'boiling heat transfer coefficient' (α_{boil}) described in Chapter 4 was used to assess the heat transfer performance of the evaporator for the various tests. The data is represented in the form of plots of the value of α_{boil} against the other process variables; the total mass flux of the process fluid through the evaporator ($\dot{m}$) and the process fluid vapour outlet quality (x). The mass flux is calculated by taking the total flowrate of the fluid on the shellside and dividing by the shellside crossflow area (including the crossflow bypass area), which is defined as the total area between the tubes over the length of one shellside baffle space (Figure 5.1).

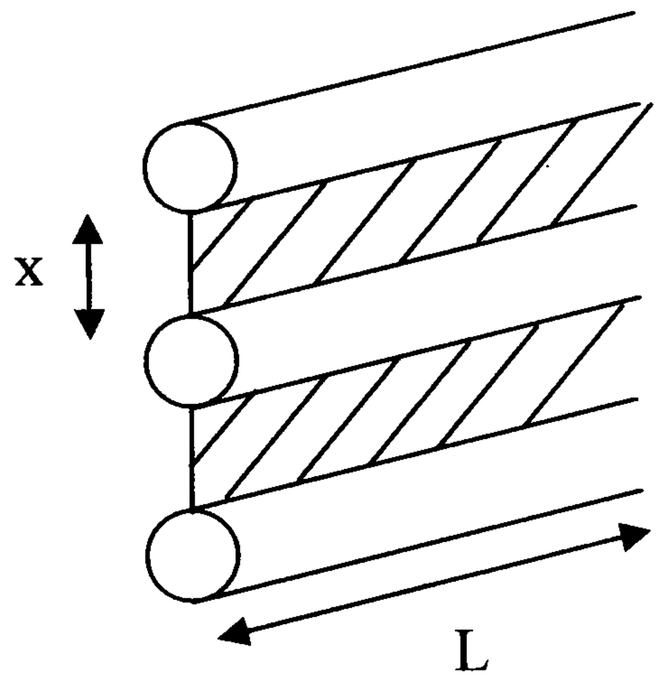

Where L is the length between shellside baffles

Crossflow area = (Number of tube gaps) L x + Bypass area

Figure 5.1 – Crossflow Area used to define Mass Flux ($\dot{m}$)

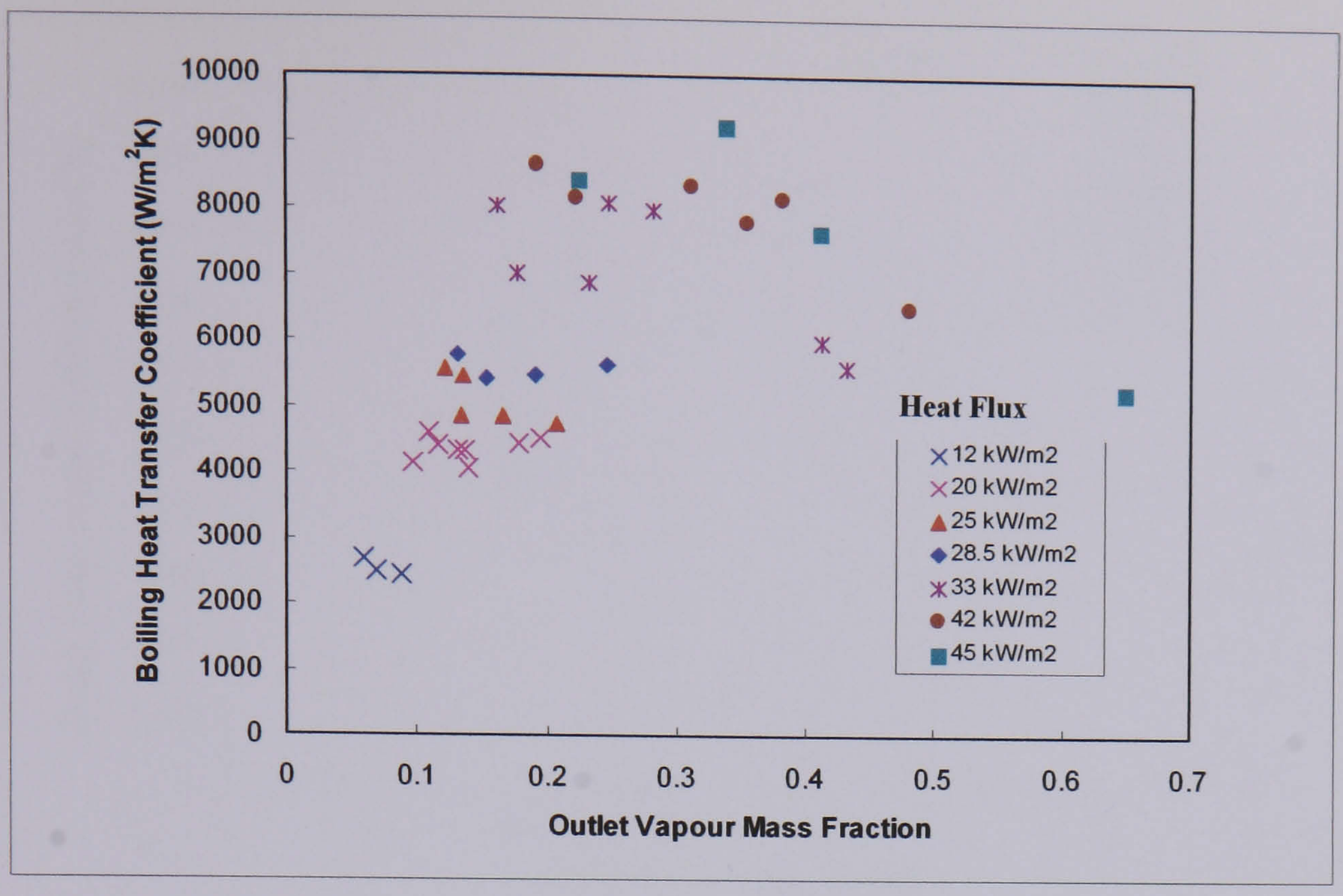

Figure 5.2(a) – Plot of α_{boil} against x for Test A (Chu et al, 1998) – (horizontal baffle)

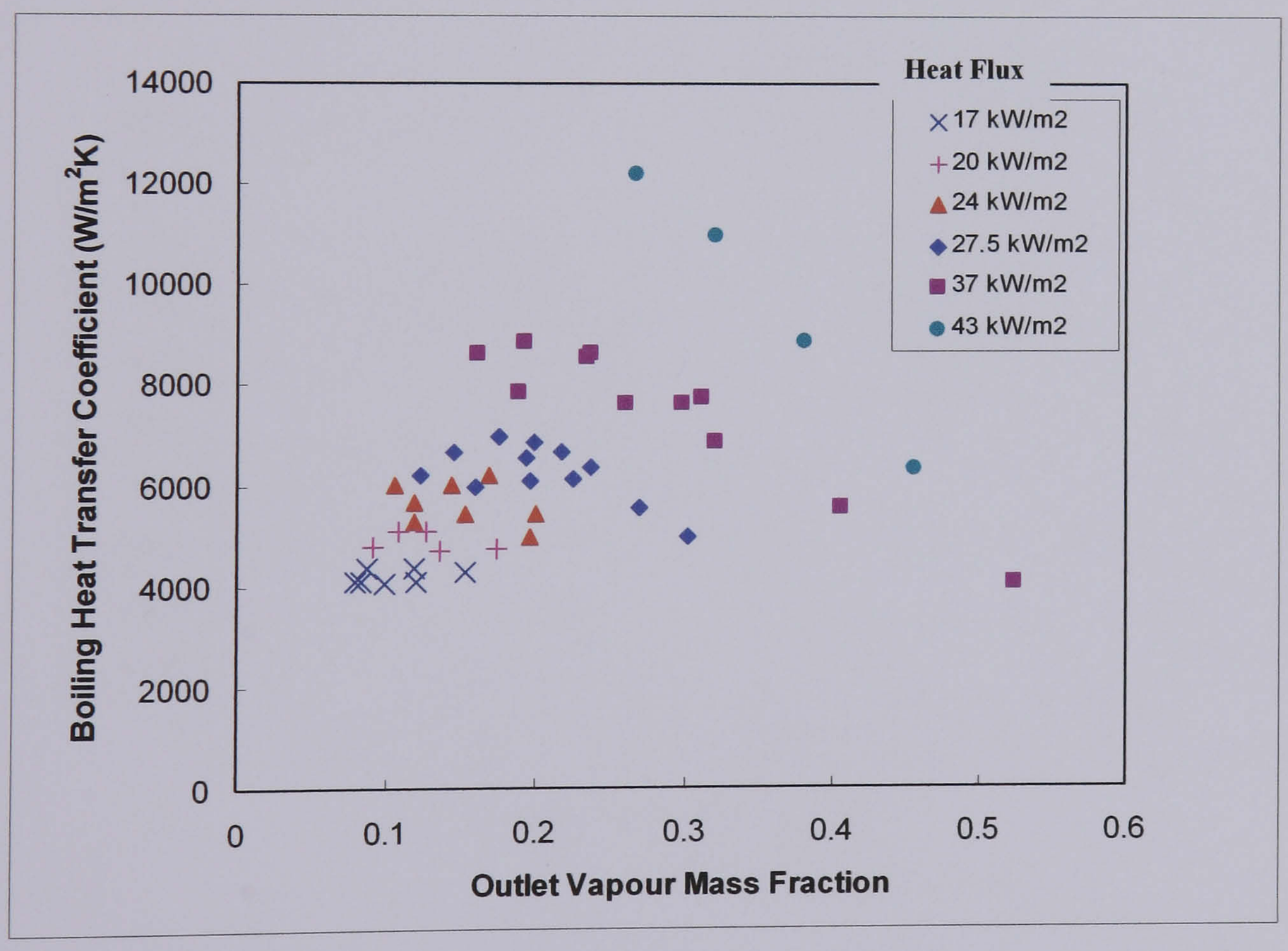

Figure 5.2(b) – Plot of α_{boil} against x for Test B (McNaught et al, 1999, 2000) – (vertical baffle)

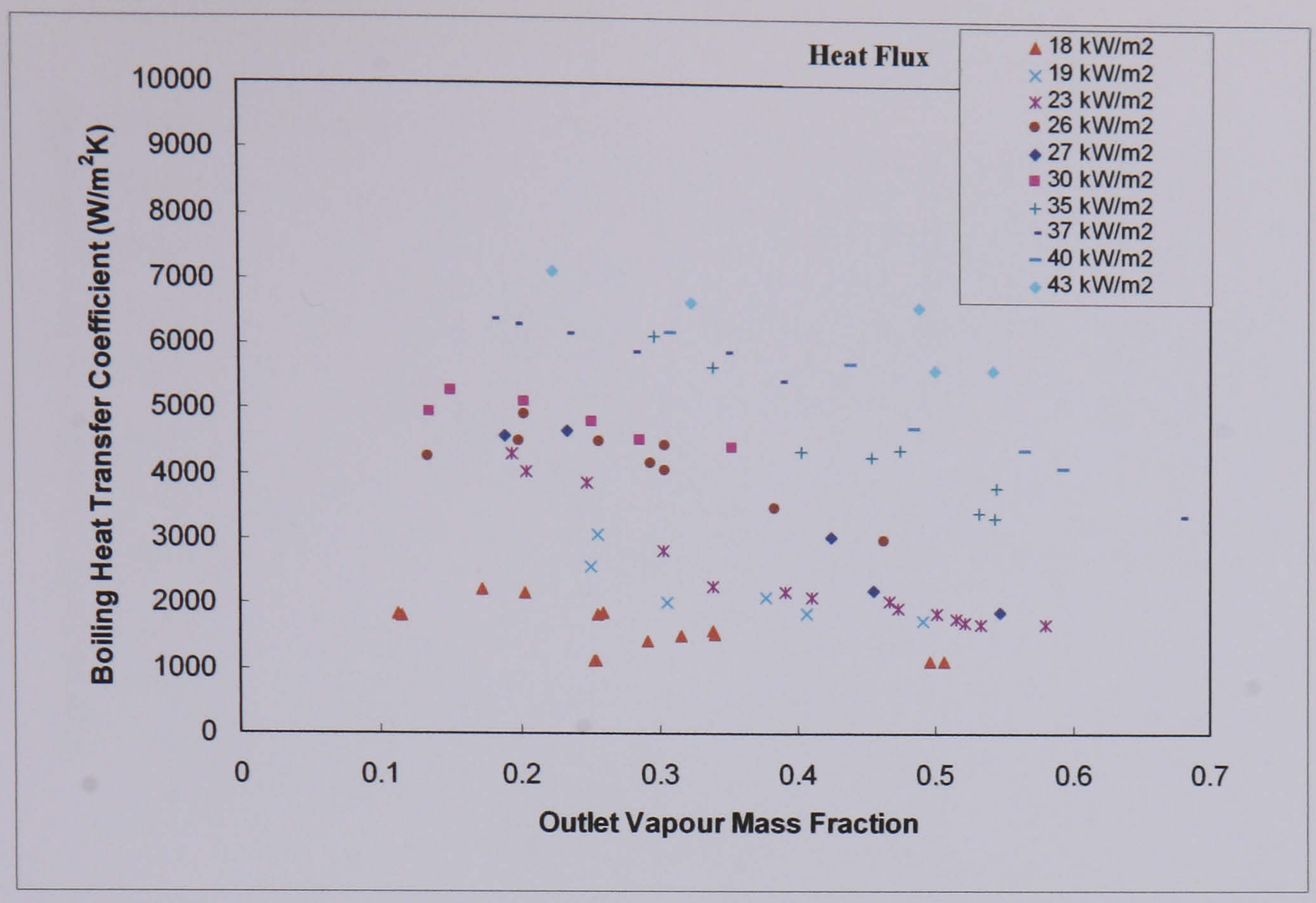

Figure 5.2(c) – Plot of α_{boil} against x for Test 1 – (horizontal baffle / sealing strips)

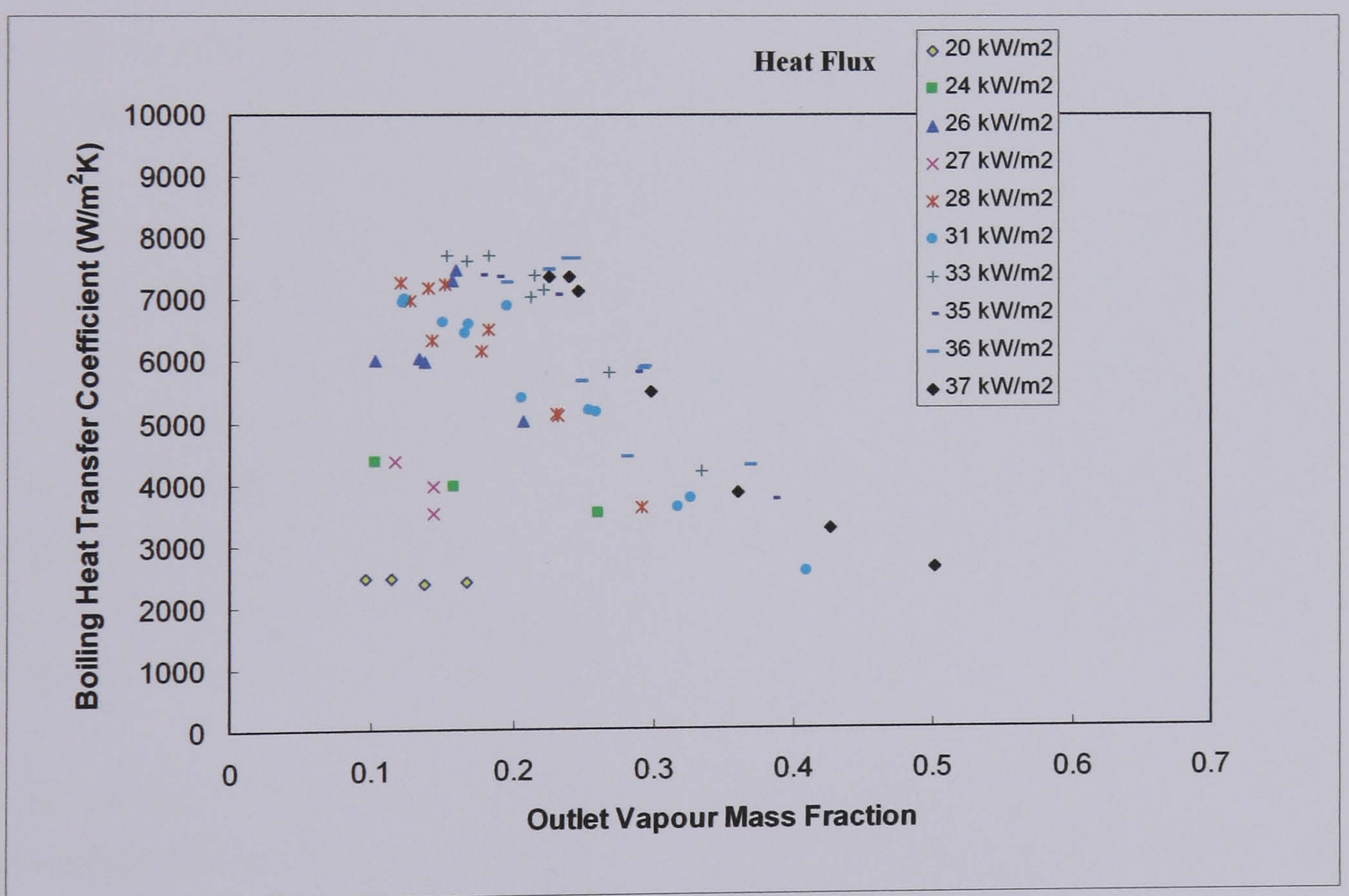

Figure 5.2(d) – Plot of α_{boil} against x for Test 2 – (vertical baffle / sealing strips)

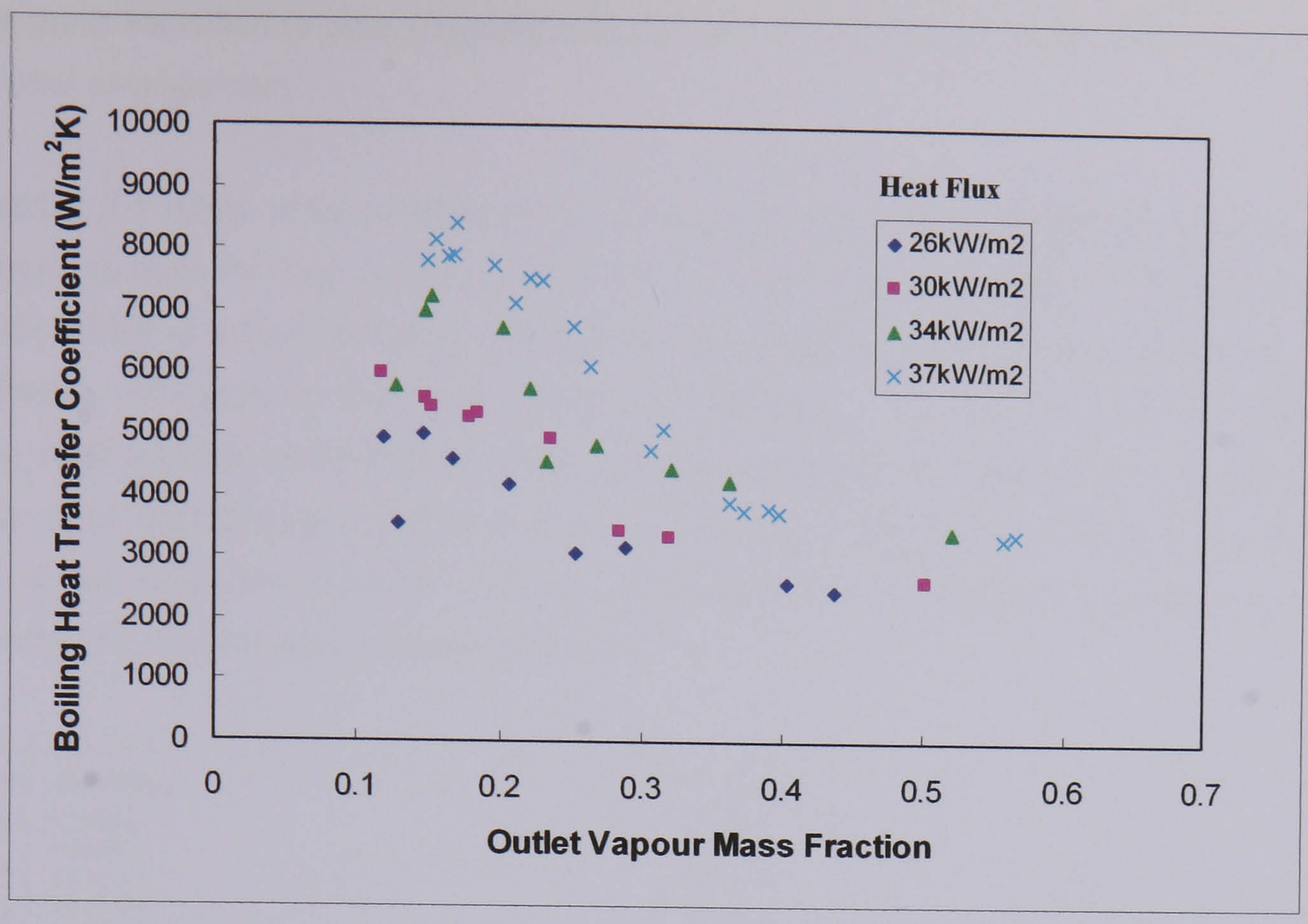

Figure 5.2(e) – Plot of α_{boil} against x for Test 3 – (vertical baffle / increased pitch)

For any given heat flux in Figure 5.2(a-e) there are points over a range of qualities. The different vapour qualities are produced by varying the mass flux of the refrigerant to the evaporator. The plots in Figure 5.2 suggest that the value of the boiling heat transfer coefficient begins to drop as the value of the outlet quality increases, particularly for the tests at the higher heat fluxes. At a constant heat flux it is reasonable to expect that the value of α_{boil} would remain reasonably constant over the full range of qualities if the dominating heat transfer process was nucleate boiling, since the coefficient due to nucleate boiling is primarily a function of the heat flux. The drop in α_{boil} would suggest that for the higher quality tests there are tubes in the tube bundle which have become surrounded by vapour contributing very little to the overall heat transfer process. The resultant loss of a number of tubes through vapour blanketing would lead to a drop in the measured value of α_{boil}.

From the comparison of Figures 5.2(a) – (e) it is evident that the orientation of the shellside baffles has an influence on the deterioration of the shellside heat transfer coefficient. The only variation in the evaporator geometry between Tests A (Figure 5.2(a)) and B (5.2(b)) was the orientation of the shellside baffles (horizontal and vertical respectively). There appears to be a sharper decline in the heat transfer coefficient as the vapour quality increases with the vertical baffle cut arrangement. This trend is also apparent in the comparison between 5.2(c) and 5.2(d) which represent test data for identical shellside geometries with horizontal and vertical baffle cuts respectively. It is therefore likely that with the vertical baffle cut arrangement there

is a sharper transition to poor evaporator performance at lower vapour qualities than with the horizontal arrangement.

To assess the effect of the sealing strips in the bypass lane, a comparison has to be made between the data for Test A (5.2(a)) and Test 1 (5.2(c)) and a similar comparison between Test B (5.2(b)) and Test 2 (5.2(c)). On examination of the figures there does not appear to be an obvious influence on the heat transfer performance. The magnitude of the measured boiling heat transfer coefficient is possibly greater without the sealing strips as the values appear to be slightly higher in Test A than in Test 1 and Test B than in Test 2. However the trend of the heat transfer data and the deterioration in heat transfer performance seem unaffected by the inclusion of sealing strips.

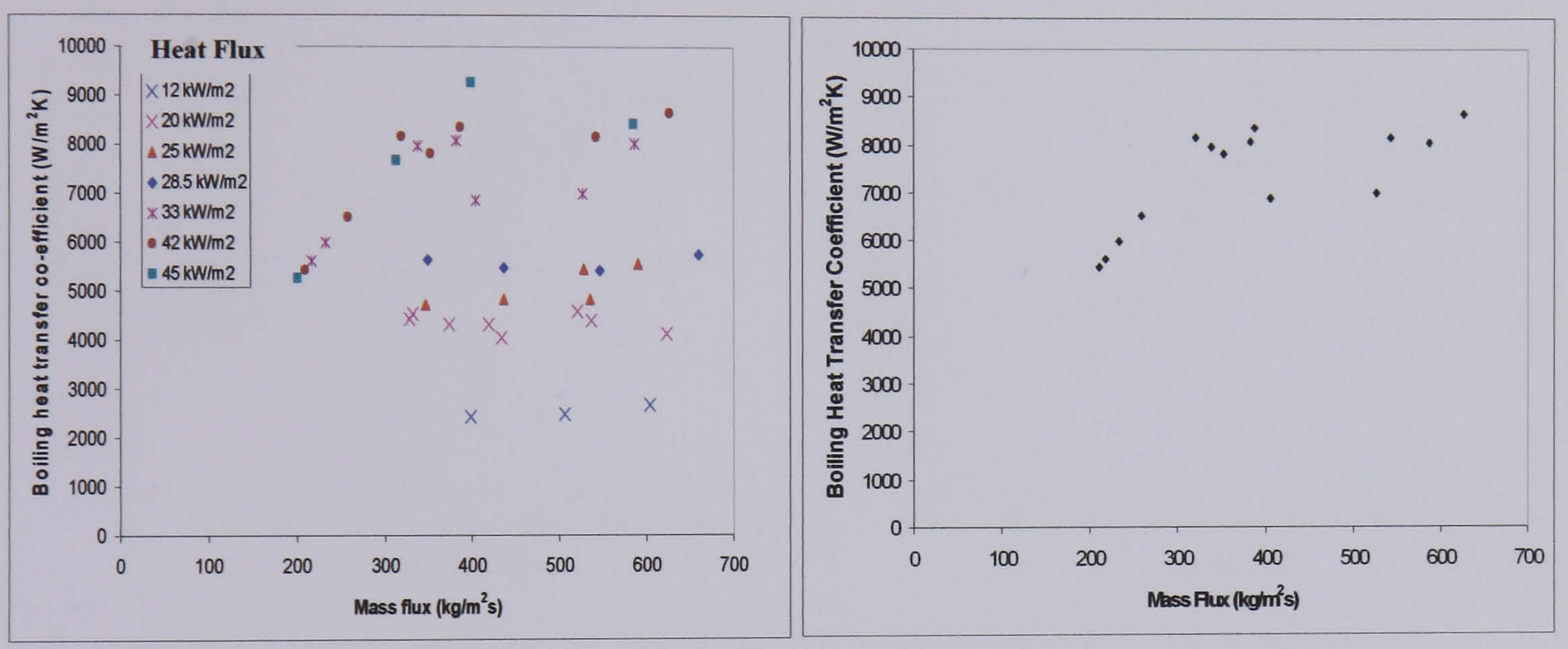

Figure 5.3(a) – Plots of α_{boil} against Mass Flux for Test A (Chu et al, 1998) – (effect of mass flux)

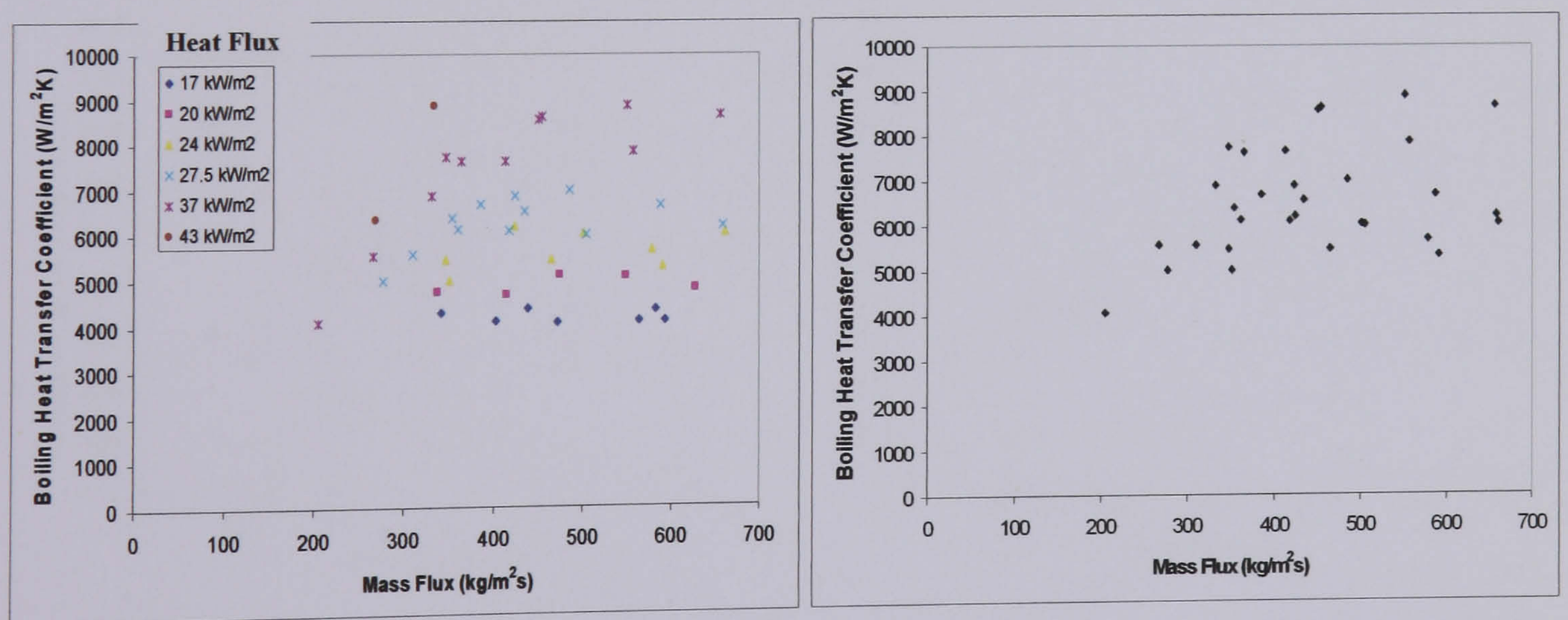

Figure 5.3(b) – Plots of α_{boil} against Mass Flux for Test B (McNaught et al, 1999, 2000) – (effect of mass flux)

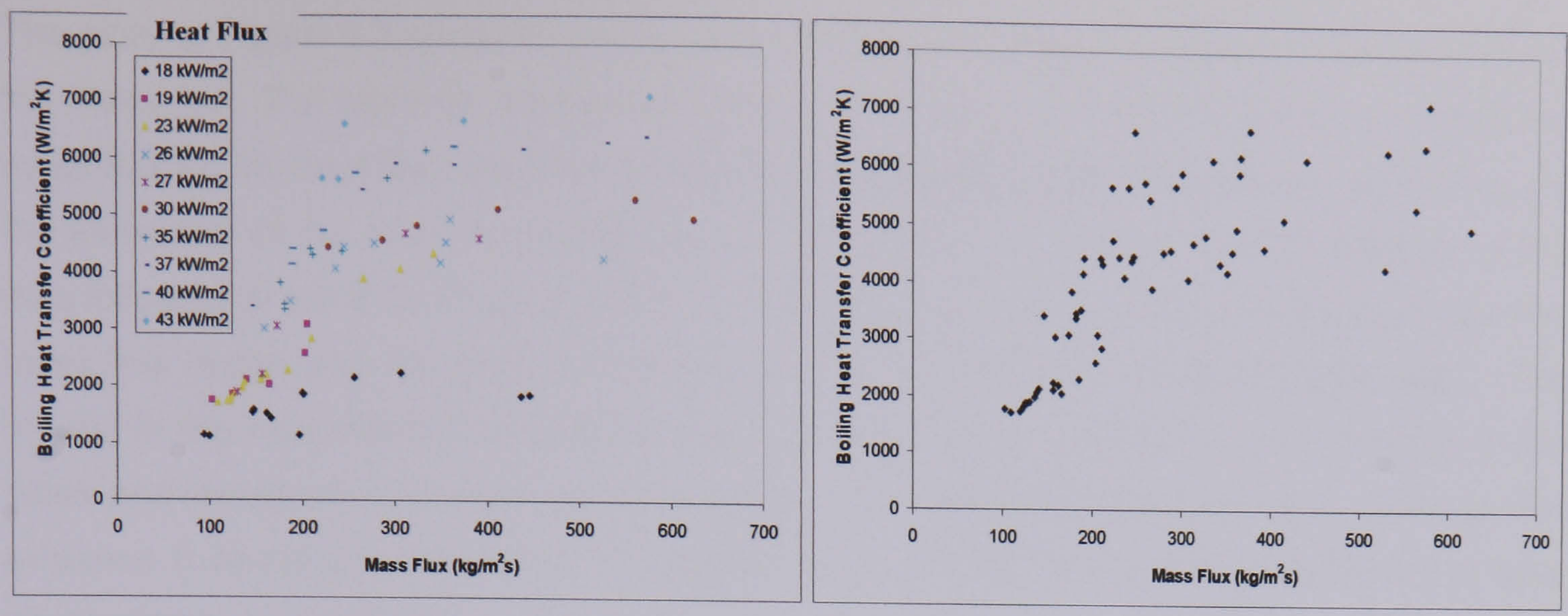

Figure 5.3(c) – Plots of α_{boil} against Mass Flux for Test 1 – (effect of mass flux)

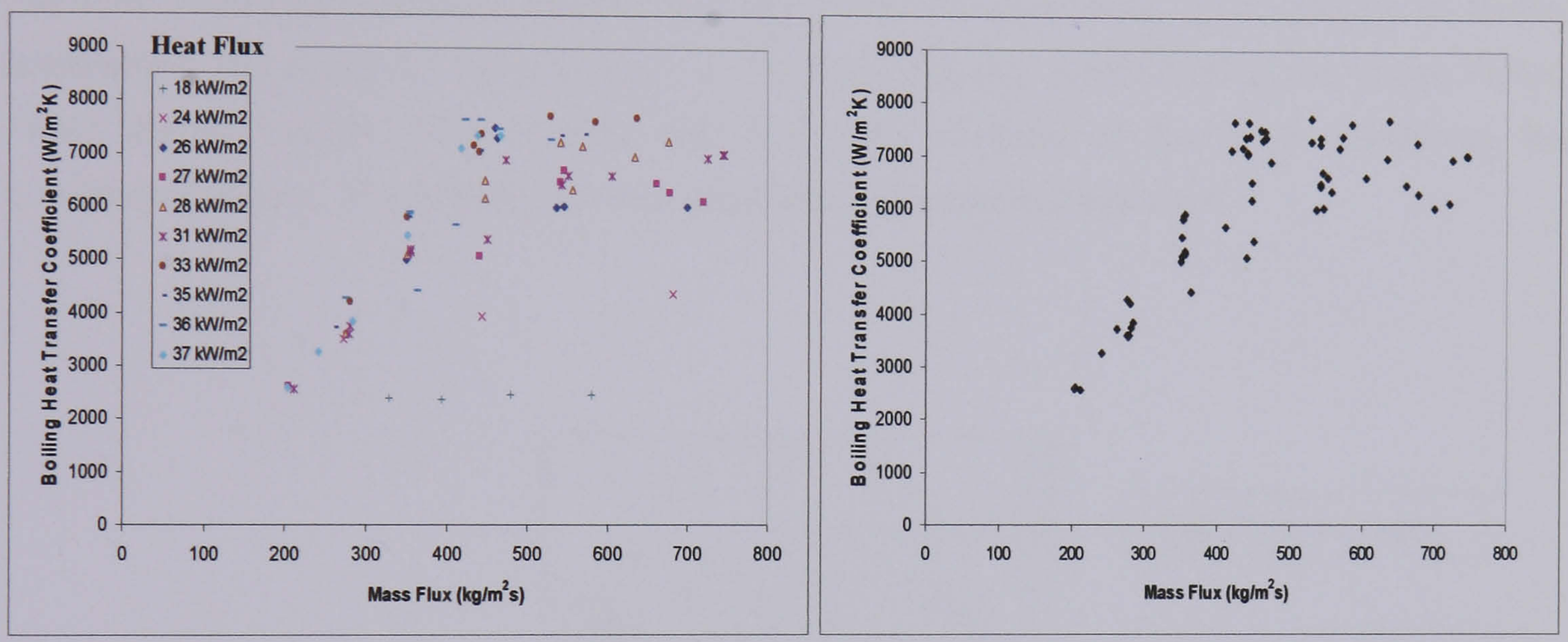

Figure 5.3(d) – Plots of α_{boil} against Mass Flux for Test 2 – (effect of mass flux)

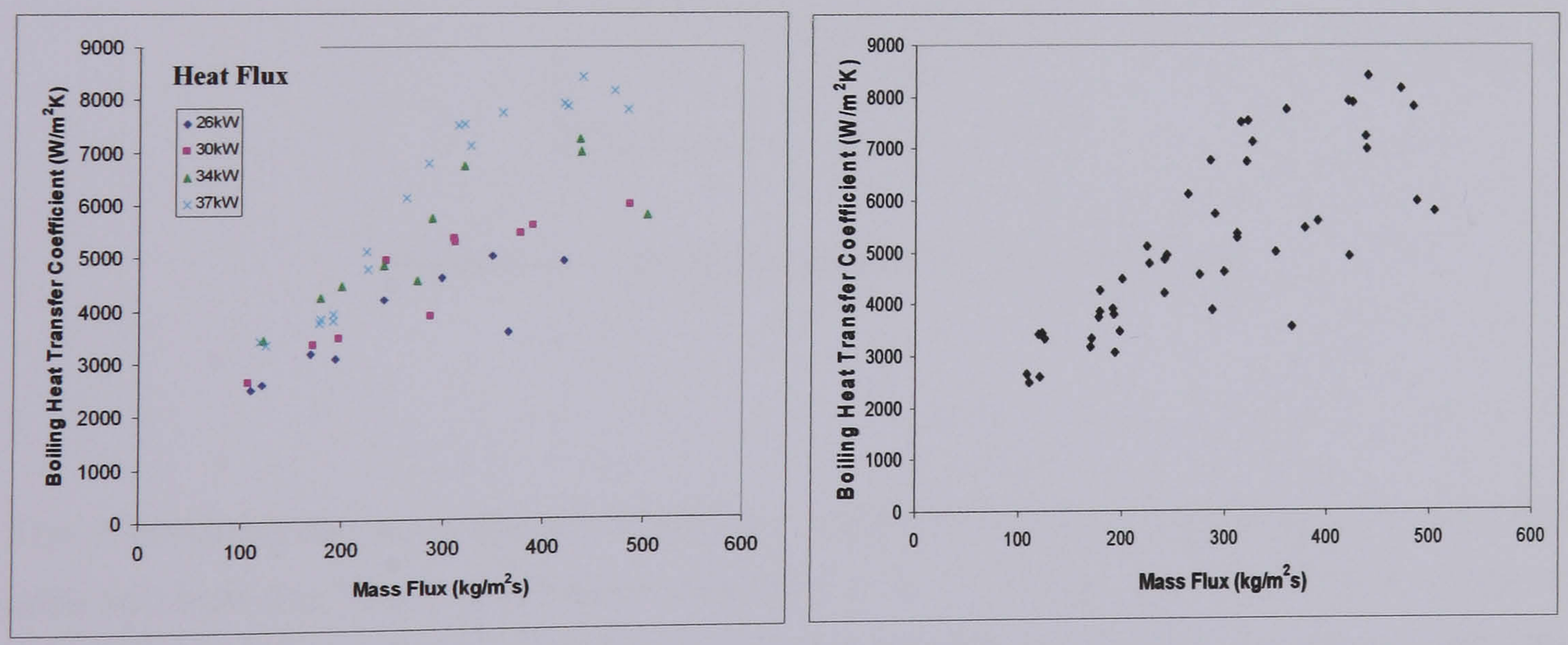

Figure 5.3(e) – Plots of α_{boil} against Mass Flux for Test 3 – (effect of mass flux)

The plots in Figure 5.3 show the value of the boiling heat transfer coefficient plotted against the mass flux. The plots on the right in 5.3(a) – (e) show the coefficient plotted against the mass flux for the heat flux runs where there is an apparent deterioration in the value of α_{boil} at the lower end of the mass flux range. It can be seen that in Tests 1 to 3 the majority of the data follows this trend. In Tests A and B only the high heat flux runs were operating in this low mass flux range and the plots in these cases are of the higher heat flux data only. The decline in the heat transfer coefficient may be due to vapour blanketing around some of the tubes and would be a concern for the designer of a shell-and-tube evaporator since on this evidence it would be undesirable to operate an evaporator under these conditions of poor heat transfer performance.

For Test 3 additional instrumentation was added to the evaporator in an attempt to further understand the apparent deterioration in the heat transfer coefficient at low mass fluxes. Three thermocouples were inserted into the outlet of three of the tubes containing the condensing steam. The tubes that were used are illustrated in Figure 5.4.

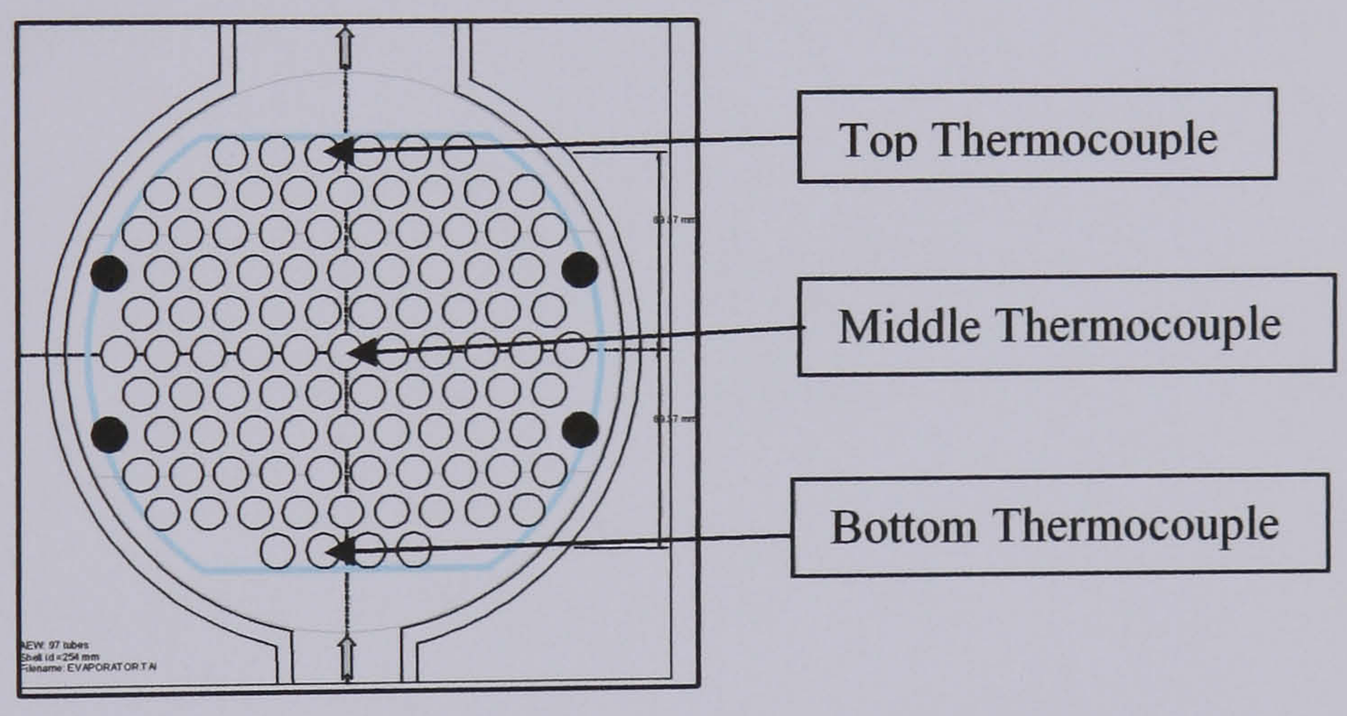

Figure 5.4 – Location of Additional Thermocouples

The thermocouples were placed in the top, middle and bottom tube rows and the results collected from the Test 3 runs were assessed. Figure 5.5 shows the relationship between the ratio of the measured temperature from each thermocouple and the steam saturation temperature at the corresponding measured tubeside outlet pressure.

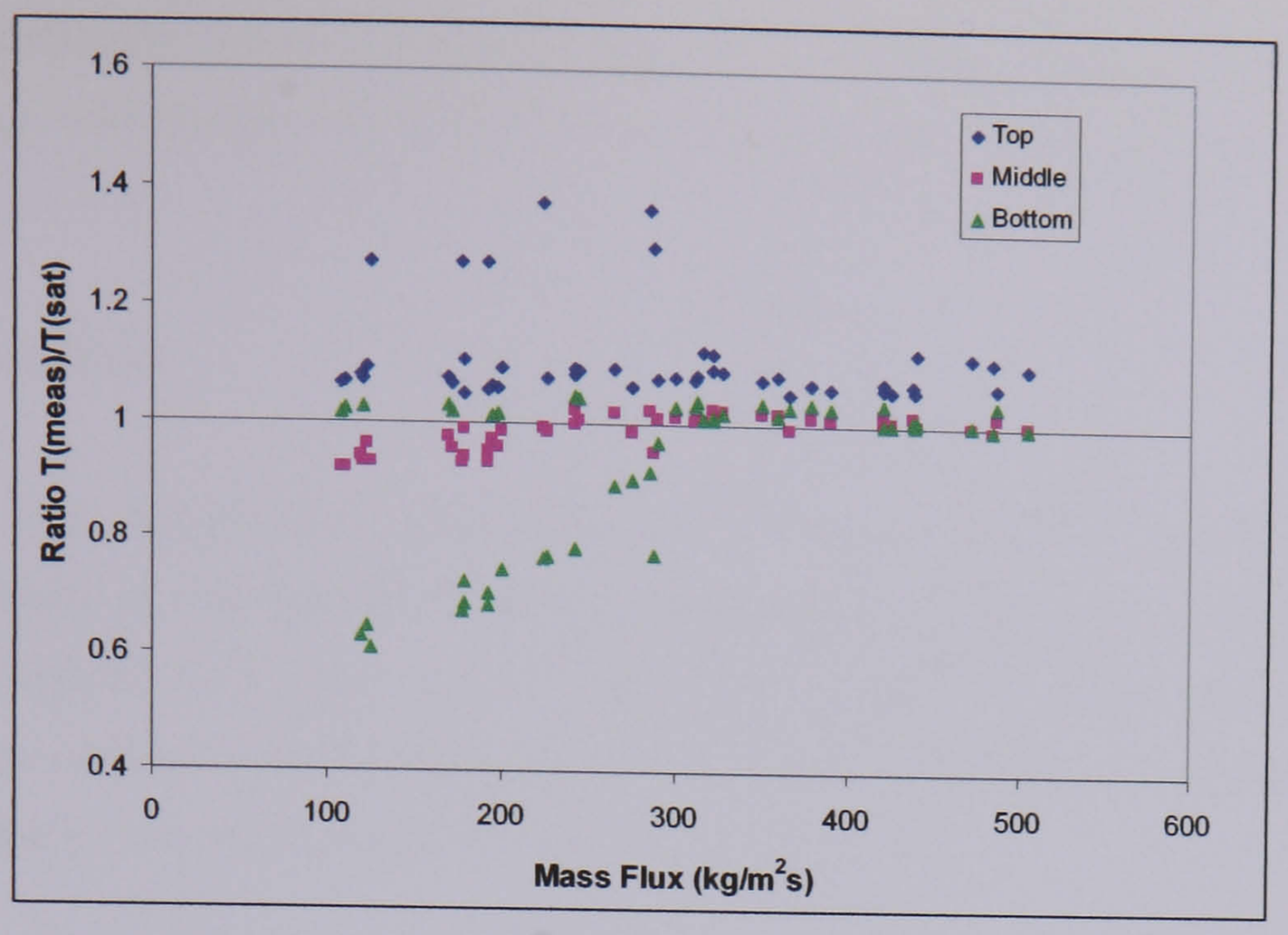

Figure 5.5 – Measured to Saturated Temperature Ratio (^{0}C) vs. Mass flux for tubeside thermocouples in Test 3

Ideally for all three tube rows the ratio should be close to unity, as in good operation the steam would be fully condensed in each tube. From Figure 5.5 it can be seen that at a mass flux around 300 kg/m^{2}s there is a transition, below which there is a drift in the ratio for the top and bottom tubeside thermocouples.

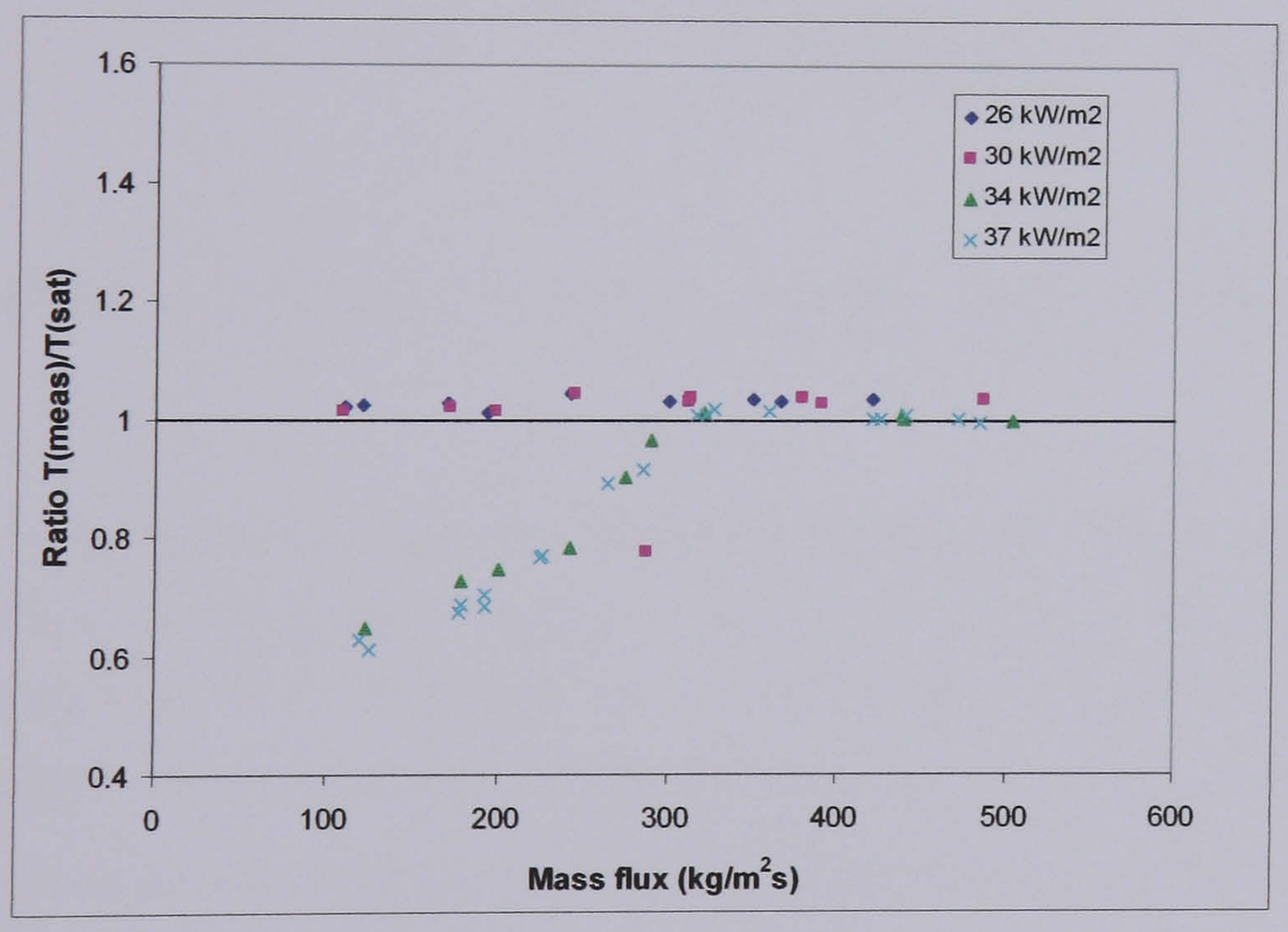

Figure 5.6 – Variation in bottom tube temperature at different heat fluxes

A closer examination of the data from the bottom thermocouple as presented in Figure 5.6 indicates that the drift in the tubeside temperature corresponds with the higher heat flux tests (34 and 37 kW/m^2). It was in these tests that the most significant deterioration in the overall shellside heat transfer coefficient was observed (Figure 5.2(e)); furthermore the transition in Figures 5.5 and 5.6 clearly corresponds with the mass flux at the deterioration in the Test 3

heat transfer coefficient shown in Figure 5.3(e). It is clear that whatever process is affecting the mean boiling heat transfer coefficient is also affecting the behaviour on the tubeside of the evaporator.

5.3.2 – Pressure Drop

The pressure drop across the evaporator was measured using two differential pressure transducers. Details of how the readings from these transducers were recorded and analysed are given in Chapter 4. In this section the results produced from the transducers are presented for two-phase boiling flows in each of the test conditions. A diagram showing the location of the two pressure transducers is given in Figure 5.7.

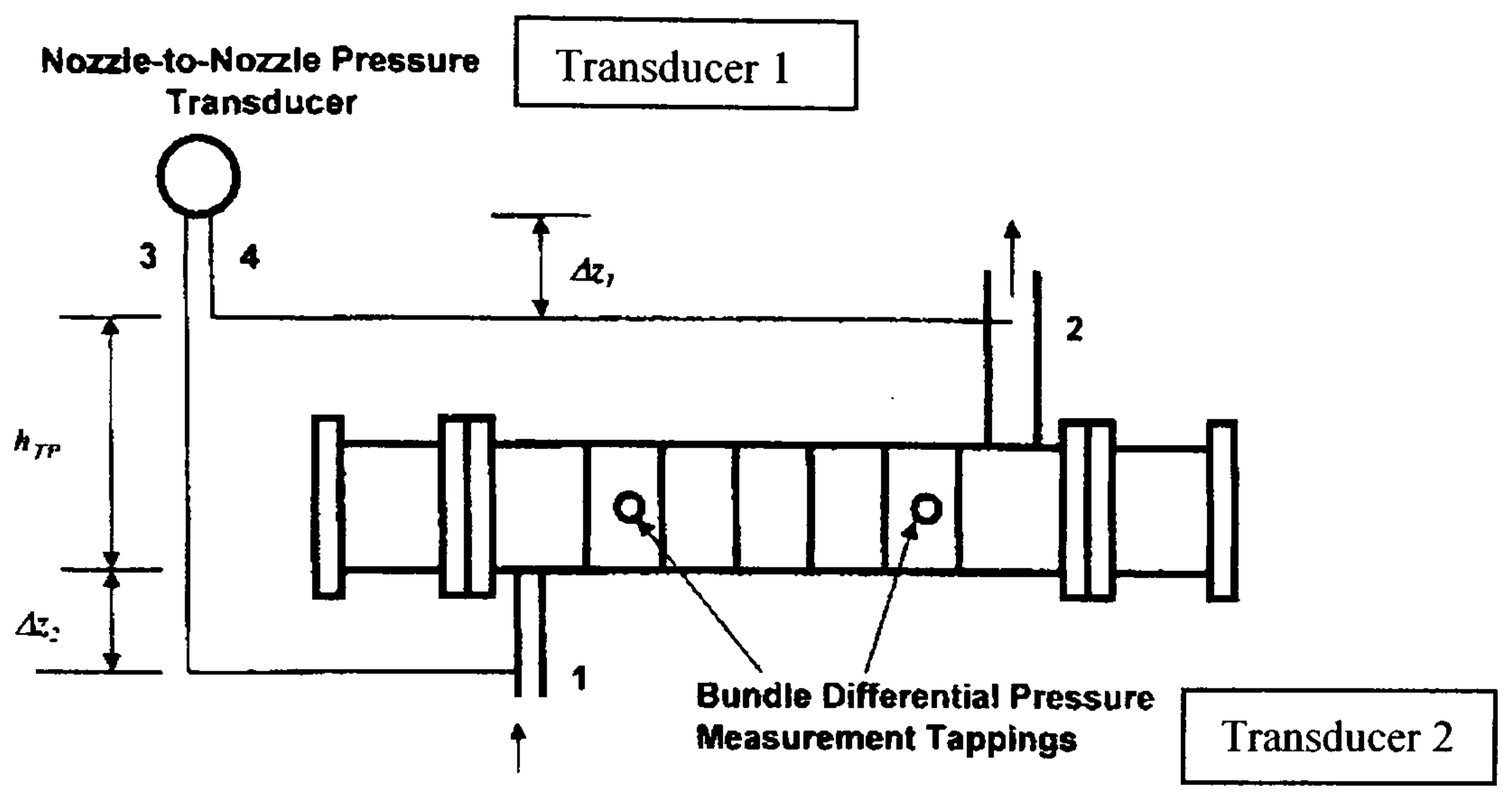

Figure 5.7 – Transducer Locations (Transducer 1 – Nozzles, Transducer 2-Shellside)

Figures 5.8(a) – (e) show the two-phase pressure drop for the various test runs for both transducers 1 and 2 plotted against the same mass flux as with the heat transfer plots. The plots give the data direct from the transducer measurements. The nozzle-to-nozzle pressure drop is represented by the Transducer 1 measurement ($\Delta p_{nozz} = p_4 - p_3$) and the pressure drop across the shellside baffle spaces is given by the reading of transducer 2 (P8).

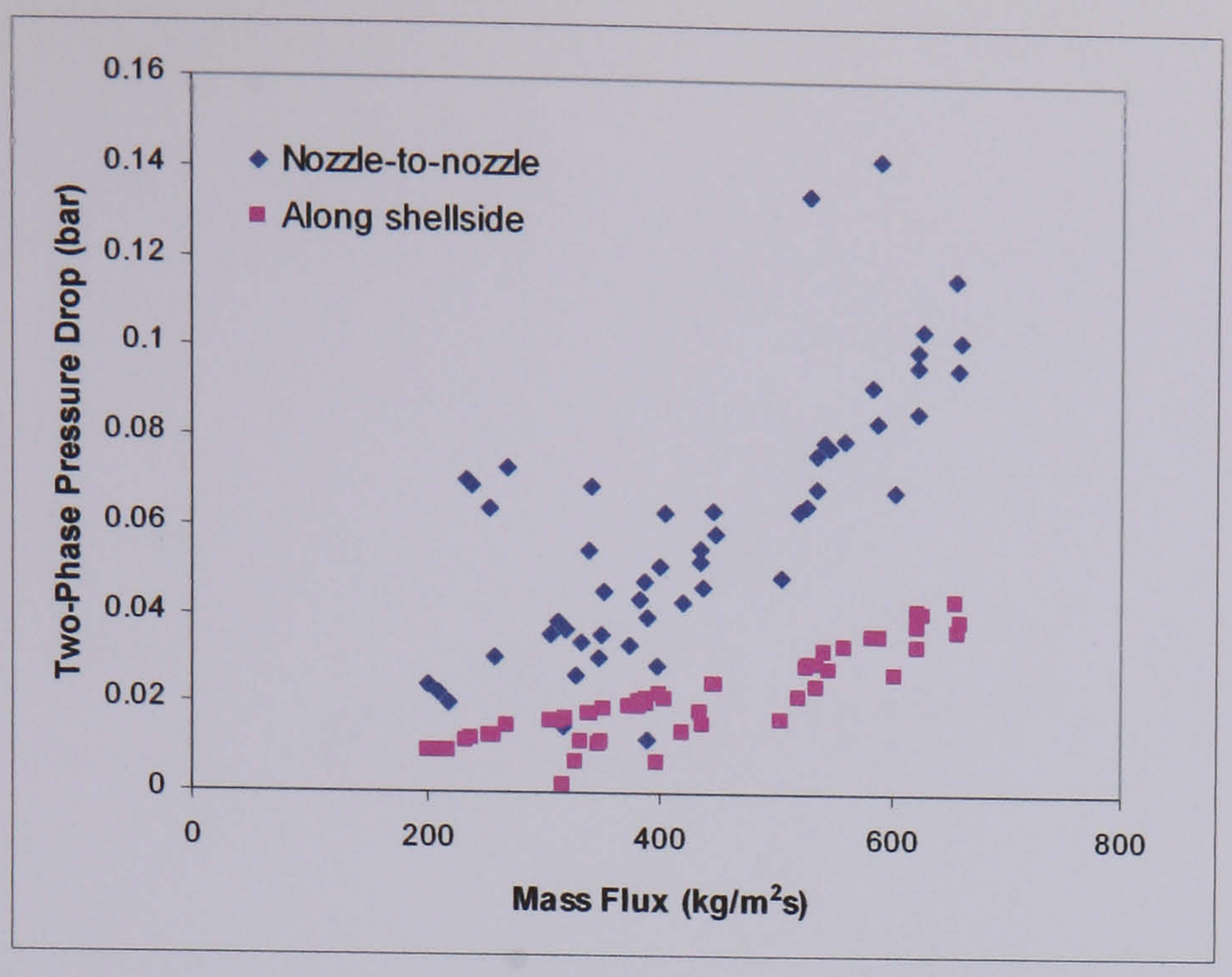

Figure 5.8(a) – Two-Phase Pressure Drop: Test A (Chu et al, 1998)

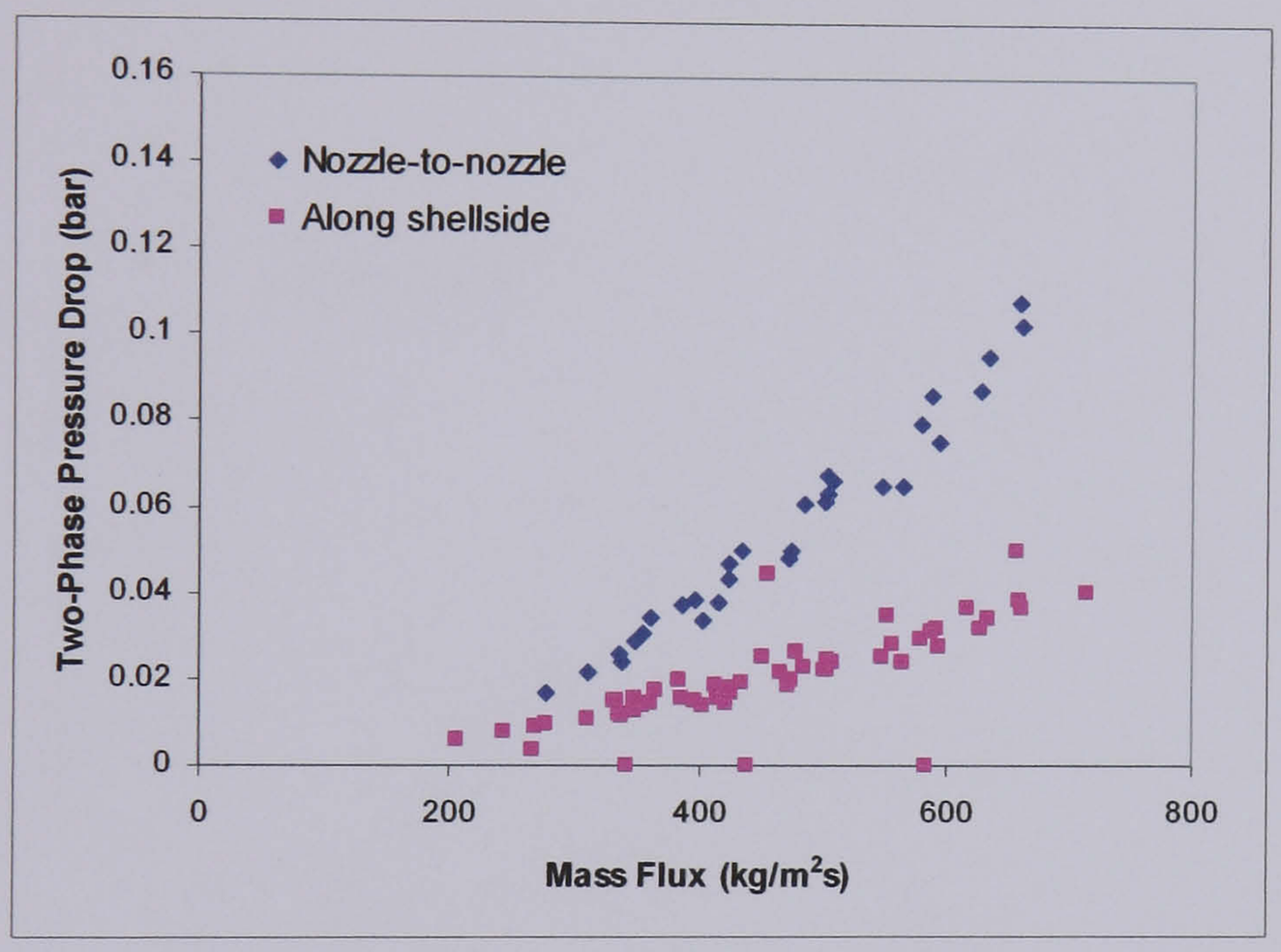

Figure 5.8(b) – Two-Phase Pressure Drop: Test B (McNaught et al 1999, 2000)

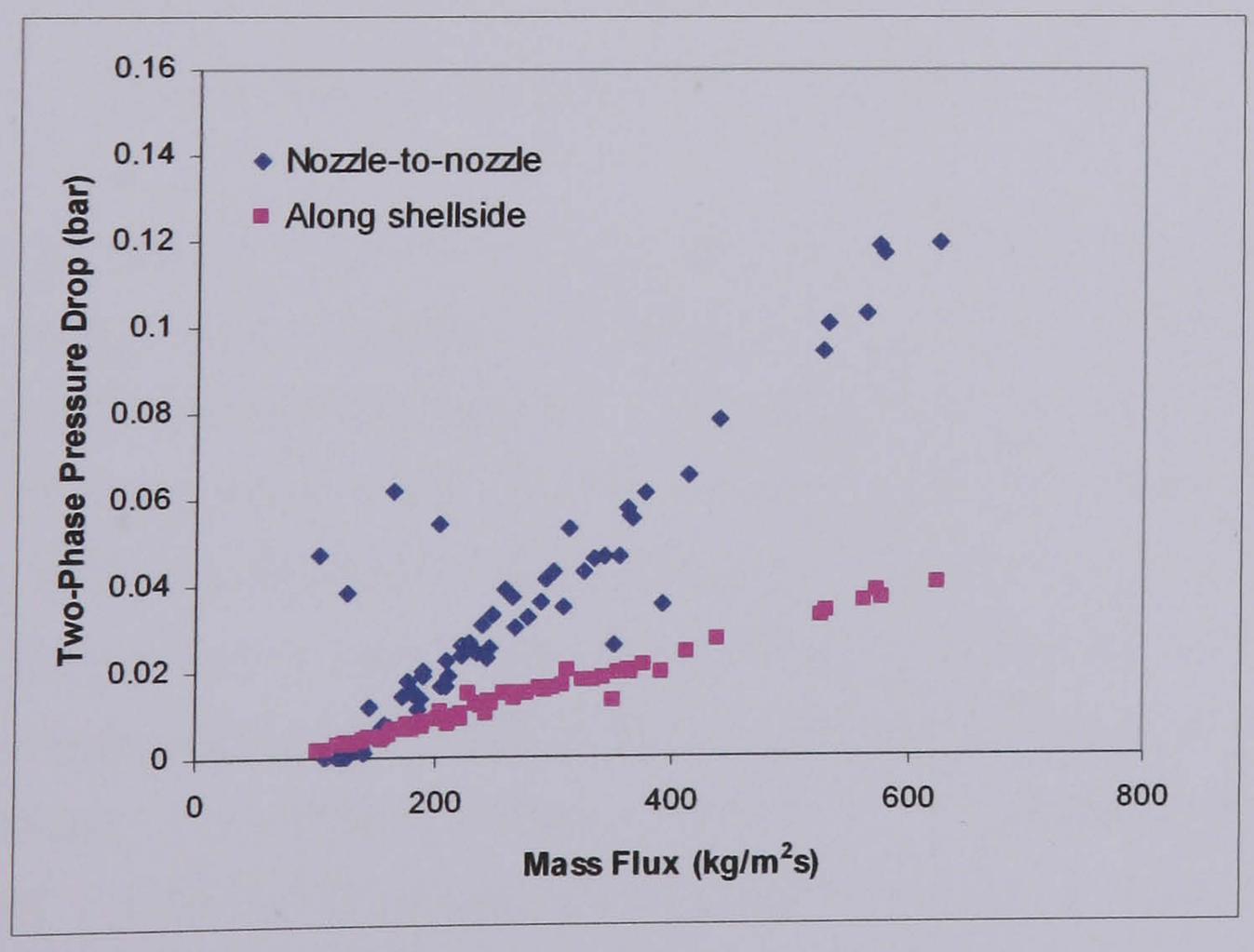

Figure 5.8(c) – Two-Phase Pressure Drop: Test 1

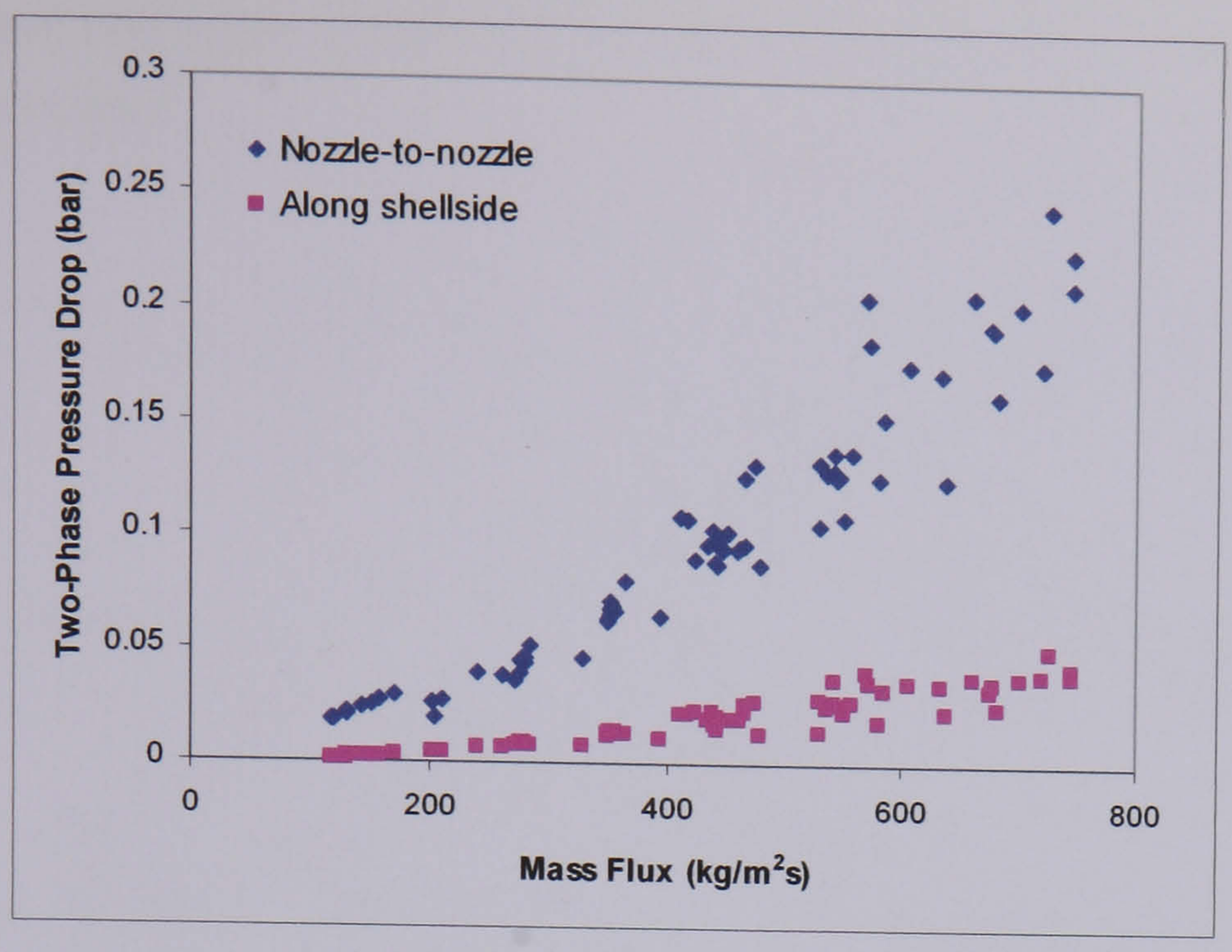

Figure 5.8(d) – Two-Phase Pressure Drop: Test 2

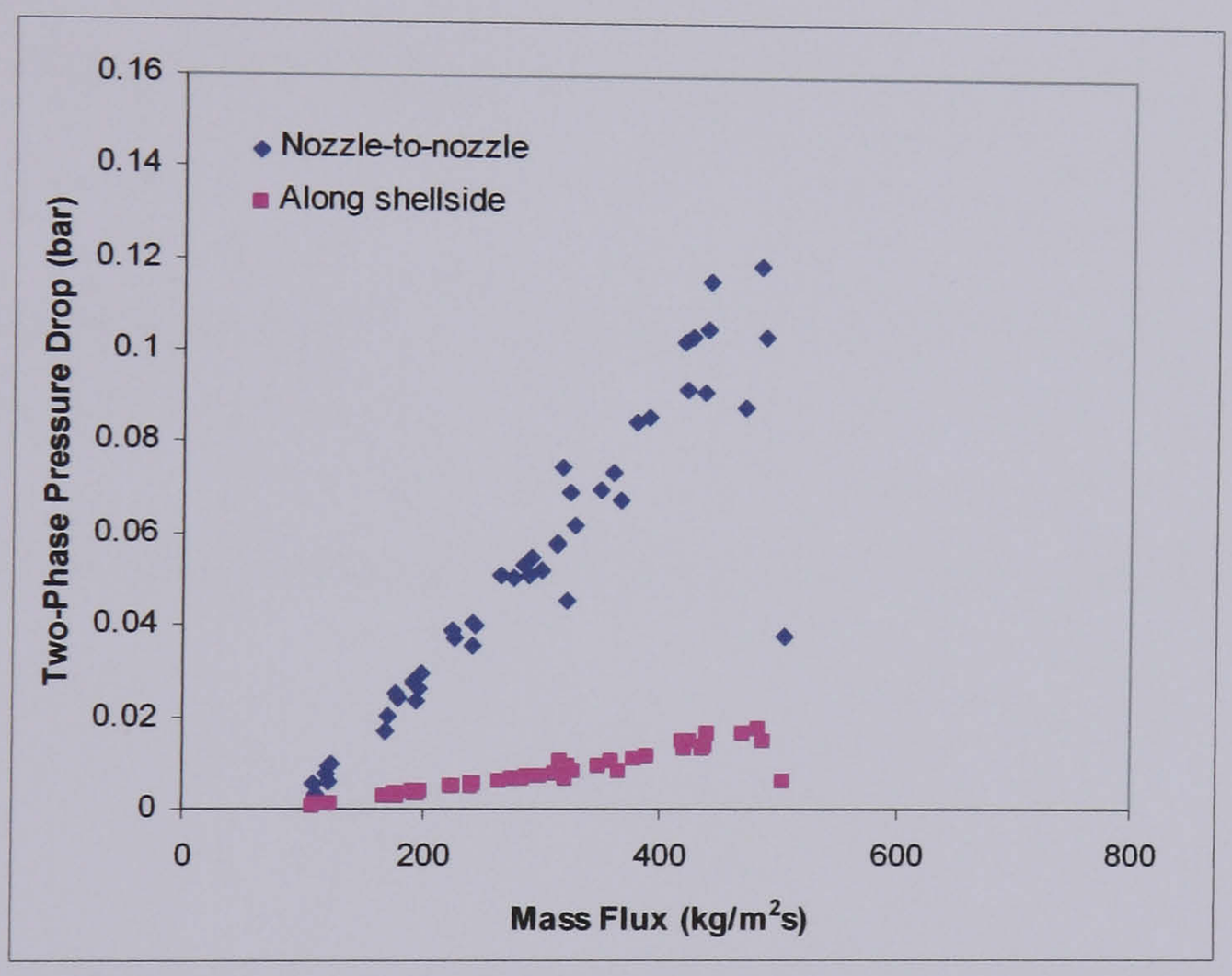

Figure 5.8(e) – Two-Phase Pressure Drop: Test 3

The pressure drop measurements show the expected trend of increasing with increasing mass flux. The reading along the shellside (Transducer 2) for Test 3 is significantly lower than the other tests, suggesting that the increase in the baffle pitch has lead to a decrease in the measured pressure drop between the shellside baffle spaces. The effect of baffle orientation on pressure drop is demonstrated by the comparison of Tests A and B and Tests 1 and 2 in Figure 5.9. The comparison of Test A and Test B shows that there is very little difference in the pressure drop between the geometries with the horizontal and the vertical baffle cuts. The pressure drop between the shellside nozzles (Transducer 1) is slightly greater for the Test 2 data than the Test 1 data indicating that the pressure drop may be greater with the vertical baffle cut, however this trend is not repeated in the baffle pressure drop (Transducer 2) data.

It appears that the orientation of the shellside baffles does not have a large effect on the measured pressure drop.

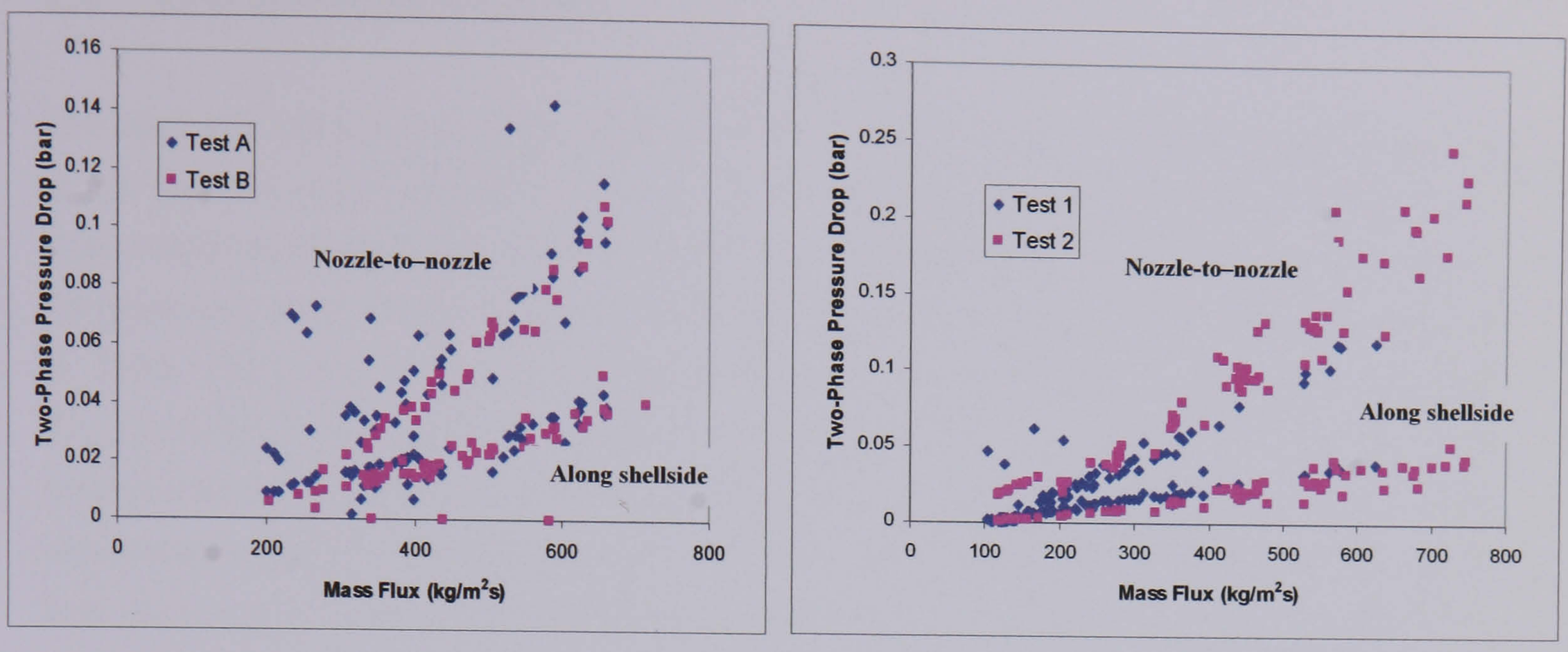

Figure 5.9 – Comparison of data for horizontal and vertical baffle orientations

The data from the nozzle-to-nozzle pressure transducer shows that the highest pressure drop exists with the geometry of Test 2.

The effect of the presence of sealing strips in the crossflow bypass is shown in Figure 5.10.

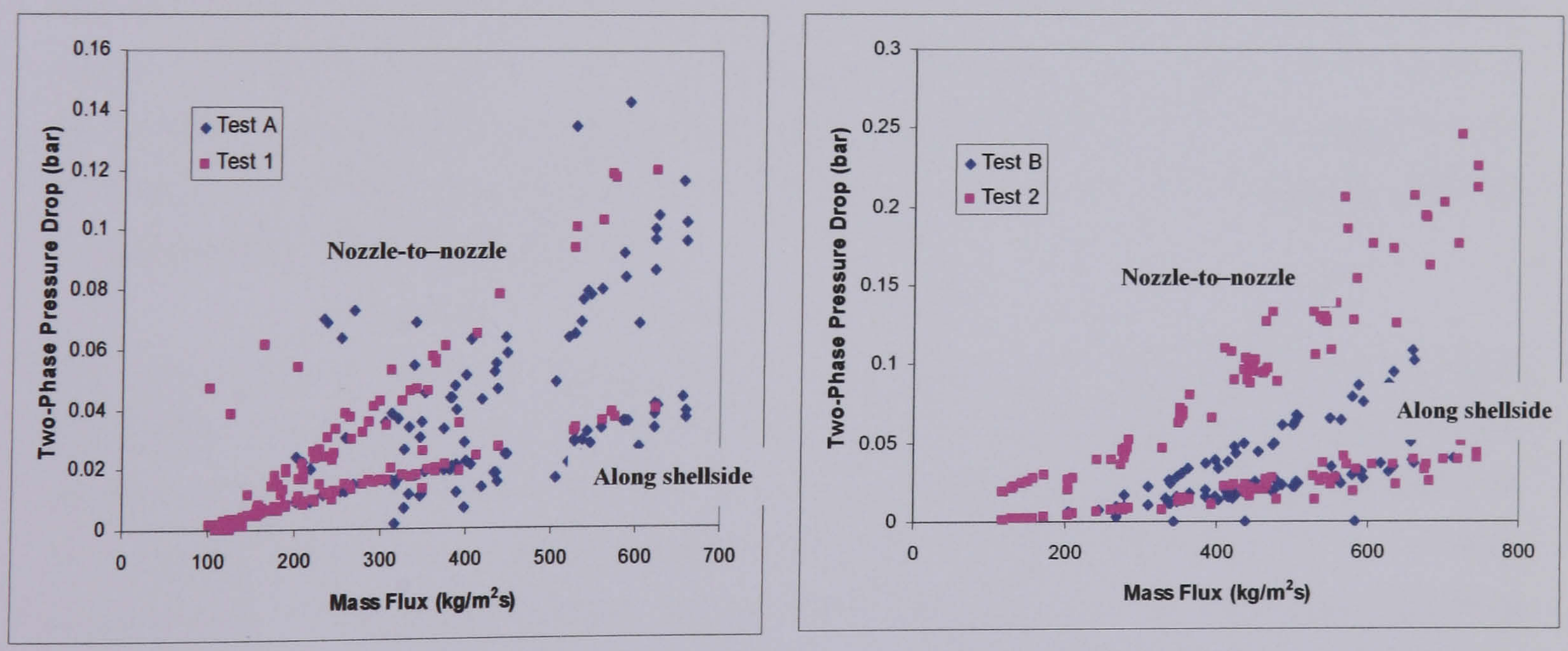

Figure 5.10 – Comparison of data for geometries with and without sealing strips

Figure 5.10 shows that the nozzle-to-nozzle pressure drop is significantly greater for the geometries with the sealing strips in the crossflow bypass (Tests 1 and 2). There is little difference in the Transducer 2 pressure drop data, although the data may be slightly greater

for Test 1 than Test A, suggesting that the sealing strips may be producing a higher pressure drop.

5.4 – Discussion of Results

The apparent deterioration of the heat transfer coefficient at the low end of the mass flux range was the most significant discovery to be made during the experimental programme. This deterioration would be of great interest to the designer of horizontal evaporators where the operating range could be within this region. HTFS reports (Chu et al, 1998; McNaught et al, 1999, 2000) suggested that the deterioration witnessed at higher outlet qualities (Figure 5.2 (a) and (b)) may be due to preferential flow of liquid in the crossflow bypass flow path. The theory implies that the flow through the crossflow path (where most of the heat transfer takes place) has a greater vapour mass fraction as a result of the liquid accumulating in the bypass lane and thus the overall heat transfer in the tube bundle is reduced (at higher qualities) as some tubes become surrounded by vapour. This type of flow separation has previously been observed in tests on a rectangular tube bundle test section with a bypass lane (Polley et al, 1973). The tests were taken in a transparent tube bundle with air/water flows and the authors noted that for certain flow conditions there was a tendency for the water to drift towards the bypass lane. During the current experimental programme it was decided to operate with sealing strips in the bypass lane to assess whether this type of phase separation was causing the poor heat transfer performance. Diagrams of the tube bundle with and without sealing strips in the bypass lane were given in Figure 3.4. As the data from Tests 1 and 2 suggest that the value of the heat transfer coefficient continues to drop at the higher vapour outlet qualities, it seems unlikely that this type of phase separation is causing the deterioration in performance. The presence of sealing strips would force bypassing liquid back into the main crossflow path which would prevent the vapour blanketing of the tube rows and cause an increase in the measured pressure drop.

The data in Figures 5.3 (c)-(e) for α_{boil} against mass flux indicate that the value of the mass flux through the evaporator is also an important factor in the apparent phase separation. An alternative hypothesis is that in the low mass flux range the dominance of gravitational forces over inertial forces could cause a separation of the phases where the liquid would flow preferentially in the bottom section of the evaporator with the top tube rows becoming surrounded by vapour. The data from Figures 5.3 (c)-(e) were re-examined to assess the possibility of a transition to gravity separated two-phase flow on the shellside. For Tests 1 to 3 the average values of the boiling heat transfer coefficient at the higher end of the mass flux range were calculated. For Test 1 the average value is around 5600 W/m^2K for Tests 2 and 3 the value is around 7000 W/m^2K. At the higher end of the mass flux range the value of α_{boil} tends to vary by as much as 15-20% from the mean value. This is mainly due to the

difference in the coefficient for tests at different heat fluxes. Figures 5.3(c)-(e) have been re-plotted in Figure 5.11. To apply a quantitative distinction between what is considered acceptable and poor heat transfer performance, the data have been separated into two categories. Data which is within 20% of the mean value at the higher mass fluxes is considered to be within an acceptable operating range, Conditions where the value of α_{boil} is more than 20% below the mean value are considered to be in the poor operating range.

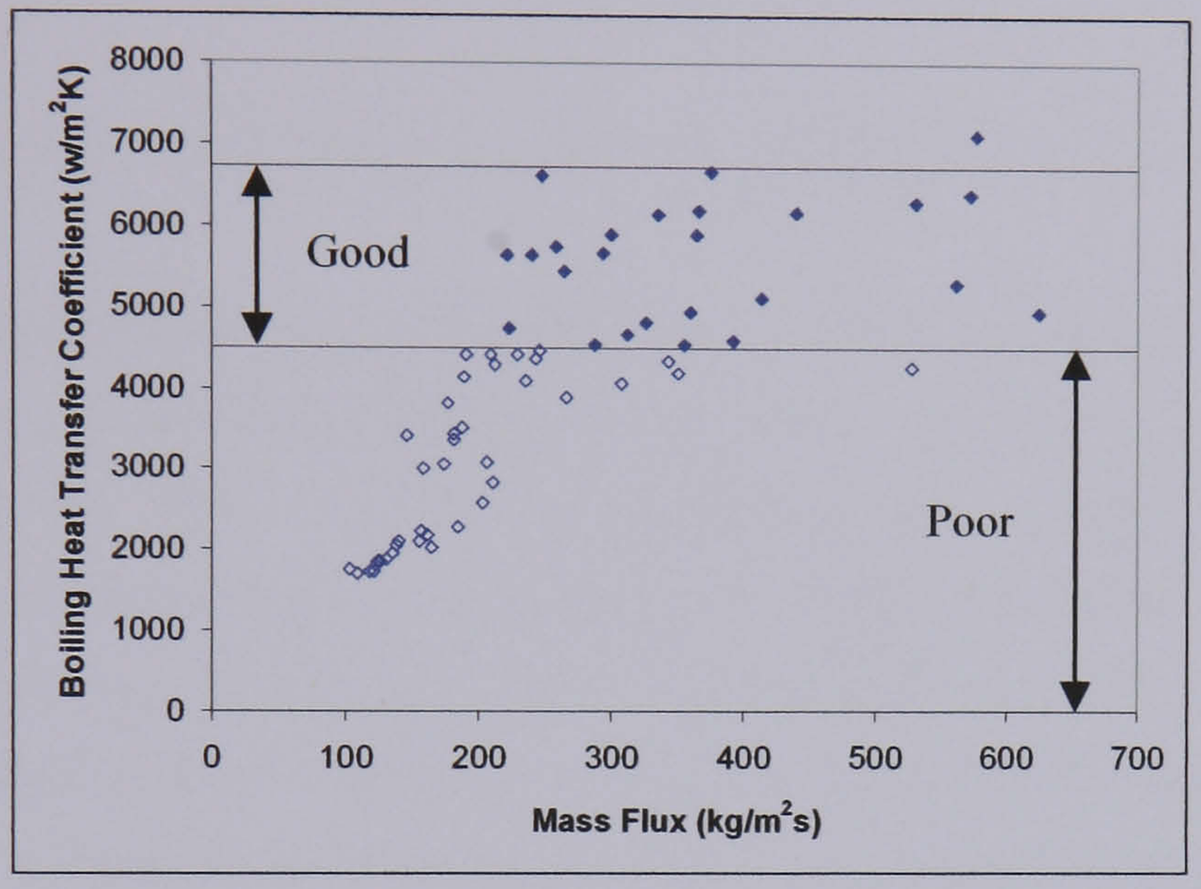

Figure 5.11(a) – Plot of Boiling Heat Transfer Coefficient for Test 1 data

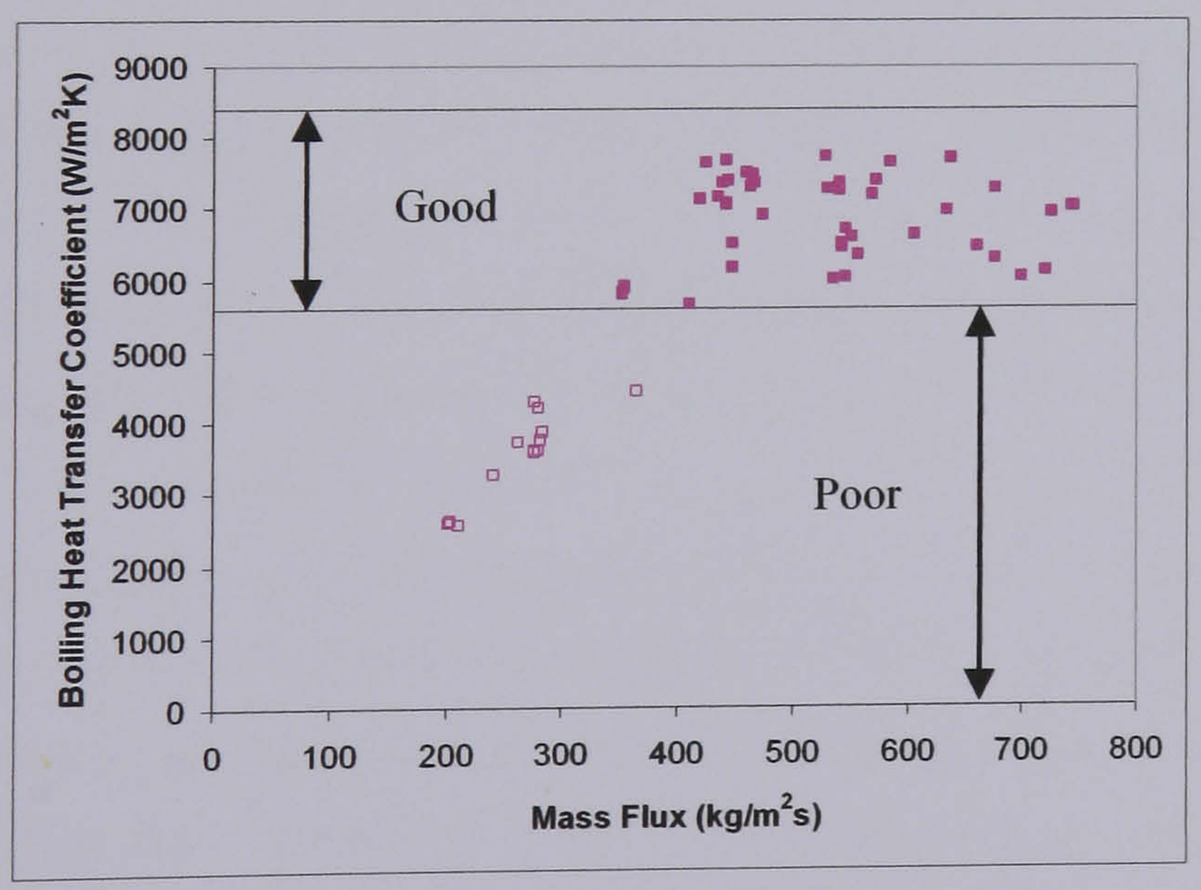

Figure 5.11(b) – Plot of Boiling Heat Transfer Coefficient for Test 2 data

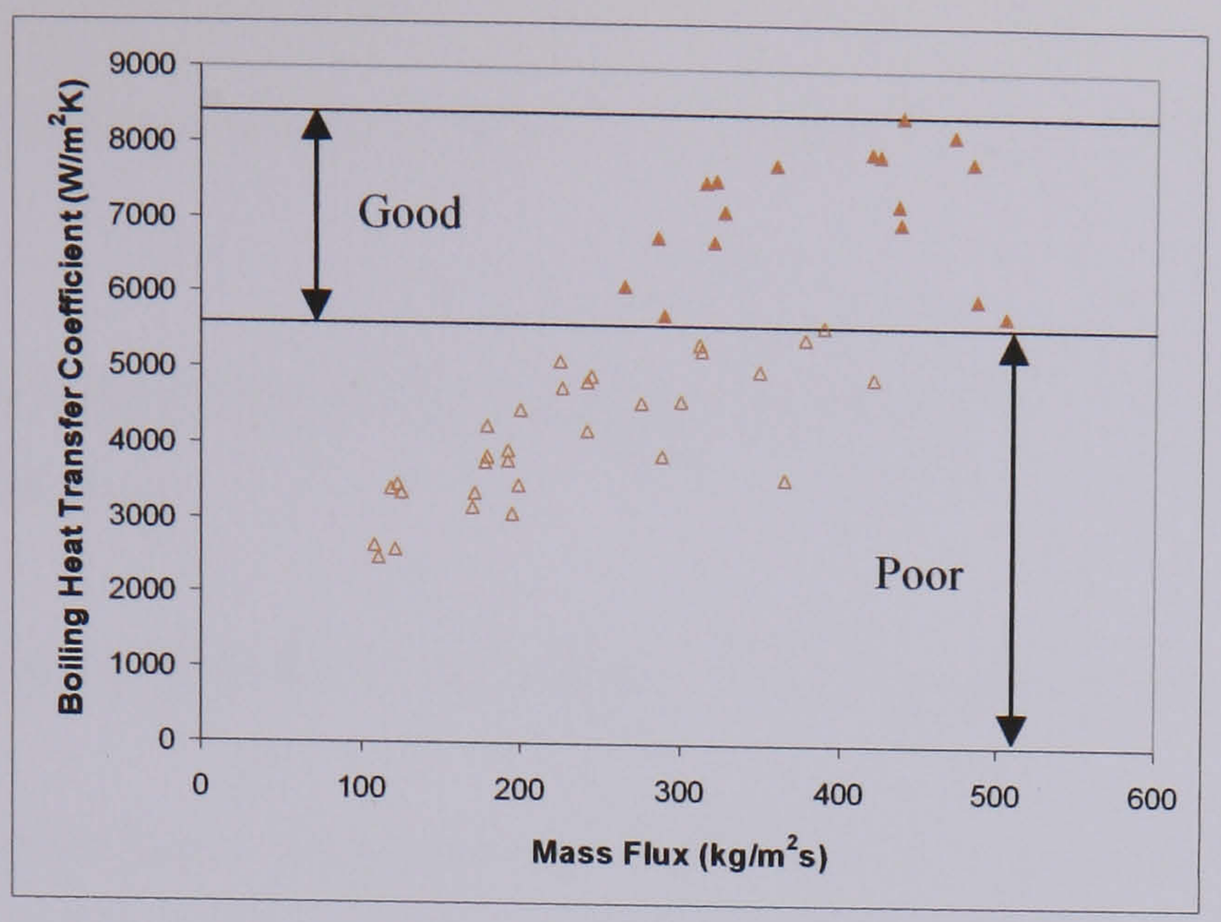

Figure 5.11(c) – Plot of Boiling Heat Transfer Coefficient for Test 3 data

Using Figure 5.11 the possibility of a transition from a homogeneous type of flow pattern to a separated type of two-phase flow pattern on the shellside was examined. The majority of the literature for two-phase flow patterns is concerned with providing maps plotted in dimensionless physical coordinates from which the likely two-phase flow pattern can be determined. There is a vast amount of literature on the subject of two-phase flow patterns in tubes. There is however a large degree of uncertainty when discussing particular two-phase flow patterns as the transitions are usually based on tests using visual observations and the distinctions between patterns in some of the literature is unclear. Indeed one literature survey (Simpson et al, 1975) covered over 300 sources on flow pattern transitions in tubes in which they found 84 different flow pattern titles. In recent times there has been a tendency to reduce the flow pattern types to around 4 or 5 main flow patterns which could be used to describe the full range of conditions. Despite the vast amount of tubeside data, there is currently very little literature on the subject of two-phase flow patterns on the shellside of shell-and-tube heat exchangers. This is not altogether surprising as there is not a lot of test data for shellside two-phase flow in the open literature. One of the few flow pattern maps designed for shellside flow is based on observational tests made of air/water flows by Grant and Murray (Grant et al, 1972, 1974; Grant, 1977; Grant et al, 1979). A diagram of their test section is shown in Figure 5.12. It is a rectangular baffled tube bundle which could possibly represent the crossflow and window flow paths of a typical shellside flow, but there is no flow area available for leakage or bypass flows. The authors produced two different flow pattern maps for the tube bundle, one with vertical and another with horizontal crossflow. To test vertical and horizontal flow they simply altered the position of the test section. This allowed them to represent the different flow patterns observed in each orientation. Figures 5.13(a) and (b) show the flow patterns observed by the authors which were used to plot the maps. The different flow patterns can be described as follows:

Spray Flow – occurring at high mass flow qualities with liquid carried along by the gas as spray.

Bubbly Flow – occurring at low mass flow qualities with gas distributed as discrete bubbles in the liquid.

Stratified Flow – where the liquid and gas phases become completely separated.

Stratified-Spray Flow – where the liquid and vapour phases are separated with liquid flowing along the bottom of the model. The gas phase is also entrained in the liquid layer in the form of bubbles with liquid droplets also carried along in the gas phase as a spray.

Intermittent Flow – where intermittent slugs of liquid are propelled through the model by a gas.

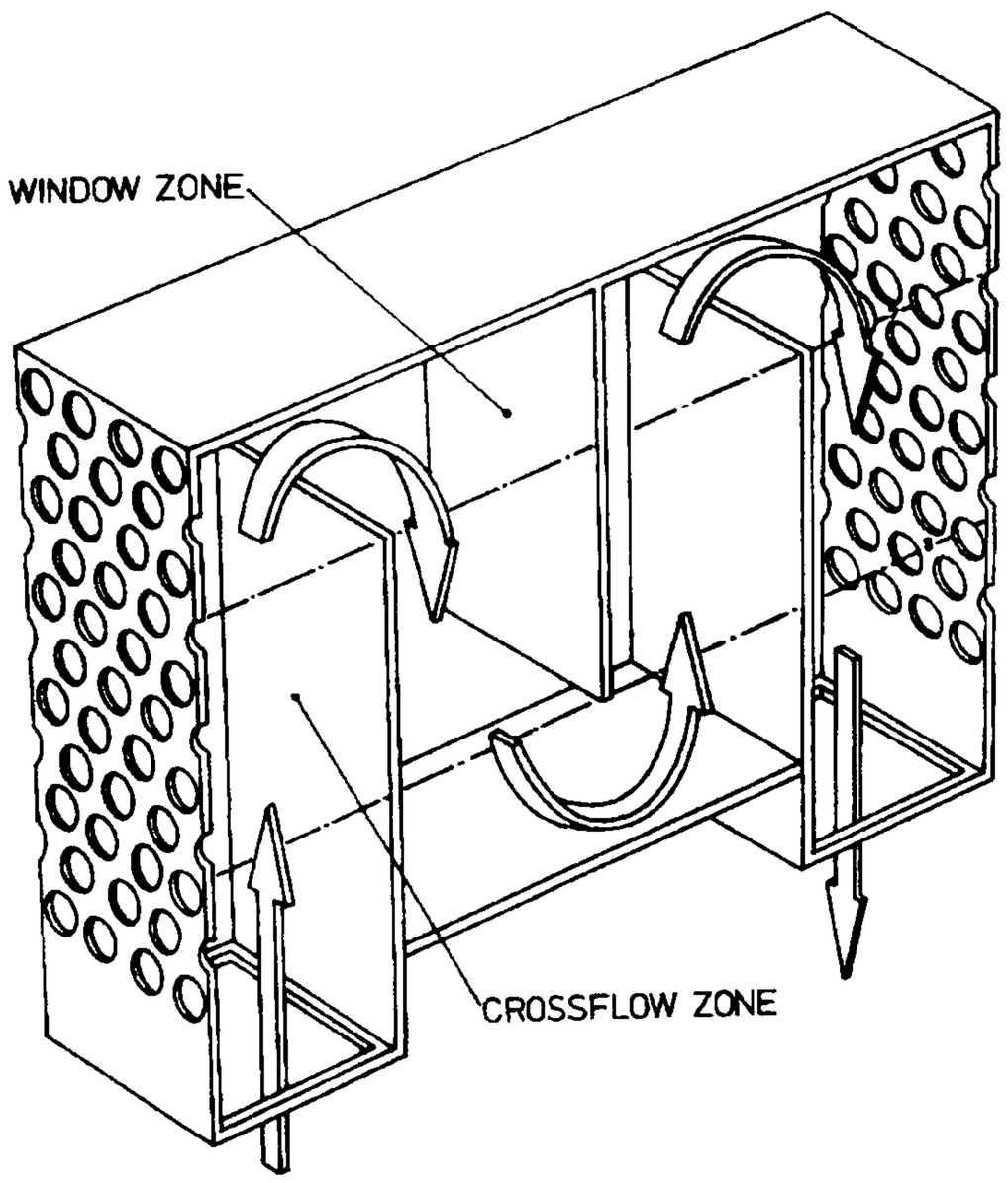

Figure 5.12 – Diagram of Test Bundle used by Grant/Murray (Grant et al, 1972, 1974)

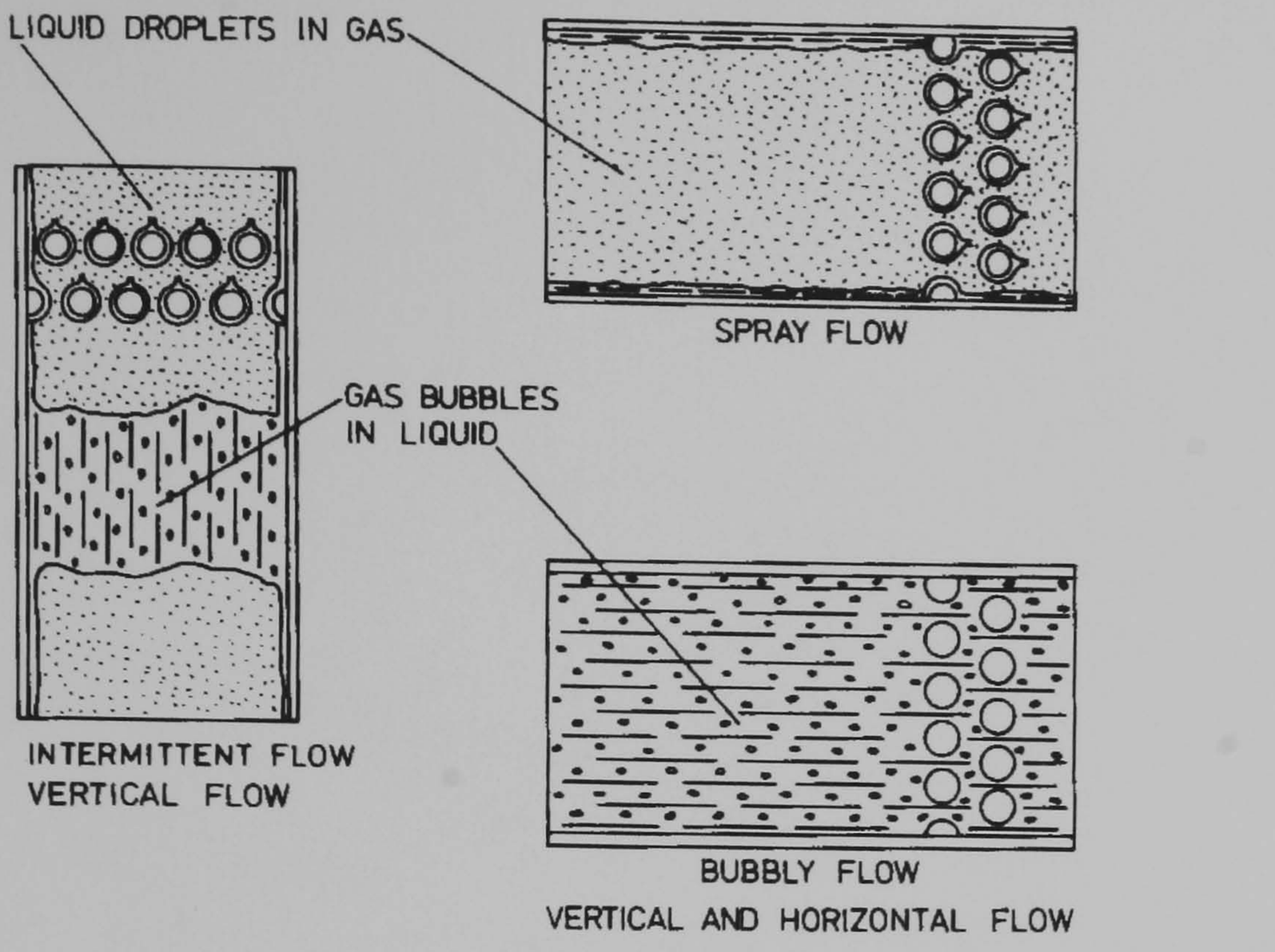

Figure 5.13(a) – Flow Patterns in Vertical Shellside Flow (Grant, 1977)

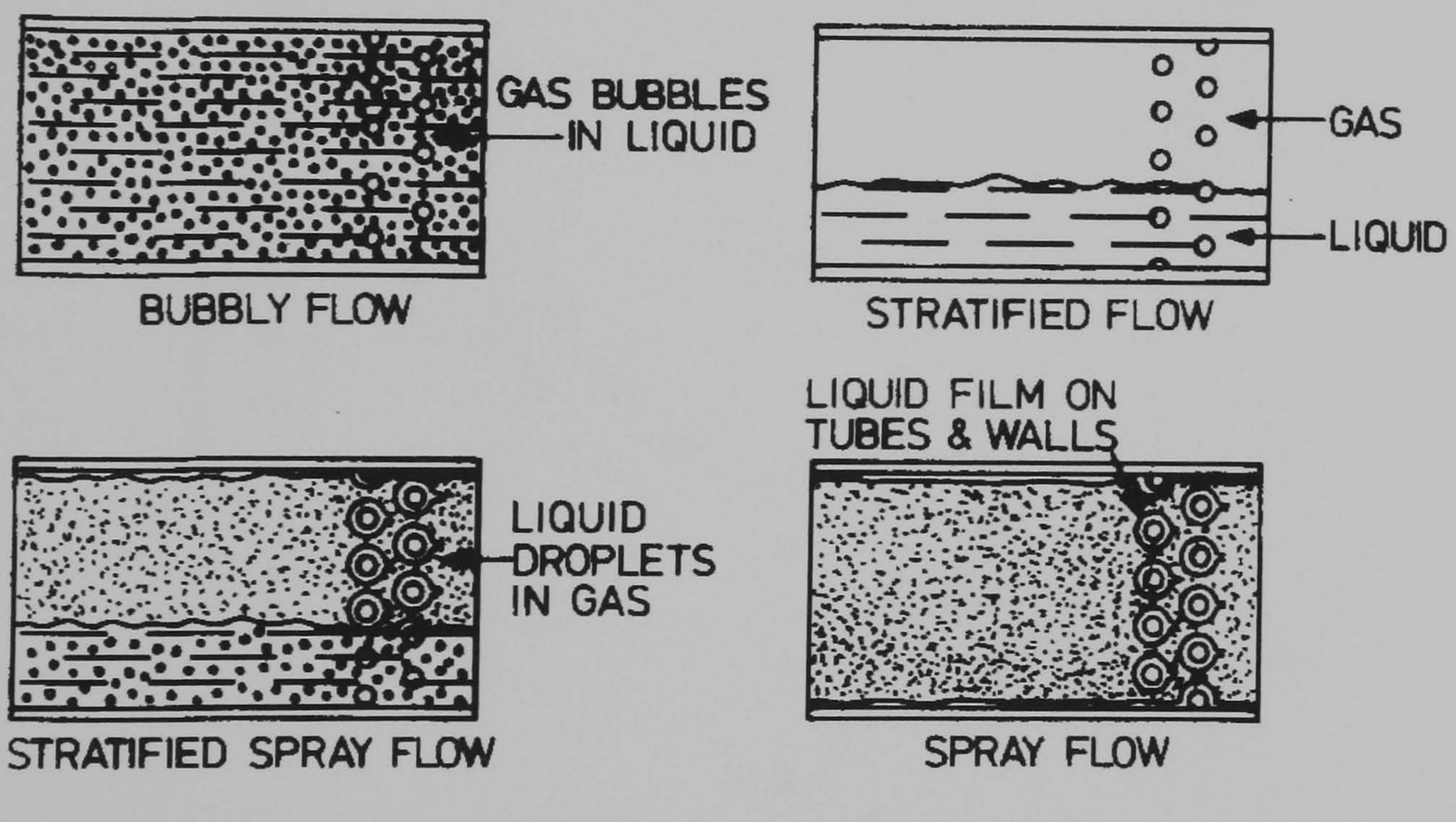

Figure 5.13(b) – Flow Patterns in Horizontal Shellside Flow (Grant, 1977)

The general flow pattern maps produced from these observations were plotted in dimensionless coordinates representing the gas and liquid phase velocities. The maps have been reproduced here (Figure 5.14(a) and (b)) for the specific reference conditions* of fluid, temperature and pressure corresponding with the test programme results from Tests 1 to 3.

The coordinates have been arranged to show the transitions in terms of the mass flux against the vapour outlet quality.

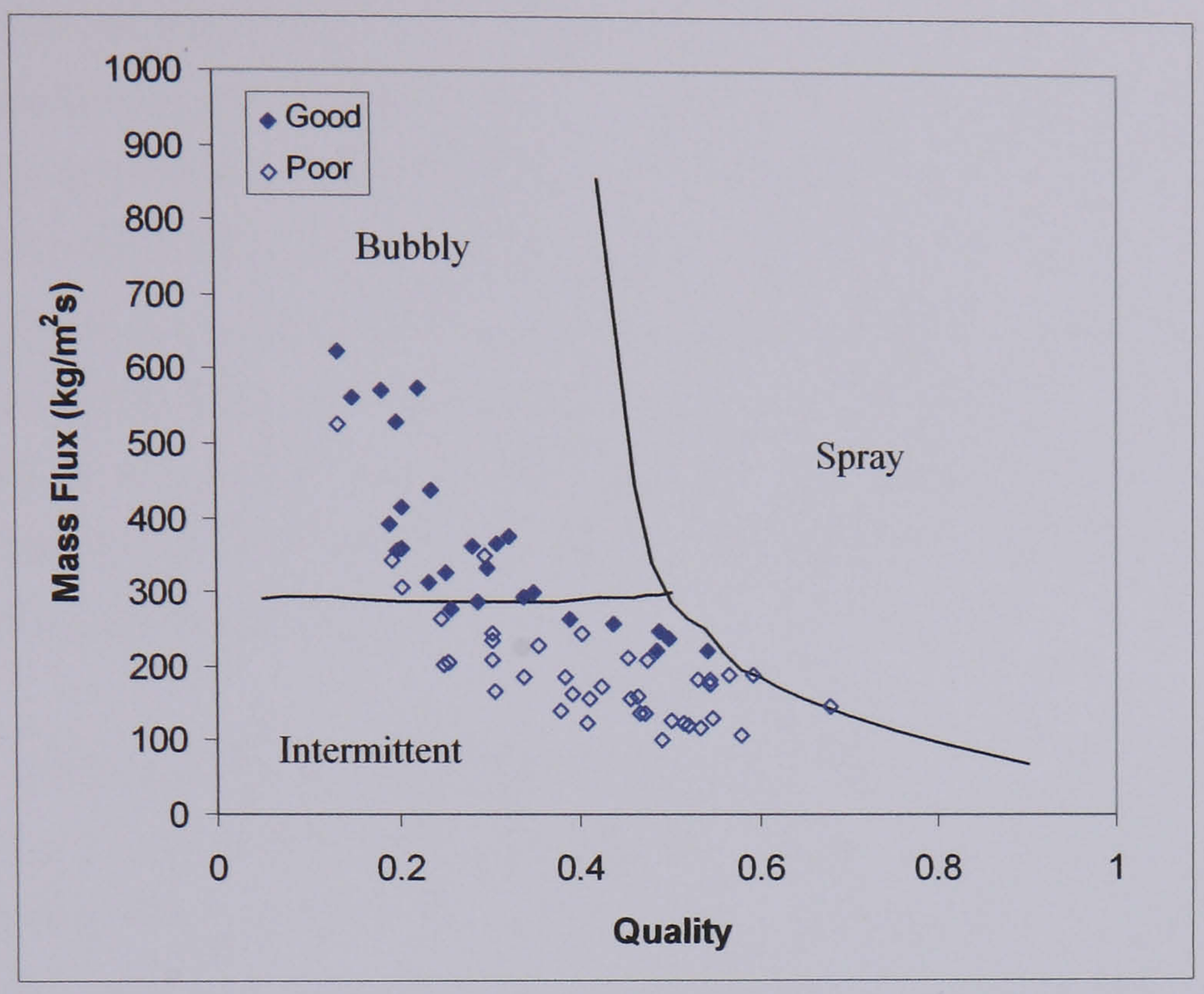

Figure 5.14(a) – Test 1 data on Shellside Vertical Crossflow Map (Grant 1977)

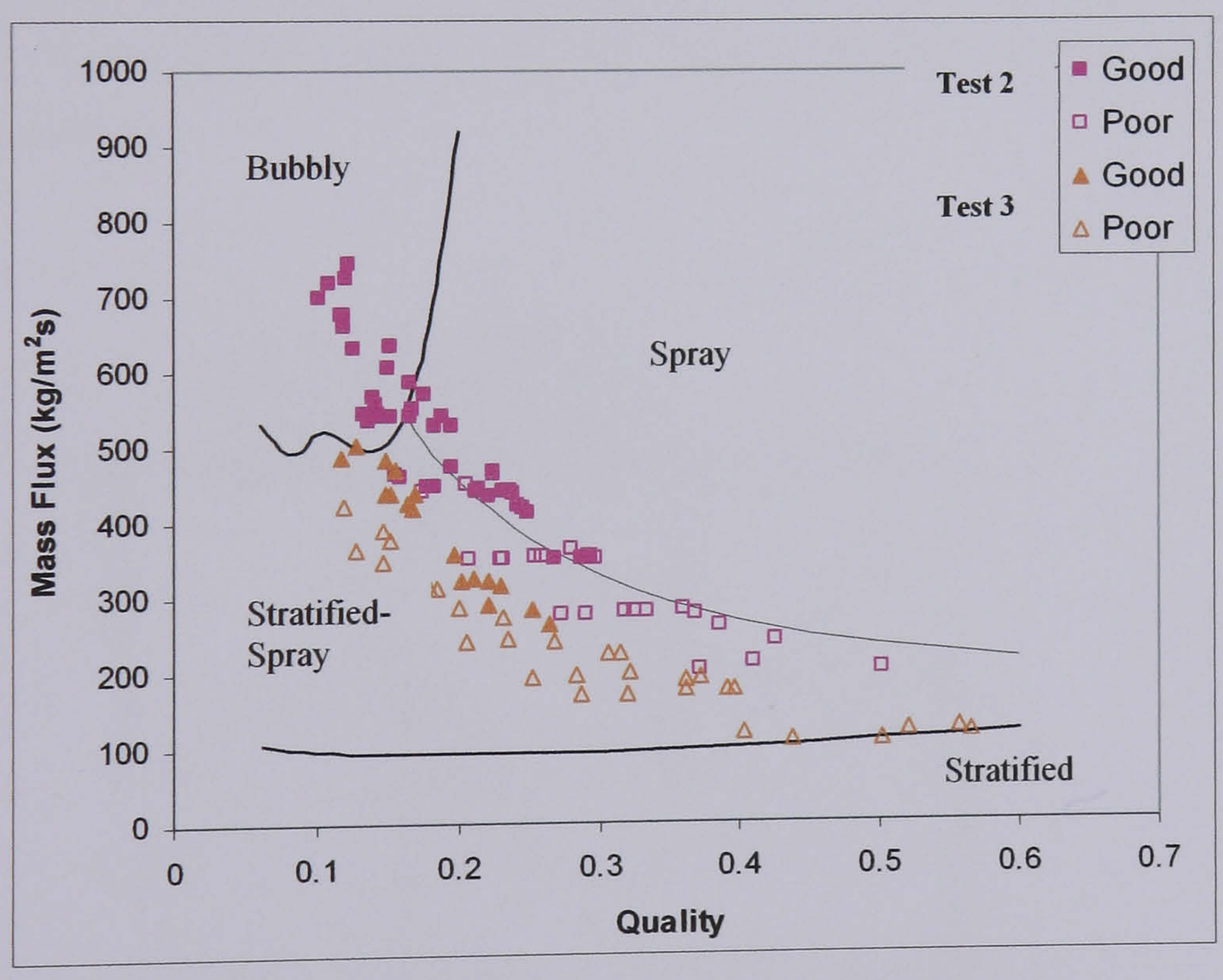

Figure 5.14(b) -Test 2 and 3 data on Shellside Horizontal Crossflow Map (Grant 1977)

*(Figure 14 plotted for saturated R-134a at P = 7bar)

Figure 5.14(a) shows the flow pattern transition lines for vertical crossflow; in addition it shows the Test 1 data arranged in terms of 'Good' and 'Poor' heat transfer as in Figure 5.11(a). The Test 1 data are plotted on this map because the geometry will produce vertical crossflow as

the baffle orientation is horizontal. From Figure 5.14(a) it appears that the transition to poorer heat transfer in the data may coincide with the flow pattern transition from bubbly to intermittent flow. Figure 5.14(b) shows the data from Tests 2 and 3 (Figures 5.11(b) and (c)) plotted next to the transition lines for horizontal crossflow (vertical baffle orientation). For the vapour outlet quality values less than 0.15 it appears that the data are possibly in the bubbly flow regime, and at greater qualities the data are very close to the transition between spray flow and stratified-spray flow. At the higher qualities the data are further into the stratified-spray regime, where a poorer heat transfer performance could be expected. When the flow pattern becomes more stratified it could lead to vapour blanketing around some of the tubes in the upper part of the bundle. Higher heat transfer coefficients would be more likely in the homogeneous flow patterns of bubbly and spray flow where it is less likely that some of the tube bundle will be short of liquid.

An additional shellside flow pattern was observed in tests in a transparent glass heat exchanger carried out for a HTFS report (Grant et al, 1987). The tests were carried out with air/water two-phase flows and the flow pattern was described as a stratified flow for the horizontal baffle cut arrangement. The flow pattern is represented in Figure 5.15. Unsurprisingly it is not on the flow pattern map in Figure 5.14(a) as it is difficult to see how this flow pattern could be produced in a test section without leakage flow paths. It is however reasonable that at the lower mass fluxes in Test 1 this flow pattern may exist in the experimental exchanger.

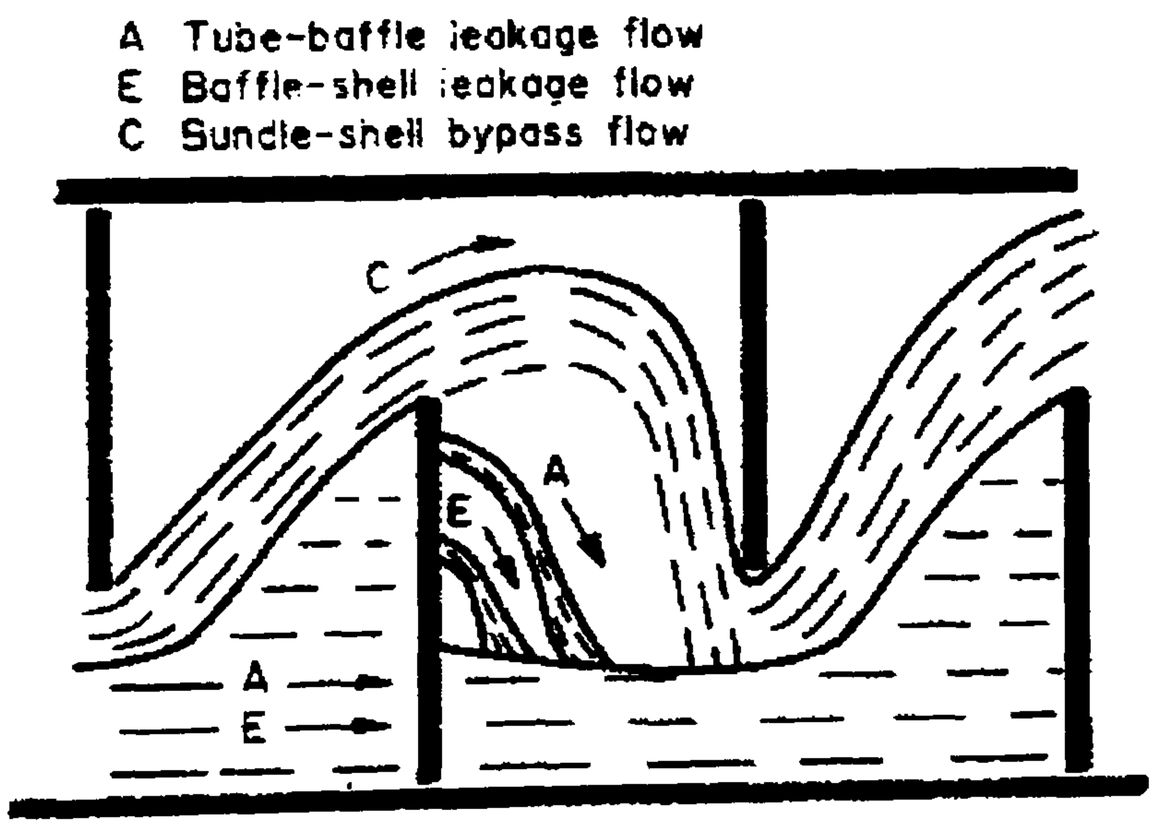

Figure 5.15 – Stratified Flow Pattern with Horizontal Baffle Orientation (Grant et al, 1987)

In Figure 5.16 the tubeside thermocouple data from Test 3 (Figure 5.5) have been re-examined applying the criteria of Figure 5.11.

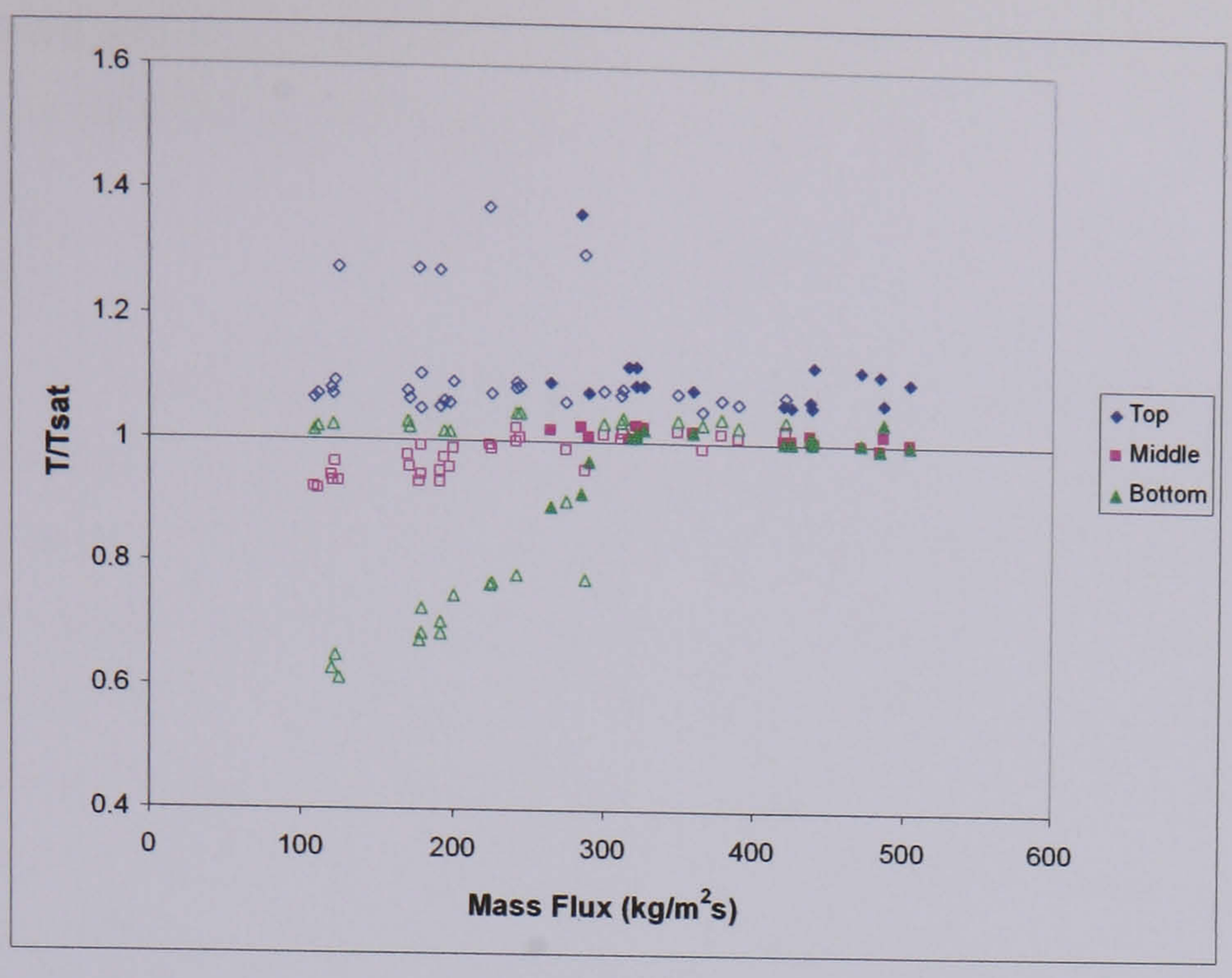

Figure 5.16 – Test 3 Tubeside Temperatures vs. Mass Flux

As was observed in Figures 5.5 and 5.6 the transition in the shellside heat transfer data corresponds closely with the deviation in the tubeside temperatures. From Figure 5.16 it can be seen that at the lower mass fluxes the temperature in the bottom tube row is significantly lower than the saturation temperature whereas the temperature in the top tube row is significantly above. This would imply that under these conditions the bottom tube is providing a greater heat duty as the incoming steam is condensed and subcooled below the saturation temperature before the exit of the tube. The opposite applies to the top tube row, where the data indicates the incoming steam does not reach the saturation temperature. This trend in the tubeside data is consistent with the hypothesis that there exists a stratified type of phase separation on the shellside. With a stratified flow pattern the top tube rows would be surrounded by vapour producing a relatively small amount of heat transfer with the incoming steam over at least some of the tube length. Surrounding the bottom tube rows would be a boiling liquid with high heat transfer rates which could explain the condensate subcooling of the bottom tube row.

The comparison of the heat transfer data with the flow pattern maps of Grant et al (Grant et al, 1979) and the tubeside temperature data for Test 3 certainly suggests that there may be a transition from a homogeneous flow pattern (bubbly/spray) to a more separated type of flow pattern (stratified-spray, stratified, intermittent). The exact physical mechanism of the transition is difficult to establish from the flow pattern maps in Figure 5.14, not least because (as with the majority of two-phase flow pattern maps) the transitions are defined in terms of general variables in the coordinates of the map. In an attempt to find further information on this possible transition point the pressure drop data of Tests 1 to 3 were re-examined. It was decided to examine the behaviour of the two-phase pressure drop multiplier. The two-phase

multiplier used was based on equation 5.1 relating the two-phase pressure drop to the pressure drop if the total flow were flowing with liquid properties.

$$\phi_{lo}^2 = \frac{\Delta P_{TP}}{\Delta P_{lo}} \tag{5.1}$$

For Tests 1 and 2 the pressure drop of the total flow with liquid properties was calculated from curve-fits to single-phase liquid pressure drop data collected over a range of mass fluxes on the experimental facility. The data for the single-phase runs for Test 1 and Test 2 are shown in Figure 5.17. The data represents the frictional pressure drop measured using differential pressure transducers 1 and 2 (Figure 5.7). For the pressure drop between the shellside nozzles (Transducer 1) the gravitational pressure drop is not included, in addition the measured pressure drop was corrected to remove an acceleration term caused by the fact that the evaporator shellside outlet nozzle was larger than the inlet nozzle.

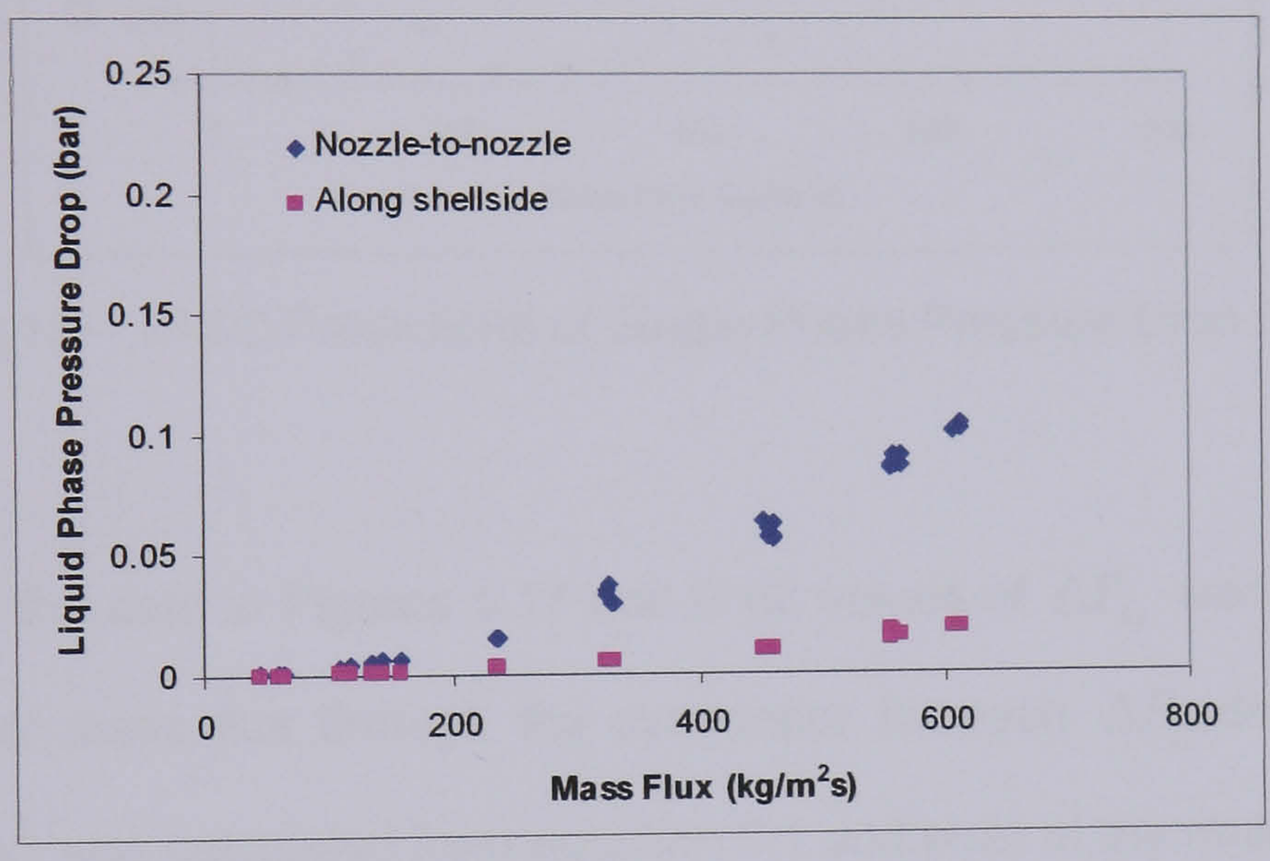

Figure 5.17(a) – Single-Phase Pressure Drop Data for Test 1

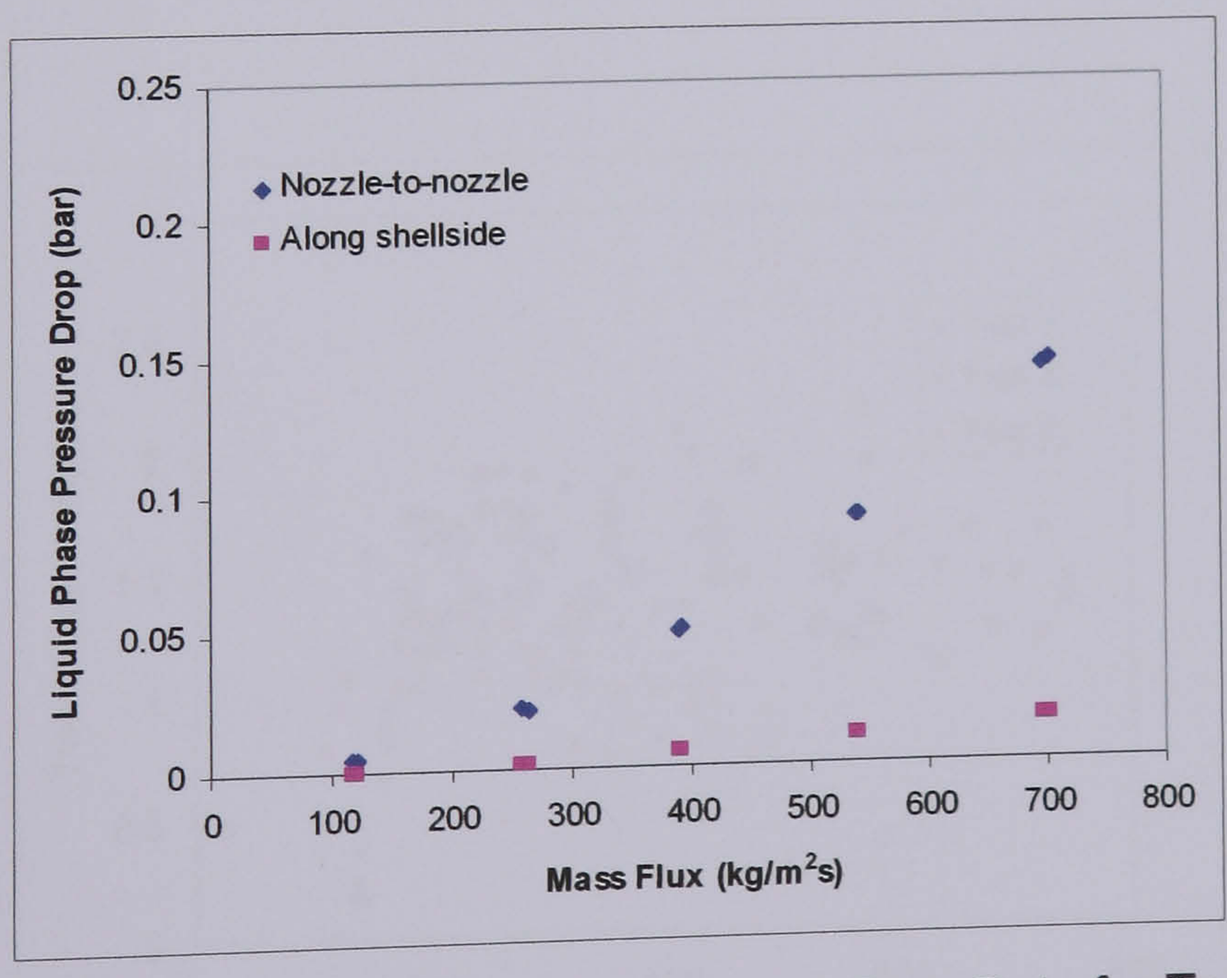

Figure 5.17(b) – Single-Phase Pressure Drop Data for Test 2

For the Test 3 geometry there was no available single-phase data so the HTFS TASC program was used to predict the single-phase predictions for this geometry (From the analysis of TASC in Chapter 6 it was observed that TASC accurately predicted the single-phase pressure drop data of Tests A, B, 1 and 2). The data of the TASC predictions for Test 3 are presented in Figure 5.18.

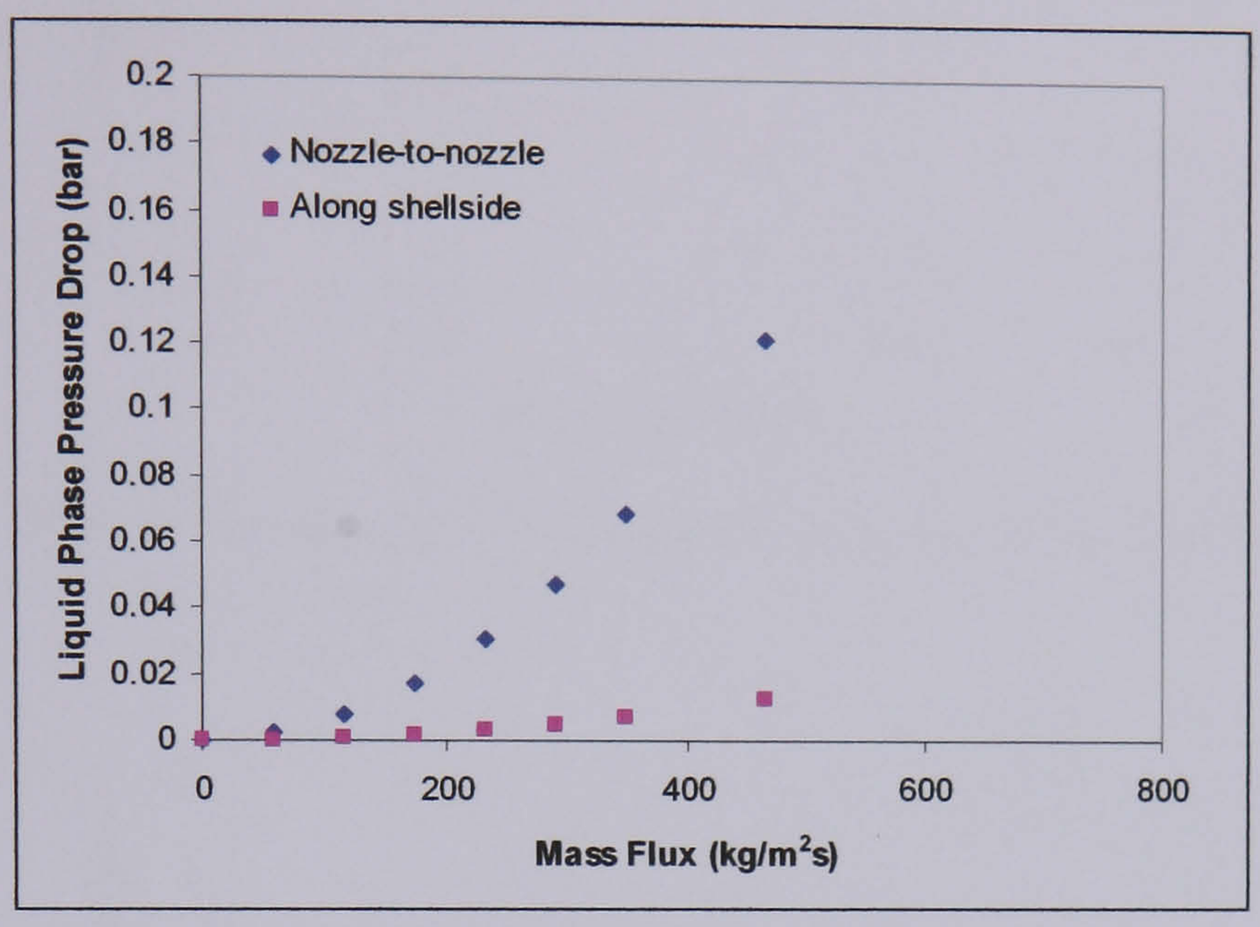

Figure 5.18 – TASC Predictions of Single-Phase Pressure Drop for Test 3

From curve fits of the data in Figures 5.17 and 5.18, values of ΔP_{lo} were calculated for the corresponding total mass flux through the evaporator for each ΔP_{TP} data point. The two-phase multiplier ϕ_{lo}^2 was calculated from equation 5.1 and plots of the multiplier against mass flux and vapour outlet quality for Tests 1, 2 and 3 are given in Figures 5.19 and 5.20.

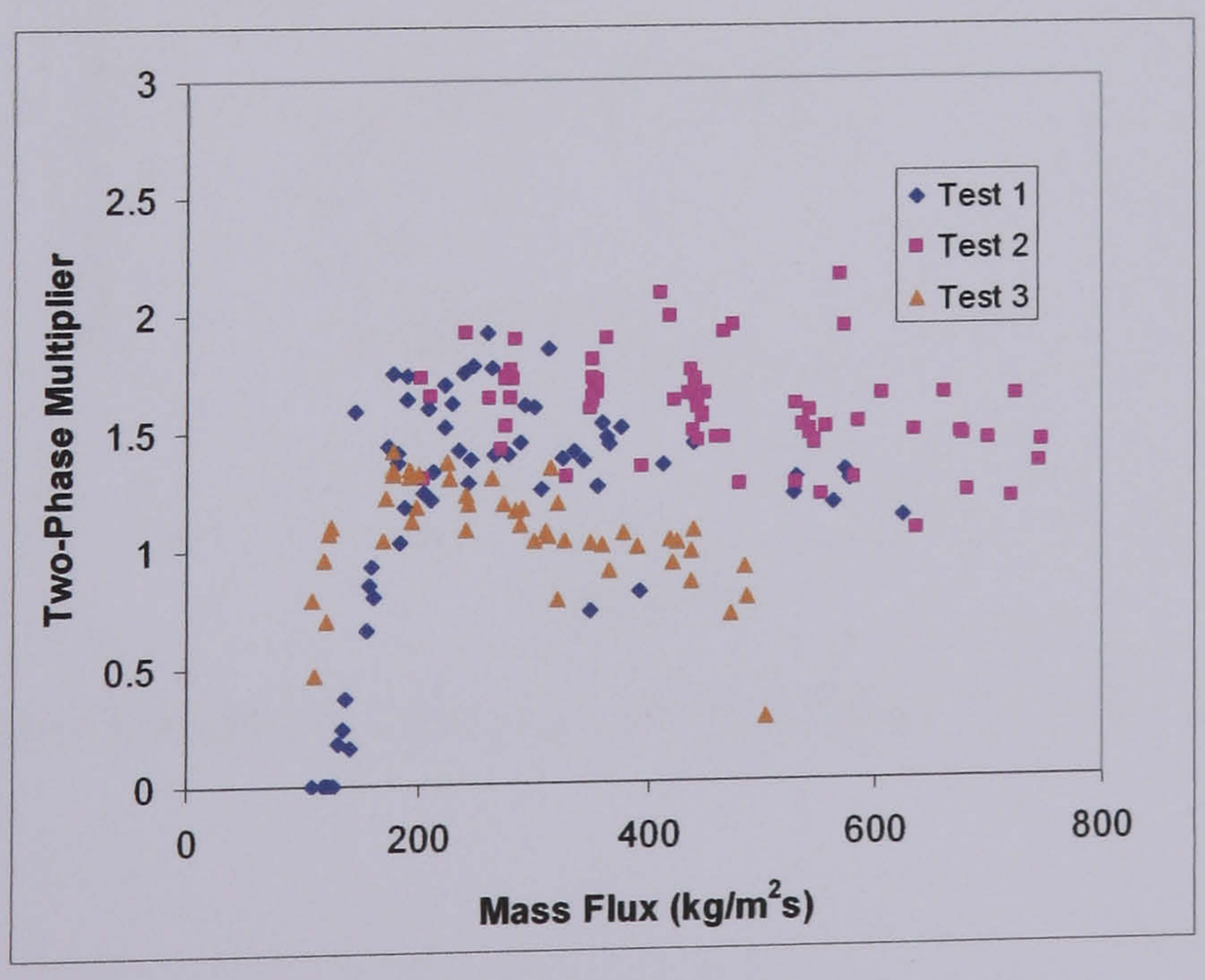

Figure 5.19(a) – Plot of Transducer 1 Pressure Drop Multiplier vs. Mass Flux for all Tests

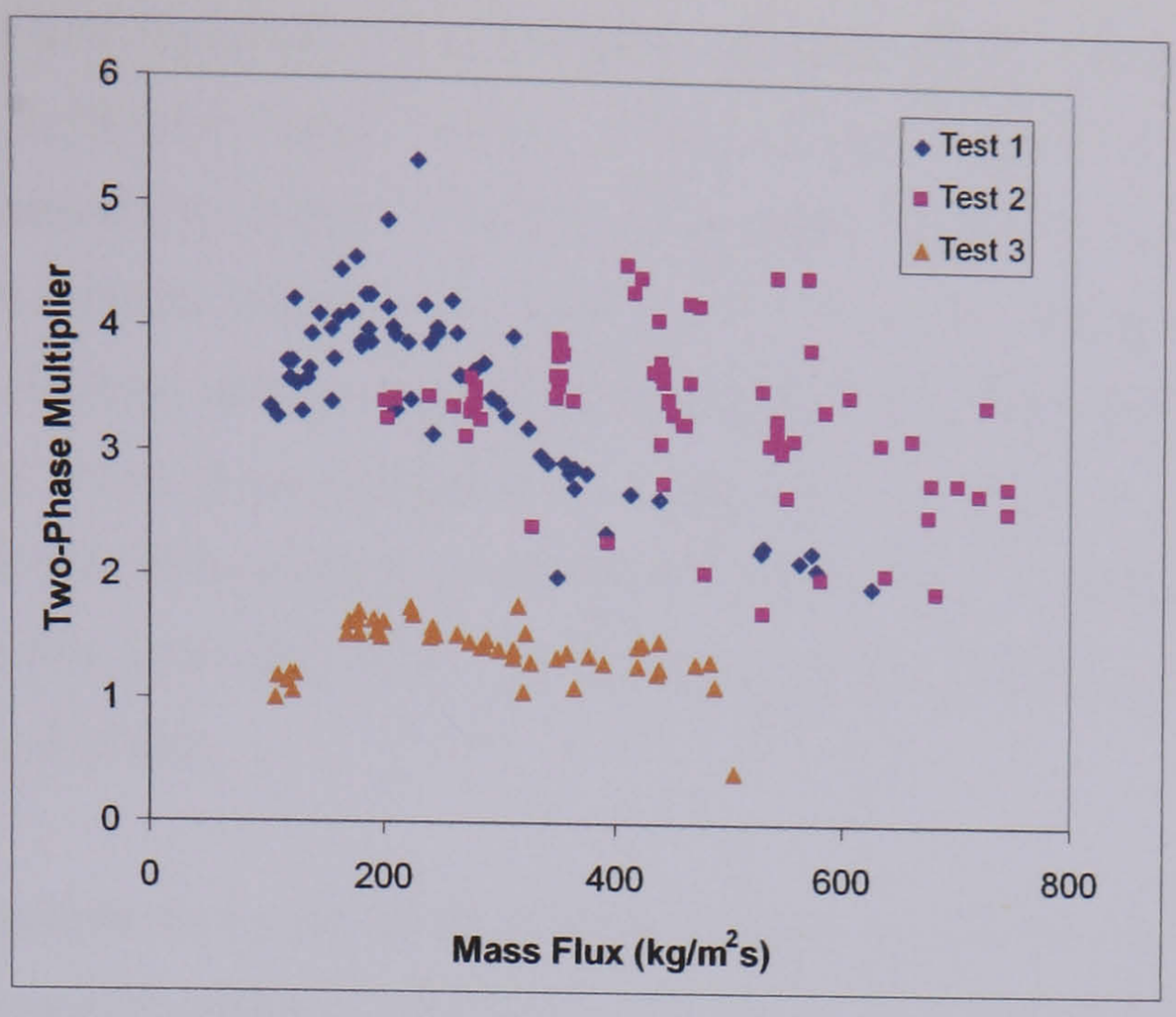

Figure 5.19(b) – Plot of Transducer 2 Pressure Drop Multiplier vs. Mass Flux for all Tests

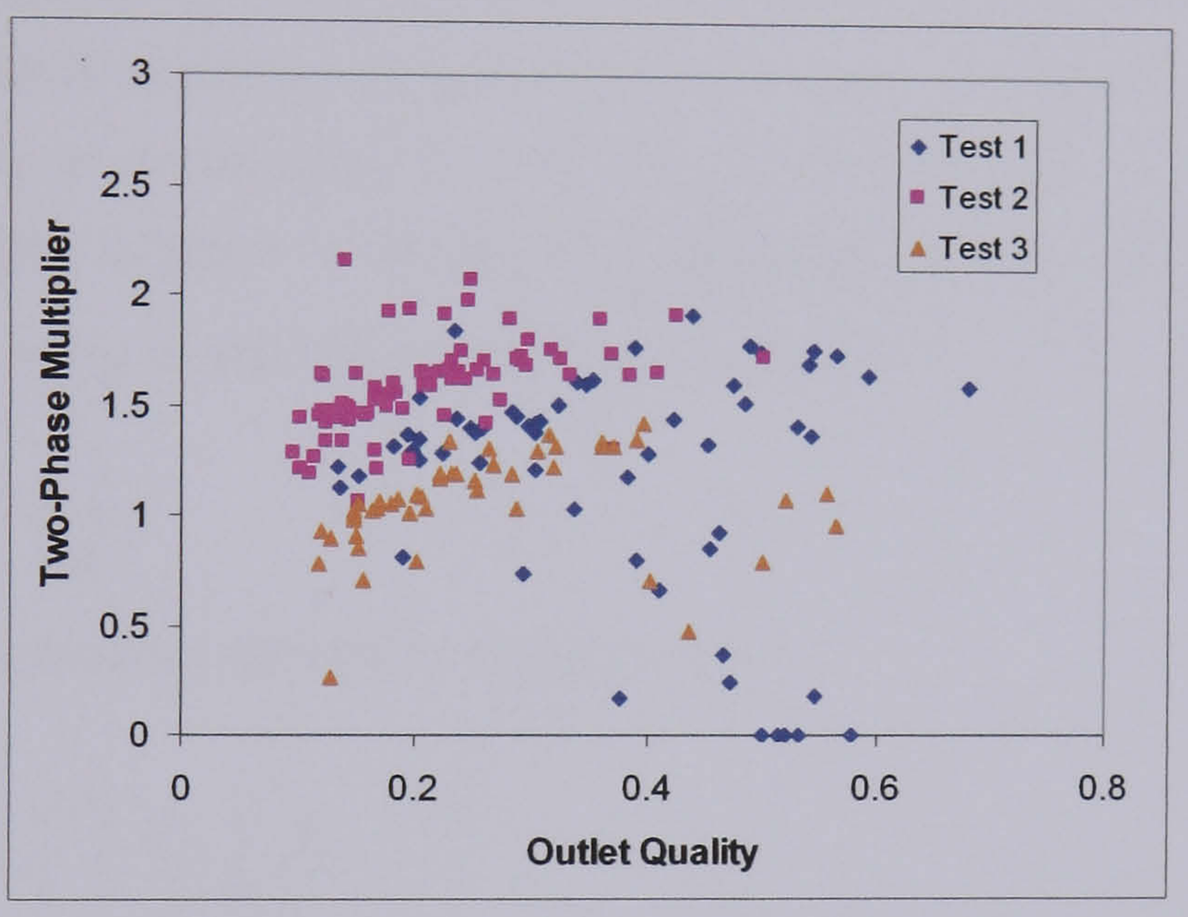

Figure 5.20(a) – Plot of Transducer 1 Pressure Drop Multiplier vs. Outlet Quality for all Tests

Figure 5.20(b) – Plot of Transducer 2 Pressure Drop Multiplier vs. Outlet Quality for all Tests

From Figures 5.19(a) and (b) it can be seen that there is an apparent peak in the value of the two-phase multiplier data from Tests 1 and 3. These peaks correspond quite closely with the mass flux of the observed transition in the heat transfer data for Tests 1 and 3 in Figure 5.11.This peak is less pronounced in the Test 2 data. For the Test 2 data a trend is more evident from Figure 5.20(b) where it appears that there is a transition in the value of the multiplier at a vapour outlet quality around 0.2. This value of the outlet quality corresponds with the beginning of the deterioration in the heat transfer data observed in Figure 5.2(d). It also corresponds to the transition from bubbly to spray or stratified-spray flow in the flow pattern map of Figure 5.14(b).

To assess the implications of these trends it was decided to examine existing correlations for predicting the two-phase multiplier. There are well established correlations for the two-phase multiplier for flow in tubes. As these correlations are based on large quantities of data it was logical to examine whether this behaviour of the two-phase multiplier was observed in tube flow before proposing an explanation for the cause on the shellside. A standard equation for the two-phase multiplier is given in equation 5.2 (Butterworth et al, 1977). It is based on the pressure drop of the liquid phase flowing alone in the tube ΔP_l.

$$\phi_l^2 = 1 + \frac{C}{X} + \frac{1}{X^2} \tag{5.2}$$

X is the Martinelli Parameter defined by equation 5.3

$$X = \left[\left(\frac{1-x}{x} \right)^{1.8} \left(\frac{\rho_g}{\rho_l} \right) \left(\frac{\eta_l}{\eta_g} \right)^{0.2} \right]^{\frac{1}{2}} \tag{5.3}$$

ρ represents the fluid density and η the fluid viscosity.

The value of C in equation 5.2 is a function of the mass flux and the fluid properties. For the purposes of this exercise the calculation procedure from the HTFS Handbook Sheet TM4 (Whalley, 1984) was adopted. The procedure for calculating the value of the multiplier for comparison with Figure 5.19 was as follows

- Select standard conditions of pressure and temperature representative of the test runs in Tests 1 – 3
- Calculate the physical properties such as density and viscosity; select a vapour quality and calculate the Martinelli parameter
- Use the methods from HTFS Handbook TM4 to calculate C
- Calculate two-phase multiplier ϕ_l^2

- Create data for a range of qualities and convert the multiplier to the total flow with liquid properties multiplier ϕ_{lo}^2 using equation 5.4.

$$\phi_{lo}^2 = \frac{m_l^2}{m_{lo}^2}\phi_l^2 \tag{5.4}$$

Since $$\Delta p_{tp} \propto \phi_{lo}^2 \frac{m_{lo}^2}{\rho} = \phi_l^2 \frac{m_l^2}{\rho} \tag{5.5}$$

This calculation procedure was carried out for vapour qualities of 0.15, 0.3 and 0.45, to represent a spread of the quality range in the data for the experimental tests. The results are plotted in Figure 5.21.

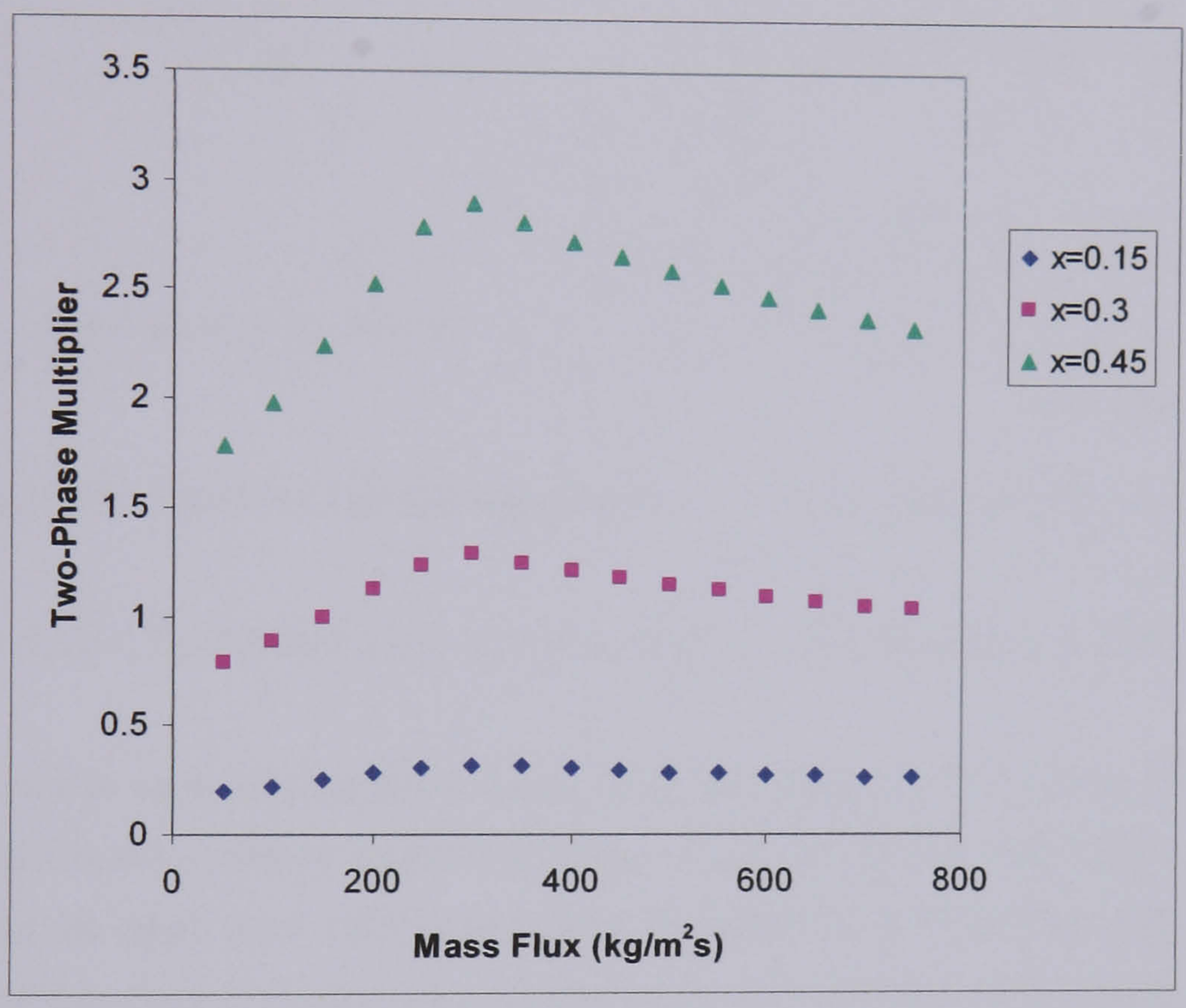

Figure 5.21 – Plot of Calculated Tubeside Two-Phase Multiplier at Different Qualities

A similar peak is observed in the predicted tube flow multiplier as is observed in the shellside data of Figure 5.19(b). As a result it was decided to examine the cause of the predicted peak in the tubeside data to help in explaining the mechanisms of a transition in the shellside data.

To enable a comparison with tubeside flow pattern maps the data of Figure 5.21 were re-plotted in terms of superficial vapour and liquid velocities using equations 5.5 and 5.6

$$\dot{v}_g = \frac{\dot{M}x}{\rho_g} \tag{5.5}$$

$$\dot{v}_l = \frac{\dot{M}(1-x)}{\rho_l} \tag{5.6}$$

To identify the location of the peak in Figure 5.21 the data were separated into two categories. In a similar manner to Figure 5.11, points corresponding to high mass flux data (>300 kg/m^{2}s) appear as full points and points at mass fluxes below the observed peak (<300 kg/m^{2}s) were plotted as hollow points. Figure 5.22(a) shows the re-plotted data of Figure 5.21. Figure 5.22(b) shows the horizontal tubeside two-phase flow pattern map of Taitel and Dukler (from Whalley, 1983).

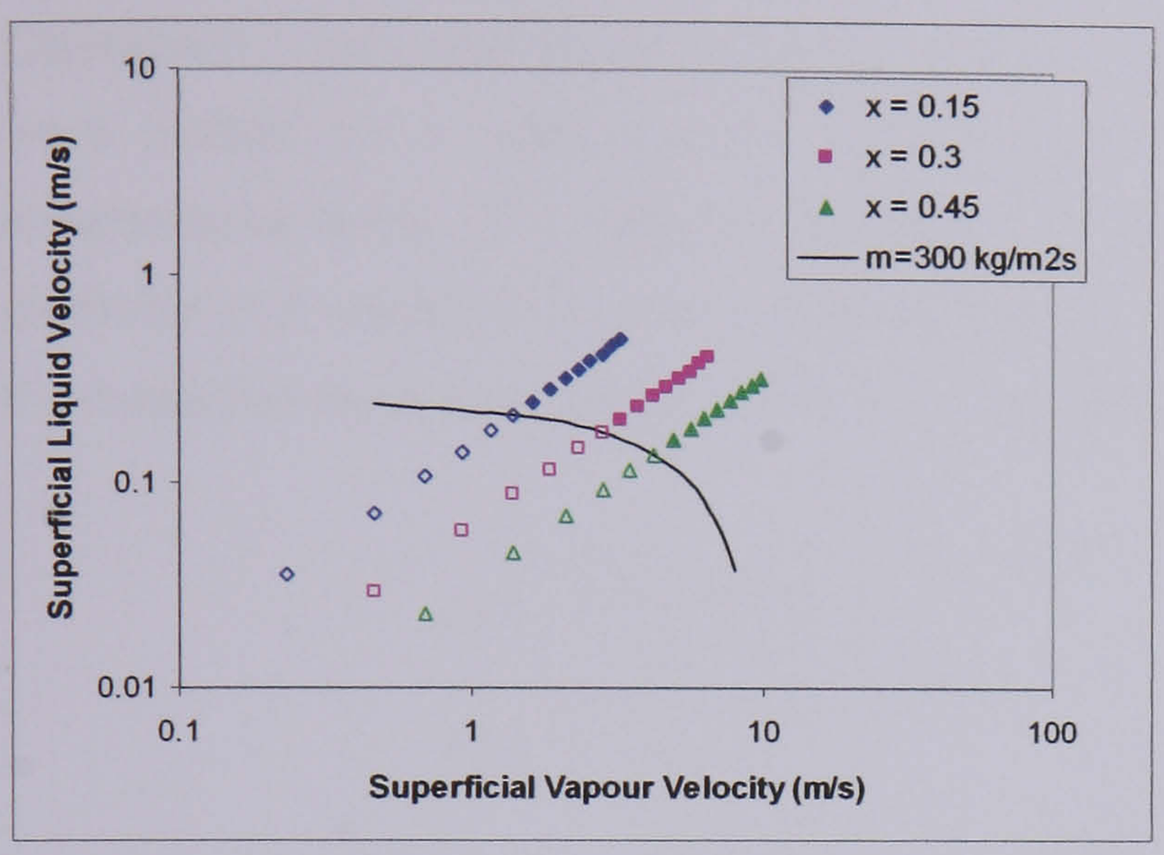

(a) – Re-plotted data in terms of phase velocities

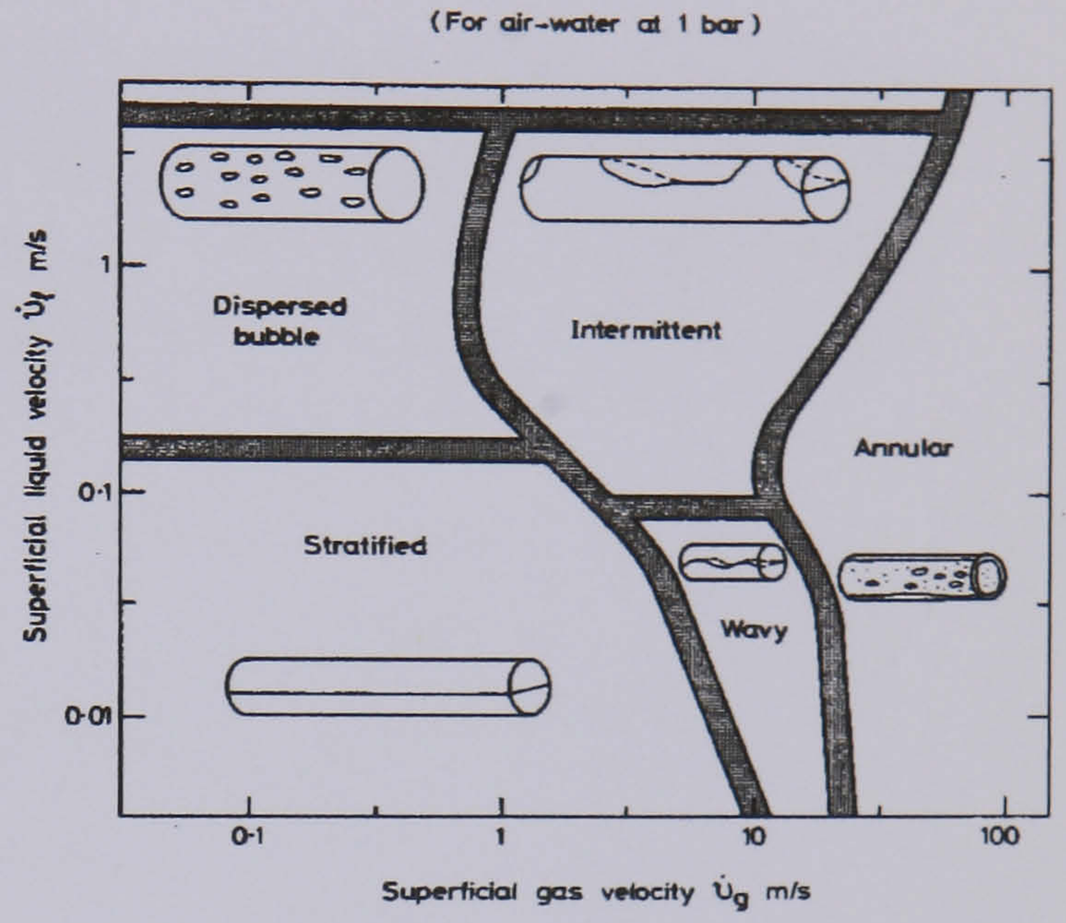

(b) – Taitel/Dukler flow pattern map

Figure 5.22 – Re-plotted mass flux data of 5.21 and tubeside flow pattern map

The transition in the data corresponds closely with the transition in the flow pattern map from stratified to dispersed bubble or intermittent flow, especially for the data at the higher vapour qualities (where the peak was more pronounced in Figure 5.21). It is clear that the peak in the two-phase multiplier data of Figure 5.21 corresponds with this type of flow pattern transition.

It was decided to make a comparison of the shellside data from Tests 1 - 3 with a correlation for deviation from stratified tubeside flow (Weisman et al, 1979) recommended by an HTFS design report (Whalley, 1983). The basic equation used to define the transition is:

$$\dot{v}_{lc} = 0.284(gD)^{0.455}\,\dot{v}_g^{\,0.091} \qquad (5.7)$$

Where $\dot{v}_{lc}$ is the critical liquid velocity of transition, g is acceleration due to gravity, D is the diameter of the tube in question and $\dot{v}_g$ the velocity of the vapour or gas phase. The liquid and vapour velocities are calculated from the mass flux and quality using equations 5.5 and 5.6. The transition criteria recommended by the HTFS report (Whalley, 1983) is the following: If relationship 5.8 is true the flow pattern is probably intermittent. If relationship 5.9 is true it is probably a stratified flow pattern. If the data is in the region of 5.10 it is unclear whether the flow pattern is stratified or intermittent.

$$\frac{\dot{v}_l}{\dot{v}_{lc}} > 2 \tag{5.8}$$

$$\frac{\dot{v}_l}{\dot{v}_{lc}} < 0.5 \tag{5.9}$$

$$0.5 < \frac{\dot{v}_l}{\dot{v}_{lc}} < 2 \tag{5.10}$$

Equation 5.7 was rearranged in terms of mass flux (M) and quality (x) and the relationships were plotted on a map (Figure 5.23) using the physical properties of the fluid in the experimental tests. The data from Tests 1 - 3 have also been plotted. The value of the diameter D in equation 5.5 was taken as twice the gap between the tubes as the flow area in the mass flux term was the crossflow + bypass area.

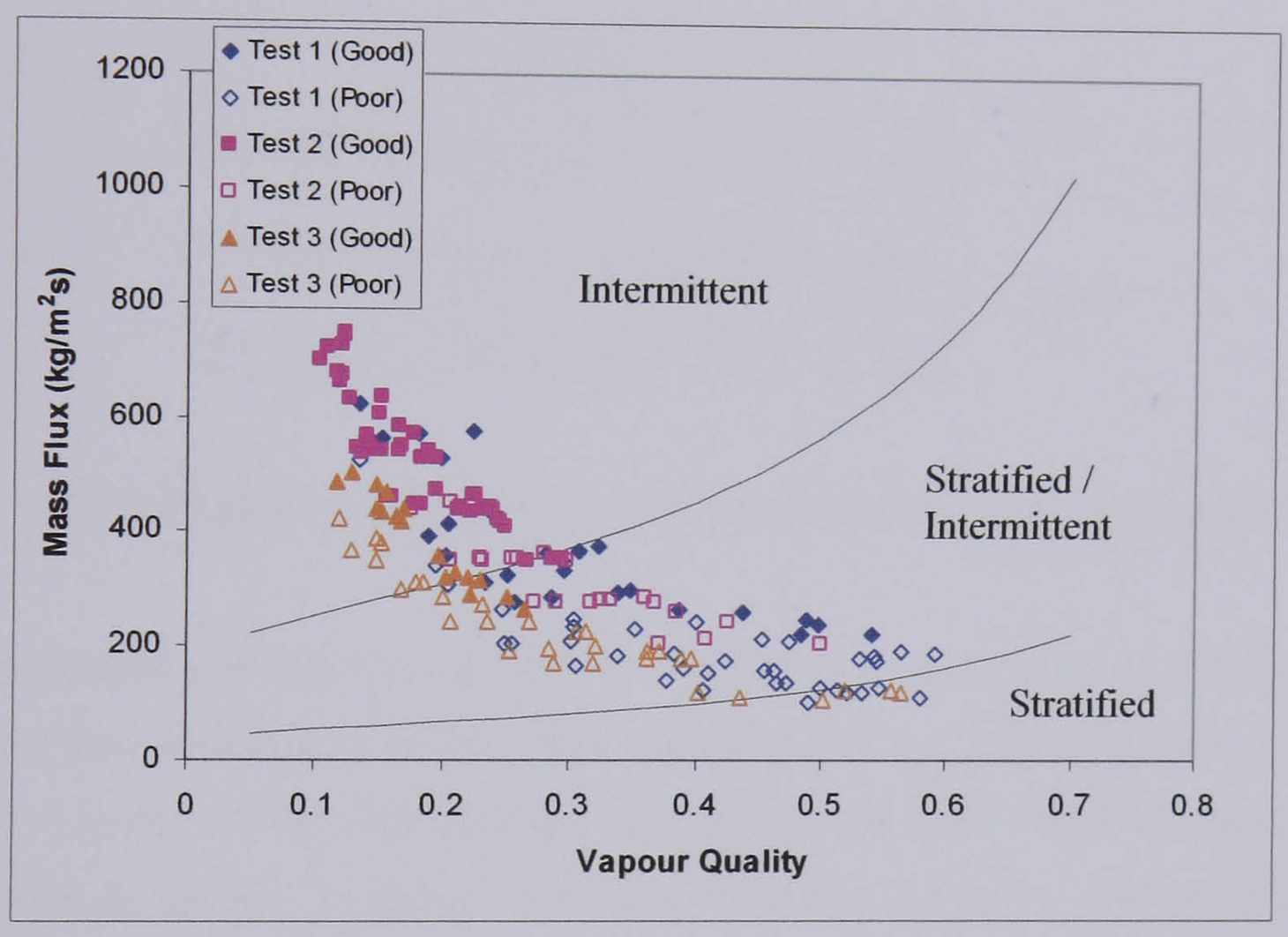

Figure 5.23 – Data from Tests 1 - 3 Plotted on Tubeside Map (Weisman et al, 1979)

Figure 5.23 shows that the data around the transition in the heat transfer results lays within the region where there is a possible transition from stratified flow, although the transition line appears to be going the opposite way from that in figure 5.14(b). It is possible that a similar transition to the tubeside case is occurring in the shellside flows however the mechanism for that transition remains unclear as intermittent flow was not observed in the shellside flow pattern map for Horizontal flow (Figure 5.14(b)).

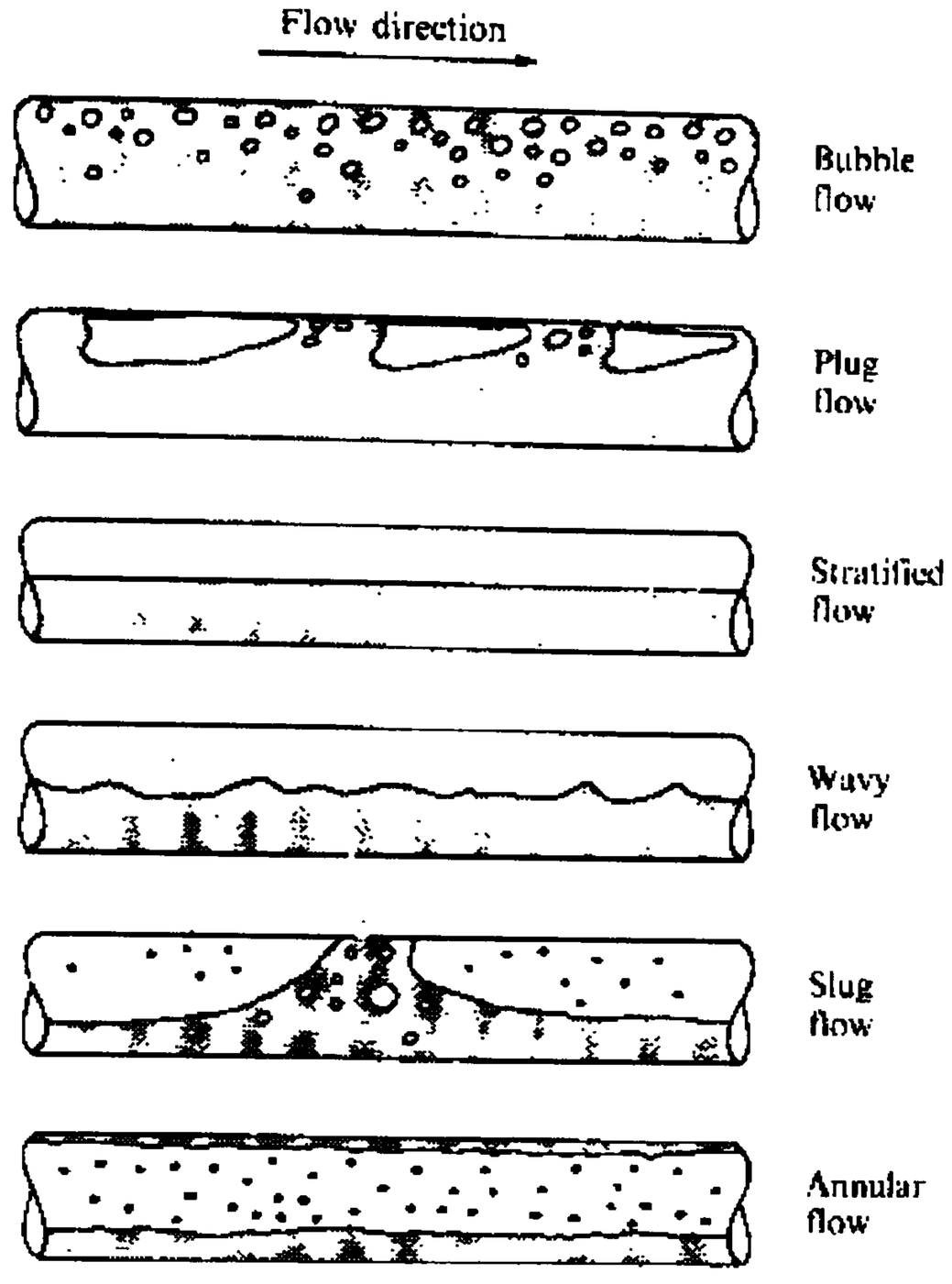

Figure 5.24 – Flow Patterns in Horizontal Tube Flow (Butterworth et al, 1977)

Figure 5.24 shows the common two-phase flow patterns in horizontal tubeside flow. Some of the flow patterns are analogous to the ones observed in the shellside flow pattern maps of Grant et al (Grant et al, 1979). The stratified flow pattern is observed once again, as is bubbly flow, annular flow is similar to spray flow and slug and plug to intermittent. In horizontal tubeside flow the transition mechanisms are clearer. From stratified flow an increase in gas velocity would cause wavy flow and then slug flow. At lower qualities bubbly flow would be dominant and at higher qualities annular flow provided the phase velocities were high enough. The homogeneous flow patterns from the maps of Figure 5.14 are essentially very similar to bubble and annular flow on the tubeside. A combination of increasing vapour qualities (from bubbly flow) and decreasing phase velocities would cause a flow pattern shift towards the direction of a stratified flow.

5.5 – Conclusion

Data from the experimental test programme were used in conjunction with data from previous tests (Chu et al, 1998; McNaught et al, 1999, 2000) to assess the effect of baffle orientation and sealing strips on shellside heat transfer and pressure drop.

A comparison of the heat transfer data suggested that an observed trend of deteriorating heat transfer coefficient was more pronounced with the vertical baffle cut arrangement. This would indicate that this geometry may be more prone to the deteriorating effect. The data for shellside pressure drop showed little difference between the horizontal and vertical baffle cut geometries.

In the tests with the inclusion of sealing strips there was significant improvement witnessed in the heat transfer performance of the evaporator and their inclusion did not prevent the deterioration in the shellside heat transfer coefficient. The data also suggested that the presence of sealing strips may lead to a slight increase in the shellside pressure drop.

Data from the experimental test programme highlighted that there is a significant decrease in the heat transfer performance of the evaporator over part of the test range. The deterioration appears to be closely related to decreasing values of the shellside mass flux and increasing values of the vapour outlet quality (especially with the vertical baffle cut orientation).

It has been proposed that the deterioration in performance may be due to a transition in the shellside two-phase flow pattern from a homogeneous type to a gravity separated stratified flow pattern. The values of mass flux and outlet quality at which deterioration occurs coincide with those predicted for the change in flow pattern on a shellside flow pattern map (Figure 5.14). In addition, measurements made of the tubeside outlet temperature at different tubes (Test 3 – Figure 5.16) are also consistent with the effect this flow pattern shift could have on tubeside heat transfer. Further support for the hypothesis is provided by the behaviour of the shellside two-phase pressure drop multiplier. There is an apparent peak in the value of the multiplier (Figure 5.19(b)) which coincides with the deterioration in the shellside heat transfer. This peak is also observed in correlations for the two-phase multiplier in horizontal tubeside flow (Figure 5.21). Flow pattern maps and transition correlations for tubeside flow suggest that the peak in the measured multiplier may be caused by a transition from a homogeneous to a stratified type of flow pattern.

CHAPTER 6 – Assessment of Existing Models

6.1 – Introduction

The literature review (Chapter 2) identified various types of models for designing shell & tube heat exchangers with boiling on the shellside. The most sophisticated of these models are computer programs which generally adopt the flow stream analysis description of shellside flow. The computer programs are usually based on correlations sometimes developed using experimental data taken from corporate test facilities. It is important that such models be tested for different experimental geometries and conditions to ensure that they produce accurate predictions beyond the range of the original test data on which the model was based. In this chapter the data collected from the experimental tests are compared with the predictions of one such program. This type of analysis is required to assess whether the current methods provide adequate prediction and to highlight any areas where the methods could be improved to more accurately predict the new data.

6.2 – The HTFS – TASC program

One of the principal software programs used in industry for the design of shell-and-tube heat exchangers is the HTFS TASC program. It is claimed by HTFS that their software is used widely throughout more than 400 leading process engineering companies. The shellside two-phase flow model is based on the flow stream type method outlined in the literature review. The following section contains more detail on the method of calculation involved in TASC. Further details of the proprietary TASC method are contained in HTFS Design Report 12 (Various Authors, 1988)

6.3 – TASC method

6.3.1 – Overall structure

The TASC program essentially carries out the thermal design of a Heat Exchanger based on the input of geometric and process variables. The program can be used to check if a proposed design will meet the process specifications or to design an exchanger based on the input of required process specifications. The principal calculations used by TASC for the thermal design of a baffled heat exchanger with boiling on the shellside are outlined in the following sections.

6.3.2 – Calculation of the required heat transfer area (A_{req})

One of the principal calculations of the TASC program is the required heat transfer area for a particular heat duty. Equation 6.1 gives the relationship for describing the rate of heat transfer through a small area of heat exchanger dA.

$$\dot{M}dh = U\Delta T dA \tag{6.1}$$

Where $\dot{M}$ is the shellside mass flowrate, dh is the change in shellside enthalpy across the area dA, U is the local overall heat transfer coefficient and ΔT is the local temperature difference. This equation (6.1) can be re-arranged and integrated to give the overall required shellside area (6.2).

$$A_{req} = \dot{M}\int_{h_{in}}^{h_{out}} \frac{dh}{U\Delta T} \tag{6.2}$$

Where h_{in} and h_{out} are the shellside inlet and outlet enthalpies. The solution of equation 6.2 requires the temperature-enthalpy profile in the exchanger. This profile is a curve of the shellside and tubeside temperatures as a function of the shellside enthalpy. In TASC, equation 6.2 is solved numerically by dividing the temperature enthalpy profile into a number of zones and using equation 6.3.

$$A_i = \dot{M}\left(\frac{dh}{U\Delta T}\right)_i \tag{6.3}$$

The equation is solved for each zone and the zonal areas summed to get A_{req} (U_i and ΔT_i are the average overall coefficient and temperature difference across the zone). The zone boundaries for the calculation are chosen such that the shellside and tubeside temperatures may be considered to vary linearly with the shellside enthalpy. The log-mean temperature difference (6.4) is used in the calculation of the zonal temperature difference ΔT_i.

$$\Delta T_i = \frac{(T-t)_2 - (T-t)_1}{\ln\dfrac{(T-t)_2}{(T-t)_1}} \tag{6.4}$$

Where $(T-t)_1$ and $(T-t)_2$ are the temperature differences between shellside and tubeside at the inlet and outlet of the zone respectively. TASC calculates the local shellside and tubeside heat transfer coefficients at the zone boundaries and uses them to calculate the local overall heat transfer coefficient using equation 6.5.

$$\frac{1}{U} = \frac{1}{\alpha_s} + r_s + \frac{y_w}{\lambda_w}\frac{d_o}{d_w} + \left(\frac{1}{\alpha_t} + r_t\right)\frac{d_o}{d_i} \tag{6.5}$$

Where;

α_s and α_t are the local shellside and tubeside heat transfer coefficients

r_s and r_t are the shellside and tubeside fouling resistances

y_w is the tube wall thickness

λ_w is the wall thermal conductivity

d_o and d_i are the tube outer and inner diameters

d_w is the tube mean diameter taken as halfway between the inner and outer diameter

The overall coefficient for the zone is calculated as the average of the local overall coefficients at each boundary (6.6)

$$U_i = \frac{(U_1 + U_2)}{2} \tag{6.6}$$

6.3.3 – Calculation of Overall Heat Transfer Coefficient and Temperature Difference

The program also calculates the average overall heat transfer coefficient and temperature difference across all the zones. These values are not actually used in the TASC program but are printed out for additional information. They are calculated using equations 6.7 and 6.8 respectively.

$$U_m = \frac{1}{A_{req}} \sum_{ZONES} U_i A_i \tag{6.7}$$

$$\Delta T_m = \frac{\dot{M}(h_{in} - h_{out})}{A_{req} U_m} \tag{6.8}$$

6.3.4 – Pressure Drop Method

The TASC program calculates the frictional, accelerational and (optionally) gravitational pressure drop. TASC calculates the pressure gradient for each of the zones of the temperature-enthalpy curve used in the required area calculation. These gradients are then multiplied by the zone length (which is known from the zone area calculation) to get the pressure drop for the zone. This method gives the pressure drop across the required exchanger (as it is based on the required area) and not the actual exchanger. When the

required and actual area is different the pressure drop across the actual exchanger is given by scaling the calculated value to the ratio of the actual tube length from the required tube length. The methods used to obtain the pressure gradients along the shellside of an exchanger are described in the following section.

6.3.5 – Shellside Frictional Pressure Drop

6.3.5 (a) – Flow Streams / Paths

The TASC shellside pressure drop is based on the stream or flow path analysis type model. The flow paths used are shown in Figure 6.1.

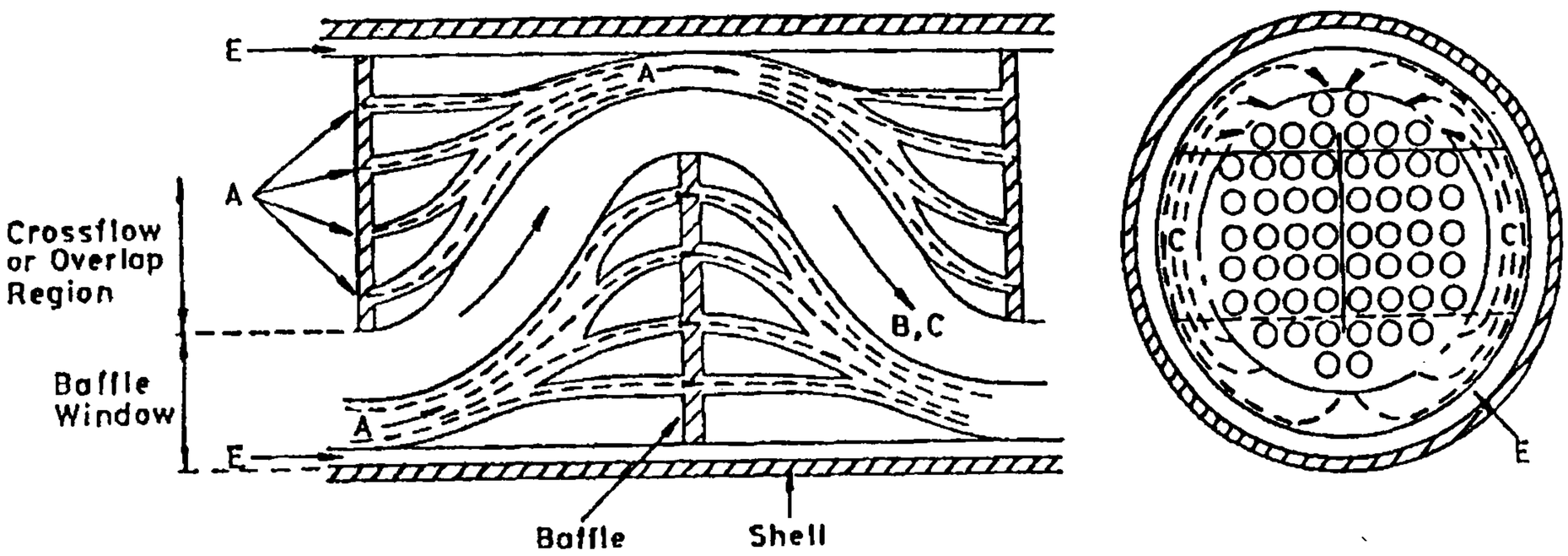

Flowstreams

A	=	Tube Baffle Leakage
B	=	Crossflow
C	=	Crossflow Bypass
E	=	Shell Baffle Leakage
W	=	A+B+C+E
	=	Window Flow in Baffle Window

Figure 6.1 – Shellside Flow Streams (Tinker, 1958)

The flow paths can be described as follows:

1(a) Crossflow

This is the flow normal to the tube bundle where most of the heat transfer takes place. The area used in the TASC calculation is at the tube bundle centre line which is calculated as the sum of the areas in between the tubes in one row as shown in Figure 6.2 (The shaded area). The total crossflow area used is the area between the tubes multiplied by the length of the zone being calculated.

$$A_{1a} = N_g l_i x \tag{6.9}$$

Where N_g is the number of gaps in the tube row and l_i is the length of the calculated zone.

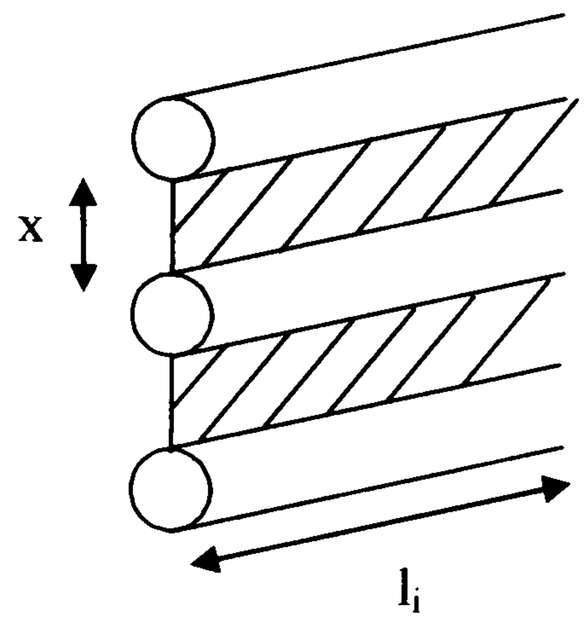

Figure 6.2 – Crossflow Area

1(b) – Crossflow Bypass

The bypass clearance is due to the necessary manufacturing clearance between the tube bundle and the shell. It allows some flow around the tube bundle rather than through it, reducing the fraction available for heat transfer.

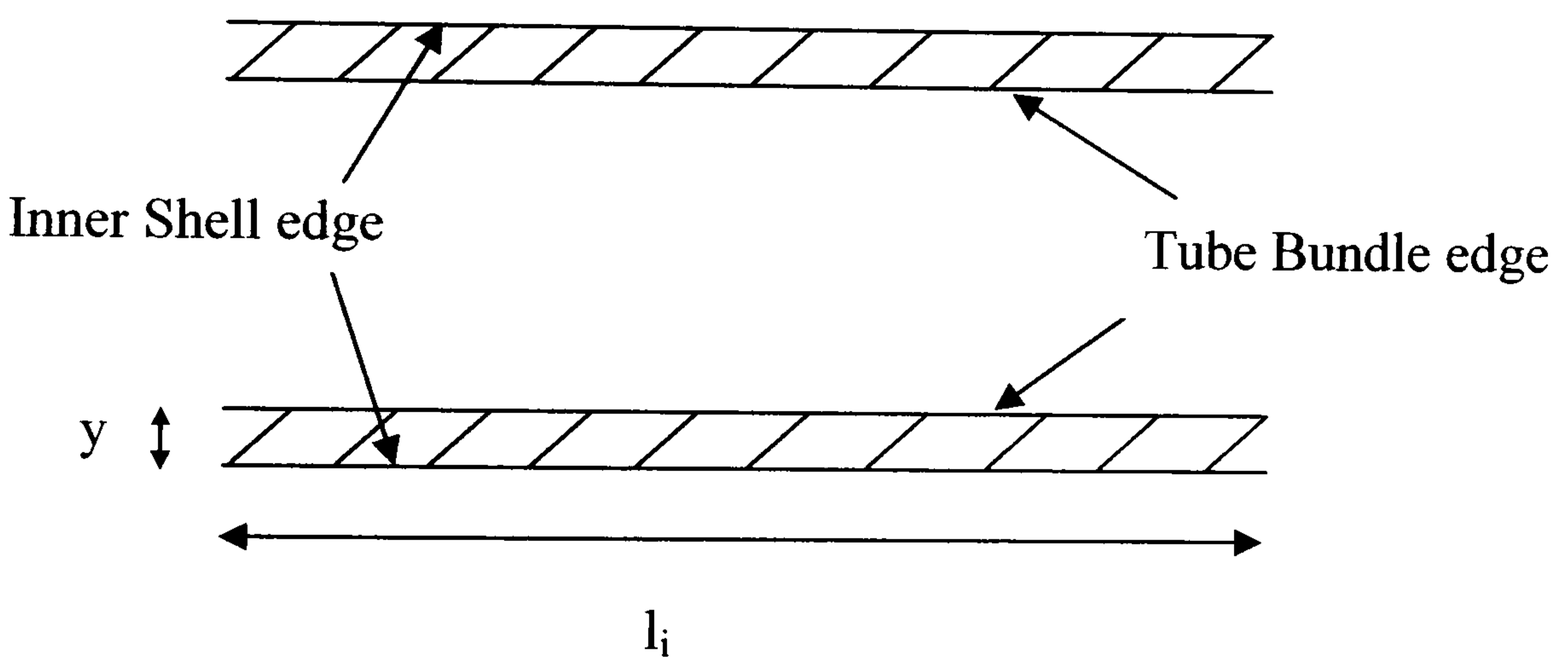

Figure 6.3 – Crossflow Bypass Area

The area associated with this stream is calculated using equation 6.10. The factor of 2 in the equation accounts for the bypass stream that exists on both sides of the tube bundle.

$$A_{1b} = 2l_i y \tag{6.10}$$

1(c) – In-line Pass Partition

The clearance due to an in-line pass partition, if present, acts in the same way as the crossflow bypass to reduce the fraction of flow available for heat transfer.

2(a) – Window Flow

The region between successive crossflow regions is where window flow occurs. Window flow is predominantly in the same direction as the tubes at 90^0 to the Crossflow. The area available for window flow is shown in Figure 6.4. It is calculated from the difference between the total area of the baffle window and the cross sectional area of the tubes in the baffle window.

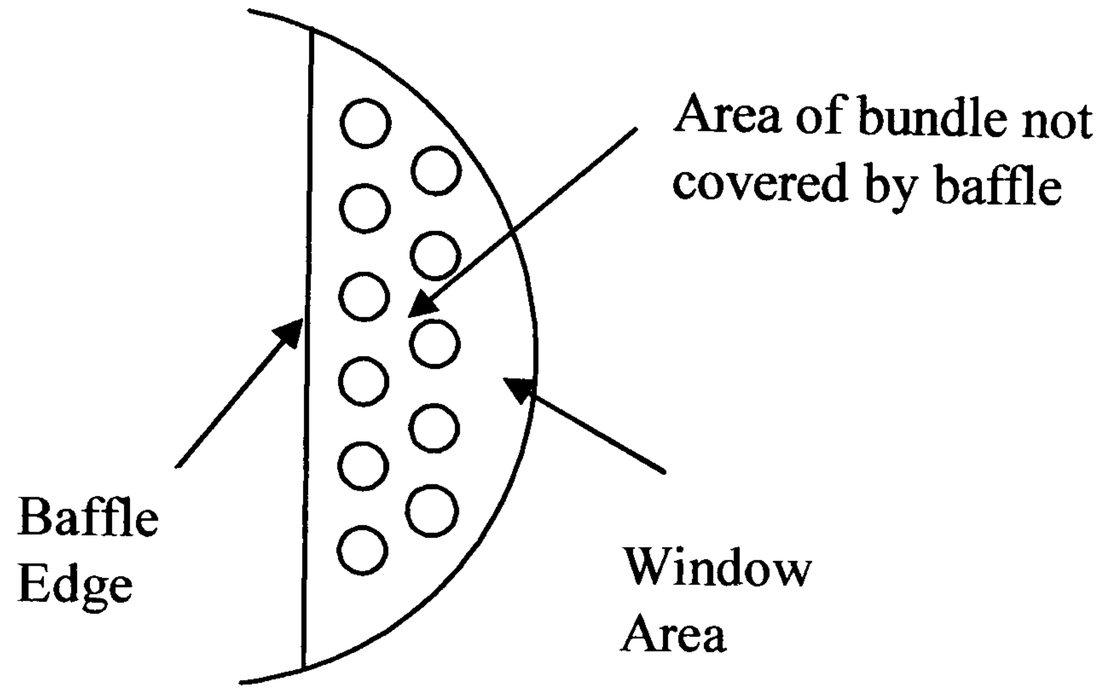

Figure 6.4 – Window Flow Area

2(b) – Window flow bypass

The window flow bypass exists for the same reason as the crossflow bypass. However, in this case the bypass flow is predominantly along the outside of the bundle rather than around it.

3(a) – Shell to Baffle Leakage

The manufacturing tolerance between the shell and the baffle acts as a leakage path. It allows flow through the compartment that is not available for heat transfer. The shell / baffle leakage area is defined as the area between the baffle outer edge and the shell where flow can leak through to the next baffle space.

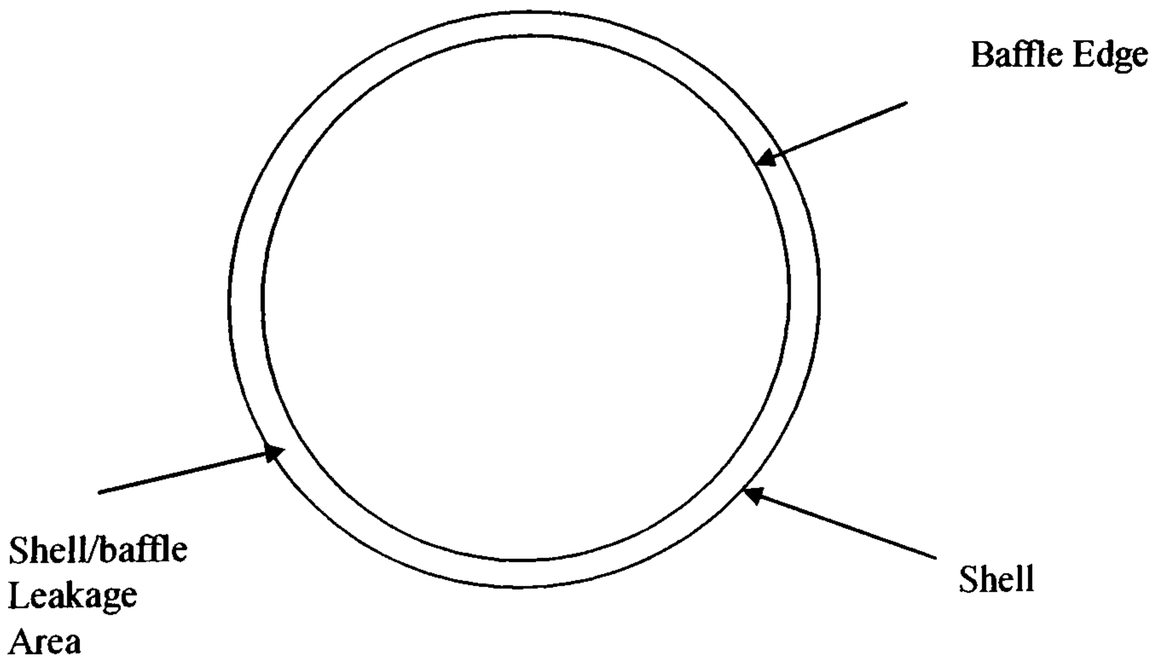

Figure 6.5 – Shell to Baffle Leakage Area

3(b) – Tube to Baffle Leakage Area

The manufacturing tolerance between the baffle and the outside of the tubes provides a further leakage path. The sum of all these small areas gives the overall area for tube/baffle leakage.

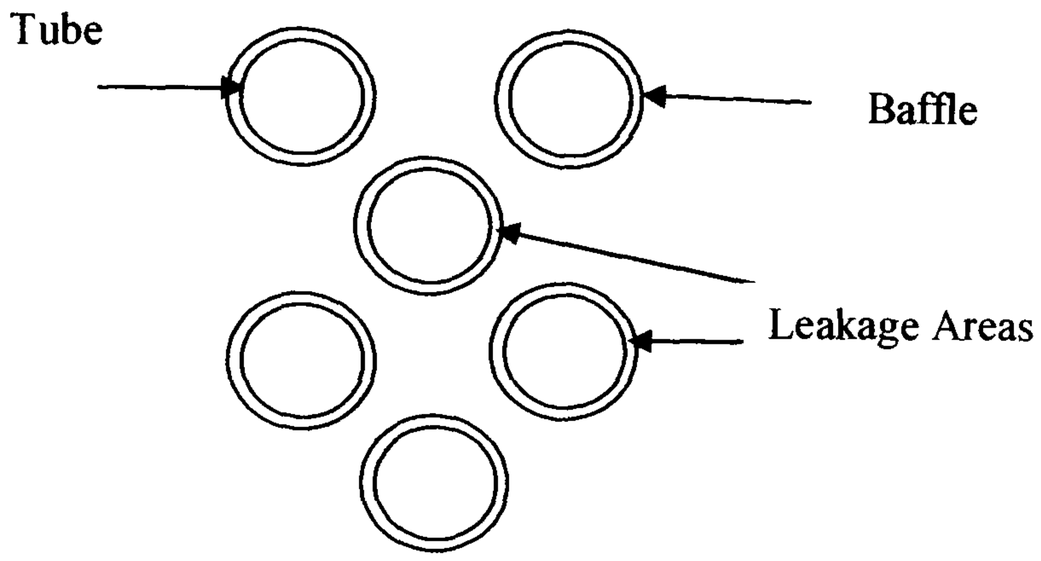

Figure 6.6 – Tube to Baffle Leakage Area

The flow stream model is based on establishing the flow distribution such that the pressure drops across parallel streams are the same. Thus for the streams shown in Figure 6.7 the following are true for pressure drop:

$$\Delta p_{total} = \Delta p_1 + \Delta p_2 = \Delta p_3 \tag{6.11}$$

$$\Delta p_{1a} = \Delta p_{1b} = \Delta p_{1c} \tag{6.12}$$

and for the mass flowrate:

$$\dot{M}_{total} = \dot{M}_1 + \dot{M}_3 \tag{6.13}$$

$$\dot{M}_1 = \dot{M}_2 \tag{6.14}$$

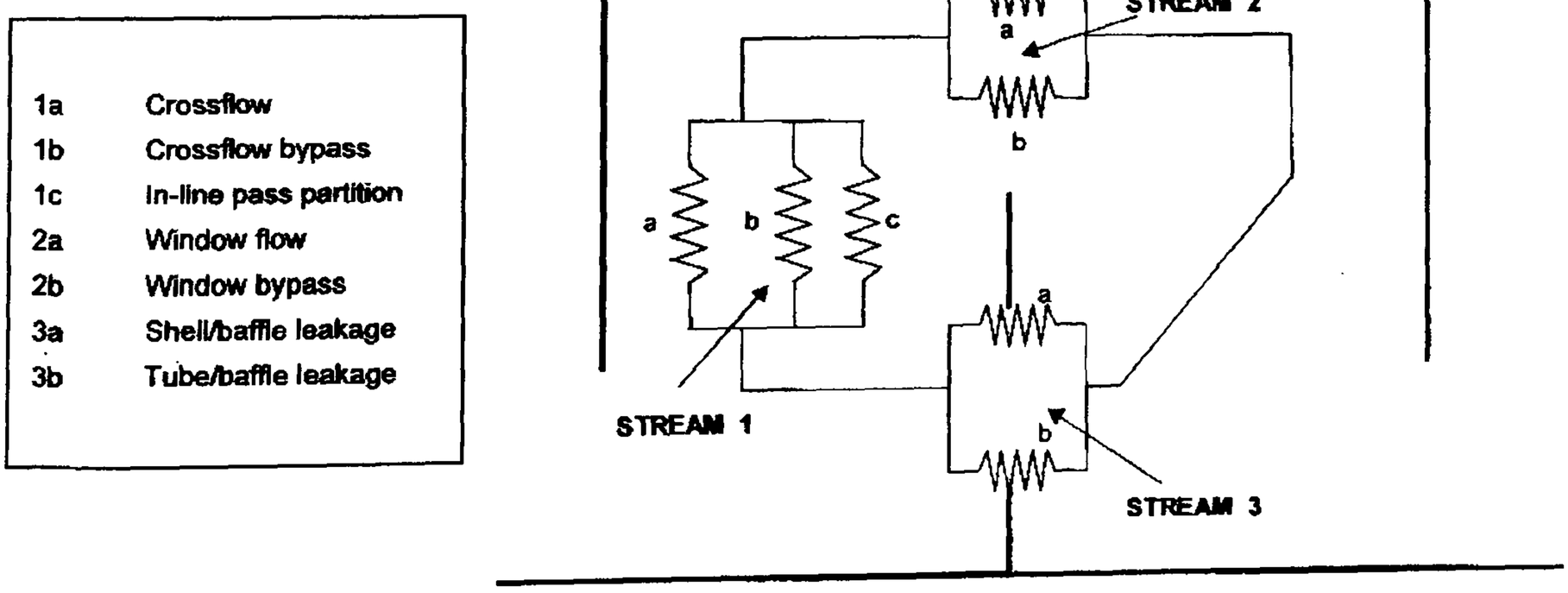

Figure 6.7 – Diagram of Flow Path Resistances in TASC Pressure Drop Model

Figure 6.7 displays the resistances in the crossflow paths (Stream 1), the window flow paths (Stream 2) and the baffle leakage paths (Stream 3). The model is based on the assumption that these three streams meet at some point in the following baffle space. Figure 6.8 contains a diagram of the flow path resistances showing the effect of the flow resistances over multiple baffle spaces. The small circular symbols at the beginning of each baffle space indicate the theoretical point at which the three streams are assumed to merge.

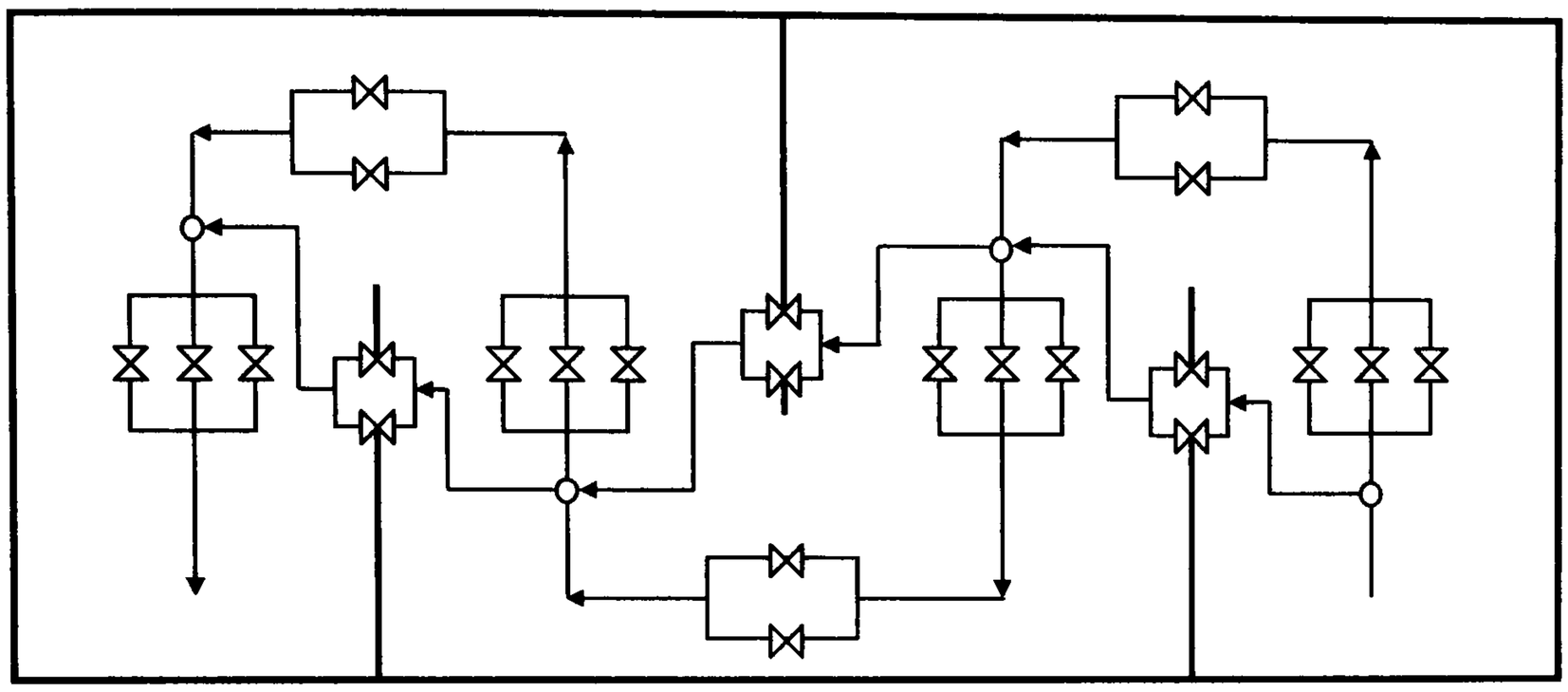

Figure 6.8 – Flow path resistances for multiple baffle spaces

For each stream in the TASC model the pressure drop can be defined in terms of mass flowrate by equation 6.15.

$$\Delta P = n\frac{\dot{M}^2}{2\rho A^2} \tag{6.15}$$

A is the area of the flow path, the expression $\frac{\dot{M}^2}{2\rho A^2}$ is defined as a 'velocity head' and n as the 'number of velocity heads' required to describe the pressure loss in the particular stream. For each of the flow streams there are relationships in TASC to calculate the value of n and subsequently the pressure drop.

6.3.5(b) – Relationships for Number of Velocity Heads Lost in Each Path

In TASC the number of velocity heads n is calculated for each flow path before the pressure drop is calculated using equation 6.15. The relationships for the number of velocity heads lost in each flow path during single-phase shellside flow are given in this section.

1(a) – Crossflow Stream

The number of velocity heads lost in the crossflow stream is calculated from the general pressure drop equation 6.16.

$$\Delta P_{1a} = 4N_c f_{1a} \frac{\dot{M}^2}{2\rho A_{1a}^2} \tag{6.16}$$

Where N_c is the number of rows crossed and f_{1a} is the single-phase friction factor.

Comparison of this equation with equation 6.15 gives equation 6.17 for the value of n.

$$n_{1a} = 4N_c f_{1a} \tag{6.17}$$

However this expression represents the number of velocity heads lost in a rectangular tube bundle where the crossflow area used is constant (the area at the circular tube bundle centre line). Equation 6.17 for n was modified by Moore (Moore, 1974) to account for the variable crossflow area in a circular tube bundle.

The friction factor for the crossflow stream f_{1a} is calculated from the correlation of Moore (Moore 1974) from previous data on crossflow test sections (Bergelin et al, 1958; Pearce, 1973). The friction factor is dependent on the tube pitch orientation and the crossflow Reynolds number, where the characteristic length used is the minimum distance between the tubes ($P_t - d_o$). The symbol P_t is the tube pitch and d_o the tube outer diameter.

1(b) – Crossflow Bypass Stream

Equation 6.16 is also used to describe the pressure drop in the crossflow bypass stream. The number of velocity heads lost is given by equation 6.18 since the area of the crossflow bypass is constant at any point in the tube bundle.

$$n_{1b} = 4N_c f_{1b} \tag{6.18}$$

When there are sealing strips in the bypass lane an additional two velocity heads are added for each pair of strips and equation 6.19 is used.

$$n_{1b} = 4N_c f_{1b} + 2N_{ss} \tag{6.19}$$

The friction factor f_{1b} is calculated using a correlation by Moore (Moore, 1974) based on the data of Bergelin (Bergelin et al, 1958).

1(c) – In-line Pass partition lane

The expressions for the number of velocity heads and friction factor in the pass partition lane are the same as those for the crossflow bypass stream.

2(a) and (b) – Window Flow and Window Bypass Streams

The window flow and window flow bypass streams are considered together in TASC. The number of velocity heads lost is calculated using the method of Wills and Johnston (Wills et al, 1981). In the method they produce expressions for losses which are described as 'geometric' and 'frictional'. The term 'geometric' applies to losses occurring due to turning of

the fluid in the window zone from one baffle space to the next. (These are irreversible losses caused by acceleration/deceleration as the fluid turns). The frictional losses are due to form drag and skin friction caused by the tubes and the shell in the window.

3(a) – Shell to Baffle Leakage Stream

The number of velocity heads lost in the shell to baffle leakage is again the sum of two terms. The expression is taken from the Moore method (Moore, 1974). One term describes the friction on the fluid as it passes between the baffle and the shell. It considers the path as flow through an annulus which is the length of the baffle thickness. The other term is considered to be due to losses caused by the directional change of the fluid as it flows round the baffle edge.

3(b) – Tube to Baffle Leakage Stream

The method used for the tube to baffle leakage stream is the same as with the shell to baffle leakage stream.

6.3.5(c) – Two-Phase

The shellside two-phase pressure drop model is developed from the single-phase model with two-phase multipliers being added to the 'frictional' and 'geometric' terms in the relationships for the number of velocity heads. The multipliers used in each flow stream are described in this section. In the Two-Phase model the flow is considered homogeneous as the vapour quality in each flow stream is assumed to be equal to the overall local quality.

1(a) – Crossflow Stream

The two-phase frictional multiplier ϕ_{lo}^2 is used to calculate the number of velocity heads lost with a two-phase flow in the crossflow stream. It is calculated using the method of Grant (Grant, 1972) and is given by equation 6.20.

$$\phi_{lo}^2 = 1 + \left\{ Y \left(\frac{\rho_l}{\rho_g} \frac{f_{go}}{f_{lo}} - 1 \right) \right\} \qquad (6.20)$$

Where f_{go} and f_{lo} are the single-phase friction factors calculated using the total mass flowrate with gas and liquid phase properties respectively. Y is given by the following:

$$x \le 0.98 \qquad Y = x + 0.15\sqrt{x} \qquad (6.21(a))$$

$$x > 0.98 \qquad Y = x + 0.15\sqrt{x} - 0.15x^{400} \qquad (6.21(b))$$

1(b) – Crossflow Bypass Stream

The crossflow bypass stream uses the same frictional two-phase multiplier as the crossflow stream. It also has an additional multiplier for the term that describes the flow directional change losses when there are sealing strips in the bypass lane. This multiplier is described as the 'non-frictional' multiplier A_f and is calculated using the zero interface-shear method (Grant, 1973) in equation 6.22.

$$A_f = \left\{1 - x + \left(x\sqrt{\frac{\rho_l}{\rho_g}}\right)\right\}^2 \tag{6.22}$$

The two-phase multipliers are used to alter the expression for the number of velocity heads in equation 6.19. The resultant expression for the number of velocity heads is equation 6.23.

$$n_{1b} = 4N_c\phi_{lo}^2 f_{lo(1b)} + 2A_f N_{ss} \tag{6.23}$$

1(c) – In-line Pass partition lane

The number of velocity heads lost in two-phase flow in the pass partition lane is given by the same expression as for the crossflow bypass, equation 6.23.

2(a) and (b) – Window Flow and Window Flow Bypass

The 'non-frictional' two-phase multiplier calculated from the zero interface-shear model (equation 6.22) is applied to the 'geometrical' loss term. The total number of velocity heads in the window and window bypass flow streams are calculated using:

$$n_2 = A_f n_{Geom} + n_{Frict} \tag{6.24}$$

Where n_{Geom} and n_{Frict} are calculated as in the single-phase case.

3(a) – Shell to Baffle Leakage

In the shell/baffle leakage stream there is a two-phase multiplier for the 'frictional' and 'geometric' terms. The frictional multiplier is calculated using equation 6.25.

$$\phi_l^2 = 1 + \frac{C}{X} + \frac{1}{X^2} \tag{6.25}$$

The parameter C is calculated by a method in the HTFS Handbook (Whalley, 1984), which is based on data of two-phase frictional pressure drop in tubes. X is the Martinelli parameter, calculated from equation 6.26.

$$X = \frac{(1-x)}{x}\sqrt{\frac{\rho_g}{\rho_l}}\sqrt{\frac{f_l}{f_g}} \tag{6.26}$$

f_l is the friction factor if the liquid phase were flowing alone in a tube. Similarly f_g is the friction factor for the gas phase. The 'geometric' multiplier is given by equation 6.27.

$$A_f = 1 - x + x\frac{\rho_l}{\rho_g} \tag{6.27}$$

The overall expression for the number of velocity heads is given by equation 6.28.

$$n_{3a} = 2\phi_l^2 f_{l(3a)} \frac{T_b}{T_{sb}} + 2.4 A_f \left(\frac{T_b}{T_{sb}}\right)^{-0.195} \tag{6.28}$$

3(b) – Tube to Baffle Leakage

The same procedure is adopted as with the shell to baffle leakage multipliers. The number of velocity heads is calculated from equation 6.29.

$$n_{3b} = 2\phi_{lo}^2 f_{l(3b)} \frac{T_b}{T_{tb}} + 2.4 A_f \left(\frac{T_b}{T_{tb}}\right)^{-0.195} \tag{6.29}$$

6.3.5(d) – Iterative Calculation Procedure for Shellside Pressure Drop

The TASC shellside pressure drop model is based on ensuring that the pressure drop and mass continuity constraints of equations 6.11-6.14 are satisfied. The procedure for calculating the shellside pressure drop is iterative and can be summarised as follows:

- Calculate flow areas in each flow stream/path.
- Estimate mass flows in each path
- Calculate number of velocity heads lost in each stream
- Use equation 6.15 to calculate each of the corresponding pressure drops
- Check equations 6.11-6.14, If they are satisfied the calculation is complete. If not the mass flowrate in each path is re-estimated and the calculation procedure repeated.

The mass flowrates are re-estimated using the following series of equations from the method of Moore (Moore, 1974). Some parameters also used in the equations are defined below.

$$S = \frac{A}{\sqrt{\frac{n}{2}}} \tag{6.30}$$

$$X_T = S_{1a} + S_{1b} + S_{1c} \tag{6.31}$$

$$\theta = \left[\left(\frac{X_T}{S_{1a}}\right)^2 \frac{N_{SS}}{N_C} + \frac{(N_C - N_{SS})}{N_C}\right]^{0.5} \tag{6.32}$$

$$A_M = \left[1 + \left(\frac{(S_{2a} + S_{2b})\theta}{X_T}\right)^2\right]^{0.5} \tag{6.33}$$

$$S_T = \frac{S_{2a} + S_{2b}}{A_M} + S_{3a} + S_{3b} \tag{6.34}$$

The new estimates of the mass flowrates are calculated as follows:

$$\dot{M}_{1a(i+1)} = \frac{1}{2}\left[\frac{\dot{M}_{TOT} A_{1a}}{S_T A_M}\frac{(S_{2a} + S_{2b})}{X_T} + \dot{M}_{1a(i)}\right] \tag{6.35}$$

$$\dot{M}_{1b(i+1)} = \frac{1}{2}\left[\frac{\dot{M}_{TOT} A_{1b}}{S_T A_M}\frac{(S_{2a} + S_{2b})}{X_T} + \dot{M}_{1b(i)}\right] \tag{6.36}$$

$$\dot{M}_{1c(i+1)} = \frac{1}{2}\left[\frac{\dot{M}_{TOT} A_{1c}}{S_T A_M}\frac{(S_{2a} + S_{2b})}{X_T} + \dot{M}_{1c(i)}\right] \tag{6.37}$$

$$\dot{M}_{2a+2b(i+1)} = \dot{M}_{1a(i+1)} + \dot{M}_{1b(i+1)} + \dot{M}_{1c(i+1)} \tag{6.38}$$

$$\dot{M}_{3a(i+1)} = \frac{1}{2}\left[\frac{\dot{M}_{TOT} A_{3a}}{S_T} + \dot{M}_{3a(i)}\right] \tag{6.39}$$

$$\dot{M}_{3b(i+1)} = \frac{1}{2}\left[\frac{\dot{M}_{TOT} A_{3b}}{S_T} + \dot{M}_{3b(i)}\right] \tag{6.40}$$

These estimates are then adjusted using the following equations to ensure that the mass balance is correct before the calculation procedure is repeated.

$$\dot{M}_{TOT(NEW)} = \dot{M}_{1a(i+1)} + \dot{M}_{1b(i+1)} + \dot{M}_{1c(i+1)} + \dot{M}_{3a(i+1)} + \dot{M}_{3b(i+1)} \tag{6.41}$$

$$\dot{M}_{1a(NEW)} = \frac{\dot{M}_{1a(i+1)}}{\dot{M}_{TOT(NEW)}}\dot{M}_{TOT} \tag{6.42}$$

$$\dot{M}_{1b(NEW)} = \frac{\dot{M}_{1b(i+1)}}{\dot{M}_{TOT(NEW)}}\dot{M}_{TOT} \tag{6.43}$$

$$\dot{M}_{1c(NEW)} = \frac{\dot{M}_{1c(i+1)}}{\dot{M}_{TOT(NEW)}}\dot{M}_{TOT} \tag{6.44}$$

$$\dot{M}_{2a+2b(NEW)} = \frac{\dot{M}_{2a+2b(i+1)}}{\dot{M}_{TOT(NEW)}}\dot{M}_{TOT} \tag{6.45}$$

$$\dot{M}_{3a(NEW)} = \frac{\dot{M}_{3a(i+1)}}{\dot{M}_{TOT(NEW)}}\dot{M}_{TOT} \tag{6.46}$$

$$\dot{M}_{3b(NEW)} = \frac{\dot{M}_{3b(i+1)}}{\dot{M}_{TOT(NEW)}} \dot{M}_{TOT} \tag{6.47}$$

6.3.6 – Accelerational pressure drop

The accelerational pressure drop due to the phase change in two-phase shellside flow, is calculated in TASC over each increment using equation 6.48.

$$\Delta P_{acc} = -\Delta MF \tag{6.48}$$

The momentum flux MF is given by equation 6.50.

$$MF = \dot{m}^2 \left\{ \frac{x^2}{\varepsilon_g \rho_g} + \frac{(1-x)^2}{(1-\varepsilon_g)\rho_l} \right\} \tag{6.49}$$

For boiling flows the phase change leads to a net drop in pressure. The void fraction term in equation 6.49 is calculated from an HTFS correlation for two-phase flow in tubes. The magnitude of the accelerational term is usually small in comparison with the frictional pressure drop calculated in section 6.3.5.

6.3.7 – Calculation of the Shellside Boiling Heat Transfer Coefficient

The TASC shellside heat transfer coefficient is calculated using equation 6.50.

$$\alpha_{boil} = \left(\alpha_{nb}^2 + \alpha_{cb}^2\right)^{1/2} \tag{6.50}$$

The expression comprises two terms; α_{nb} which describes the heat transfer due to the process of nucleate boiling and α_{cb} which describes the heat transfer due to convective boiling. The two terms are calculated independently and combined to produce the overall local coefficient. The calculation of the overall shellside coefficient was described in section 6.3.2. The coefficient calculated here is for use in equation 6.5 when calculating the overall coefficient for one shellside zone.

6.3.7(a) – Calculation of the nucleate boiling coefficient α_{nb}

The nucleate boiling coefficient is calculated using the method of Stephan-Abdelsalam (Stephan et al, 1978). The method contains a correlation comprising of a number of dimensionless groups containing fluid physical properties and process conditions such as fluid temperature and heat flux. The method of the correlation is described below.

Firstly the mean bubble diameter is calculated from equation 6.51.

$$d_b = 0.0146 \times 35B \tag{6.51}$$

Where B is the Laplace constant defined by equation 6.52.

$$B = \left(\frac{2\sigma}{g_n \left(\rho_l - \rho_g \right)} \right)^{1/2} \tag{6.52}$$

σ is the surface tension and g_n the acceleration due to gravity.

Equation 6.53 is then used to calculate the thermal diffusivity.

$$a = \frac{\lambda_l}{\rho_l c_{pl}} \tag{6.53}$$

λ_l is the liquid thermal conductivity and c_{pl} the liquid specific heat capacity.

The dimensionless parameters used in the correlation for the nucleate boiling coefficient are given the symbols X_1 , X_2, X_4, X_5 and X_{13}. They are calculated using equations 6.54 – 6.58.

$$X_1 = \frac{q d_b}{\lambda_l T} \tag{6.54}$$

$$X_2 = \frac{a^2 \rho_l}{d_b \sigma} \tag{6.55}$$

$$X_4 = \frac{\Delta h_l d_b^2}{a^2} \tag{6.56}$$

$$X_5 = \frac{\rho_g}{\rho_l} \tag{6.57}$$

$$X_{13} = \frac{\rho_l - \rho_g}{\rho_l} \tag{6.58}$$

Where q is the heat flux, T the fluid temperature and Δh_l the latent heat at that temperature.

The parameters above are combined to calculate the nucleate boiling coefficient in equation 6.59.

$$\alpha_{nb} = \frac{\lambda_l}{d_b} \times 0.23 X_1^{\,0.674} X_5^{0.297} X_4^{0.371} X_{13}^{(-1.73)} X_2^{0.35} \tag{6.59}$$

Of the dimensionless parameters in equation 6.59, X_1 is the most significant and generally the value of the nucleate boiling coefficient can be considered to be a function of the heat flux q.

6.3.7(b) – Calculation of the coefficient due to convective boiling α_{fc}

In the calculation of the boiling heat transfer coefficient in TASC it is assumed that the crossflow stream is the only one that makes a significant contribution to the heat transfer process. The coefficient due to convective boiling describes the influence the two-phase flow

characteristics in the crossflow can have on the value of the boiling coefficient. The coefficient is based on the HTFS method (McNaught, 1994). The method involves calculating the single-phase liquid convective heat transfer coefficient and multiplying by an enhancement factor F which describes the extra convection obtained due to the presence of the two-phase flow. The method is outlined in the following equations. Firstly, the single-phase heat transfer coefficient is calculated using the HTFS method (Wills, 1985). The principal correlation used is equation 6.60.

$$\alpha_l = a\frac{\lambda_b}{d_o}\mathrm{Re}_{1a}^{m}\,\mathrm{Pr}_b^{0.34} \tag{6.60}$$

The constants a and m are dependent on the value of the Reynolds number and on the tube bundle configuration. Equation 6.60 is solved in the following manner:

The mean bundle width is calculated from 6.61.

$$L_R = \frac{A_c}{L_b} - d_o \tag{6.61}$$

A_c is the crossflow area and L_b the space between shellside baffles.

The longitudinal and transverse pitches for a 30° layout are given by;

$$P_x = 0.866P_t \text{ and } P_y = P_t \tag{6.62}$$

Where P_t is the tube pitch.

The number of gaps is estimated with equation 6.63.

$$N_g = \frac{L_R}{P_y} \tag{6.63}$$

The minimum crossflow area is then calculated with equation 6.64.

$$A_m = N_g\left(P_y - d_0\right)L_b \tag{6.64}$$

The crossflow Reynolds number is calculated using the crossflow mass flowrate which is obtained from the resolved calculation of the shellside pressure drop model (equation 6.42).

$$\mathrm{Re}_{1a} = \frac{\dot{M}_c d_o}{\eta_b A_m} \tag{6.65}$$

η_b is the liquid viscosity at the bulk temperature.

The Prandtl number is given by equation 6.66.

$$\mathrm{Pr}_b = \frac{c_{pb}\eta_b}{\lambda_b} \tag{6.66}$$

The constants a and m in equation 6.60 are then given by the following relationships;

$$\mathrm{Re}_{1a} < 300 \qquad a = 1.309 \qquad m = 0.36 \tag{6.67(a))}$$

$$300 < \mathrm{Re}_{1a} < 200000 \qquad a = 0.273 \qquad m = 0.635 \tag{6.67(b))}$$

$$\mathrm{Re}_{la} > 200000 \qquad a = 0.124 \qquad m = 0.7 \tag{6.67(c)}$$

The value for α_l is then obtained from equation 6.60. A proprietary method for the enhancement factor for two-phase flow is then applied to give:

$$\alpha_{cb} = F\alpha_l \tag{6.68}$$

6.3.7(c) – Combined Boiling Coefficient

The combined shellside heat transfer coefficient is obtained from equation 6.50. The value of the heat transfer coefficient due to nucleate boiling is generally larger than the contribution due to the convective term and the highest heat transfer coefficients are obtained when the process of nucleate boiling is dominating.

6.4 – Generation of comparisons of experimental data with TASC

In order to produce a correct assessment of the predictions from the TASC program it was necessary to apply some further processing to the measured experimental data. Some of these adjustments were outlined in Chapter 4. In this section a description is given of the adjustments required to ensure a fair comparison of the TASC predictions for pressure drop and heat transfer with the experimental data in Chapter 5.

6.4.1 – Pressure drop

This section deals with the amendments required for comparing predictions of TASC with the experimental pressure drop data measured by transducer 1 and transducer 2 (Chapter 5). A diagram showing the transducer tapping points is given in Figure 6.9.

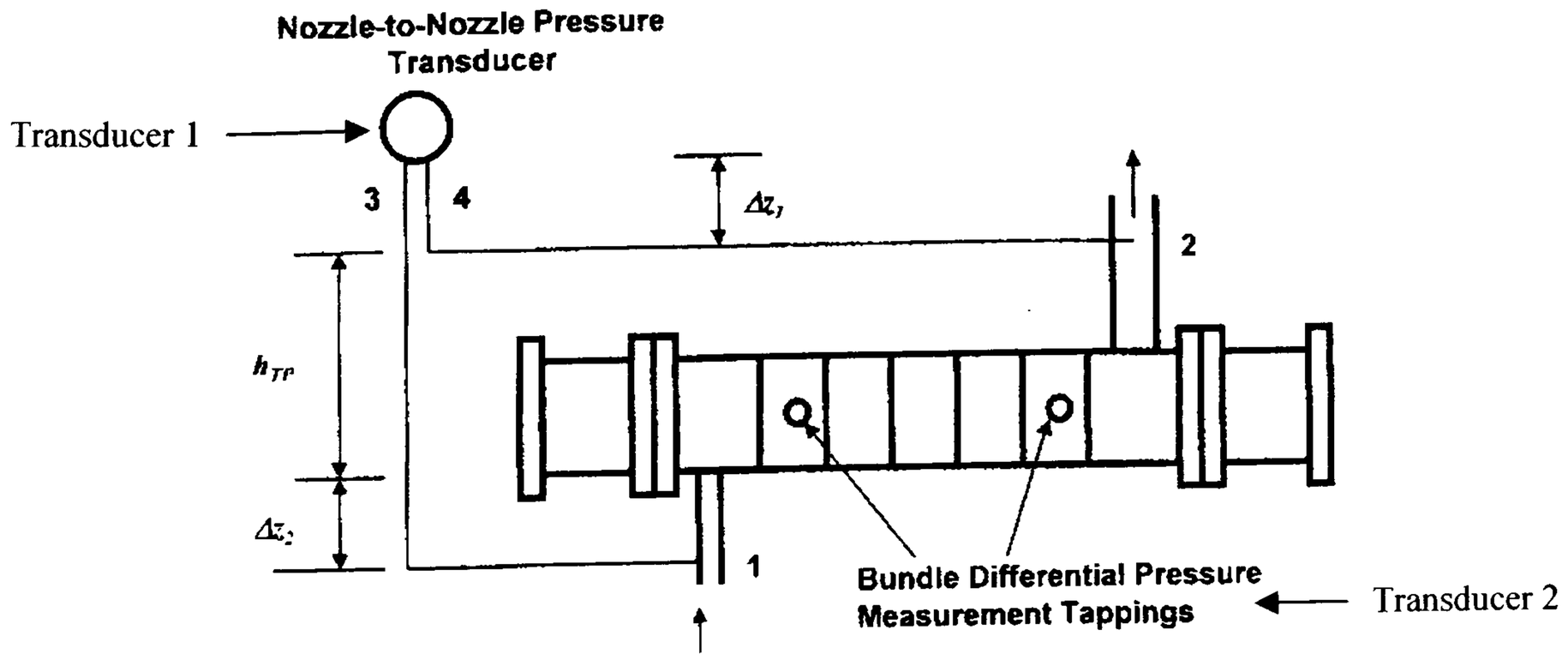

Figure 6.9 – Location of Pressure Transducer Tapping Points in Experimental Tests

6.4.1(a) – Generation of transducer 1 comparison

Since the pressure tappings are flush with the wall Transducer 1 measures the STATIC pressure drop between the inlet and outlet shellside nozzles. The measurement includes:

- Irreversible losses due to friction
- Accelerational change due to phase change
- Gravitational head due to the change in elevation across the pressure connections Allowance must be made for the fact that the shellside fluid has a different density from the liquid in the transmission lines from the nozzles to the transducer.
- Change in static pressure due to the fact the outlet nozzle is a larger diameter than the inlet nozzle.

The TASC prediction of the total pressure drop between the nozzles includes:

- The pressure drop due to irreversible losses calculated from the shellside model in 6.3.5.
- Accelerational change due to phase change
- The pressure drop in the end zones (1st and last baffle spaces)
- The pressure drop at the nozzles. The value reported in TASC is the stagnation pressure drop, i.e. the irreversible loss.
- Optionally the gravitational pressure drop.

The desired pressure drop to compare with TASC (when the TASC prediction of the gravity term is included) is the stagnation pressure drop ΔPo_{12} between points 1 and 2 in Figure 6.9. This value was calculated using equation 4.16 from the procedure outlined in Chapter 4

6.4.1(b) – Generation of transducer 2 comparison

The TASC program outputs values for the irreversible pressure drop across the length of the tube bundle. This pressure drop includes the pressure drop across the mid-spaces (as calculated in section 6.3.5) and the pressure drop across the end-zones (1st and last baffle space) where there are no leakage streams. To compare the experimental data with predictions of TASC the following method is adopted;

- Obtain the overall irreversible bundle pressure drop from the TASC output.
- Subtract the value of the pressure drop in the end zones (TASC produces an output that expresses the pressure drop in the end zones as a percentage of the total bundle pressure drop.
- Multiply the result by 0.8 to account for the fact that transducer 2 only covers 4/5 of the shellside between endzones.

6.4.2 – Heat Transfer

The heat transfer experimental data can be easily compared with the predictions of TASC using a term called the Area Ratio. TASC outputs the value of the area ratio which is defined by equation 6.69.

$$A_{Ratio} = \frac{A_{actual}}{A_{req}} \tag{6.69}$$

Where A_{actual} is the experimental heat exchanger surface area and A_{req} is the calculated required heat transfer area to perform the duty. The A_{req} term is calculated using equation 6.2. The accuracy of the TASC prediction to the experimental data can be observed from this ratio. If the ratio is greater than unity it suggests TASC is over-predicting the heat transfer rate as it predicts a smaller exchanger could produce the measured value. Similarly a ratio less than unity implies TASC is under-predicting the heat transfer rate.

6.5 – Comparison of TASC with Experimental Data

The data collected from the experimental facility were examined in Chapter 5. In this section the predictions of the TASC program are compared with the heat transfer and pressure drop data of the various tests. Details of the individual tests can be found in Chapter 5.

6.5.1 – Pressure Drop

6.5.1(a) – Single-Phase

Figures 6.10 – 6.13 show the TASC predictions plotted against the measured experimental values (Processed as in section 6.4) for the tests involving the single-phase liquid flowing on the shellside.

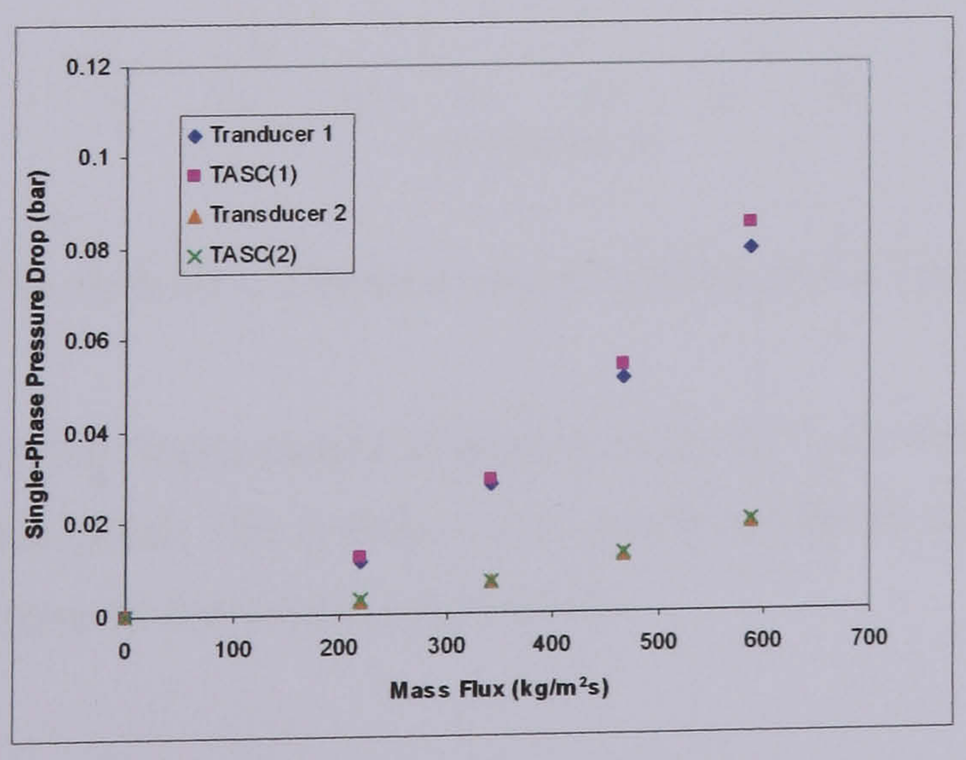

Figure 6.10 – Single-Phase Predictions for Test A (Chu et al, 1998)

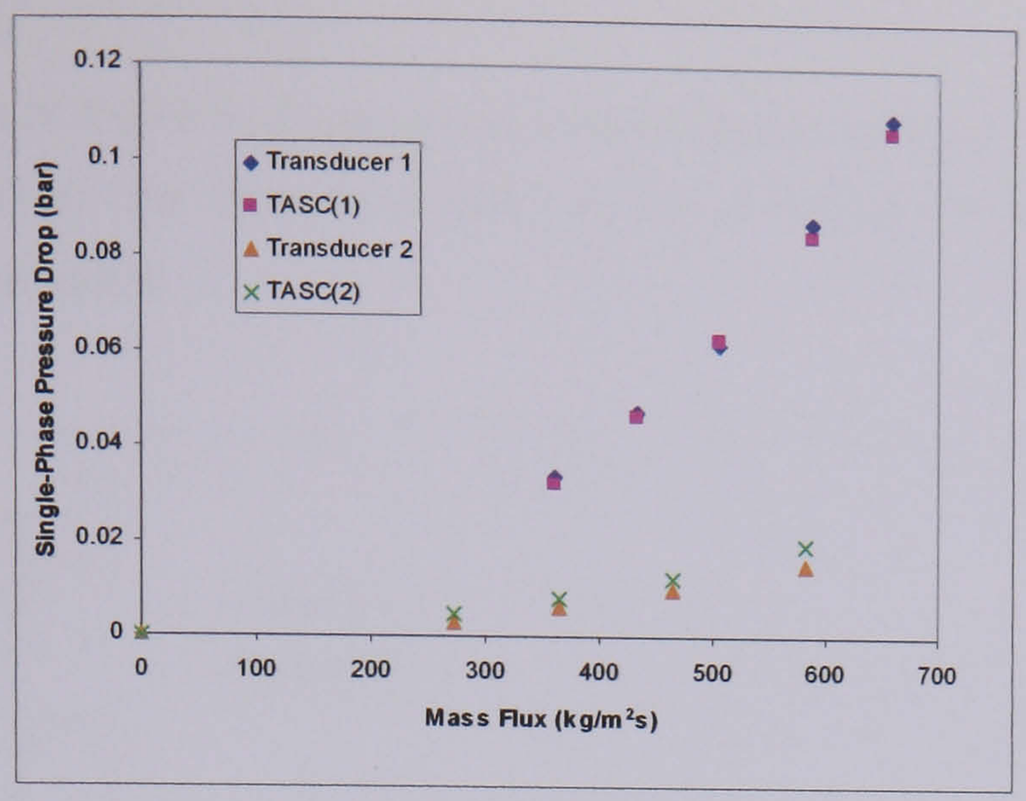

Figure 6.11 – Single-Phase Predictions for Test B (McNaught et al, 1999,2000)

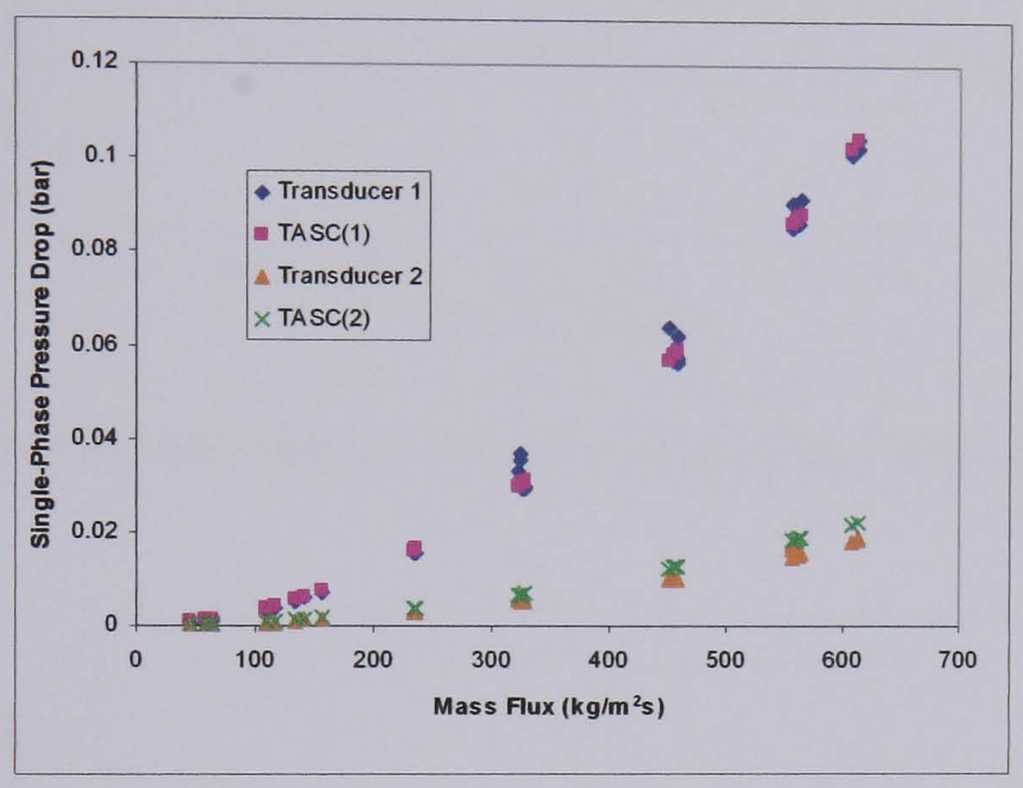

Figure 6.12 – Single-Phase Predictions for Test 1

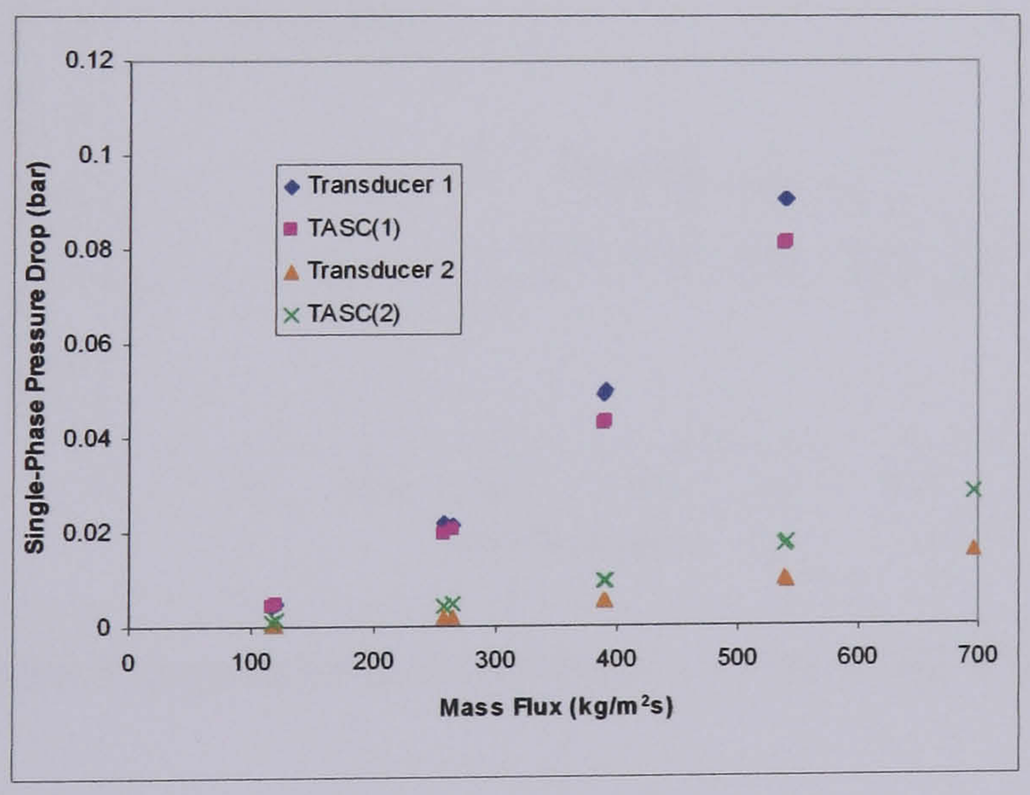

Figure 6.13 – Single-Phase Predictions for Test 2

The TASC prediction of the liquid phase pressure drop for both Transducer points 1 and 2 appears to be reasonably good. The trends are correctly predicted and the absolute values of the pressure drop are close to the TASC predictions.

6.5.1(b) – Two-Phase

The TASC predictions of the two-phase pressure drop data are shown in Figures 6.14 – 6.18. The data is presented in the form of a ratio of the predicted TASC value to the actual measured experimental value.

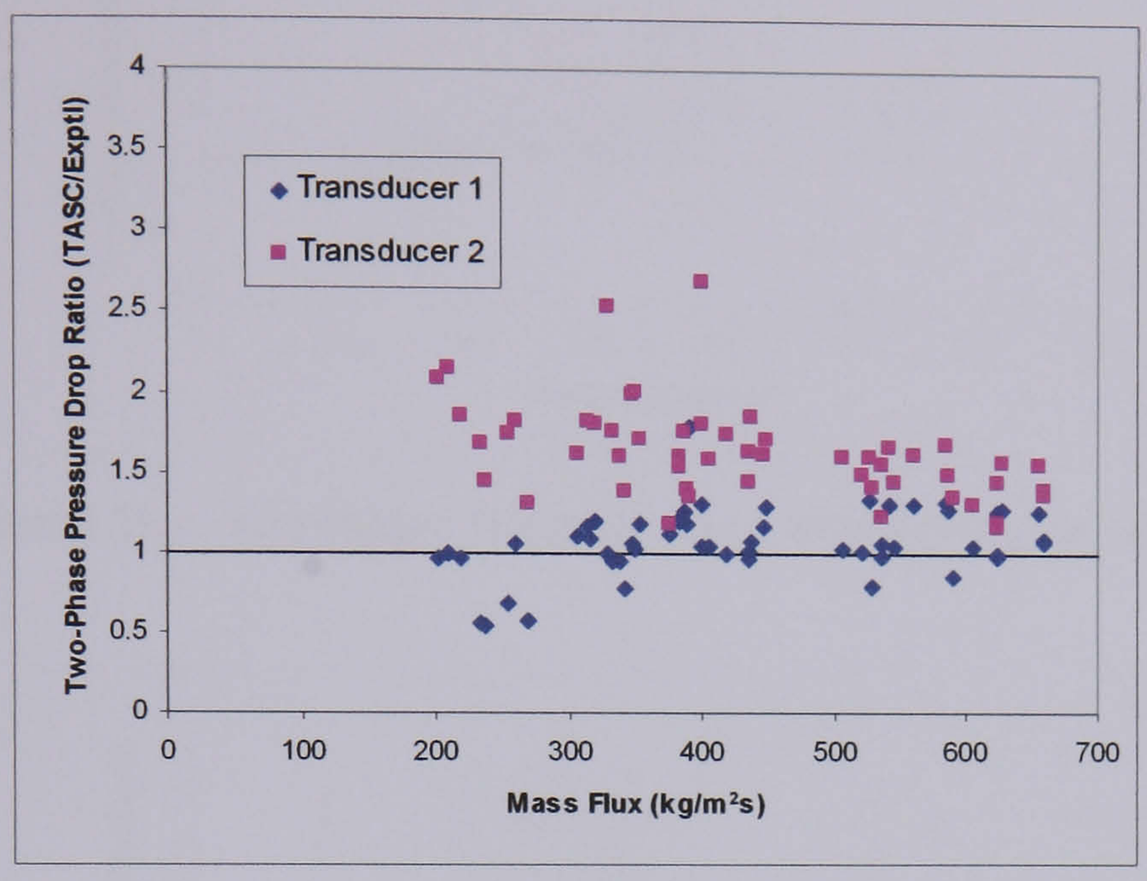

Figure 6.14 – Two-Phase Pressure Drop Predictions for Test A (Chu et al, 1998)

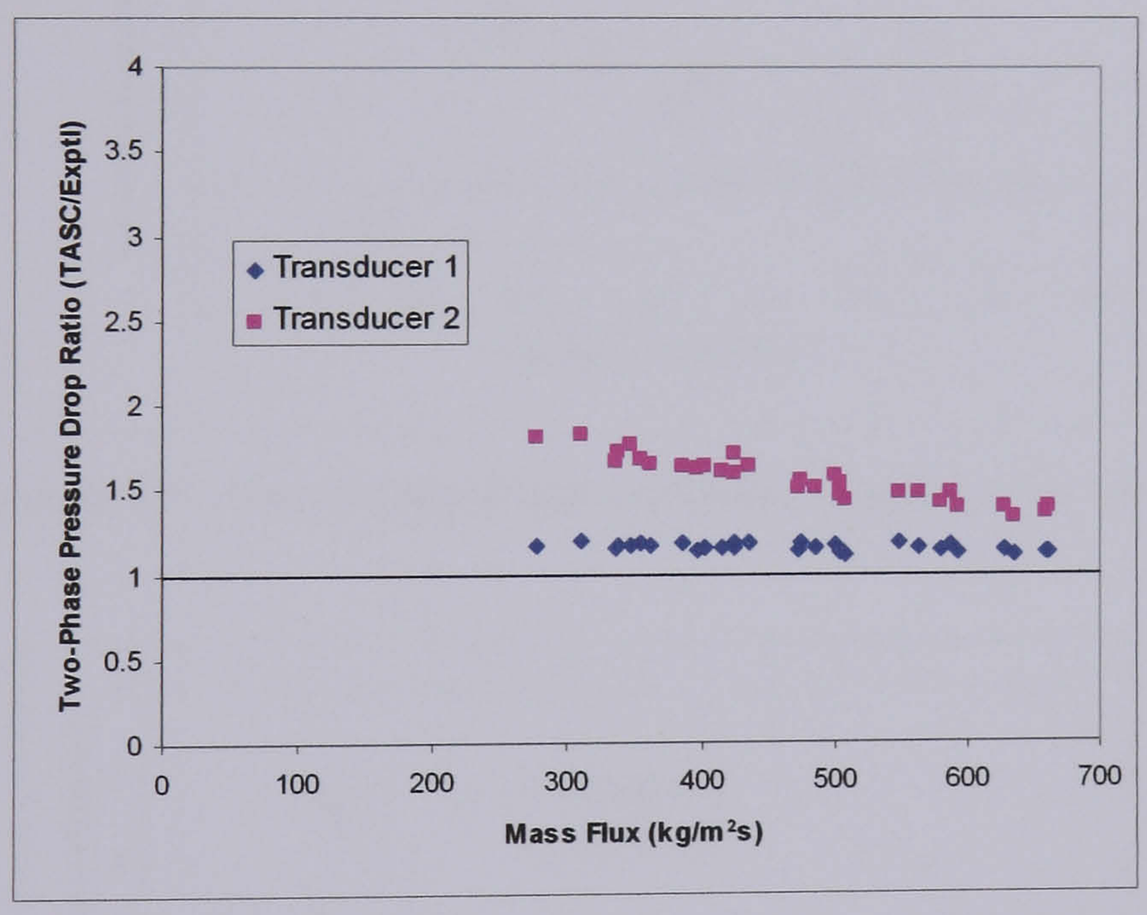

Figure 6.15 – Two-Phase Pressure Drop Predictions for Test B (McNaught et al, 1999, 2000)

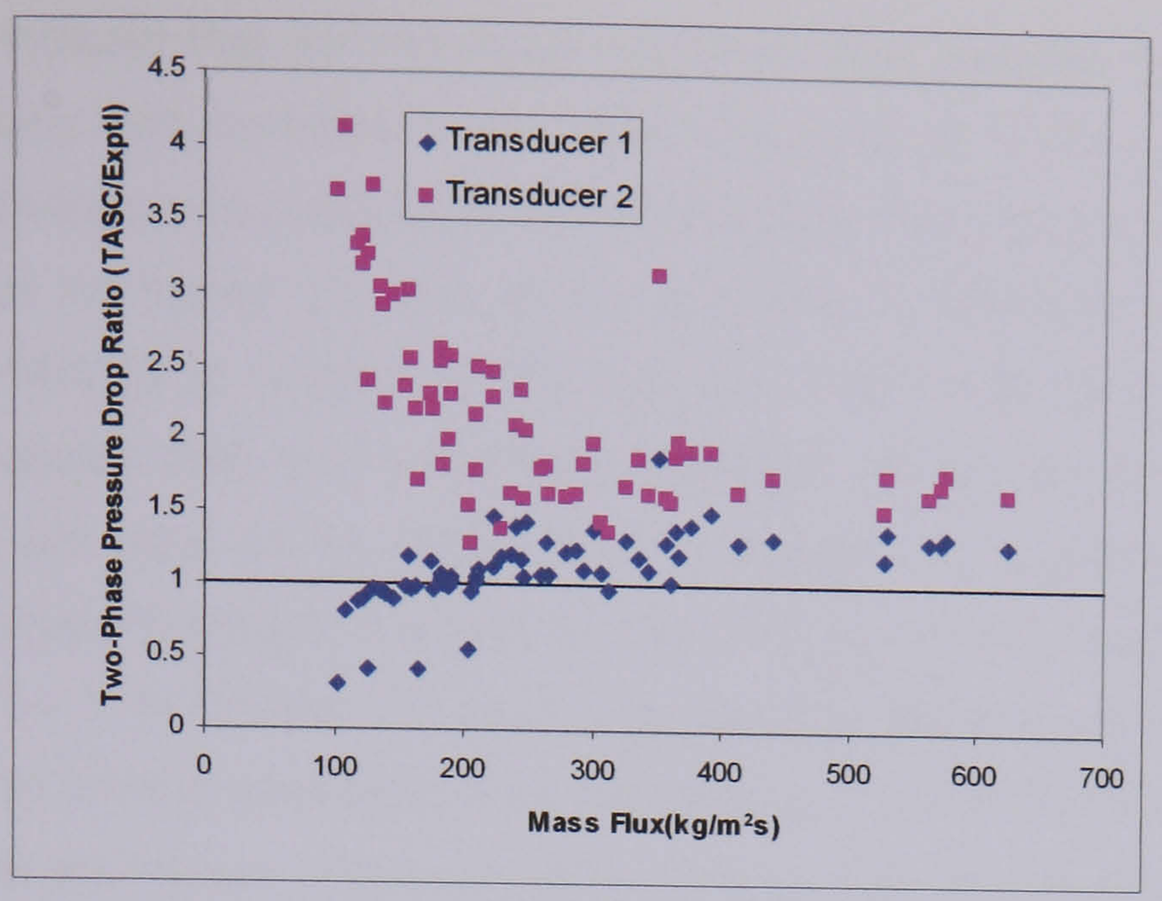

Figure 6.16 – Two-Phase Pressure Drop Predictions for Test 1

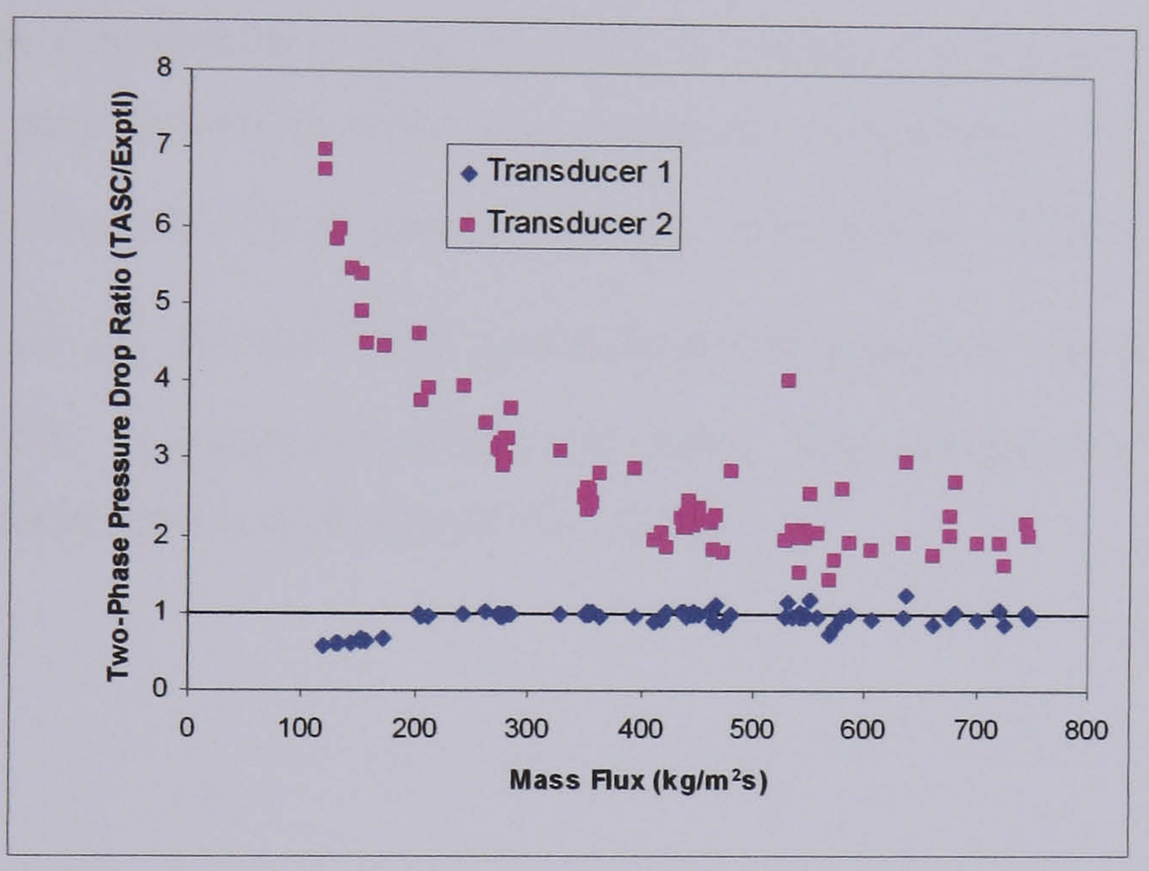

Figure 6.17 – Two-Phase Pressure Drop Prediction for Test 3

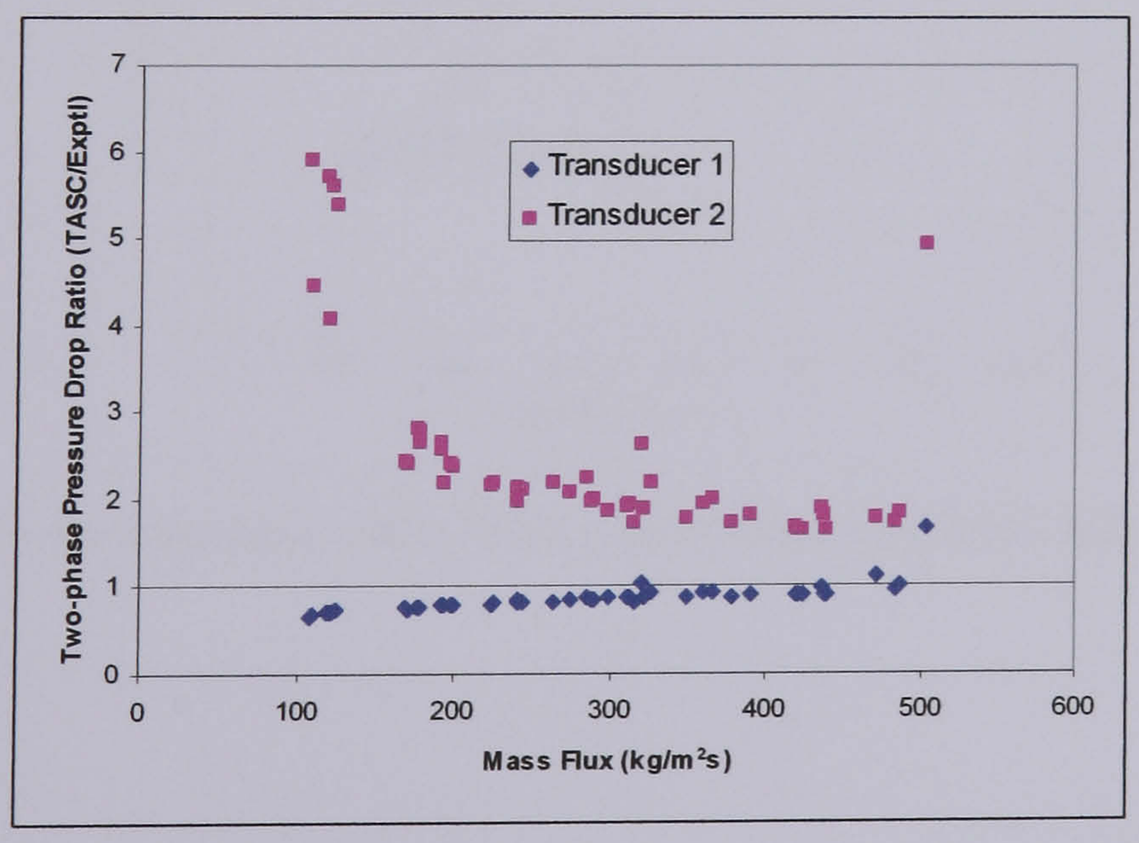

Figure 6.18 – Two-Phase Pressure Drop Prediction for Test 3

Figures 6.14–6.18 indicate that the two-phase pressure drop between the shellside nozzles (Transducer 1) is fairly well predicted. It was seen from Chapter 5 (Figures 5.8(a) – (e)) that the measured nozzle-to-nozzle pressure drop is much larger than the shellside pressure drop. It would appear that the higher accuracy of the prediction of the nozzle-to-nozzle pressure drop in Figures 6.14-6.18 is caused by the fact that TASC can more accurately predict pressure drop in nozzles than in the shellside geometry. In general the predictions of the Transducer 2 data are poor as the TASC method appears to over-predict the two-phase shellside pressure drop. This trend is extremely apparent at the low mass fluxes especially in the data for Tests 1 - 3. In Chapter 5 it was proposed that there could be a change in two-phase flow pattern to a more separated flow pattern at the low mass fluxes. The TASC flow model assumes that the vapour quality in each shellside flow stream is equal to the overall quality at that point in the shell (i.e – a homogeneous flow pattern with uniform quality). A change to a more separated type of two-phase flow pattern may be causing a decrease in the measured two-phase pressure drop causing TASC to produce such a large over-prediction. In Chapter 5 a peak was observed when the measured two-phase pressure drop multiplier based on the total flow with liquid properties (ϕ_{lo}^2) was plotted against mass flux (Figure 5.18(b)). The value of ϕ_{lo}^2 for the TASC predictions was evaluated for the test conditions to assess whether TASC correctly predicted this trend. The comparison of the TASC and experimental values are shown in Figures 6.19 - 6.21.

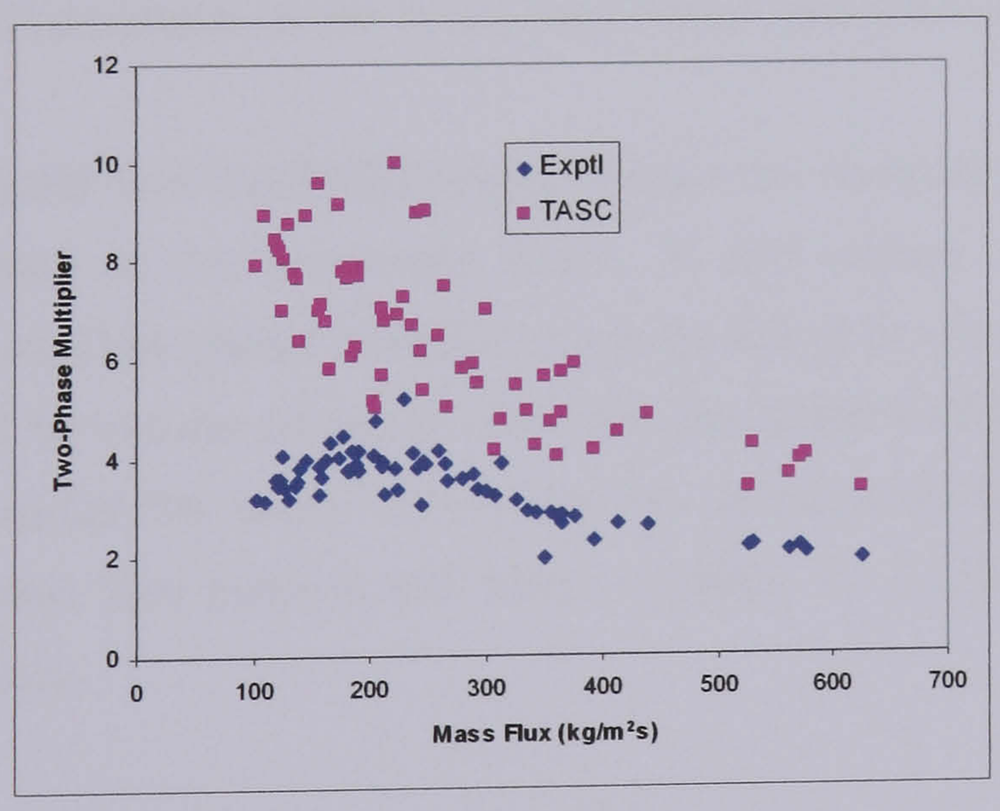

Figure 6.19 – Comparison of the TASC Two-Phase Multiplier with Test 1 data

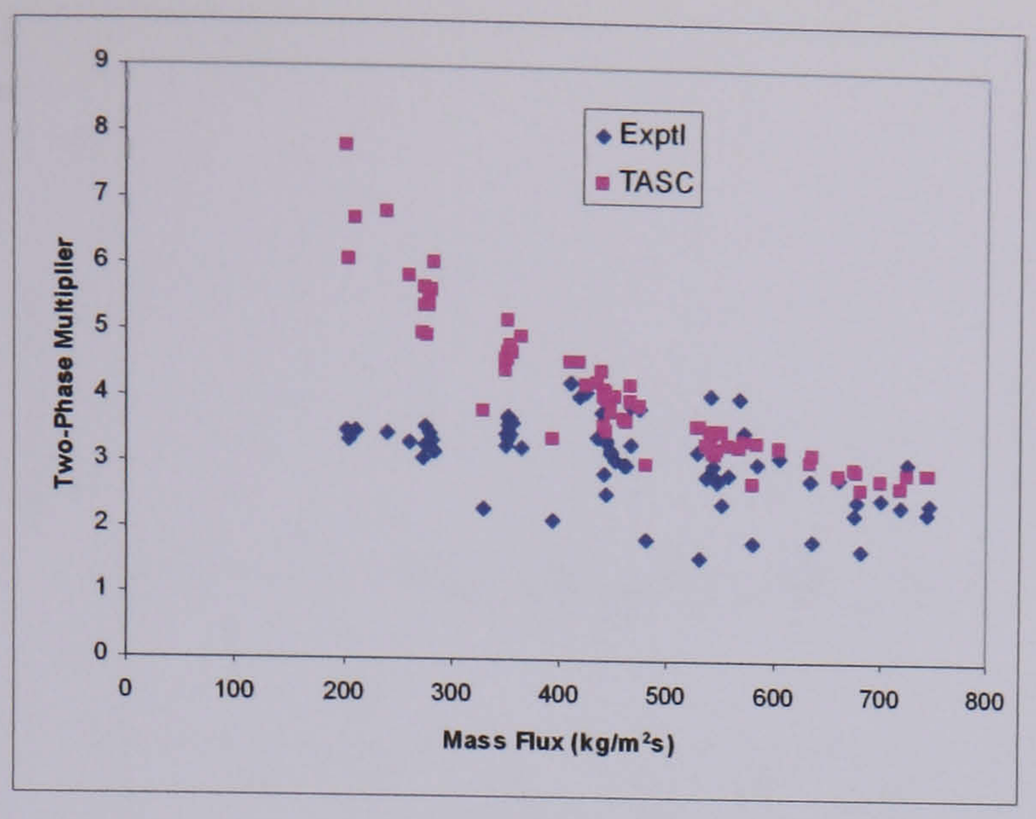

Figure 6.20 – Comparison of the TASC Two-Phase Multiplier with Test 2 data

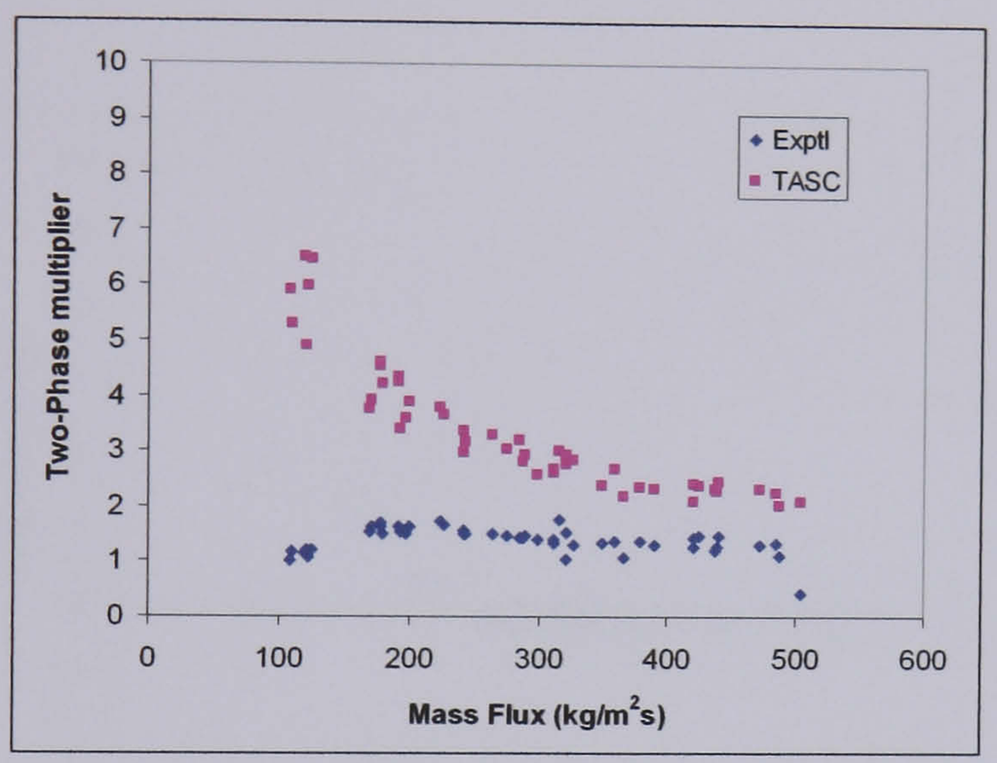

Figure 6.21 – Comparison of the TASC Two-Phase Multiplier with Test 3 data

Figures 6.19 - 6.21 indicate that the TASC program does not correctly predict the trend of the two-phase multiplier data at the low mass fluxes. It was shown in Chapter 5 that this behaviour of the measured two-phase multiplier could be linked to a change in two-phase flow pattern, as is predicted by in-tube pressure drop and flow pattern correlations. The failure of the TASC model to predict the same trend may be attributed to the fact that the model assumes a homogeneous flow pattern and does not allow for a change in two-phase flow pattern at low mass fluxes.

6.5.2 – Heat Transfer

In Chapter 5 it was observed that the value of the boiling heat transfer coefficient dropped at the low mass fluxes indicating that a flow pattern transition may be occurring causing vapour blanketing around some of the tubes. Figures 6.22 – 6.26 contain plots of the TASC area ratio against mass flux for all the experimental tests. The area ratio term is described in section 6.4.2.

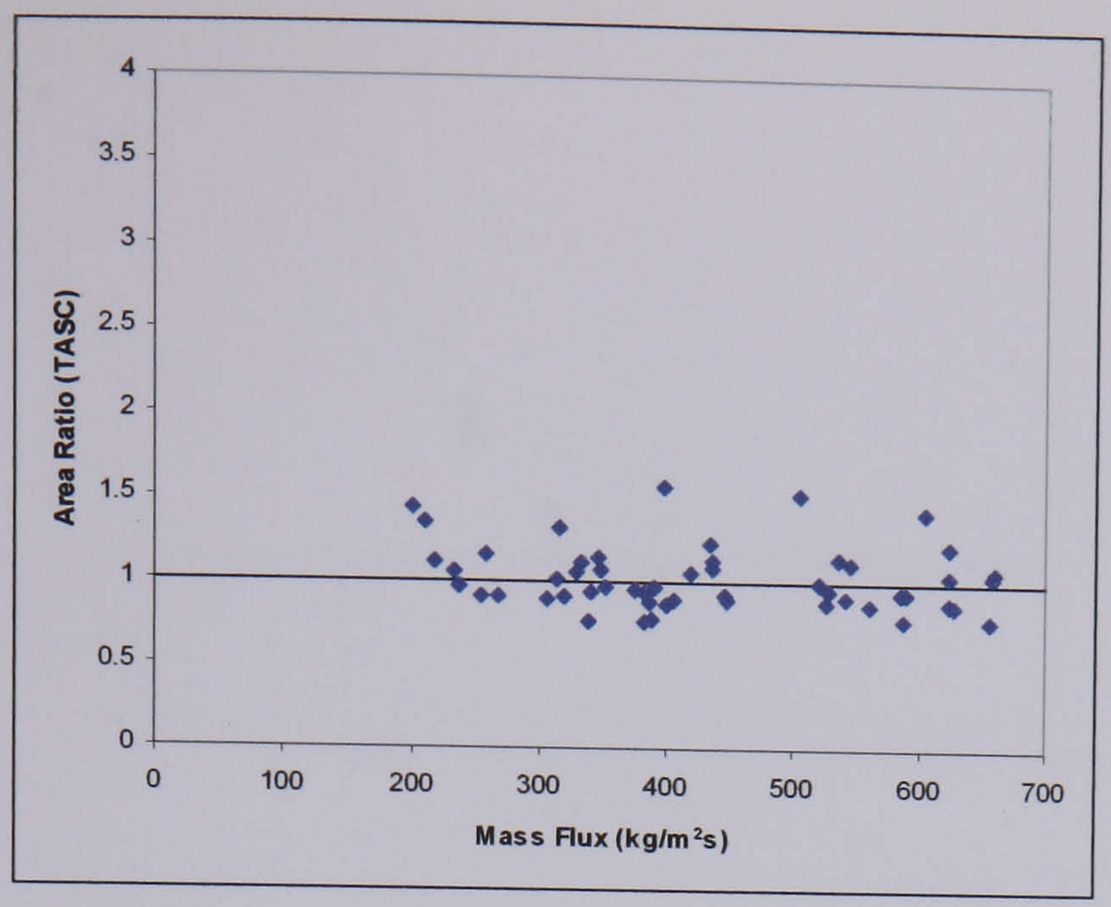

Figure 6.22 – TASC Area Ratio for Test A (Chu et al, 1998) – horizontal baffle

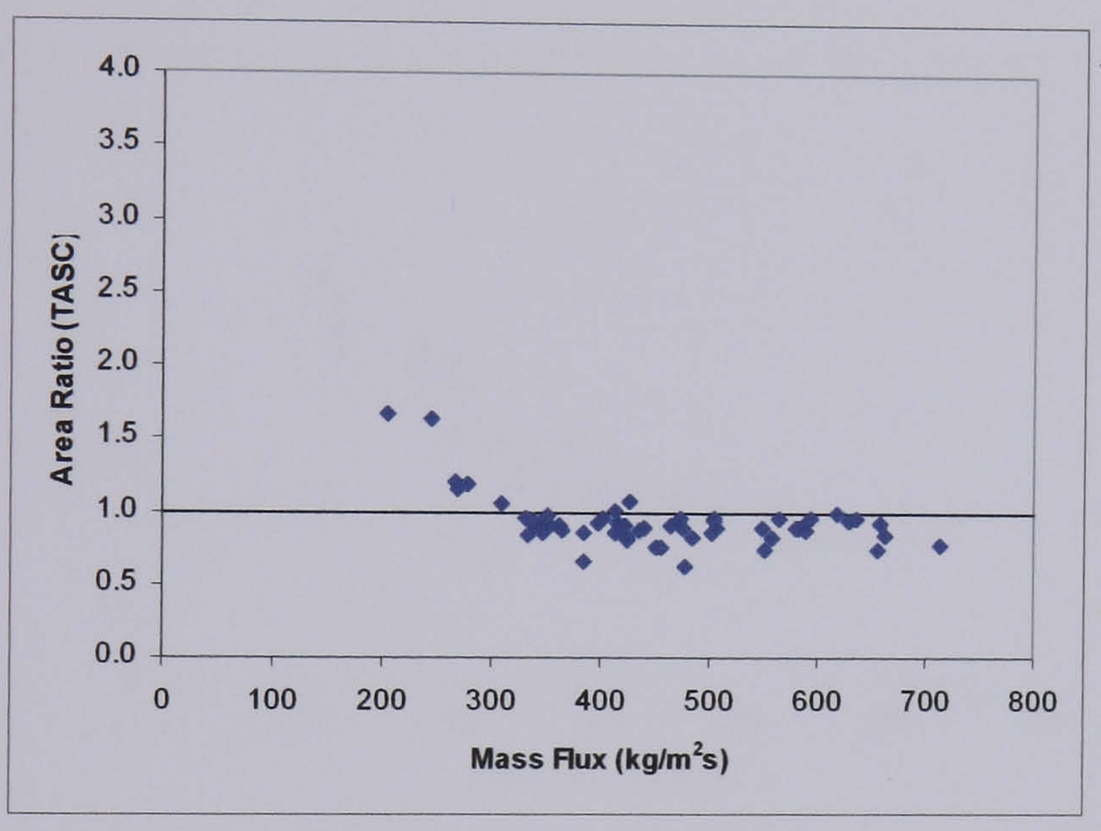

Figure 6.23 – TASC Area Ratio for Test B (McNaught et al, 1999, 2000) – vertical baffle

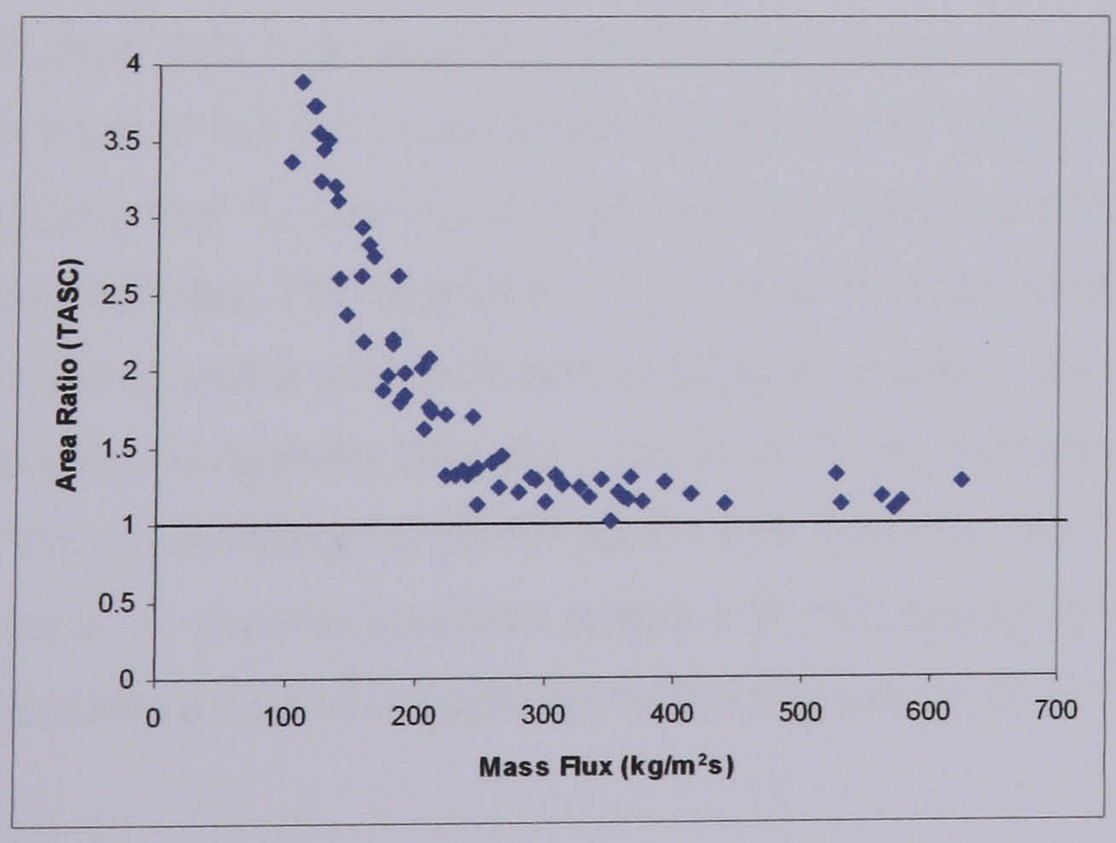

Figure 6.24 – TASC Area Ratio for Test 1 – horizontal baffle / sealing strips

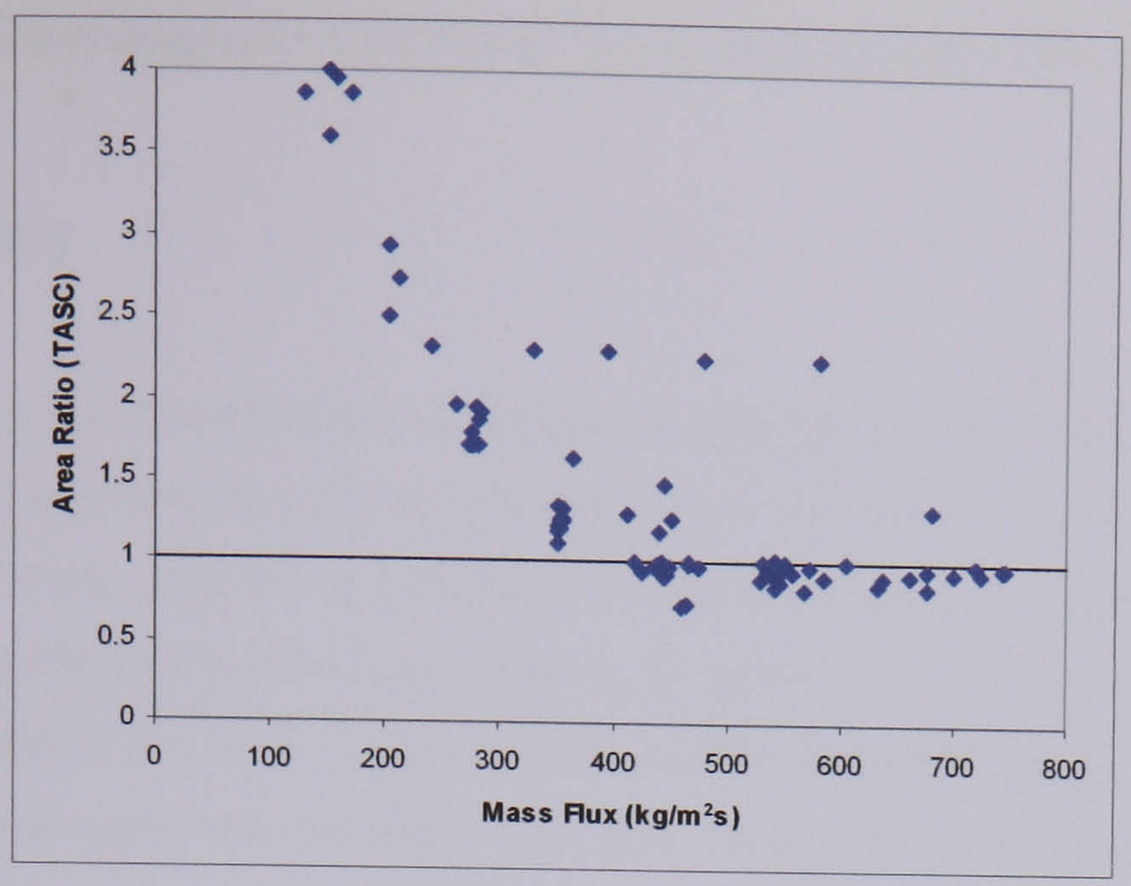

Figure 6.25 – TASC Area Ratio for Test 2 – vertical baffle / sealing strips

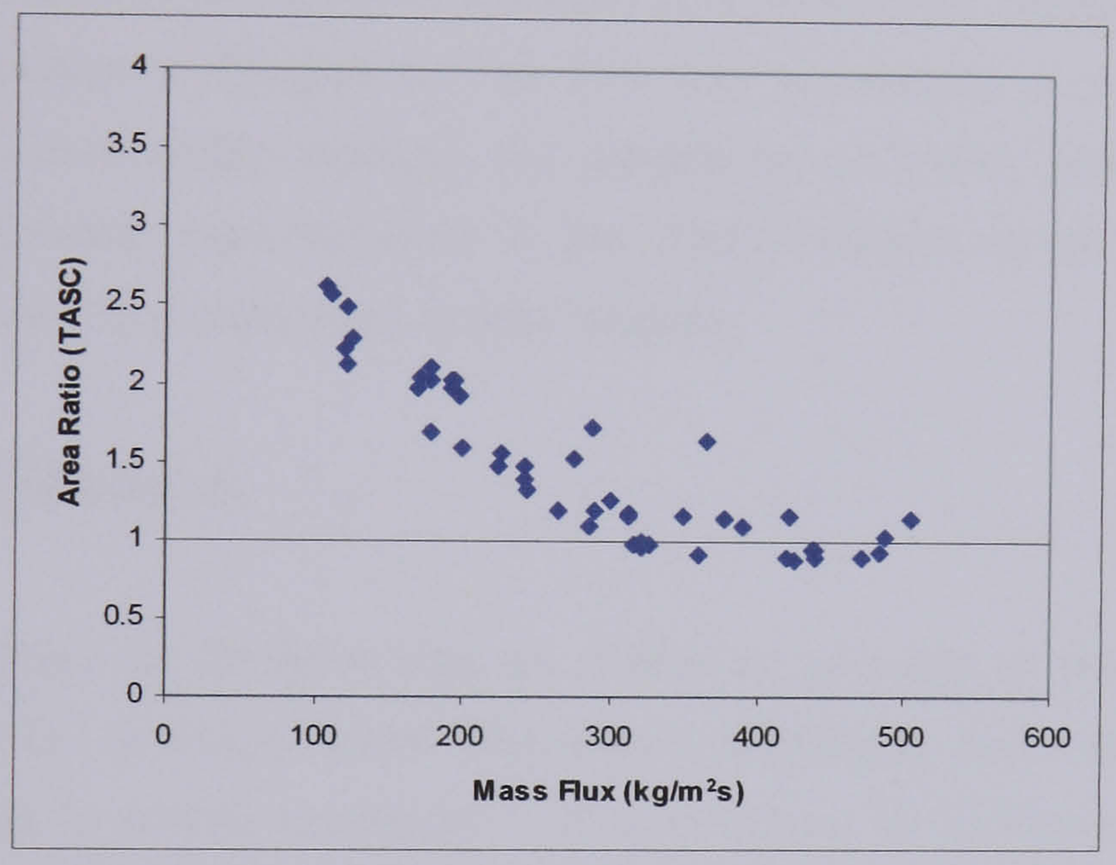

Figure 6.26 – TASC Area Ratio for Test 3 – vertical baffle increased pitch

As with the pressure drop data it is clear that TASC does not predict the deterioration in the heat transfer performance at the low mass fluxes (especially for Tests 1 - 3). The plots of the TASC area ratio indicate that for the majority of the data TASC produces reasonably good predictions of the heat transfer. The prediction of the heat transfer coefficient is only poor at the low mass flux values where it was indicated in Chapter 5 that there could be a change in the two-phase flow pattern. It appears that the main area for improvement in the TASC model would be to predict this deterioration in performance and describe the mechanism that could cause such deterioration. A general shellside model with this capability would be very useful for the design of evaporators which may operate within this low mass flux range.

CHAPTER 7 – Development of New Shellside Model (Model-A)

7.1 – Introduction

The Analysis of the experimental data in Chapter 5 highlighted that there was a transition to a poorer heat transfer performance of the test exchanger at lower mass fluxes. The hypothesis was proposed that there may be a transition in the two-phase flow pattern causing vapour blanketing around some of the tubes and leading to a decrease in the measured heat transfer coefficient. In Chapter 6 the HTFS Shell-&-tube heat exchanger design program TASC was assessed against the experimental data from the current project and against previous test data (Chu et al, 1998; McNaught et al, 1999, 2000). The TASC program failed to predict the trends in the heat transfer and pressure drop experimental data over the low mass flux range. It was decided to create a new general shellside two-phase flow model based on the HTFS TASC method described in Chapter 6. The aim was to produce a model which would be accurate enough to reasonably replicate the predictions of TASC, whilst remaining flexible enough to allow possible improvements to the TASC method to be assessed. The new shellside model (Model A) is described in this Chapter.

7.2 – Method of Model-A

The calculation method for Model-A was as similar as possible to the method outlined in Chapter 6 for the TASC shellside model. There were simplifying assumptions required to limit the size of the model to enable modification of its structure for further analysis. This section refers to Chapter 6 where the methods of TASC are directly replicated and highlights other areas where the procedure in Model-A differs from TASC.

7.2.1 – Shellside frictional pressure drop

Model-A uses the flow stream model of TASC described in section 6.3.5. The flow streams used are the same as those described in that section, where the flow distribution through each stream is determined based on the equality of pressure drop in parallel flow paths. This model is based on equations 7.1 – 7.4 which refer to the TASC flow path resistances shown in Figure 7.1.

$$\Delta p_{total} = \Delta p_1 + \Delta p_2 = \Delta p_3 \tag{7.1}$$

$$\Delta p_{1a} = \Delta p_{1b} = \Delta p_{1c} \tag{7.2}$$

$$\dot{M}_{total} = \dot{M}_1 + \dot{M}_3 \tag{7.3}$$

$$\dot{M}_1 = \dot{M}_2 \tag{7.4}$$

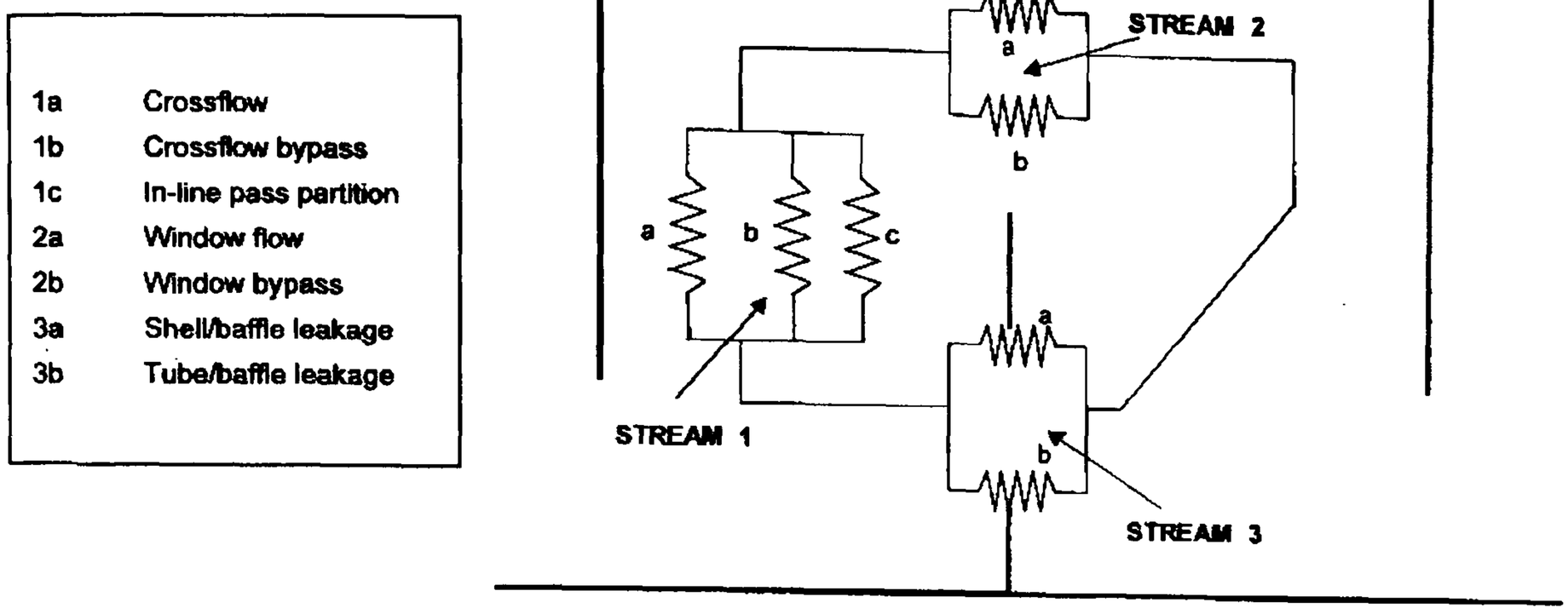

Figure 7.1 – Diagram of Flow Path Resistances in TASC Pressure Drop Model

The calculation of the pressure drop in each flow stream is given by equation 7.5(6.15).

$$\Delta P = n\frac{\dot{M}^2}{2\rho A^2} \tag{7.5}$$

The area term is calculated using the flow area definitions in 6.3.5(a). The correlations used for determining the number of velocity heads (n) lost in each stream are identical to those described in section 6.3.5(b) for single-phase and 6.3.5(c) for two-phase flows. Also the iterative procedure outlined for the calculation of the shellside pressure drop is the same as described in 6.3.5(d) namely:

- Calculate flow areas in each flow stream/path.
- Estimate mass flows in each path
- Calculate number of velocity heads lost in each stream
- Use equation 7.5 to calculate each of the corresponding pressure drops
- Check equations 7.1-7.4, If they are satisfied the calculation is complete. If not the mass flowrate in each path is re-estimated and the calculation procedure repeated.

The equations used for re-estimating the mass flowrates are equations 6.31-6.48 as in TASC. The principal difference between Model-A and the TASC shellside model is the zones over which the shellside pressure drop is calculated. In TASC the shellside pressure drop is calculated by summing the pressure drop over all the incremental area zones of the Temperature-enthalpy profile as described in Section 6.3.2.

It is important to note that the TASC shellside pressure drop is not calculated over incremental zones of equal length. Instead the zone boundaries are chosen based on the temperature-enthalpy data of the shellside and tubeside fluids. In Model-A the zone boundaries are not chosen from temperature-enthalpy profiles of the fluids, but are fixed as equal length increments over the shellside. For comparison with the test data the increments were set as the distance between shellside baffles. The flow areas calculated represented the flow area for each stream in each baffle space. The experimental exchanger was divided into seven zones for Tests 1 and 2 (figure 7.2(a)) and five zones for Test 3 (figure 7.2(b)).

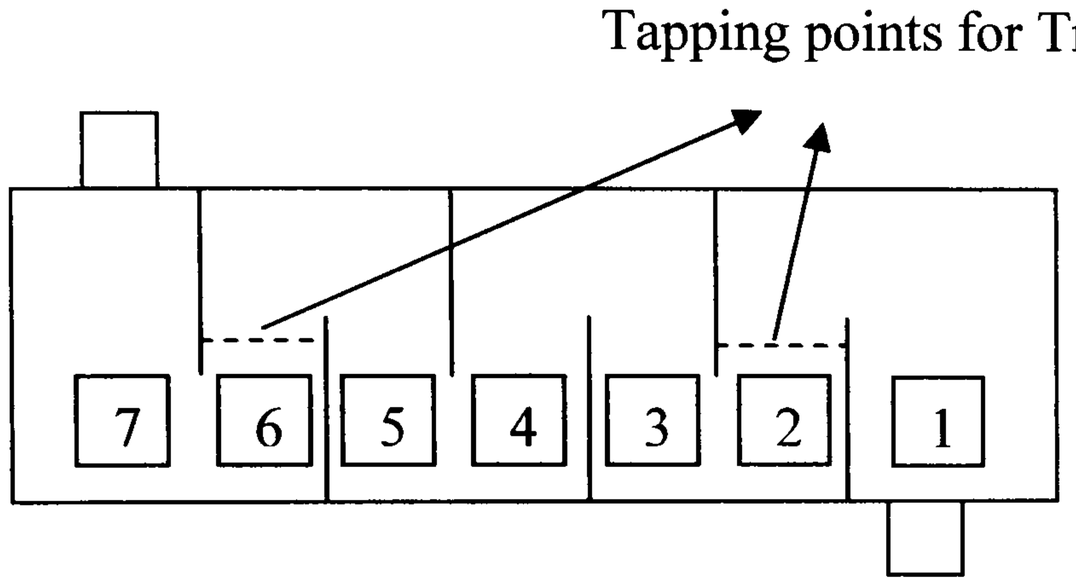

(a) – Baffle zone lengths for Tests 1 and 2

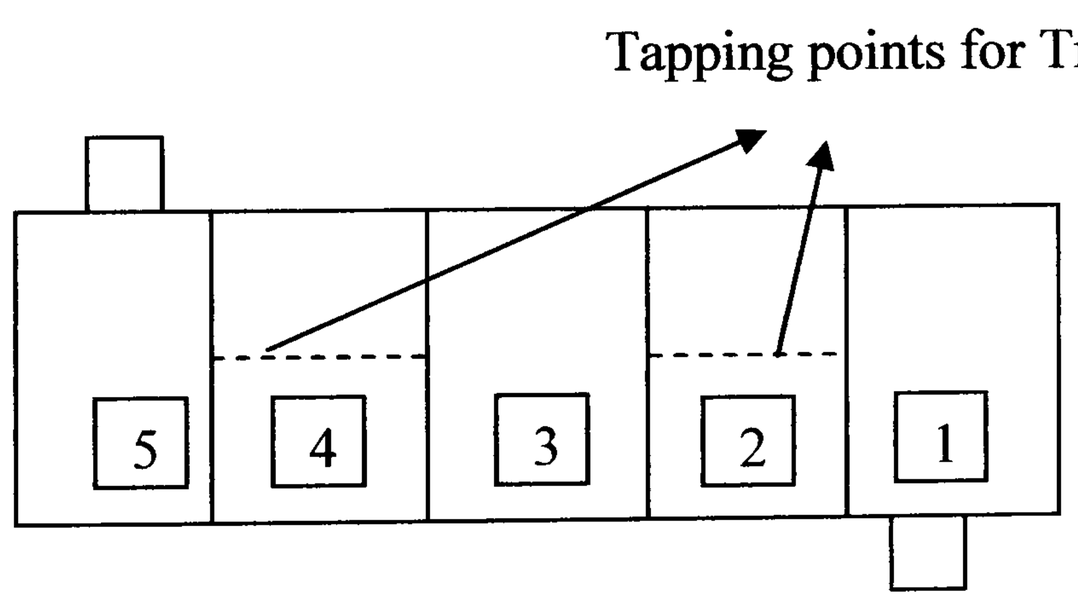

(b) – Baffle zone lengths for Test 3

Figure 7.2 – Zone lengths used in Shellside Pressure Drop Model-A

The pressure drop was calculated in each of the zones between the transducer tapping points. The total pressure drop for comparison with the predictions of TASC and the experimental data for Transducer 2 was generated using equations 7.6 (Tests 1 and 2) and 7.7 (Test 3).

$$\Delta P_{TOT} = \frac{\Delta P_2}{2} + \Delta P_3 + \Delta P_4 + \Delta P_5 + \frac{\Delta P_6}{2} \tag{7.6}$$

$$\Delta P_{TOT} = 0.7\Delta P_2 + \Delta P_3 + 0.7\Delta P_4 \tag{7.7}$$

The terms for the pressure drop in the zones containing the tapping points were scaled to represent the length of the baffle zone that was covered by the pressure drop measurement. An additional simplification of Model-A was required for the pressure drop in boiling two-phase shellside flow. An assumption was made for the vapour quality in each zone to enable the calculation of the number of velocity heads lost in each flow path. It was assumed that there is a step increase in vapour quality at each shellside zone between inlet and outlet. The vapour outlet quality from the evaporator that was calculated in the experimental test runs (Chapter 4) was used to calculate the quality in each shellside zone using equation 7.8.

$$x_i = \left(\frac{x_{Outlet}}{N_{Zones}} \right) \times i \qquad (7.8)$$

In summary, the main difference between the TASC shellside pressure drop model and Model-A is the zones over which the total pressure drop is calculated. The TASC model is based on increments tied to temperature-enthalpy profiles which specify the local conditions of the shellside fluid and the area over which the pressure drop is calculated. Model-A uses standard length increments and makes assumptions of the fluid conditions (primarily vapour quality) in each zone to calculate the pressure drop.

The reason for this simplification in the calculation method of Model-A was to reduce the number of shellside increments and consequently the size of the calculation for the overall shellside pressure drop. It was desirable to keep the number of shellside increments relatively small to ensure that the calculation wouldn't become excessively large as amendments were made to try to improve the Model.

The principal consequence of reducing the number of shellside increments was that there was a far less gradual increase in the vapour quality along the length of the exchanger. With an increasing number of incremental zones the increase in vapour quality along the exchanger becomes linear. In Model-A there is a step increase in the vapour quality at each baffle space with the value calculated using equation 7.8. This quality that is used to calculate the pressure drop is possibly slightly higher than the value obtained from a strictly linear calculation as it represents the quality at the outlet of each baffle zone.

7.2.2 – Accelerational pressure drop

It was decided to omit the accelerational pressure drop calculation from Model-A as it is largely insignificant in comparison with the calculation of the shellside frictional pressure drop. The accelerational pressure drop throughout the experimental test range was always less than 10% of the total pressure drop.

7.2.3 –Boiling Heat Transfer Coefficient

The shellside boiling heat transfer coefficient is calculated using the same method as the TASC model. Equation 7.9 gives the coefficient where α_{nb} is the contribution due to nucleate boiling calculated from the Stephan-Abdelsalam correlation (6.60) and α_{cb} is the coefficient due to forced convective boiling calculated from the HTFS method outlined in section 6.3.7(b).

$$\alpha_{Model-A} = \alpha_{boil} = \left(\alpha_{nb}^2 + \alpha_{cb}^2\right)^{1/2} \tag{7.9}$$

The calculation of α_{cb} requires a knowledge of the mass flowrate in the crossflow path. As with TASC, this is obtained from the iterative solution of the shellside flow stream model (see section 6.3.7(b). The calculation of α_{nb} requires a knowledge of the heat flux (q). The procedure for the calculation of the heat flux and hence α_{nb} is an iterative one which can be summarised as follows:

- Input the shellside and tubeside fluid temperatures, tube wall thermal conductivity and geometric details.
- Estimate the heat flux (q) – (Initial estimate q_i taken as 10000 W/m^2)
- Calculate the tubeside heat transfer coefficient α_t
- Using q_i and the crossflow mass flowrate, calculate α_{nb} and α_{cb} and hence α_{boil}
- Calculate the overall heat transfer coefficient U using equation 7.10

$$\frac{1}{U} = \frac{1}{\alpha_s} + r_s + \frac{y_w}{\lambda_w}\frac{d_o}{d_w} + \left(\frac{1}{\alpha_t} + r_t\right)\frac{d_o}{d_i} \tag{7.10}$$

- Re-calculate the heat flux using equation 7.11

$$q_{i+1} = U\left(T_{tubeside} - T_{shellside}\right) \tag{7.11}$$

- If q_{i+1} is approximately equal to q_i then the calculation is complete. If not the calculation is repeated using q_{i+1} as the heat flux estimate.

The procedure above requires the calculation of the tubeside heat transfer coefficient α_t. This was calculated using the Boyko and Kruzhilin (Boyko et al, 1967) method which can be described as follows; Firstly the condensate Prandtl number and Reynolds number based on the total flow with liquid properties are calculated using equations 7.12 and 7.13.

$$\mathrm{Pr}_l = \frac{c_{pl}\eta_l}{\lambda_l} \tag{7.12}$$

$$\mathrm{Re}_{lo} = \frac{4\dot{M}_c}{\pi d_i \eta_l} \tag{7.13}$$

Where c_{pl} is the specific heat capacity of the liquid, η_l is the viscosity, λ_l the thermal conductivity, d_i the tube internal diameter and $\dot{M}_c$ the condensate mass flowrate (obtained from the experimental test data). Then the heat transfer coefficient assuming the total fluid flowing with liquid properties is calculated from equation 7.14.

$$\alpha_{t(lo)} = 0.021 \frac{\lambda_l}{d_i} \mathrm{Re}_{lo}^{0.8} \mathrm{Pr}_l^{0.43} \tag{7.14}$$

Finally the condensate heat transfer coefficient is calculated from equation 7.15.

$$\alpha_t = \alpha_{t(lo)} \left[1 + x \left(\frac{\rho_l}{\rho_g} - 1 \right) \right]^{1/2} \tag{7.15}$$

The method recommends using a mean coefficient over the tube length which is the average of the result of equation 7.15 with the inlet and outlet qualities. For Model-A it was assumed that there was complete condensation in the tubes from the vapour at inlet (i.e $x_{in} = 1$ and $x_{out} = 0$). Hence the tubeside coefficient was calculated using equation 7.16.

$$\alpha_t = \frac{1}{2} \left[\alpha_{t(lo)} \left(\frac{\rho_l}{\rho_g} \right)^{1/2} + \alpha_{t(lo)} \right] \tag{7.16}$$

7.3 – Comparison of Model-A with TASC and Experimental Data

Model-A as described above was written in a computer program (Appendix C) and used to calculate predictions for the data from the experimental tests. In this section the predictions of Model-A are compared with those of TASC and with the experimental data.

7.3.1 – Single-phase pressure drop

Figure 7.3 and Figure 7.4 show comparisons of single-phase pressure drop for Model-A, TASC and the Experimental data for all the single phase liquid shellside tests.

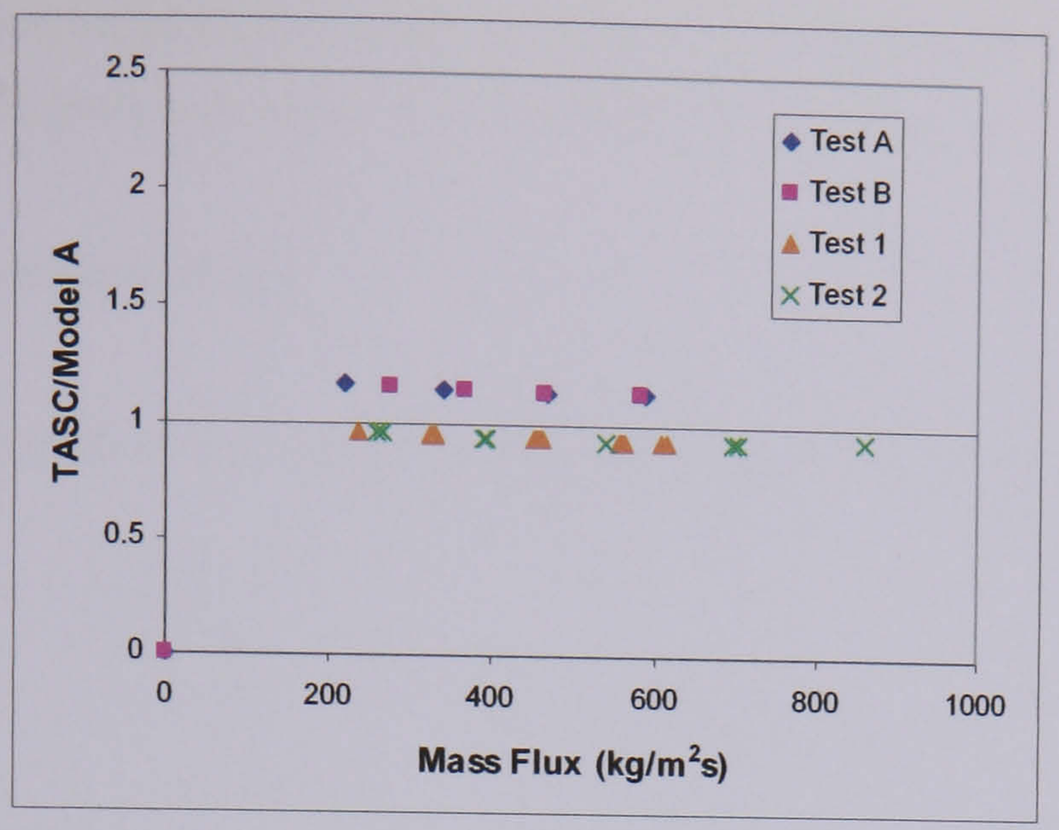

Figure 7.3 – Comparison of Model-A and TASC single-phase pressure drop predictions (all tests)

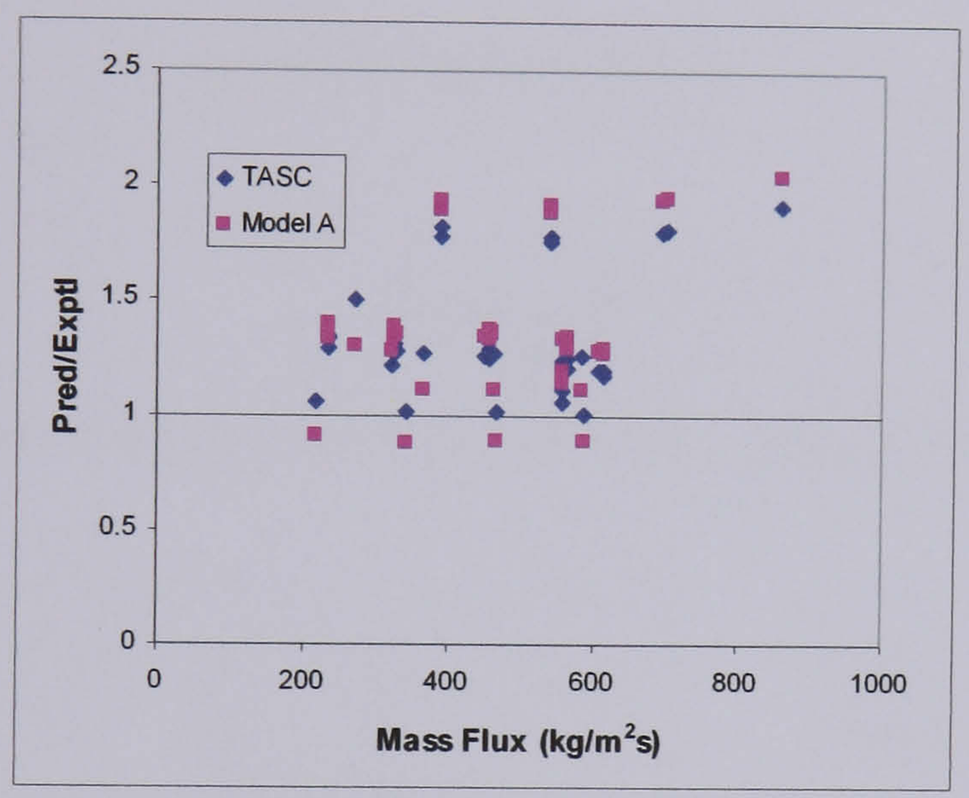

Figure 7.4 – Ratio of TASC and Model-A predictions to experimental data for single-phase pressure drop (all tests)

The data in the figures are for the pressure Transducer 2 and measures the pressure drop between the baffle spaces 2 and 6. Figure 7.3 plots the ratio of the TASC prediction to the Model-A prediction for the all the test data. It can be seen from Figure 7.3 that Model-A predicts a slightly greater pressure drop for Tests 1 and 2 than TASC does and a slightly smaller pressure drop for Tests A and B. The Model-A predictions are within $\pm 15\%$ of those of TASC. It is likely that the difference in the two predictions is caused by the different incremental boundaries for the pressure drop calculation. The method in TASC assumes a small temperature change along the shell as the temperature enthalpy curve is used to produce the shellside zone increments from which the pressure drop is calculated, whereas Model-A assumes a constant shellside temperature for the single-phase tests. Figure 7.4 shows a comparison of TASC and Model-A with the single-phase experimental data. It can be seen that the method of TASC can over-predict the measured value by as much as 90%. The trend of the Model-A data matches closely with that of TASC and it appears that there is a

much greater difference between the predictions and the experimental data (Figure 7.4) than there is between the predictions of the individual models (Figure 7.3)

7.3.2 – Two-phase pressure drop

Figures 7.5 and 7.6 show the same plots for the two-phase pressure drop of Transducer 2.

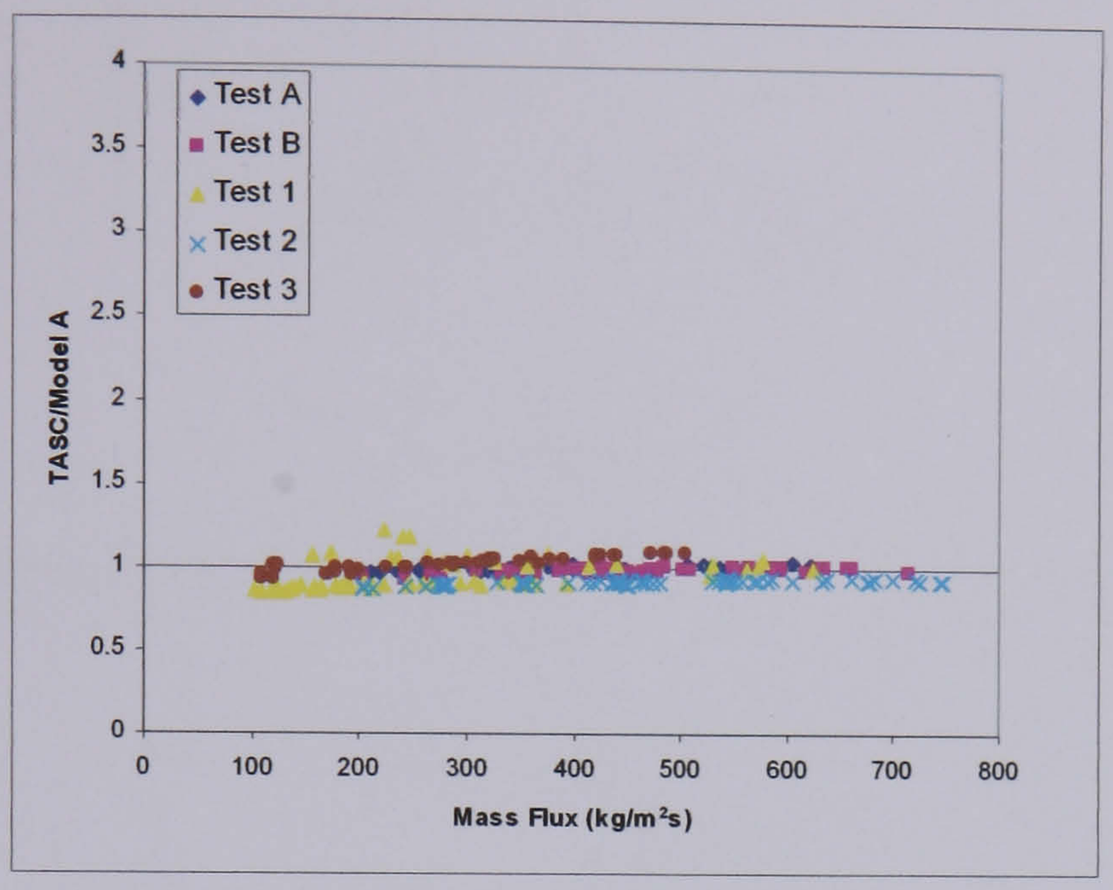

Figure 7.5 – Comparison of Model-A and TASC two-phase pressure drop predictions (all tests)

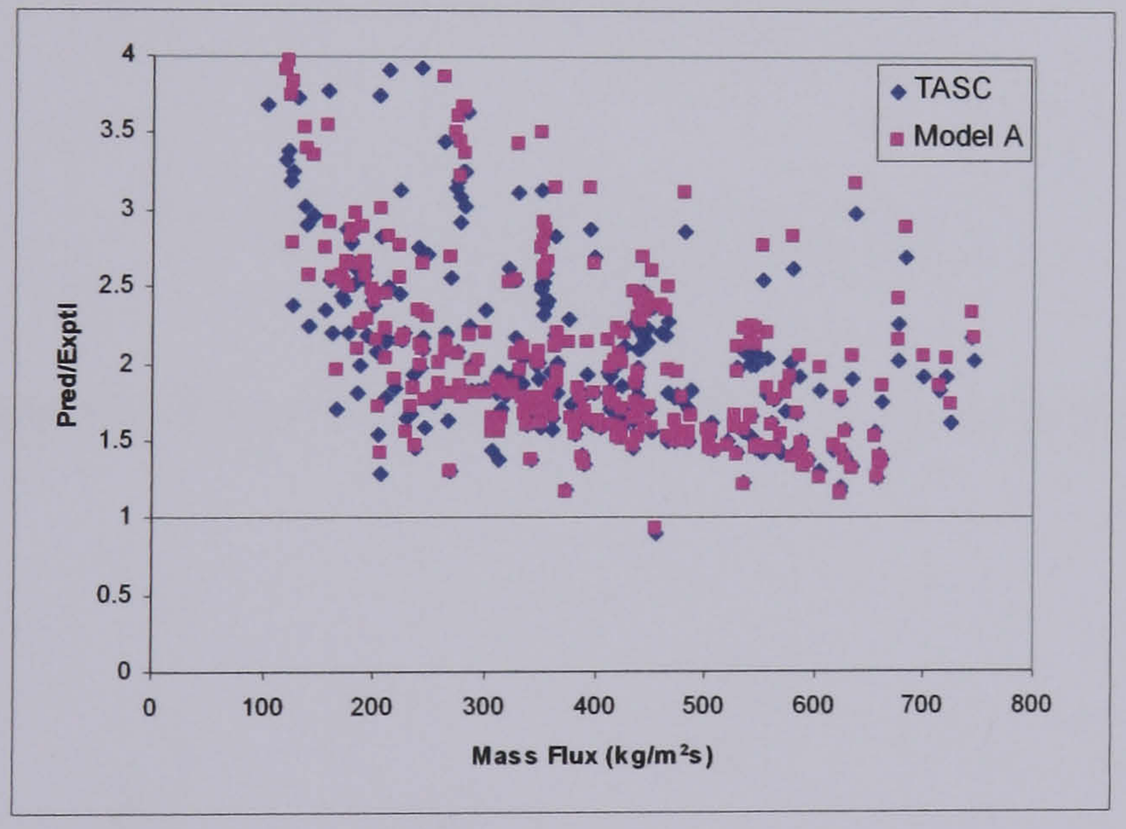

Figure 7.6 – Ratio of TASC and Model-A predictions to experimental two-phase pressure drop (all tests)

The data in Figures 7.5 and 7.6 indicate that there is a good agreement (within 25%) between the predictions of Model-A and those of TASC when compared with the accuracy of the predicted values (in figure 5.7 TASC can over-predict the experimental value by as much as 400%). The pressure drop predicted is very slightly greater for the Model-A predictions in Tests 1 and 2 but in general the results and the trends of the TASC data are repeated by Model-A. The plots for the two-phase multiplier shown in Chapter 6 (Figures 6.18 - 6.20) have

been reproduced with the two-phase multiplier from Model-A produced for comparison. The results are shown in Figures 7.7 - 7.9.

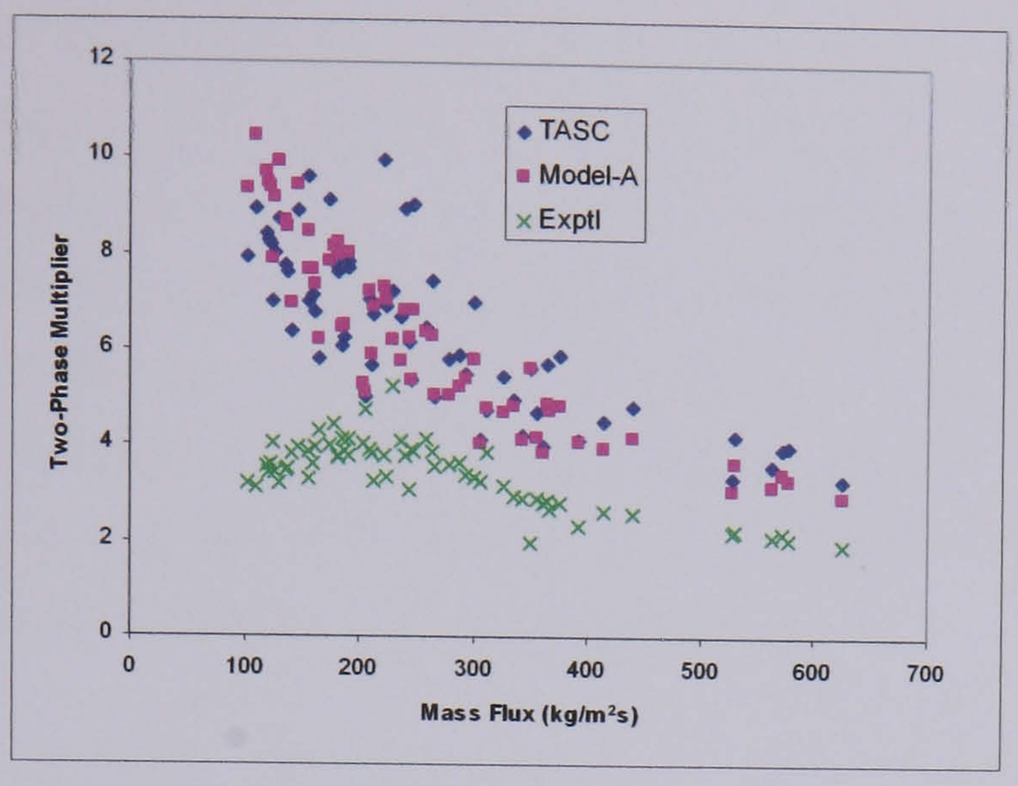

Figure 7.7 – Comparison of TASC and Model-A with Experimental Two-Phase Multiplier (Test 1)

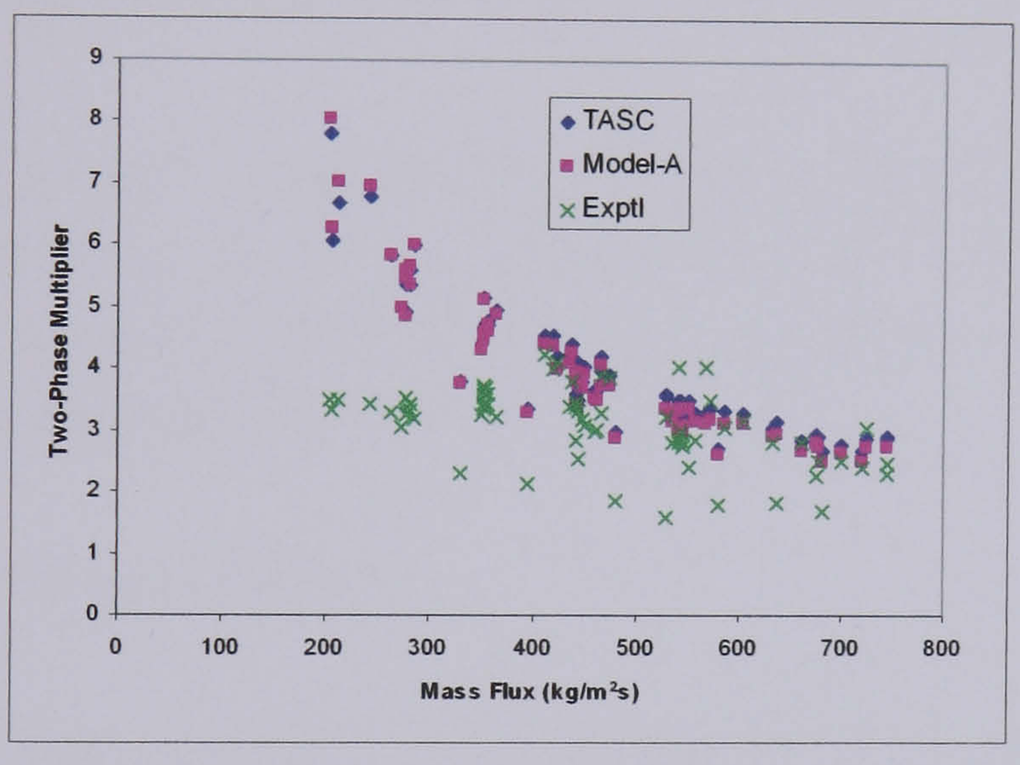

Figure 7.8 – Comparison of TASC and Model-A with Experimental Two-Phase Multiplier (Test 2)

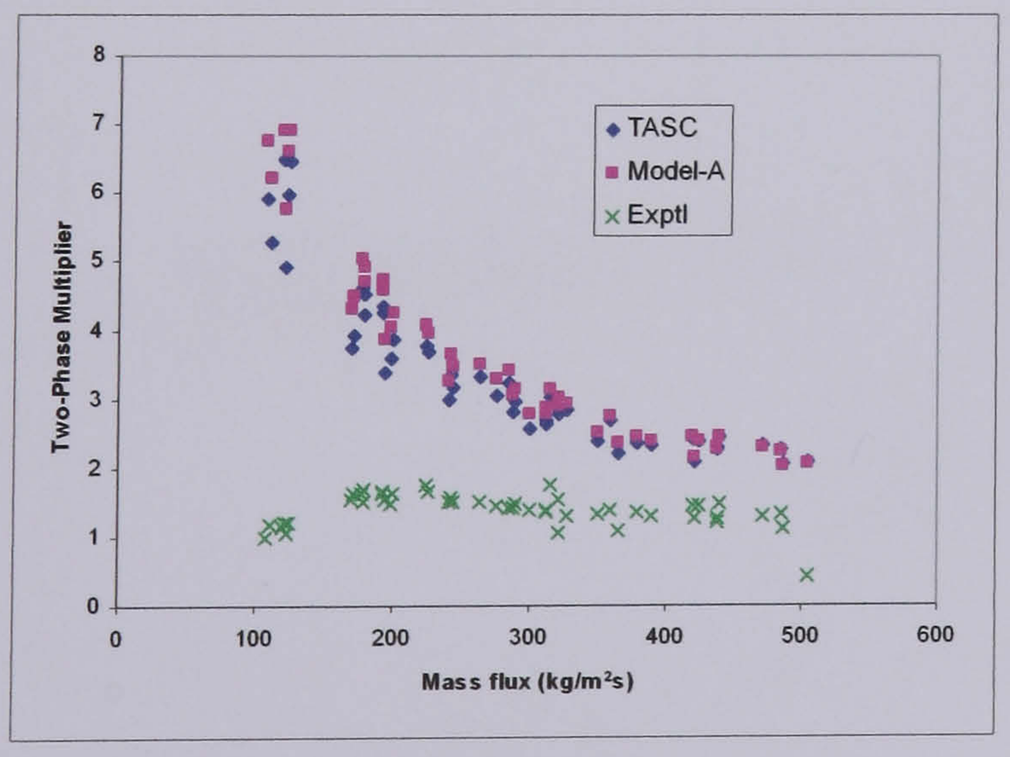

Figure 7.9 – Comparison of TASC and Model-A with Experimental Two-Phase Multiplier (Test 3)

It is evident that Model-A produces the same trend in the two-phase multiplier as in the TASC predictions. There are slight differences in the value of the multipliers calculated. As the correlations used in Model-A and TASC are identical, It is likely that the cause of the difference between the TASC and Model-A predictions is the assumptions on which Model-A is based. It was highlighted before that the principal difference between the models was regarding the increments over which the shellside pressure drop is calculated. A consequence of the Model-A approach was that the vapour quality may be slightly higher than in the calculations of TASC. From equation 7.17 it can be seen that the value of the two-phase pressure drop multiplier increases with increasing vapour quality. The slightly larger vapour quality values in the Model-A calculations may explain why the pressure drop predictions of the model are generally larger than those in TASC.

$$\phi_{lo}^2 = 1 + \left[\left(x + 0.15\sqrt{x} \right) \left(\frac{\rho_l}{\rho_g} \frac{f_{go}}{f_{lo}} - 1 \right) \right] \qquad (7.17)$$

f_{go} and f_{lo} are the single-phase vapour and liquid friction factors respectively.

Despite the slight difference in the incremental calculation method, the predictions of Model-A are replicating the predictions of TASC to a reasonable degree. The similarity in the trends of the predictions would suggest that changes which improve the predictions of Model-A would likely produce a similar improvement in TASC.

7.3.3 – Boiling Heat Transfer Coefficient

Figures 7.10 and 7.11 show comparisons of the boiling heat transfer coefficient predictions.

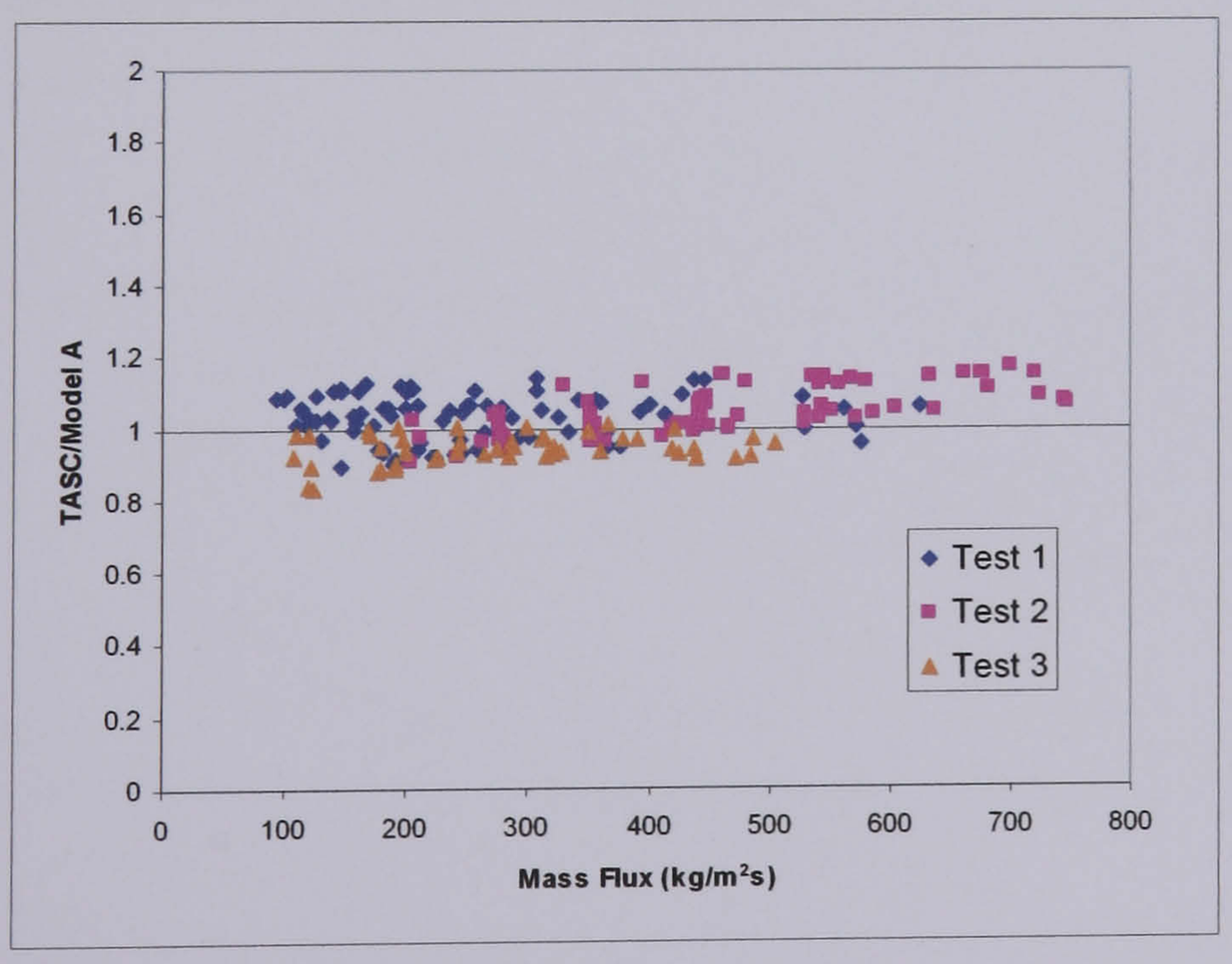

Figure 7.10 – Ratio of TASC to Model-A Predictions for Boiling Coefficient (Tests 1 - 3)

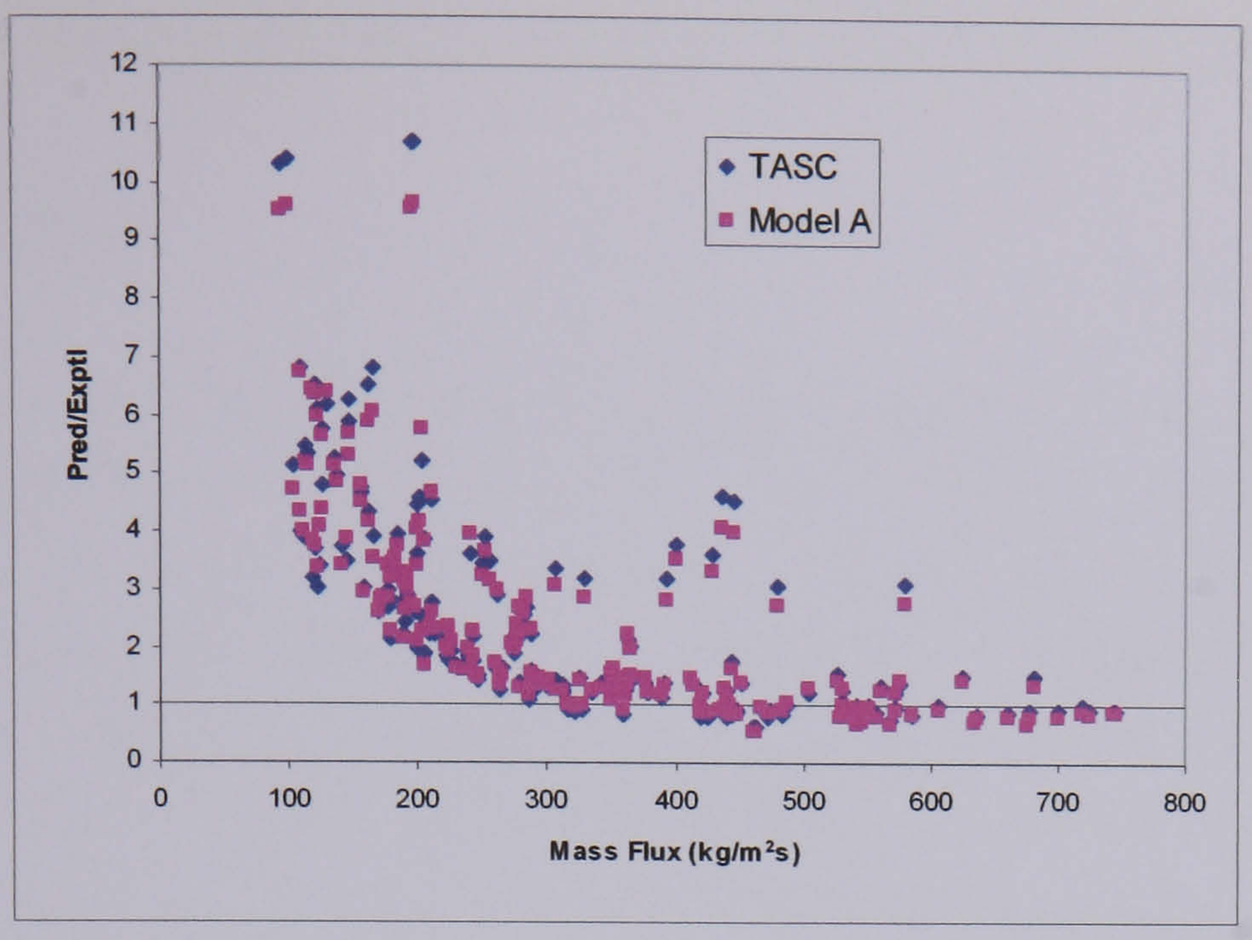

Figure 7.11 – Ratio of Predicted to Experimental Boiling Coefficient (Tests 1 - 3)

Figures 7.10 and 7.11 highlight that the method for predicting the boiling heat transfer coefficient in Model-A gives a prediction within 15-20% of the TASC value. The trend of poorer prediction of the experimental data at the lower mass fluxes is equally apparent in the Model-A predictions. The reason the ratios at the lower mass fluxes are so large are that the predictions are very sensitive to the mean temperature difference. The predicted values are generated using the measured temperature difference which is large in this range as it corresponds with a low measured boiling coefficient.

From the data in figures 7.3 – 7.11 it is clear that Model-A is sufficiently accurate to assume that a change resulting in the improvement of the prediction of Model-A would be likely to have a similar effect if applied to the TASC model.

CHAPTER 8 – Development of Stratified Shellside Model (Model-B)

8.1 – Introduction

The experimental data analysis (Chapter 5) and subsequent comparison with TASC (Chapter 6) highlighted that there was a requirement for a new shellside two-phase flow model for predicting the heat transfer coefficient and pressure drop during low mass fluxes. A hypothesis was presented that the drop in the heat transfer coefficient may be caused by a separation of the liquid and vapour phases leading to dryout and vapour blanketing around some of the tubes. In Chapter 5 the data was assessed against flow pattern maps for shellside crossflow (Grant, 1977). In both vertical and horizontal crossflow the transition in the heat transfer data was close to the map boundaries between the homogeneous flow patterns (Bubbly/Spray) and the separated flow patterns (Stratified/Stratified-Spray/Intermittent). An examination of the literature revealed that there is currently very little information on mechanisms of flow pattern transition in shellside geometries. Further analysis using the two-phase multiplier and heat transfer data identified that the poor performance data were within a range where a transition to a stratified pattern was predicted by a correlation based on observations of horizontal tubeside flow. It was decided to create a shellside stratified flow model to test the assumption that this type of flow pattern could cause the performance deterioration witnessed in the data of the experimental tests. Two types of stratified flow were identified in Chapter 5. The different types witnessed in previous tests are dependent on the shellside baffle orientation. Figure 8.1 shows a stratified type of flow that has been witnessed in shellside tests with a horizontal baffle orientation (Grant et al, 1987) whereas Figure 8.2 shows the type of stratified flow observed with a vertical baffle orientation (Grant, 1977).

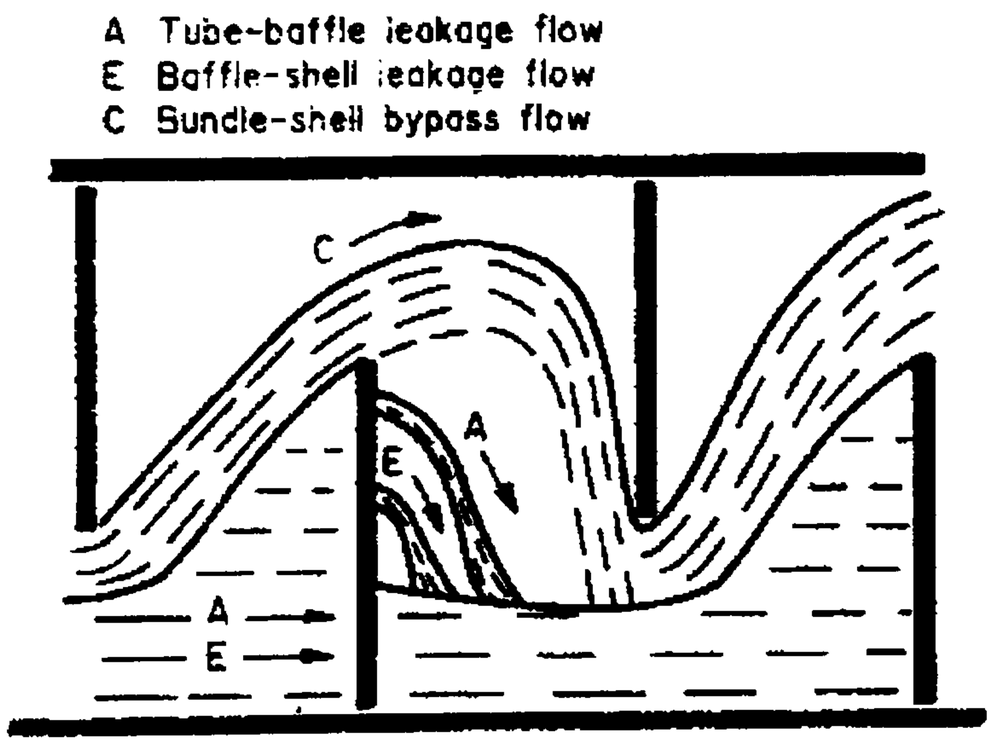

Figure 8.1 – Stratified Flow in Horizontal Baffle-Orientation (Grant et al, 1987)

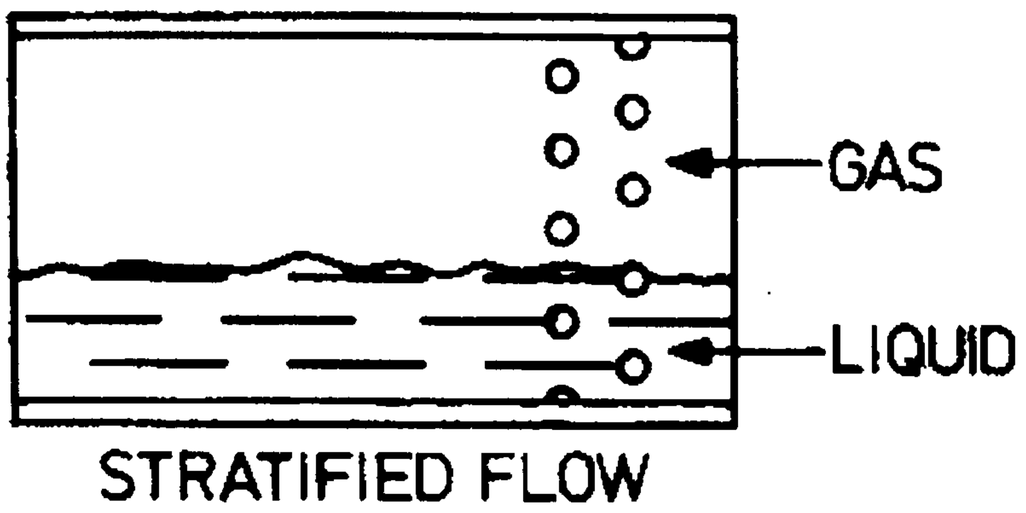

Figure 8.2 – Stratified Flow in Vertical Baffle-Orientation (Grant, 1977)

The type of stratified flow in Figure 8.2 is simpler due to the predominant flow direction being from side to side with the vertical baffle orientation. This motion allows the phases to separate more easily due to gravity than with the horizontal orientation which forces the flow up and down along the shellside. It was decided to base the Stratified flow model (Model-B) on the type of flow shown in Figure 8.2 as it would be easier to model whilst still being able to achieve the objective of assessing whether this type of phase separation would cause the observed deterioration in performance.

8.2 – Model-B Method

8.2.1 – Overall structure

The Model-B method involves modifying the method of Model-A (Chapter 7) to describe stratified shellside flow. The principal assumptions on which Model-B is based can be summarised as the following:

- The shellside is divided into the same incremental zones as in Model-A
- As in Model-A there is a step increase in vapour quality across each zone in two-phase flow.
- There is a complete separation of the liquid and vapour phases such that the liquid occupies the bottom part of the shell and the vapour occupies the top.
- The pressure drop in each of the phases are equal and equal to the overall pressure drop, i.e.

$$\Delta P_{TOT} = \Delta P_{LIQ} = \Delta P_{VAP} \tag{8.1}$$

  Interface shear is assumed negligible compared to the pressure drop caused by the effect of the shell and tube geometry.
- Boiling occurs in the liquid pool at the bottom section of the shell, heat transfer in the upper section is given by the single-phase vapour coefficient.

The basis of the stratified flow in Model-B is that the vapour and liquid occupy a volume of the shell such that the pressure drop across each of the two-phases is equal. This method requires the separate calculation of the liquid and vapour phase pressure drops on the shellside. The method of the TASC model and Model-A described in Chapters 6 and 7 involved the calculation of the shellside pressure drop by iterative calculations of the individual pressure drops in each of the shellside flow paths. For Model-B this calculation procedure becomes more complicated as a separate pressure drop calculation is carried out for each phase. In Chapter 6 it was observed in the TASC model that the pressure drop in each flow path was calculated using equation 8.2

$$\Delta P = n\frac{\dot{M}^2}{2\rho A^2} \tag{8.2}$$

Relationships existed for the parameter n in each of the shellside flow paths. In Model-B additional relationships dependent on the shellside void fraction exist for the calculation of the flow area term A. The flow area used in the pressure drop calculation is not the area of the flow path (as in TASC and Model-A) but the area of the particular phase in the flow path, since the pressure drop being calculated is that of one phase. The calculation procedure in Model-B begins with an estimation of the void fraction ε_g. From this the flow areas occupied by the liquid and vapour phases in each flow path are determined using the procedures described in section 8.2.2.

8.2.2 – Modified Flow Areas

All the flow areas in Model-B are calculated from corrections used to the flow path areas from the homogeneous Model-A. The calculation of the flow areas begins with an estimation of the void fraction. The void fraction is defined by equation 8.3 based on the flow situation in Figure 8.3.

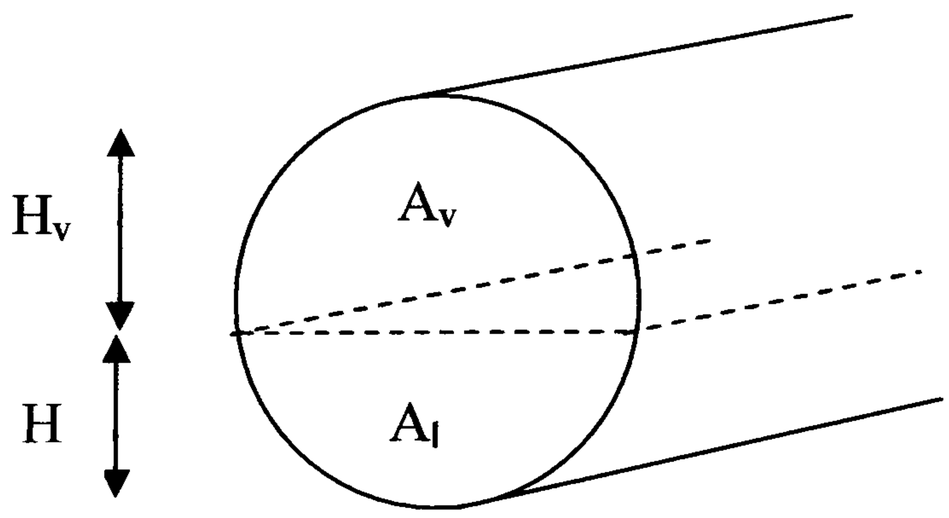

Figure 8.3 – Phase areas in stratified two-phase flow

$$\varepsilon_g = \frac{A_v}{A_l + A_v} \tag{8.3}$$

The height of the phase interface from the base of the shell is calculated using the following geometrical relationships for the area of a segment in a circular cross section.

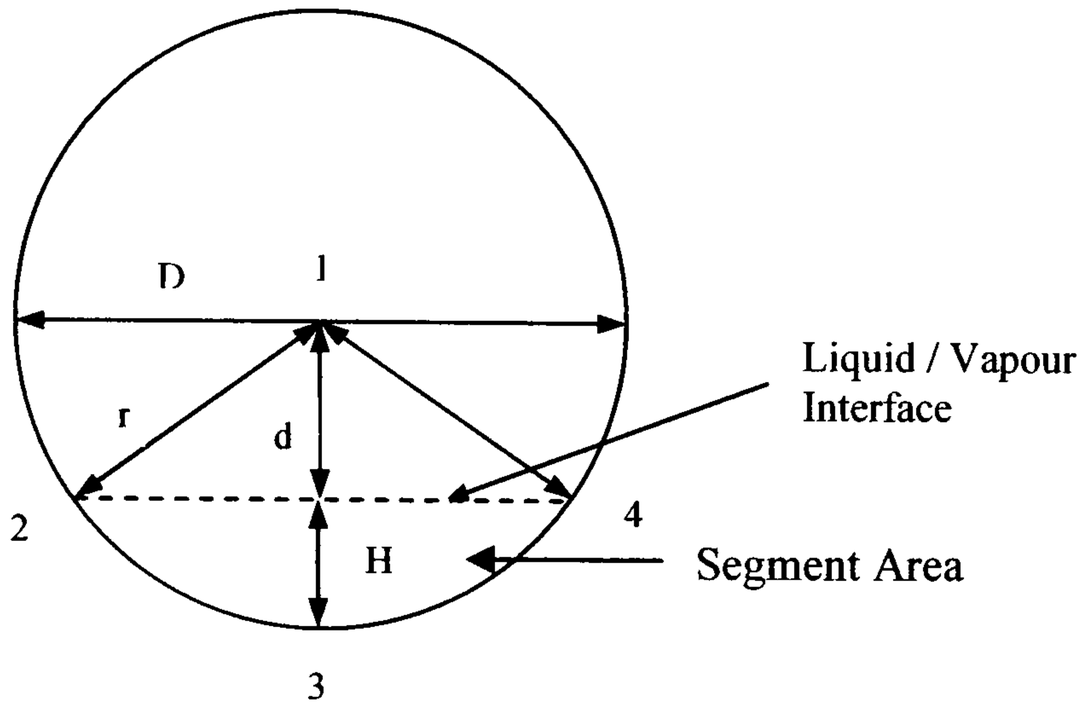

Figure 8.4 – Circular cross section with segment area

$$A_{Segment} = A_{Sector(1,2,3,4)} - A_{Triangle(1,2,4)} \tag{8.4}$$

$$A_{Segment} = r^2 \cos^{-1}\frac{r-H}{r} - (r-H)\sqrt{2rH - H^2} \tag{8.5}$$

The area of the segment is known from the void fraction. If the void fraction is greater than 0.5 the segmental area calculated is that of the liquid phase and the height H obtained from 8.5 is the liquid height above the base of the shell. If the void fraction is less than 0.5 then the segmental area used is the vapour area and the height of the interface above the base of the shell is given by subtracting the calculated value of H from the shell diameter D, i.e. $H_l = H$ if $\varepsilon_g > 0.5$ and $H_l = D - H$ if $\varepsilon_g < 0.5$.

1(a) – Crossflow Area

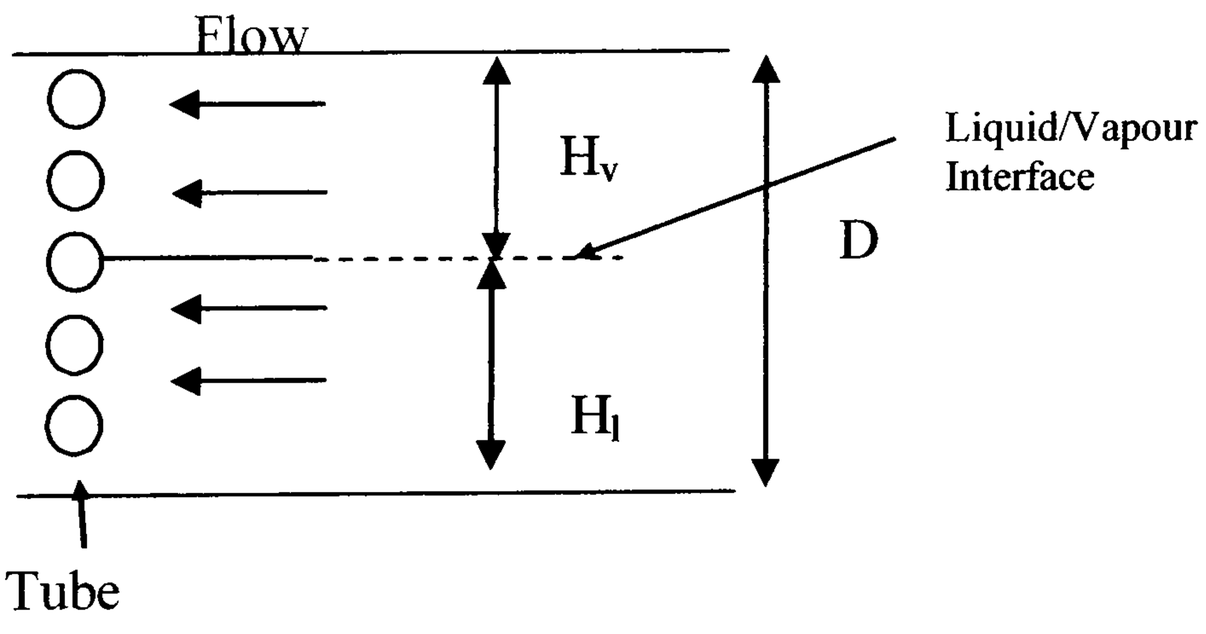

Figure 8.5 – Diagram of fraction of crossflow area covered by each phase

The area in the crossflow path is calculated by correcting the crossflow area of Model-A using the height of the vapour or liquid phases depending on which phase pressure drop is being calculated.

$$A_{1a(Model-B)} = A_{1a(Model-A)} \frac{H_{Phase}}{D} \tag{8.6}$$

1(b) – Crossflow Bypass

For the crossflow bypass flow stream the area is dependent on the predominant flow direction and hence the baffle orientation (Figure 8.6). With the horizontal baffle orientation (cut) the predominant flow direction is in the vertical up-and-down direction and there is a bypass flow path on either side of the tube bundle in each phase. With the vertical baffle orientation the flow direction is from side-to-side and there is only one crossflow bypass flow area available in each phase. Therefore the flow area for the horizontal orientation is the same as that used in Model-A and for the vertical baffle orientation it is calculated as half the bypass flow area of Model-A.

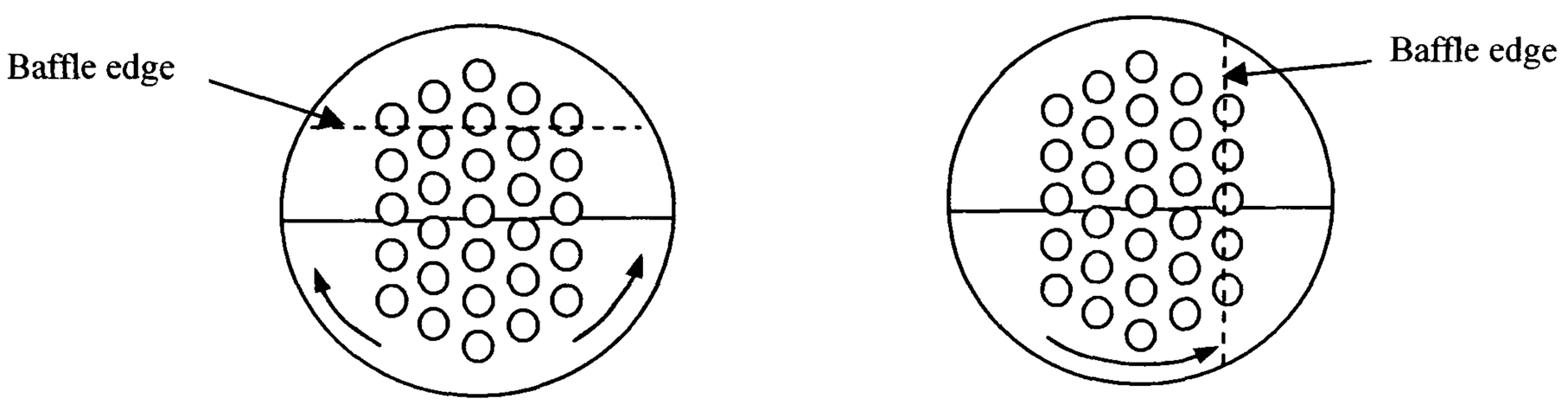

Figure 8.6 – Crossflow bypass areas for Model-B, horizontal and vertical baffle-orientations

2(a) and 2(b) – Window Flow and Window Flow Bypass

The terms for the flow areas of the window flow and window flow bypass are considered together in the TASC and Model-A methods. In Model-B the window flow area requires the most adjustment from Model-A as the relationship between phase height and window flow area is not simple. A diagram of the available window area with the vertical baffle orientation is shown in Figure 8.7.

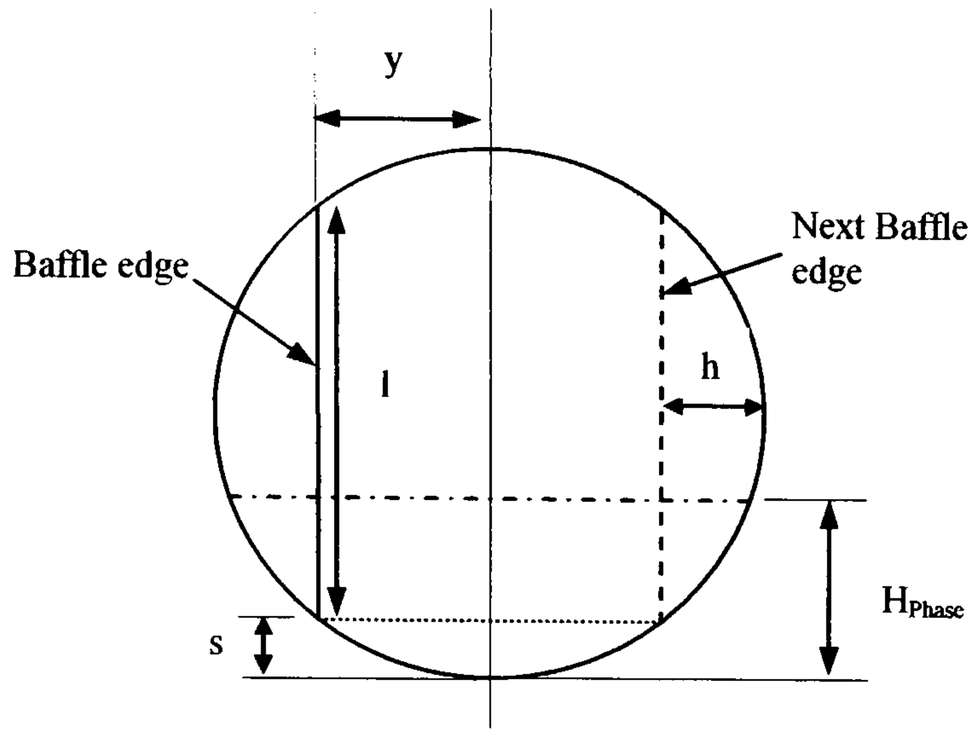

Figure 8.7 – Parameters used in the calculation of window flow area (Vertical baffle-cut)

With the vertical baffle orientation the location of the baffle window is at the side of the shell. The predominant flow in the side-to-side direction means that flow can enter through the window area of one baffle and exit through the window area of the next baffle. After the height of the phase, H_{Phase} is established from the void fraction, the window flow area of the phase can be calculated. The baffle-cut in an exchanger is usually specified as a percentage. The baffle cut in the experimental exchanger was 30%. This means that the distance between the baffle edge and the shell h is 30% of the shell internal diameter. The area of the segment of the baffle window can be calculated by using the value of h in equation 8.5, giving:

$$A_{Seg(Win)} = r^2 \cos^{-1}\frac{r-h}{r} - (r-h)\sqrt{2rh-h^2} \tag{8.7}$$

Where r is the shell radius. The chord length l in Figure 8.7 can be calculated from 8.8.

$$l = 2\left(r^2 - y^2\right)^{1/2} \tag{8.8}$$

The height above the base of the shell at which the baffle window begins is given by:

$$s = \frac{D-l}{2} \tag{8.9}$$

Thus the area of the baffle below the baffle window can be calculated from:

$$A_{Below} = r^2 \cos^{-1}\frac{r-s}{r} - (r-s)\sqrt{2rs-s^2} \tag{8.10}$$

If the area of the phase in the calculation is less than the area calculated from equation 8.10 then the window flow area will be zero as the flow will not have penetrated the window region. If the phase height is greater than s, the window area will continue to increase until the phase height is equal to (D-s) at which point the window area for the phase will equal the total

area calculated as in Model-A. The equations for calculating the Model-B window flow area with the vertical baffle orientation are given below.

If $H_{Phase} < s$

$$A_{2a(Model-B)} = 0 \tag{8.11}$$

If $s < H_{Phase} < r$

$$A_{2a(Model-B)} = \frac{\left[\left(A_{Phase} - A_{Below}\right)/2 - y\left(H_{Phase} - s\right)\right]}{A_{Seg(Win)}} A_{2a(Model-A)} \tag{8.12}$$

If $r < H_{Phase} < D - s$

$$A_{2a(Model-B)} = A_{2a(Model-A)} - \frac{\left[\left(\frac{\pi D^2}{4} - A_{Phase} - A_{Below}\right)/2 - y\left(D - H_{Phase} - s\right)\right]}{A_{Seg(Win)}} A_{2a(Model-A)} \tag{8.13}$$

If $H_{Phase} > D - s$

$$A_{2a(Model-B)} = A_{2a(Model-A)} \tag{8.14}$$

Equation 8.13 calculates the area of the phase that occupies more than half the shell by subtracting the window area of the smaller phase from the total available window area. Equations 8.11 – 8.14 describe the window flow area for one phase with the vertical baffle orientation. With the horizontal baffle orientation the calculation is slightly different. Figure 8.8 shows the location of the baffle windows with the horizontal baffle cut.

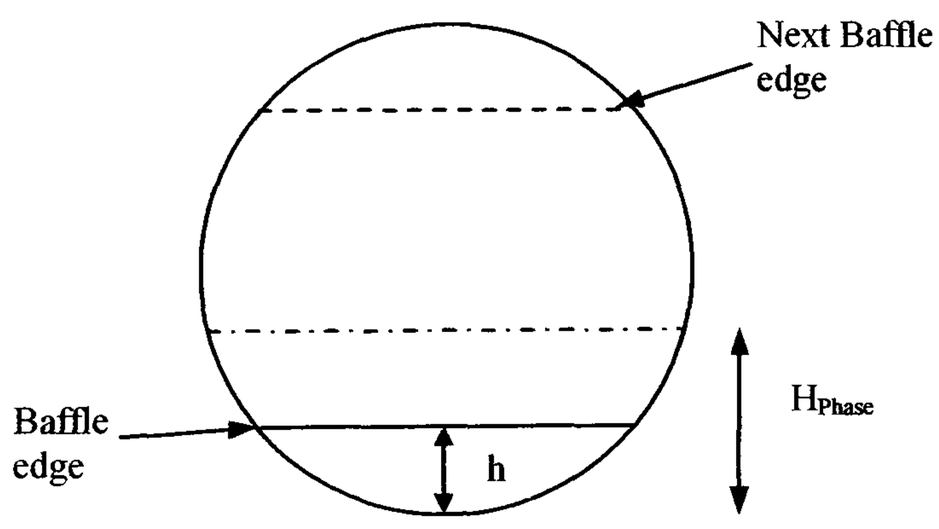

Figure 8.8 – Baffle windows with horizontal orientation

The baffle windows are at the top and bottom of the shell as opposed to at the sides. This means that only one of the baffle windows will be occupied if the phase height is insufficient to reach the other window. If the height of the phase is less than the height of the window h the

flow area is calculated from the area of the segment covered (equation 8.15). If the phase height is greater than h but still not enough to reach the top baffle window, the flow area is half of that calculated by Model-A (as one of the baffle windows is full and the other empty). If the phase height is sufficient to reach the second baffle window, the segment area not occupied by the phase is calculated and used to determine the area occupied by subtracting from the Model-A flow area. The equations for calculating the window flow area in the horizontal baffle case are presented in 8.15 – 8.19.

If $0 < H_{Phase} < h$

$$A_{2a(Model-B)} = \frac{r^2 \cos^{-1}\frac{r - H_{Phase}}{r} - (r - H_{Phase})\sqrt{2rH_{Phase} - H_{Phase}^2}}{A_{Seg(Win)}} \frac{A_{2a(Model-A)}}{2} \quad (8.15)$$

If $h < H_{Phase} < (D - h)$

$$A_{2a(Model-B)} = \frac{A_{2a(Model-A)}}{2} \quad (8.16)$$

If $H_{Phase} > (D - h)$

$$H_U = D - H_{Phase} \quad (8.17)$$

$$A_{2a(U)} = \frac{r^2 \cos^{-1}\frac{r - H_U}{r} - (r - H_U)\sqrt{2rH_U - H_U^2}}{A_{Seg(Win)}} \frac{A_{2a(Model-A)}}{2} \quad (8.18)$$

$$A_{2a(Model-B)} = A_{2a(Model-A)} - A_{2a(U)} \quad (8.19)$$

3(a) – Shell to Baffle Leakage

The area available for shell to baffle leakage flow in stratified flow depends on the fraction of the leakage area covered by the phase. The leakage path exists around the edge of the baffle and the fraction of the total leakage path will be proportional to the ratio of the arc S created by the phase to the circumference of the shell (Figure 8.9). When the height of the phase H_{Phase} is less than the shell radius r the arc of the segment can be calculated using 8.20.

$$S = 2r \cos^{-1}\frac{r - H_{Phase}}{r} \quad (8.20)$$

The area of the shell to baffle leakage flow path is calculated from 8.21.

$$A_{3a(Model-B)} = \frac{S}{2\pi r} A_{3a(Model-A)} \tag{8.21}$$

If the phase height is greater than the shell radius equation 8.20 is used to calculate the arc of the segment not occupied by the phase and the area of the flow path is calculated from 8.22.

$$A_{3a(Model-B)} = \frac{2\pi r - S}{2\pi r} A_{3a(Model-A)} \tag{8.22}$$

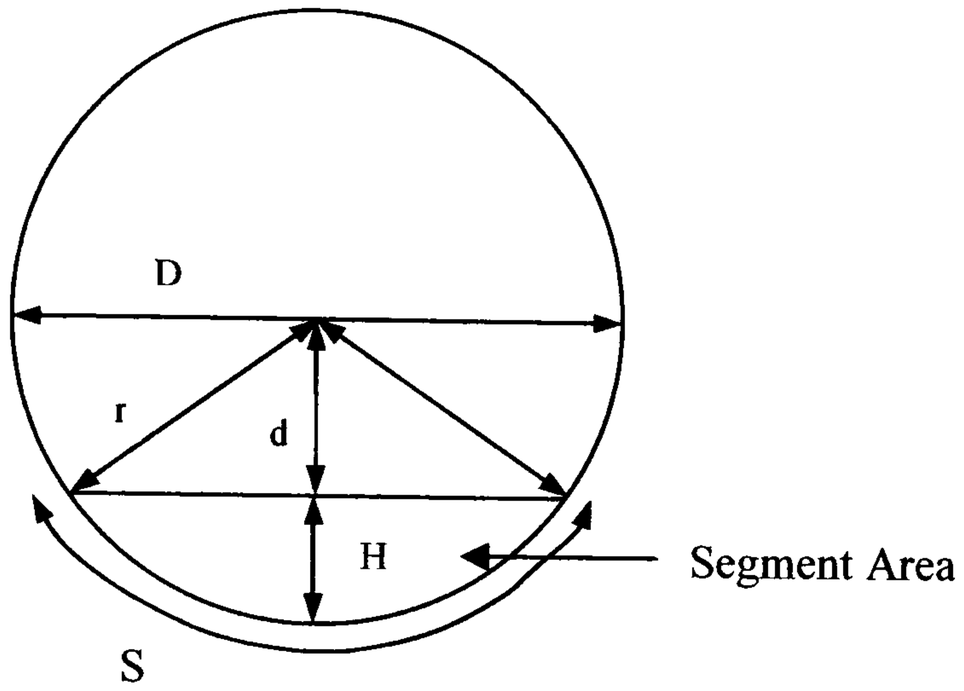

Figure 8.9 – Diagram indicating arc created by segment

3(b) – Tube to Baffle Leakage

As the tube to baffle leakage area is directly related to the number of tubes covered by the phase, the available area can be calculated from the fraction of the total tubes covered. The number of tubes covered is proportional to the cross sectional area submerged by the phase, therefore equation 8.23 is used for the tube to baffle leakage area.

$$A_{3b(Model-B)} = \frac{A_{Phase}}{\pi r^2} A_{3b(Model-A)} \tag{8.23}$$

8.2.3 – Calculation Procedure

As described in section 8.2.1 Model-B produces the result where the liquid phase and vapour phase pressure drops are equal. The calculation procedure of the stratified flow model (Model-B) is adopted for each shellside baffle space as in Model-A, and can be described as follows:

- Input variables such as mass flowrate, temperature and vapour quality.
- Assume stratified separation of the liquid and vapour phases and make an initial estimation of the void fraction
- Calculate the modified flow areas from those used in Model-A using the procedures described in 8.2.2.

- Calculate the single-phase liquid and vapour phase pressure drops using the correlations for single-phase flow from Model-A with the modified flow areas for Model-B.
- Output the values of the liquid and vapour phase pressure drops. If they are equal the calculation is finished and the values of the total pressure drop and void fraction are stored. If they are not equal the void fraction is re-estimated using the iterative method of false position and the calculation repeated.

It should be noted that in the above procedure there is no correlation for the calculation of void fraction. The value of the void fraction is fixed by the two assumptions that the phases are completely separated in a stratified flow pattern and that the pressure drop in the liquid and vapour phases are equal. The void fraction value which satisfies these two assumptions is calculated by iterating the above procedure using the method of false position (Perry et al, 1997). The method is based on equation 8.24.

$$b_{i+1} = b_i - \frac{b_i - b_0}{f(b_i) - f(b_0)} f(b_i) \qquad (8.24)$$

The value will converge on a solution if b_i and b_0 are established for which the values of $f(b_i)$ and $f(b_0)$ have opposite signs. The liquid and vapour pressure drops calculated in Model-B are functions of the void fraction ε_g. From the initial void fraction estimate, values of the liquid and vapour pressure drops are calculated and the constraint for pressure drop equality of the two phases checked. Equation 8.24 is adopted for the model in 8.25 and used to calculate new void fraction estimates.

$$\varepsilon_{g(i+1)} = \varepsilon_{g(i)} - \frac{\varepsilon_{g(i)} - \varepsilon_{g(0)}}{(\Delta P_l - \Delta P_v)_i - (\Delta P_l - \Delta P_v)_0} (\Delta P_l - \Delta P_v)_i \qquad (8.25)$$

Where $(\Delta P_l - \Delta P_v)$ represents the difference between the liquid and vapour phase shellside pressure drops from the calculation of Model-B. A solution for the void fraction is obtained when the value of ε_g is determined for which the pressure difference between the phases $(\Delta P_l - \Delta P_v)$ is equal to zero (for the practical purposes of the model 1Pa difference is small enough to assume equality). For the method to be effective initial estimates are required for the void fraction which produce values of $(\Delta P_l - \Delta P_v)_1$ and $(\Delta P_l - \Delta P_v)_0$ with opposite signs.

8.2.4 – Shellside Pressure Drop with Stratified Flow (Model-B)

The predictions of shellside pressured drop from Model-B are produced using the same shellside increments as Model-A. The increments are of length equal to the experimental evaporator shellside baffle spaces (Figure 8.10). As with Model-A the assumption was made that there was a step increase in the vapour quality at each successive increment. For each increment there is an iterative calculation to produce a void fraction and stratified pressure drop result. The total shellside pressure drop for comparison with Model-A, TASC and the experimental data is produced in the same way as Model-A using equation 8.26 for Tests 1 and 2 and 8.27 for Test 3.

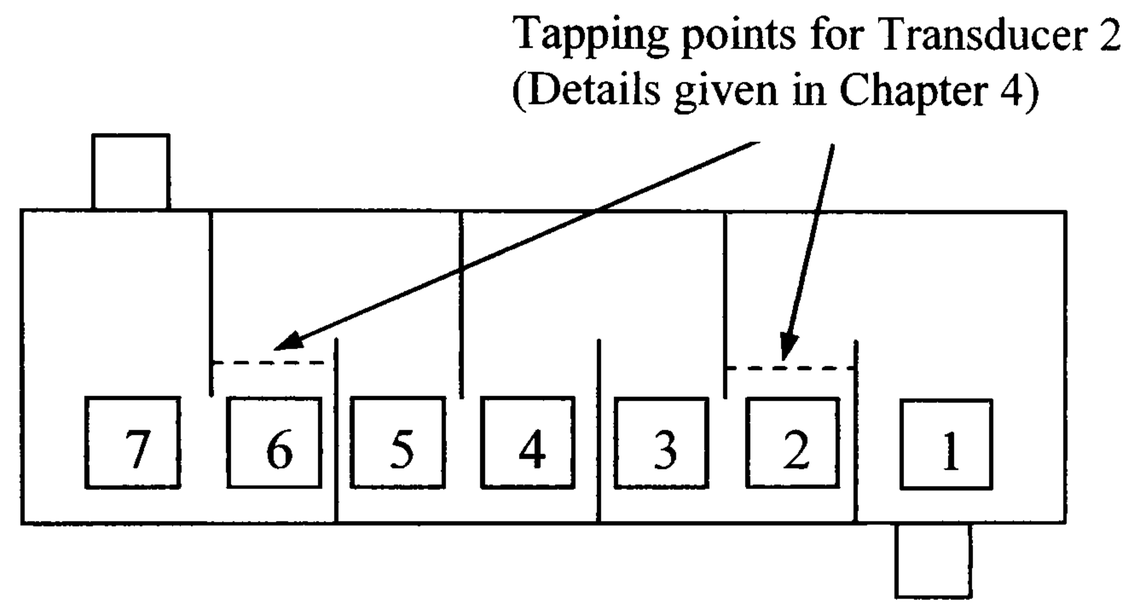

(a) – Test 1 and Test 2

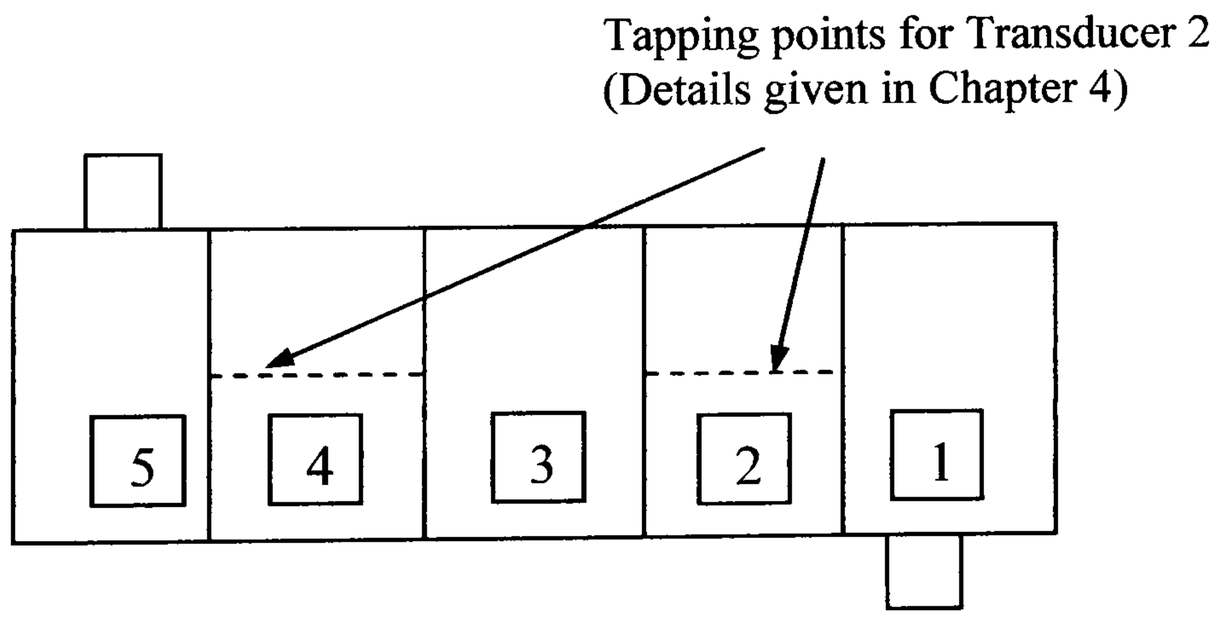

(b) – Test 3

Figure 8.10 – Shellside increments for pressure drop calculation

$$\Delta P_{TOT} = \frac{\Delta P_2}{2} + \Delta P_3 + \Delta P_4 + \Delta P_5 + \frac{\Delta P_6}{2} \tag{8.26}$$

$$\Delta P_{TOT} = 0.7\Delta P_2 + \Delta P_3 + 0.7\Delta P_4 \tag{8.27}$$

8.2.5 – Heat Transfer Coefficient in Model-B

One of the principal assumptions of the stratified flow model outlined in 8.2.1 was that boiling occurred in the liquid pool in the bottom section of the shell and the heat transfer in the top section would be due to the single-phase vapour. The heat transfer coefficient in Model-B is calculated using equations 8.28 and 8.29.

$$\alpha_{Model-B} = \frac{\sum_{i=0}^{N_{Bspace}} \alpha_{Bspace_i}}{N_{Bspace}} \tag{8.28}$$

N_{Bspace} is the number of shellside baffle spaces (7 for Tests 1 and 2, and 5 for Test 3) and α_{Bspace} is the heat transfer coefficient calculated in each baffle space using equation 8.29.

$$\alpha_{Bspace} = \varepsilon_g \alpha_g + (1 - \varepsilon_g)\alpha_{Model-A} \tag{8.29}$$

The value of ε_g is obtained from the resolution of the stratified flow model in each baffle space. The single-phase vapour coefficient α_g is calculated using the HTFS method for shellside single-phase flow (Wills, 1985). The method is identical to that for the calculation of the single-phase liquid coefficient α_l outlined in Chapter 6(6.3.6(b)), with the only difference being the use of vapour physical properties in place of liquid.

8.3 – Comparison of Model-B with Model-A, TASC and Experimental Data

The stratified model described in this chapter was written in Microsoft Excel Visual Basic computer code (Appendix C) and used to calculate values for comparison with other models (Model-A and TASC) and experimental data. Predictions were generated for the two-phase pressure drop with stratified flow between the tapping locations of Transducer 2 in the experimental evaporator. The location of the tapping points is indicated in Figure 8.10. Predictions were also created for the shellside heat transfer coefficient with stratified flow based on equation 8.28. These predictions were used for comparison with the measured boiling heat transfer coefficient of the experimental tests and with the predictions of TASC and Model-A.

8.3.1 – Two-Phase Pressure Drop

Figures 8.11 - 8.13 show comparisons of the two-phase pressure drop Model-B predictions against those of Model-A, TASC and the experimental data for Tests 1 - Test 3. The Test

measurements were made using the shellside pressure drop transducer as indicated in Figure 8.10.

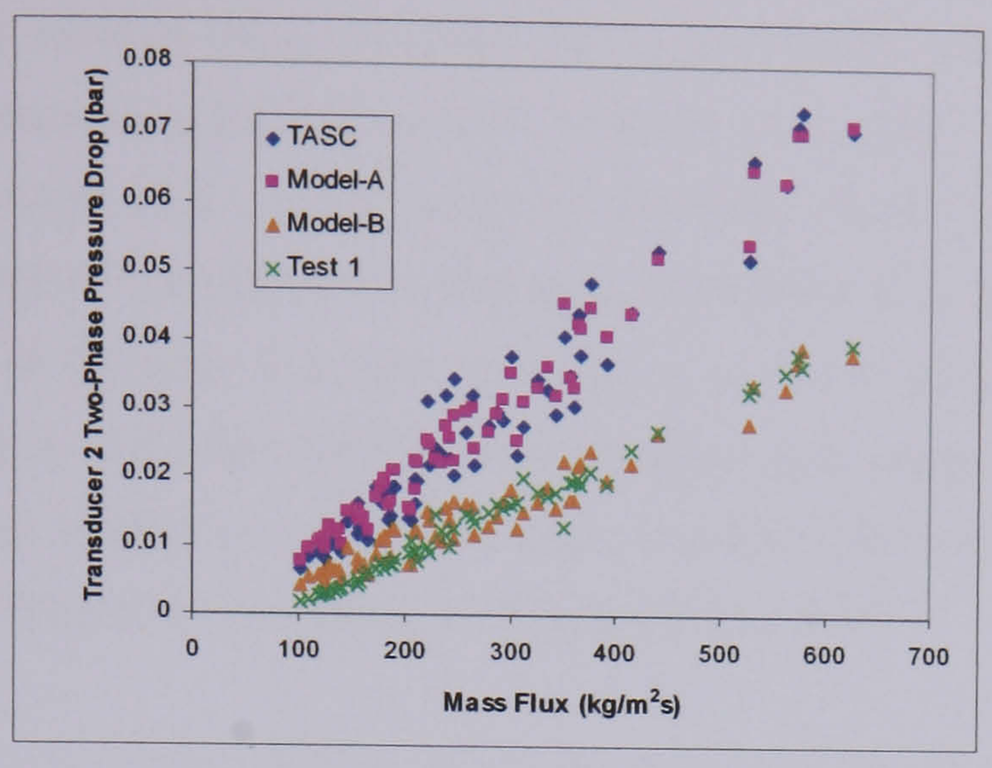

Horizontal baffle cut

Figure 8.11 – Pressure drop predictions of TASC, Model-A, Model-B and Test 1 data (Shellside Transducer 2)

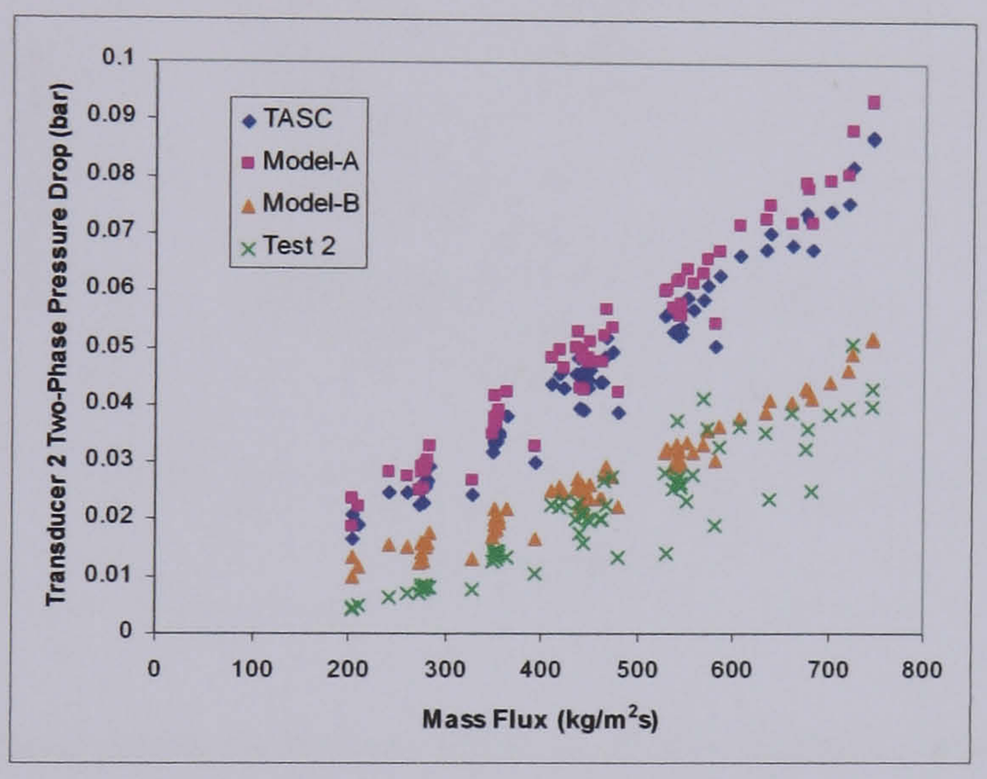

Vertical baffle cut

Figure 8.12 – Pressure drop predictions of TASC, Model-A, Model-B and Test 2 data (Shellside Transducer 2)

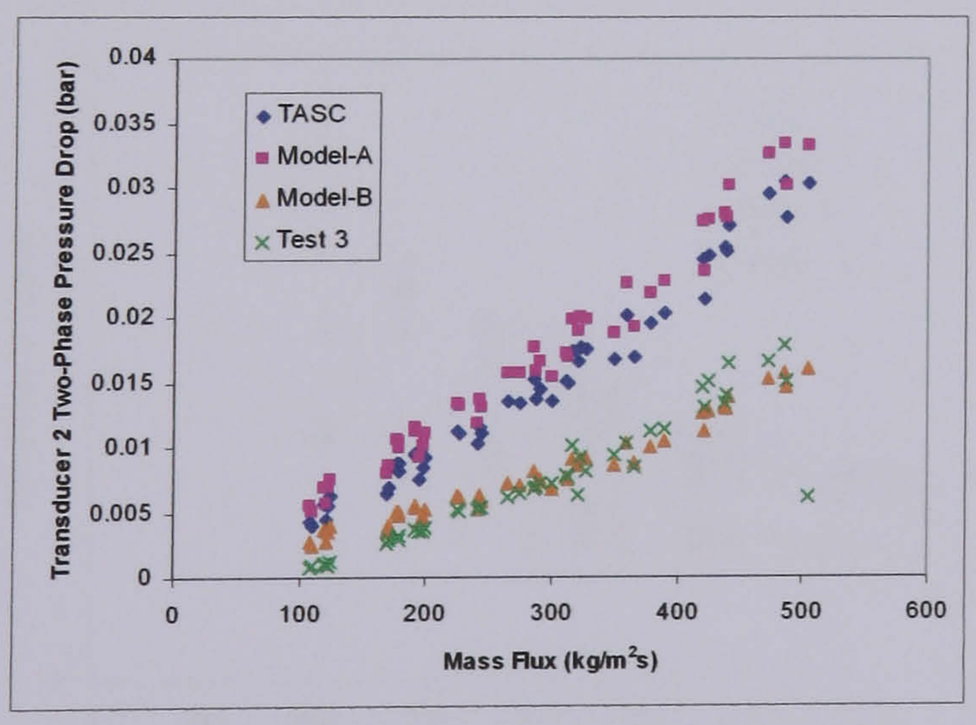

Vertical baffle cut

Figure 8.13 – Pressure drop predictions of TASC, Model-A, Model-B and Test 3 data (Shellside Transducer 2)

Figures 8.11 - 8.13 indicate that for the Transducer 2 experimental data the stratified flow model (Model-B) gives a much more satisfactory prediction of the pressure drop than the homogeneous flow models used in TASC and Model-A. In Chapters 6 and 7 it was observed that the homogeneous models over-predicted the experimental data for Transducer 2 but produced a more satisfactory prediction of the Transducer 1 data. The data comparison in Figures 8.11 - 8.13 indicate that for the length of the tube bundle between the Transducer tapping points the shellside flow pattern is best described with the stratified flow model. In the experimental analysis of Chapter 5 it was observed that there was a peak when the two-phase multiplier (based on total flow with liquid properties) was plotted against the mass flux. The two-phase multiplier data from the Transducer 2 measurements are plotted against the predictions of Model-B, Model-A and TASC in Figures 8.14 - 8.16.

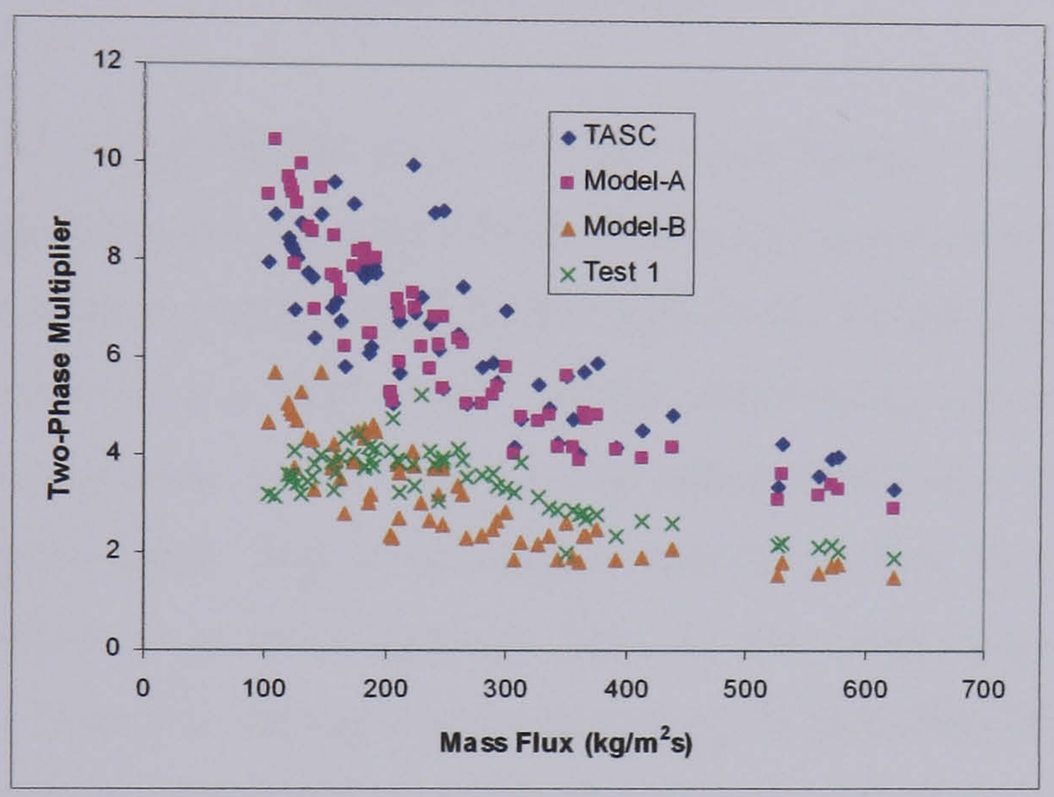

Horizontal baffle cut

Figure 8.14 – Two-phase pressure drop multiplier of TASC, Model-A, Model-B and Test 1 data (Shellside Transducer 2)

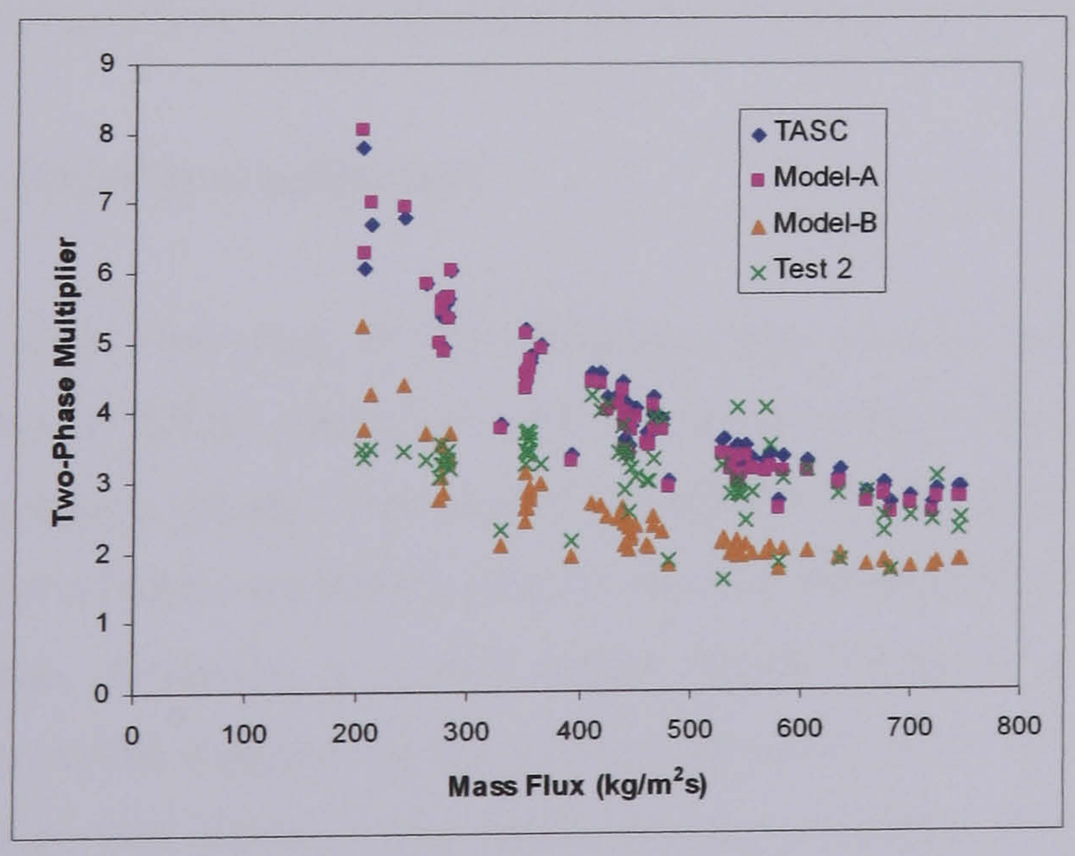

Vertical baffle cut

Figure 8.15 – Two-phase pressure drop multiplier of TASC, Model-A, Model-B and Test 2 data (Shellside Transducer 2)

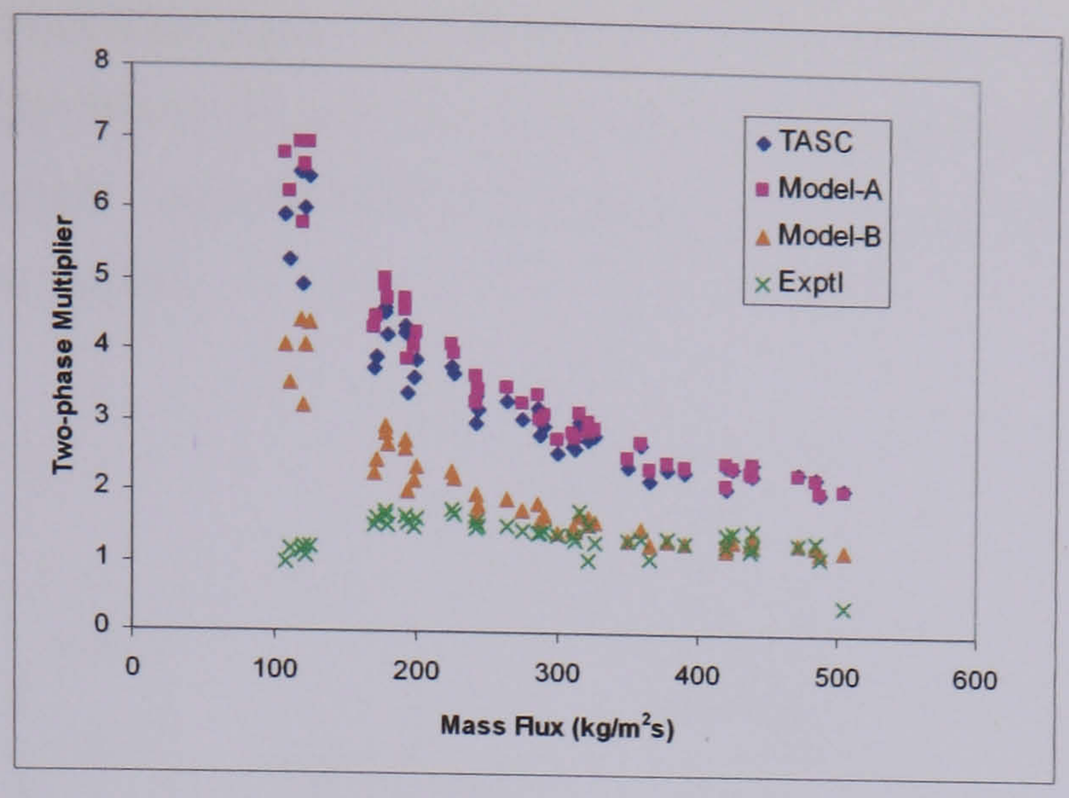

Vertical baffle cut

Figure 8.16 – Two-phase pressure drop multiplier of TASC, Model-A, Model-B and Test 3 data (Shellside Transducer 2)

The data in Figure 8.14 suggests that at the higher mass fluxes the experimental two-phase multiplier lies in a range between the predictions of the homogeneous models (TASC, Model-A) and the predictions of the stratified flow model (Model-B). Model-B generally gives a better prediction of the multiplier for the Test 1 data. At the lower mass flux end the peak observed in the experimental data causes a shift where the stratified model is more likely to give a good prediction of the multiplier value. This could support the theory that there is a transition from a homogeneous flow pattern to a more stratified flow, as the experimental data appears to be moving in the direction from the homogeneous(Model-A) to stratified(Model-B) predictions as the mass flux decreases. This trend is even more evident in the Test 2 data (Figure 8.15). At the higher mass flux values the homogeneous models give a better prediction whereas at the lower end the experimental data is better predicted by Model-B. Figure 8.16 indicates that the prediction of the Test 3 experimental multiplier is poor for all three models at the low mass flux range and Model-B produces the best prediction at the high mass fluxes.

8.3.2 – Boiling Heat Transfer Coefficient

Figures 8.17 - 8.19 show the plots of the shellside heat transfer coefficient predictions of Model-B against those of TASC, Model-A, and the experimental data. For the Test 1 data (Figure 8.17) at mass fluxes greater than about 200kg/m^{2}s the homogeneous models (TASC, Model-A) probably give a better prediction of the heat transfer coefficient as Model-B tends to under-predict the data. However at lower mass fluxes Model-B clearly gives a better prediction of the data trends supporting the theory that there is a transition to stratified flow around this mass flux. For Test 2 the homogeneous models clearly produce a better representation of the data at the higher mass fluxes than Model-B. At the lower mass fluxes however the predictions of Model-B are much closer to the experimental data. Figure 8.19

indicates that for the Test 3 data also, the lower end of the mass flux range is better predicted with the stratified model (Model-B) and the higher end with the homogeneous models (TASC, Model-A). This once again supports the theory that there is a transition from homogeneous to a stratified type of flow pattern.

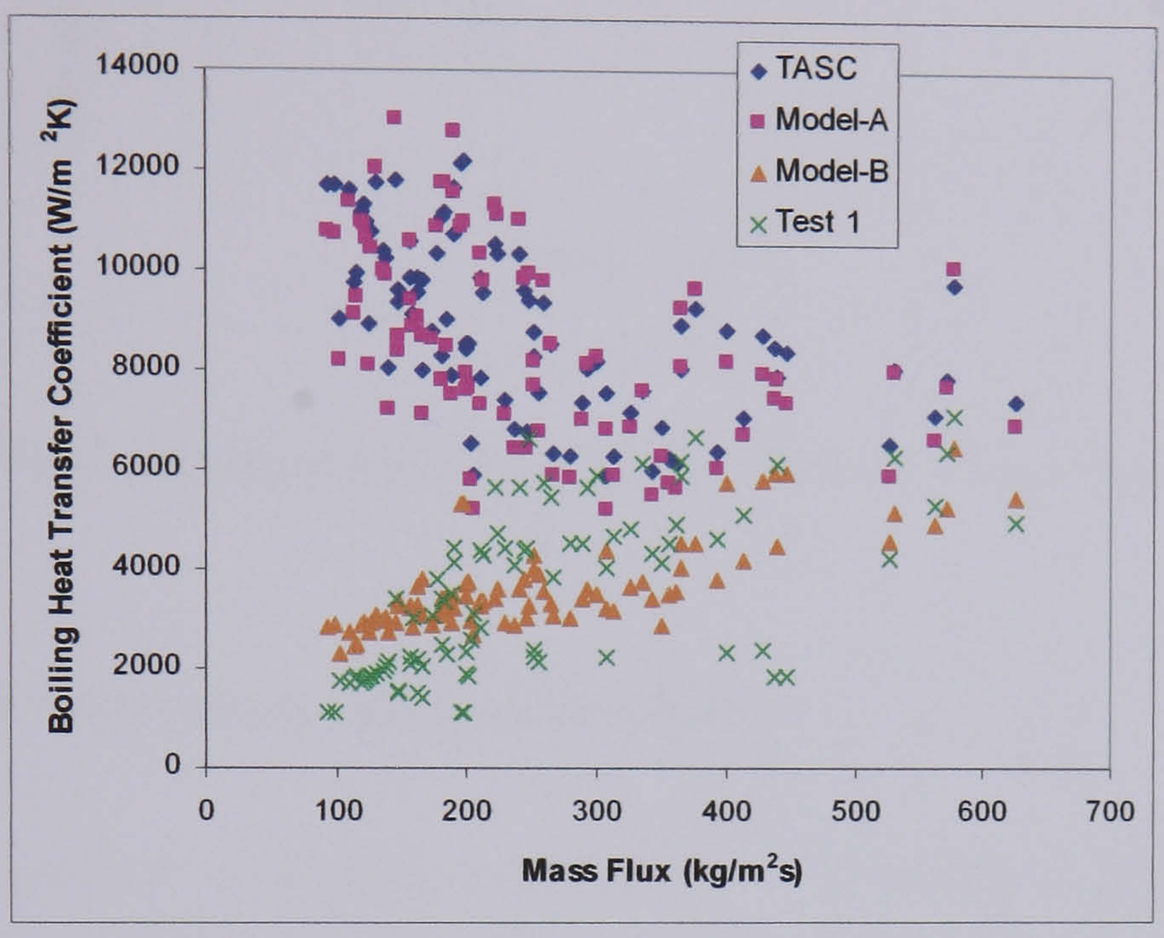

Horizontal baffle cut

Figure 8.17 – Heat transfer predictions of TASC, Model-A, Model-B and Test 1 data

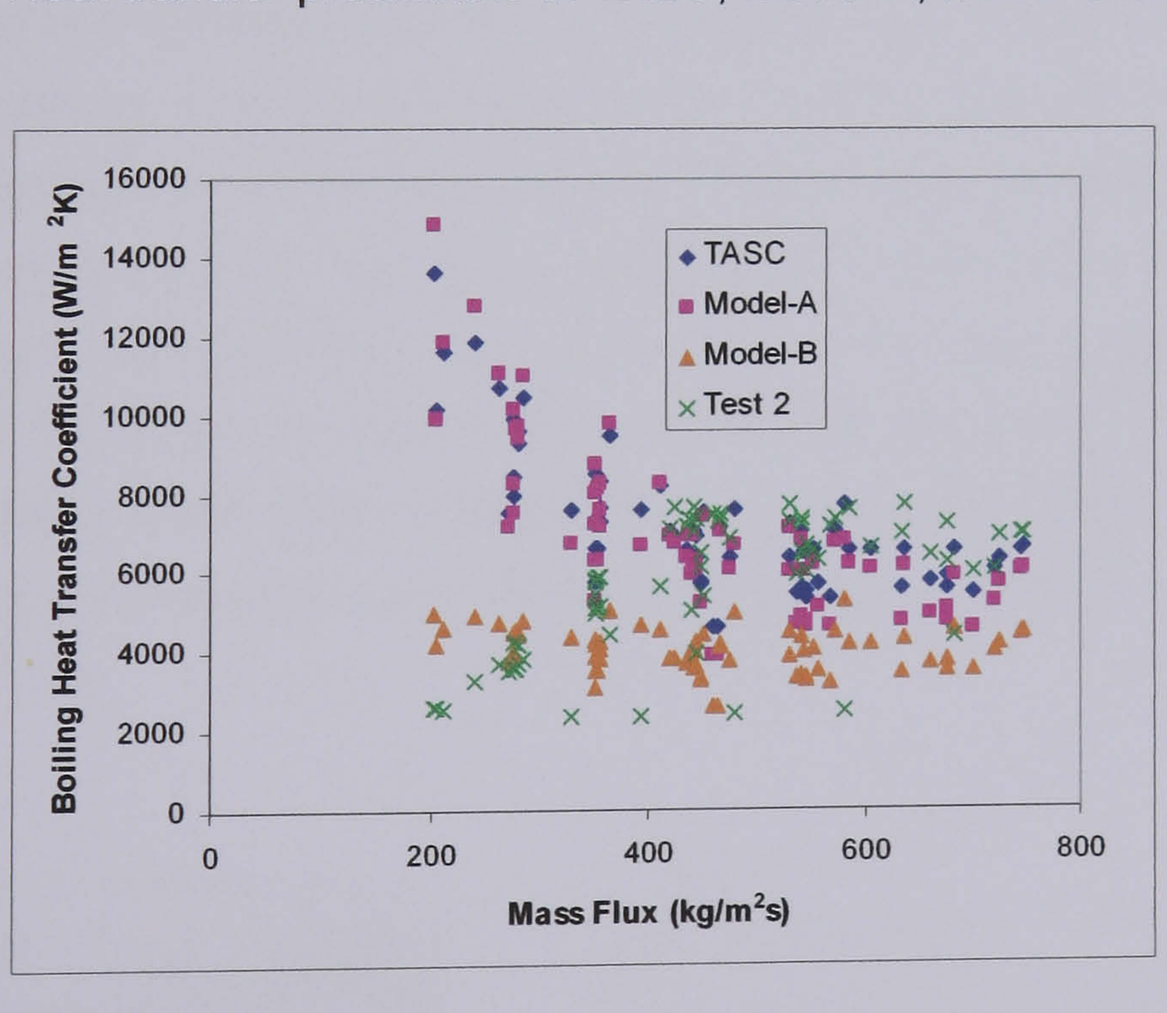

Vertical baffle cut

Figure 8.18 – Heat transfer predictions of TASC, Model-A, Model-B and Test 2 data

Vertical baffle cut

Figure 8.19 – Heat transfer predictions of TASC, Model-A, Model-B and Test 3 data

8.3.3 – Discussion – Alternative explanation of data?

The experimental pressure drop data in figures 8.11-8.13 suggests that the stratified flow model gives the best prediction over the whole of the experimental range. In contrast the heat transfer data in figures 8.17-8.19 suggests that there is a transition between stratified flow at the low mass fluxes and homogeneous flow at the higher mass fluxes. Thus it would appear that there is an apparent contradiction between the heat transfer and pressure drop data. One possible explanation is that the flow is mainly stratified over the whole range but there is sufficient entrainment of liquid in the vapour phase at high mass fluxes to ensure the upper tubes are fully wetted. Provided the majority of the tubes remain wet, nucleate and convective boiling could still be the dominant heat transfer process. The lower mass flux range where the transition in the heat transfer data is observed could represent where the flow becomes completely stratified and the upper tube rows are surrounded by vapour. A potential scenario is shown in Figure 8.20.

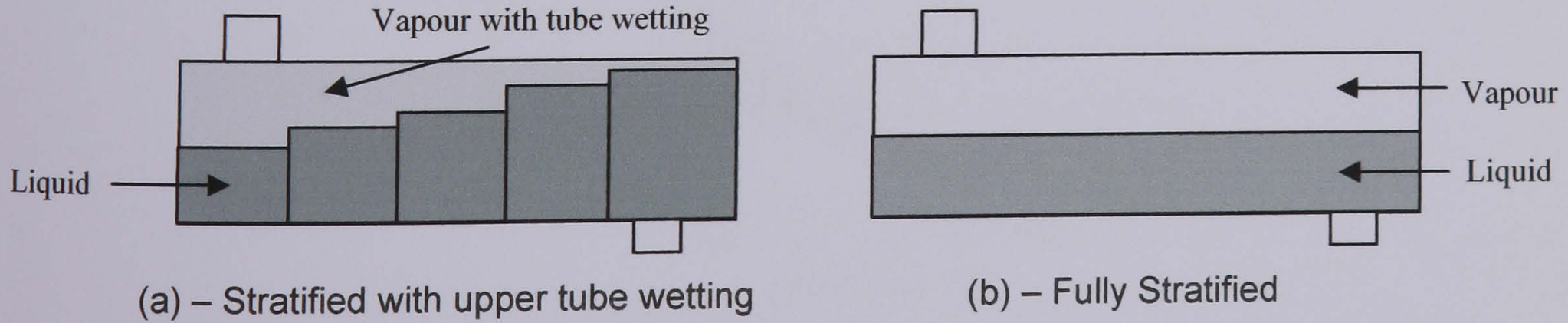

(a) – Stratified with upper tube wetting

(b) – Fully Stratified

Figure 8.20 – Potential stratified flow types at high and low mass fluxes

For the high mass flux tests the flow is predominantly stratified but with the tubes in the upper part of the bundle wet due to entrainment of liquid in the vapour phase (Figure 8.20(a)). At the lower mass fluxes the flow is completely stratified with a constant liquid level throughout the shellside.

The basis of the stratified flow model (Model-B) was that the vapour and liquid phases were distributed such that the frictional pressure drop in each phase was equal. In the lower mass flux range there is generally a larger change in the height of the vapour/liquid interface between the first and last baffle spaces from the stratified flow predicted by Model-B. In this range there is a possibility that the gravitational pressure drop becomes an important contributory factor to the phase distribution. The resulting increase in the importance of the gravitational term could imply that the liquid and vapour phases separate in the manner of Figure 8.20(b) to maintain an equal pressure drop in the liquid and vapour.

Assuming a flow distribution as in Figure 8.20(a), Model-B was used to calculate the interface height predicted in the first and last baffle spaces for all the experimental test data. These heights were then used to calculate the gravitational pressure drop in the liquid phase from equation 8.30.

$$\Delta P_{grav} = \rho_l g_n \left(H_{1st} - H_{last} \right) \tag{8.30}$$

The values of the gravitational pressure drop in the liquid phase between the first and last baffle spaces were used to assess the significance of the gravitational term in the low mass flux range. The values calculated using equation 8.30 were compared with the frictional pressure drop predicted using Model-B. The results of the comparison are presented in Figure 8.21.

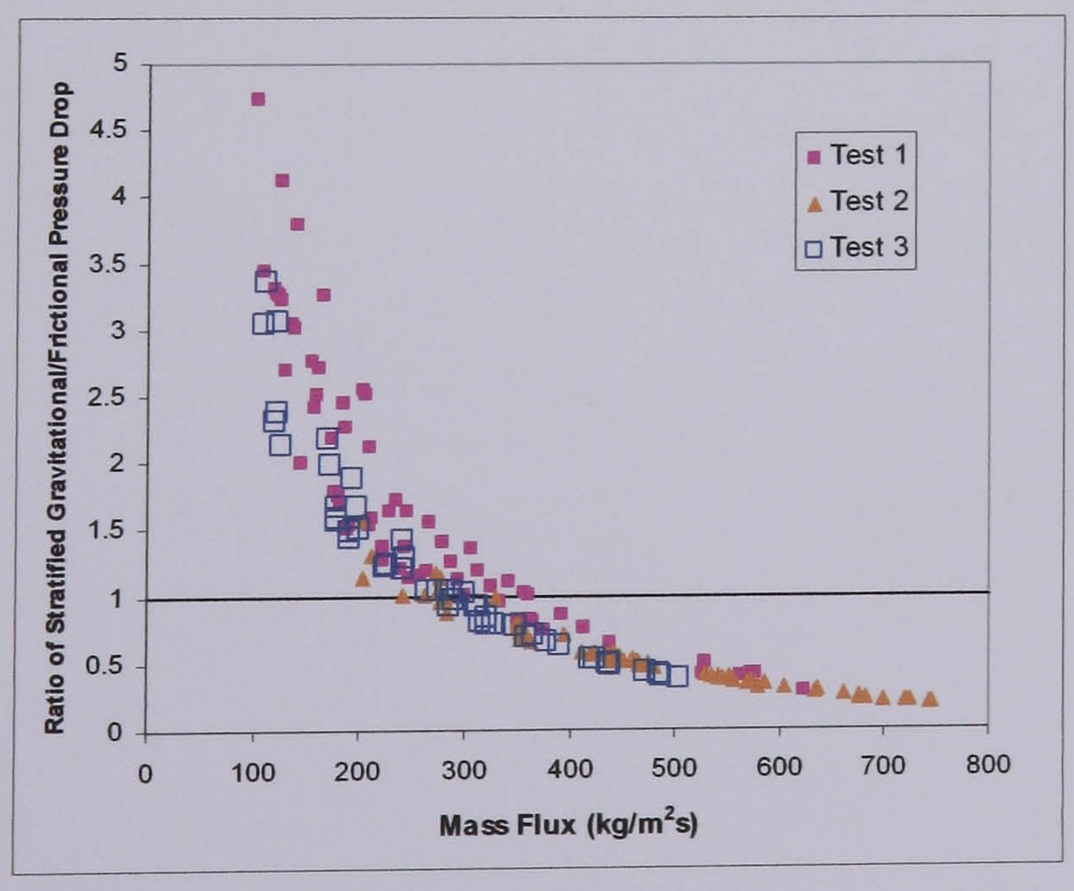

Figure 8.21 – Ratio of gravitational to Model-B frictional pressure drop (all tests)

It is clear from Figure 8.21 that the gravitational component becomes more significant than the frictional component at the low mass fluxes (< 300 kg/m^2s) suggesting that the gravitational forces become more important than the frictional forces at these mass fluxes. This may suggest that the type of flow shown in Figure 8.20(b) is more likely to be occurring at the lower mass fluxes in the experimental tests.

8.4 – Conclusion

The comparisons of the heat transfer and pressure drop data with the predictions of Model-B highlight that there is evidence of a transition to a stratified type of two-phase flow. Model-B vastly improves the prediction of the heat transfer coefficient at the low mass flux range of the experimental tests where a decrease in evaporator performance had been observed. This supports the hypothesis that a transition to stratified flow had occurred in the experimental tests. The Model-B pressure drop predictions would suggest that the flow may be stratified throughout the whole of the experimental test range. Comparison of the heat transfer and pressure drop data indicates that the flow may be stratified but with sufficient liquid in the vapour phase at high mass fluxes to ensure that heat transfer performance expected from a homogeneous flow can be obtained. Whether the flow at the high mass flux range is indeed stratified or homogeneous, it is clear from the Model-B analysis that a shellside model that could predict the onset of a completely separated stratified flow at lower mass fluxes would be a very useful and significant improvement on the current design methods.

CHAPTER 9 – Further model development; flow-pattern transition (Model-C)

9.1 – Introduction

The experimental data (Chapter 5) and subsequent shellside models (Chapters 7 and 8) suggested that there had been a transition to separated flow during the programme on the test evaporator. The analysis of Model-B, described in Chapter 8 showed that an improved prediction of the heat transfer and pressure drop data was obtained at the lower mass fluxes when a stratified flow pattern was assumed in place of the usual homogeneous pattern assumed by the current design methods such as TASC. The greatest benefit to the design process would be obtained from a model that could predict the onset of the completely stratified flow pattern and which could be used to prevent operation with this type of flow. In Chapter 5 it was shown that a correlation used for the prediction of transition to stratified flow in tubes (Weisman et al, 1979) gave a reasonable representation of the observed transition in the shellside data. In this chapter, potential transition criteria are examined and assessed for inclusion in a shellside model (Model-C) which predicts the shellside flow pattern and calculates the corresponding heat transfer and pressure drop data. For analysis, the shellside data presented in the graphs in this section are grouped in terms of observed heat transfer performance as in Section 5.4.

9.2 – Potential Models

An assessment of the open literature (See Chapter 5) revealed that there was very little information on the subject of flow pattern transitions in two-phase shellside flow. The only available shellside maps were based on very limited air/water tests in ideal geometries. In addition the transitions are described in terms of dimensionless groups which are empirically correlated to experimental data. There is far more information on the subject of flow pattern transition in tubeside flow, which is in turn based on a far larger range of experimental data. The shellside maps presented in Chapter 5 (Grant, 1977) gave a reasonably good representation of the transition in the experimental data. However due to the limited data on which the flow pattern maps are based and also in the inherent limitations due to the empirical nature of the model, it was decided to examine the possibility of adapting a tubeside model to describe the transition. In this section some tubeside models are examined which have a theoretical basis for describing the flow pattern transition.

9.2.1 – Method of Chen (Chen et al, 1997)

In Chapter 5 the Test 1 data for the horizontal baffle orientation were plotted on the shellside flow map for vertical crossflow of Grant et al (Grant, 1977). The plot is shown again in Figure 9.1. The transition in the heat transfer data corresponds closely with the transition from bubbly flow to intermittent flow. It was decided to examine a tubeside model used for the prediction of transition to bubbly flow in order to assess the applicability to the prediction of the shellside flow pattern. The theoretical model of Chen (Chen et al, 1997) was examined as it is applicable to several geometries and is possibly quite adaptable for inclusion in a general shellside model. The method is described by the authors as a general model for transition to dispersed bubble flow. The assumption made in applying it to the shellside data is that the mechanism of break-up into bubble flow can be used to describe the transition between a well mixed bubble flow and an intermittent or stratified flow. The transition to a stratified flow may be more closely related to bubble coalescence than break-up, however it is assumed that the transition point as represented in the flow pattern maps describes the transition between flow patterns in both directions regardless of the original flow pattern. The model is based on the hypothesis that the dispersed bubble flow pattern can exist when the turbulent frictional forces in the liquid phase are greater than the buoyant gravitational forces in the vapour phase. The applicability of this method in the shellside case will depend on how accurately this transition describes the predominance of frictional over gravitational forces in the shellside case. A diagram showing dispersed bubble flow in horizontal and vertical tubes is shown in Figure 9.2.

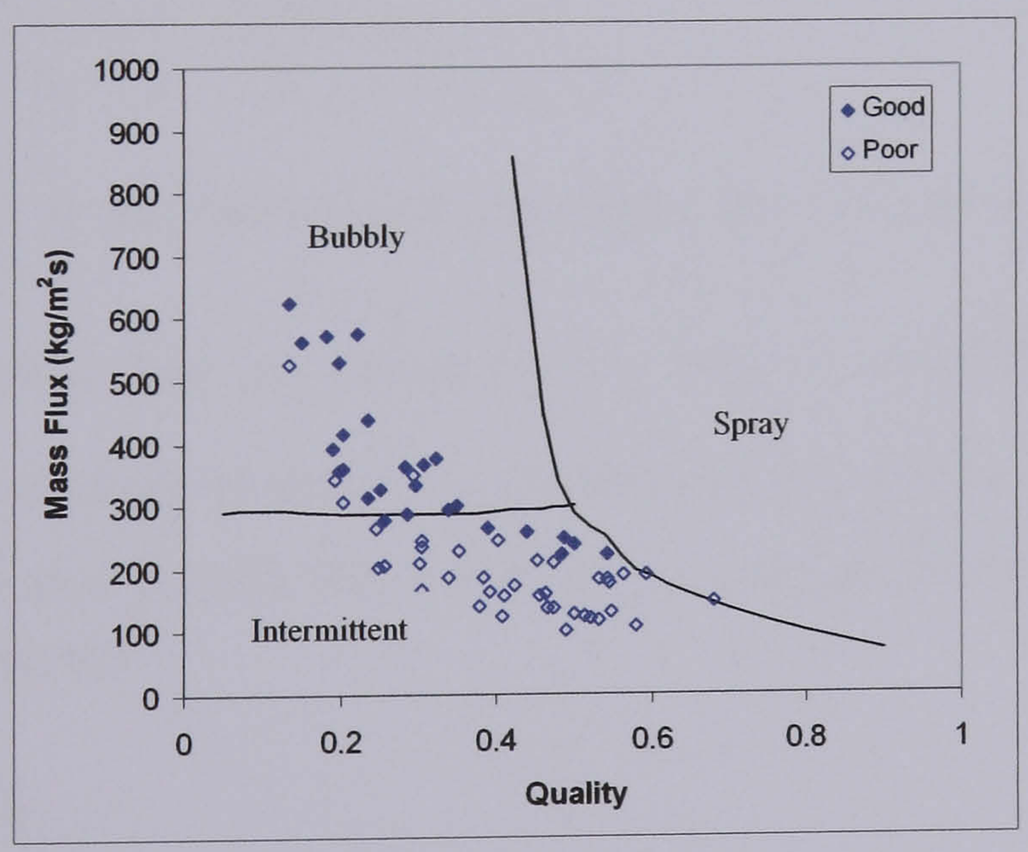

Figure 9.1 – Test 1 data on flow pattern map for vertical crossflow (Grant, 1977)

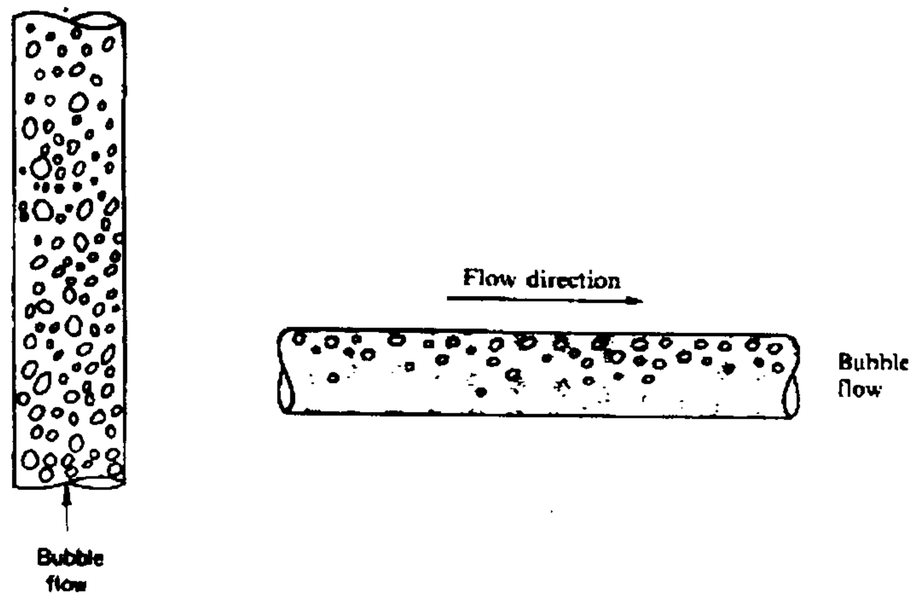

Figure 9.2 – Bubble flow in vertical and horizontal tubeside flow

The method is based on the occurrence of dispersed bubble flow at high liquid flowrates where there is a uniform distribution of the gas phase in the form of finely dispersed bubbles in a continuous flowing liquid phase. The dispersed bubbles behave as rigid spheres rising vertically in rectilinear motion. The flow is considered as a homogenous flow. According to Chen, dispersed bubble flow is caused when the liquid flow rate is sufficiently high to cause the gas phase to be broken up into small spherical bubbles, i.e. when the turbulent forces in the liquid overcome the gas-liquid interfacial tension. An increase in gas flowrate requires a further increase in the liquid flowrate to disperse the gas phase. The transition to bubbly flow is assumed to occur when the turbulent kinetic energy of the incoming liquid phase is greater than the total surface free energy of dispersed bubbles with a critical diameter to retain a spherical shape. The total turbulent kinetic energy of the incoming liquid flow is calculated using equation 9.1.

$$E_T = \frac{3}{2} C_L \left(\frac{D_H u_{Sl}}{\eta_l} \right)^{-n} \frac{\rho_l u_{Sl}^2}{2} A u_{Sl} \qquad (9.1)$$

The term $C_L \left(\frac{D_H u_{Sl}}{\eta_l} \right)^{-n}$ is the friction factor for liquid flow in a smooth pipe at superficial velocity u_{Sl}. For turbulent flow the values for C_L and n of 0.046 and 0.2 were used respectively, and the hydraulic diameter D_H is calculated as 4 times the area divided by the wetted perimeter. The total surface free energy of discrete gas bubbles in dispersed bubble flow is given by equation 9.2.

$$E_S = \frac{6\sigma}{d} A u_{Sg} \qquad (9.2)$$

The average diameter of the bubbles existing in the dispersed bubble flow can be calculated by equating equations 9.1 and 9.2. However, the method is based on the assumption that dispersed bubble flow only exists when the bubbles are small enough to retain their spherical shape and prevent the process of agglomeration due to bubble deformation. The critical

diameter first proposed by Brodkey (Brodkey, 1967) and later modified by Barnea (Barnea 1982, 1986) is used in the transition model and calculated using equation 9.3.

$$d_c = 2\left[\frac{0.4\sigma}{(\rho_l - \rho_g)g}\right]^{1/2} \tag{9.3}$$

A diameter larger than that calculated in the above equation would lead to deformation of the gas bubble from its spherical shape. This critical bubble diameter is used to define the minimum surface free energy at which dispersed bubble flow can exist by combining equations 9.2 and 9.3 to give equation 9.4.

$$E_{S(\min)} = 3Au_{Sg}\left[2.5(\rho_l - \rho_g)\sigma g\right]^{1/2} \tag{9.4}$$

Equations 9.1 and 9.4 are equated to define the transition boundary to dispersed bubble flow. The resultant equation is rearranged (equation 9.5) for representation in the flow pattern coordinates of superficial gas and liquid phase velocities.

$$\frac{u_{Sl}}{u_{Sg}} = 12.65\frac{Y_L}{Eo^{1/2}} \tag{9.5}$$

Where;

$$Y_L = \frac{(\rho_l - \rho_g)g}{\frac{4C_L}{D_H}\left(\frac{D_H u_{Sl}}{\eta_l}\right)^{-n}\frac{\rho_l u_{Sl}^2}{2}} \tag{9.6}$$

Eo is a modified Eotvos number given by:

$$Eo = \frac{g(\rho_l - \rho_g)D_H^2}{\sigma} \tag{9.7}$$

It was decided to apply the method of Chen to the shellside flow case, to assess the possibility of its use in predicting the observed transition in the data. In order to apply the method to shellside flow it was necessary to amend the values used for the parameter D_H and the friction factor C_L in equations 9.1 and 9.6. The hydraulic diameter used for shellside flow was taken as twice the minimum gap between the tubes in crossflow. This diameter is often used for calculating Reynolds number in shellside crossflow. The value of the parameter C_L was calculated from HTFS correlations for frictional pressure drop over tube banks in crossflow (Wills, 1984). The parameter is largely a function of crossflow Reynolds number and tube bundle geometry. For the range of experimental tests on the current evaporator geometry, the crossflow Reynolds number was found to vary between values of 9500 and 65000. In this region there were not large deviations in the calculated value of C_L. For simplification it was decided to apply an average Reynolds number of 37000 for the purpose of evaluating the Chen model. The value of C_L calculated using the HTFS method is defined

in terms of the number of tube rows in crossflow, where the characteristic number used is defined by equation 9.8.

$$N_{Cr} = \frac{L_{Cr}}{d_o} \tag{9.8}$$

L_{Cr} is the length of the tube bundle in the crossflow direction and d_o is the tube outer diameter. From the geometry of the experimental evaporator it was decided to base the calculation on having 7 tube rows in crossflow. From the evaporator dimensions this gave a value of $L_{Cr} = 0.1397$ m with a tube diameter $d_o = 0.01588$ m. The value given by equation 9.8 in this case is 8.80. This must then be multiplied by C_L calculated from the HTFS correlations to give the appropriate value of C_L for use in the Chen method. For the current evaporator geometry and test conditions the value of $C_L = 34.7$ was calculated. This is evidently far greater than the $C_L = 0.046$ used in the Chen method. The difference can be attributed to the fact that the turbulent forces involved in a flow across banks of tubes are likely to be very much greater than those involved in flow through a smooth tube.

The transition to dispersed bubble flow predicted by the adapted Chen model is plotted in figure 9.3(a) for the characteristic conditions of the experimental tests (R-134A at 700kPa). Also plotted are the transition lines to bubbly flow of the shellside flow pattern maps for horizontal and vertical crossflow (Figure 5.13) of Grant and Murray (Grant, 1977). These transition lines have been converted into the coordinates of the superficial phase velocities for comparison with the predictions of the Chen method. Figure 9.3(b) shows a comparison of the Chen transition to bubbly flow with the experimental shellside data of Tests 1 – 3. The data points in Figure 9.3(b) have been separated into the categories of acceptable and poor heat transfer performance defined in Chapter 5 (section 5.4).

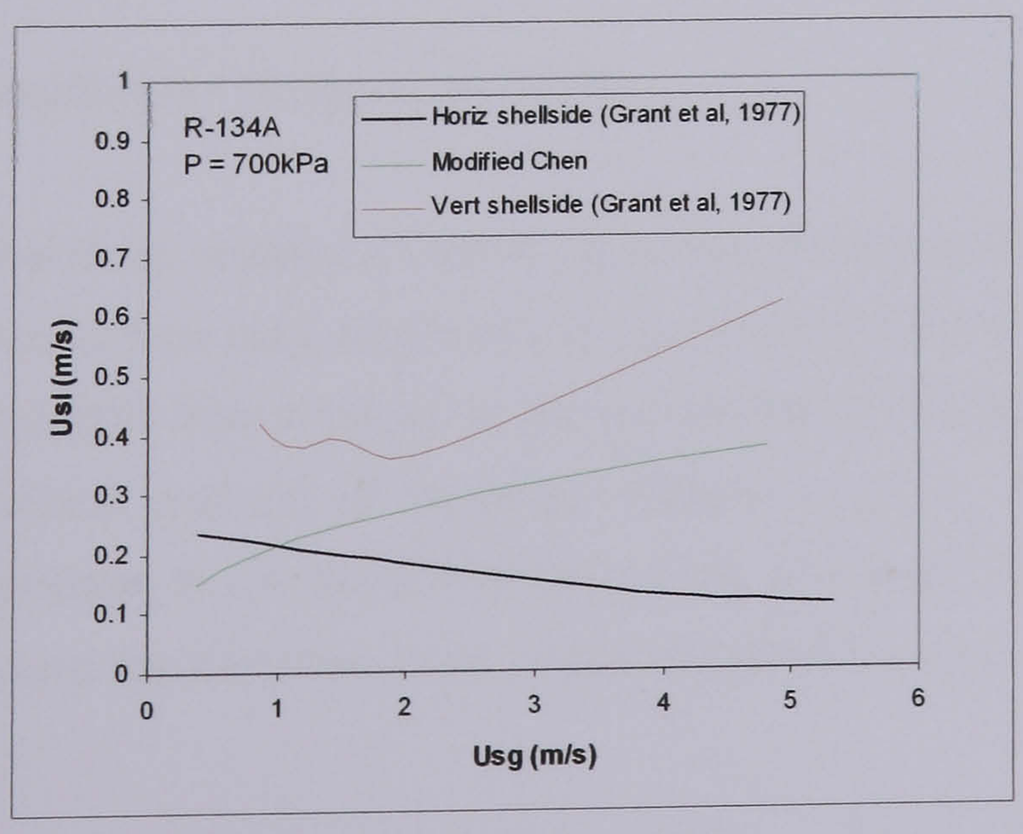

Figure 9.3(a) – Chen (Chen et al, 1997) and Shellside (Grant, 1977) transition to bubbly flow

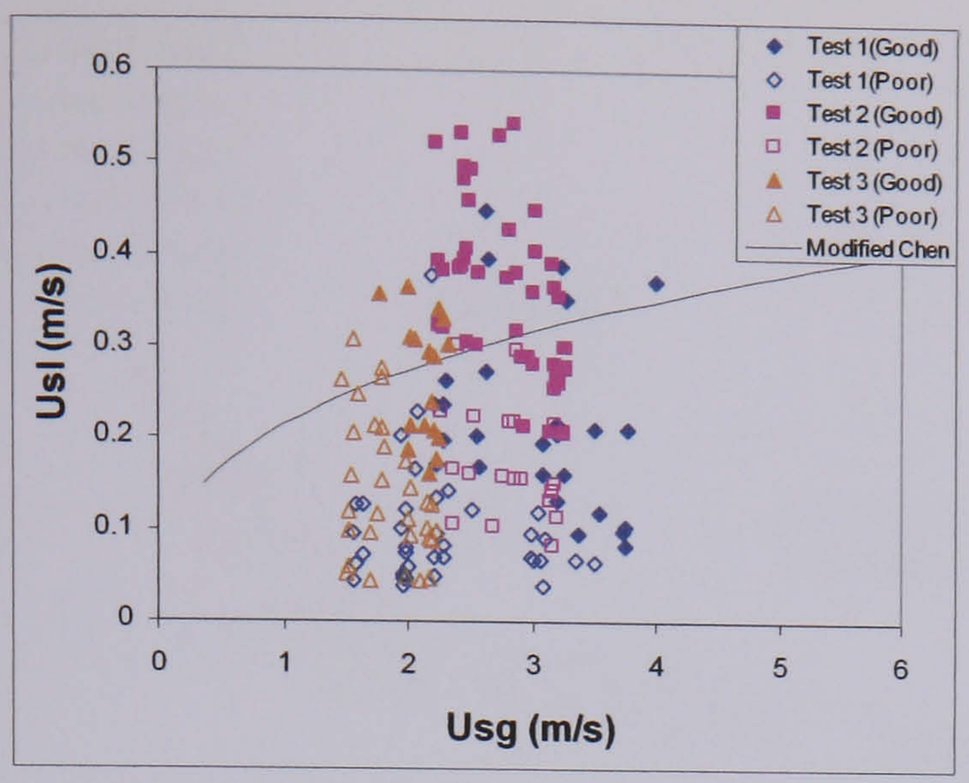

Figure 9.3(b) – Chen transition (Chen et al, 1997) and data for Tests 1 -3

From Figure 9.3(a) it can be seen that the adapted Chen model produces a prediction for transition to bubbly flow between the predictions of the two shellside lines. At lower superficial vapour velocities (<2 m/s) the model of Chen predicts the opposite trend (increasing u_{sl} with increasing u_{sg}) to the transitions of the shellside maps. Figure 9.3(b) indicates that the Chen method tends to over predict the value of u_{sl} at which the transition occurs. In total only 50% of the data considered as 'good' in the analysis of section 5.4 (the solid data points) appear above the transition line in figure 9.3(b). In addition it appears that the prediction becomes worse as the value of u_{sg} increases. This may indicate that the trend of increasing u_{sl} of transition with increasing u_{sg} could be inaccurate for the shellside case. The Chen method is based on the principle that an increasing gas velocity requires a larger liquid velocity to break-up the gas phase into discrete bubbles; however the transition in the shellside data does not repeat this trend. This may suggest that the Chen model may not be applicable to the shellside case as the turbulent kinetic energy of the liquid phase may not be the controlling mechanism in the transition to homogeneous flow.

9.2.2 – Method of Taitel/Dukler (Taitel et al, 1976)

From the analysis of the Chen method it seems clear that the apparent flow pattern transition in the shellside data may not be best explained by the physical mechanisms used to describe the onset of dispersed bubble flow in tubes. In the discussion of Chapter 5 (section 5.4) it was observed that the tubeside method of Weisman (Weisman et al, 1979) gave reasonable agreement with the transition in the experimental results. The graph in Figure 9.4 shows the experimental test data and the transition lines of the Weisman method.

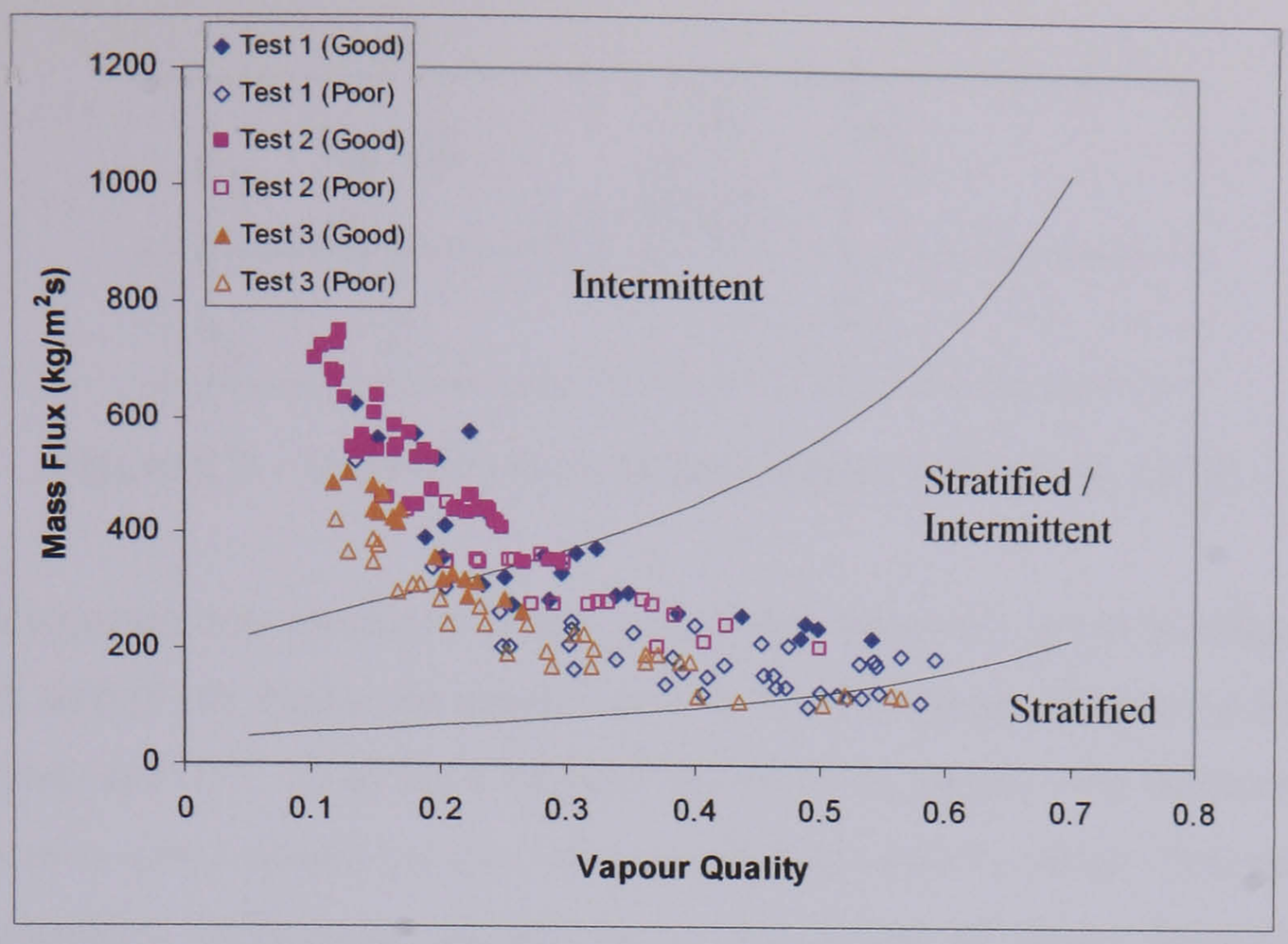

Figure 9.4 – Experimental test data and transition to stratified flow (Weisman et al, 1979)

In figure 9.4, 69% of the good heat transfer data (solid data points) are above, and 78% of the poor heat transfer data points are below the transition line between intermittent and stratified/intermittent flow. The transition line from the Weisman method appears to be closer to describing the point of transition in the data than the Chen method. The Weisman method describes the transition from stratified flow to intermittent flow in horizontal two-phase flow in tubes. The reasonably close relationship between the transition in the shellside data and the transition in the tubeside model suggests that a more accurate representation of the shellside data may be obtained from close examination of the mechanisms behind the deviation from stratified flow in tubes. The Weisman method (described in Chapter 5) is an empirical model based on experimental data collected from two-phase flow in tubes. The empirical nature of the method gives rise to inherent limitations in terms of application to a general shellside model. To counter this limitation it was decided to examine a more theoretical approach to describe the transition from stratified flow in tubes. The method of Taitel/Dukler (Taitel et al, 1976) is a very popular criterion for determining tubeside two-phase flow patterns. The paper describes theoretical mechanisms for transition between the five basic flow regimes; smooth-stratified, stratified-wavy, intermittent, annular-dispersed and dispersed-bubble flow. It was decided to examine the transition between stratified and intermittent flow in the Taitel/Dukler method as this transition had produced good correlation with the experimental data using the Weisman method. The authors base the model on the idea that an increase in the liquid flowrate during stratified flow will eventually cause a wave large enough to form a blockage in the pipe causing the onset of intermittent flow. The model begins by considering a stratified flow with a wave existing on the surface over which the gas flows (Figure 9.5)

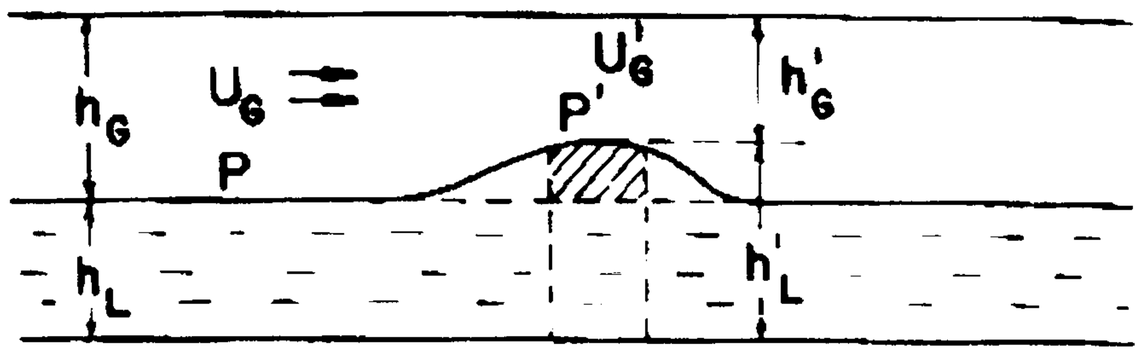

Figure 9.5 – Instability for a solitary wave (Taitel et al, 1976)

As the gas accelerates the pressure in the gas phase over the wave decreases due to the Bernoulli effect, which will make the wave more inclined to grow. The force of gravity on the wave will compete with this trend as it causes the wave to decay. The authors define criteria for the stability of a wave based on the Kelvin-Helmholtz theory (Milne-Thomson, 1960). For waves of infinitesimal amplitude formed on a flat sheet of liquid flowing between two horizontal parallel plates relationship 9.9 applies. This describes the velocity of the gas phase at which waves will begin to grow.

$$u_g > \left[\frac{g(\rho_l - \rho_g)h_g}{\rho_g}\right]^{1/2} \tag{9.9}$$

Here h_g is the distance between the equilibrium liquid level and the upper plate. The authors extend this theory, firstly for the case of a wave of finite amplitude, then for the wave in pipe geometry. The gas velocity which defines the transition from stratified to intermittent flow in tubes is given by equation 9.10.

$$u_{g(Crit)} = C_2\left[\frac{(\rho_l - \rho_g)g_n A_g}{\rho_g \dfrac{dA_l}{dh_l}}\right]^{1/2} \tag{9.10}$$

Where A_g is the cross sectional flow area of the vapour in the stratified flow without the wave, A_l and h_l are the corresponding liquid phase area and height, g_n is the acceleration due to gravity and C_2 is given by:

$$C_2 = 1 - \frac{h_L}{D} \tag{9.11}$$

D is the diameter of the tube corresponding with the liquid height h_l. A superficial gas velocity value higher than that predicted by relationship 9.10 would cause a departure from stratified flow. The assumption made on applying this type of transition to the shellside is that the velocity high enough to cause a departure from stratified flow in the tubeside case could be high enough to cause a transition from stratified flow in the shellside case. To assess how the model of Taitel/Dukler compares with the shellside data it was essential to generate

predictions of the critical gas velocity from equation 9.10 for the shellside case. The superficial gas velocity of a particular flow can be determined from equation 9.12.

$$u_{sg} = \frac{\dot{m}x}{\rho_g} \tag{9.12}$$

For shellside flow the mass flux $\dot{m}$ is based on the minimum-crossflow and bypass areas and x is the vapour mass quality. The value of u_{sg} obtained from equation 9.12 is compared with the value from 9.10. If the velocity is greater than that of equation 9.10 the method predicts intermittent flow and a smaller velocity implies stratified flow. However, calculation of the critical gas velocity from equation 9.10 requires knowledge of the void fraction in the pipe (or shell) geometry. For the current comparison the shellside geometry was used. An attempt was made to create a map (as in Figure 9.4) of the predictions of the Taitel/Dukler model on which the shellside data could also be plotted. The shellside data thus far has been presented in most cases on the coordinates of mass flux against vapour quality and so it was attempted to create a line tracing the quality and mass flux values corresponding to the predicted transition of the Taitel/Dukler method for the experimental conditions. The method involved an iterative calculation on the shellside mass flux to obtain the critical value for the transition. It can be seen that the regime transition based on the Taitel/Dukler method can be obtained by equating 9.10 and 9.12 as in 9.13.

$$\frac{\dot{m}x}{\rho_g} = C_2\left[\frac{(\rho_l - \rho_g)g_n A_g}{\rho_g \dfrac{dA_l}{dh_l}}\right]^{1/2} = u_{g(Crit)} \tag{9.13}$$

This equation contains the terms C_2, A_g and $\frac{dA_l}{dh_l}$ which are all functions of the shellside void fraction ε_g. The void fraction, in turn is a function of the shellside mass flux and vapour quality, therefore the calculation procedure is an iterative one. To create the predictions of the Taitel/Dukler model for the shellside case the following procedure is adopted.

- Set vapour quality, estimate mass flux.
- Put values into stratified shellside model described in Chapter 8 (Model-B) to obtain shellside void fraction.
- From shellside void fraction calculate values of C_2, A_g and $\frac{dA_l}{dh_l}$
- Calculate $u_{g(Crit)}$ then re-calculate mass flux from 9.13. If mass flux is different from estimate, repeat calculation with new mass flux.

From the resolution of Model-B, the void fraction is obtained, as is the height of the stratified surface (from method described in Chapter 8). The value of C_2 is obtained from equation 9.11, A_g is obtained from the void fraction and the total cross sectional area of the shell using the shell internal diameter. The value of the rate of change of the liquid phase area with the liquid phase height $\frac{dA_l}{dh_l}$ is estimated numerically using equation 9.14.

$$\frac{dA_l}{dh_l} \approx \frac{\Delta A_l}{\Delta h_l} = \frac{A_{l2} - A_l}{h_{l2} - h_l} \tag{9.14}$$

Where A_l is the area covered by the liquid phase of height h_l and h_{l2} is a height marginally greater than that of the liquid phase. For the purpose of this calculation the value of h_{l2} was fixed as 1cm larger than that of the calculated phase height h_l (It was found that this difference was sufficiently small to represent $\frac{dA_l}{dh_l}$ at any given stratified interface height).

For a range of vapour qualities the mass flux was calculated that corresponds with the Taitel/Dukler transition. Also a map was created containing the superficial liquid and vapour velocities as they are often used for two-phase flow pattern maps. The superficial gas velocity was calculated using equation 9.12 and the corresponding liquid velocity using 9.15.

$$u_{sl} = \frac{\dot{m}(1-x)}{\rho_g} \tag{9.15}$$

Figures 9.6 and 9.7 show the data for the horizontal and vertical baffle orientations (again plotted in terms of 'good' and 'poor' heat transfer defined in section 5.4) with the transition lines of the Taitel/Dukler method. Both maps were created for the experimental conditions of R-134A at 700kPa.

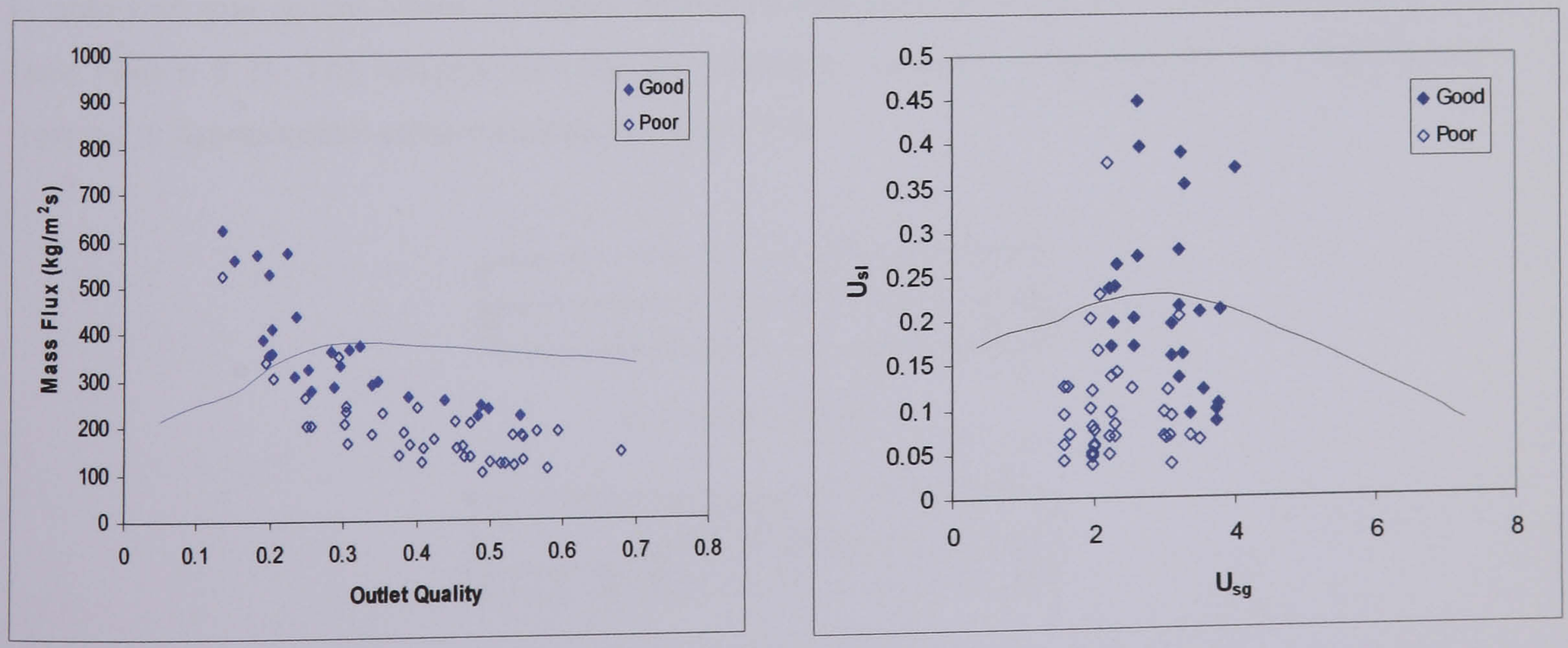

Figure 9.6 – Test 1 data (Horizontal baffle) and transition line of Taitel/Dukler method

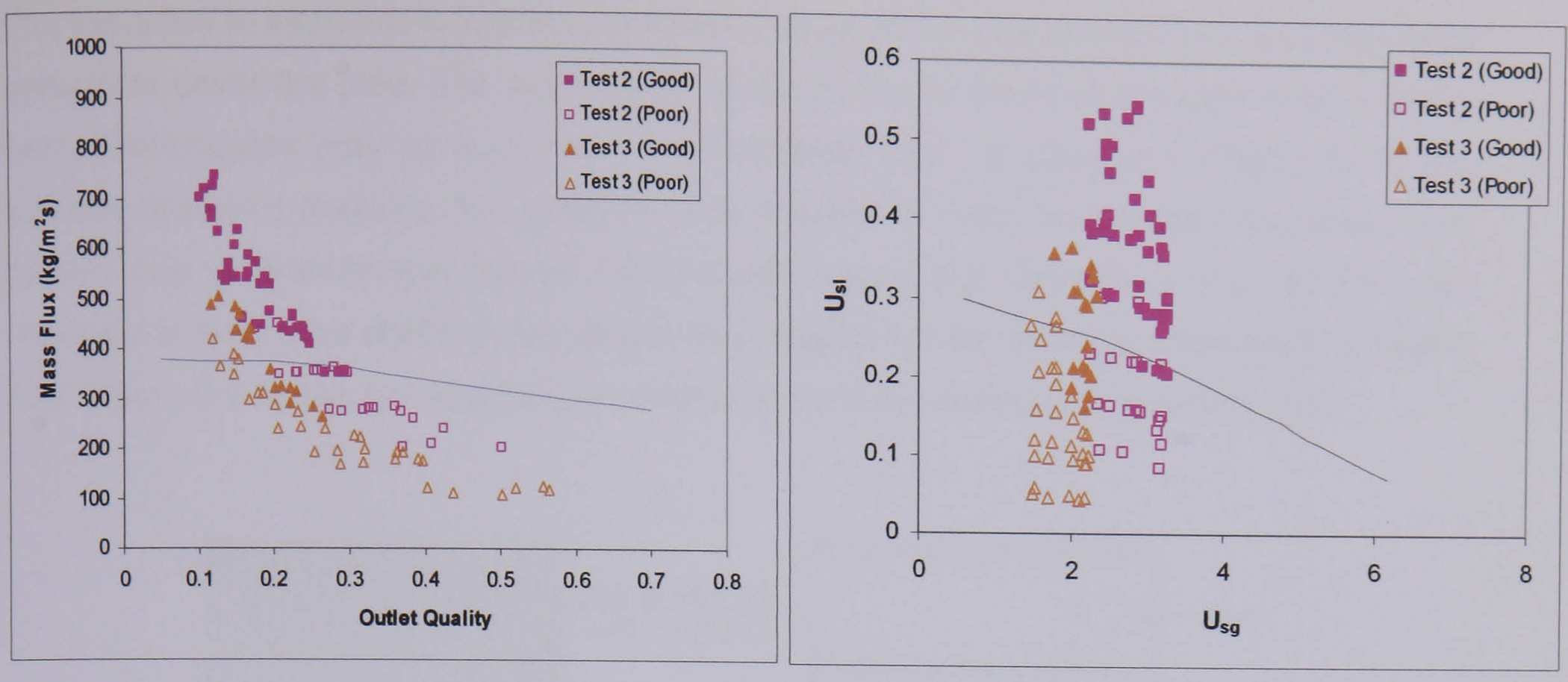

Figure 9.7 – Test 2 and 3 data (Vertical baffle) and transition line of Taitel/Dukler method

From the figures it is apparent that the transition criterion of the Taitel/Dukler method gives a good representation of the transition in the shellside data, with 68% of the 'good' data points above the transition line and 95% of the poor data points below. The best agreement is obtained with the data for the vertical baffle orientation (Figure 9.7) as 82% of the 'good' data points are above and 95% of the 'poor' data below the transition line in this case. The success of the prediction with this baffle geometry is not surprising as this orientation promotes flow in the horizontal plane on which the theoretical model is based. The applicability of the Taitel/Dukler analysis to the horizontal baffle orientation is more questionable as the flow direction is forced up and down between the shellside baffle spaces. Despite this the transition in the horizontal orientation data is also reasonably well represented by the Taitel/Dukler and Weisman methods (Figures 9.6 and 9.4). This is possibly because a similar mechanism is causing the onset/departure from stratified flow; however a poorer agreement is obtained due to the more complex nature of the stratified flow with this baffle orientation (see Figure 8.1). The mechanism for the tubeside transition proposed by the Taitel/Dukler method is represented schematically in Figure 9.8.

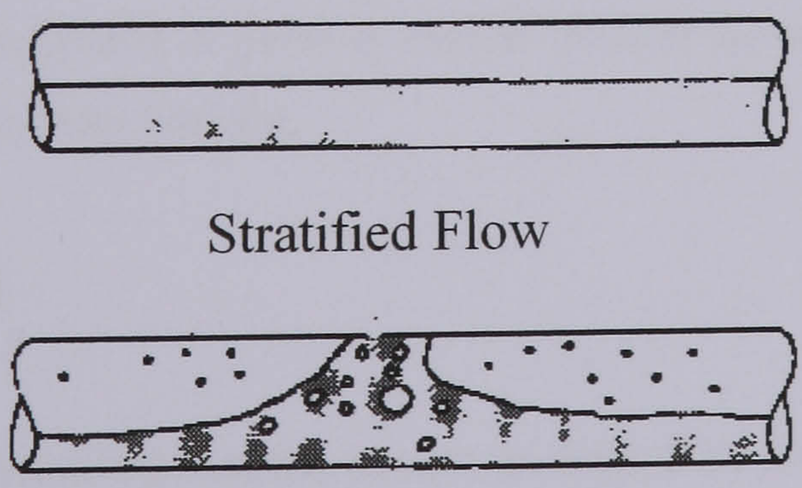

Figure 9.8 – Transition from Stratified to Intermittent Flow in Tubes

The transition to intermittent flow occurs when a wave on the stratified surface becomes large enough to cover the pipe. The applicability of the model to the shellside data implies that a similar mechanism may be occurring in the shellside flow. In Chapter 5 (Figure 5.12) the typically observed shellside flow patterns were presented. From the shellside two-phase flow pattern map of Grant/Murray (Grant, 1977) it was evident that intermittent flow had not been observed in horizontal shellside two-phase flow despite the fact that it is observed in tubeside flow. Figure 9.9 shows the flow patterns represented in the shellside flow pattern map.

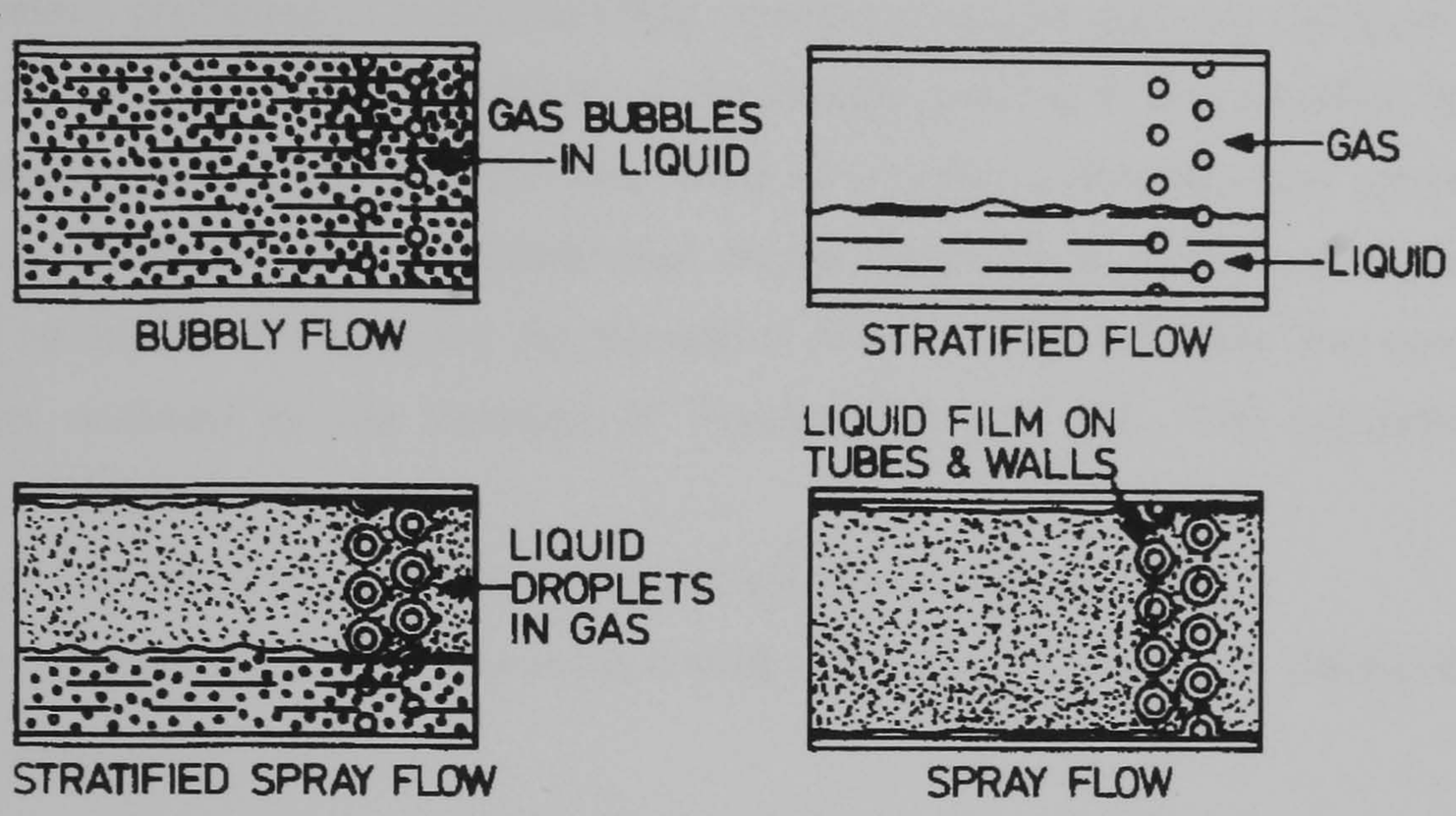

Figure 9.9 – Flow Patterns observed in horizontal two-phase flow (Grant, 1977)

The mechanism of transition between the shellside flow patterns in Figure 9.9 is less clear than in the tubeside case (Figure 9.8). The application of the Taitel/Dukler tubeside method to the shellside case is based on the assumption that a vapour phase velocity sufficient to cause a transition from stratified flow in the tubeside case (Figure 9.8) would be sufficient to cause a departure from stratified flow in the shellside case (Figure 9.9). Whether this transition was to be to stratified-spray, bubbly or spray flow would be dependent on the local conditions of vapour quality and void fraction. The success of the method of Taitel/Dukler in representing the transition in the shellside data highlighted that it may be a useful indicator in a general shellside model. As a result the models described in Chapter 7 (Model-A) and Chapter 8 (Model-B) were amended to create a general model (Model-C) which includes the possibility of a change in the two-phase flow pattern.

9.3 – Model-C Method

The analysis of Chapter 8 indicated that the pressure drop data for the experimental tests was best predicted by the stratified flow model, Model-B across the whole range. By contrast the heat transfer prediction would benefit from the inclusion of a transition criterion which

describes the point at which the flow was sufficiently separated to cause liquid wetting of the upper rows of the tube bundle. Thus it was decided to create a flow model which attempts to define the point at which the flow ceases to be completely stratified.

The calculation method adopted in Model-C was to apply the transition criteria of the Taitel/Dukler tubeside method to the general shellside model. This is achieved by applying the criteria to the input data, predicting the shellside flow pattern and altering the calculation procedure accordingly.

If the flow pattern predicted is a stratified flow, the heat transfer data are calculated using the model described in Chapter 8 (Model-B). If the model predicts a non-stratified flow pattern, the homogeneous TASC style model described in Chapter 7 (Model-A) is applied. For the pressure drop predictions the stratified flow model, Model-B is assumed to give the best prediction. The method for applying the transition criteria to the shellside flow runs is exactly the same as outlined in the creation of Figures 9.6 and 9.7. The procedure can be summarised as follows:

- Input vapour quality and mass flux and all other input parameters
- Put values into stratified shellside model described in Chapter 8 (Model-B) to obtain shellside void fraction.
- From shellside void fraction calculate values of C_2, A_g and $\frac{dA_l}{dh_l}$
- Calculate $u_{g(Crit)}$, also calculate u_{sg} from (9.12). If $u_{sg} > u_{g(Crit)}$ then the flow pattern is assumed non-stratified, if u_{sg} is not greater than $u_{g(Crit)}$ the flow is assumed stratified.

9.3.1 – Allowance for Entrainment

In addition to the allocation of the homogeneous pattern (Model-A) or the stratified pattern (Model-B) there is also an allowance made for the fraction of entrainment of liquid in the vapour phase. The purpose for allowing entrainment of the liquid phase was to smooth the transition in the heat transfer data in order to describe the process of wetting an increasing fraction of the tubes in the upper tube bundle.

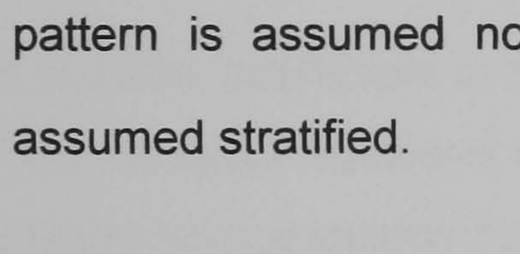

(a) – Completely stratified

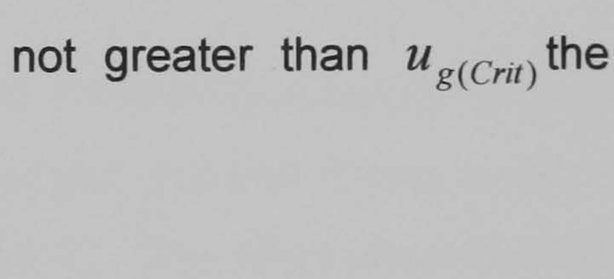

(b) – Flow with liquid entrainment

Figure 9.10 – Completely Stratified flow and Stratified flow with entrainment

An entrainment parameter E was defined that describes the fraction of the tubes in the upper bundle that are surrounded by liquid. A value of $E = 0$ implies that the flow is completely stratified as in figure 9.10(a) with no wetting of the upper tube bundle, whereas $E = 1$ implies that all of the tubes in the upper bundle are surrounded by liquid. Equations 9.16 – 9.18 were used to control the range of gas superficial velocities over which the transition from no tube wetting in the upper bundle to complete tube wetting occurs.

$$\text{If } u_{sg} < Low_{bc} u_{g(Crit)} \text{ Then } E = 0 \tag{9.16}$$

$$\text{If } u_{sg} > Up_{bc} u_{g(Crit)} \text{ Then } E = 1 \tag{9.17}$$

$$\text{If } Low_{bc} u_{g(Crit)} < u_{sg} < Up_{bc} u_{g(Crit)} \text{ Then } E = \left(\frac{\dfrac{u_{sg}}{u_{g(Crit)}} - Low_{bc}}{Up_{bc} - Low_{bc}} \right) \tag{9.18}$$

Up_{bc} and Low_{bc} are the upper and lower boundary conditions which must be chosen to define the range of data over which entrainment occurs. Appropriate values of the boundary conditions are examined in section 9.4. The equation for E in (9.18) represents a linear interpolation of tube wetting due to liquid entrainment in the vapour phase between the lower and upper boundary conditions.

9.3.2 – Calculation of Shellside Heat Transfer Coefficient

The heat transfer coefficient in the model with transition (Model-C) is based on defining the stage of the transition between the completely stratified heat transfer model of Model-B and the completely homogeneous heat transfer model, Model-A. The entrainment wetting factor, E is used to calculate the shellside heat transfer coefficient using equation 9.19.

$$\alpha_{Model-C} = E\alpha_{Model-A} + (1 - E)\alpha_{Model-B} \tag{9.19}$$

9.3.3 – Calculation of Shellside Pressure Drop

In Model-C the calculation of shellside pressure drop is undertaken using the stratified flow model, Model-B. The analysis of Chapter 8 suggested that this gave the best predictions throughout the full range of data. The assumption in using this method is that there is sufficient liquid entrainment at the higher mass fluxes to produce a flow pattern as in Figure 9.10(b). In this case the flow pattern is predominantly stratified and there is little deviation between the pressure drop calculated with a small fraction of liquid entrainment and that calculated by the fully stratified model. This approach is in contrast to that adopted for the heat transfer coefficient in which it is assumed that the homogeneous style heat transfer

model (Model-A) can be adopted at higher mass fluxes. The reason for the difference in approach is that with a small fraction of liquid entrainment (sufficient for tube wetting in the upper rows) the heat transfer mechanisms of homogeneous flow can be sustained and the heat transfer performance is effectively the same as in the homogeneous flow case. In contrast a large fraction of liquid entrainment in the vapour phase would be required to produce a pressure drop in the range as would be expected for homogeneous flow.

9.4 – Comparison of Model-C and previous models with experimental data

The transition criterion of the tubeside method of Taitel/Dukler was combined with the shellside flow models described in the previous chapters. Model-A for homogeneous flow and Model-B for stratified shellside flow were combined to create Model-C which accounts for both flow types. In this section the predictions of Model-C are compared with the experimental test data and with Model-A and Model-B to analyse the potential improvements of the shellside model with flow pattern transition. The comparisons are made with all of the test data for the shellside heat transfer coefficient (α). The data for the shellside pressure drop is not examined in this section as Model-B is used to calculate the pressure drop across the full range. In each of the comparisons the range over which the transition occurs is also examined. In each of the Figures Model-C is applied with 5 different sets upper and lower boundary conditions relevant to equations 9.16 – 9.18. The boundary conditions tested were as follows:

$$Low_{bc} = 0.95 \text{ and } Up_{bc} = 1.05 \tag{9.20}$$

$$Low_{bc} = 0.75 \text{ and } Up_{bc} = 1.25 \tag{9.21}$$

$$Low_{bc} = 0.5 \text{ and } Up_{bc} = 1.5 \tag{9.22}$$

$$Low_{bc} = 0.25 \text{ and } Up_{bc} = 1.75 \tag{9.23}$$

$$Low_{bc} = 0.05 \text{ and } Up_{bc} = 1.95 \tag{9.24}$$

Figures 9.11 - 9.13 show comparisons of the shellside heat transfer Model-C predictions against those of Model-A, Model-B and the experimental data for Tests 1-3. In each figure the letters (a) – (e) show the Model-C predictions with the entrainment boundary conditions taken from equations 9.20-9.24. It can be seen from Figure 9.11 that the best prediction of the Test 1 heat transfer data is obtained using Model-C with the boundary conditions taken from equation 9.23. For Test 2 and Test 3 (figures 9.12 and 9.13) the best agreement with the heat transfer data is obtained using Model-C with the boundary conditions defined by equations 9.20 or 9.21. These results would suggest that for the horizontal baffle arrangement (Test 1) the transition to completely stratified flow is more gradual. With the vertical baffle arrangement (Tests 2 and 3); the transition to complete stratification is much sharper. This result is unsurprising as the vertical baffle cut promotes flow in the horizontal side to side direction

where gravitational separation is easier than with the horizontal baffle which produces vertical up-and-down shellside flow.

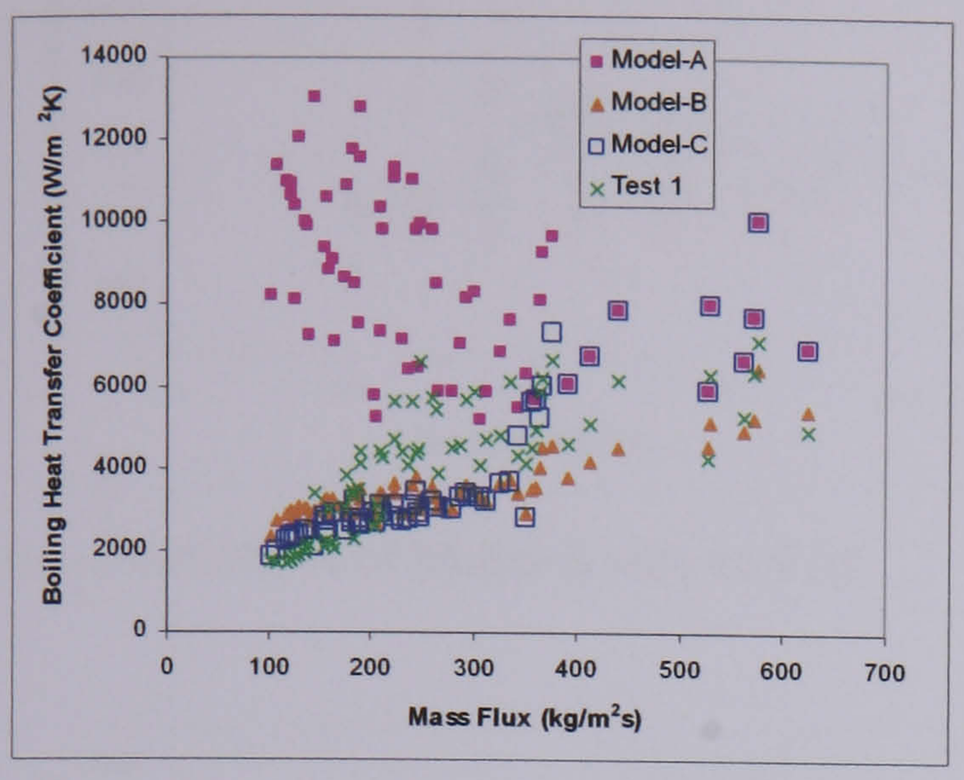

(a) – Predictions of Model-C with eq.9.20

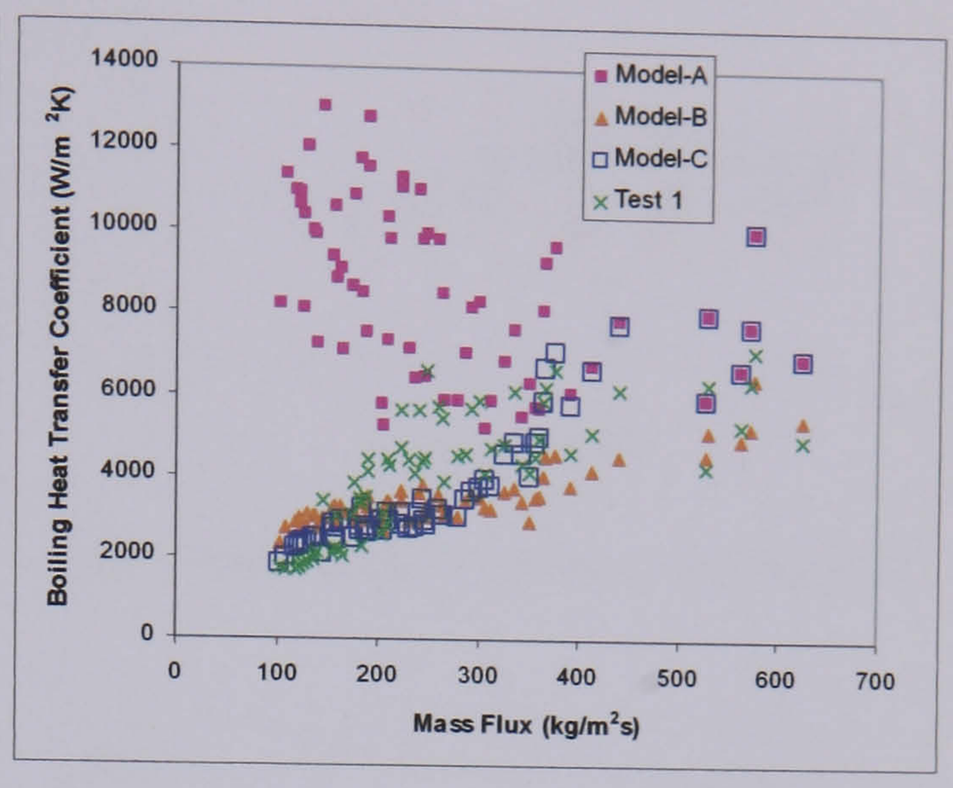

(b) – Predictions of Model-C with eq.9.21

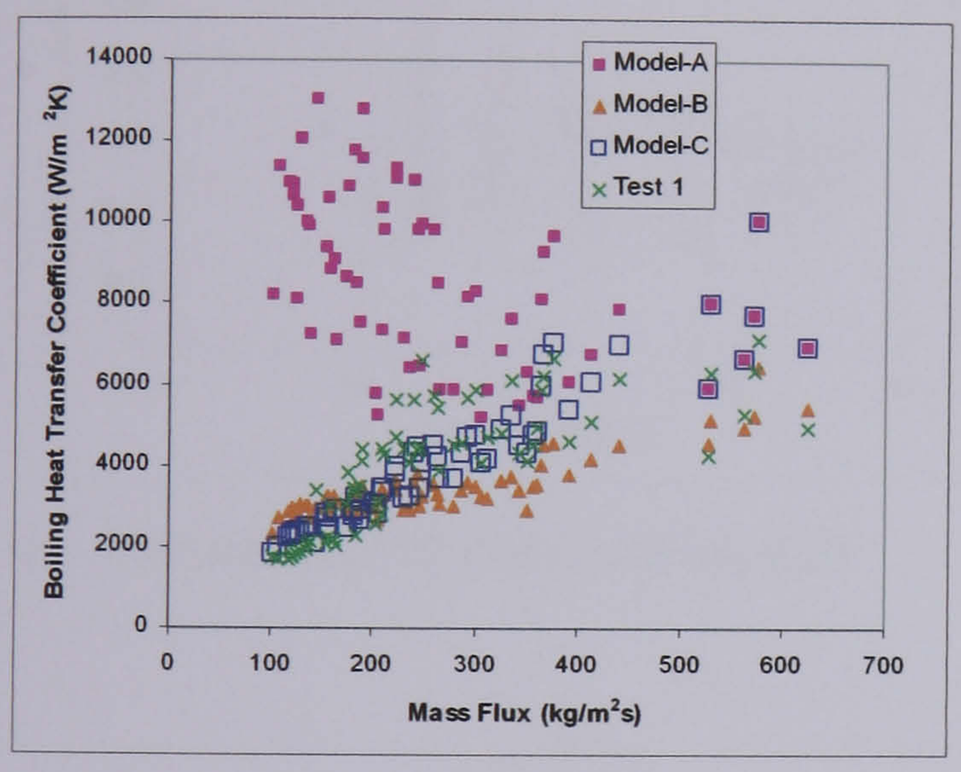

(c) - Predictions of Model-C with eq.9.22

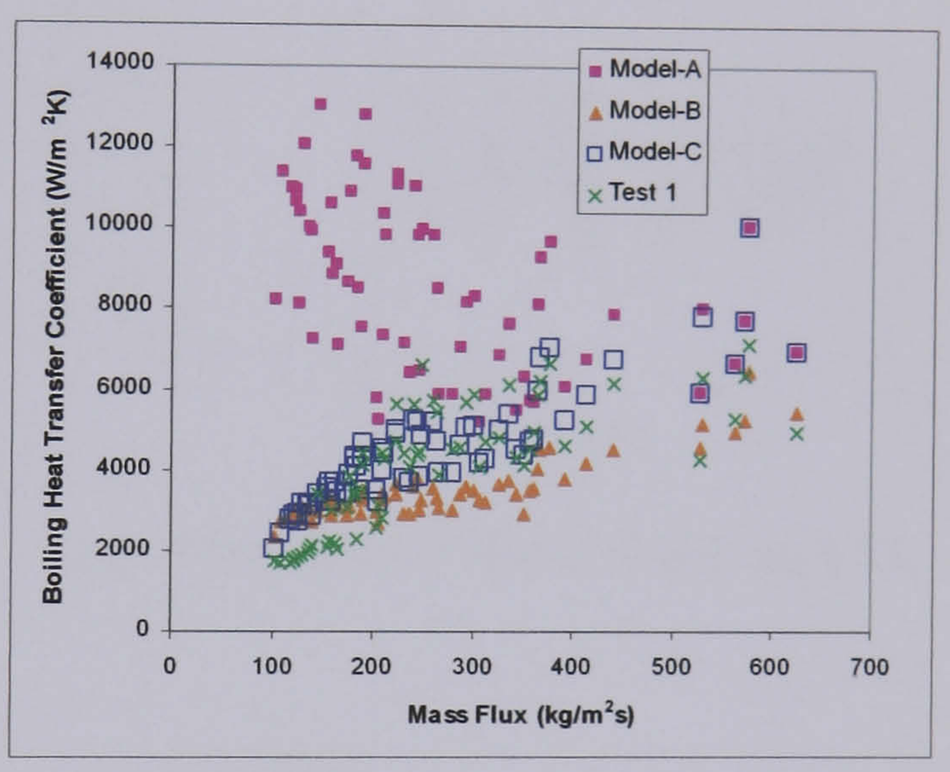

(d) - Predictions of Model-C with eq.9.23

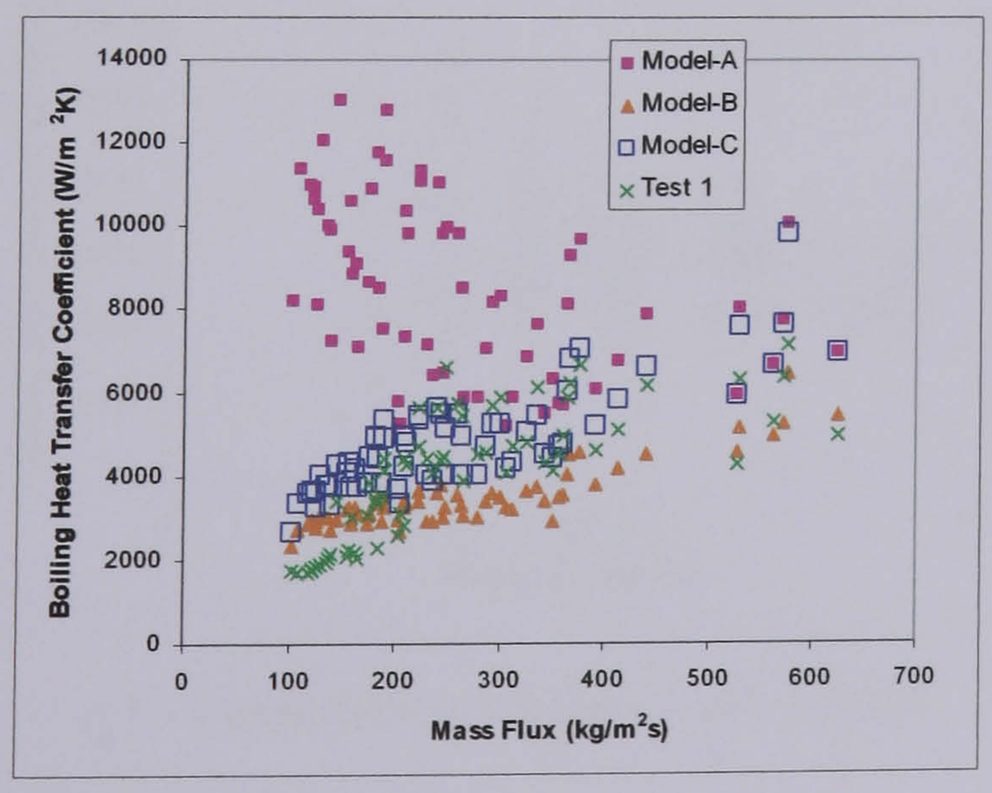

(e) - Predictions of Model-C with eq.9.24

Figure 9.11 – Heat transfer predictions of Model-A, Model-B, Model-C and Test 1 data

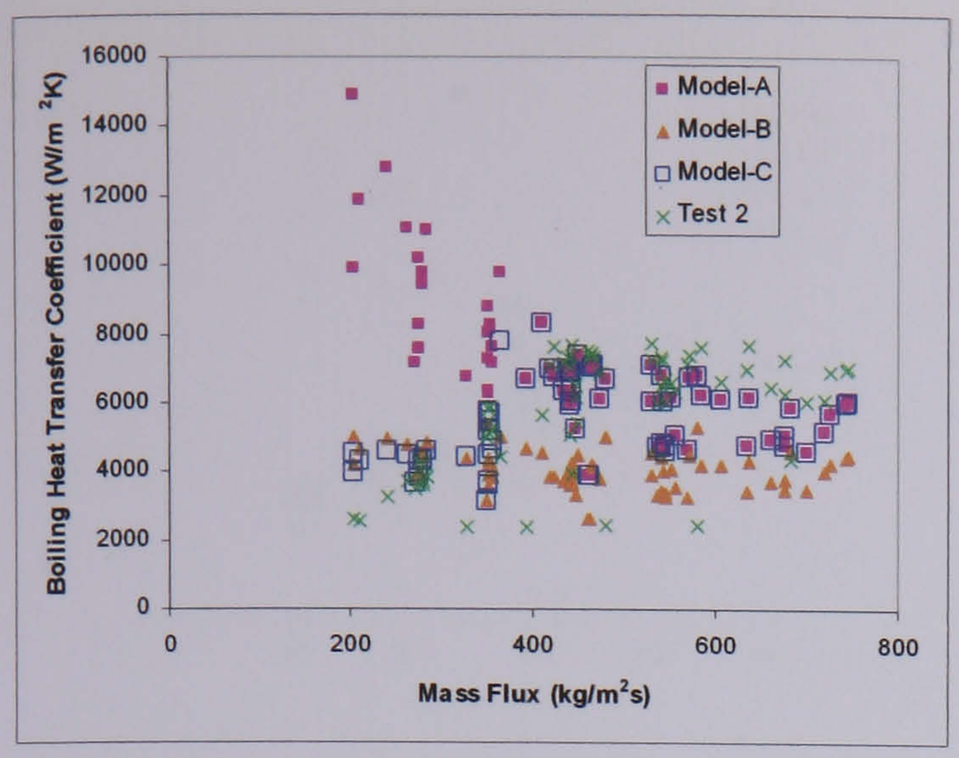

(a) – Predictions of Model-C with eq.9.20

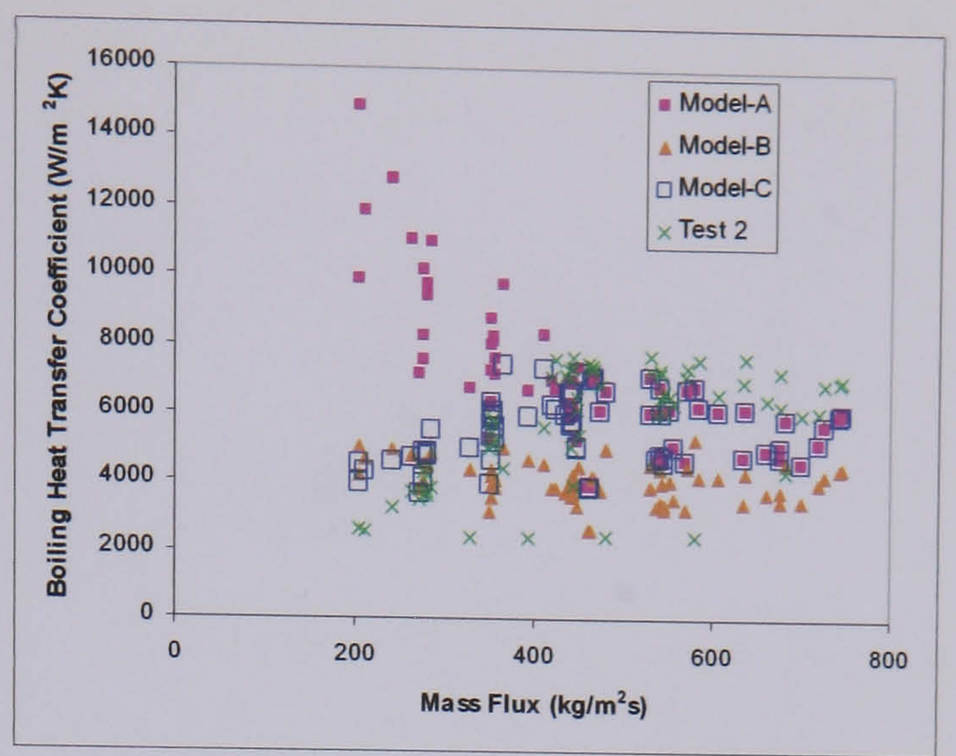

(b) – Predictions of Model-C with eq.9.21

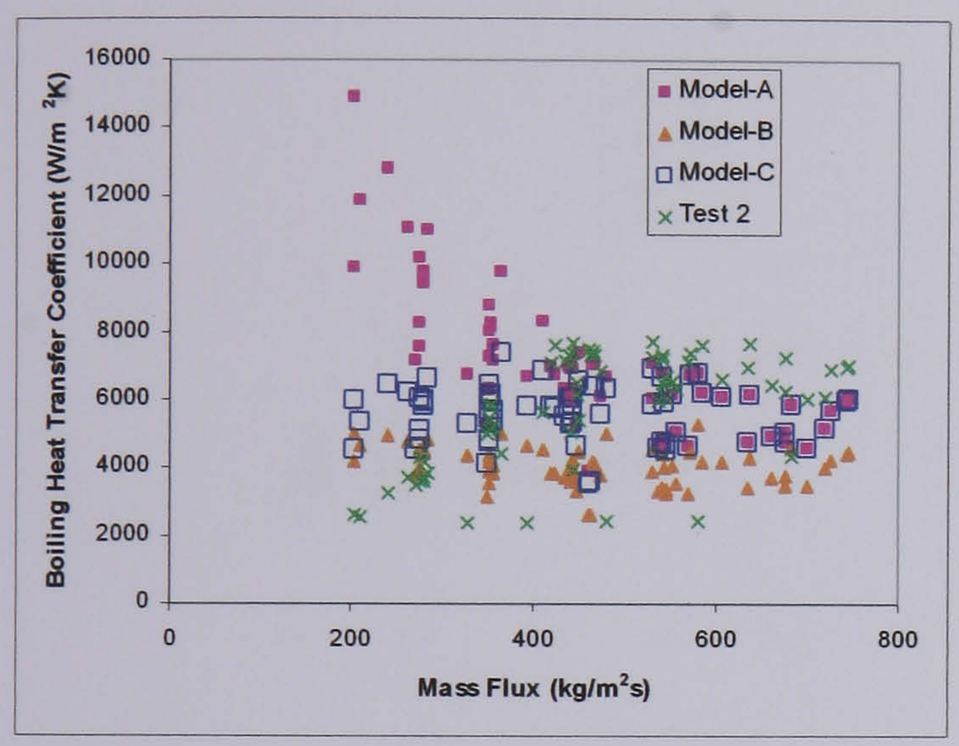

(c) - Predictions of Model-C with eq.9.22

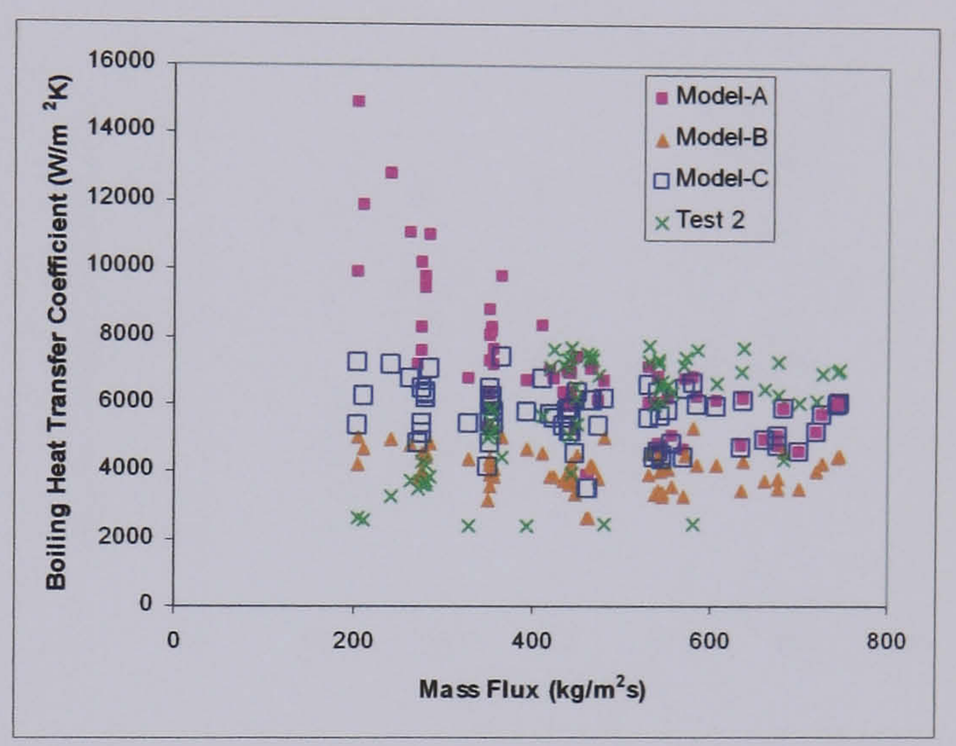

(d) - Predictions of Model-C with eq.9.23

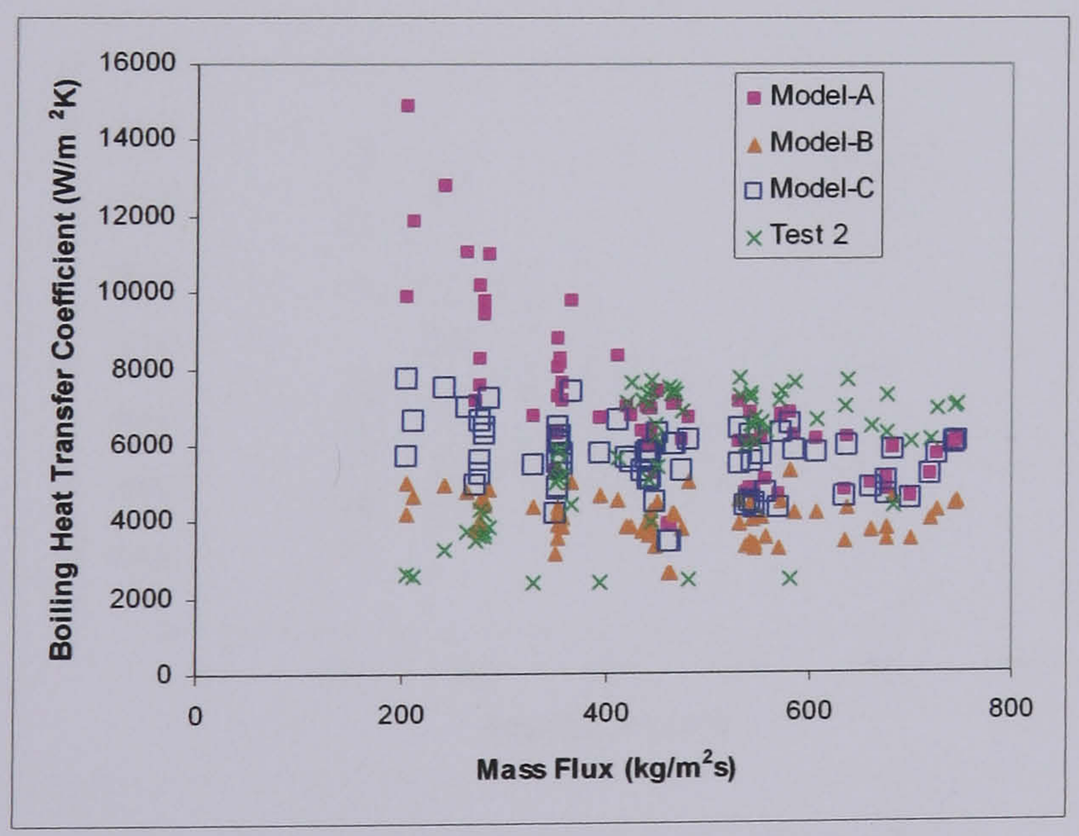

(e) - Predictions of Model-C with eq.9.24

Figure 9.12 – Heat transfer predictions of Model-A, Model-B, Model-C and Test 2 data

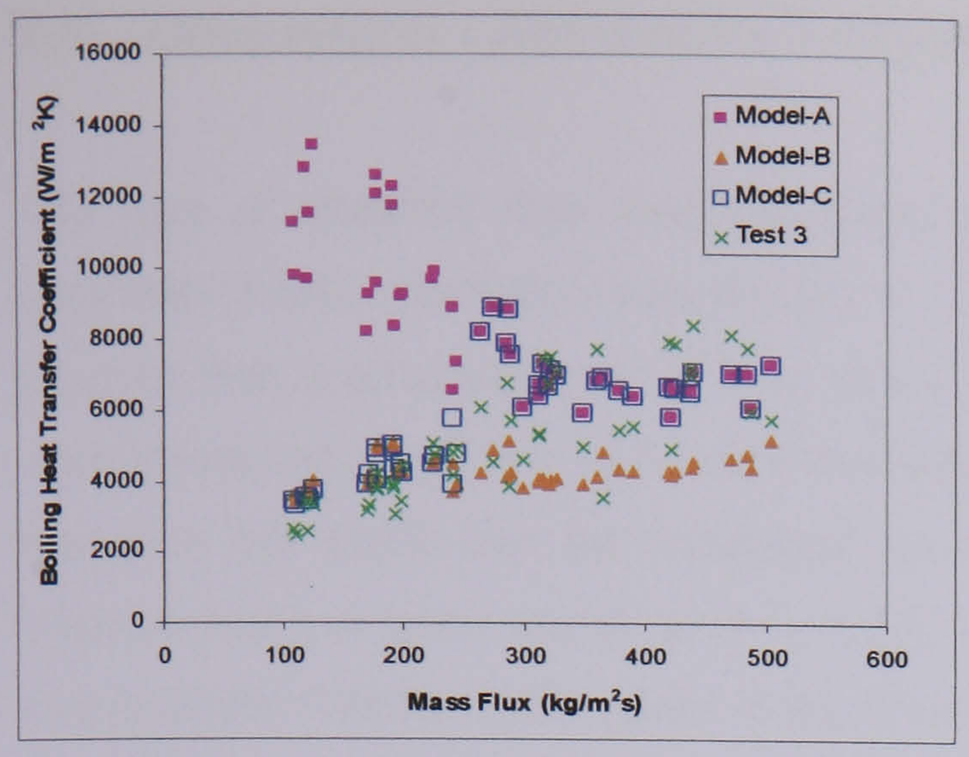

(a) – Predictions of Model-C with eq.9.20

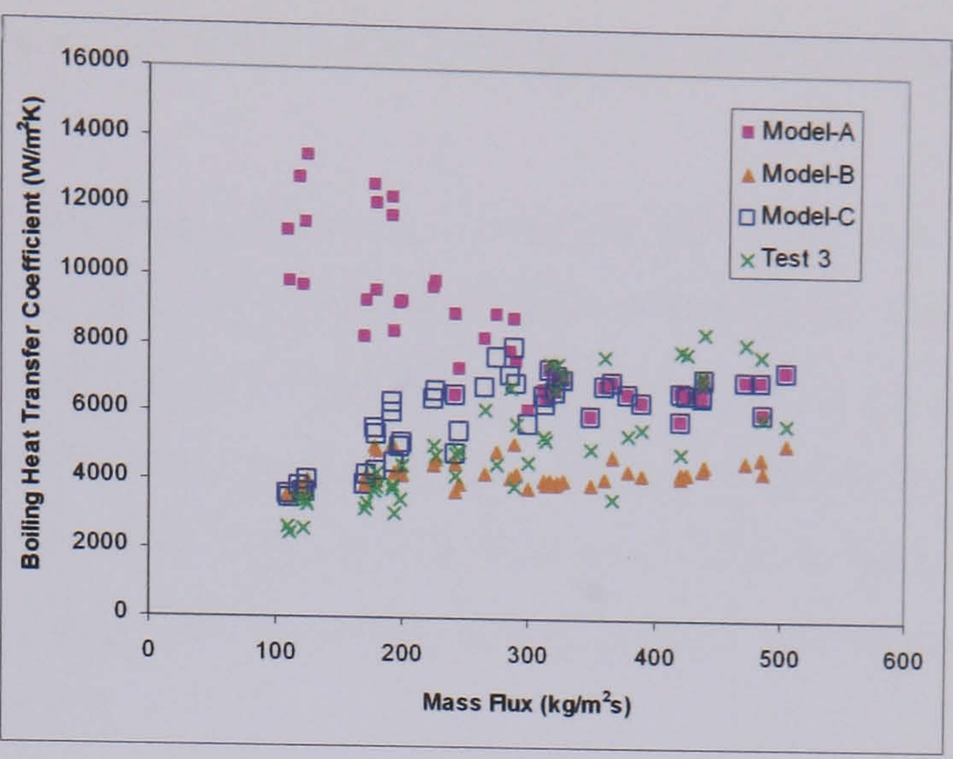

(b) – Predictions of Model-C with eq.9.21

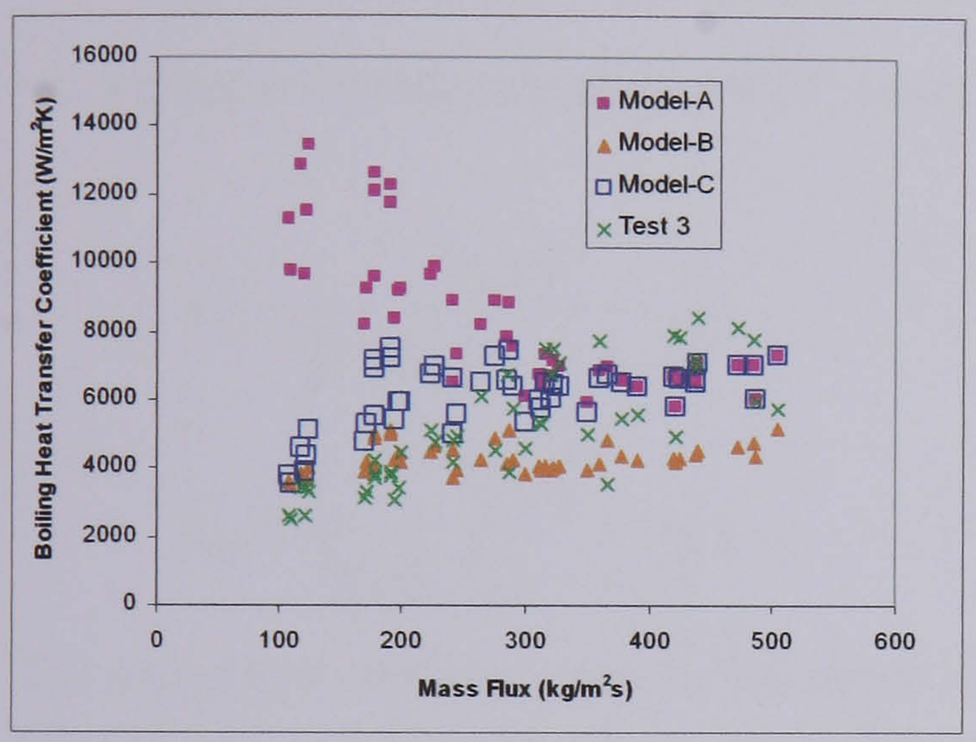

(c) - Predictions of Model-C with eq.9.22

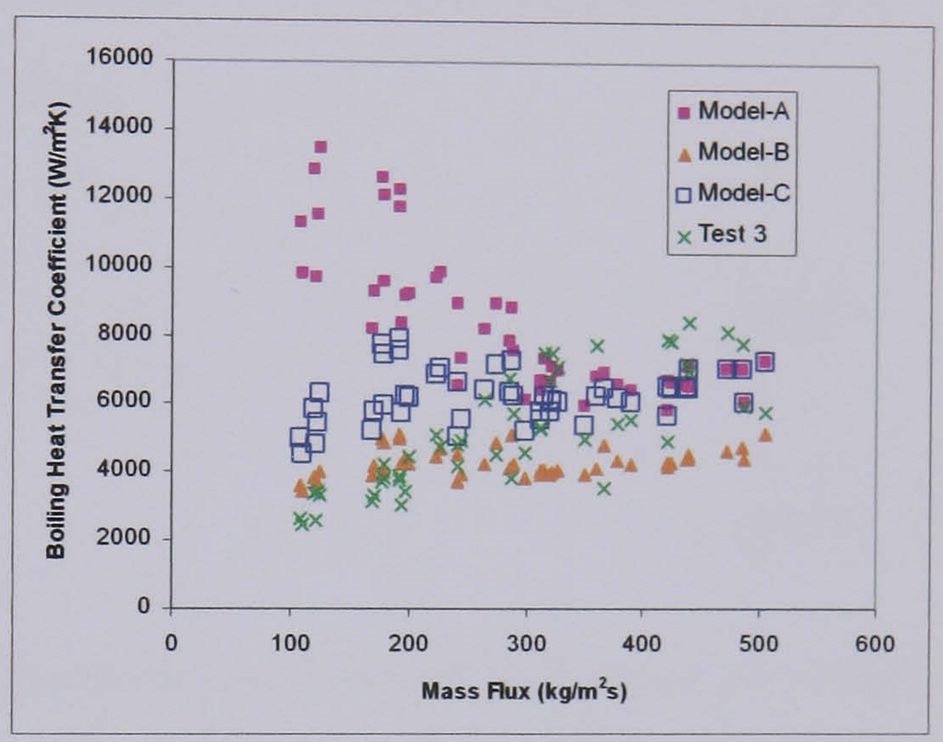

(d) - Predictions of Model-C with eq.9.23

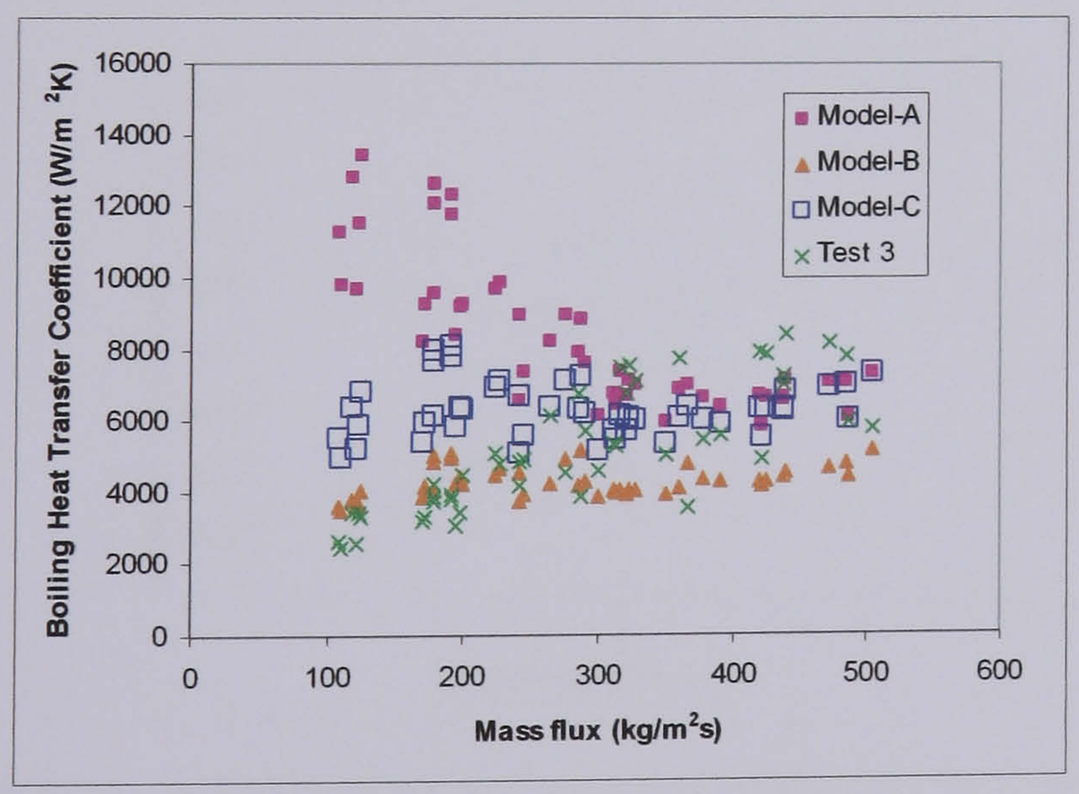

(e) - Predictions of Model-C with eq.9.24

Figure 9.13 – Heat transfer predictions of Model-A, Model-B, Model-C and Test 3 data

9.5 – Discussion - Alternative Transition Criterion for Horizontal Baffle Cut?

The type of stratified flow that had been previously observed (Grant et al, 1987) with a horizontal baffle orientation was shown in Figure 8.1. The representation in the figure would suggest that a stratified type of flow could persist if the liquid and vapour phase velocities were insufficient to lift the liquid over the baffle into the upper window. Failure of the liquid to flow over the baffle can be envisaged as a flooding type of phenomenon, and a general criterion that has been successfully used to quantify the flooding point in uniform channels is that of Wallis (Wallis, 1969) given in equation 9.25.

$$\left(\dot{v}_{lo}^{*}\right)^{0.5} + \left(\dot{v}_{go}^{*}\right)^{0.5} = C \tag{9.25}$$

C is a constant, and the dimensionless superficial liquid and vapour velocities $\dot{v}_{lo}^{*}$ and $\dot{v}_{go}^{*}$ are defined in equations 9.26 and 9.27 respectively.

$$\dot{v}_{lo}^{*} = \frac{\dot{v}_{lo}\rho_{l}^{0.5}}{\left[g_n d_{eq}\left(\rho_l - \rho_g\right)\right]^{0.5}} \tag{9.26}$$

$$\dot{v}_{go}^{*} = \frac{\dot{v}_{go}\rho_{g}^{0.5}}{\left[g_n d_{eq}\left(\rho_l - \rho_g\right)\right]^{0.5}} \tag{9.27}$$

The equivalent diameter used in the above equations was taken as four times the crossflow area divided by the wetted perimeter at the minimum tube gap. Figure 9.14 shows a plot of the Test 1 data against the Wallis flooding parameter C defined in equation 9.25.

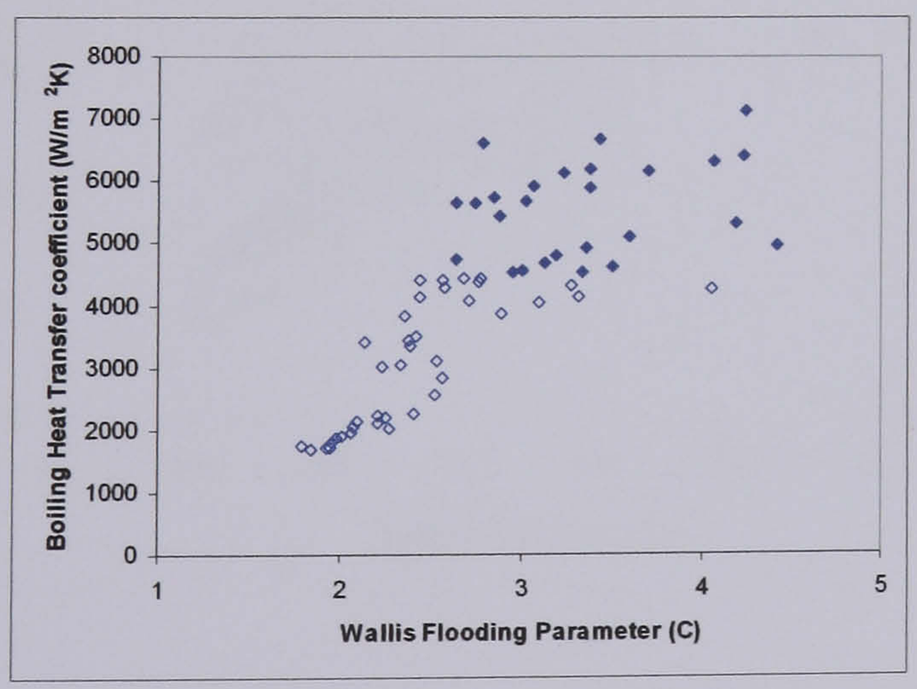

Figure 9.14 – Shellside Heat Transfer Coefficient for Test 1 data

The observed transition in the shellside heat transfer data coincides with a value of C around 2.5 – 3.5. The parameter is a better tool for defining the transition than the mass flux as it is dimensionless and can be applied to a wider range of conditions. It was decided to examine the effect of introducing this transition criterion in place of the Taitel/Dukler model for the case

with the horizontal baffle orientation. The values of C = 2.5, 3 and 3.5 were tested for the transition from completely stratified shellside flow. As with the Taitel/Dukler model an allowance for entrainment was made and the boundaries around the transition were chosen as those in equations 9.28 – 9.30 as these were found to produce the best fit to the spread of data.

$$\text{If } C < 0.5\,C_{Crit} \quad \text{Then } E = 0 \tag{9.28}$$

$$\text{If } C > 1.5 C_{Crit} \quad \text{Then } E = 1 \tag{9.29}$$

$$\text{If } 0.5 C_{Crit} < C < 1.5 C_{Crit} \quad \text{Then } E = \left(\frac{\frac{C}{C_{Crit}} - 0.5}{1.5 - 0.5} \right) \tag{9.30}$$

The values of heat transfer coefficient were then calculated by Model-C with these transition boundaries applied in place of the Taitel/Dukler method. Comparisons of the heat transfer predictions using both transition criteria are shown in Figures 9.15 – 9.17.

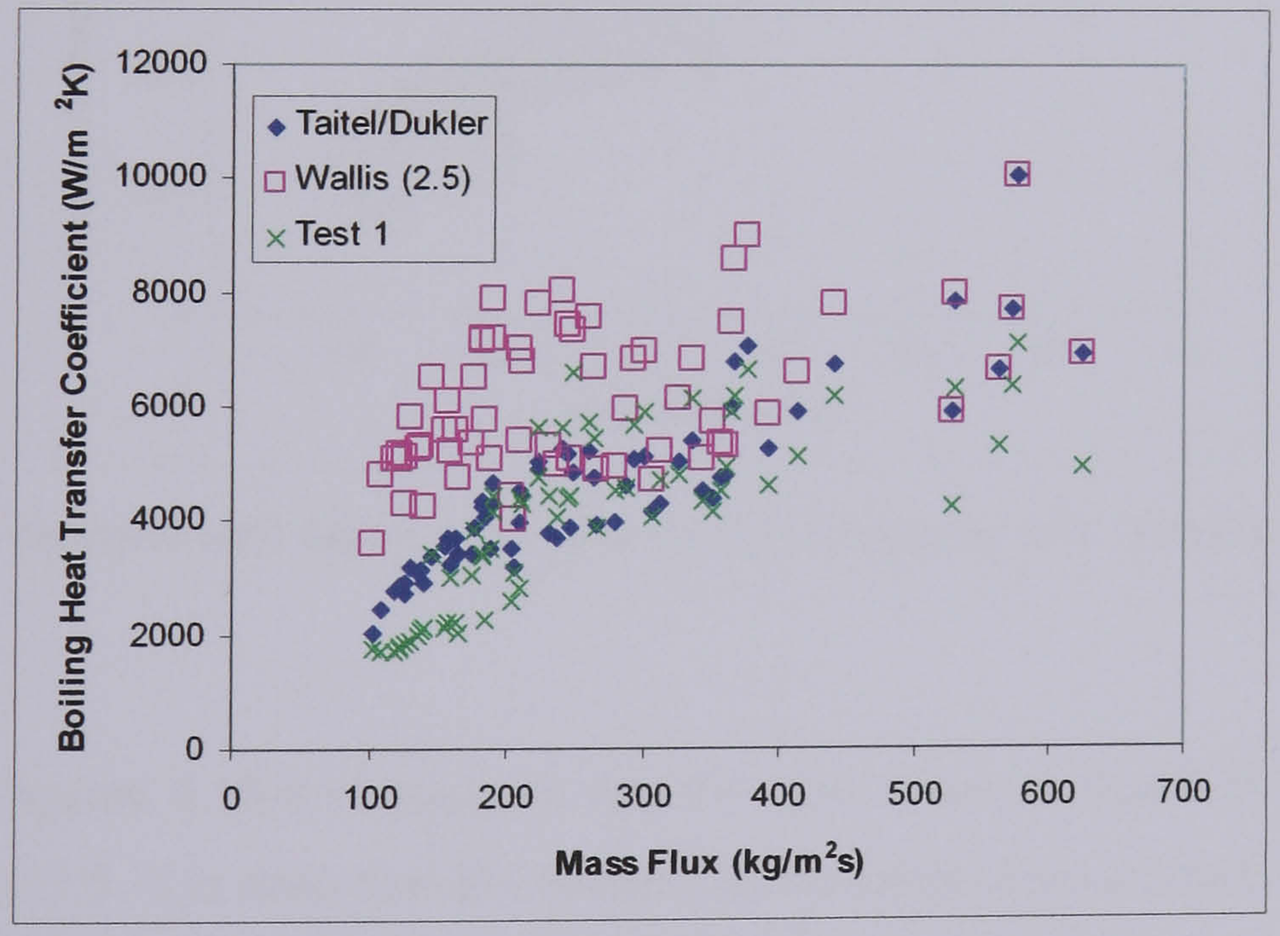

Figure 9.15 - Model-C with Wallis parameter C = 2.5 compared with Taitel/Dukler transition

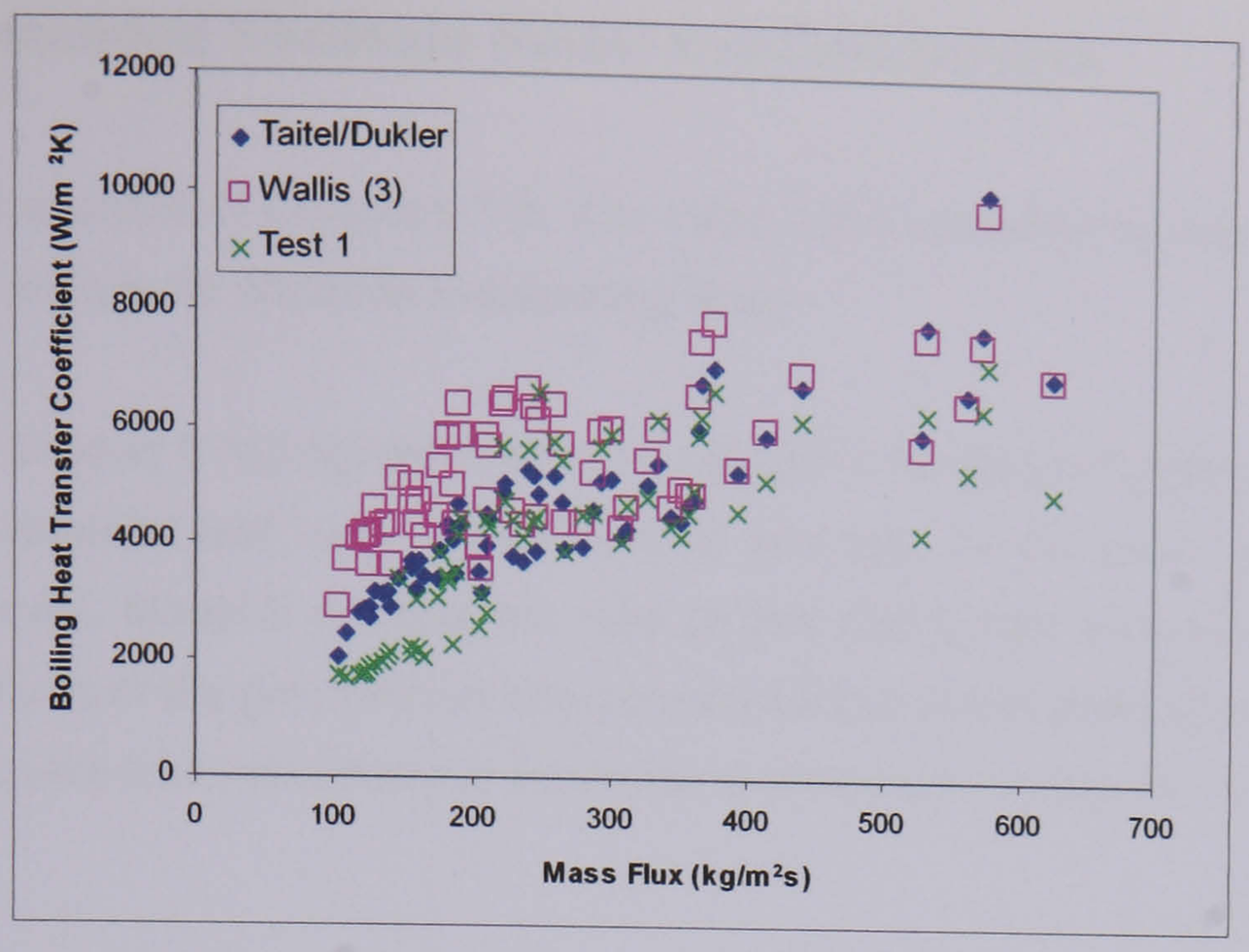

Figure 9.16 - Model-C with Wallis parameter C = 3 compared with Taitel/Dukler transition

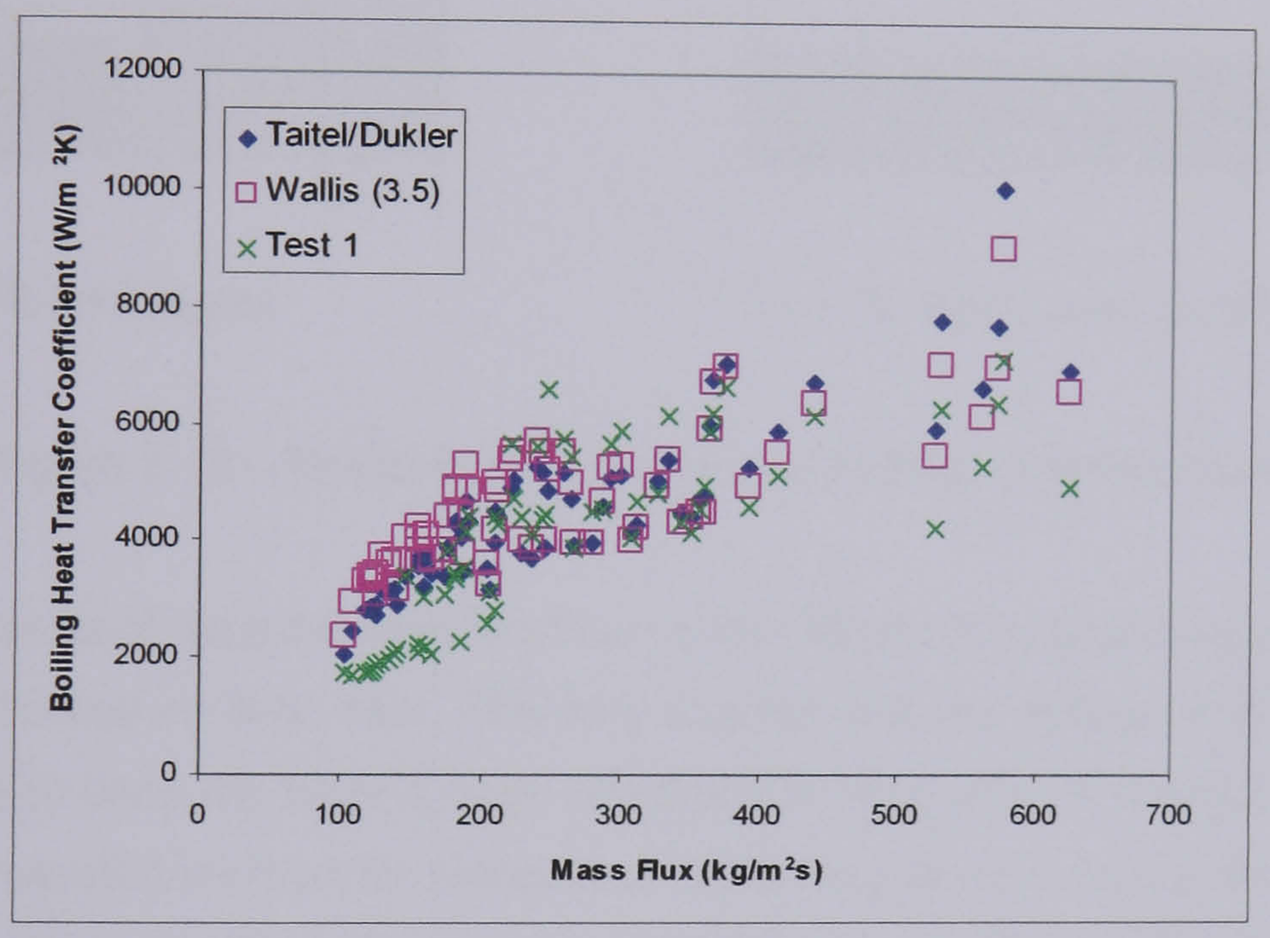

Figure 9.17 - Model-C with Wallis parameter C = 3.5 compared with Taitel/Dukler transition

The results in Figures 9.15-9.17 suggest that the best result is obtained using the Wallis parameter of $C = 3.5$. It is likely that the Wallis flooding parameter provides a closer physical relation to what is actually occurring in the experimental tests with the horizontal baffle orientation. However in the absence of more data in this range for tests with this baffle orientation, the applicability of the value of C equal to 3.5 for the transition is questionable in a general shellside model.

9.6 – Recommended Shellside Model and Conclusions

From the model analysis of Chapters 7-9, it is clear that improvements can be made to the current design methods for shellside evaporating flows.

The analysis of Chapter 8 highlighted that there may exist two different types of stratified flow during the experimental test runs (Figure 8.20(a) and (b)). At the lower mass fluxes, the stratified flow model, Model-B predicts the type of flow distribution shown in Figure 9.18(a). However an analysis of the gravitational component of liquid phase pressured drop in Chapter 8 indicated the profile was more likely to be similar to that shown in Figure 9.18(b).

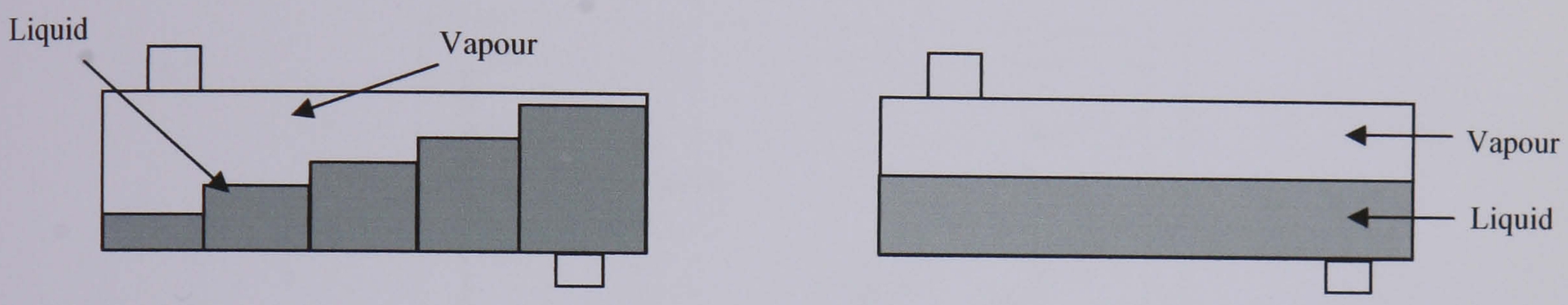

(a) – Model-B flow layout

(b) – Constant level stratified flow

Figure 9.18 – Model-B and constant liquid level stratified flows

Over the entire range of data the stratified flow model (Model-B) has given good predictions of the experimental pressure drop data. This may suggest that the change in profile from Figure 9.18(a) and 9.18(b) does not have a large affect on the prediction of shellside pressure drop. Thus the recommended method for calculating shellside pressure drop over the full range of the data is that of the stratified flow model, Model-B. The shellside heat transfer coefficient predicted using Model-B is also recommended for tests with low mass fluxes. The close agreement of the heat transfer predictions with the experimental test data in the low mass flux range would imply that the average shellside void fraction predicted by the Model-B profile (Figure 9.18(a)) is very similar to the actual experimental void fraction.

The fact that the pressure drop data is also well represented by the stratified model at the high mass fluxes suggests that there is not a major change in the distribution of the liquid and vapour phases. Despite this, the heat transfer data suggests that a larger part of the tube bundle is operating in the nucleate boiling regime at the high mass fluxes suggesting there may be liquid entrainment in the vapour phase in the upper tube rows. The heat transfer data in this range is best predicted using the homogeneous TASC style method which assumes nucleate and convective boiling are the dominating heat transfer mechanisms.

The transition between the stratified and homogeneous heat transfer regimes can be modelled using a correlation developed for deviation from stratified flow in horizontal tubes (Taitel et al, 1976). Furthermore, an allowance for gradual entrainment of liquid in the vapour phase around the transition point can improve the prediction of the heat transfer coefficient (especially in the horizontal baffle cut geometry). As a result the recommended method for calculating the shellside heat transfer coefficient is Model-C with equation 9.23 for the horizontal baffle cut and Model-C with equation 9.21 for the vertical baffle cut geometry.

Comparisons of the predictions of the recommended pressure drop model and those of TASC with the data from Tests 1-3 are shown figures 9.19-9.21.

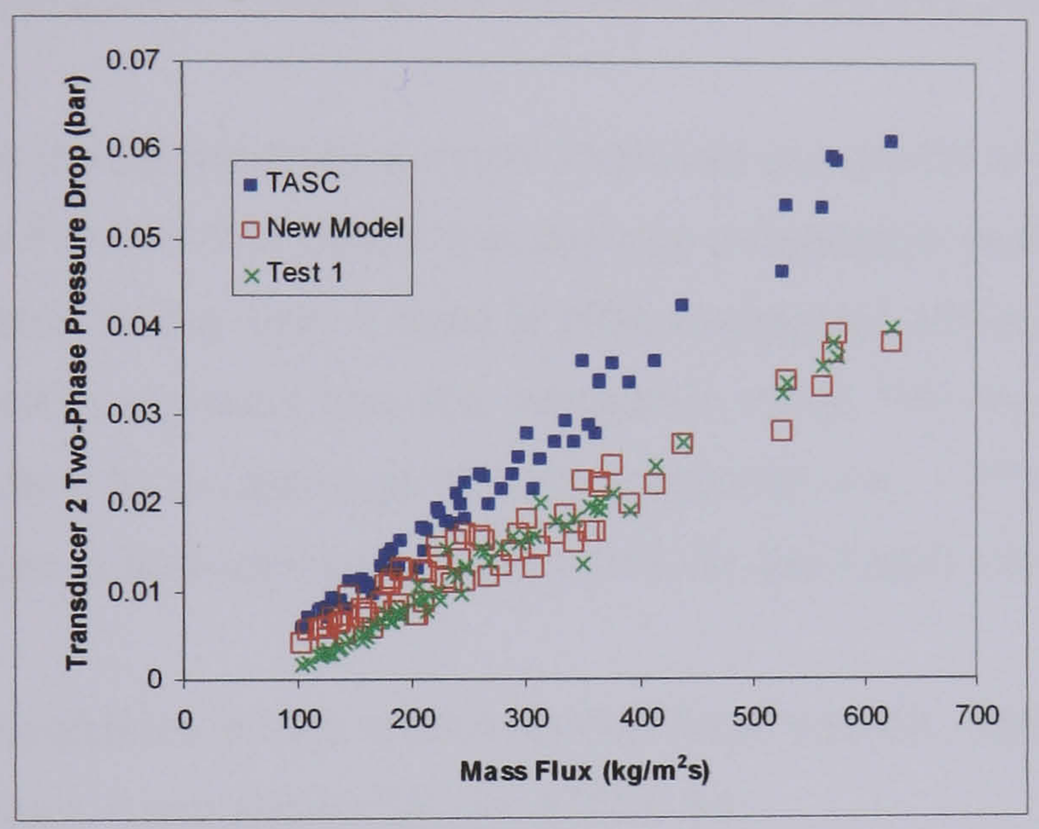

Figure 9.19 – Comparison of New Model and TASC pressure drop predictions with Test 1 data

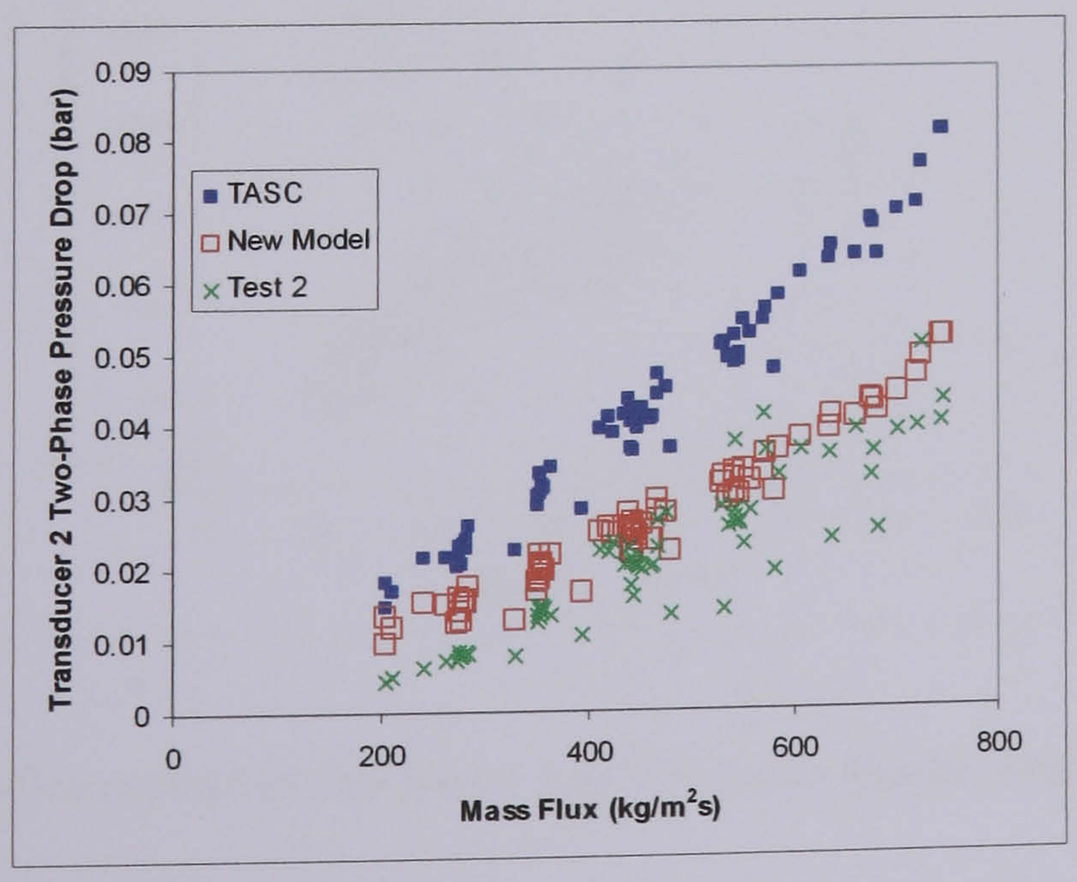

Figure 9.20 – Comparison of New Model and TASC pressure drop predictions with Test 2 data

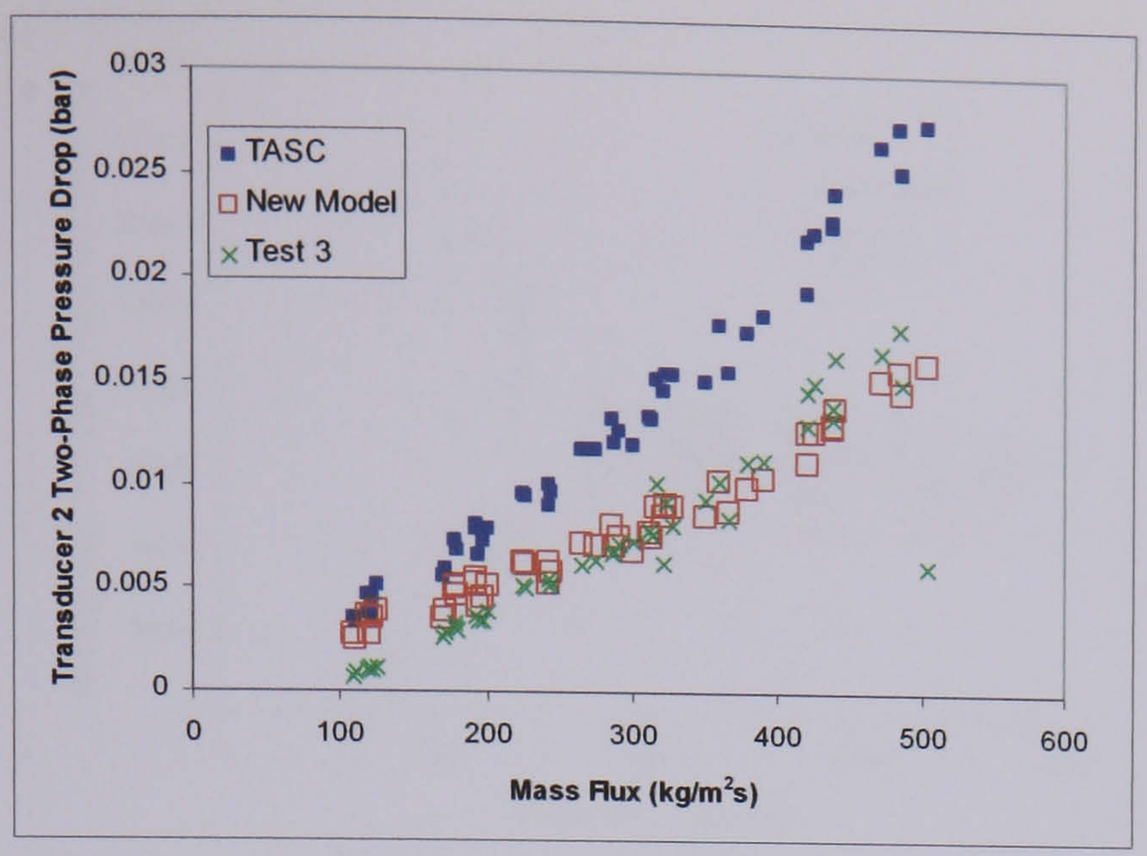

Figure 9.21 – Comparison of New Model and TASC pressure drop predictions with Test 3 data

It is clear that the new model provides a much improved prediction of the shellside pressure drop for all three tests For the new model the average percentage deviation of the prediction from the measured value in the Test 1 data is 39% compared with an average deviation of 90% between the TASC prediction and the measured value. For the Test 2 data the new model prediction deviates by an average of 42% compared with 122% for TASC, and in the Test 3 data the deviation is 46% compared with 119% for the TASC value.

Comparisons of the predictions of the recommended heat transfer model and those of TASC with the data from Tests 1-3 are shown figures 9.22-9.24.

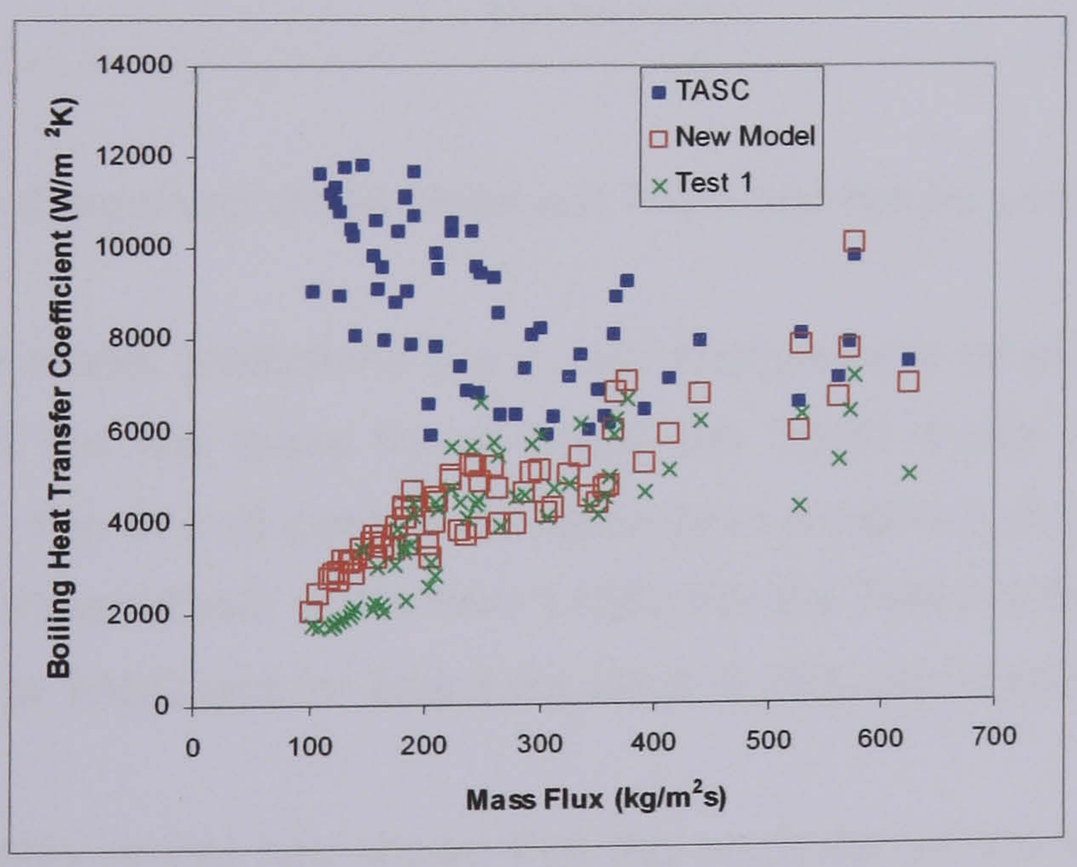

Figure 9.22 – Comparison of New Model and TASC heat transfer predictions with Test 1 data

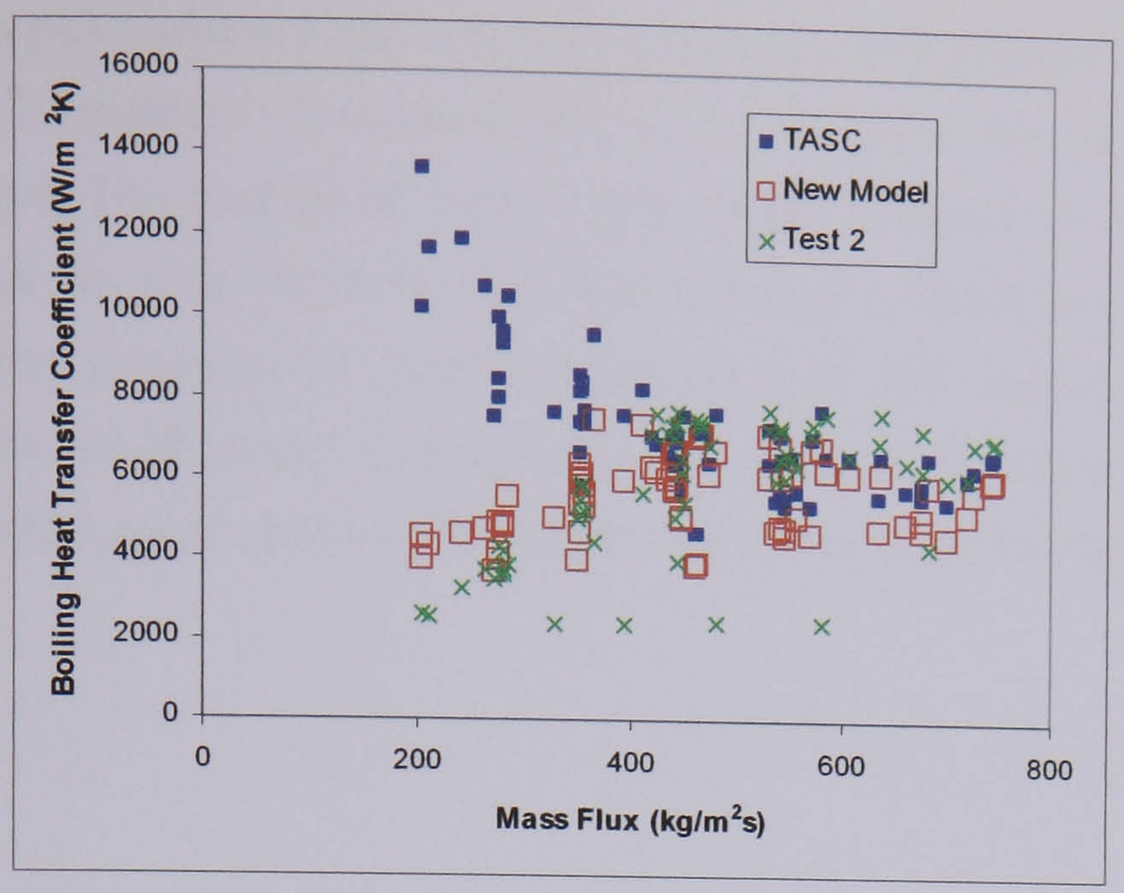

Figure 9.23 – Comparison of New Model and TASC heat transfer predictions with Test 2 data

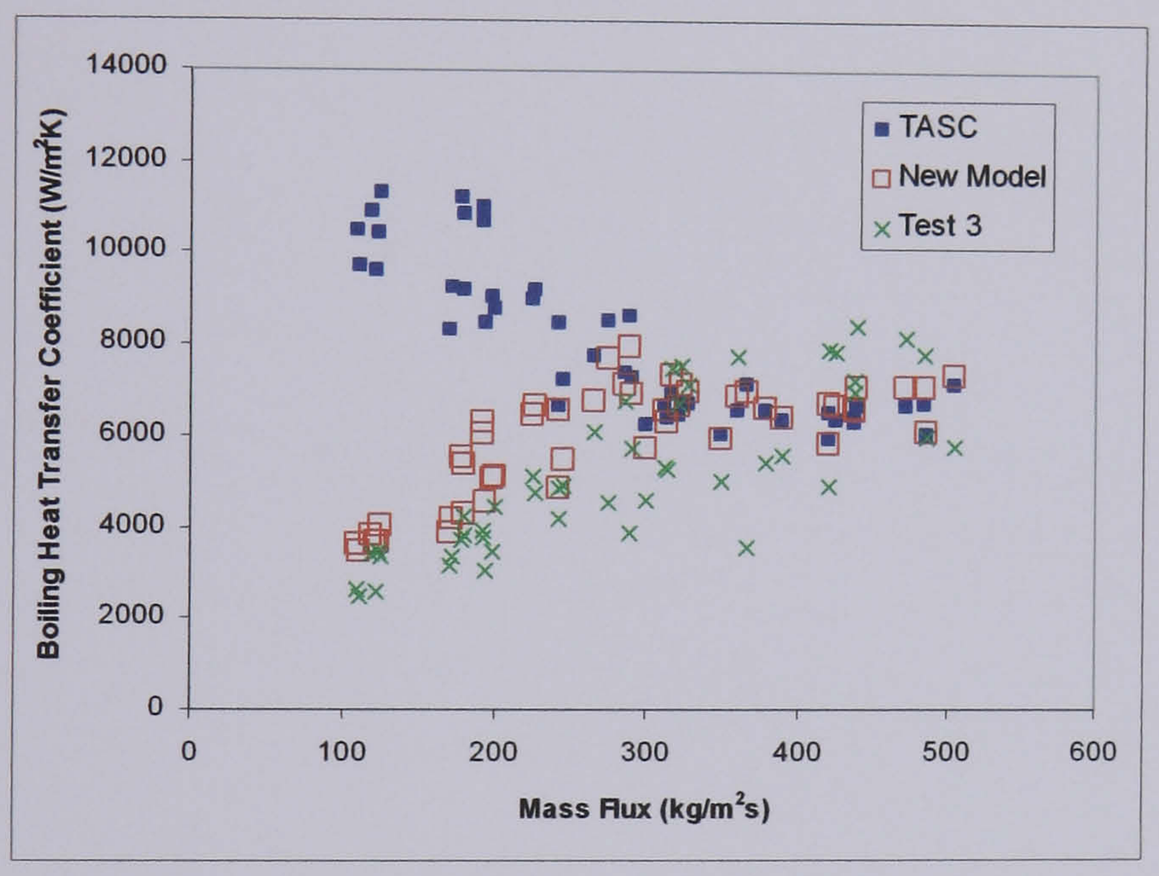

Figure 9.24 – Comparison of New Model and TASC heat transfer predictions with Test 3 data

Once again the new model predictions are a vast improvement on those of TASC. This is especially evident at the low mass fluxes where the TASC model does not predict the transition in the data. The overall average deviation from prediction of the new model is 24% for the Test 1 data compared with 168% from TASC. For the Test 2 data the deviation is 29% compared with 64% for TASC and for Test 3 the value is 26% compared with 88% of TASC.

The analysis of the new model has shown that the prediction of the shellside data can be improved with the inclusion of a tubeside model for the transition from stratified to intermittent flow. The data for the shellside heat transfer coefficient in all the tests have been improved by including the transition model of Taitel/Dukler (Taitel et al, 1976) for horizontal two-phase flows in tubes. Furthermore improved prediction can be obtained by defining a boundary

around the transition point where there is a gradual entrainment of liquid in the vapour phase. The effect of baffle orientation (horizontal/vertical) seems to be important in describing the nature of the transition. The method of Taitel/Dukler model is based on a mechanism derived from horizontal flows so it is not surprising that the sharp transition in vertical baffle cut (horizontal flow case) provides the best agreement with this model. The more gradual transition between the stratified and homogeneous flow patterns with the horizontal baffle cut can be attributed to the type of stratified flow observed in this geometry (Figure 8.1).

CHAPTER 10 – Conclusions and Recommendations for Future Work

10.1 – Conclusions

- A wide range of data has been produced for evaporating shellside flows in three different test geometries. The data provides a wide range of boiling heat transfer and pressure drop data which was previously unavailable in the open literature. The experimental test programme has examined the influence of shellside geometric features such as the inclusion of sealing strips in the crossflow bypass stream, the orientation of the shellside baffles (horizontal/vertical) and the number of shellside baffles and baffle pitch. The data produced can be used for the analysis of design methods for shell-and-tube heat exchangers with boiling on the shellside.
- It has been identified that current design methods fail to predict a deterioration in the heat transfer performance at low mass fluxes and produce a poor prediction of shellside pressure drop over a wide range of conditions. Evidence from the examination of two-phase flow pattern maps and the behaviour of the two-phase pressured drop multiplier data would suggest that there is a change in the shellside flow pattern that is not predicted by current design methods. It has been highlighted that this change may be towards a fully separated stratified flow with the upper tube rows surrounded by vapour.
- A new model has been developed which describes the transition in the heat transfer data and predicts the onset of this transition. It is based on the hypothesis that at lower mass fluxes the upper tube rows are surrounded by vapour whereas at higher mass fluxes the entire tube bank is fully wetted. The transition point is modelled using a method for transition from stratified to intermittent flow in horizontal tubes (Taitel et al, 1976). In addition the new model has been further developed to allow for a gradual wetting of the upper tube rows around the transition point. The predictions of the heat transfer and pressure drop data of the new model are a vast improvement on those of the best available current design software.

10.2 – Recommendations for future work

- Tests in which the shellside flow could be visualised would be useful in enabling accurate description of the physical mechanisms that cause the transition in the shellside heat transfer data.
- Further tests on an evaporator with a horizontal baffle cut would be useful in determining if the Wallis flooding parameter is a useful tool for describing the transition with this geometry.

References

Barnea, D.; Shoham, O.; Taitel, Y. – 'Flow pattern transition for vertical downward two-phase flow', Chemical Engineering Science (37), pp 741 – 744, 1982

Barnea, D; Taitel, Y. – Flow pattern transition in two-phase gas-liquid flows, in Encyclopedia of Fluid Mechanics, Vol.3 pp 403 – 474, Gulf publishing company, Houston, 1986

Bergelin, O.P; Bell, K.J; Leighton, M.D. – 'Heat transfer and fluid friction during flow across banks of tubes – IV, the effect of internal leakage within segmentally baffled heat exchangers', Transactions of the A.S.M.E. Vol. 80, (1) pp 53 – 60, 1958.

Brodkey, R.S. – 'The phenomena of fluid motions', Addison-Wesley, Reading, MA, 1967

Butterworth, D. - 'A Comparison of Some Void-Fraction Relationships for Co-Current Gas Liquid Flow', International Journal of Multiphase Flow, Vol.1, p845-850, 1975.

Butterworth, D; Hewitt, G.F. - 'Two-Phase Flow and Heat Transfer', UKAEA Research Group, Harwell Series, Oxford University Press, 1977.

Butterworth, D; Hewitt, G.F; Moore, M.J.C. - 'Shell and Tube Heat Exchangers with Single Phase Flow', HTFS Design Report. 2, 1971

Chen, X.T., Cai, X.D., Brill, J.P. – 'A general model for transition to dispersed bubble flow', Chemical Engineering Science, Vol. 52, (23) pp 4373 – 4380, 1997

Chenoweth, J.M.; Martin, M.W. - 'Turbulent Two-Phase Flow', Petrol. Refiner. Vol.34(10), 151-155, Oct. 1955

Chisolm, D. - 'A Theoretical Basis for the Lockhart-Martinelli Correlation for Two-Phase Flow', Int. Journ. Heat. Mass Transfer Vol.10 p1767-1778, 1967.

Chisolm, D. - 'Pressure Gradients Due to Friction During the Flow of Evaporating Two-Phase Mixtures in Smooth Tubes and Channels', Int. Journ. Heat. Mass Transfer Vol.16 p347-358, 1973.

Chu, C.M.; McNaught, J.M. – Shellside boiling in a TEMA E-Shell: Horizontally cut baffles, HTFS RS Report RS1028, 1998

Collier, J.G. - 'Convective Boiling and Condensation', McGraw Hill, 1972.

Collier, J.G.; Hewitt,G. - Transactions of the Institution of Chemical Engineers, Vol.39(127), 1961.

Cornwell, K. – 'The influence of bubbly flow on boiling flow in a tube bundle', International Journal of Heat and Mass Transfer, Vol.33, No.12, pp2579-2584, 1990

Cornwell, K; Schuller, R.B – 'A study of boiling outside a tube bundle using high speed photography', International Journal of Heat and Mass Transfer', Vol.25, No.5, pp683-690, 1982.

Cotchin, C.D. - 'Shell Side Two-Phase Pressure Drop for Side-to-Side Flow in Segmentally Baffled Shell-and-Tube Heat Exchangers', HTFS Research Symposium, RS324, 1980.

Diehl, J.E; Unruh, C.H. - 'Two-Phase Pressure Drop for Horizontal Cross-Flow through Tube Banks', ASME Paper 58-HT-20, 1958.

Dowlati, R; Chan, A.M.C; Kawaji, M. - 'Hydrodynamics of Two-Phase Flow Across Horizontal In-Line and Staggered Tube Bundles', Transactions of the ASME, Journal of Fluids Engineering, Vol.114, p450-456, Sept. 1992

Dowlati, R; Kawaji, M; Chan, A.M.C. - 'Pitch-to-Diameter Effect on Two-Phase Flow Across an In-line Tube Bundle', AIChE Journal 36(5), p765-772, May 1990.

Dowlati, R; Kawaji, M; Chisolm, D; Chan, A.M.C. - 'Void Fraction Prediction in Two-Phase Flow across a Tube Bundle', AIChE Journal 38(4), p619-622, April 1992

Dowlati, R; Kawaji, M; Chan, A.M.C - 'Two-Phase Crossflow and Boiling Heat Transfer in Horizontal Tube Bundles', ASME, Journal of Heat Transfer, Vol.118, p124-131, Feb. 1996.

Fair, J.R. - 'What You Need To Design Thermosiphon Reboilers', Petrol. Refiner, Vol. 39(2), p105-123, Feb 1960

Fair, James.R; Klip, Abraham - 'Thermal Design of Horizontal Reboilers', Chemical Engineering Progress 79(3), p86-96, March 1983

Farrant, P – 'An introduction to uncertainty analysis for heat transfer experiments', Internal NEL report, Jan. 2002

Feenstra, P.A; Weaver, D.S; Judd, R.L. - 'An Improved Void Fraction Model for Two-Phase Cross-flow in Horizontal Tube Bundles', International Journal of Multiphase Flow, 26, p1851-1873, 2000.

Grant, I.D.R. - 'Pressure Drop on the Shell-Side of Shell-and-Tube Heat Exchangers in Single and Two-Phase Flows', HTFS Design Report 16, May 1977.

Grant, I.D.R; Chisolm, D. - 'Two-Phase flow on the Shell-side of a Segmentally Baffled Shell-and-Tube Heat Exchanger', Transactions of the ASME: Journal of Heat Transfer, 101(1), 38-42, February 1979.

Grant, I.D.R; Cotchin, C.D. - 'Liquid Hold-up on the Shell-side of Segmentally Baffled Shell-and-Tube Heat Exchangers', HTFS Research Symposium, RS424, March 1982.

Grant, I.D.R; Cotchin, C.D.; Graham, D. - 'Void Fraction and Pressure Drop Measurements for Two-Phase Upflow across a Horizontal Tube Bundle', HTFS, RS643, 1986.

Grant, I.D.R; Cotchin, C.D; White – 'Two-phase up-and-down flow on the shellside of a baffled shell-and-tube heat exchanger', HTFS RS report, RS742, 1987

Grant, I.D.R; Cotchin, C.D; White – 'Shellside two-phase flow past segmental baffles with air sparging', HTFS RS report, RS798, 1989

Grant, I.D.R; Finlay, I.C; Harris, D. - Flow and Pressure Drop during Vertically Upward Two-Phase Flow past a Tube Bundle with and without Bypass Leakage. NEL report, 1974

Grant, I.D.R. and Murray, I. - 'Shell-side Performance of Segmentally Baffled Shell and Tube Heat Exchangers by Divided Flow Method', HTFS Design Report 24, 1972.

Grant, I.D.R. and Murray, I. - 'Pressure Drop on the Shell-side of a Segmentally Baffled Shell-and-Tube Heat Exchanger with Vertical Two-Phase Flows', NEL report 500, 1972.

Grant, I.D.R. and Murray, I. - 'Pressure Drop on the Shell-side of a Segmentally Baffled Shell-and-Tube Heat Exchanger with Horizontal Two-Phase Flows', NEL report 560, 1974.

Hassan, Y.A. and Blanchat, T.K. – 'A new heat transfer correlation and flow regime map for tube bundles', Transactions of the ASME, Journal of engineering for gas turbines and power, Vol.112, pp150-156, January 1990.

Hills, J.H - 'The behaviour of a pilot-scaled horizontal thermosyphon reboiler', Institution of Chemical Engineers, Trans. of the IChemE, Vol.75A, p652-656, October 1997.

Hughmark, G.A. - 'Designing Thermosiphon Reboilers', Chemical Engineering Progress, Vol 65 (7), p67-70, July 1969

Ishihara, K.; Palen, J.W. and Taborek, J. - 'Critical Review of Correlations for Predicting Two-Phase Flow Pressure Drop across Tube Banks', Heat Transfer Engineering, Vol.1, no.3, Jan-Mar. 1980

Jensen, M.K. and Hsu, J.T. – 'A parametric study of boiling heat transfer in a horizontal tube bundle', Transactions of the ASME, Journal of heat transfer, Vol.110, pp976-981, November 1988.

Kern, D.Q. - 'Process Heat Transfer', McGraw-Hill, 1950.

Leong, L.S. and Cornwell, K. – 'Flow boiling heat transfer coefficients in a kettle reboiler tube bundle', Chemical Engr, Vol. 343 (219), 1979.

Levy, S. - 'Prediction of Two-Phase Annular Flow with Liquid Entrainment', Int. Journ. Heat Mass. Transfer (9), p171-188, 1966

Lockhart, R.W; Martinelli, R.C. - 'Proposed Correlation of Data for Isothermal Two-Phase, Two-Component Flow in Pipes', Chem. Eng. Progress Vol.45(1), p39-48, 1949.

Martin, G.R.; Sloley, A.W. - 'Effectively Design and Simulate Thermosyphon Reboiler Systems' – Part I, Hydrocarbon Processing, p101-110, June 1995

Martin, G.R.; Sloley, A.W. - 'Effectively Design and Simulate Thermosyphon Reboiler Systems' – Part II, Hydrocarbon Processing, p67-78, July 1995

McKee, H.R. - 'Thermosiphon Reboilers – A Review', Industrial and Engineering Chemistry, Vol.62, No.12, December 1970

McNaught, J.M. – 'HTFS Handbook BM9', 1994

McNaught, J.M.; Chu, C.M. – 'Shellside boiling in a TEMA E-shell: Vertically cut baffles', HTFS RS Report, RS1049, 1999

McNaught, J.M; Clark, T – 'Shellside boiling in a TEMA E-shell: Increased heat flux', HTFS RS Report, RS1066, 2000

Milne-Thomson, L.M. – 'Theoretical Hydrodynamics', Macmillan, New York, 1960

Moore, M.J.C - 'Pressure Drop and Heat Transfer Calculations on the Shell Side of Shell and Tube Heat Exchangers', AERE report, R7666, February 1974.

Motinski, I.L. – 'Application of the rule of corresponding states for the calculation of heat transfer and critical heat flux', Br. Chem. Eng. Vol. 10 (8) pp 523 – 530, 1963

Noghrehkar, G.R; Kawaji, M; Chan, A.M.C. – 'Investigation of two-phase flow regimes in tube bundles under cross-flow conditions', International journal of multiphase flow, Vol. 25, pp857-874, 1999

Palen, J.W.; Hewitt, G.F. - 'Shell and Tube Reboilers' – handbook of heat exchanger design, Section 3.6. Hemisphere Publishing, 1990.

Palen, J.W.; Taborek, J. - 'Solution of Shell Side Flow Pressure Drop and Heat Transfer by Stream Analysis Method', Chem. Eng. Progress Symposium Series, Heat Transfer- Philadelphia, 92(65) p53-63, 1969

Perry, R.H. and Green, D.W. – 'Perry's chemical engineers' handbook', 7th edition, McGraw-Hill, New York, 1997.

Polley, G.T.; Grant, I.D.R. - 'Pressure Drop Prediction for Two-Phase Upward Flow through a Tube Bundle with Bypassing', NEL internal report 1973

Robson, B – 'Physprop', Physical property database software program, NEL, 1999

Robson, B – 'Data acquisition software for heat transfer facilities', NEL, 1998

Roser, R; Thonon, B. and Mercier, P. – 'Experimental investigations on boiling of n-pentane across a horizontal tube bundle: two-phase flow and heat transfer characteristics', International journal of refrigeration, Vol.22, pp536-547, 1999.

Schrage, D.S; Hsu, J.T; Jensen, M.K. - 'Two-Phase Pressure Drop in Vertical Crossflow across a Horizontal Tube Bundle', AIChE Journal 34(1), p107-115, Jan. 1998.

Shellene, K.R.; Sternling, C.V; Church, D.M.; Snyder, N.H. - 'Experimental Study of a Vertical Thermosiphon Reboiler'- Chemical Engineering Symp. Series, Vol.64(82), Heat Transfer- Seattle, 1968

Simpson, H.C.; Rooney, D.H.; Grattan, E.; Bradford, A.M.; Callander, T.M.S; Al-Samarrae, F. – 'Flow patterns in two-phase flow', HTFS Design report 41, 1975

Stephan, K; Abdelsalam, M. – 'Heat transfer correlations for natural convection boiling', International journal of Heat and Mass transfer, Vol.23, pp 73-87, 1980

Taborek, J. – 'Design methods for heat transfer equipment', Heat exchangers: Design and theory sourcebook, Hemisphere, Washington, 1974.

Taitel, Y.; Dukler, A.E. – 'A model for predicting flow regime transitions in horizontal and near horizontal gas-liquid flow', AIChE Journal, Vol. 22, (1) pp 47-55, 1976

Tinker, T.S. - 'Shell side characteristics of shell and tube heat exchangers – A simplified rating system for commercial heat exchangers'. Trans. of the ASME, Vol.80 (1), p36-49,1955.

Tong, L.S. – 'Boiling Heat Transfer and Two-Phase Flow', Wiley, New York, 1965

Various Authors - 'HTFS Design Report 12', TASC 3: Shell-and-Tube Heat Exchanger Program, HTFS, 1988.

Wallis, G.B. – 'One-dimensional two-phase flow', McGraw-Hill, New York, 1969

Weisman, J.; Duncan. D.; Gibson. J.; Crawford, T. – 'Effects of fluid properties and pipe diameter on two-phase flow patterns in horizontal lines', Int. Journal of Multiphase Flow, Vol.5, pp 437 – 462.

Whalley, P.B. – 'HTFS Handbook BE2', 1977

Whalley, P.B. – 'HTFS Handbook TM4', 1984

Whalley, P.B. – 'Flow Patterns in two-phase flow – Part 4: The transition from stratified to intermittent flow in horizontal flow', HTFS Design Report 41, 1983

Wills, M.J.N. - 'HTFS Handbook SM4', 1985

Wills, M.J.N.; Johnston, D. – 'The calculation of single-phase window pressure drop in single segmentally baffled shell-and-tube heat exchangers', HTFS RS Report, RS369.

Xu, G.P; Tou, K.W; Tso, C.P. - 'Two-Phase Void Fraction and Pressure Drop in Horizontal Crossflow across a Tube Bundle', ASME, Journal of Heat Transfer, Vol.120, p140-145, March 1998

Yilmaz, Salim.B - 'Horizontal Shellside Thermosyphon Reboilers' – Special Report, Chemical Engineering Progress, p64-70, November 1987.

Zivi, S.M. – 'Estimation of steady state steam void fraction by means of the principle of minimum entropy production', Journal of Heat Transfer (86c), pp 417 - 429

Zuber, N.; Findlay, J.A. - 'Average Volumetric Concentration in Two-Phase Flow Systems', ASME, Journal of Heat Transfer, Vol.87 (453), 1965.

Appendix A: Results of Uncertainty Analysis

A1 – Introduction

A summary of the outcomes of the uncertainty analysis was provided in Chapter 4 (Section 4.3). The purpose of this Appendix is to describe the procedure that was used in calculating the uncertainties and to provide a detailed list of the standard uncertainties for the measured and calculated parameters produced from the experimental data.

A2- Procedure

2.1 – Introduction

Whenever a measurement is made, the value obtained is simply the best estimate of the true value that can be obtained. In practice, the true value may be slightly greater or less than this estimate. The 'uncertainty' of a measured result is defined as a quantity that characterises the dispersion of the values that could reasonably be attributed to the measured variable (Farrant, 2002). This section describes the procedures that were used to quantify the uncertainties that are likely to occur during the process of measuring the experimental test data.

2.2 – Measurement Uncertainties

The uncertainty in a measurement is the quantity used to define the likely deviation of the measurement from the true value. The measured values from each instrument in the test run output reports are the mean values calculated from the 10 scans of the data acquisition unit. The assumption is made that there is a normal distribution of results around this mean value (The assumption of a normal distribution is standard practice in the absence of contrary information). The mean value of the measured parameter is given by equation A1.

$$\bar{y} = \frac{1}{n}\sum_{i=1}^{n} y_i \qquad \text{(A1)}$$

where n is the number of measurements (in this case 10) and y is the measured parameter. If an additional measurement were made at the same conditions the uncertainty in the measurement could be expressed by the standard deviation given by equation A2.

$$s(y) = \sqrt{\frac{\sum_{i=1}^{n}(y_i - \bar{y})^2}{n-1}} \qquad \text{(A2)}$$

This deviation is defined as the **'Standard Uncertainty'** of the measurement and is an estimate of the deviation between the new measurement and the average value. When there is a normal distribution of the data, 68% of measurements will fall within the range covered by the standard deviation from the mean value.

In the case of the measurements made through the data collection system (section 3.5), the standard uncertainty calculated will be slightly different. Equation A2 describes the likely standard deviation of a new measurement from the previously calculated mean value. However, the process of collecting a new measurement using the data acquisition unit and acquisition software involves reading each instrument 10 times and recording the measurement as the average of the 10 values. Therefore the likely deviation between this new average measurement and the previous average is much smaller than if a single measurement were taken (i.e with a normal distribution, a single measurement is much more likely to deviate from the true value than an average of 10 measurements). The standard uncertainty of this new average measurement in relation to the previous average can be calculated from equation A3.

$$s(\bar{y}) = \frac{s(y)}{\sqrt{n}} \qquad \text{(A3)}$$

This equation was applied to all the measurements made on the experimental facility using the data collection system. The equation describes the standard uncertainty of the measurement which covers the range which will encapsulate 68% of the data. Common practice when dealing with standard uncertainties is to multiply this uncertainty by a coverage factor to ensure that it covers more of the data points. Each of the calculated standard uncertainties of the test measurements were multiplied by a factor of 2. This coverage factor ensures that the quoted uncertainty value will cover a range (sometimes referred to as the confidence level) within which 95.4% of the data distribution will fall. The parameter which is the standard uncertainty multiplied by the coverage factor is defined as the **'Expanded Uncertainty'** of the measurement.

2.3 – Instrument Uncertainties

The uncertainty in the measurement is not the only consideration in determining the accuracy of the result. Another factor of key importance is the uncertainty associated with the instrument. This is the uncertainty associated with the instrument's ability to read/produce the correct value (e.g. how accurately a thermocouple can determine the temperature). The uncertainty of the instrument is usually quoted by the manufacturer and is often presented in one of two forms. If the terms 'accuracy, tolerance or hysteresis' are used it is assumed that the instrument uncertainty has a normal distribution with a confidence level of 95.4% (i.e a

coverage factor of 2). Where the terms 'limit, tolerance limit or drift between calibrations' are used, a rectangular distribution is assumed. A rectangular distribution implies that the true value could lie anywhere within a given range and is not more likely to be close to an average value (as in a normal distribution). The standard uncertainty calculated for a rectangular distribution is given by equation A4.

$$u(i) = \frac{a}{\sqrt{3}} \qquad \text{(A4)}$$

where a is the manufacturer's tolerance limit.

2.4 – Experimental Facility Instrument Uncertainties

Before examining the uncertainty associated with individual data points on the experimental facility, it is worth looking at the instrument uncertainties of the principal measurements. Table A1 lists the principal measurements made with the instrument identifications corresponding to those in Figure 3.1. The flow meters on the facility were calibrated to be within a maximum of 1% drift from previous calibrations. Therefore a rectangular distribution is assumed and the instrument standard uncertainty is calculated using equation A4 with the value of a taken as 1% of the top operating flowrate for each flow meter. For the temperature instruments the spread is represented in terms of manufacturer's tolerance. Therefore a normal distribution is assumed with a coverage factor of 2. The standard uncertainty is given by the quoted tolerance divided by 2. The pressure transducers in the facility were calibrated in a similar manner to the flow meters and likewise a rectangular distribution is assumed with the standard uncertainty calculated using equation A4. The value of a is calculated at 1% of the top operating pressure reading.

Parameter	Instrument I.D.	Distribution type	Top of range reading or manufacturers tolerance	Standard Instrument Uncertainty
Flow	F1	Rectangular	2.0 (l/s)	0.0115 (l/s)
Flow	F2	Rectangular	4.0 (l/s)	0.02309 (l/s)
Flow	F4	Rectangular	2.0 (l/s)	0.0115 (l/s)
Flow	F5	Rectangular	12.0 (l/s)	0.0693 (l/s)
Flow	F9	Rectangular	6.0 (l/s)	0.0346 (l/s)
Temperature	PRT1	Normal	0.05 (°C)	0.025 (°C)
Temperature	PRT2	Normal	0.05 (°C)	0.025 (°C)
Temperature	PRT3	Normal	0.05 (°C)	0.025 (°C)
Temperature	PRT4	Normal	0.05 (°C)	0.025 (°C)
Temperature	PRT5	Normal	0.05 (°C)	0.025 (°C)
Temperature	T3	Normal	0.5 (°C)	0.25 (°C)
Temperature	T14	Normal	0.5 (°C)	0.25 (°C)
Temperature	T15	Normal	0.5 (°C)	0.25 (°C)
Pressure	P1	Rectangular	0.2 (bar)	0.00115(bar)
Pressure	P3	Rectangular	6 (bar)	0.0346 (bar)
Pressure	P4	Rectangular	6 (bar)	0.0346 (bar)
Pressure	P8	Rectangular	0.15 (bar)	0.00087(bar)
Pressure	P9	Rectangular	0.78 (bar)	0.0045 (bar)

Table A1 – Experimental Facility Instrument Uncertainties

2.5 – Additional Instrument Uncertainty in Flow Measurement

The process of collecting flow measurements from the facility is illustrated in Figure A1. Each of the flow meters is wired to a separate channel in the frequency-to-voltage converter before the signal is sent to the data acquisition unit. An instrument uncertainty was attributed to the converter unit to account for any uncertainty in the measurement of the frequency output by the flow meter.

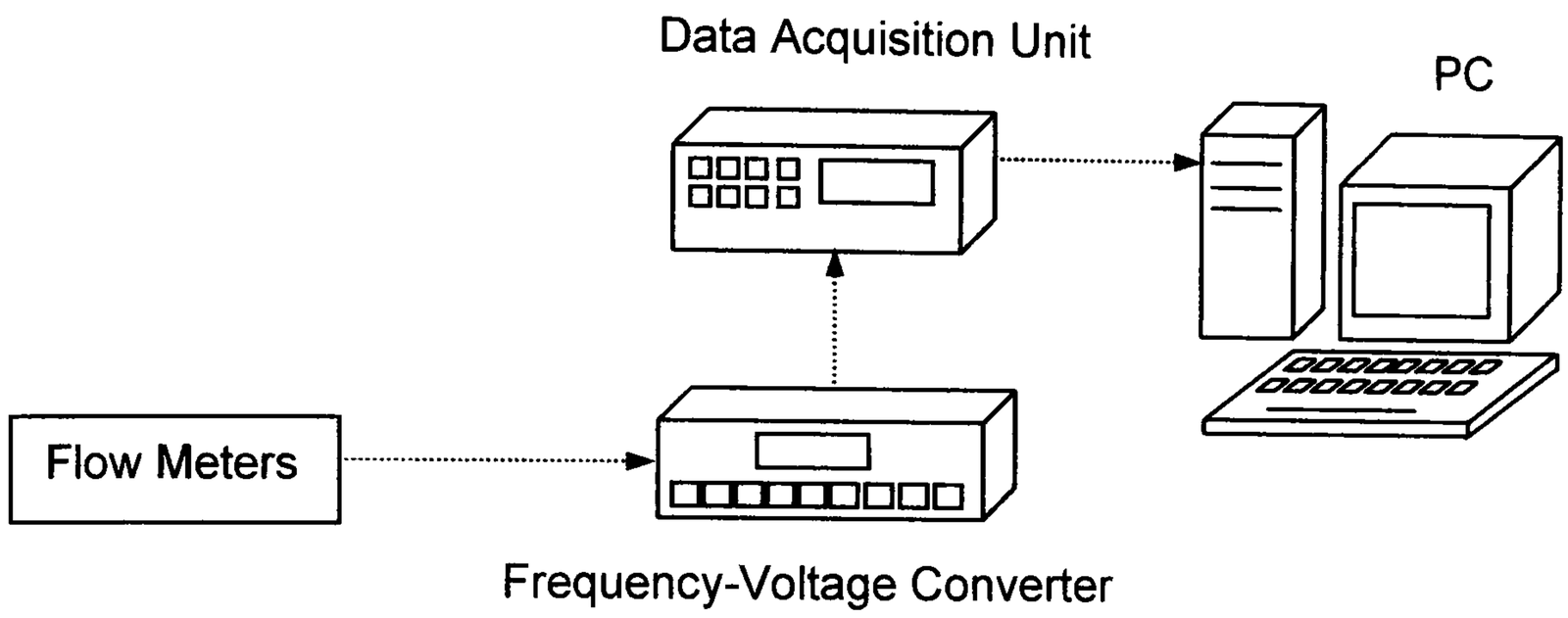

Figure A1 – Flow measurement data collection system

The frequency-to-voltage converter operates over a frequency range of 0-1200Hz. In calibration tests the frequency signal from two of the channels was noted to drift at the lower end of the range and this had an effect on the output flowrate produced. The drift was checked using a 'Fluke 702 Documenting Process Calibrator'. The calibrator was used to produce a signal of known frequency which was compared with the frequency produced by the converter. From the data a curve fit was made of the true frequency to the displayed frequency. The curve fit was used to process the flowrate values from these measurements. The two channels affected were those which were connected to flow meters F1 and F2. These were responsible for the measurements of the refrigerant flowrate to the evaporator and the cooling water flow to the first condenser respectively. The curve-fits used to generate the true frequency from the measured value are shown in Figures A2 and A3. For flow meter F1 the curve fit is split at 160Hz (0.617 l/s) with different curves being used to determine the true frequency at values above and below the split. The same procedure is used for F2 with the split at 160Hz which in this case corresponds to a flowrate of 3.55 l/s. The uncertainty used for the estimation of the frequency was taken as the maximum deviation of any data point from the curve fit line. This uncertainty was translated to an uncertainty in the flow and would be considered along with the instrument uncertainty when determining the overall uncertainty in a flow measurement from instruments F1 and F2. Numerical values calculated for the uncertainty of the curve fits are given in Table A2.

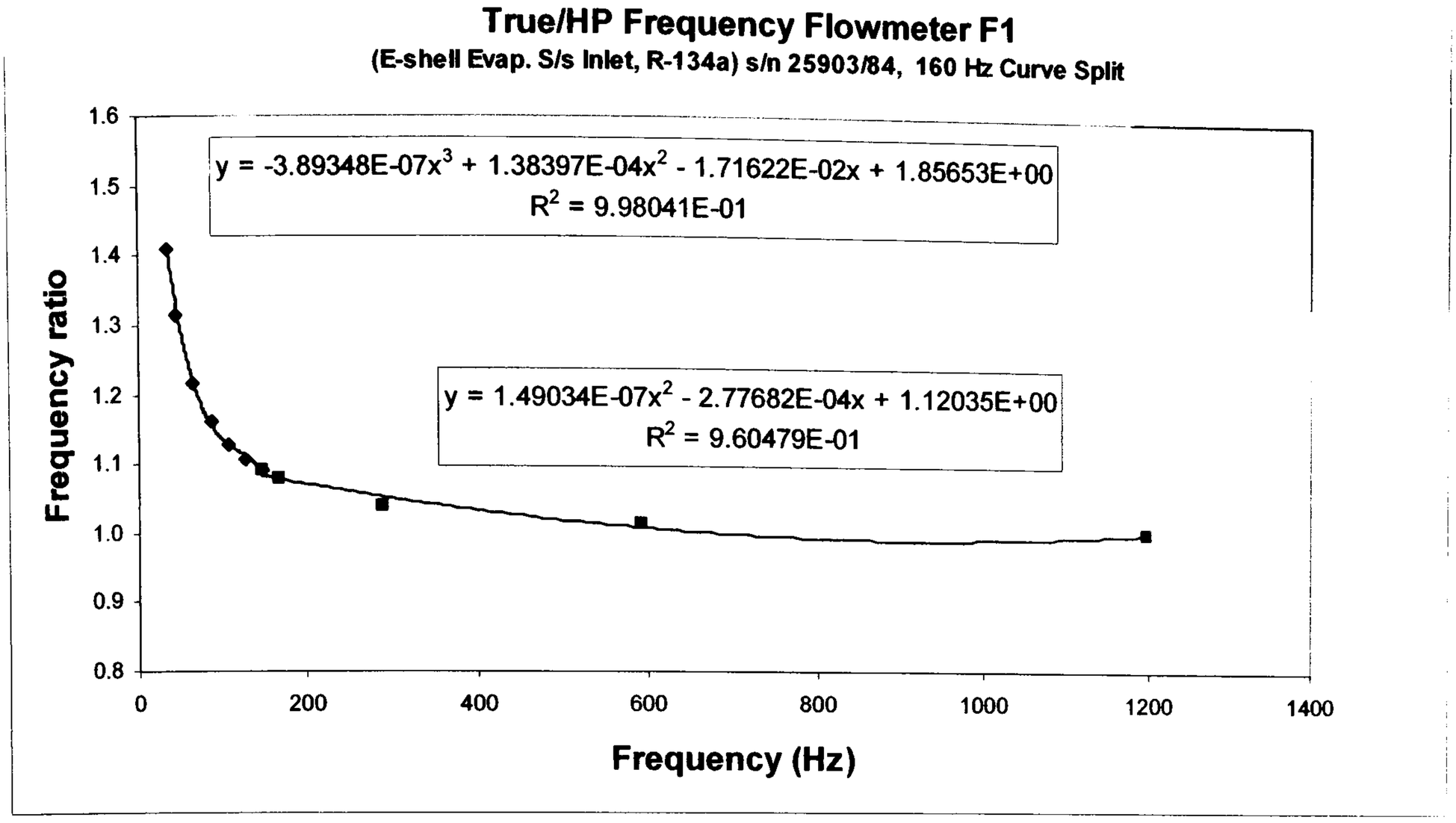

Figure A2 – Curve-fit used to produce flow meter data from F1

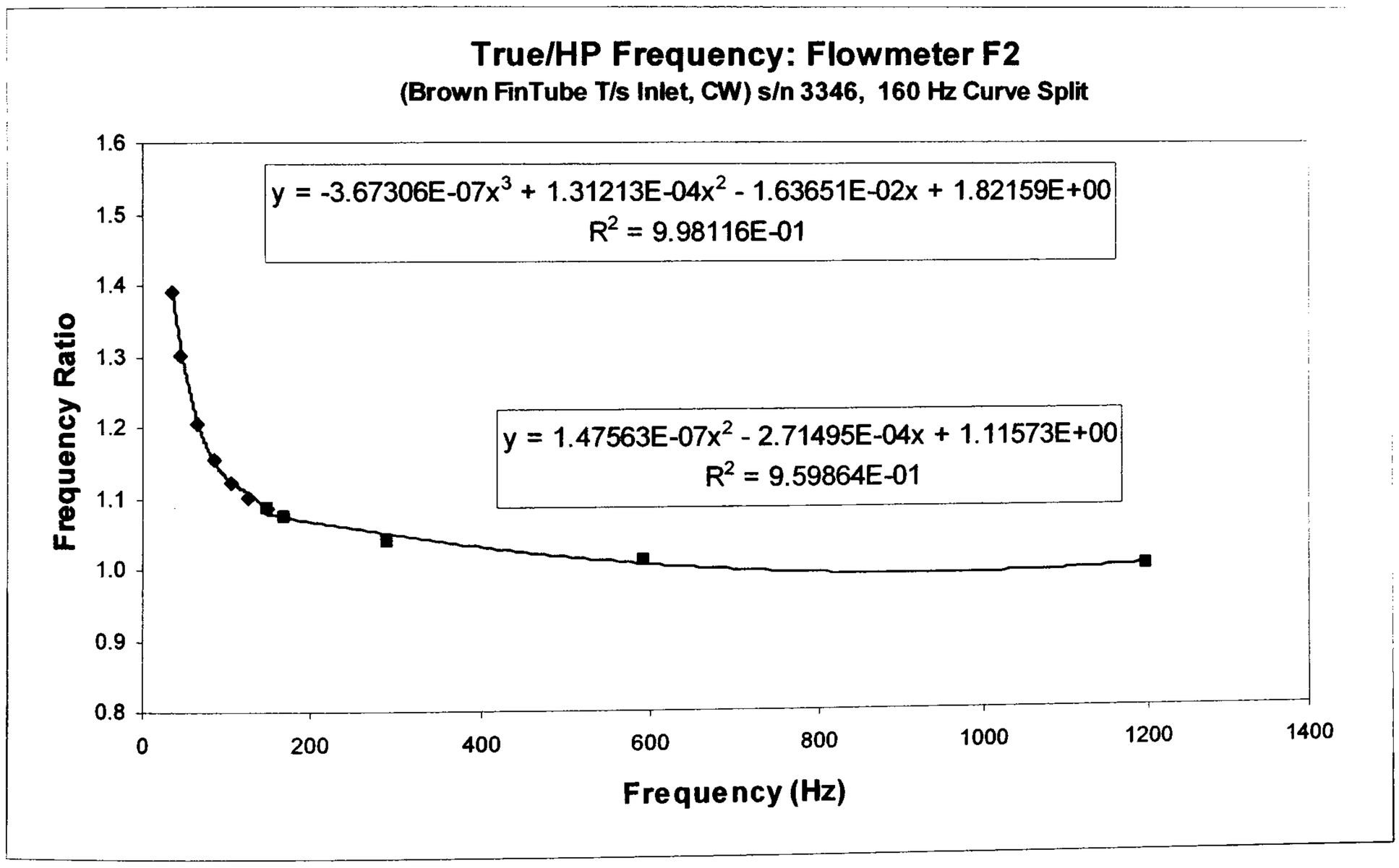

Figure A3 – Curve-fit used to produce flow meter data from F2

Flow meter	Instrument Uncertainty (l/s)	Conversion Uncertainty < 160Hz (l/s)	Conversion Uncertainty > 160Hz (l/s)
F1	0.024	0.0028	0.0148
F2	0.144	0.0132	0.0724

Table A2 – Instrument and Frequency conversion uncertainties for flow meters 1 and 2

2.6 – Combining Uncertainties

The previously described analysis considers examples of independent uncertainty as the value of the measurement uncertainty is independent of the instrument uncertainty. When uncertainties are independent of each other they can be combined by a method known as 'root sum of squares' or 'summation in quadrature'. Equation A5 is used to calculate the combined standard uncertainty, which can be multiplied by a coverage factor of 2 to give the combined expanded uncertainty. It is the combined expanded uncertainty of each measurement which is used to describe the overall uncertainty in an experimental value.

$$u_c = \sqrt{u_m^2 + u_i^2} \qquad \text{(A5)}$$

where u_c is the combined standard uncertainty, u_m is the measurement standard uncertainty (standard deviation) and u_i is the instrument standard uncertainty. For the calculated combined standard uncertainty in measurements made on flow meters F1 and F2 equation A6 was used.

$$u_c = \sqrt{u_m^2 + u_i^2 + u_{conv}^2} \qquad \text{(A6)}$$

Here the value of u_{conv} is taken from table A2 and is chosen depending on the flowrate being measured. For a flowrate of 0.60 l/s being measured by F1 the value of u_{conv} would be 0.0028 l/s, since this corresponds to a frequency of less than 160 Hz.

2.7 – Multi-Parameter Uncertainties

In the case of calculated parameters such as the shellside outlet vapour quality (equation 4.2) or the steam heat load (equation 3.1) a different approach to combining uncertainties is employed. For example, in calculating the heat received by the coolant flow in one of the condensers it is important to know the uncertainty involved in the value of the coolant flowrate and also the uncertainties associated with the inlet and outlet coolant temperatures. In many calculations the uncertainty in a particular parameter will have a more significant influence on the calculation than an identical uncertainty in another. Sensitivity coefficients are introduced in order to account for the importance of each parameter in the overall calculation. The sensitivity co-efficient is a measure of how much a change in a particular parameter effects the overall calculated value. Equation A7 is the general equation for the sensitivity co-efficient.

$$c_i = \frac{\partial y_i}{\partial x_i} = \frac{\Delta y_i}{\Delta x_i} \qquad \text{(A7)}$$

where y is the calculated value and x is the parameter being measured. A suitable increment to choose when calculating the sensitivity co-efficient is the standard uncertainty of the

parameter. The overall combined standard uncertainty for the calculated value is given by equation A8.

$$u_c(y) = \sqrt{\sum_{i=1}^{n} (c_i u(x_i))^2} \qquad \text{(A8)}$$

2.8 - Example calculation of combined expanded multi-parameter uncertainty – Q_{Steam}

This section provides a sample calculation of the uncertainty in the steam heat load as an example of the calculation procedure for determining the overall uncertainty in a calculated value. It is assumed that the uncertainties associated with the estimation of physical properties (such as enthalpy from the temperature measurements and steam saturation temperature from the pressure measurement) are negligible in comparison with the combined measurement and instrument uncertainties. The equation for the calculation of steam heat load in the evaporator is given below.

$$Q_{steam} = \frac{W_c}{t}\left[\left(h_{gin} - h_{gsat}\right) + \left(\Delta h_{cond}\right) + \left(h_{lsat} - h_{lout}\right)\right] \qquad \text{(A9)}$$

W_c is the weight of condensate collected, t is the collection time, h_{gin} and h_{gsat} are the specific gas enthalpies at the inlet and saturation temperatures. Δh_{cond} is the latent heat of condensation and h_{lsat} and h_{lout} are the specific liquid enthalpies at the saturation temperature and outlet temperature respectively. The important measurements for the calculation of the steam heat load are the condensate weight, the collection time the steam side inlet and outlet temperatures and the steam pressure at outlet (used for the calculation of Tsat.). For the steam condensate weight, the weigh scales used have a tolerance of $\pm 1g$ and a rectangular distribution is assumed. Therefore the standard uncertainty is given by equation A4, and is 0.000577kg. Similarly the collection time uncertainty is $\pm 1s$ and the standard uncertainty is 0.577s. The standard instrument uncertainties for the steam side inlet and outlet temperatures and the steam outlet pressure are given in Table A1 and are 0.25°C, 0.25°C and 0.00115 bar respectively. For the current example the following data was used:

Weight Condensate: 5.166kg

Collection Time: 114.68 seconds

Steam Inlet Temp. (T14): 99.36 °C with a measurement standard uncertainty of 0.011 °C

Steam Outlet Temp. (T15): 31.01 °C with a measurement standard uncertainty of 0.0113 °C

Steam Outlet Pressure (P1): 0.0518 bar with a measurement standard uncertainty of $1x10^{-6}$ bar.

The combined standard uncertainties for each measured point are given by equation A5 and the instrument standard uncertainties are given in Table A1. For the steam inlet temperature the following gives the standard uncertainty:

$$u_c = \sqrt{u_m^2 + u_i^2}$$

$$u_c = \sqrt{0.011^2 + 0.25^2}$$

$$u_c = 0.25\ ^{\circ}C$$

In a similar manner the following standard uncertainties are obtained:

Steam side outlet temperature: u_c = 0.25°C

Steam side outlet Pressure: u_c = 0.00115 bar

Weight of condensate collected: u_c = 0.000577kg

Collection time: u_c = 0.577 seconds.

Using the equations for steam heat load and for the calculation of sensitivity coefficients:

$$Q_{steam} = \frac{W_c}{t}\left[\left(h_{gin} - h_{gsat}\right) + \left(\Delta h_{cond}\right) + \left(h_{lsat} - h_{lout}\right)\right]$$

$$c_i = \frac{\partial y_i}{\partial x_i} = \frac{\Delta Q_i}{\Delta x_i}$$

The calculation for the sensitivity coefficient of the steam inlet temperature would be done as follows:

$$Q_{steam}(T_1) = \frac{W_c}{t}\left[\left(h_{gin}(T_1) - h_{gsat}\right) + \left(\Delta h_{cond}\right) + \left(h_{lsat} - h_{lout}\right)\right]$$

$$Q_{steam}(T_1) = \frac{5.166}{114.68}\left[\left(2676 - 2560\right) + \left(2419.68\right) + \left(140.42 - 129.9\right)\right]$$

$$Q_{steam}(T_1) = 114.6977kW$$

Using T_2 = 99.36 + 0.25 = 99.61 °C

$$Q_{steam}(T_2) = \frac{5.166}{114.68}\left[\left(2676.5 - 2560\right) + \left(2419.68\right) + \left(140.42 - 129.9\right)\right]$$

$$Q_{steam}(T_2) = 114.7309kW$$

Therefore the sensitivity coefficient for the steam inlet temperature is given by:

$$c_{steam\,in} = \frac{\Delta Q_i}{\Delta x_i} = \frac{114.7309 - 114.6977}{0.25} = 0.1327$$

Using the same method the following sensitivity coefficients are calculated:

$$c_{weight} = 22.21$$

$$c_{time} = 0.995$$

$$c_{Pressure} = 0.7204$$

$$c_{Tout} = 0.18914$$

The calculated sensitivity coefficients are used to calculate the overall uncertainty in the steam heat load by combining them with the standard uncertainties and taking the sum of the squares using equation A8.

$$u_c(Q) = \sqrt{\left(u(Wt) \times c_{Weight}\right)^2 + \left(u(t) \times c_{time}\right)^2 + \left(u(T_{in}) \times c_{Tin}\right)^2 + \left(u(P_t) \times c_{Pt}\right)^2 + \left(u(T_{out}) \times c_{Tout}\right)^2}$$

This gives a value of the standard uncertainty in the steam heat load of:

$$u_c(Q) = 0.583kW$$

Thus the combined expanded uncertainty is given as twice this value with a confidence limit of 95.4%. The steam heat load calculated from this particular set of data can therefore be represented as:

$$Q_{Stteam} = 114.7 \pm 1.17kW$$

A3 - Calculated Uncertainty Data

This section contains of the uncertainty analysis produced using the procedure outlined above. Figures A4 – A13 contain plots of the experimental data that were presented in Chapter 5 (Figures 5.2, 5.3, 5.5 and 5.8). The plots display error bars which correspond to the range of ± the expanded uncertainty in the value. Tables A3 – A14 give the principal measured and calculated data and the standard uncertainties which correspond to this data. The headings in the data columns represent the following:

F1 – Refrigerant volumetric flowrate from accumulator to evaporator

F9 – Refrigerant volumetric flowrate from separator to evaporator

Wt – Steam condensate weight collected

Time – Recorded time of condensate collection

PRT3 – R-134A evaporator outlet temperature

P9 – Differential pressure drop between shellside nozzles

P1 – Measured pressure in steam outlet header

P8 – Differential pressure drop across shellside baffle spaces

Tsat – Steam saturation temperature corresponding to P1

Qsteam – Steam heat load

x(outlet) – Evaporator exit vapour mass fraction

m – Mass flux to evaporator

boil htc – Shellside boiling heat transfer coefficient

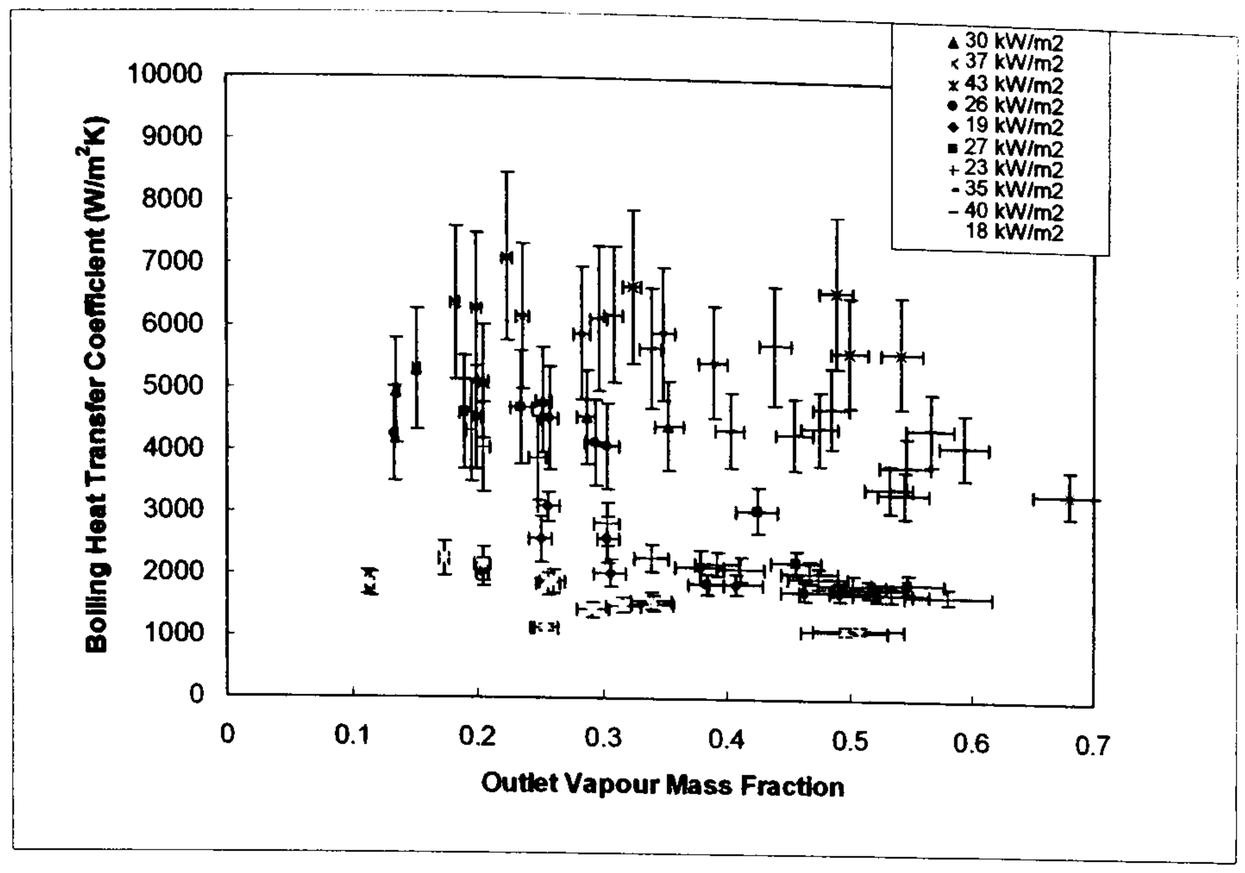

Figure A4 – Figure 5.2(c) data for Test 1 re-plotted with expanded uncertainties

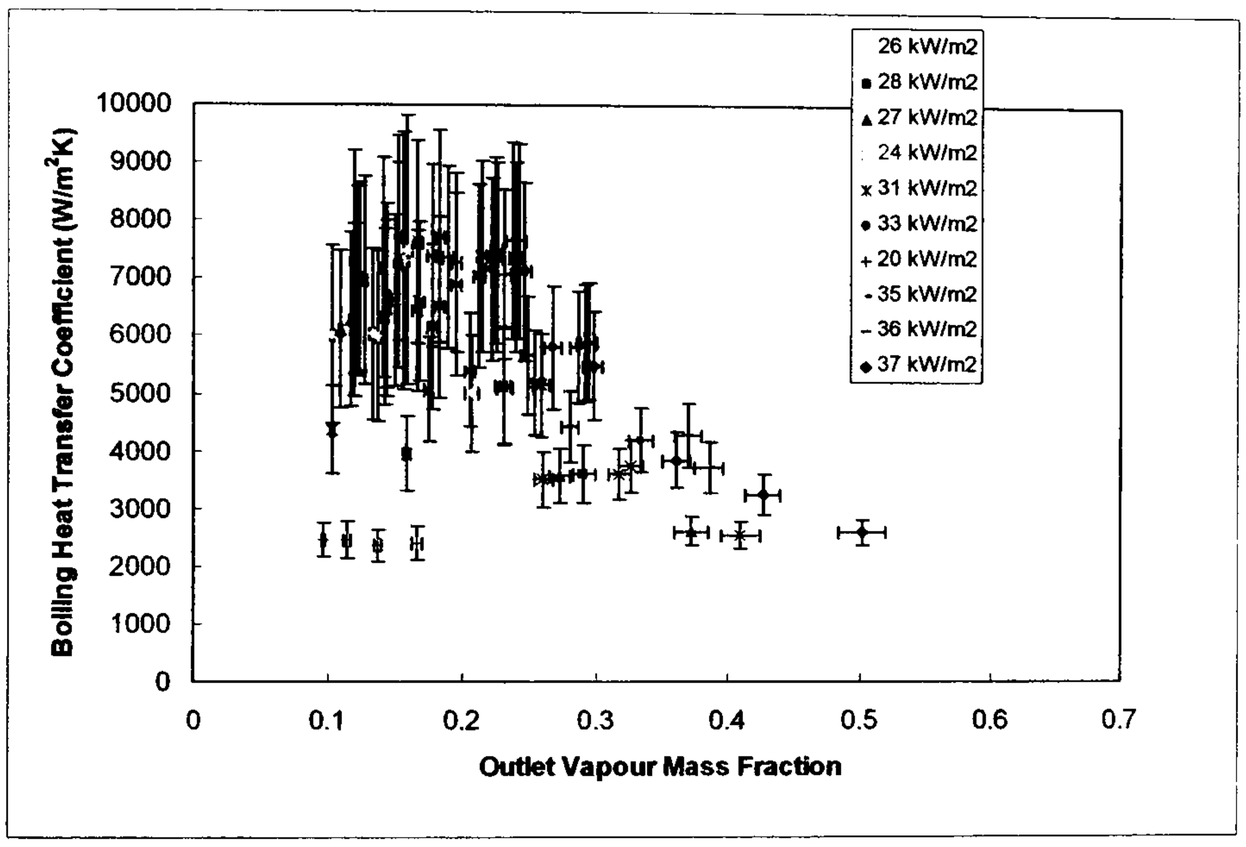

Figure A5 – Figure 5.2(d) data for Test 2 re-plotted with expanded uncertainties

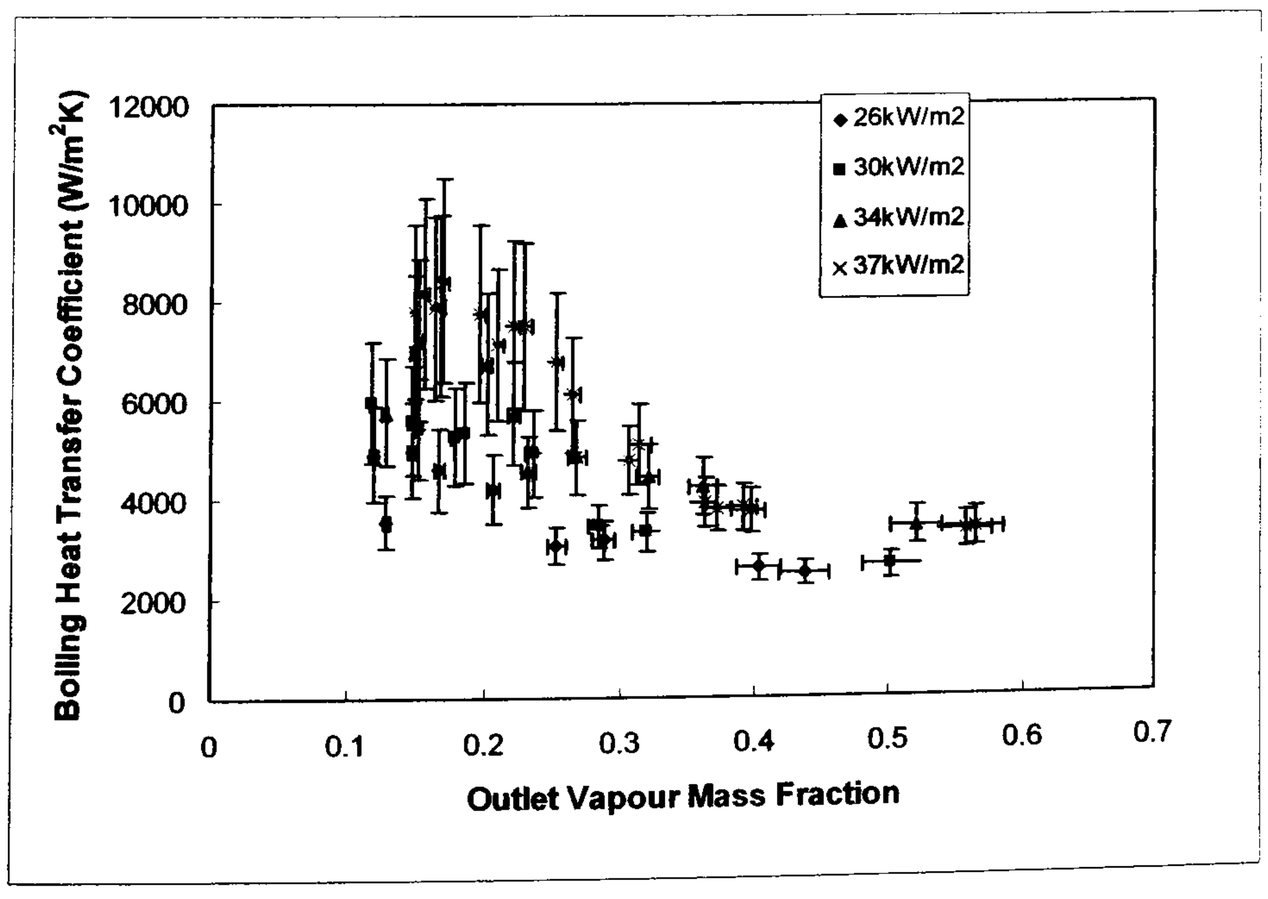

Figure A6 – Figure 5.2(e) data for Test 3 re-plotted with expanded uncertainties

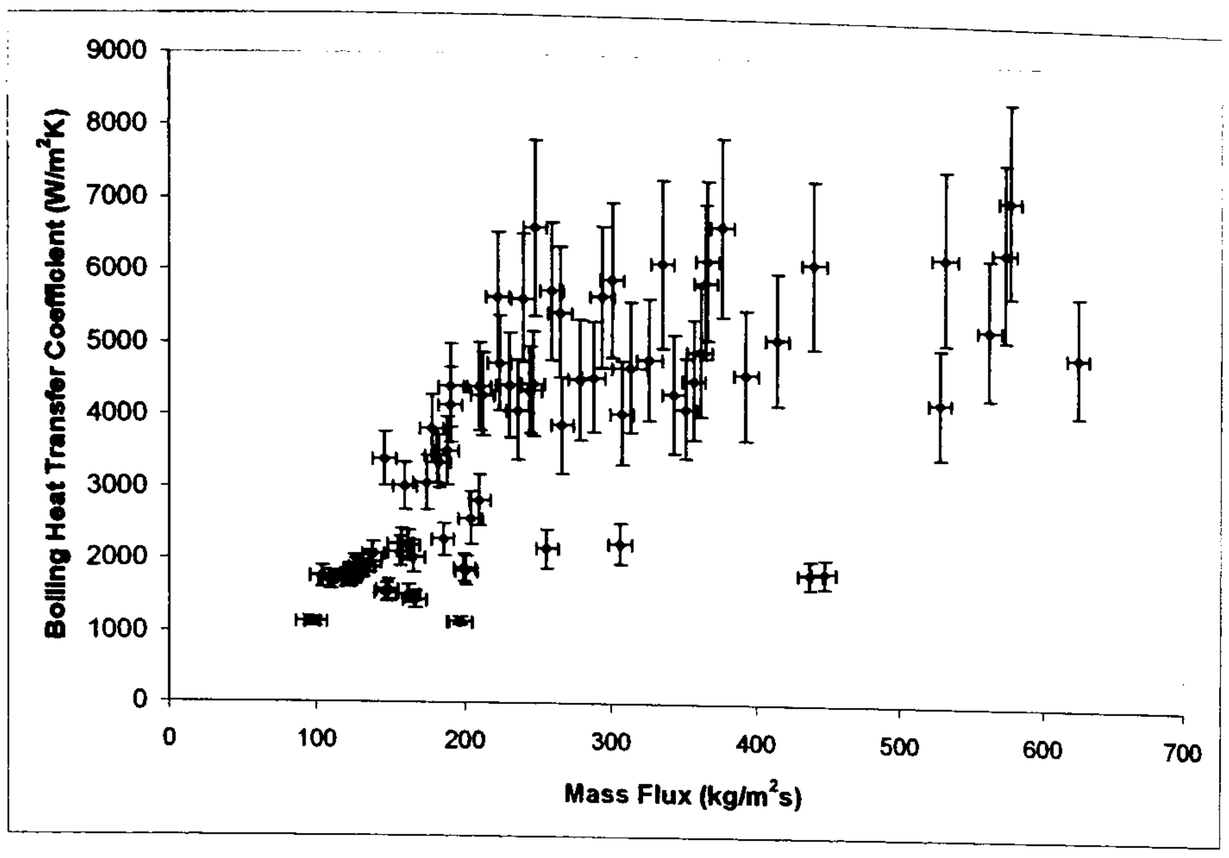

Figure A7 – Figure 5.3(c) data for Test 1 re-plotted with expanded uncertainties

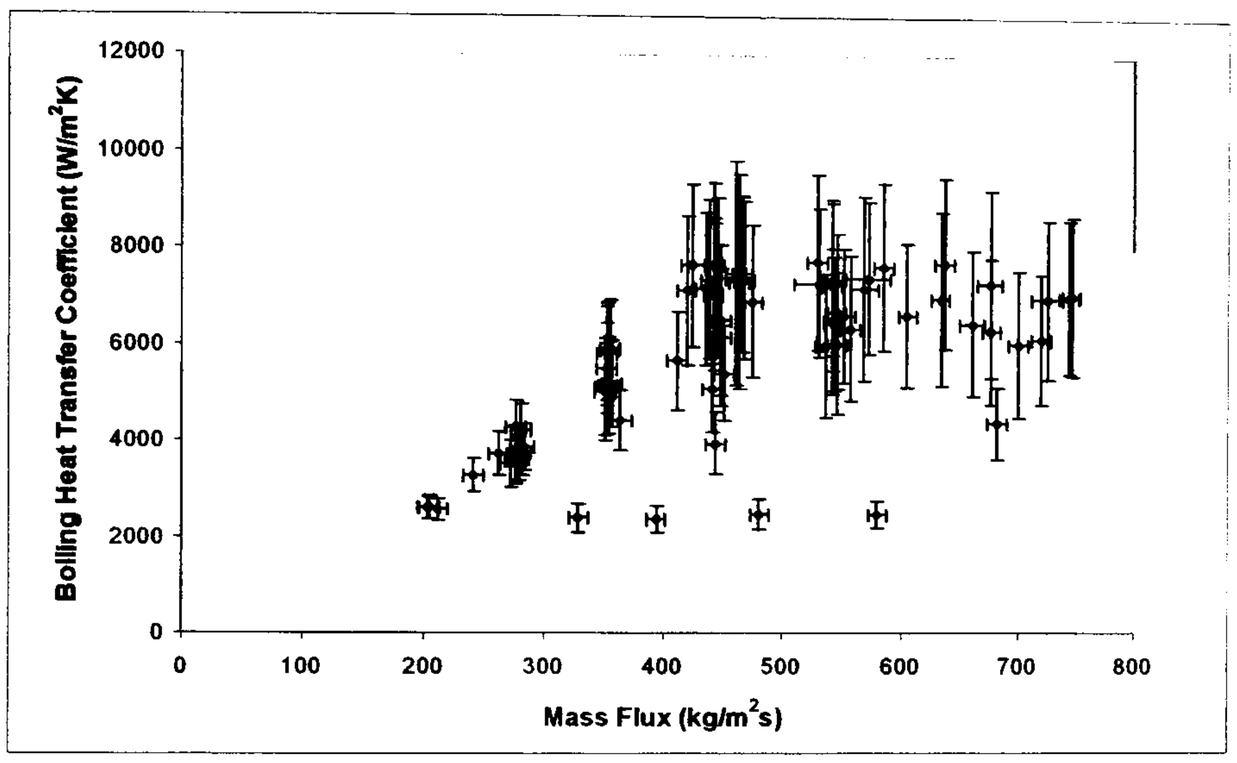

Figure A8 – Figure 5.3(d) data for Test 2 re-plotted with expanded uncertainties

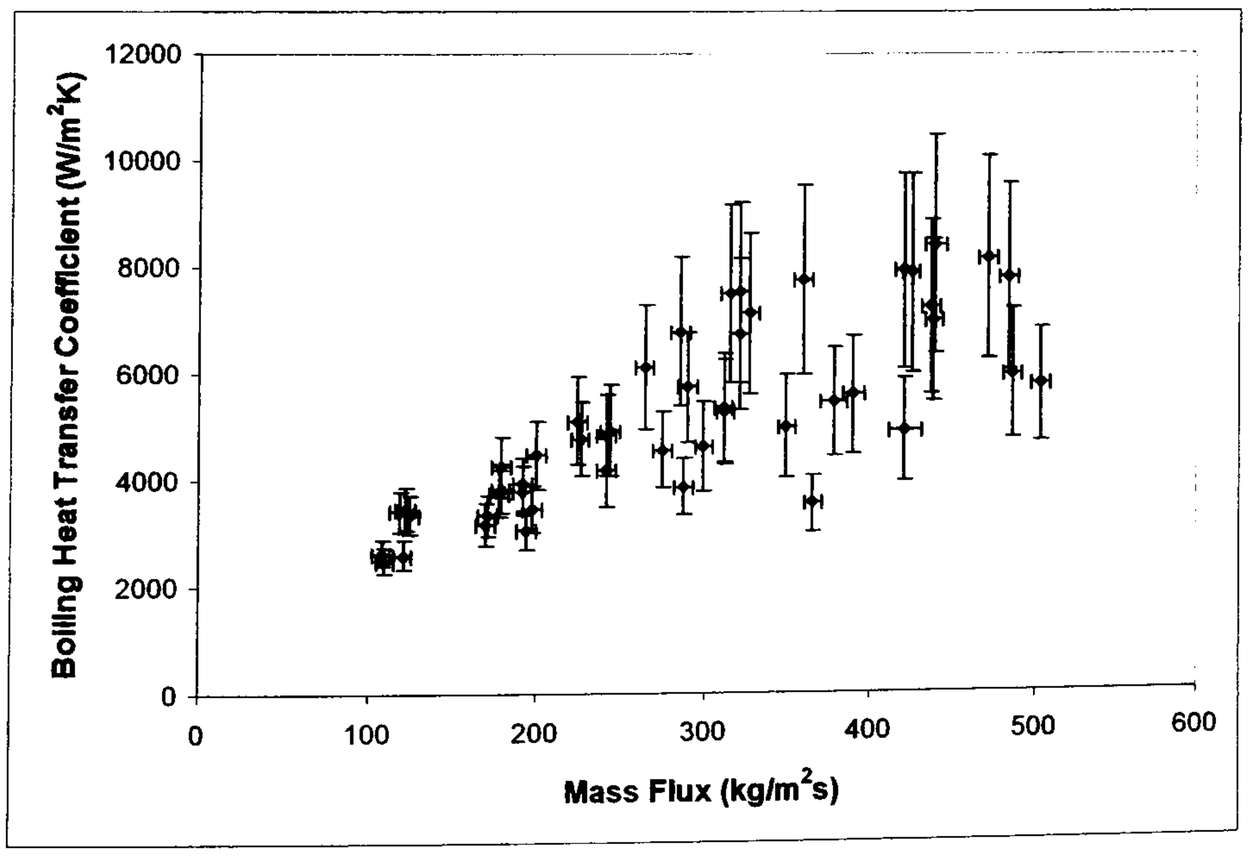

Figure A9 – Figure 5.3(e) data for Test 3 re-plotted with expanded uncertainties

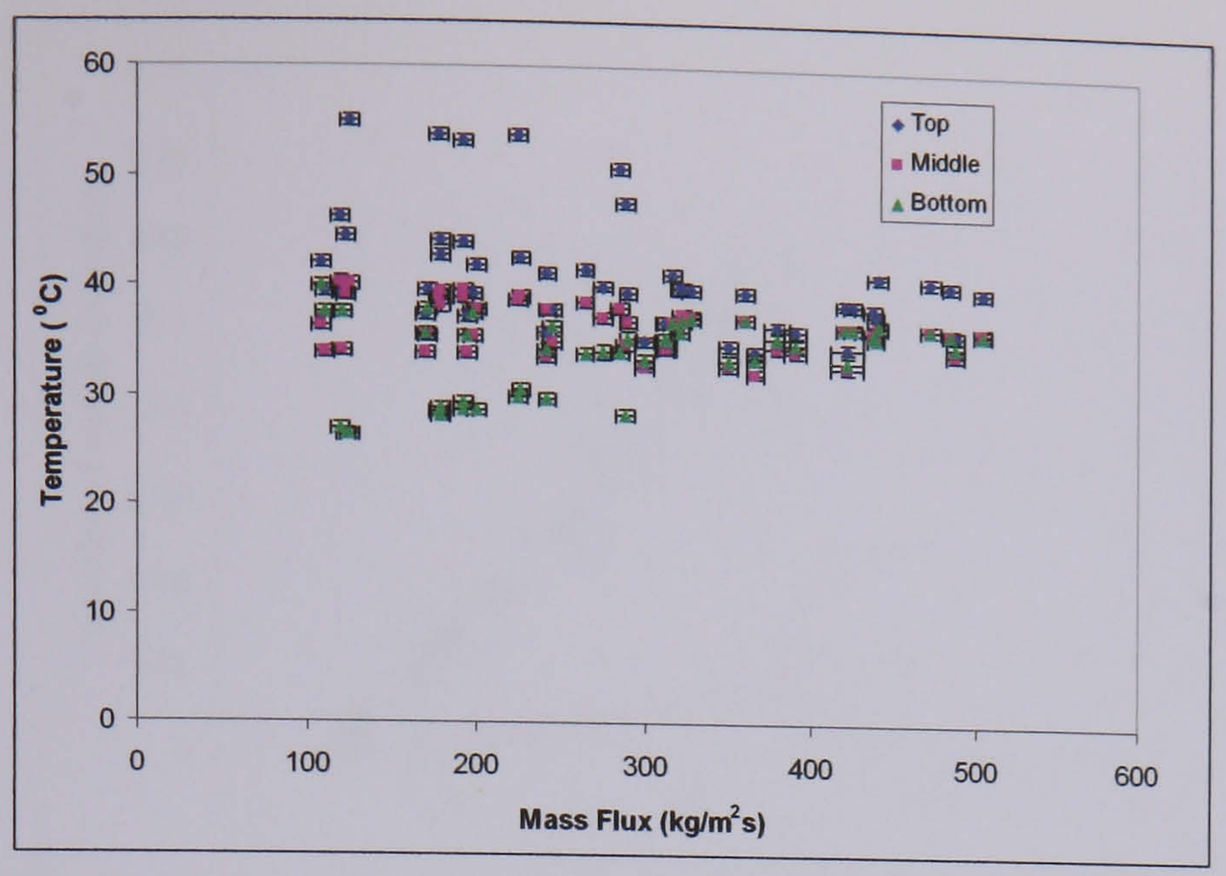

Figure A10 – Figure 5.5 data for Test 3 re-plotted with expanded uncertainties

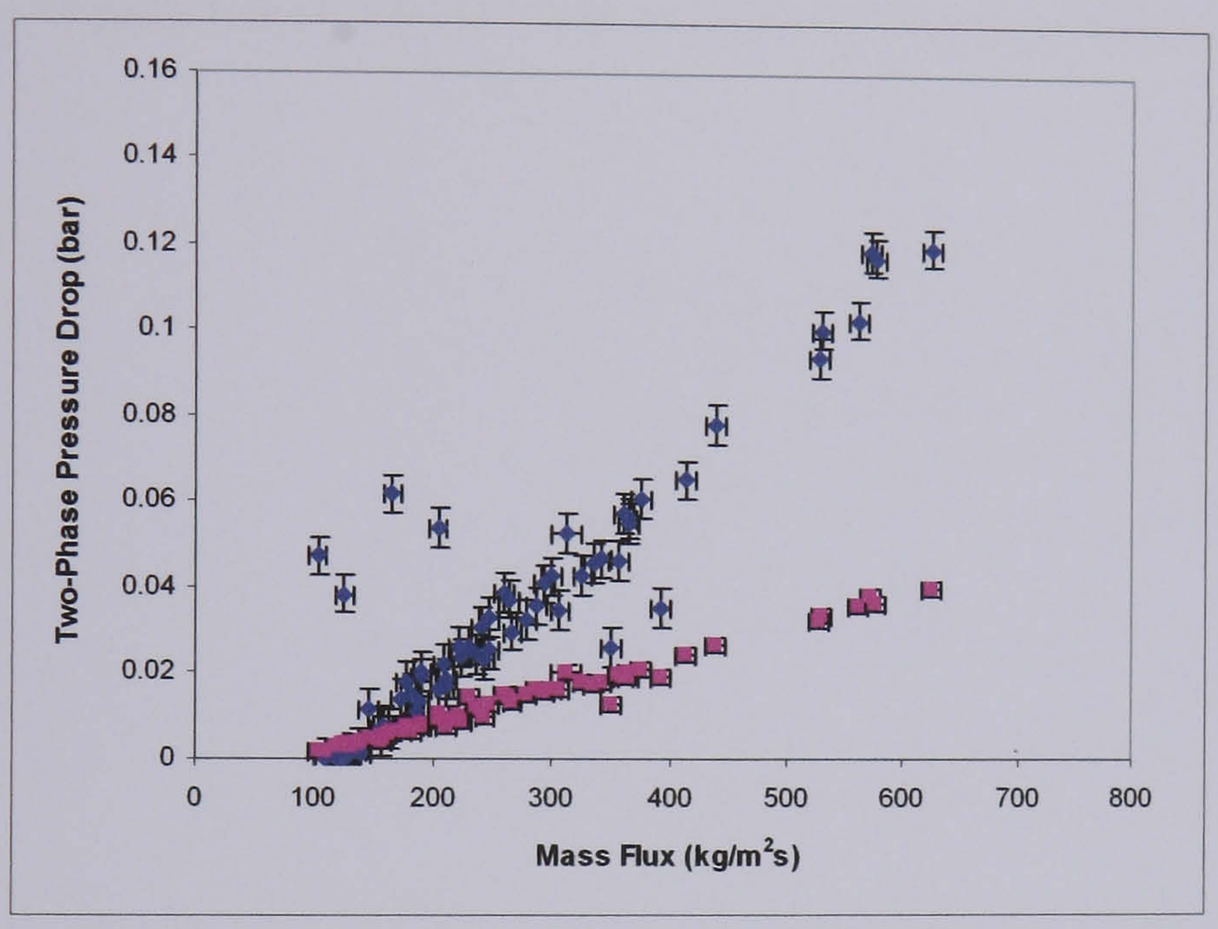

Figure A11 – Figure 5.8(c) data for Test 1 re-plotted with expanded uncertainties

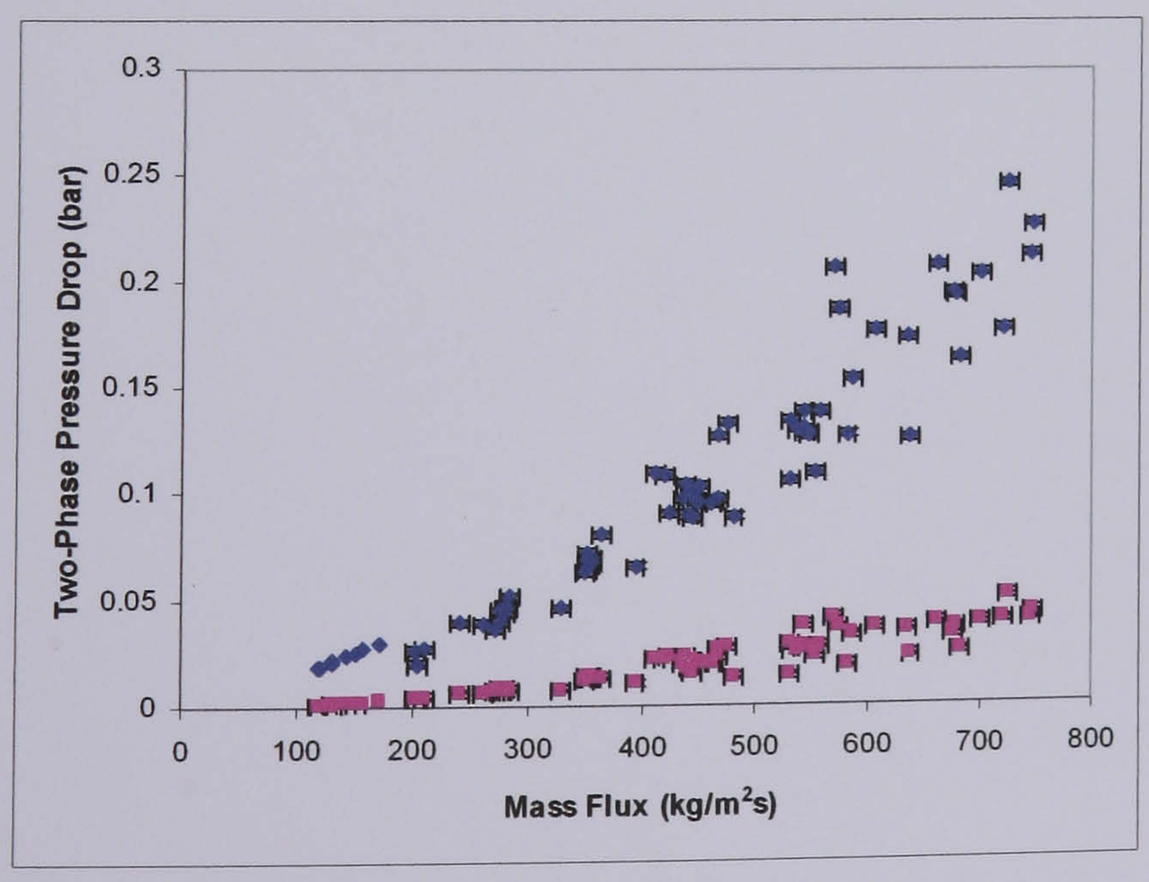

Figure A12 – Figure 5.8(d) data for Test 2 re-plotted with expanded uncertainties

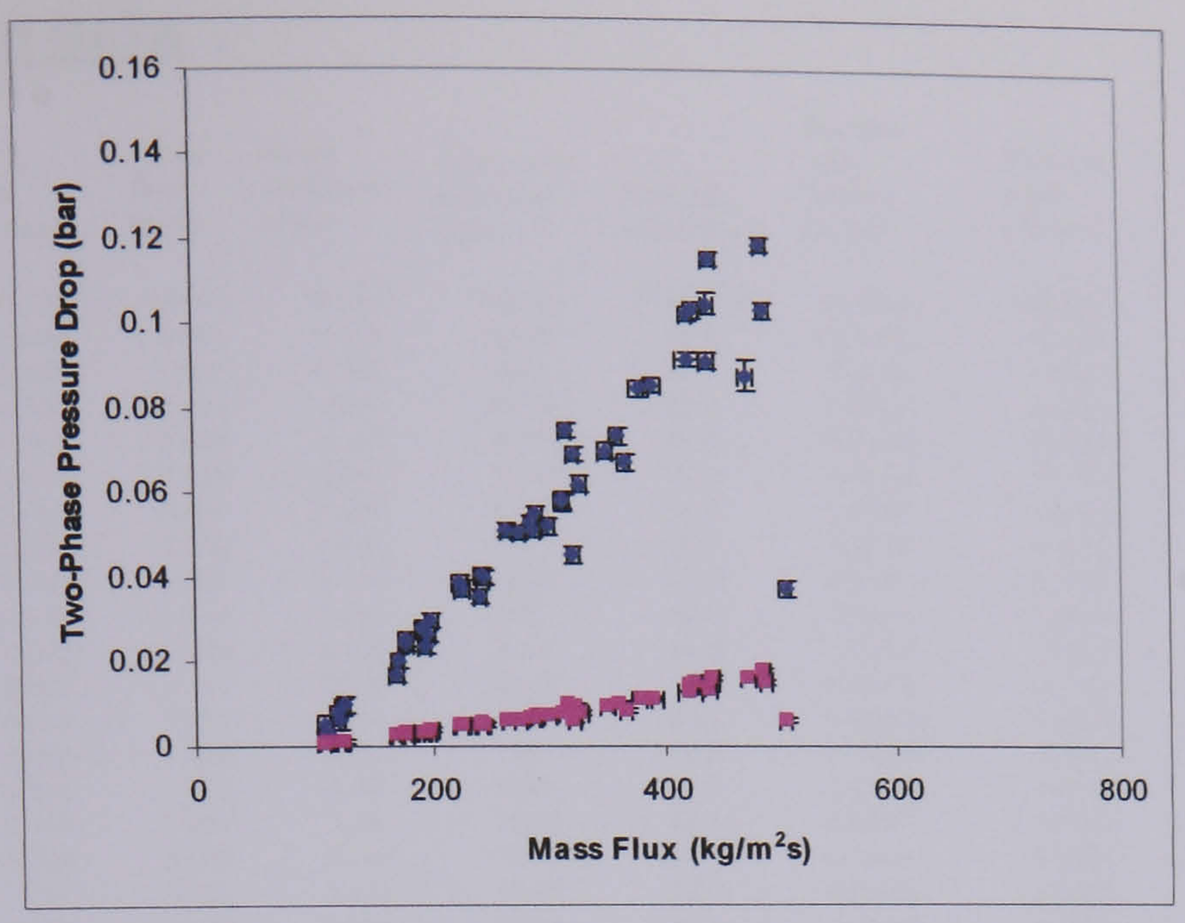

Figure A13 – Figure 5.8(e) data for Test 3 re-plotted with expanded uncertainties

TABLE A3 : TEST 1 DATA

R134a flow, feed	R134a flow re-circ	Steam condensate weight	Condensate collection time	Shellside outlet temp	Pressure drop between nozzles	Tubeside outlet pressure	Pressure drop along shellside
F1 (l/s)	F9 (l/s)	Wt (kg)	Time (s)	PRT3 (^{0}C)	P9 (bar)	P1 (bar)	P8 (bar)
0.499	0.834	5.166	114.68	22.7	0.00111	0.0518	0.004
0.485	1.469	5.105	113.2	22.7	0.0165	0.0441	0.0107
0.658	0.575	5.06	80.74	21.7	0.00107	0.0673	0.0029
0.674	3.042	5.142	80.63	21.8	0.03537	0.0428	0.01912
0.649	2.314	5.005	79.09	22.1	0.05285	0.043	0.02015
0.655	0.829	5.087	81.51	21.6	0.00695	0.05958	0.00432
0.667	0.982	5.068	78.43	22.1	0.01416	0.0522	0.00645
0.944	1.608	5.116	61.08	27.8	0.03727	0.0653	0.0145
0.949	1.947	5.332	62.4	27.3	0.04267	0.0627	0.01606
0.929	2.584	5.167	61.9	27.4	0.05613	0.0624	0.02017
0.923	3.317	5.098	61.19	27.6	0.07822	0.0621	0.02684
0.919	4.201	5.106	59.92	27.8	0.10056	0.0629	0.03355
0.924	4.605	5.265	63	27.9	0.11883	0.0623	0.03836
0.747	1.454	5.08	76.67	25.2	0.02636	0.0546	0.0147075
0.773	1.984	5.08	76.35	25.2	0.03576	0.0542	0.01616
0.724	2.398	5.113	75.91	25.2	0.04286	0.0534	0.0179
0.75	3.216	5.151	74.98	25.4	0.06532	0.0533	0.02419
0.739	4.646	5.063	73.71	25.4	0.1028	0.0528	0.03568
0.747	5.245	5.103	74.92	25.66	0.11963	0.05452	0.03999
1.093	2.587	5.084	51.85	32.15	0.06091	0.0831	0.0211
1.101	1.324	5.127	51.3	32.47	0.03319	0.08556	0.01264
1.102	1.256	5.136	52.07	33.32	0.03079	0.0943	0.01168
1.103	1.082	5.167	51.3	33.44	0.02599	0.0959	0.01
1.143	4.584	5.278	52.18	36.15	0.11733	0.1011	0.03658
0.626	2.759	5.173	89.04	22.72	0.04627	0.0443	0.01954
0.645	2.008	5.131	86.89	23.02	0.03251	0.0454	0.01492
1.666	1.666	5.012	85.02	22.72	0.02606	0.0459	0.01298
0.637	1.609	5.123	86.07	23.22	0.02425	0.0478	0.01214
0.689	4.33	4.752	84.09	23.24	0.09401	0.0461	0.03251
0.45	1.109	5.04	118.97	20.43	0.06174	0.0464	0.0063
0.453	0.515	5.029	116.22	20.11	0.04725	0.05016	0.0018
0.439	0.743	5.033	113.81	20.34	0.0385	0.05	0.0034
0.46	1.464	4.992	117.82	20.49	0.05395	0.0415	0.009
0.681	2.787	5.035	85.25	26.56	0.05747	0.0536	0.01942
0.672	0.855	5.111	83.32	26	0.00781	0.0647	0.0049
0.652	1.15	5.081	85.69	26.09	0.01336	0.0595	0.0073
0.676	1.691	5.235	85.74	26.17	0.02553	0.0553	0.01272
0.58	2.673	4.521	82.28	22.21	0.04675	0.04267	0.01809
0.595	1.931	4.918	90.41	21.96	0.02981	0.0435	0.01342
0.578	2.362	4.107	81.13	25.18	0.03475	0.0495	0.01633
0.583	1.412	4.221	80.64	22.19	0.01669	0.0494	0.00907
0.592	1.164	4.613	87.88	22.16	0.0113	0.0541	0.0076
0.579	0.958	4.376	82.71	21.9	0.00692	0.056	0.00555
0.592	0.885	4.982	93.75	21.81	0.00537	0.0571	0.005
0.582	0.727	4.966	90.96	21.91	0.00245	0.0595	0.0036
0.594	0.692	4.857	90.85	21.85	0.00156	0.0602	0.0034
0.578	0.617	4.815	90.08	21.77	0	0.0622	0.0029
0.585	0.581	5.013	94.09	21.7	0	0.0632	0.0029
0.584	0.565	4.855	90.85	21.7	0	0.06486	0.0027
0.588	0.54	4.846	90.84	21.68	0	0.065	0.0027
0.578	0.456	4.923	90.57	21.68	0	0.067	0.002
0.874	1.182	5.317	66.96	29.39	0.01865	0.07671	0.0078
0.889	1.146	5.14	61.4	29.42	0.02209	0.0785	0.00918
0.89	1.475	5.179	64.43	29.44	0.02319	0.0768	0.00974
0.892	0.827	5.163	64.1	29.29	0.01787	0.08128	0.00744
0.886	0.874	5.459	68	29.19	0.01501	0.0855	0.00664
0.941	0.821	5.231	65.7	28.92	0.01461	0.08483	0.0066
0.887	2.362	5.478	68.06	29.4	0.04582	0.0673	0.01752
0.89	1.955	5.249	64.65	29.37	0.04099	0.0692	0.01551
0.92	0.503	5.129	60.09	31.27	0.01151	0.09991	0.0045
1.055	0.809	5.143	55.31	32.84	0.01889	0.1029	0.00727
1.049	1.481	5.493	59.54	31.33	0.03883	0.0817	0.0148
0.986	2.585	5.577	60.75	31.27	0.05519	0.07902	0.01915
0.992	0.871	5.486	60.69	31.28	0.02018	0.09009	0.00805
0.973	1.207	5.51	60.69	31.11	0.02349	0.08703	0.00893
0.493	1.907	4.379	102.05	18.11	0.08191	0.0398	0.01299
0.478	1.397	5.057	118.03	18.34	0.07042	0.0435	0.00912
0.461	0.92	4.913	118.53	18.2	0.04999	0.0468	0.0047
0.475	2.399	4.456	101.55	18.27	0.09251	0.04007	0.01613
0.474	1.411	5	117.92	18.33	0.07254	0.0437	0.0097
0.479	1.038	4.993	118.25	18.19	0.06103	0.049	0.0095
0.448	1.396	4.985	118.09	17.42	0	0.0587	0.02773
0.422	0.456	4.922	118.75	17.61	0	0.0585	0.0279
0.45	1.106	4.523	112.82	17.6	0.00685	0.0474	0.0063
0.466	3.719	5.007	121.88	18.03	0.05533	0.0421	0.02265
0.445	1.392	4.977	118.8	17.41	0	0.0583	0.0277
0.455	0.472	4.89	118.53	17.46	0	0.058	0.0282
0.451	0.92	4.772	113.8	17.64	0.00274	0.0467	0.0044

TABLE A4 : STANDARD UNCERTAINTIES IN TEST 1 DATA

R134a flow, feed	R134a flow re-circ	Steam condens weight	Condensate collection time	Shellside outlet temp	Pressure drop between nozzles	Tubeside outlet pressure	Pressure drop along shellside
F1 (l/s)	F9 (l/s)	Wt (kg)	Time (s)	PRT3 (^{0}C)	P9 (bar)	P1 (bar)	P8 (bar)
0.011881638	0.034815226	0.000577	0.577	0.025002	0.002252385	0.001154701	0.00087
0.011881638	0.034711669	0.000577	0.577	0.02500242	0.002255216	0.001154809	0.000870052
0.01877161	0.034692939	0.000577	0.577	0.0250045	0.002251775	0.001154701	0.00087
0.018774273	0.035332704	0.000577	0.577	0.02500288	0.002253939	0.001154701	0.00088784
0.018774273	0.053276636	0.000577	0.577	0.02500338	0.002263469	0.001154701	0.000873876
0.01877161	0.034692939	0.000577	0.577	0.02500288	0.002251846	0.00115477	0.000870092
0.018774273	0.034711669	0.000577	0.577	0.02500338	0.002251722	0.001154701	0.000870282
0.01877161	0.034646789	0.000577	0.577	0.02500288	0.002252645	0.00115477	0.000870092
0.018774273	0.034677082	0.000577	0.577	0.02500338	0.002253284	0.001154701	0.000870144
0.01877161	0.034646789	0.000577	0.577	0.02500128	0.002255961	0.001154701	0.000870144
0.018774273	0.034922772	0.000577	0.577	0.025005119	0.002259383	0.001154701	0.000870465
0.01877161	0.039196939	0.000577	0.577	0.02500288	0.002261612	0.001154701	0.000871659
0.01877161	0.03560337	0.000577	0.577	0.02500338	0.002255768	0.001154701	0.000870144
0.018774273	0.034646789	0.000577	0.577	0.02500128	0.00225284	0.001154701	0.000870144
0.01877161	0.034642459	0.000577	0.577	0.02500338	0.002253053	0.001154701	0.000870575
0.018774273	0.034646789	0.000577	0.577	0.025005119	0.002252645	0.001154701	0.000870368
0.01877161	0.034642459	0.000577	0.577	0.02500338	0.02077836	0.001154701	0.000872072
0.018774273	0.034677082	0.000577	0.577	0.02500338	0.002253533	0.001154701	0.000870207
0.018774273	0.034664102	0.000577	0.577	0.025002	0.002261612	0.00115477	0.000874494
0.018774273	0.034677082	0.000577	0.577	0.0250045	0.002259124	0.001154701	0.000870827
0.018774273	0.034654004	0.000577	0.577	0.02500392	0.002252041	0.001154809	0.000870144
0.018774273	0.034654004	0.000577	0.577	0.02500338	0.002253167	0.001154701	0.000870092
0.018774273	0.034677082	0.000577	0.577	0.02500338	0.002253533	0.001154701	0.00087
0.018782261	0.034884094	0.000577	0.577	0.02500338	0.002253799	0.001154701	0.000870465
0.01877161	0.034733269	0.000577	0.577	0.025005119	0.002256158	0.001154701	0.000870465
0.01877161	0.034646789	0.000577	0.577	0.025002	0.002257211	0.001154701	0.000870575
0.01877161	0.034654004	0.000577	0.577	0.02500288	0.002256776	0.001154701	0.000870465
0.01877161	0.034642459	0.000577	0.577	0.02500392	0.002255768	0.001154701	0.000870282
0.01877161	0.034664102	0.000577	0.577	0.02500288	0.00225284	0.001154701	0.000870971
0.011885846	0.034642459	0.000577	0.577	0.02500392	0.002251746	0.001154701	0.00087
0.011881638	0.034664102	0.000577	0.577	0.025	0.002251846	0.001154809	0.00087
0.011881638	0.034646789	0.000577	0.577	0.025002	0.002252308	0.001154701	0.00087
0.011885846	0.034646789	0.000577	0.577	0.025	0.002252234	0.001154701	0.00087
0.01877161	0.034848242	0.000577	0.577	0.025	0.002253284	0.001154701	0.000870207
0.01877161	0.034646789	0.000577	0.577	0.025	0.002252467	0.001154701	0.00087
0.01877161	0.034642459	0.000577	0.577	0.02500338	0.002251746	0.001154701	0.000870092
0.01877161	0.034664102	0.000577	0.577	0.02500288	0.002252041	0.001154701	0.000870092
0.011881638	0.034664102	0.000577	0.577	0.025011517	0.002254232	0.001154809	0.000870575
0.011881638	0.034664102	0.000577	0.577	0.02503869	0.002255041	0.001154701	0.000870092
0.011881638	0.034677082	0.000577	0.577	0.025008818	0.002252467	0.001154701	0.000870207
0.011881638	0.034654004	0.000577	0.577	0.025005119	0.002253533	0.001154701	0.000870144
0.011881638	0.034646789	0.000577	0.577	0.025014576	0.002252166	0.001154701	0.00087
0.011885846	0.034642459	0.000577	0.577	0.025014576	0.002251746	0.001154701	0.000870144
0.011885846	0.034642459	0.000577	0.577	0.025021771	0.002252041	0.001154701	0.00087
0.011881638	0.034646789	0.000577	0.577	0.025008818	0.002251846	0.001154701	0.00087
0.011881638	0.034654004	0.000577	0.577	0.025007999	0.002251746	0.001154701	0.00087
0.011881638	0.034654004	0.000577	0.577	0.025013516	0.002251666	0.001154701	0.00087
0.011881638	0.034664102	0.000577	0.577	0.025005119	0.002251666	0.001154701	0.00087
0.011885846	0.034654004	0.000577	0.577	0.025010578	0.002251666	0.001154809	0.00087
0.011881638	0.034664102	0.000577	0.577	0.025013516	0.002251666	0.001154701	0.00087
0.011881638	0.034664102	0.000577	0.577	0.025011517	0.002251666	0.001154701	0.00087
0.01877161	0.034646789	0.000577	0.577	0.025017994	0.002252234	0.00115474	0.00087
0.018774273	0.034815226	0.000577	0.577	0.025011517	0.002252234	0.001154701	0.000870827
0.01877161	0.034785054	0.000577	0.577	0.025015675	0.002251686	0.001155324	0.000870144
0.01877161	0.034677082	0.000577	0.577	0.025025907	0.002251846	0.001154857	0.000870144
0.018774273	0.034642459	0.000577	0.577	0.025017994	0.002252554	0.001154701	0.000870144
0.018774273	0.034642459	0.000577	0.577	0.025017994	0.002251888	0.001154809	0.00087
0.018774273	0.034664102	0.000577	0.577	0.025020472	0.002254704	0.001154701	0.000870282
0.018774273	0.034654004	0.000577	0.577	0.025020472	0.002254232	0.001154701	0.000870144
0.018774273	0.034884094	0.000577	0.577	0.025030402	0.002251888	0.001155324	0.00087
0.018782261	0.034664102	0.000577	0.577	0.025028863	0.002251986	0.001155225	0.000870144
0.018814179	0.034815226	0.000577	0.577	0.025023109	0.002257211	0.001154701	0.00087
0.018814179	0.034646789	0.000577	0.577	0.025024488	0.002253664	0.00115477	0.000870144
0.018782261	0.034664102	0.000577	0.577	0.025017994	0.002251775	0.001154809	0.000870144
0.01877161	0.034733269	0.000577	0.577	0.025008818	0.002251808	0.001154809	0.000870144
0.011881638	0.034664102	0.000577	0.577	0.025007999	0.002257895	0.001154701	0.000870282
0.011885846	0.034692939	0.000577	0.577	0.025016814	0.002252101	0.001154701	0.000870092
0.011881638	0.034642459	0.000577	0.577	0.025016814	0.002252041	0.001154701	0.00087
0.011881638	0.035396327	0.000577	0.577	0.0250045	0.002254232	0.001154809	0.000870368
0.011881638	0.034692939	0.000577	0.577	0.025009678	0.002263469	0.001154701	0.00087
0.011881638	0.034646789	0.000577	0.577	0.025011517	0.002252308	0.001154701	0.00087
0.011881638	0.037099865	0.000577	0.577	0.025007219	0.002251666	0.001154701	0.000870144
0.011881638	0.034848242	0.000577	0.577	0.025015675	0.002251666	0.001154701	0.00087
0.011881638	0.034711669	0.000577	0.577	0.025011517	0.002251722	0.001154701	0.00087
0.011885846	0.036878178	0.000577	0.577	0.025024488	0.002253664	0.001154701	0.000870282
0.011885846	0.039196939	0.000577	0.577	0.025014576	0.002251666	0.001154701	0.00087
0.011885846	0.034664102	0.000577	0.577	0.025021771	0.002251666	0.001154701	0.00087
0.011885846	0.034733269	0.000577	0.577	0.025058252	0.002252467	0.001154701	0.00087

TABLE A5 : CALCULATED VALUES FROM TEST 1 DATA

Tsat (^{0}C)	Qsteam (kW)	x (outlet)	m (kg/m^{2}s)	boil htc (W/m^{2}K)
33.52050781	110	0.377186845	140.2343507	2138.467231
30.6640625	110	0.255857926	205.5648322	3102.134123
38.26660156	152	0.546315643	130.1065046	1896.194014
30.13671875	156	0.18948844	391.9954595	4610.160894
30.22460938	155	0.234360863	312.2801471	4692.326589
36.02539063	152	0.454911226	156.6391783	2226.208924
33.65234375	158	0.423715953	173.7934399	3062.431211
37.71728516	213	0.388141198	264.2515663	5446.868334
36.97021484	218	0.348085105	300.3489585	5902.986562
36.88232422	213	0.282342194	364.2234299	5894.293128
36.79443359	213	0.23489029	439.3184667	6162.545972
37.03613281	217	0.198315079	530.1598823	6300.769848
36.86035156	213	0.181468031	572.3279291	6386.594208
34.44335938	169	0.352602493	229.7793274	4424.660362
34.31152344	170	0.28648525	287.824446	4549.920015
34.04785156	172	0.251554247	325.9296048	4810.386428
34.02587891	175	0.203444835	413.7838074	5110.690809
33.87207031	176	0.150962517	561.8320229	5302.919497
34.44335938	174	0.134980988	624.65546	4952.298705
42.24365234	248	0.322898166	375.6829965	6661.589323
42.79296875	253	0.488052044	247.297983	6612.896888
44.68261719	249	0.499175219	239.7783553	5638.215662
44.99023438	254	0.541603379	222.0962299	5646.963071
46.04492188	255	0.223080677	576.725408	7122.758648
30.75195313	149	0.19872695	356.0873911	4530.361064
31.19140625	151	0.257156503	278.8298353	4518.169949
31.3671875	151	0.293904893	350.5120199	4133.526383
32.0703125	152	0.303420059	235.9104514	4082.374724
31.45507813	145	0.133772757	527.1426557	4257.161983
31.54296875	108	0.305173181	165.1318508	2030.51013
32.94921875	110	0.490031084	102.6295872	1756.236066
32.88330078	113	0.406679089	125.2328769	1860.940356
29.609375	108	0.249734589	203.7568993	2576.565123
34.13574219	150	0.203229726	360.5142623	4935.374212
37.56347656	156	0.462554118	159.0179571	3016.391085
36.02539063	151	0.382651941	187.6028661	3504.009919
34.68505859	156	0.303513493	246.3621376	4451.595697
30.09277344	141	0.194369756	342.7303754	4326.187342
30.42236328	139	0.247317049	266.3357032	3875.669475
32.70751953	129	0.203743324	306.9482905	4060.300612
32.68554688	134	0.30264216	210.202386	2825.488202
34.28955078	130	0.33801628	185.0370023	2278.33026
34.92675781	135	0.391335242	162.0871069	2193.378936
35.27832031	135	0.410195653	155.8018881	2107.765627
36.02539063	139	0.465927077	138.0388012	2064.589234
36.24511719	136	0.472662866	135.6378568	1966.529058
36.81640625	136	0.501156246	126.0701978	1863.723047
37.12402344	135	0.514198367	123.0366459	1797.023975
37.60742188	135	0.521170777	121.2428011	1732.639221
37.65136719	135	0.532412456	119.0340473	1720.78097
38.17871094	138	0.579540437	109.1145434	1702.774786
40.72753906	202	0.453455467	211.8068598	4299.414161
41.16699219	213	0.47439651	209.6230535	4406.128736
40.74951172	204	0.401821161	243.6001934	4367.114125
41.82617188	204	0.544736378	177.1468668	3818.988999
42.79296875	204	0.530781987	181.4307365	3437.393552
42.6171875	202	0.543305464	181.7953732	3353.309055
38.26660156	205	0.29646458	334.6975467	6139.507672
38.79394531	206	0.338392492	293.1077946	5666.834603
45.78125	216	0.679432875	145.6963201	3400.399307
46.39648438	235	0.592511028	189.8520485	4141.563243
41.9140625	234	0.438281373	258.9870158	5739.104539
41.29882813	233	0.307898205	365.6230211	6199.229046
43.80371094	229	0.564795424	190.7401753	4415.184466
43.14453125	230	0.484316323	223.3211127	4730.952822
28.88427734	110	0.203527026	255.9533845	2162.980024
30.42236328	110	0.258949363	199.8294687	1885.421754
31.71875	106	0.338085615	147.2412143	1584.598554
28.99414063	113	0.172817659	306.3612135	2243.828712
30.51025391	109	0.25528578	200.9011087	1848.969865
32.50976563	108	0.315636396	161.7461376	1513.210637
35.76171875	108	0.254252623	197.052131	1140.913161
35.71777344	106	0.50638982	93.77249801	1136.838886
31.93847656	103	0.291267172	166.1893578	1434.338383
29.85107422	106	0.112050224	446.4226708	1853.707951
35.62988281	107	0.253020535	196.3097771	1139.996066
35.54199219	105	0.495115248	99.04888765	1124.942628
31.67480469	107	0.339235455	146.4133268	1535.349946
29.9609375	106	0.114411695	436.8476568	1829.61029

TABLE A6 : STANDARD UNCERTAINTY IN CALCULATED VALUES FROM TEST 1 DATA

Tsat (^{0}C)	Qsteam (kW)	x (outlet)	m (kg/m^{2}s)	boil htc (W/m^{2}K)
0.395507813	0.577105982	0.009636958	3.87006875	113.5622385
0.439453125	0.588986165	0.004536965	3.859776742	245.5220165
0.329589844	1.12389843	0.014670052	4.16234607	73.1917092
0.483398438	1.166018363	0.002106564	4.220796544	454.0767655
0.461425781	1.178838136	0.004282237	5.953480001	453.5830766
0.3515625	1.114477098	0.010306378	4.163602747	100.2454265
0.395507813	1.206289395	0.008660746	4.159213735	188.1170676
0.329589844	1.992347499	0.005514284	4.080343464	452.2058187
0.329589844	1.992492712	0.004498588	4.089746307	530.7094362
0.329589844	1.962781105	0.003272679	4.085588798	535.3847998
0.329589844	1.981784841	0.00251152	4.108333303	581.3286546
0.329589844	2.068613385	0.002111127	4.500346389	603.2308119
0.329589844	1.931467234	0.001763829	4.166567458	617.9594582
0.395507813	1.265069674	0.005621491	4.113988017	362.8818652
0.395507813	1.275663411	0.003843349	4.113480178	381.7547136
0.395507813	1.297077392	0.003041579	4.114027406	421.309701
0.373535156	1.339744684	0.00212853	4.110988573	456.3066667
0.373535156	1.363529941	0.001373982	4.114403945	488.0077941
0.3515625	1.329099824	0.001175946	4.10993558	419.7145133
0.263671875	2.722600463	0.003762538	4.025765049	618.3687287
0.263671875	2.805028978	0.00701693	4.019319388	607.2360955
0.219726563	2.719291821	0.007325633	4.007833649	443.8558025
0.241699219	2.817003536	0.008305627	4.008260881	449.8124446
0.219726563	2.776788434	0.0022945	3.990075649	675.049446
0.439453125	0.96093439	0.00223407	4.15335044	421.4910159
0.439453125	1.001003984	0.003491375	4.141538957	417.0033891
0.439453125	1.020746368	0.004478747	4.146014171	348.7794798
0.439453125	1.017131202	0.004700385	4.138601246	345.261122
0.439453125	0.987531729	0.001212737	4.140504457	382.3846086
0.439453125	0.526220538	0.006564616	3.879374838	111.7838771
0.395507813	0.546988104	0.01630955	3.885074918	78.51640771
0.417480469	0.571053402	0.011016186	3.880693363	89.34395
0.483398438	0.533610281	0.004453953	3.879126666	186.1408659
0.373535156	1.012613063	0.002282821	4.114875775	453.4129529
0.307617188	1.069441888	0.010004468	4.103582165	165.6919588
0.3515625	1.008958924	0.007161523	4.102036849	233.5485482
0.373535156	1.041240197	0.004498564	4.103007412	369.6048703
0.461425781	0.981132929	0.002285492	3.860821043	410.8984124
0.461425781	0.883825513	0.003502618	3.86369864	337.8481675
0.417480469	0.90950389	0.002616791	3.827129553	359.7765988
0.395507813	0.946381247	0.005305383	3.859993033	174.4067102
0.373535156	0.868944028	0.0067	3.859616244	114.8402175
0.3515625	0.928089547	0.008584658	3.862349642	102.3702254
0.3515625	0.823447999	0.009372984	3.863394346	94.67908023
0.3515625	0.87012519	0.011668513	3.86251613	90.2032981
0.329589844	0.852758682	0.012260421	3.863932815	80.70076173
0.3515625	0.85917264	0.013749056	3.864861663	75.21786919
0.329589844	0.81979535	0.014562645	3.866682457	68.36721973
0.307617187	0.850044327	0.014951742	3.865818158	61.98942984
0.307617188	0.84873597	0.015593322	3.866914981	60.63290861
0.3515625	0.867059453	0.018014521	3.866913322	63.15810564
0.263671875	1.714932468	0.007450941	4.059521506	289.5783016
0.263671875	1.968440129	0.007801072	4.074519184	301.6341155
0.285644531	1.803792583	0.005977462	4.07140222	302.7904431
0.263671875	1.812976689	0.010437228	4.063570781	234.0475656
0.263671875	1.702018083	0.009909787	4.061880005	192.9532599
0.263671875	1.747081102	0.010491592	4.065423516	184.5653473
0.329589844	1.717696171	0.003495598	4.06114307	583.0903489
0.307617188	1.821539182	0.004391251	4.060602349	491.780642
0.241699219	2.035266148	0.01491672	4.056100836	187.4273496
0.219726563	2.405727907	0.010460456	4.015600695	260.5018647
0.263671875	2.235919475	0.006173845	4.051068843	476.4130436
0.263671875	2.182874544	0.003460091	4.036765813	550.2001159
0.219726562	2.142028238	0.009884201	4.036549705	286.8053272
0.219726562	2.153737961	0.007454938	4.044541585	330.6038581
0.505371094	0.621247888	0.003045192	3.908012467	136.5147398
0.461425781	0.53670831	0.004771966	3.908426809	98.89551742
0.439453125	0.515799054	0.008293248	3.904775049	70.17063311
0.483398438	0.637991226	0.002234415	3.980124438	139.7141287
0.461425781	0.531597287	0.004682946	3.90839628	95.73196328
0.439453125	0.526094798	0.007126978	3.905328246	63.79952024
0.3515625	0.521298116	0.005024978	4.162915909	32.31135342
0.3515625	0.508364556	0.018446721	3.932268157	32.57146705
0.439453125	0.522937448	0.006423706	3.918591918	59.25678778
0.461425781	0.499210251	0.001084434	4.133272579	97.94565461
0.373535156	0.514884648	0.005291016	4.377123317	33.83954707
0.3515625	0.507940419	0.017743184	3.915507876	32.08569625
0.439453125	0.542309313	0.008334252	3.920460396	65.93432446

TABLE A7 : TEST 2 DATA

R134a flow, feed	R134a flow re-circ	Steam condensate weight	Condensate collection time	Shellside outlet temp	Pressure drop between nozzles	Tubeside outlet pressure	Pressure drop along shellside
F1 (l/s)	F9 (l/s)	Wt (kg)	Time (s)	PRT3 (^{0}C)	P9 (bar)	P1 (bar)	P8 (bar)
0.659	3.742	5.013	85.08	22.66	0.09553	0.0388	0.02028
0.658	3.719	4.932	82.83	22.69	0.09449	0.03885	0.02004
0.693	2.636	4.915	84.15	22.57	0.06282	0.04265	0.0126
0.655	4.541	4.901	83.48	22.92	0.128	0.04137	0.02596
0.662	4.437	5.134	86.56	22.91	0.12921	0.04159	0.02552
0.669	5.984	4.984	86.07	22.64	0.20333	0.04054	0.0386
0.732	4.699	4.856	75.25	24.11	0.206	0.04375	0.04122
0.712	5.742	4.91	75.08	24.22	0.19408	0.0442	0.03258
0.769	5.283	5.001	77.78	24.21	0.17285	0.04433	0.03548
0.743	4.578	4.984	78.54	24.19	0.1379	0.04517	0.02781
0.742	3.53	4.654	70.36	23.98	0.09591	0.04504	0.02003
0.734	3.539	4.948	77.34	24.04	0.09522	0.04524	0.02016
0.734	2.636	4.959	75.14	24.02	0.06655	0.04863	0.01319
0.73	2.622	5.105	77.23	24.03	0.0644	0.04875	0.01332
0.733	1.901	4.886	74.81	23.97	0.04476	0.05557	0.00781
0.768	5.704	4.899	77.55	24.49	0.19293	0.04591	0.03604
0.808	6.155	5.105	71.95	25.98	0.24572	0.05074	0.0508
0.824	6.346	5.003	67.72	26.25	0.22649	0.05243	0.04314
0.837	6.314	4.945	67.23	26.16	0.21224	0.052	0.04
0.843	4.973	5.004	68.98	26.06	0.1764	0.05237	0.03632
0.837	4.374	5.023	69.98	25.99	0.138	0.05208	0.0277
0.826	3.504	5.002	67	26.05	0.10271	0.05678	0.01966
0.829	2.583	4.886	65.69	25.89	0.06937	0.05715	0.01368
0.8	1.881	5.013	68.98	25.76	0.04655	0.0653	0.00812
0.812	1.215	4.857	69.49	25.46	0.02719	0.07586	0.0049
0.773	4.456	5.015	76.07	27.61	0.12801	0.0533	0.02677
0.724	4.538	5.02	80.41	27.46	0.12682	0.05287	0.02633
0.713	4.509	5.006	80.58	26.91	0.13004	0.05174	0.02608
0.748	6.188	5.009	80.63	27.04	0.17683	0.05298	0.03952
0.716	3.53	5.023	82	27.02	0.0893	0.05561	0.01751
0.732	1.933	5.106	85.79	26.72	0.03974	0.06138	0.00787
0.719	1.249	5.01	82.17	26.48	0.02027	0.07161	0.0044
0.518	3.219	4.91	112.7	21.99	0.06534	0.04787	0.01049
0.479	4.075	4.923	110.01	22.06	0.08841	0.04792	0.01359
0.521	4.986	4.956	110.18	22.15	0.12735	0.04832	0.01924
0.512	2.61	4.935	110.73	22.09	0.04597	0.0484	0.00784
0.908	4.397	5.026	68.66	26.53	0.10917	0.05384	0.02317
0.842	3.722	5.165	69.21	26.54	0.13263	0.05362	0.02746
0.854	3.333	4.985	63.6	26.54	0.09657	0.05424	0.02027
0.865	3.379	4.969	65.97	26.4	0.09847	0.05306	0.02075
0.881	2.541	5.002	69.92	26.3	0.06755	0.05697	0.01441
0.845	1.86	5.253	70.25	26.31	0.04616	0.06695	0.00829
0.885	4.803	5.023	64.93	29.65	0.15383	0.06275	0.03285
0.869	5.311	5.059	65.41	29.2	0.1252	0.06108	0.02361
0.884	4.249	5.013	65.25	29.01	0.13358	0.06028	0.02837
0.884	3.424	5.005	66.08	29.07	0.09669	0.06077	0.02068
0.868	2.549	5.478	72.89	29.2	0.06554	0.06575	0.01403
0.841	1.884	4.997	65.8	29.34	0.04394	0.07541	0.00852
0.784	5.583	5.012	80.47	27.04	0.20722	0.05221	0.03893
0.649	5.887	5.019	90.3	25.45	0.163	0.0514	0.02497
0.652	3.593	5.098	90.62	24.63	0.08775	0.05123	0.01589
0.65	1.954	4.976	85.24	24.23	0.03612	0.05306	0.00718
0.971	4.31	5.098	63.55	30.73	0.12987	0.06816	0.03742
0.945	4.635	5.108	64.04	30.71	0.18632	0.06786	0.0362
0.977	3.33	4.998	62.67	30.97	0.10243	0.06967	0.02127
0.923	2.513	5.065	62.45	30.69	0.06877	0.07316	0.01459
0.971	1.583	5.076	63.88	30.67	0.03889	0.08776	0.00714
0.929	4.246	5.109	62.28	31.11	0.10549	0.0705	0.014
0.963	3.586	4.968	59.87	31.09	0.12667	0.07018	0.02671
0.968	3.352	4.998	59.98	31.07	0.09942	0.06975	0.02092
0.963	2.493	5.269	66.84	31.02	0.06854	0.0751	0.01461
0.959	2.505	5.101	61.35	31.07	0.06835	0.0753	0.01462
0.968	1.726	5.2	64.54	30.87	0.04507	0.08365	0.00848
0.945	3.189	4.896	59.87	30.71	0.09026	0.06784	0.0233
0.907	3.058	4.986	60.03	27.18	0.1096	0.06249	0.02252
0.954	2.556	5.061	61.96	27.2	0.08015	0.06875	0.01351
0.944	3.096	4.996	60.31	27.31	0.10814	0.05814	0.0222
0.97	3.257	5.016	59.65	27.25	0.1038	0.05781	0.02296
0.953	2.439	4.999	58.99	27.24	0.071662	0.06437	0.01433
0.952	1.786	5.101	61.95	27.16	0.05161	0.07391	0.00809
0.943	1.383	5.032	59.76	27.18	0.03944	0.08252	0.00631
0.949	1.01	5.091	60.85	27.02	0.02655	0.09471	0.00453
0.944	3.56	5.132	60.52	27.39	0.09679	0.05854	0.02271

TABLE A8 : STANDARD UNCERTAINTIES IN TEST 2 DATA

R134a flow, feed	R134a flow re-circ	Steam condensate weight	Condensate collection time	Shellside outlet temp	Pressure drop between nozzles	Tubeside outlet pressure	Pressure drop along shellside
F1 (l/s)	F9 (l/s)	Wt (kg)	Time (s)	PRT3 (^{0}C)	P9 (bar)	P1 (bar)	P8 (bar)
0.0188	0.034642459	0.000577	0.577	0.025023109	0.000873474	0.001154701	0.000296215
0.018774273	0.034646789	0.000577	0.577	0.025017994	0.00086769	0.001154701	0.000289781
0.01877161	0.034677082	0.000577	0.577	0.025009678	0.000869624	0.001154701	0.000288952
0.01877161	0.034654004	0.000577	0.577	0.025007999	0.000889357	0.001154701	0.000293638
0.01877161	0.034664102	0.000577	0.577	0.025025907	0.000889357	0.001154701	0.00029205
0.01877161	0.036770912	0.000577	0.577	0.025016814	0.000871554	0.001154701	0.000311486
0.01877161	0.053276636	0.000577	0.577	0.025046038	0.00086769	0.001154701	0.000290763
0.01877161	0.046904157	0.000577	0.577	0.025015675	0.002851106	0.001154701	0.000646702
0.01877161	0.034646789	0.000577	0.577	0.02503198	0.000882698	0.001154701	0.000288952
0.01877161	0.034642459	0.000577	0.577	0.025030402	0.000873067	0.001154701	0.000289522
0.01877161	0.034654004	0.000577	0.577	0.025015675	0.000873067	0.001154701	0.000290075
0.01877161	0.034646789	0.000577	0.577	0.025025907	0.000921952	0.001154701	0.000289108
0.01877161	0.034646789	0.000577	0.577	0.025017994	0.000900464	0.001154701	0.000289108
0.01877161	0.034654004	0.000577	0.577	0.025020472	0.000867321	0.001154701	0.000288744
0.01877161	0.034646789	0.000577	0.577	0.025020472	0.000881496	0.001154701	0.000288744
0.01877161	0.035332704	0.000577	0.577	0.025040467	0.001011062	0.001154701	0.000312687
0.01877161	0.058992372	0.000577	0.577	0.025014576	0.000904923	0.001154701	0.000289298
0.01877161	0.034884094	0.000577	0.577	0.025027365	0.000897082	0.001154701	0.000350747
0.01877161	0.035834341	0.000577	0.577	0.02503198	0.001334319	0.001154701	0.000337021
0.01877161	0.034711669	0.000577	0.577	0.025021771	0.001002994	0.001154701	0.000289781
0.01877161	0.034646789	0.000577	0.577	0.025036953	0.00101434	0.001154701	0.000294233
0.01877161	0.034654004	0.000577	0.577	0.025012497	0.000904923	0.001154701	0.000288692
0.01877161	0.034642459	0.000577	0.577	0.025040467	0.000870222	0.001154701	0.000288692
0.01877161	0.034646789	0.000577	0.577	0.025020472	0.000866998	0.001154701	0.000288831
0.01877161	0.034646789	0.000577	0.577	0.025033597	0.000866721	0.001154701	0.000288692
0.01877161	0.034677082	0.000577	0.577	0.025021771	0.000871554	0.001154701	0.000295522
0.01877161	0.034654004	0.000577	0.577	0.025027365	0.000866231	0.001154701	0.000291587
0.01877161	0.034654004	0.000577	0.577	0.025044141	0.000876148	0.001154701	0.000290075
0.01877161	0.034664102	0.000577	0.577	0.02503869	0.00101434	0.001154701	0.000407607
0.01877161	0.035332704	0.000577	0.577	0.025021771	0.000878684	0.001154701	0.000289108
0.01877161	0.034785054	0.000577	0.577	0.025040467	0.000868105	0.001154701	0.000288831
0.01877161	0.034692939	0.000577	0.577	0.025013516	0.0008675	0.001154701	0.000288744
0.011881638	0.034664102	0.000577	0.577	0.025011517	0.000877637	0.001154701	0.000288692
0.011881638	0.034664102	0.000577	0.577	0.025007999	0.000893088	0.001154701	0.00029205
0.011881638	0.034757733	0.000577	0.577	0.025014576	0.000873474	0.001154701	0.000294861
0.011881638	0.034646789	0.000577	0.577	0.025017994	0.000878684	0.001154701	0.000288744
0.01877161	0.040442552	0.000577	0.577	0.025011517	0.000876633	0.001154701	0.000292546
0.01877161	0.03666606	0.000577	0.577	0.025012497	0.000871204	0.001154701	0.000324689
0.01877161	0.034646789	0.000577	0.577	0.025021771	0.000868565	0.001154701	0.000289108
0.01877161	0.034654004	0.000577	0.577	0.025011517	0.000873067	0.001154701	0.000294861
0.01877161	0.034664102	0.000577	0.577	0.025005779	0.000874761	0.001154701	0.000289298
0.01877161	0.034641016	0.000577	0.577	0.025020472	0.000866491	0.001154701	0.000288831
0.01877161	0.034677082	0.000577	0.577	0.025020472	0.000898752	0.001154701	0.000288831
0.01877161	0.034848242	0.000577	0.577	0.025007219	0.002784903	0.001154701	0.000317763
0.01877161	0.034711669	0.000577	0.577	0.025015675	0.000893088	0.001154701	0.000291587
0.01877161	0.034692939	0.000577	0.577	0.025013516	0.000870865	0.001154701	0.000289108
0.01877161	0.034664102	0.000577	0.577	0.025016814	0.000866854	0.001154701	0.000289522
0.01877161	0.034642459	0.000577	0.577	0.025007999	0.000867892	0.001154701	0.000288952
0.01877161	0.046904157	0.000577	0.577	0.025024488	0.000896262	0.001154701	0.000375624
0.01877161	0.034785054	0.000577	0.577	0.025015675	0.002575439	0.001154701	0.000398777
0.01877161	0.034664102	0.000577	0.577	0.025012497	0.000886564	0.001154701	0.000289522
0.01877161	0.034646789	0.000577	0.577	0.025024488	0.000926367	0.001154701	0.000288831
0.01877161	0.034884094	0.000577	0.577	0.02503198	0.002036881	0.001154701	0.000712526
0.01877161	0.091555448	0.000577	0.577	0.025019213	0.001540807	0.001154701	0.000309165
0.01877161	0.034646789	0.000577	0.577	0.025036953	0.001942935	0.001154701	0.000476795
0.01877161	0.034642459	0.000577	0.577	0.025013516	0.000882698	0.001154701	0.000291587
0.01877161	0.034654004	0.000577	0.577	0.025046038	0.000866721	0.001154701	0.000288952
0.01877161	0.098622513	0.000577	0.577	0.025019213	0.000870222	0.001154701	0.000288692
0.01877161	0.038482463	0.000577	0.577	0.025040467	0.003612313	0.001154701	0.000294233
0.01877161	0.034711669	0.000577	0.577	0.02503198	0.000891564	0.001154701	0.000295522
0.01877161	0.034642459	0.000577	0.577	0.025028863	0.000878155	0.001154701	0.000290075
0.01877161	0.034646789	0.000577	0.577	0.025023109	0.000868813	0.001154701	0.000289298
0.01877161	0.034654004	0.000577	0.577	0.02504995	0.000878684	0.001154701	0.000288831
0.01877161	0.04234265	0.000577	0.577	0.025035255	0.000871915	0.001154701	0.000288831
0.01877161	0.03646368	0.000577	0.577	0.025030402	0.000968342	0.001154701	0.000377655
0.01877161	0.043082479	0.000577	0.577	0.025016814	0.000880912	0.001154701	0.000293076
0.01877161	0.034815226	0.000577	0.577	0.025012497	0.000881496	0.001154701	0.000315172
0.01877161	0.034815226	0.000577	0.577	0.02503198	0.001001402	0.001154701	0.000305897
0.01877161	0.034785054	0.000577	0.577	0.025015675	0.000942993	0.001154701	0.000292546
0.01877161	0.034654004	0.000577	0.577	0.025013516	0.000873891	0.001154701	0.000289108
0.01877161	0.034654004	0.000577	0.577	0.025019213	0.000870222	0.001154701	0.000290075
0.01877161	0.034654004	0.000577	0.577	0.025025907	0.000866998	0.001154701	0.000288744
0.01877161	0.035332704	0.000577	0.577	0.025024488	0.000882698	0.001154701	0.000288692

TABLE A9 : CALCULATED VALUES FROM TEST 2 DATA

Tsat (^{0}C)	Qsteam (kW)	x (outlet)	m (kg/m^{2}s)	boil htc (W/m^{2}K)
28.44482422	151	0.156280348	463.0504793	7306.509329
28.46679688	153	0.158877316	460.4834629	7490.49601
30.09277344	150	0.206988289	350.3557971	5005.439569
29.56542969	151	0.132663434	546.26481	6028.888736
29.65332031	153	0.136889908	536.0833709	5989.648966
29.21386719	149	0.102556956	700.0367246	6023.899819
30.53222656	165	0.140211971	568.8971809	7171.65731
30.70800781	168	0.119721067	675.8277514	7269.762241
30.75195313	165	0.126766001	633.7519634	6966.127798
31.10351563	163	0.141974413	557.2376097	6342.394299
31.03759766	170	0.18262204	447.670782	6502.94729
31.10351563	165	0.177906724	447.6930286	6158.656142
32.37792969	170	0.230352375	353.1051446	5140.681159
32.421875	170	0.231312292	351.2083427	5111.681972
34.77294922	168	0.290763084	276.0302034	3609.65529
31.3671875	162	0.116850583	677.1488357	6287.351618
33.14697266	180	0.121207103	725.154765	6940.236773
33.74023438	189	0.123405515	746.0807889	7012.139447
33.58642578	188	0.123297321	744.3139662	7005.740344
33.69628906	186	0.150031821	605.5498501	6613.487877
33.60839844	184	0.1655638	542.6774739	6446.250707
35.16845703	192	0.205450866	450.844723	5407.12166
35.27832031	191	0.258425717	355.4394697	5151.01024
37.71728516	186	0.317642902	279.4022889	3605.195189
40.5078125	179	0.408924924	211.4430242	2559.148502
34.02587891	167	0.151960717	541.7743117	7229.02079
33.87207031	159	0.143330262	545.4536212	6693.302312
33.4765625	159	0.143547584	542.2515142	6489.758305
33.91601563	159	0.108943914	719.9368758	6112.399908
34.79492188	157	0.174640855	440.7504983	5069.47163
36.59667969	153	0.273051997	276.8991412	3578.641
39.43115234	156	0.371670729	204.6340178	2617.157636
32.11425781	112	0.137081746	393.9851719	2370.04755
32.11425781	115	0.114198672	480.0186899	2463.394939
32.29003906	116	0.096133614	580.3130227	2471.509044
32.29003906	114	0.166376619	329.0476126	2393.768338
34.22363281	187	0.167707275	551.5308473	6596.491928
34.13574219	190	0.194770769	474.4783483	6889.491906
34.35546875	200	0.22138352	435.2850228	7155.49959
33.95996094	192	0.211931423	441.4051257	7036.354578
35.234375	183	0.254046647	356.0233864	5191.044684
38.17871094	190	0.325734238	281.4181767	3739.328022
36.9921875	197	0.166372608	585.4771071	7623.895522
36.50878906	197	0.152386997	637.0486305	7700.26125
36.24511719	196	0.182479897	529.4464675	7712.905269
36.39892578	193	0.214389354	444.2651928	7386.808928
37.84912109	192	0.267443883	352.2322282	5795.585087
40.41992188	194	0.333199176	280.7719673	4203.420183
33.65234375	159	0.119340689	660.8763103	6451.109968
33.38867188	143	0.102381635	681.812775	4367.345487
33.30078125	145	0.158406096	443.9516143	3946.682655
33.95996094	148	0.260414484	272.6683043	3512.346417
38.53027344	204	0.188639427	541.6680262	7356.362133
38.44238281	203	0.177020764	572.3738844	7390.220565
38.92578125	203	0.230817133	441.4166721	7059.845003
39.84863281	206	0.28699758	352.4741346	5816.39107
43.27636719	202	0.385174876	262.0134375	3718.19606
39.14550781	209	0.195236033	530.1315404	7275.760741
39.05761719	211	0.224775044	466.0343033	7466.472964
38.92578125	212	0.237574755	442.6030441	7653.692199
40.33203125	209	0.292215815	354.1408251	5874.119646
40.37597656	212	0.294266122	354.9020705	5905.052899
42.35351563	205	0.368741942	276.1942103	4281.256381
38.44238281	208	0.242613689	424.0490391	7642.324829
36.90429688	212	0.248269926	411.3732243	5660.969244
38.66210938	209	0.28037014	364.1433639	4427.885743
35.5859375	212	0.24617594	418.9818018	7117.020794
35.49804688	215	0.239346916	438.4587117	7355.715215
37.45361328	217	0.297784535	351.856902	5479.804204
40.02441406	211	0.360089665	284.0885777	3852.832223
42.08984375	215	0.425483428	241.3251248	3264.279611
44.77050781	213	0.500826722	203.3514428	2595.592128
35.71777344	217	0.22534688	466.9838847	7350.768428

TABLE A10:STANDARD UNCERTAINTY IN CALCULATED VALUES FROM TEST 2 DATA

Tsat (^{0}C)	Qsteam (kW)	x (outlet)	m (kg/m^{2}s)	boil htc (W/m^{2}K)
0.505371094	1.023684993	0.001504937	4.145764896	1119.161768
0.505371094	1.062216854	0.001544405	4.145920305	1167.354579
0.439453125	1.02206869	0.002411423	4.150036537	506.7048591
0.461425781	1.03683262	0.001176568	4.143618268	738.7628075
0.483398438	1.011450403	0.001204128	4.14467189	744.0213008
0.483398438	0.991556231	0.000831377	4.344409973	765.4723783
0.439453125	1.258725112	0.001636014	5.917167533	953.4775757
0.439453125	1.27862969	0.001171746	5.290542593	972.6761268
0.439453125	1.214946355	0.001088323	4.126717719	905.4443053
0.439453125	1.187628997	0.001274871	4.126509239	760.8692865
0.439453125	1.380095775	0.001891552	4.130156766	781.7388478
0.439453125	1.216261249	0.001782494	4.128730437	711.8322315
0.439453125	1.28833315	0.002668605	4.12893056	507.1443335
0.439453125	1.25594503	0.00267066	4.129467257	501.5743704
0.373535156	1.273867884	0.004025312	4.129529533	244.5982593
0.439453125	1.196584587	0.000992189	4.186434846	752.4556532
0.395507813	1.440959906	0.001323192	6.447489651	821.2891961
0.395507813	1.592622148	0.001086143	4.122491235	822.1438887
0.373535156	1.597207381	0.001102052	4.211005227	798.8394868
0.395507813	1.536507391	0.001374892	4.109007195	742.2719318
0.395507813	1.499580722	0.001564158	4.103912933	698.3297404
0.373535156	1.623569494	0.002113135	4.103732439	493.8005717
0.3515625	1.648430366	0.003033313	4.104674319	442.4715136
0.329589844	1.528674519	0.00432472	4.106703312	225.241545
0.307617188	1.452733812	0.007054632	4.110523449	116.9428475
0.373535156	1.176648672	0.001347468	4.085746877	881.2657107
0.395507813	1.055882021	0.001237644	4.085596502	801.820166
0.395507813	1.049263708	0.001240353	4.092716741	761.0082636
0.395507813	1.047796507	0.000837651	4.092127784	680.3301687
0.3515625	1.013579819	0.001706473	4.153297125	454.5048838
0.329589844	0.938498064	0.003729626	4.106983954	233.124632
0.285644531	0.997237843	0.006547179	4.101636544	124.4820947
0.417480469	0.531582559	0.001381294	3.86341155	141.4052758
0.439453125	0.559605945	0.000985735	3.862651455	155.3380365
0.395507813	0.560315028	0.000733814	3.87101705	145.1511514
0.439453125	0.553631957	0.001941475	3.860486334	147.7754139
0.3515625	1.444192209	0.001668168	4.635630347	693.9809413
0.395507813	1.462117083	0.001949989	4.282518219	791.2965391
0.3515625	1.667191827	0.002284087	4.096755129	794.6090584
0.373535156	1.546973445	0.002166193	4.099221979	795.2188379
0.3515625	1.38385741	0.002931912	4.101383514	451.424661
0.307617188	1.431298256	0.004364009	4.099107375	233.7979948
0.329589844	1.604277552	0.001504467	4.059080944	872.818351
0.329589844	1.593669032	0.001341612	4.080579388	888.7727217
0.3515625	1.588110701	0.001709664	4.070588483	916.5117911
0.329589844	1.545368238	0.00216326	4.068033802	827.3038718
0.329589844	1.388415979	0.00299325	4.063652618	531.3863643
0.263671875	1.543619608	0.004404319	4.059813867	278.3160853
0.395507813	1.053045696	0.001119018	5.244197168	751.4594455
0.395507813	0.839574876	0.000763365	4.123647948	380.7829575
0.417480469	0.847545302	0.001494713	4.122823391	323.3519948
0.373535156	0.931659687	0.003581658	4.126228847	242.7477032
0.307617188	1.694113072	0.001767973	4.063427696	790.4916324
0.307617188	1.671989269	0.003074829	9.58686656	798.2938222
0.307617188	1.7063447	0.002361675	4.038737004	734.2486726
0.263671875	1.737651268	0.00328167	4.042009301	483.6267818
0.263671875	1.654614278	0.005468771	4.043270826	220.9700718
0.307617188	1.76531377	0.003819696	10.2844505	772.4336964
0.307617188	1.856904975	0.002404653	4.386642875	807.8676372
0.307617188	1.861751526	0.002446229	4.043251966	844.7550669
0.263671875	1.577918885	0.003244782	4.037623022	502.2476279
0.285644531	1.811618656	0.003350574	4.037347315	505.26422
0.263671875	1.66349465	0.004984595	4.040618669	284.9516796
0.307617188	1.832000213	0.002905818	4.751149485	839.6407114
0.3515625	1.861820252	0.002745979	4.255152836	509.3409564
0.307617188	1.768240689	0.003767087	4.875498075	312.852311
0.3515625	1.852711061	0.002627079	4.102155508	773.0422487
0.3515625	1.901517375	0.002511776	4.102949879	820.6226207
0.329589844	1.930226533	0.00348729	4.100272097	469.3337547
0.307617188	1.778466525	0.004822121	4.089317748	242.4570915
0.285644531	1.877087622	0.006401765	4.089041646	177.0331461
0.219726563	1.82218036	0.008698074	4.091100146	111.000048
0.3515625	1.889605882	0.002293134	4.14844918	818.9153696

TABLE A11 : TEST 3 DATA

R134a flow, feed	R134a flow re-circ	Steam condensate weight	Condensate collection time	Shellside outlet temp	Pressure drop between nozzles	Tubeside outlet pressure	Pressure drop along shellside
F1 (l/s)	F9 (l/s)	Wt (kg)	Time (s)	PRT3 (°C)	P9 (bar)	P1 (bar)	P8 (bar)
0.608	4.566	4.989	83.49	23.07	0.06736	0.04914	0.00846
0.675	4.287	4.915	75.3	24.27	0.06997	0.04817	0.00944
0.646	5.334	5.1	80.13	24.45	0.09193	0.0484	0.01304
0.663	3.593	5.023	78.76	24.19	0.05213	0.04873	0.00729
0.678	2.75	5.246	82.17	24.01	0.03572	0.04976	0.00518
0.669	2.08	5.316	84.59	23.84	0.02388	0.05612	0.00348
0.651	1.755	5.066	79.59	23.85	0.01695	0.05554	0.00266
0.664	1.051	5.04	79.31	23.82	0.00592	0.06157	0.0011
0.667	0.897	5.264	84.37	23.81	0.00333	0.0623	0.00091
0.763	3.695	4.989	70.47	25.81	0.05776	0.05334	0.00765
0.743	6.208	5.203	72.06	26.06	0.10341	0.05252	0.01512
0.775	4.791	5.569	76.85	25.89	0.08551	0.05327	0.01135
0.756	4.644	5.036	69.2	25.87	0.08486	0.05383	0.01123
0.759	3.687	5.096	69.54	25.77	0.05834	0.05402	0.00787
0.724	2.758	5.568	74.15	25.66	0.0401	0.0558	0.00531
0.766	2.053	5.353	74.37	25.6	0.02624	0.06311	0.00348
0.726	1.716	5.084	71.52	25.55	0.02037	0.06332	0.00287
0.741	0.802	5.421	75.35	25.32	0.00535	0.07186	0.00074
0.855	3.086	5.103	62.34	27.21	0.0508	0.06543	0.00645
0.858	3.748	5.292	64.26	27.54	0.04545	0.05806	0.00633
0.927	6.308	5.269	65.53	27.6	0.03769	0.06043	0.00615
0.814	5.465	5.427	63.77	27.83	0.09154	0.05844	0.01339
0.844	5.452	5.367	64.93	27.81	0.10507	0.05822	0.01396
0.834	3.325	5.338	64.54	27.62	0.05514	0.0615	0.00722
0.835	2.635	5.116	60.53	27.58	0.04076	0.06622	0.00544
0.864	2.004	5.101	61.46	27.52	0.02991	0.06756	0.00388
0.886	1.68	5.2	62.34	27.47	0.02401	0.06876	0.00292
0.873	0.884	5.103	60.47	27.3	0.00927	0.07663	0.001
0.908	3.796	5.204	59.32	28.4	0.06216	0.06136	0.00808
0.91	3.721	5.066	55.47	28.45	0.06925	0.06171	0.0093
0.902	5.214	5.021	56.79	28.64	0.10342	0.06067	0.01511
0.899	5.151	5.129	56.79	28.66	0.10236	0.06082	0.0146
0.914	4.261	5.005	55.47	28.61	0.07353	0.06129	0.0103
0.901	2.902	5.313	58.72	28.56	0.05129	0.06605	0.0062
0.911	2.344	5.065	56.47	28.53	0.03746	0.07248	0.00506
0.907	1.852	5.057	55.37	28.56	0.02795	0.08075	0.00362
0.913	1.657	5.099	55.26	28.53	0.02431	0.08205	0.00327
0.916	0.798	5.009	55.47	28.38	0.0078	0.08575	0.00101
0.901	5.425	5.023	52.39	28.49	0.11556	0.06128	0.01641
0.914	5.871	5.098	54.21	28.49	0.08813	0.06121	0.01658
0.906	6.06	5.009	54.43	28.41	0.11879	0.06106	0.01778
0.939	3.601	5.002	53.66	28.22	0.07484	0.06162	0.0102
0.934	3.166	5.098	54.87	28.18	0.05312	0.06341	0.00679
0.917	2.306	5.003	54.49	28.16	0.03891	0.07017	0.0052
0.956	1.802	5.005	53.94	28.09	0.02746	0.08127	0.00362
0.908	1.646	5.106	54.21	28.08	0.02549	0.08264	0.00312
0.951	0.844	4.998	53.88	27.94	0.00988	0.08671	0.00116
0.759	3.345	5.026	67.67	25.71	0.05122	0.0614	0.0069

TABLE A12 : STANDARD UNCERTAINTIES IN TEST 3 DATA

R134a flow, feed	R134a flow re-circ	Steam condensate weight	Condensate collection time	Shellside outlet temp	Pressure drop between nozzles	Tubeside outlet pressure	Pressure drop along shellside
F1 (l/s)	F9 (l/s)	Wt (kg)	Time (s)	PRT3 (^{0}C)	P9 (bar)	P1 (bar)	P8 (bar)
0.011885846	0.03500857	0.000577	0.577	0.025245217	0.000925249	0.001154701	0.000288744
0.01877161	0.034757733	0.000577	0.577	0.025064896	0.000940508	0.001154701	0.000289108
0.01877161	0.0671744	0.000577	0.577	0.025168711	0.000930933	0.001154701	0.000290763
0.01877161	0.034815226	0.000577	0.577	0.025223719	0.000887246	0.001154701	0.000288692
0.018774273	0.034654004	0.000577	0.577	0.025199206	0.000868565	0.001154701	0.000288692
0.018774273	0.034642459	0.000577	0.577	0.025245217	0.000871204	0.001154701	0.000288692
0.018774273	0.034642459	0.000577	0.577	0.025056117	0.000876148	0.001154701	0.000288692
0.018774273	0.034642459	0.000577	0.577	0.025089619	0.000868105	0.001154701	0.000288692
0.018774273	0.034646789	0.000577	0.577	0.025071897	0.0008666	0.001154701	0.000288692
0.018774273	0.034646789	0.000577	0.577	0.025263115	0.0008666	0.001154701	0.000288692
0.018774273	0.03666606	0.000577	0.577	0.025079254	0.000870222	0.001154701	0.000288831
0.018774273	0.044632947	0.000577	0.577	0.0251761	0.000868105	0.001154701	0.000288831
0.018774273	0.05375872	0.000577	0.577	0.025042284	0.000887246	0.001154701	0.000289522
0.018774273	0.034646789	0.000577	0.577	0.025203194	0.000905845	0.001154701	0.000290763
0.018774273	0.034654004	0.000577	0.577	0.025258583	0.000883943	0.001154701	0.000288744
0.018774273	0.034646789	0.000577	0.577	0.025042284	0.000866393	0.001154701	0.000288692
0.018774273	0.034641146	0.000577	0.577	0.025172386	0.000866998	0.001154701	0.000288692
0.018774273	0.034642459	0.000577	0.577	0.025140724	0.000868329	0.001154701	0.000288692
0.018774273	0.034646789	0.000577	0.577	0.025076762	0.000872288	0.001154701	0.000289298
0.018774273	0.03500857	0.000577	0.577	0.02532556	0.000925249	0.001154701	0.000290763
0.018774273	0.035462656	0.000577	0.577	0.025112248	0.000985904	0.001154701	0.000298485
0.018774273	0.03575472	0.000577	0.577	0.02513412	0.001052239	0.001154701	0.000311486
0.018774273	0.034922772	0.000577	0.577	0.025211287	0.001168348	0.001154701	0.000301037
0.018774273	0.034677082	0.000577	0.577	0.0251761	0.000873474	0.001154701	0.000289108
0.018774273	0.034664102	0.000577	0.577	0.025137402	0.0008675	0.001154701	0.000288692
0.018774273	0.034654004	0.000577	0.577	0.025081786	0.000871204	0.001154701	0.000288831
0.018774273	0.034646789	0.000577	0.577	0.025069523	0.000866231	0.001154701	0.000288692
0.018774273	0.034642459	0.000577	0.577	0.025137402	0.000873474	0.001154701	0.000288692
0.018774273	0.034711669	0.000577	0.577	0.025112248	0.000892321	0.001154701	0.000288744
0.018774273	0.036987836	0.000577	0.577	0.025187477	0.000879225	0.001154701	0.000288952
0.018774273	0.034848242	0.000577	0.577	0.025168711	0.000930933	0.001154701	0.000289298
0.018774273	0.034964267	0.000577	0.577	0.025150924	0.000872288	0.001154701	0.000288831
0.018774273	0.03500857	0.000577	0.577	0.025115254	0.000878155	0.001154701	0.000288675
0.018774273	0.034964267	0.000577	0.577	0.025147485	0.000888643	0.001154701	0.000288692
0.018774273	0.034677082	0.000577	0.577	0.025161478	0.000871204	0.001154701	0.000288692
0.018774273	0.034664102	0.000577	0.577	0.025199206	0.000871915	0.001154701	0.000288692
0.018774273	0.034646789	0.000577	0.577	0.025154403	0.000869624	0.001154701	0.000288692
0.018774273	0.034642459	0.000577	0.577	0.025147485	0.000867892	0.001154701	0.000288692
0.018774273	0.039049968	0.000577	0.577	0.025245217	0.000893088	0.001154701	0.000291158
0.018774273	0.04011982	0.000577	0.577	0.02509231	0.001852899	0.001154701	0.000352552
0.018774273	0.034815226	0.000577	0.577	0.025161478	0.000901336	0.001154701	0.000290763
0.018774273	0.034733269	0.000577	0.577	0.025168711	0.000919802	0.001154701	0.000288952
0.018774273	0.034884094	0.000577	0.577	0.025183645	0.000869624	0.001154701	0.000288831
0.018774273	0.034692939	0.000577	0.577	0.025030402	0.000869624	0.001154701	0.000288744
0.018774273	0.034654004	0.000577	0.577	0.025058252	0.000872672	0.001154701	0.000288692
0.018774273	0.034642459	0.000577	0.577	0.025100618	0.000877129	0.001154701	0.000288692
0.018774273	0.034654004	0.000577	0.577	0.025356577	0.000866998	0.001154701	0.000288692
0.018774273	0.034757733	0.000577	0.577	0.025121385	0.000866998	0.001154701	0.000289522

TABLE A13 : CALCULATED VALUES FROM TEST 3 DATA

Tsat (^{0}C)	Qsteam (kW)	x (outlet)	m (kg/m^{2}s)	boil htc (W/m^{2}K)
32.57568359	146	0.128356369	365.7852386	3552.255949
32.22412109	159	0.147102967	349.510968	4996.414648
32.29003906	155	0.119199748	420.9827384	4916.643618
32.421875	155	0.167000332	299.855931	4607.549461
32.79541016	154	0.206264989	241.6529772	4195.806852
34.97070313	152	0.252975071	193.8887964	3066.991243
34.75097656	153	0.287763731	169.6915555	3163.538688
36.640625	153	0.402806097	120.9674987	2595.600266
36.86035156	150	0.436536961	110.3200889	2481.439795
34.04785156	171	0.178951028	312.5138442	5274.623548
33.76220703	175	0.11741632	486.8965015	5968.514533
34.00390625	176	0.147575577	390.0889912	5588.076781
34.20166016	177	0.152247471	378.4786795	5444.879043
34.26757813	178	0.185198679	311.7115764	5345.708607
34.83886719	181	0.235879151	244.2088311	4924.423833
37.08007813	173	0.283756197	197.7465801	3460.14979
37.16796875	171	0.318941357	171.3276002	3339.534366
39.49707031	172	0.501482858	108.3324758	2633.652975
37.73925781	196	0.232331315	275.0564613	4555.241773
35.5859375	198	0.201556211	321.1325389	6725.746034
36.2890625	193	0.127609696	504.3313907	5773.15397
35.67382813	204	0.151688046	437.3707262	7231.69719
35.62988281	198	0.148165306	438.5828871	6993.032041
36.61865234	198	0.221634758	289.8936874	5731.413754
37.98095703	202	0.268171933	241.8992986	4841.774122
38.35449219	198	0.320671277	199.9710588	4459.451954
38.66210938	199	0.361300765	178.9425519	4241.396696
40.70556641	201	0.520221656	122.592301	3446.08395
36.57470703	210	0.210294286	327.0653958	7122.929656
36.68457031	219	0.220835436	321.9381471	7523.461233
36.37695313	212	0.163965468	424.9129432	7874.75909
36.42089844	216	0.168262221	420.3005098	7921.67839
36.55273438	216	0.19643346	359.5710732	7746.775469
37.91503906	216	0.264042589	264.2837813	6115.140536
39.67285156	214	0.305534348	226.2231667	4766.95752
41.69433594	218	0.361996052	191.7325671	3910.17394
42.00195313	220	0.390174486	178.6155264	3832.556515
42.83691406	215	0.564587439	119.1807119	3405.507658
36.55273438	230	0.169597955	439.7147568	8413.632931
36.53076172	225	0.155846172	471.6194475	8155.072942
36.48681641	220	0.148766473	484.3249465	7790.112401
36.640625	223	0.229366392	315.8448191	7493.554617
37.16796875	222	0.251997725	285.2708431	6771.205314
39.05761719	220	0.31426555	224.2650741	5103.347652
41.82617188	222	0.37164119	191.952064	3790.519099
42.13378906	225	0.396206694	177.7597222	3743.423794
43.05664063	221	0.556636797	124.988836	3332.930342
36.59667969	179	0.201159349	287.7876842	3870.435207

TABLE A14 : STANDARD UNCERTAINTY IN CALCULATED VALUES OF TEST 3 DATA

Tsat (^{0}C)	Qsteam (kW)	x (outlet)	m (kg/m^{2}s)	boil htc (W/m^{2}K)
0.417480469	0.976796644	0.001133895	2.613899841	264.5178372
0.417480469	1.181530785	0.001374137	2.78261146	478.1825607
0.439453125	1.084345057	0.001499648	4.910254302	485.5479677
0.417480469	1.104227388	0.001663803	2.786828973	416.5135505
0.417480469	1.059638194	0.002332073	2.778427676	350.8131252
0.3515625	1.008188286	0.003351288	2.779139544	181.8352934
0.395507813	1.085754564	0.004245537	2.779044232	203.6529087
0.3515625	1.083078584	0.007959236	2.779285049	133.6017928
0.329589844	0.999658156	0.009440998	2.779635727	120.4653274
0.373535156	1.362311797	0.001798859	2.762578373	487.5586166
0.373535156	1.359876825	0.001009102	2.885707146	607.2624712
0.395507813	1.281076689	0.001479476	3.393674611	551.565812
0.373535156	1.425301712	0.001807501	3.991148318	511.9369867
0.395507813	1.428707441	0.00185566	2.762922325	506.5932493
0.395507813	1.372991047	0.002625866	2.764273755	433.6746188
0.3515625	1.305941083	0.003718804	2.7643224	218.2584226
0.307617188	1.339214752	0.004646606	2.764395353	192.0667744
0.307617188	1.282072748	0.010732897	2.766437221	125.21542
0.3515625	1.765236833	0.002551773	2.75040847	350.2667926
0.3515625	1.730173501	0.002048783	2.769764859	708.851221
0.3515625	1.654936064	0.001139051	2.797339613	539.3294304
0.373535156	1.801760815	0.00141052	2.813216278	821.1550726
0.3515625	1.71878651	0.001358014	2.762223177	760.5914389
0.329589844	1.7265326	0.002332374	2.748696934	518.9613483
0.329589844	1.875066183	0.003137255	2.748221032	380.93958
0.307617188	1.812127389	0.004220841	2.74810451	322.3394041
0.307617188	1.794861026	0.005135027	2.74808899	287.9963832
0.285644531	1.864019907	0.009873103	2.74928783	199.0941807
0.329589844	1.990327531	0.002177478	2.743997233	756.3676941
0.3515625	2.213862773	0.002427657	2.883712891	846.6891313
0.3515625	2.095227725	0.001630979	2.750321102	929.3671675
0.3515625	2.140122978	0.001676047	2.757237532	917.038925
0.3515625	2.187719644	0.002050932	2.760336628	894.9243126
0.3515625	2.069052862	0.002972208	2.757997184	583.0147344
0.263671875	2.123170226	0.003749684	2.740673007	347.146618
0.263671875	2.196379084	0.004860532	2.739598662	242.1265975
0.263671875	2.22216278	0.005464875	2.738798785	233.7008497
0.263671875	2.163311788	0.010758807	2.739831659	190.9936099
0.3515625	2.459311094	0.001809839	3.011948844	1031.857055
0.329589844	2.331984889	0.001628677	3.079162015	958.6653928
0.329589844	2.273098791	0.001493748	2.750395645	882.3830743
0.3515625	2.334918828	0.002504709	2.746894334	842.8926364
0.3515625	2.274529898	0.002820407	2.756460873	701.6656389
0.307617188	2.254633396	0.003891728	2.744894685	405.3094492
0.263671875	2.289275056	0.005044332	2.743110129	229.874394
0.263671875	2.311134	0.005541525	2.742485944	224.8268668
0.263671875	2.286084015	0.010270608	2.7444016	183.0821529
0.3515625	1.48023227	0.002122024	2.770265476	264.7294957

Appendix B: Further Geometric Details of Experimental Evaporator

In this appendix figures are presented which give further details on the test geometries and location of instrumentation during the experimental tests.

Tube Bundle Layout

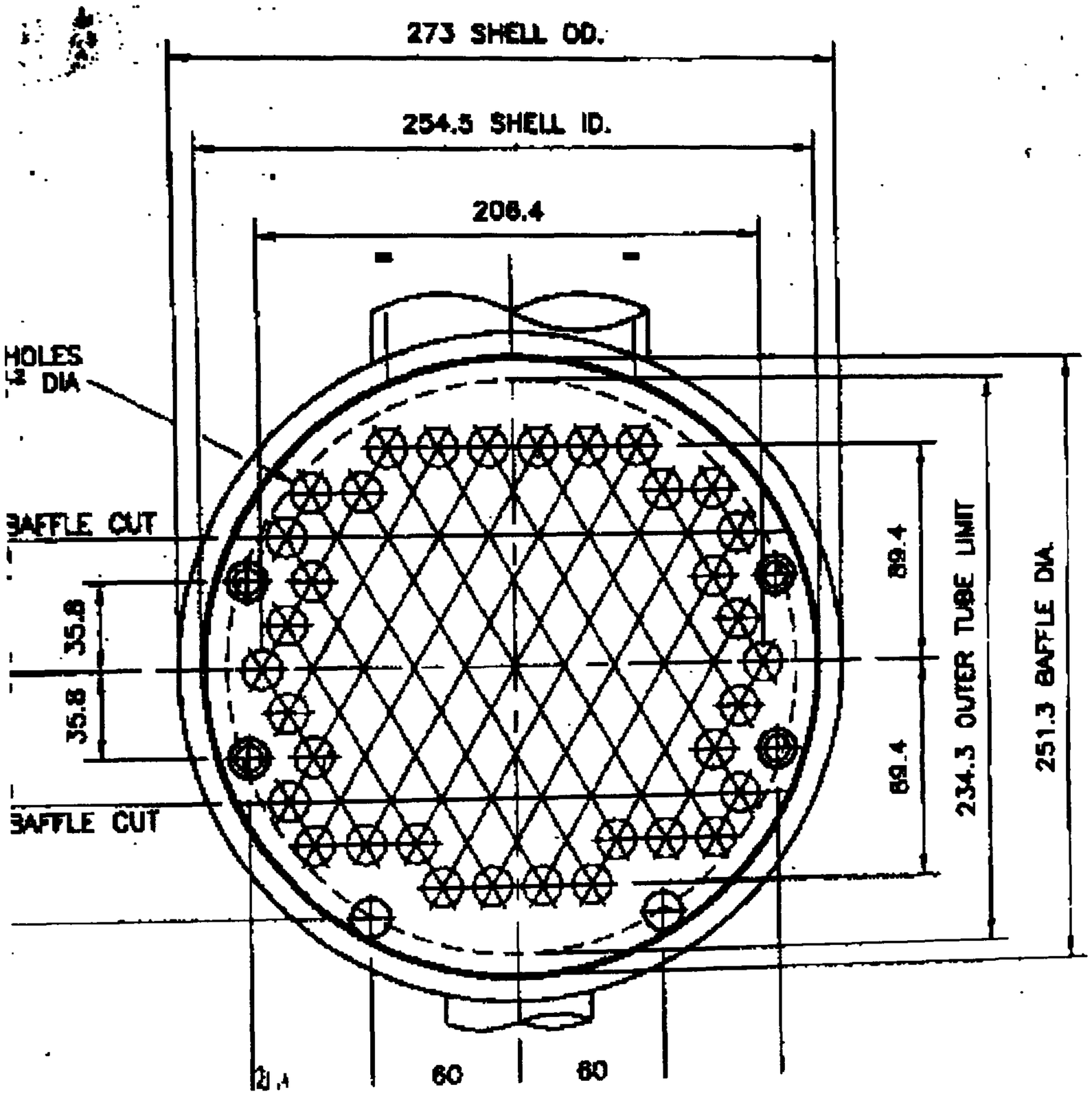

Figure B1 – Dimensions of Tube Bundle Layout (with horizontal baffle cut)

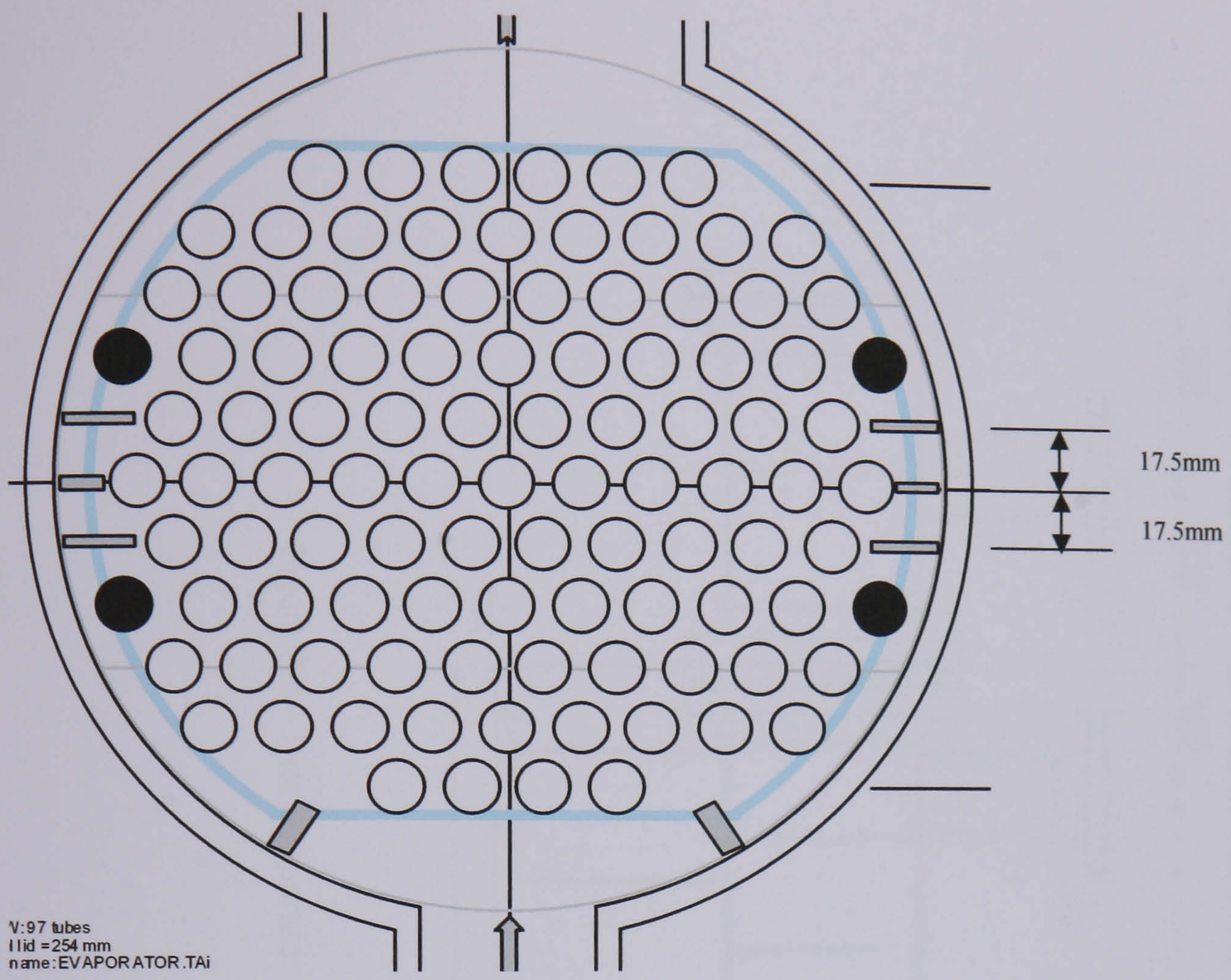

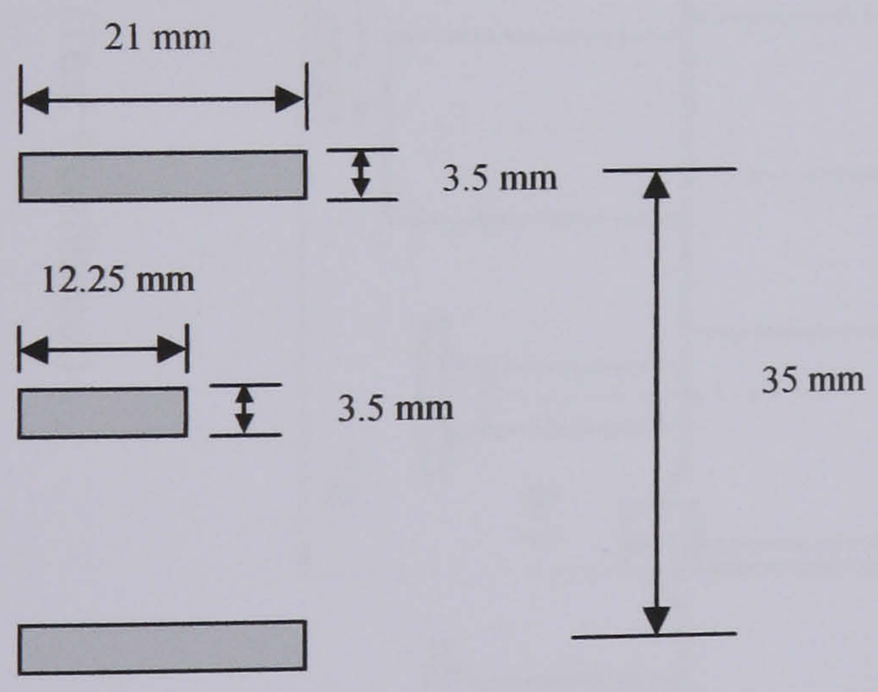

Figure B2 – Location and Dimension of Sealing Strips (Tests 1 and 2)

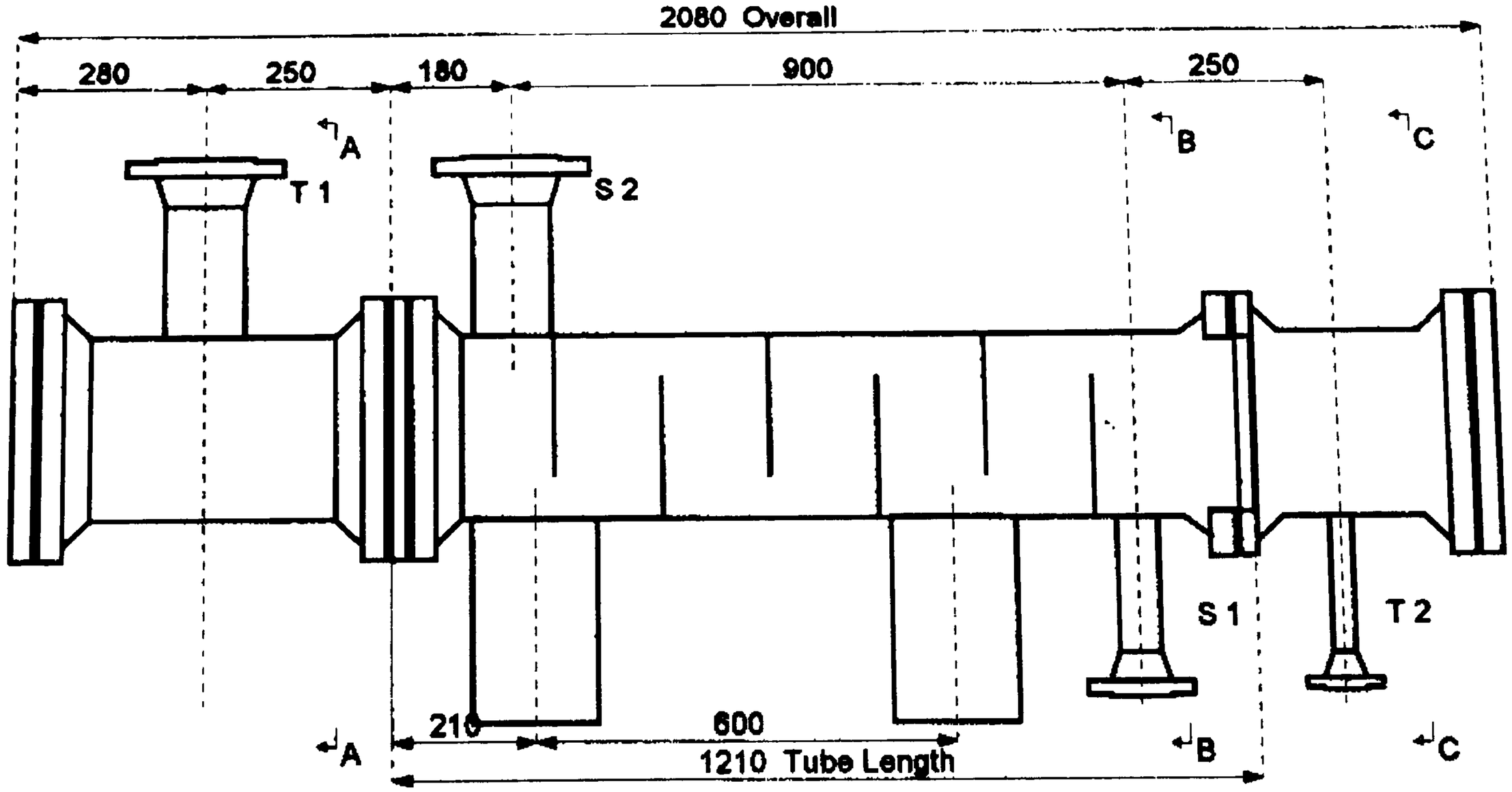

Figure B3 – Test Evaporator Dimensions (Test 1 baffle cut)

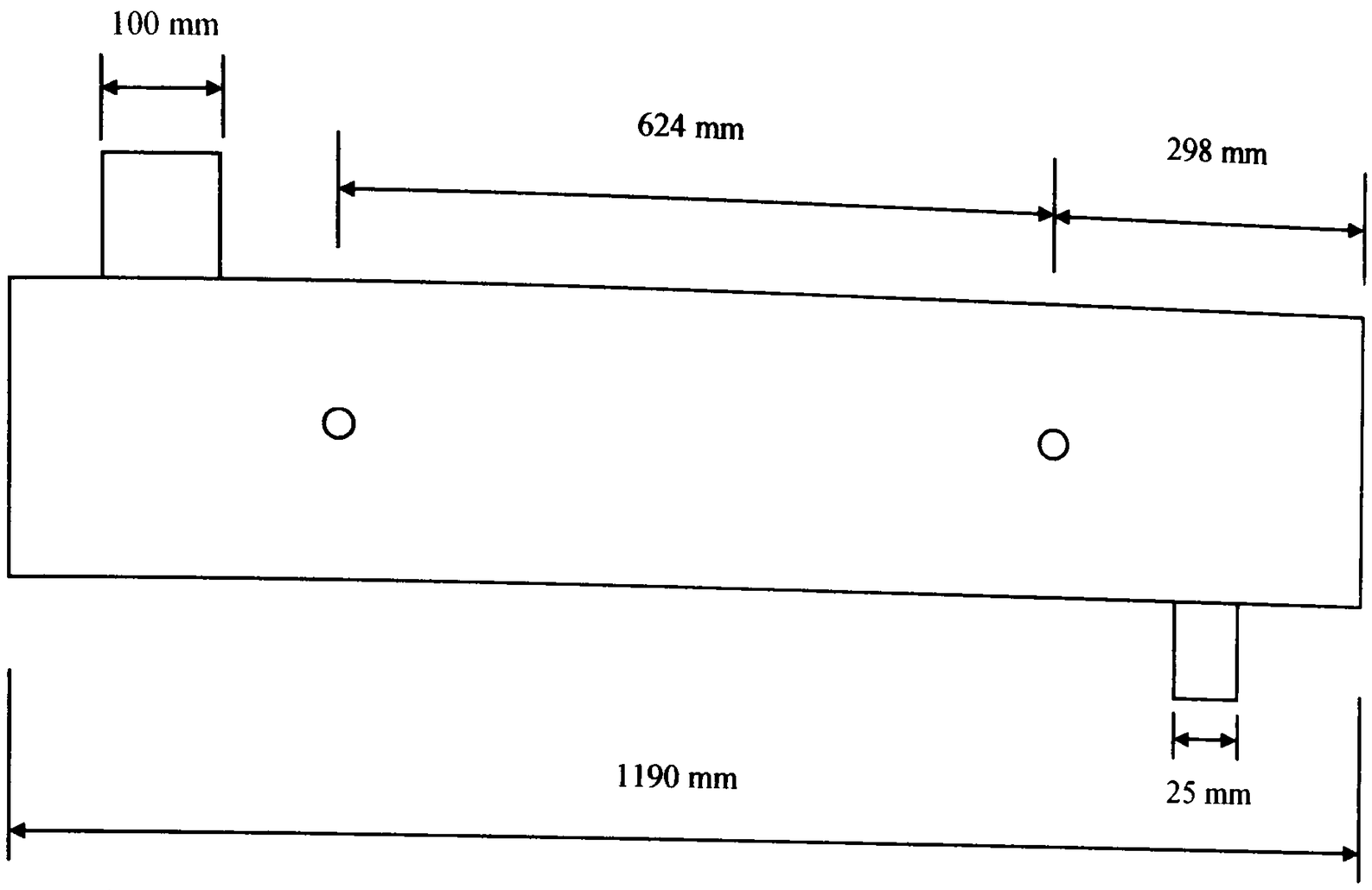

Figure B4 – Location of Shellside Pressure Transducer

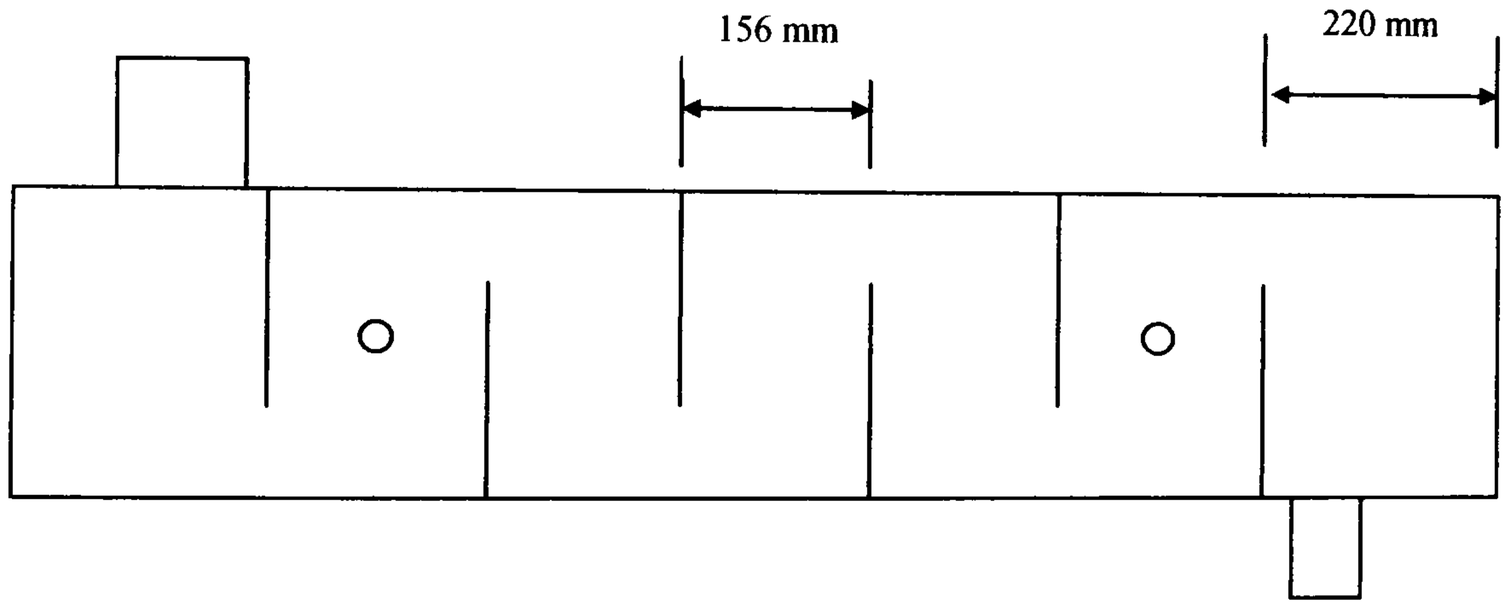

Figure B5 – Shellside Baffle Layout - Test 1 (Horizontal Cut)

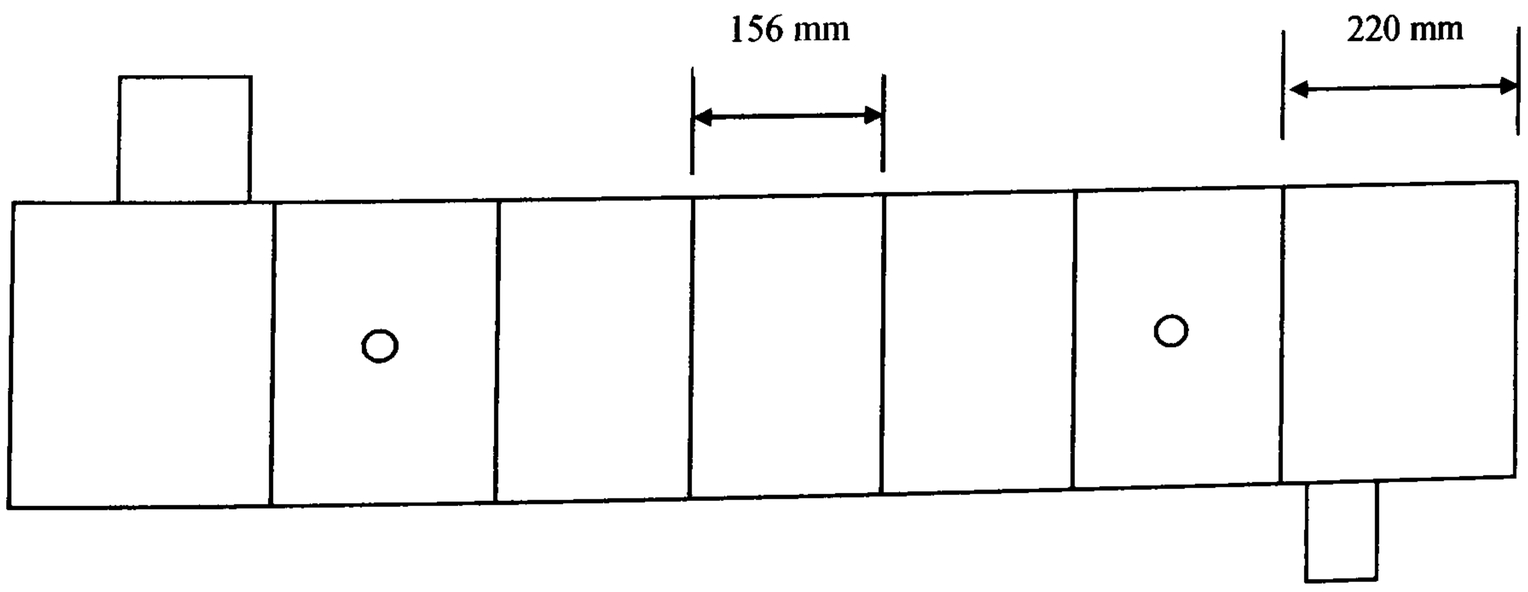

Figure B6 – Shellside Baffle Layout - Test 2 (Vertical Cut)

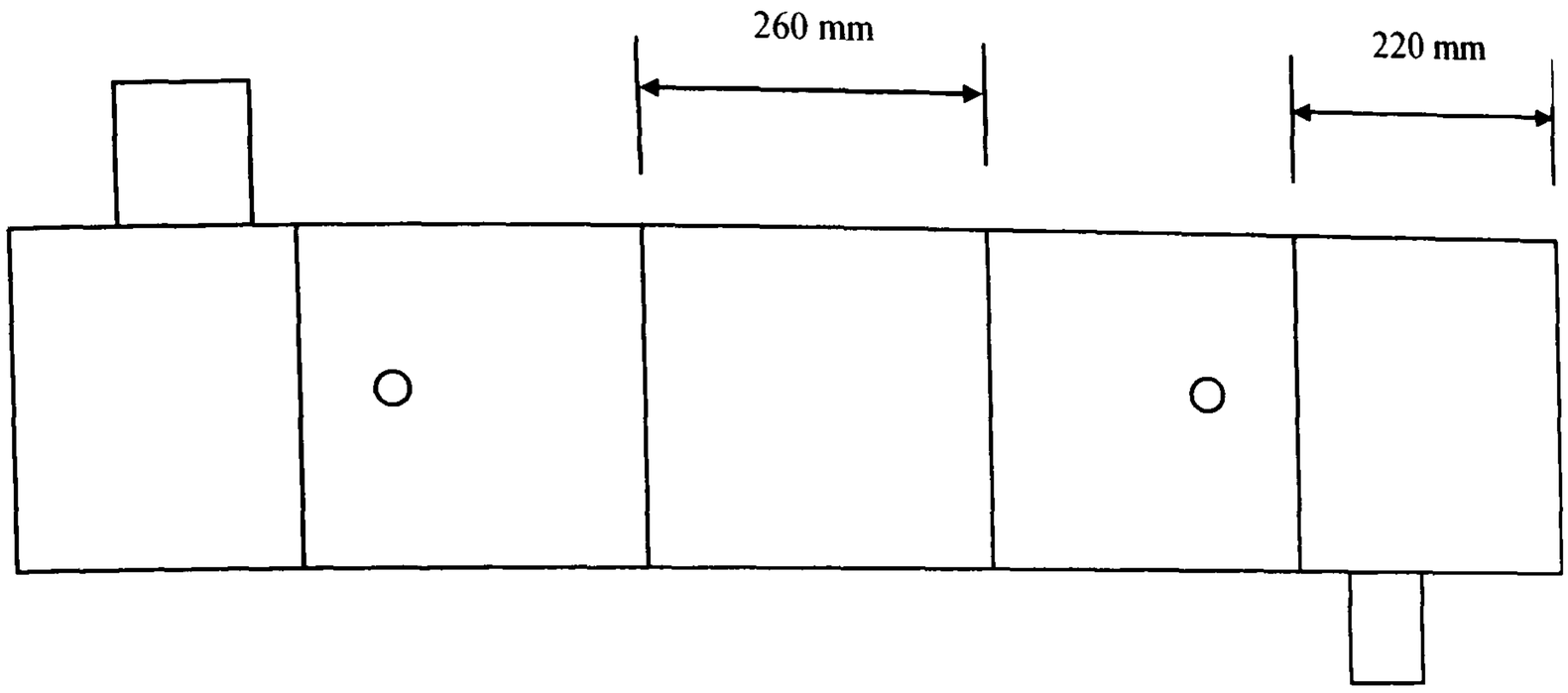

Figure B7 – Shellside Baffle Layout – Test 3 (Vertical Cut)

Appendix C: VBA Computer Code for Shellside Models (A – C)

In this appendix the principal subroutines of computer code that were written to produce the results of the shellside models are presented. It should be noted that these subroutines form only part of the overall models as they are designed to link to other sub-routines which are not presented here as they contain many of the proprietary design methods used in the HTFS TASC program. The code is presented here for the purpose of demonstrating how the models were set-up to be used in conjunction with the TASC style design methods.

Model-A Heat Transfer

The function (htboil) which was used to produce the iterative calculation of the shellside boiling heat transfer coefficient is presented below. Also presented are the functions for calculating the nucleate boiling coefficient (htnuc) and the tubeside condensing heat transfer coefficient (htcond).

Function C1 – htboil

```
Function fn_htboil(Thot, Tcold, x, MFLUX, ALPHAL,
FLOWCOND)
'
'DESC: Returns shellside boiling heat transfer co-efficient
'------------------
'INPUT:
'       Thot = hot stream temperature (tube side)
'       Tcold = cold stream temperature (shell side)
'       x = vapour quality
'       MFLUX = mass flux (kg/m2s)
'        ALPHAL = single-phase liquid coefficient from HTFS
method
'       FLOWCOND = mass flowrate condensate (kg/s)
'------------------
'NOTES:
'------------------
'HISTORY:
' Mod.  Date     By       Description
' 0   20/01/03  G.Doo
'
'_____________________________________
'LOCAL DECLARATIONS
'Error Handler
On Error GoTo Err_fn_htboil
'------------------------------
'initial estimate of heat flux q
qinit = 10000
q = qinit
'set initial number of iterations
n = 0
'tube wall heat transfer co-eff
htwall = 288828
'tubeside co-eff multiplied by tube outer to inner diameter
ratio for U calculation
htcond = fn_htcond(FLOWCOND, Thot) * 15.88 / 13.4
'iterative loop for boiling co-eff
Do
HTBOIL = fn_htcomb(Tcold, q, x, MFLUX, ALPHAL)
'calculating overall co-efficient U
invU = (1 / htwall + 1 / htcond + 1 / HTBOIL)
U = 1 / invU
're-calculating heat flux
q1 = U * (Thot - Tcold)
Conver = Abs((q1 - q) / q1)
q = q1
n = n + 1
Loop Until Conver < 0.05 Or n = 50
'Set returning value
 fn_htboil = HTBOIL
'_____________________________
'Exit before error handler
 Exit Function
'eeeeeeeeeeeeeeeeeeeeeeeee
Err_fn_htboil:
 fn_htboil = 0  'Return value if problem occurs
'_____
'eeeeeeeeeeeeeeeeeeeeeeeee
'___________
End Function
```

Function C2 – htnuc

```
Function fn_htnuc(Tcold, q)
'DESC: Returns nucleate boiling heat transfer co-efficient
'THIS FUNCTION IS CALLED BY fn_htboil
'-----------
'INPUT:    q = heat flux (w/m2)
'          Tcold = cold stream temperature (shell side)
'SOURCES:
'  1. Based on Stephan-Abdelsalam method for nucleate boiling
'       Int. Journal Heat and Mass Transfer Vol. 23 pp73-87, 1980.
'-----------
'HISTORY:
' Mod.  Date     By       Description
' 0   20/01/03  G.Doo
'_____________________________________
'LOCAL DECLARATIONS
'Error Handler
On Error GoTo Err_fn_htnuc
'-------------------------
'calculating nucleate boiling co-efficient
'Laplace constant
B = (2 * fn_PropR134a(Tcold, 14) / (9.81 * (fn_PropR134a(Tcold, 1) - fn_PropR134a(Tcold, 6)))) ^ 0.5
'bubble diameter
Db = 0.0146 * 35 * B
'thermal diffusivity
Thdiff = fn_PropR134a(Tcold, 4) / (fn_PropR134a(Tcold, 1) * fn_PropR134a(Tcold, 2))
'parameters in stephan-abdelsalam correlation
X1 = q * Db / (fn_PropR134a(Tcold, 4) * (Tcold + 273))
X2 = Thdiff ^ 2 * fn_PropR134a(Tcold, 1) / (fn_PropR134a(Tcold, 14) * Db)
X4 = (fn_PropR134a(Tcold, 11)) * Db ^ 2 / Thdiff ^ 2
X5 = fn_PropR134a(Tcold, 6) / fn_PropR134a(Tcold, 1)
X13 = (fn_PropR134a(Tcold, 1) - fn_PropR134a(Tcold, 6)) / fn_PropR134a(Tcold, 1)
'correlation
HTCNU = fn_PropR134a(Tcold, 4) / Db * 0.23 * X1 ^ 0.674 * X5 ^ 0.297 * X4 ^ 0.371 * X13 ^ (-1.73) * X2 ^ 0.35
htnuc = HTCNU
'Set returning value
 fn_htnuc = htnuc
'_____________________________
'Exit before error handler
  Exit Function
'eeeeeeeeeeeeeeeeeeeeeeeeee
Err_fn_htnuc:
  fn_htnuc = 0  'Return value if problem occurs
'_____
'eeeeeeeeeeeeeeeeeeeeeeeeee
'_________
End Function
```

Function C3 – htcond

```
Function fn_htcond(FLOWCOND, Thot)
'DESC: Returns heat transfer co-efficient for tubeside condensation
'THIS FUNCTION IS CALLED BY fn_htflux
'-----------
'INPUT:    FLOWCOND = mass flowrate of condensate in one tube
'          Thot = Condensate Temperature
'SOURCES:
'  1. use methods from:HTFS Handbook CM9 for condensation in uniform channels
'  2. Based on BOYKO-KRUZHILIN method, Int. Journal Heat and Mass Transfer
'     Vol. 10 pp361-373 (1967)
'HISTORY:
' Mod.  Date     By       Description
' 0   15/01/03  G.Doo
'_____________________________________
'LOCAL DECLARATIONS
'Error Handler
On Error GoTo Err_fn_htcond
'---------------------------------
'condensate properties
Cl = fn_PropWat(Thot, 2) / 1000
VISCL = fn_PropWat(Thot, 3)
kl = fn_PropWat(Thot, 4)
'tube internal diameter (m)
D = 0.0134
'Calculation of the condensate Prandtl number
Prl = Cl * VISCL / kl
RELO = 4 * FLOWCOND / (3.14159 * D * VISCL)
'assuming that total flow with condensate properties
'using Mikheev (1956)
hlo = 0.021 * kl / D * RELO ^ 0.8 * Prl ^ 0.43
'calculation of local co-efficent at tube inlet and outlet
'assuming quality of 1 at inlet and quality of 0 at outlet
RHOL = fn_PropWat(Thot, 1)
RHOG = fn_PropWat(Thot, 6)
hlin = hlo * (RHOL / RHOG) ^ 0.5
hlout = hlo
'mean co-efficient
htmean = (hlin + hlout) / 2
htcond = htmean
'Set returning value
  fn_htcond = htcond
'_____________________________
'Exit before error handler
  Exit Function
'eeeeeeeeeeeeeeeeeeeeeeeeee
Err_fn_htcond:
  fn_htcond = 0  'Return value if problem occurs
'_____________
End Function
```

Model-B – Flow Model

For the stratified flow model (Model-B) three sub-routines have been presented. The sub-routine (Stratified) is presented which contains the basic assumption of equal pressure drop across the phases and the iterative void fraction solution of the shellside pressure drop. Also shown is the function (ArfStrat) which contains the modification to the Model-A flow areas for use in the stratified model. Finally a function which uses the stratified flow model to produce an average shellside void fraction (AverageVF) is also presented.

Function C4 – Stratified

```
Function fn_Stratified(TEMP, QUALITY, FLOW, SS, OUT,
BCUT)
'
'DESC: Returns liquid phase height and stratified pressure
drop in side-side flow
'----------------
'INPUT:    TEMP = Temperature
'          QUALITY = vapour mass fraction
'          FLOW = flowrate
'          SS = number of pairs of sealing strips
'          OUT = desired output
'             1 = Stratified Pressure Drop (no-shear)
'             2 = Void Fraction
'             3 = Stratified liquid height
'          BCUT = baffle cut orientation (1=horizontal,
2=vertical)
'----------------
'NOTES:
----------------
'HISTORY:
' Mod.  Date     By       Description
' 0   24/05/02  G.Doo
'
'-------------------------------------------------
'LOCAL DECLARATIONS
'Error Handler
On Error GoTo Err_fn_Stratified
'---------------------------------
'carrying out iterative calculation to determine void fraction
'that produces pressure drop equality
'branch for single phase
If QUALITY = 0 Then
VF = 0
Stratified = fn_Pdflow(0, TEMP, 0, FLOW, SS, 1, 0, 1, BCUT,
0, 0)
ElseIf QUALITY = 1 Then
VF = 1
Stratified = fn_Pdflow(1, TEMP, 1, FLOW, SS, 1, 1, 1, BCUT,
0, 0)
Else
'set initial values
VF1 = 0.95
VF2 = 0.05
n = 0
FLOWL = (1 - QUALITY) * FLOW
FLOWV = QUALITY * FLOW
Do
'calculate pressure drops for each phase with respective void
fractions
PDL1 = fn_Pdflow(0, TEMP, QUALITY, FLOWL, SS, 1, VF1,
1, BCUT, 0, 0)
PDV1 = fn_Pdflow(1, TEMP, QUALITY, FLOWV, SS, 1, VF1,
1, BCUT, 0, 0)
DP1 = PDL1 - PDV1
PDL2 = fn_Pdflow(0, TEMP, QUALITY, FLOWL, SS, 1, VF2,
1, BCUT, 0, 0)
PDV2 = fn_Pdflow(1, TEMP, QUALITY, FLOWV, SS, 1, VF2,
1, BCUT, 0, 0)
DP2 = PDL2 - PDV2
'iterative method of false position
VF3 = (VF1 * DP2 - VF2 * DP1) / (DP2 - DP1)
DP = Abs(DP2)
If VF3 > 0.99 Then
VF2 = 0.75
Else
VF2 = VF3
End If
n = n + 1
Loop Until DP < 1 Or n = 30
End If
'total area
 'geometrical details
   DS = 0.254     'Inner Shell diameter
   RS = DS / 2    'Inner Shell Radius
   DT = 0.01588   'Tube outer diameter
   'cross sectional area of shell
   AREAT = 3.14159 * DS ^ 2 / 4
   AREAL = (1 - VF2) * AREAT
   AREAV = VF2 * AREAT
If VF2 > 0.5 Then
AREA = AREAL
```

```
Else
AREA = AREAV
End If
'ITERATIVE CALCULATION
'-------------------------------
'set initial limits of calculation as shell radius and min height
h1 = 0.127
h2 = 0.0001 'initial min phase height
Do
'calculating areas
COSTERM1 = (RS - h1) / RS
INVCOS1 = Atn(-COSTERM1 / Sqr(-COSTERM1 * COSTERM1 + 1)) + 2 * Atn(1)
A1 = RS ^ 2 * INVCOS1 - (RS - h1) * (2 * RS * h1 - h1 ^ 2) ^ 0.5
COSTERM2 = (RS - h2) / RS
INVCOS2 = Atn(-COSTERM2 / Sqr(-COSTERM2 * COSTERM2 + 1)) + 2 * Atn(1)
A2 = RS ^ 2 * INVCOS2 - (RS - h2) * (2 * RS * h2 - h2 ^ 2) ^ 0.5
'differences between areas and required phase area
dA1 = A1 - AREA
dA2 = A2 - AREA
'using iterative method of false position
h3 = (h1 * dA2 - h2 * dA1) / (dA2 - dA1)
h2 = h3
Loop Until dA2 > -0.00001
If VF2 > 0.5 Then
HLIQ = h2
Else
HLIQ = DS - h2
End If
Stratheight = HLIQ
If QUALITY > 0 Then
If QUALITY < 1 Then
'set desired output
If OUT = 1 Then
Stratified = PDL2
ElseIf OUT = 2 Then
Stratified = VF2
Else
Stratified = Stratheight
End If
End If
End If
'Set returning value
 fn_Stratified = Stratified
'-------------------------------
'Exit before error handler
 Exit Function
Err_fn_Stratified:
 fn_Stratified = 0  'Return value if problem occurs
'eeeeeeeeeeeeeeeeeeeeeeeeee
'-----------
End Function
```

Function C5 – ArfStrat

```
Function fn_ArfStrat(PHASE, TEMP, IFR, FLOW, QUALITY, LEVEL, AREA, VF, BCUT)
'Desc:  Outputs flow area for stratified flow
'Amended 19.06.02 flow area calcs for tube baffle and window
'-----------------------------------------
'Input:
'     PHASE = 0-Liquid, 1-Vapour, 2-Two-Phase
'     TEMP = Temperature
'     IFR = Flow path (as described above)
'     FLOW = Flowrate of gas, liquid or two-phase
'     QUALITY = Vapour mass fraction
'       LEVEL = 1-Xsectional area covered by phase is less than half overall area
'             2-Xsectional area covered by phase is more than half overall area
'     VF = Vapour void fraction
'     BCUT = baffle cut orientation (1=horizontal, 2=vertical)
'-------------------------------------------------
'calculating overall flow areas vapour and liquid
RHOL = fn_PropR134a(TEMP, 1)
RHOG = fn_PropR134a(TEMP, 6)
'Liquid and vapour flowrates
ML = FLOW * (1 - QUALITY)
MV = FLOW * QUALITY
'total area
 'geometrical details
   DS = 0.254     'Inner Shell diameter
   RS = DS / 2    'Inner Shell Radius
   DT = 0.01588   'Tube outer diameter
   'cross sectional area of shell
   AREAT = 3.14159 * DS ^ 2 / 4
'vapour area
AREAV = VF * AREAT
'liquid area
AREAL = AREAT - AREAV
'calculating height of phase in heat exchanger
'ITERATIVE CALCULATION
'-------------------------------
'set initial limits of calculation as shell radius and min height
h1 = 0.127
h2 = 0.0001 'initial min phase height
If AREAV > AREAL Then
Areq = AREAL
Else
Areq = AREAV
End If
Do
'calculating areas
COSTERM1 = (RS - h1) / RS
INVCOS1 = Atn(-COSTERM1 / Sqr(-COSTERM1 * COSTERM1 + 1)) + 2 * Atn(1)
```

```
A1 = RS ^ 2 * INVCOS1 - (RS - h1) * (2 * RS * h1 - h1 ^ 2) ^
0.5
COSTERM2 = (RS - h2) / RS
INVCOS2 = Atn(-COSTERM2 / Sqr(-COSTERM2 *
COSTERM2 + 1)) + 2 * Atn(1)
A2 = RS ^ 2 * INVCOS2 - (RS - h2) * (2 * RS * h2 - h2 ^ 2) ^
0.5
'differences between areas and required phase area
dA1 = A1 - Areq
dA2 = A2 - Areq
'using iterative method of false position
h3 = (h1 * dA2 - h2 * dA1) / (dA2 - dA1)
h2 = h3
Loop Until dA2 > -0.00001
h = h2
'calculating flow areas for each flow path
Select Case IFR
'
-------------------------------------------------------
Case 1  'crossflow
'constraint for less/more than half full case
If LEVEL = 1 Then
fn_ArfStrat = fn_Arf(1) * h / DS
Else
fn_ArfStrat = fn_Arf(1) - fn_Arf(1) * h / DS
End If
'
-------------------------------------------------------
Case 2  'Crossflow bypass
If BCUT = 1 Then
fn_ArfStrat = fn_Arf(2)
Else
fn_ArfStrat = fn_Arf(2) / 2
End If
'
-------------------------------------------------------
Case 3  'In-line pass partition
fn_ArfStrat = fn_Arf(3)
'
-------------------------------------------------------
Case 4  'Window Flow
'baffle geometric details for window flow
'area of window flow segment with 30% baffle cut
Asegwin = 0.3 * 3.14159 * RS ^ 2
'use iterative calculation to get distance from shell to baffle
edge
'ITERATIVE CALCULATION
'
-------------------------
'set initial limits of calculation as shell radius and min height
hW1 = 0.127
hW2 = 0.0001 'initial min window height
AWreq = Asegwin
Do
'calculating areas
COSTERMW1 = (RS - hW1) / RS
INVCOSW1 = Atn(-COSTERMW1 / Sqr(-COSTERMW1 *
COSTERMW1 + 1)) + 2 * Atn(1)
AW1 = RS ^ 2 * INVCOSW1 - (RS - hW1) * (2 * RS * hW1 -
hW1 ^ 2) ^ 0.5
COSTERMW2 = (RS - hW2) / RS
INVCOSW2 = Atn(-COSTERMW2 / Sqr(-COSTERMW2 *
COSTERMW2 + 1)) + 2 * Atn(1)
AW2 = RS ^ 2 * INVCOSW2 - (RS - hW2) * (2 * RS * hW2 -
hW2 ^ 2) ^ 0.5
'differences between areas and required window area
dAW1 = AW1 - Asegwin
dAW2 = AW2 - Asegwin
'using iterative method of false position
hW3 = (hW1 * dAW2 - hW2 * dAW1) / (dAW2 - dAW1)
hW2 = hW3
Loop Until dAW2 > -0.00001
'branch for different baffle cut orientation
'HORIZONTAL BAFFLE CUT
If BCUT = 1 Then
If LEVEL = 1 Then
If h < hW2 Then
fn_ArfStrat = 0.5 * (A2 / Asegwin) * fn_Arf(4)
Else
fn_ArfStrat = 0.5 * fn_Arf(4)
End If
ElseIf LEVEL = 2 Then
If h < hW2 Then
fn_ArfStrat = fn_Arf(4) - 0.5 * (A2 / Asegwin) * fn_Arf(4)
Else
fn_ArfStrat = 0.5 * fn_Arf(4)
End If
End If
'VERTICAL CUT
ElseIf BCUT = 2 Then
'distance from centre of shell to baffle edge
dist = RS - hW2
'chord length
l = 2 * (RS ^ 2 - dist ^ 2) ^ 0.5
'height of baffle cut above base of shell
x = (DS - l) / 2
'area of segment beneath baffle cut
COSTERMbaf = (RS - x) / RS
INVCOSbaf = Atn(-COSTERMbaf / Sqr(-COSTERMbaf *
COSTERMbaf + 1)) + 2 * Atn(1)
Asegbaf = RS ^ 2 * INVCOSbaf - (RS - x) * (2 * RS * x - x ^
2) ^ 0.5
'area covered by liquid/vapour phase
COSTERMPHASE = (RS - h) / RS
INVCOSPHASE = Atn(-COSTERMPHASE / Sqr(-
COSTERMPHASE * COSTERMPHASE + 1)) + 2 * Atn(1)
Aseg1 = RS ^ 2 * INVCOSPHASE - (RS - h) * (2 * RS * h - h
^ 2) ^ 0.5
If Aseg1 < Asegbaf Then
If LEVEL = 1 Then
fn_ArfStrat = 0
Else
fn_ArfStrat = fn_Arf(4)
End If
ElseIf Aseg1 > Asegbaf Then
```

```
'accounting for half empty/full case
If LEVEL = 1 Then
fn_ArfStrat = (((Aseg1 - Asegbaf) * 0.5 - dist * (h - x)) /
Asegwin) * fn_Arf(4)
Else
fn_ArfStrat = ((Asegwin - ((Aseg1 - Asegbaf) * 0.5 - dist * (h -
x))) / Asegwin) * fn_Arf(4)
End If
End If
End If
'
_____
_
Case 5  'Shell-Baffle Leakage
'need to calculate arc length submerged
COSTERMleak = (RS - h) / RS
INVCOSleak = Atn(-COSTERMleak / Sqr(-COSTERMleak *
COSTERMleak + 1)) + 2 * Atn(1)
'length of arc
S = DS * INVCOSleak
'overall circumference of shell
CIRC = 3.14159 * DS
If LEVEL = 1 Then
fn_ArfStrat = (S / CIRC) * fn_Arf(5)
Else
fn_ArfStrat = ((CIRC - S) / CIRC) * fn_Arf(5)
End If
'
_____
Case 6  'Tube-Baffle Leakage
'area submerged
COSTERMPHASE = (RS - h) / RS
INVCOSPHASE = Atn(-COSTERMPHASE / Sqr(-
COSTERMPHASE * COSTERMPHASE + 1)) + 2 * Atn(1)
Asub = RS ^ 2 * INVCOSPHASE - (RS - h) * (2 * RS * h - h ^
2) ^ 0.5
If LEVEL = 1 Then
fn_ArfStrat = (Asub / AREAT) * fn_Arf(6)
Else
fn_ArfStrat = ((AREAT - Asub) / AREAT) * fn_Arf(6)
End If
'
_____
Case 7  'Crossflow sealing strip row
'based on assumption same as crossflow
'constraint for less/more than half full case
If LEVEL = 1 Then
fn_ArfStrat = fn_Arf(1) * h / DS
Else
fn_ArfStrat = fn_Arf(1) - fn_Arf(1) * h / DS
End If
'
_____
End Select
End Function
```

Function C6 – AverageVF

```
Function fn_averageVF(PHASE, TEMP, QUALITY, FLOW,
SS, STRAT, BCUT)
'DESC: Outputs average stratified VF Between Baffle
Spaces 2 and 6
'NOTES:
-----------
'HISTORY:
' Mod.  Date     By       Description
' 0   30/01/03  G.Doo
'
_____
'LOCAL DECLARATIONS
'Return value
'Error Handler
On Error GoTo Err_fn_averageVF
'-----------------------------------
'set up quality for each baffle space between 2 and 6
 QUAL2 = (QUALITY / 7) * 2
 QUAL3 = (QUALITY / 7) * 3
 QUAL4 = (QUALITY / 7) * 4
 QUAL5 = (QUALITY / 7) * 5
 QUAL6 = (QUALITY / 7) * 6
'for non-stratified homogeneous flow
If STRAT = 0 Then
averageVF = 0
'for stratified flow
ElseIf STRAT = 1 Then
'calculating VF in each baffle space
 VF2 = fn_Stratified(TEMP, QUAL2, FLOW, SS, 2, BCUT)
 VF3 = fn_Stratified(TEMP, QUAL3, FLOW, SS, 2, BCUT)
 VF4 = fn_Stratified(TEMP, QUAL4, FLOW, SS, 2, BCUT)
 VF5 = fn_Stratified(TEMP, QUAL5, FLOW, SS, 2, BCUT)
 VF6 = fn_Stratified(TEMP, QUAL6, FLOW, SS, 2, BCUT)
End If
'average void fraction
averageVF = (VF2 + VF3 + VF4 + VF5 + VF6) / 5
'Set returning value
 fn_averageVF = averageVF
'
_____
'Exit before error handler
 Exit Function
'eeeeeeeeeeeeeeeeeeeeeeeee
Err_fn_averageVF:
 fn_averageVF = 0  'Return value if problem occurs
'
_____
'eeeeeeeeeeeeeeeeeeeeeeeee
'
_____
End Function
```

Model-C – Flow Model

For Model-C, the code which uses the Taitel/Dukler transition is presented (Transition). Also shown are the smaller sub-routines dA/dL and Hliq which are also used in the calculation.

Function C7 – Transition

```
Function fn_Transition(TEMP, QUALITY, FLOW, SS, BCUT,
AVVF, HLIQ, AREA)
'DESC: Returns Two-Phase flow pattern from Taitel/Dukler
Method
'----------------
'INPUT:    TEMP = Temperature
'          QUALITY = vapour mass fraction
'          FLOW = flowrate
'          SS = number of pairs of sealing strips
'          HLIQ = stratified liquid height
'          BCUT = Baffle orientation 1=Horizontal 2=Vertical
'            AREA = Crossflow and bypass area used for mass
flux
'----------------
'NOTES:
"----------------
'HISTORY:
' Mod.  Date     By       Description
' 0   15/06/03   G.Doo
'
'-------------------------------------------------------
'LOCAL DECLARATIONS
"Error Handler
On Error GoTo Err_fn_Transition
'-------------------------------
'calculating liquid height if stratified flow exists
'calculate gradient dA/dL
dAdL = fn_dAdL(HLIQ)
'total area
 'geometrical details
   DS = 0.254      'Inner Shell diameter
   RS = DS / 2     'Inner Shell Radius
   DT = 0.01588    'Tube outer diameter
   'cross sectional area of shell
   AREAT = 3.14159 * DS ^ 2 / 4
AG = AVVF * AREAT
RHOG = fn_PropR134a(TEMP, 6)
RHOL = fn_PropR134a(TEMP, 1)
MFLUX = FLOW / AREA
ug1 = QUALITY * MFLUX / RHOG
ug2 = (1 - HLIQ / DS) * (((RHOL - RHOG) * 9.81 * AG) /
(RHOG * dAdL)) ^ 0.5
TRANS = ug1 / ug2
If TRANS < 0.95 Then
E = 0
Elseif TRANS > 1.05 Then
E = 1
Else
E = (TRANS - 0.95) / (1.05 - 0.95)
End If
'Set returning value
 fn_Transition = E
'
'-------------------------------
'Exit before error handler
 Exit Function
'eeeeeeeeeeeeeeeeeeeeeeeee
Err_fn_Transition:
 fn_Transition = 0  'Return value if problem occurs
'
'_____
'eeeeeeeeeeeeeeeeeeeeeeeee
'
'__________
End Function
```

Function C8 - dAdL

```
Function fn_dAdL(h)
'Desc:  Outputs rate of change of area in pipe with liquid
height
'---------------------------------------
'Input:
'     h = Liquid height
'-----------------------------------------
'total area
 'geometrical details
   DS = 0.254      'Inner Shell diameter
   RS = DS / 2     'Inner Shell Radius
   DT = 0.01588    'Tube outer diameter
   'cross sectional area of shell
   AREAT = 3.14159 * DS ^ 2 / 4
If h < RS / 2 Then
COSTERM = (RS - h) / RS
INVCOS = Atn(-COSTERM / Sqr(-COSTERM * COSTERM +
1)) + 2 * Atn(1)
A = RS ^ 2 * INVCOS - (RS - h) * (2 * RS * h - h ^ 2) ^ 0.5
Else
h1 = DS - h
COSTERM = (RS - h1) / RS
INVCOS = Atn(-COSTERM / Sqr(-COSTERM * COSTERM +
1)) + 2 * Atn(1)
A1 = RS ^ 2 * INVCOS - (RS - h1) * (2 * RS * h1 - h1 ^ 2) ^
0.5
```

```
A = AREAT - A1
End If
h2 = h + 0.01
If h2 < RS / 2 Then
COSTERM2 = (RS - h2) / RS
INVCOS2 = Atn(-COSTERM2 / Sqr(-COSTERM2 *
COSTERM2 + 1)) + 2 * Atn(1)
A2 = RS ^ 2 * INVCOS2 - (RS - h2) * (2 * RS * h2 - h2 ^ 2) ^
0.5
Else
h22 = DS - h2
COSTERM2 = (RS - h22) / RS
INVCOS2 = Atn(-COSTERM2 / Sqr(-COSTERM2 *
COSTERM2 + 1)) + 2 * Atn(1)
A22 = RS ^ 2 * INVCOS2 - (RS - h22) * (2 * RS * h22 - h22 ^
2) ^ 0.5
A2 = AREAT - A22
End If
difA = A2 - A
difH = h2 - h
dAdL = difA / difH
fn_dAdL = dAdL
End Function
```

Function C9 - Hliq

```
Function fn_Hliq(AVVF)
'Desc:  Outputs stratified liquid height for transition model
'
'-----------------------------------------------
'Input:
'     AVVF = Average void fraction
'-----------------------------------------------
'total area
 'geometrical details
   DS = 0.254      'Inner Shell diameter
   RS = DS / 2     'Inner Shell Radius
   DT = 0.01588    'Tube outer diameter
   'cross sectional area of shell
   AREAT = 3.14159 * DS ^ 2 / 4
'phase areas
AREAV = AVVF * AREAT
AREAL = (1 - AVVF) * AREAT
If AVVF > 0.5 Then
A = AREAL
Elself AVVF < 0.5 Then
A = AREAV
End If
'set initial limits
h1 = 0.127
h2 = 0.0001 'initial min phase height
Do
'calculating areas
COSTERM1 = (RS - h1) / RS
INVCOS1 = Atn(-COSTERM1 / Sqr(-COSTERM1 *
COSTERM1 + 1)) + 2 * Atn(1)
A1 = RS ^ 2 * INVCOS1 - (RS - h1) * (2 * RS * h1 - h1 ^ 2) ^
0.5
COSTERM2 = (RS - h2) / RS
INVCOS2 = Atn(-COSTERM2 / Sqr(-COSTERM2 *
COSTERM2 + 1)) + 2 * Atn(1)
A2 = RS ^ 2 * INVCOS2 - (RS - h2) * (2 * RS * h2 - h2 ^ 2) ^
0.5
'differences between areas and required phase area
dA1 = A1 - A
dA2 = A2 - A
'using iterative method of false position
h3 = (h1 * dA2 - h2 * dA1) / (dA2 - dA1)
h2 = h3
Loop Until dA2 > -0.00001
h = h2
If AVVF > 0.5 Then
HLIQ = h
Else
HLIQ = DS - h
End If
fn_Hliq = HLIQ
End Function
```

The final sub-routines presented (Pdbundle and PdTest3) in this section are used by all the shellside models for calculating the pressure drop between the shellside baffle spaces. The purpose of the sub-routines is to select the method of calculating pressure drop.

Function C10 – Pdbundle

```
Function fn_Pdbundle(PHASE, TEMP, QUALITY, FLOW, SS, STRAT, BCUT, E)
'DESC: Outputs Total Bundle Pressure Drop Between Baffle Spaces 2 and 6
'NOTES:
'----------
'HISTORY:
' Mod.  Date     By       Description
' 0   24/10/01  G.Doo    Initial Version
'
'_____
'LOCAL DECLARATIONS
'Return value
'Error Handler
On Error GoTo Err_fn_Pdbundle
'----------
'set up quality for each baffle space between 2 and 6
 QUAL2 = (QUALITY / 7) * 2
 QUAL3 = (QUALITY / 7) * 3
 QUAL4 = (QUALITY / 7) * 4
 QUAL5 = (QUALITY / 7) * 5
 QUAL6 = (QUALITY / 7) * 6
'for non-stratified homogeneous flow
If STRAT = 0 Then
'calculating pressure drop in each baffle space
 PD2 = 0.5 * fn_Pdflow(PHASE, TEMP, QUAL2, FLOW, SS, 0, 0, 1, BCUT, 1, QUAL2)
 PD3 = fn_Pdflow(PHASE, TEMP, QUAL3, FLOW, SS, 0, 0, 1, BCUT, 1, QUAL3)
 PD4 = fn_Pdflow(PHASE, TEMP, QUAL4, FLOW, SS, 0, 0, 1, BCUT, 1, QUAL4)
 PD5 = fn_Pdflow(PHASE, TEMP, QUAL5, FLOW, SS, 0, 0, 1, BCUT, 1, QUAL5)
 PD6 = 0.5 * fn_Pdflow(PHASE, TEMP, QUAL6, FLOW, SS, 0, 0, 1, BCUT, 1, QUAL6)
'for stratified flow
Elseif STRAT = 1 Then
'calculating pressure drop in each baffle space
If E = 0 Then
 PD2 = 0.5 * fn_Stratified(TEMP, QUAL2, FLOW, SS, 1, BCUT)
 PD3 = fn_Stratified(TEMP, QUAL3, FLOW, SS, 1, BCUT)
 PD4 = fn_Stratified(TEMP, QUAL4, FLOW, SS, 1, BCUT)
 PD5 = fn_Stratified(TEMP, QUAL5, FLOW, SS, 1, BCUT)
 PD6 = 0.5 * fn_Stratified(TEMP, QUAL6, FLOW, SS, 1, BCUT)
Else
 PD2 = 0.5 * fn_Entrained(TEMP, QUAL2, FLOW, SS, 1, BCUT, E)
 PD3 = fn_Entrained(TEMP, QUAL3, FLOW, SS, 1, BCUT, E)
 PD4 = fn_Entrained(TEMP, QUAL4, FLOW, SS, 1, BCUT, E)
 PD5 = fn_Entrained(TEMP, QUAL5, FLOW, SS, 1, BCUT, E)
 PD6 = 0.5 * fn_Entrained(TEMP, QUAL6, FLOW, SS, 1, BCUT, E)
End If
End If
'summing pressure drop
PDTOTAL = PD2 + PD3 + PD4 + PD5 + PD6
'Set returning value
 fn_Pdbundle = PDTOTAL
'_____
'Exit before error handler
 Exit Function
'eeeeeeeeeeeeeeeeeeeeeeeeee
Err_fn_Pdbundle:
 fn_Pdbundle = 0  'Return value if problem occurs
'_____
'eeeeeeeeeeeeeeeeeeeeeeeeee
'_____
End Function
```

Function C11 – PdTest3

```
Function fn_PdTest3(PHASE, TEMP, QUALITY, FLOW, SS, STRAT, BCUT, E, TEST)
'DESC: Outputs Total Bundle Pressure Drop Between Baffle Spaces 2 and 4
'----------
'NOTES:
'Calculates bundle pressure drop with test 3 baffle geometry
'----------
'HISTORY:
' Mod.  Date     By       Description
' 0   24/10/03  G.Doo    Initial Version
'
'_____
'LOCAL DECLARATIONS
'
'Return value

'Error Handler
```

```
On Error GoTo Err_fn_PdTest3
'-------------------------------
'set up quality for each baffle space between 2 and 4
'
 QUAL2 = (QUALITY / 5) * 2
 QUAL3 = (QUALITY / 5) * 3
 QUAL4 = (QUALITY / 5) * 4

'
'for non-stratified homogeneous flow
If STRAT = 0 Then

'calculating pressure drop in each baffle space
'
 PD2 = 0.7 * fn_Pdflow(PHASE, TEMP, QUAL2, FLOW, SS,
0, 0, 1, BCUT, 1, QUAL2, TEST)
 PD3 = fn_Pdflow(PHASE, TEMP, QUAL3, FLOW, SS, 0, 0,
1, BCUT, 1, QUAL3, TEST)
 PD4 = 0.7 * fn_Pdflow(PHASE, TEMP, QUAL4, FLOW, SS,
0, 0, 1, BCUT, 1, QUAL4, TEST)

'
'for stratified flow
Elself STRAT = 1 Then

'calculating pressure drop in each baffle space
'
'
'
If E = 0 Then
 PD2 = 0.7 * fn_Stratified(TEMP, QUAL2, FLOW, SS, 1,
BCUT, TEST)
 PD3 = fn_Stratified(TEMP, QUAL3, FLOW, SS, 1, BCUT,
TEST)
 PD4 = 0.7 * fn_Stratified(TEMP, QUAL4, FLOW, SS, 1,
BCUT, TEST)

'
Else

 PD2 = 0.7 * fn_Entrained(TEMP, QUAL2, FLOW, SS, 1,
BCUT, E, TEST)
 PD3 = fn_Entrained(TEMP, QUAL3, FLOW, SS, 1, BCUT,
E, TEST)
 PD4 = 0.7 * fn_Entrained(TEMP, QUAL4, FLOW, SS, 1,
BCUT, E, TEST)

End If


End If
'summing pressure drop
PDTOTAL = PD2 + PD3 + PD4
```

```
'Set returning value
 fn_PdTest3 = PDTOTAL
'
'-------------------------------
'Exit before error handler
 Exit Function
'eeeeeeeeeeeeeeeeeeeeeeeee
Err_fn_PdTest3:
 fn_PdTest3 = 0  'Return value if problem occurs
'
'-------
'eeeeeeeeeeeeeeeeeeeeeeeee
'
'----------
End Function
```